Investigation of DNA double-strand break-associated histone post-translational modifications using targeted mass spectrometry

A thesis submitted to the University of Sussex for the degree of Doctor of Philosophy

Zuzanna Kozik

October 2018

Declaration

I hereby declare that this thesis has not been, and will not be, submitted in whole or in part to another University for the award of any other degree.

Zuzanna Kozik

Acknowledgments

I would like to thank Dr Steve Sweet and Dr Velibor Savic for offering me the opportunity to undertake this work, and for all of the guidance during the course of this project. I would also like to thank Prof Penny Jeggo for overtaking my supervision after Steve left. I am very grateful to everyone in GDSC, and in particular Dr Jo Murray and Prof Tony Carr, for their continual support and assistance and for making GDSC such an enjoyable place to work. Finally, I would like to thank my friends and family and everyone who has helped me during past four years, this would not be possible without you.

UNIVERSITY OF SUSSEX

ZUZANNA KOZIK

DOCTOR OF PHILOSOPHY GENOME STABILITY

INVESTIGATION OF DNA DOUBLE-STRAND BREAKS ASSOCIATED HISTONE POST-TRANSLATIONAL MODIFICATIONS USING TARGETED MASS SPECTROMETRY TECHNIQUES

Summary

DNA double strand breaks (DSBs) pose a major threat to the maintenance of genetic integrity. Cells have evolved response pathways to detect, signal and repair those lesions. Alterations in the factors involved in these pathways may lead to disease development, such as cancer. Several histone modifiers have previously been shown to be recruited to the sites of DSBs, but their role in the repair process still remains unclear. It has been proposed that the cellular response to DSBs leads to changes in phosphorylation, methylation, acetylation and ubiquitination and other post-translational modifications (PTMs) of histones at the site of damage. Some of these modifications are known epigenetic markers involved in maintaining cellular identity. It has been proposed that DSB-induced alterations to the epigenetic code introduce a potential window of opportunity for pathological changes to occur.

Here, I have developed a chromatin immunoprecipitation followed by mass spectrometry (ChIP-MS) method to enrich for mono-nucleosomes containing Ser139-phosphorylated H2AX (γH2AX). I utilise targeted mass spectrometry to quantify histone PTMs associated with γH2AX formed after ionising radiation (IR)

damage of HEK293 cells, as well as wild type and ATM deficient 1BR fibroblasts. Surprisingly, few local changes in histone PTMs associated with γH2AX containing mono-nucleosomes were found. A damage-dependent increase in H2A(X) lysine15 ubiquitination (H2A(X) K15Ub) was detected and I gained insight into the dynamics of this important PTM. We found that γH2AX levels are maximal within 30 min of IR exposure after 3 Gy whilst H2A(X) K15Ub reaches maximal level at 4-8 h. A dose-response analysis revealed that whilst γH2AX levels increase linearly with dose, the level of H2A(X) K15Ub peaks at ~3 Gy and is substantially diminished after 40 Gy, demonstrating that the response is not linear with dose and becomes saturated at higher doses. Furthermore, our preliminary data suggests that contrary to previous reports ATM-dependent late repairing DSBs are not enriched in constitutive heterochromatin marks. I discuss the clinical significance of these findings.

53BP1	p53 binding protein 1
Ac	Acetylation
ADD	ATRX, DNMT3 and DNMT3L domain
AEBSF	4-(2-aminoethyl) benzenesulfonyl fluoride hydrochloride
Alt-NHEJ	Alternative NHEJ
AP	Apurinic/Apyrimidinic
APLF	Aprataxin and PNK-like factor
APTX	Aprataxin
ARR	Access-Repair-Restore model
A-T	Ataxia telangiectasia disorder
ATM	Ataxia telangiectasia mutated
ATP	Adenosine tri-phosphate
ATR	Ataxia telangiectasia and Rad3 related
BAH	Bromo adjacent homology domain
Bax	Bcl-2 associated X protein
Bcl-2	B-cell lymphoma 2
BER	Base excision repair
BRCT	BRCA1 C-terminal domain
BrD	Bromo-domain
c-Abl	Cellular Abelson tyrosine-protein kinase 1
CHK1/2	Checkpoint kinase 1/2
ChIP	Chromatin immunoprecipitation
CK2	Casein kinase 2
CPT	Camptothecin

CtIP	CtBP-interacting protein
DDA	Data-dependent acquisition
DDR	DNA damage response
DNA	Deoxyribonucleic acid
DNA-PK	DNA-dependent protein kinase
DNA-PKcs	DNA-dependent protein kinase catalytic subunit
DSB	Double-strand break
DUB	De-ubiquitinating enzyme
EXO1	Exonuclease 1
FA	Formic acid
FAT	Focal adhesion kinase
FAT-C	Focal adhesion kinase C-terminal
FEN1	Flap endonuclease 1
FHA	Forkhead-associated domain
γH2AX	Histone H2AX pSer139
GFP	Green fluorescent protein
HDAC	Histone deacetylase
HEAT	Huntington, elongation factor 3 (EF3), the 65 kDa alpha regulatory subunit of protein phosphatase 2A (PP2A) and the yeast PI3-kinase TOR1
HP1	Heterochromatin protein 1
HR	Homologous recombination
hTERT	Human telomerase reverse transcriptase
IP	Immunoprecipitation
IR	Ionising radiation

KAP-1	Kruppel associated box domain protein 1
LC-MS/MS	Liquid chromatography tandem mass spectrometry
LET	Linear energy transfer
LIG3	DNA Ligase 3
LTQ	Linear trap quadrupole
MBT	Malignant brain tumour repeat
MDC1	Mediator of DNA damage checkpoint protein 1
Me1/2/3	Mono-/di-/tri-methylation
MEF	Mouse embryonic fibroblast
MNase	Micrococcal nuclease
MMEJ	Microhomology-mediated end joining
MRN	Mre11-Rad50-Nbs1
NCS	Neocarzinostatin
NER	Nucleotide excision repair
NHEJ	Non-homologous end joining
PAXX	Paralog of XRCC4 and XLF
PAR	Poly(ADP-ribose)
PARG	Poly(ADP-ribose) glycohydrolase
PARP	Poly(ADP-ribose) polymerase
PHD	Plant homeodomain
PHF8	PHD finger protein 8
PI3K	Phosphatidylinositol 3-kinase-related kinase
PMSF	Phenylmethylsulfonyl fluoride
PNKP	Polynucleotide kinase/phosphatase

PRC1	Polycomb repressive complex 1
PTIP	PAX-interacting protein 1
PTM	Post-translational modification
PUMA	p53 upregulated modulator of apoptosis
PWWP	‘Proline-Tryptophan- Tryptophan- Proline’ domain
RAD51	Radiation sensitive protein 51
RAG1/2	Recombination activating gene 1/2
RFP	Red fluorescent protein
RIF1	Rap1-interacting factor 1 homolog
RNA	Ribonucleic acid
RNF168	Ring finger protein 168
RNF8	Ring finger protein 8
RPA	Replication protein A
RT	Radiation therapy
SDS	Sodium dodecyl sulphate
SCID	Severe combined immunodefiency
SRM	Selective reaction monitoring
SSA	Single-strand annealing
SRM	Selected reaction monitoring
SSB	Single-strand break
SSBR	Single-strand break repair
SUMO	Small ubiquitin-like modifier
TAD	Topologically associating domain
TDP1	Tyrosyl-DNA phosphodiesterase 1

TDP2	Tyrosyl-DNA phosphodiesterase 2
TEAB	Triethylammonium bicarbonate
TFA	Trifluoroacetic acid
TIP60	60 kDa Tat-interactive protein
TOP1	DNA topoisomerase 1
TOP2	DNA topoisomerase 2
TOP3	DNA topoisomerase 3
Ub	Ubiquitination
UV	Ultraviolet
WD40	‘Tryptophan-Asparagine’ dipeptide 40 motif
XLF	XRCC4-like factor
XRCC4	X-ray cross complementing group 4
Zn-CW	Zinc finger-‘Cysteine and Tryptophan’ domain

Index of Figures

Index of tables

1 CHAPTER ONE: INTRODUCTION

1.1 DNA DAMAGE AND ITS CONSEQUENCES

The genetic information of a eukaryotic cell is packaged into chromatin, which is a highly condensed structure composed of DNA, histones and other associated proteins. Besides being encoded by the DNA sequence, the information required for the proper functioning of the organism is also determined by the pattern of DNA and histone modifications known as epigenetic marks.

Every day we are exposed to a range of genotoxic agents, which pose a major threat to the integrity of genetic information. It has been shown that a variety of exogenous and endogenous toxins or exposures, such as ultra violet (UV) light, ionizing radiation (IR) or replication stress to name a few, can induce DNA lesions.

DNA double-strand breaks (DSBs) are particularly dangerous. If not repaired correctly, these lesions can have profound consequences to the health of the affected cell, tissue or even the whole organism. For instance, mutations to the genetic code can impact on crucial cellular pathways involved in the regulation of cell cycle, DNA repair and apoptosis, which are important for prevention and accumulation of chromosomal aberrations and consequently contribute to the development of a disease state, such as cancer, neurodegeneration, immunodeficiency and premature ageing (Jackson and Bartek, 2009). Therefore, faithful repair of DSBs is crucial for human health.

In order to prevent the formation and propagation of those pathogenic changes, the cell has evolved DNA damage response (DDR) pathways that allow the recognition of DNA damage and signal it to the cell. This signaling triggers the activation of a cell cycle arrest, which allows time for the repair of the break. Depending on the stage of the cell cycle and the type of lesion, different repair pathways may be preferred. The choice of repair pathway can be also influenced by the chromatin state, as well as by existing histone post-translational modifications (PTMs) (Aymard *et al.*, 2014). The signaling of damage and the repair process itself also require modification of the chromatin structure.

Specific histone PTMs act to signal damage to the regions flanking the break, recruit factors that protect naked DNA ends or relax chromatin to allow access

of the repair machinery (Lukas, Lukas and Bartek, 2011). Additionally, some histones might be exchanged with their variants or even whole nucleosomes might be removed from the site of damage (Mehrotra *et al.*, 2011; Xu *et al.*, 2012; Adam, Polo and Almouzni, 2013). Once the repair has occurred, the chromatin must be restored to its previous state.

A range of histone PTMs have been reported to play a role in the cellular response to DNA damage. Also, several histone modifiers, which are often mutated in cancer, have been reported to be recruited to the sites of breaks. However, in most cases the exact role or consequence of the PTM in the subsequent DNA repair process is still to be elucidated. This thesis focuses on the impact of DNA DSBs on the surrounding chromatin environment.

1.2 SOURCES OF DNA DSBS

DNA DSBs are the most dangerous cytotoxic lesions. If they are not repaired correctly, they may lead to pathogenic changes, which in turn may contribute to development of disease states, such as cancer. If they are not repaired at all, they may lead to cell death. Enhanced cell death can cause stem cell depletion and is particularly dangerous if a given cell is for example a post-mitotic neuron, as this may contribute to neurodegeneration (Espada and Ermolaeva, 2016; McKinnon, 2017). DSBs arise, when the sugar-phosphate backbone of both strands of DNA are broken in close proximity to each other. This may lead to physical dissociation and separation of damaged DNA ends, and potentially to chromosomal rearrangements. Chromosomal translocations are known to cause loss-of-function in tumour suppressor genes or gain-of-function in proto-oncogenes, further contributing to cancer development (Haber and Fearon, 1998). It has been estimated that on average ~10 DSBs per cell may arise spontaneously every day, induced by both internal and external factors sources (Jan H J Hoeijmakers, 2009).

1.2.1 Endogenous sources of DSBs

1.2.1.1 Topoisomerases

DSBs can be induced during normal physiological processes, such as transcription and DNA replication, which can produce superhelical tension in DNA. This torsional stress needs to be relieved and it may be lifted by a family of enzymes known as topoisomerases, of which there are three types: 1A (TOP3α/β), 1B (TOP1) and 2 (TOP2α/β) (Pommier *et al.*, 2016). Although the TOP1 family is known to introduce a cleavage in a single strand of DNA, there are several instances where this lesion may be converted to a DSB. Some drugs used in cancer therapy, such as Camptothecin, function to trap TOP1 complexes on DNA (Pommier *et al.*, 2006). It has been proposed that if the DNA replication or transcription machinery encounters and collides with poised TOP1 complexes, it may lead to DSB formation (Cristini *et al.*, 2016). Another possibility is that if two poised TOP1 complex-induced SSBs are positioned in close proximity on DNA, this may lead to the separation of DNA ends and conversion to a DSB. In addition, a multitude of exogenous and endogenous DNA lesions, as well as drugs can lead to TOP1 cleavage complex (TOP1cc) trapping, consequently leading to DSB formation and activation of DDR signalling (Pommier *et al.*, 2006).

On the other hand, TOP2 family enzymes alleviate transcriptionally induced torsional stress by introducing a transient cleavage to both of the strands of the DNA phosphodiester backbone, followed by rapid re-ligation of the ends (John L Nitiss, 2009). This process does not usually activate the DDR response. However in some cases, for instance in the presence of TOP2 poisons, the TOP2 cleavage complex (TOP2cc) is stabilised onto DNA preventing the re-ligation step, subsequently leading to the formation of a cytotoxic lesion and activation of DDR signalling (John L. Nitiss, 2009). In non-replicating cells, TOP2-induced breaks have been shown to be a frequent cause of translocations in the regions of highly transcribed genes (Schwer *et al.*, 2016; Wei *et al.*, 2016). Consistently, inhibition of transcription reduces the rate of translocation, while depletion of TDP2 (5'-tyrosyl DNA phosphodiesterase),

which is involved in the removal of TOP2 prior to DNA ends re-ligation, increases in the translocation occurrence (Gómez-Herreros *et al.*, 2017).

1.2.1.2 R-loops

Another potential source of endogenous DSBs are R-loops, which are RNA:DNA hybrids associated with ssDNA forming during transcription. Although for the most part these structures are resolved by RNA processing factors, high levels of transcription may lead to their accumulation. Exposed ssDNA can serve as a substrate for cytosine deamination by the APOBEC enzyme, which can then activate the BER (base excision repair) pathway, consequently leading to DSB formation (Stork *et al.*, 2016). Alternatively, R-loops may lead to activation of the transcription-coupled nucleotide excision repair (TC-NER) machinery, which can remove the hybrid, generating a DSB upon encounter with the replication fork (Stork *et al.*, 2016). R-loops can be also resolved by removing RNA itself through the action of RNase H nuclease or through RNA displacement by the Senataxin (SETX) helicase (Mischo *et al.*, 2011; Skourti-Stathaki, Proudfoot and Gromak, 2011; Sollier *et al.*, 2014).

Interestingly, we have recently demonstrated that depletion of SETX leads to increased misprocessing of R-loops in the proximity of DSBs, which may lead to large deletions and subsequently increased genomic instability (Brustel *et al.*, 2018) (the publication is attached to this thesis). Furthermore, SETX deficiency has been linked to the development of neurological diseases, highlighting it is important in the process of resolving R-loops (Yüce and West, 2013; Groh *et al.*, 2017).

1.2.1.3 Antibody diversification

In higher eukaryotes programmed DSBs can also be introduced during the development of the immune system. The adaptive immune response requires the generation of a repertoire of immunoglobulins (Ig) that can recognise and neutralise a plethora of antigens. This can be generated via pathways known as V(D)J recombination and class switch recombination (CSR) (Jung and Alt, 2004; Hwang, Alt and Yeap, 2015). Diversity is achieved via distinctive processes involving breakage and re-joining of DNA segments. This is achieved via action

of recombination activating enzymes, RAG1 and RAG2, whose expression is restricted to immature lymphocytes. Importantly, the DSBs introduced through the action of RAG proteins have to be repaired through a specific pathway, known as DNA non-homologous end joining (NHEJ) (Dudley *et al.*, 2005). NHEJ has been shown to be required for the development of B and T cells and consequently, patients deficient in the components of this pathway display immunodeficiency, as well as increased radiosensitivity (Woodbine, Gennery and Jeggo, 2014).

1.2.2 Exogenous sources of DSBs

DNA damage can also arise due to external agents, such as ionising radiation (IR) and radiomimetic drugs. IR is a type of high-energy radiation that is able to release electrons from atoms and molecules, thereby ionising them. IR can be categorised into α- and β-particles, neutrons, and X- and γ-rays. The units of radiation are commonly expressed in gray (Gy), which is the measure of the amount of radiation absorbed by 1 kg of animal tissue (Dunne-Daly, 1999).

DNA is highly susceptible to IR. IR is able to induce several types of DNA breaks, particularly DSBs. Charged particles may ionise DNA directly or may ionise water, consequently producing highly reactive hydroxyl (-OH) species, which can then react with DNA. Additionally, reactive oxygen species (ROS) generated by IR can also induce several other types of DNA breaks, such as abasic sites and single strand breaks (SSBs).

Importantly, IR-induced breaks can be very complex, containing multiple type of lesions in close proximity, posing an additional challenge for the repair machinery. Collectively, these lesions contribute to cell death and mitotic failure, and these detrimental consequences are often exploited for radiation therapy (Lomax, Folkes and O'Neill, 2013).

1.2.3 The importance of DNA damaging agents in the cancer therapy treatments

Cancer cells are particularly susceptible to DNA damage, hence IR and radiomimetic drugs are frequently used during treatment of cancer patients. This sensitivity arises as a consequence of the greater cycling capacity of tumour cells caused by inactivated checkpoint responses, resulting in uncontrolled proliferation and increase in genomic instability. In addition to that, downregulation of DDR pathways, for which synthetic lethality can be exploited, further sensitises tumour cells to DNA damage (Pearl *et al.*, 2015; Jeggo, Pearl and Carr, 2016). Treatment with DNA damaging agents aims to reduce the tumour size or to eliminate residual tumour cells.

Radiation therapy (RT) is the most commonly prescribed cancer treatment. The optimum IR dose depends on the type of cancer. The goal of RT is to deliver maximal IR dose to the tumour, while sparing normal tissue. A typical RT regime delivers daily doses of 1.5-3 Gy over several weeks and the limit of RT is decided based on the response of normal tissue that also receives some IR (Hickey *et al.*, 2016; Yarnold, 2018). IR dose size and dose fractionation are important concepts in radiotherapy. Numerous studies have shown that reducing of the dose per fraction delays normal tissue toxicity and allows delivery of higher total doses to tumours, while improving patient survival (Bernier, Hall and Giaccia, 2004). However the molecular basis of this phenomenon are still not completely understood.

Nonetheless, one of the downsides of RT is that IR unavoidably reaches normal tissue, as well as tumour. Subsequently, this may contribute to the formation of chromosomal abnormalities and increased risk of new malignancies. High RT doses are known to produce toxicity, which may contribute to poor patient's prognosis (Brown, Mutter and Halyard, 2015). Additionally, some patients (5-10%) appear to respond abnormally to RT, with severe cases of radiation induced toxicity leading to patients death (Rogers *et al.*, 2000; Pollard and Gatti, 2009). Therefore, RT regimens based on the individual patient/tumour capability

to repair IR-induced breaks could improve the decision for the most suitable treatment for cancer patients, as well as treatment safety.

1.3 DNA REPAIR OCCURS IN THE CONTEXT OF CHROMATIN

Nucleosomes are thought to provide a repressive background to cellular processes that require direct access to DNA, sterically hindering recognition sequences of DNA binding factors, such as RNA polymerases (Orphanides and Reinberg, 2000). Therefore, the processes that entail DNA substrates, such as transcription, replication and repair, require mechanisms which alleviate this repression. Indeed, a plethora of chromatin modifying enzymes has been shown to be involved in processes capable of modulating chromatin accessibility through covalent histone PTMs and nucleosomal remodelling. These processes have been widely studied in the background of transcription and replication, and more recently in the context of DDR and repair.

In recent years, a model for the chromatin response to DNA damage has been proposed, and is referred to as the “access-repair-restore” (ARR) model (Smerdon and Conconi, 1999; Green and Almouzni, 2003; Polo and Almouzni, 2015). In this model, recognition of a DNA break is followed by transient opening of the chromatin achieved via nucleosome mobilisation, chromatin remodelling and histone PTMs, which then allows the access of the repair machineries to the DNA lesion. Once the damage has been repaired, chromatin must be restored to its original state, to ensure preservation of the genetic and epigenetic integrity of the genome. In the past years, several examples of compliance with the ARR model have been demonstrated for the repair of DNA lesions during the nucleotide excision repair (NER) and DSB repair pathways.

Several covalent modifications of histone tails have currently been reported to change in response to DNA DSBs. These include, but are not limited to, phosphorylation of serine and threonine residues, as well as acetylation, ubiquitination and methylation of lysine residues. These alterations have the potential to impact the chromatin structure, as well as to act as a binding platforms for the recruitment of the DNA damage repair machinery.

In this section, I will introduce the concept of the chromatin and discuss our current knowledge regarding its structure and regulation in the context of the DNA damage response.

1.3.1 Chromatin structure

Genetic information of a eukaryotic cell is packaged into chromatin, which is a complex between DNA and associated proteins, of which the most abundant are histones. The repeating unit of chromatin, the nucleosome, consists of 145-147 base pairs (bp) of DNA wrapping 1.65 superhelical turns around an octamer of histone proteins, two of each: H2A, H2B, H3 and H4 (**Figure 1.1**) (Luger *et al.*, 1997). Additionally, the linker histone H1 wraps another 20 bp, resulting in two full turns around the nucleosome. The structure of the histones, canonical nucleosome core and the many alternatives containing variant histones and post-translationally modified residues have been determined, allowing us to gain an insight into the mechanism of chromatin regulation (Koyama and Kurumizaka, 2018).

1.3.1.1 Nucleosome structure

Each nucleosome is composed of the 'core', linker DNA and in most cases, a linker histone, together forming the elementary repeating unit of chromatin. The core is composed of four pairs of histones, which are small (11-15 kDa), basic proteins that are very highly conserved between species. Each of the histones contain a dimerising central histone-fold domain, composed of four α-helices and two loops, spanned by N- and C-terminal unstructured regions known as histone tails. The histone core is involved in mediating stable histone-histone contacts through "handshake" interactions to form the core octamer, as well as forming numerous histone-DNA interactions serving to compact DNA into the nucleus (Mariño-Ramírez *et al.*, 2005).

H3/H4 and H2A/H2B dimers associate with each other through α-helical dimerization domains. H3/H4 dimers interact via the H3/H3 interface, forming stable tetramers in solutions. On the other hand, H2A/H2B dimers associate with H3/H4: H3/H4 tetramers via interactions between H2B:H4, forming a symmetrical tetramer. Importantly, the H2B:H4 interactions are relatively weak

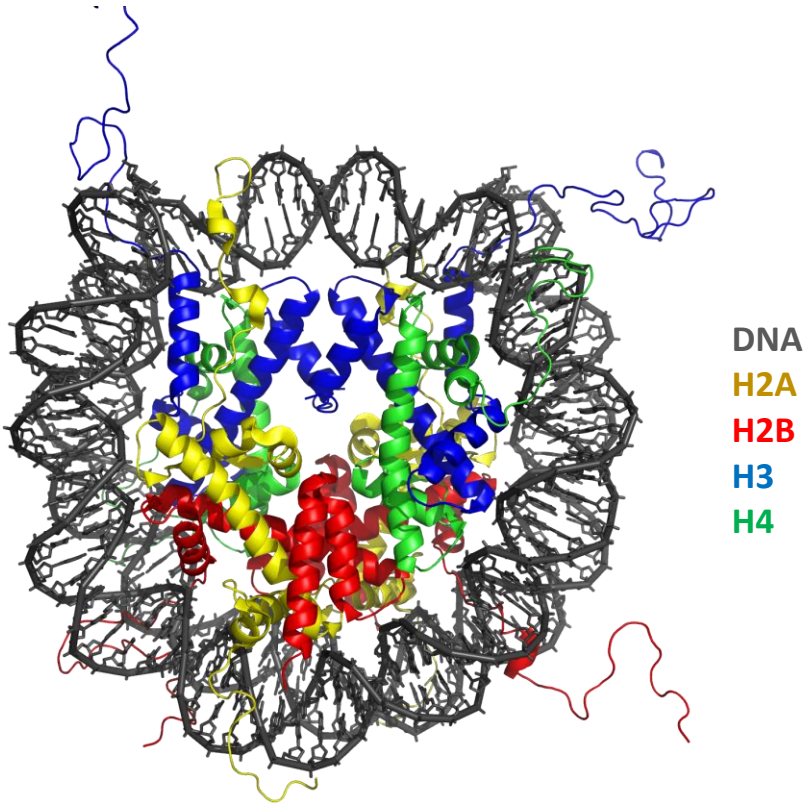

Figure 1.1 Structure of the nucleosome. Nucleoprotein complex consisting of 147 bp of DNA wrapped around a histone octamer composed of two copies of each: H2A, H2B, H3 and H4. Flexible, unstructured regions protruding from the nucleosome are histone tails. Adapted from: Ordu, Lusser and Dekker, 2016.

and the entire octamer only forms when wrapped by DNA (McGinty and Tan, 2015).

Flexible histone tails protrude from the nucleosome core and are easily accessible to the enzymes that deposit post-translational modifications (PTM), which play an important role in the regulation of the nucleosomal structure and dynamics, as well as contribute to the epigenetic regulation of cell fate (Bannister and Kouzarides, 2011). The tails adopt random coil conformations when not associated with DNA or when free in solution. They contain an abundance of lysine and arginine residues, as well as glycine, alanine and threonine, which greatly contribute to their unstructured conformation.

PTMs of histone tails may alter condensed chromatin structure, thereby playing a role in access to genes; serve as a binding platform for cellular machinery or signal specific cellular events (Kouzarides, 2007). Specific genomic regions may contain different patterns of histone PTMs and the combinatorial effect of these modifications has been termed the “histone code” (Strahl and Allis, 2000).

1.3.1.2 Core and variants histones

The majority of core histones are synthesised during S phase of the cell cycle to allow rapid compaction of the DNA behind the replication fork. However, replication-independent histone variants may also be incorporated into the chromatin in other stages of the cell cycle.

Incorporation of histone variants into the nucleosome may lead to profound changes in chromatin properties and in this way impact upon DNA compaction, replication, transcription and repair. Proteins which facilitate exchange of components of the nucleosome, histone chaperones, may recognise both canonical and variant histones, while some have evolved to recognise specific histones.

Out of the four core histones, H2B shows very little functional diversification, while H4 is the only histone that has a single isoform. However, several paralogues of H2A and H3, as well as linker histone H1 are known (**Figure 1.2**). These have different properties and functions. For instance the H3 variant,

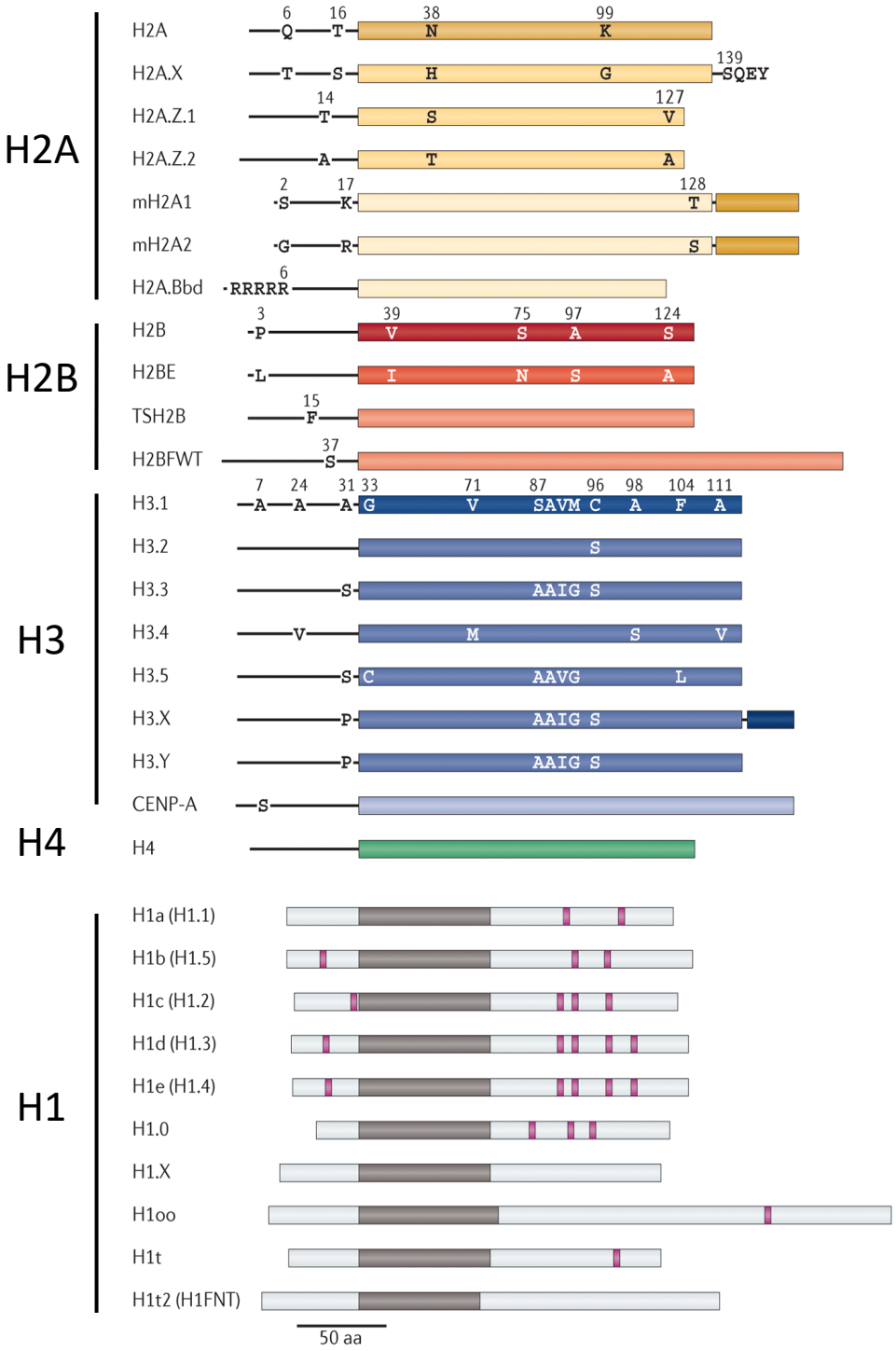

Figure 1.2 Variants of core histones. Black lines represent unstructured N-terminal tails. Key differences in amino acids amongst the H2A, H2B and H3 variants are depicted. Amino acids in the variants of H1 are not shown due to the high sequence divergence. Figure adapted from: Maze *et al.*, 2014.

CENP-A, is incorporated into specialised nucleosomes, which play a role in kinetochore assembly, while CenH3 is found at the centromeres. CenH3 has been revealed to assemble into centromeric nucleosomes independently of DNA sequence, signifying an example of epigenetic inheritance. Another example is histone H3.3, which is expressed in all cell cycle stages, is incorporated into the nucleosome in a replication-independent manner and is known to be enriched in transcriptionally active genes. Interestingly, H3.3 has been shown to be important for the maintenance of genomic stability following DNA damage.

It has been revealed that following UV-C irradiation and prior to repair, the histone chaperone HIRA deposits new histone H3.3, leading to its accumulation at the sites of DNA damage in active genes. There H3.3 variant replaces core H3 and primes chromatin for later reactivation of transcription (Adam, Polo and Almouzni, 2013). To further underscore the importance of this variant in maintaining genomic stability and in the response to DNA damage, mutations in the N-terminal tail of this variant have been associated with increased UV sensitivity, and linked to several paediatric cancers, such as glioblastomas, chondroblastomas and giant cell tumours of the bone (Schwartzentruber *et al.*, 2012; Wu *et al.*, 2012; Behjati *et al.*, 2013).

Similarly, some H2A variants have been linked to the DDR. Like H3.3, the H2AZ variant was also shown to be rapidly incorporated into the chromatin flanking DNA breaks, with the loss of the specific histone chaperones that facilitate H2AZ exchange lead to inefficient RAD51 foci formation, and subsequently to defects in homologous recombination (HR) (Alatwi and Downs, 2015).

Another DNA damage related histone variant, macroH2A.1, has been recently demonstrated to promote DSB repair. The recruitment and incorporation of this variant has been shown to induce chromatin condensation, which facilitates accumulation of BRCA1 and DSB repair via HR (Khurana *et al.*, 2014). One of the best described DNA damage-associated histone variants is H2AX. It is now well established that in response to DNA damage, H2AX is phosphorylated on serine 139 (generating what is commonly referred to as γH2AX), where it serves as a signalling molecule and a binding platform for the recruitment of the cellular

machinery that enables timely and efficient DNA repair (Rogakou *et al.*, 1998a). This will be discussed in detail later.

1.3.2 Regulation of chromatin structure and function through histone PTMs

Histone tails are the substrate for a range of cellular enzymes catalysing covalent modifications (**Figure 1.3**). The structure and function of chromatin can be regulated via multiple PTMs. These serve to modulate interactions between histones and DNA, and subsequently allow or restrict the access of the cellular machinery to genes, signal specific cellular events or provide binding platforms for the proteins involved in the regulation of DNA related processes. The most common histone modifications include acetylation, methylation and ubiquitination of lysine residues, and phosphorylation of serine and threonine residues (**Figure 1.4**); however, a plethora of other post-translationally modified residues have also been reported (Bannister and Kouzarides, 2011; Lawrence, Daujat and Schneider, 2016).

Importantly, several of these modifications, as well as histone variants have been implicated in the response to DNA DSBs (**Tables 1.1 and 1.2**).

1.3.2.1 Acetylation

Histones are covalently modified by the addition of an acetyl moiety to the ε-amino group of lysine residues (**Figure 1.4**) by the class of enzymes known as histone acetyltransferases (HATs), and this modification can be reversed by the action of histone deacetylases (HDACs). HATs utilise acetyl-CoA as a cofactor to catalyse the transfer of the acetyl group to the lysine residue, the addition of which neutralises the positive charge on a lysine and consequently opens the chromatin structure by weakening of the interactions between the histones tails and DNA.

There are two major classes of HATs: type-A and type-B. Type-A HATs are present in the cell nucleus and are often found within large multiprotein

complexes involved in the regulation of transcription through modifications of nucleosomal histones. On the other hand, type-B HATs are cytoplasmic and only capable of modifying free, newly synthesised histone H4 at lysine 5 and 12. This pattern of acetylation plays a role in the deposition of the histones into chromatin, after which the marks are apparently removed (Parthun, 2007). The positive charge on lysine residues may be restored by the action of HDACs. Their action is thought to stabilise local chromatin architecture, leading to the repression of transcription.

Apart from its ability to neutralise the lysine charge, the acetyl group may also serve as a binding platform for the recruitment of proteins containing bromodomains (BrD), which are the readers of this modification. Interestingly, several DDR proteins contain BrDs, suggesting a role for acetylation of histones in the repair process (Chiu, Gong and Miller, 2017).

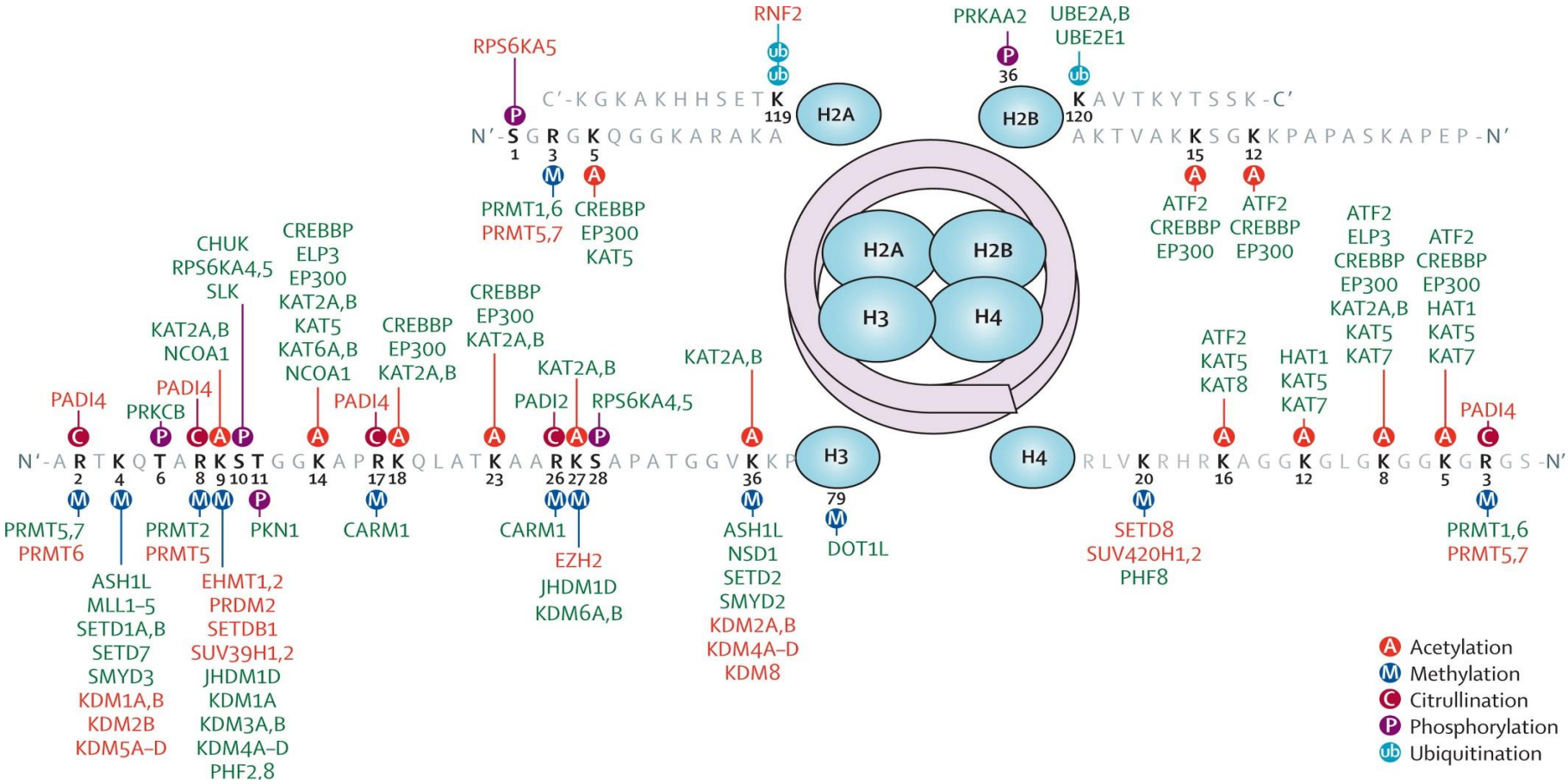

Figure 1.3 Major histone PTMs and histone modifiers. Enzymes in green and red are associated with transcriptional activation and repression respectively. Figure adapted from: Huynh and Casaccia, 2013.

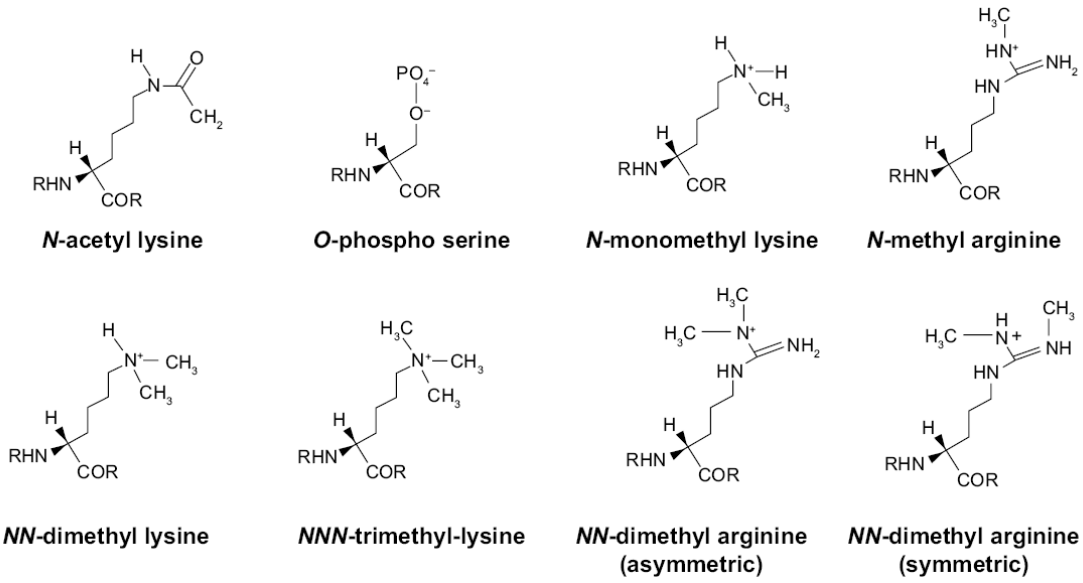

Figure 1.4 Chemical structures of common histone modifications.

Figure adapted from: Osamor *et al.*, 2016.

Modification	Histone	Residue	Change following damage induction
Acetylation	H2AX	K5	**Increase by WB and MS after IR** (Xie *et al.*, 2010; Ikura *et al.*, 2015)
		K36	**No change after IR** (Jiang, Xu and Price, 2010) **Increase by MS after IR** (Jiang, Xu and Price, 2010)
	H3	K9	**Decrease by WB and IF after Phleo, IR and laser micro-irradiation** (Tjeertes, Miller and Jackson, 2009; Meyer *et al.*, 2016a)
		K14	**No change by WB after Phleo** (Tjeertes, Miller and Jackson, 2009)
		K18	**Increase with ChIP-qPCR after I-SceI** (Ogiwara *et al.*, 2011) **No change by WB after Phleo** (Tjeertes, Miller and Jackson, 2009)
		K23	**No change by WB after Phleo** (Tjeertes, Miller and Jackson, 2009)
		K56	**Decrease by WB after Phleo** (Tjeertes, Miller and Jackson, 2009) **Not changed by ChIP-qPCR after AsiSI** (Clouaire *et al.*, 2018)
	H4	K16	**Increase with WB and IF after IR** (Gupta *et al.*, 2005; Sharma *et al.*, 2010) **Decrease by WB and IF after Bleocin; and by ChIP-qPCR after I-SceI** (K. Hsiao and Mizzen, 2013) **No change by ChIP-qPCR after AsiSI** (Clouaire *et al.*, 2018)
Phosphorylation	H2AX	S139	**Increase by WB, IF, ChIP, MS** (Rogakou *et al.*, 1999a; Savic *et al.*, 2009a; Hatimy *et al.*, 2015)
	H4	S1	**Increase by ChIP-qPCR after AsiSI** (Clouaire *et al.*, 2018)
Methylation	H3	K4me2/3	**No change by ChIP-qPCR after AsiSI or by WB after Phleo** (Clouaire *et al.*, 2018; Tjeertes, Miller and Jackson, 2009) **Decrease with IF and ChIP-qPCR after laser micro-irradiation and AsiSI** (Mosammaparast *et al.*, 2013; Gong *et al.*, 2017)
	H3	K9me2/3	**No change by ChIP-qPCR after AsiSI** (Clouaire *et al.*, 2018; Tjeertes, Miller and Jackson, 2009) **Increase with ChIP-qPCR after I-SceI or p84-ZFN** (S. Fnu *et al.*, 2011; Ayrapetov *et al.*, 2014a)
	H3	K36me2	**No change by ChIP-qPCR after AsiSI** (Clouaire *et al.*, 2018) **Increase by WB after IR, increase by ChIP-qPCR after I-SceI** (Sheema

			Fnu *et al.*, 2011)
	H3	H36me3	**No change by ChIP-qPCR after AsiSI** (Clouaire *et al.*, 2018) **Constitutive K36me3 increased at HR-dependent breaks** (Pfister *et al.*, 2014; Clouaire *et al.*, 2018)
	H3	K79me2	**Decreased by ChIP-qPCR after AsiSI** (Clouaire *et al.*, 2018) **No change by WB after Phleo** (Tjeertes, Miller and Jackson, 2009) **No change by WB after IR** (Huyen *et al.*, 2004)
	H4	K20me1	**Increased by ChIP-qPCR after AsiSI and I-SceI** (Pei *et al.*, 2011; Tuzon *et al.*, 2014; Clouaire *et al.*, 2018) **No change by WB after IR**
Ubiquitination	H2A(X)	K15	**Increase by FK2 antibody and MS; mutational studies show defect in DDR** (Stewart *et al.*, 2009; Gatti *et al.*, 2012; Mattiroli, J. H. a Vissers, *et al.*, 2012)
	H2B	K120	**Decreased by ChIP-qPCR after AsiSI** (Clouaire *et al.*, 2018)
	H4	K91	**Increased by WB** (Yan, Dutt, Xu, Graves, Juszczynski, John P Manis, *et al.*, 2009)

Table 1.1 An overview of selected mammalian DDR/repair histone PTMs implicated in DDR and repair. WB = western blot; IF = immunofluorescence; ChIP = chromatin immunoprecipitation; p84-ZFN, AsiSI and I-SceI = DSB-inducing nucleases; IR = ionising radiation; Phleo = phleomycin

	Histone variant	Change following damage induction
	H2AZ	**Decreased by ChIP-qPCR after AsiSI** (Clouaire *et al.*, 2018) **Rapidly incorporated and removed from chromatin, shown by laser micro-irradiation** (Alatwi and Downs, 2015; Gursoy-Yuzugullu, Ayrapetov and Price, 2015)
	macroH2A1.1	**Increase by ChIP-qPCR after AsiSI and I-SceI** (Khurana *et al.*, 2014; Clouaire *et al.*, 2018)
H3	H3.1	**No change with ChIP-qPCR after I-SceI** (Ogiwara *et al.*, 2011) **Decreased by ChIP-qPCR after AsiSI** (Clouaire *et al.*, 2018)
	H3.3	**Increase by IF after UV** (Adam, Polo and Almouzni, 2013)

Table 1.2. An overview of histone variants implicated in DDR and repair.

1.3.2.2 Methylation

Chromatin function can also be regulated through methylation of histone basic residues. In contrast to acetylation, methylation does not change the charge of the amino acids; and therefore it is considered that the function of this mark is exerted by effector molecules that are able to bind it. Location and degree of the methylation status has been linked to regulation of transcription, both activation and suppression; maintenance of genomic integrity, and propagation of epigenetic memory. Lysine, as well as arginine residues can be modified by addition of a methyl moiety in several ways. Lysines can be mono (me1), di- (me2) or tri-methylated (me3), while arginine residues can be mono-methylated and symmetrically or asymmetrically di-methylated **(Figure 1.4**) (Zhang and Reinberg, 2001; Bedford and Clarke, 2009).

Three families of methyltransferases are able to catalyse the addition of the methyl group from S-adenosylmethionine to histone residues. SET-domain-containing and DOT1-like proteins methylate lysines, while arginine residues are modified by protein arginine N-methyltransferases (PRMTs) (Greer and Shi, 2012). Some methyltransferases can be recruited directly to specific DNA sequences (Woo *et al.*, 2010) or their targeting to specific genomic loci can be facilitated by long and small non-coding RNAs (Verdel, 2004; Rinn *et al.*, 2007; Ogawa, Sun and Lee, 2008; Gupta *et al.*, 2010; Woo *et al.*, 2010). Additionally, interplay between DNA methylation and histone deacetylation has been shown to play a role in orchestrating histone methylation (Fuks, 2005).

Interestingly, methylation of histones can also be regulated by co-occurring histone marks. For example, a combinatorial pattern of histone modifications can influence the binding properties of the methyltransferases promoting co-occurrence of certain marks, such as H2B ubiquitination and H3K4 methylation (Krogan *et al.*, 2003; Kim *et al.*, 2009). Conversely, some combinations of histone marks may mutually exclude others, for example H3K4me3 recruits an enzyme, PHF8, which then removes a methyl group from H3K9me2 (Horton *et al.*, 2010).

Methyl marks can be recognised by ‘reader’ proteins containing methyl-binding motifs, such as PHD, chromo, tudor, PWWP, WD40, BAH, ADD, ankyrin repeat,

MBT and Zn-CW domains (Hyun *et al.*, 2017). Depending on the histone residue, binding of the methyl 'reader' proteins can regulate multiple complex cellular metabolic pathways, impact on chromatin structure, influence transcription, induce cell cycle arrest, senescence, apoptosis, autophagy and more (Hyun *et al.*, 2017). Interestingly, several DDR factors contain methyl binding domains, which suggests possibly a role for methylation during DNA repair (Wei *et al.*, 2018).

Importantly, several methylated histone residues, as well as histone methyl transferases have been implicated in the DDR and the choice of repair pathways. For instance, pre-existing H3K36me2 has been shown to promote non-homologous end joining (NHEJ) pathway, while H3K36me3 has been shown to be required for the repair of DSBs by HR, and consequently a reduction in H3K36 methylation levels was shown to lead to repair defects and increased genomic instability (Fnu *et al.*, 2011; Aymard *et al.*, 2014; Pfister *et al.*, 2014).

Histone H3K9 residue methylation has also been shown to be an important player during the DDR and repair. However, studies reporting methylation changes in this mark are often conflicting. For instance, di- and trimethylation of histone lysine9 (H3K9me2/3) has been reported to increase, decrease and remain unchanged at the sites of DNA DSBs (Falk *et al.*, 2007; Young, McDonald and Hendzel, 2013; Ayrapetov *et al.*, 2014a; Jiang *et al.*, 2015; Wu *et al.*, 2015).

Another interesting histone residue involved in the DDR is H4K20. H4K20me2 serves as a binding platform for the DDR mediator protein, 53BP1 (Botuyan *et al.*, 2006a; Wilson *et al.*, 2016), which has been shown to be important for the regulation of the choice between HR and NHEJ pathways (Kakarougkas *et al.*, 2013). This modification is deposited progressively into newly synthesised nucleosomes throughout the G2, M and G1 phases of the cell cycle. It is very abundant, and has been shown to constitute over 80% of all H4K20 modifications (Pesavento *et al.*, 2008). It has been proposed that 53BP1 binding to the damaged chromatin behind the replication fork is weakened as the

dilution of H4K20me2 between ‘new’ and ‘old’ chromatin reduces its ability to bind nucleosomes, and subsequently cells are more likely to repair DSBs using homology directed repair (Pellegrino *et al.*, 2017).

1.3.2.3 Phosphorylation

Protein phosphorylation involves the transfer of the γ-phosphate group from ATP to serine (S) (**Figure 1.4**), threonine (T) or tyrosine (Y) of the target protein. This modification is deposited by multiple protein kinases and it is reversible by protein phosphatases. The phospho-moiety adds negative charge to proteins, which can change their structure and functional activity. In addition, the phosphate-moiety can serve as a binding platform for the recruitment and retention of other protein factors.

Phosphorylation is a key cellular regulatory mechanism activated in response to multiple extra- and intra-cellular stimuli, including DNA damage. Several kinases have been implicated in DDR to DSBs, most importantly ataxia-telangiectasia mutated (ATM), ataxia-telangiectasia and Rad3-related (ATR) and DNA protein kinase (DNA-PK), all of which are members of the phosphoinositide 3-kinase (PIKK) family. They are all crucial in the early stages of DDR signalling, where amongst other targets, they phosphorylate the histone variant H2AX on S139 (Rogakou *et al.*, 1998b; Stiff *et al.*, 2004). Their role will be discussed in more detail later.

DNA damage-induced phosphorylation of S/T residues serves to recruit proteins containing phospho-binding motifs, such as 14-3-3, Polo-box domains, WD40 repeats, BRCA1 carboxy-terminal (BRCT) and Forkhead-associated (FHA) domains (Reinhardt and Yaffe, 2013). These proteins are involved in the assembly of DDR complexes, DNA repair and the regulation of the cell cycle.

A.

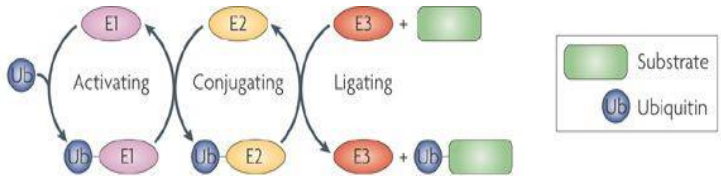

B.

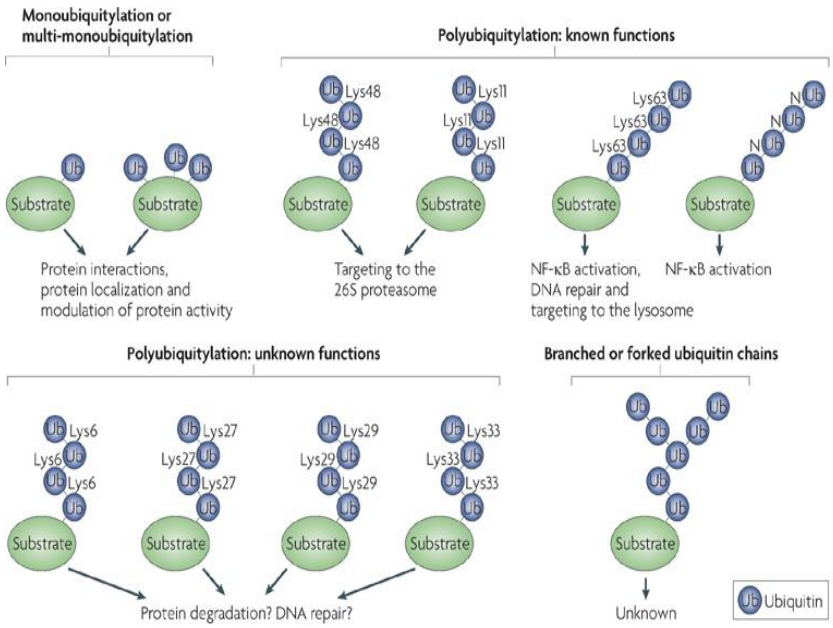

Figure 1.5 Schematic representation of the ubiquitination reaction. A) The ubiquitination reaction occurs in three steps, catalysed by specialised enzymes: an ubiquitin activating enzyme (E1), an ubiquitin conjugating enzyme (E2) and an ubiquitin ligating enzyme (E3). B) Additional ubiquitin molecules can be ligated to the lysine chains of previously attached ubiquitin molecules resulting in different molecular outcomes. Figure adapted from: Dikic, Wakatsuki and Walters, 2009.

1.3.2.4 Ubiquitination

In addition to acetylation and methylation, lysine residues of histones can be also ubiquitinated. This modification involves addition of a single or multiple ubiquitin residues to specific lysine residues linked via an isopeptide bond. Ubiquitin is a 76-residue polypeptide that is attached to target proteins in a three-step process catalysed by E1, E2 and E3 ubiquitin ligases (**Figure 1.5 A**). A range of outcomes in ubiquitin signalling cascades can be achieved through different E3 ligases. Additionally, ubiquitin is rich in lysine residues that can be further modified with additional ubiquitin molecules, forming varied poly-ubiquitin chains and branches adding another layer of complexity to ubiquitin signalling (**Figure 1.5 B**).

Protein ubiquitination has been shown to play a role in the regulation of cellular processes, such as stem cell maintenance and differentiation, cell cycle regulation, protein degradation, transcription and DNA repair (Cao and Yan, 2012). Ubiquitination of the histones H1, H2A and H2B and H4 have been described in the literature to play a role in the response to DNA DSBs, specifically to promote the local relaxation of the chromatin fibre and recruitment of DDR factors to the sites of breaks (Doil *et al.*, 2009a; Pinato *et al.*, 2009; Yan, Dutt, Xu, Graves, Juszczynski, John P. Manis, *et al.*, 2009; Yan *et al.*, 2013; Thorslund *et al.*, 2015a).

The importance of ubiquitin signalling during DDR is further emphasised by the link between the defects in this response and human diseases (Stewart *et al.*, 2009; Tessadori *et al.*, 2017).

1.3.3 The effect of chromatin compaction on DSB repair

Nucleosomal DNA complexes commonly referred to as “beads-on-a-string” structure, constitute the first level of chromatin condensation. However, in order to fit an average eukaryotic genome into the nucleus, additional levels of condensation must also be achieved. It has been proposed that chromatin becomes arranged into higher order structures in a hierarchical manner to

ultimately form mitotic chromosomes (Woodcock and Ghosh, 2010) (**Figure 1.6**). In the interphase nucleus, chromatin is broadly categorised into two major states according to its condensation level. Compacted chromatin, or heterochromatin, is transcriptionally inactive, whereas open regions are known as euchromatin and are transcriptionally active (Babu and Verma, 1987).

Heterochromatin consists of two distinct forms, facultative and constitutive, which are distinguished by their pattern of histone PTMs. Facultative heterochromatin is enriched in H3K27me2/3 and H2AK119Ub, two gene silencing histone marks. Facultative heterochromatin is known to contain genes, and can adopt open and transcriptionally active conformations, depending on the cell type and developmental stage (Trojer and Reinberg, 2007). Constitutive heterochromatin is enriched in H3K9me2/3 and H4K20me3 histone marks, which denote gene-poor, repetitive and late replicating DNA sequences (Saksouk, Simboeck and Déjardin, 2015).

Transcriptional repression and compaction of constitutive heterochromatin is achieved through the action of several factors. DNA methylation by DNA methyl transferases leads to gene silencing, while H3K9 methylation promotes local compaction of chromatin; at the same time, marks promoting transcription (e.g. H3K4me3) are removed (Katan-Khaykovich and Struhl, 2005; Saksouk, Simboeck and Déjardin, 2015). This condensation is achieved via action of several proteins. Notably, H3K9me2/3 promotes the recruitment of the heterochromatin binding protein HP1 (heterochromatin protein 1), which subsequently recruits KAP1 (KRAB (Kruppel-associated box) domain-associated protein 1) which then promotes heterochromatin assembly (Kwon and Workman, 2011; Jang *et al.*, 2018). Additionally, HP1 serves as scaffold for recruitment of chromatin modifiers, such as H3K9 methyltransferases and histone deacetylases, the combined action of which leads to heterochromatin spreading and maintenance (Saksouk, Simboeck and Déjardin, 2015).

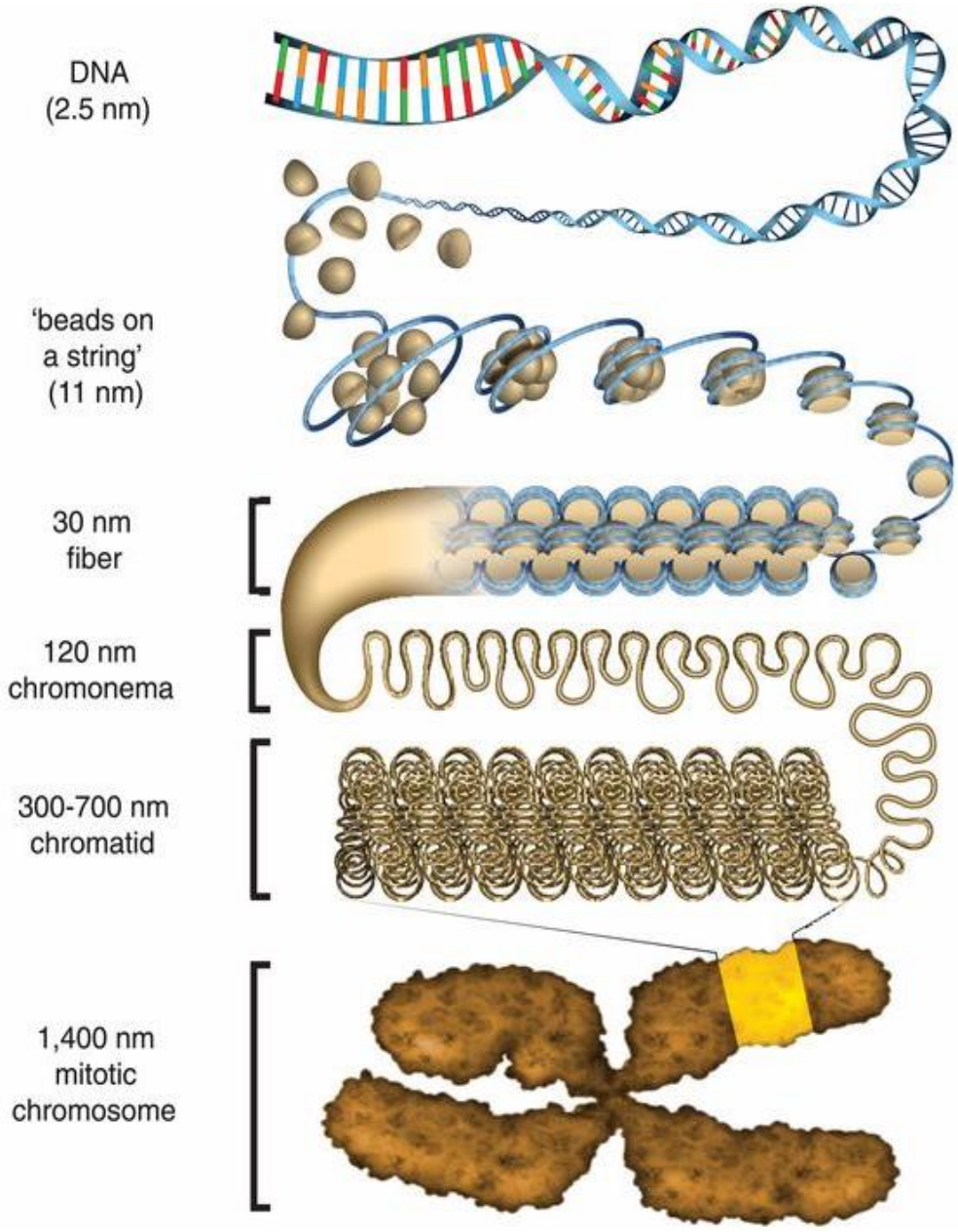

Figure 1.6 Schematic representation of the hierarchical model of chromatin compaction. The model assumes sequential condensation of the primary DNA structure into nucleosomes, the 30 nm fibre, up to the mitotic chromosome. Figure adapted from: Ou *et al.*, 2017b.

Interestingly, it has been demonstrated that the rate of repair of DSBs is not the same in eu- and hetero-chromatin. Based on that information a model has been proposed, which postulates that biphasic repair kinetics (which has been observed in many studies) consists of a fast component that repairs the majority (>80%) of the breaks within the first few hours following break induction, while the remaining breaks are repaired by a slow component and is dependent on ATM signalling, as well as the DNA damage mediator proteins MDC1, RNF8, RNF168 and 53BP1 (**Figure 1.7 A**) (Goodarzi *et al.*, 2008a; Noon *et al.*, 2010). Consequently, cells lacking functional ATM show a specific defect in the repair of slow component breaks. It has been suggested that chromatin provides a barrier for the DNA repair process and that the local compaction state of the chromatin may impact on repair efficiency (Goodarzi, Noon and Jeggo, 2009). In accordance with that, immunofluorescence (IF) studies have shown that γH2AX foci co-localise with heterochromatin markers, such as H3K9me3 or DAPI dense chromocenters in mouse cells (**Figure 1.7 B**), at late time points (24h) following damage induction. ATM has been shown to be required for the relaxation of heterochromatin via phosphorylation of KAP1 S824. Furthermore, relaxation of the heterochromatin structure through the knock-down of KAP1, HP1 or HDAC1/2 has been shown to alleviate the requirement for ATM activity, consistent with the idea that the condensed chromatin provides a barrier to repair processes (Goodarzi *et al.*, 2008a).

Interestingly, H3K9 methyltransferases, as well as HP1 and KAP1 compacting factors have also been shown to be rapidly recruited to the sites of DSBs, suggesting a role for chromatin compaction during DDR (Ayoub *et al.*, 2008; Sun *et al.*, 2009). Indeed, *de novo* H3K9 tri-methylation at the site of DSBs has been also demonstrated using chromatin-immunoprecipitation (ChIP) studies (Ayrapetov *et al.*, 2014a). This raises the question whether the defect associated with late repairing, ATM-dependent DSB repair represents the repair of DSBs within pre-existing heterochromatin or in regions that become heterochromatinised as a result of the DDR.

A.

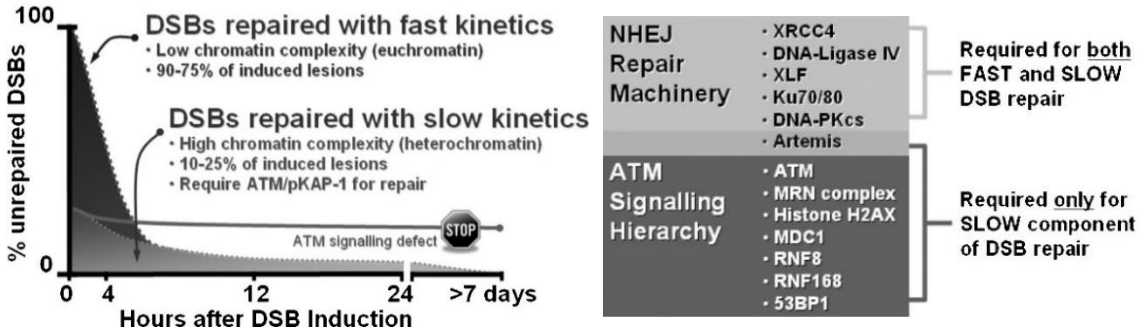

B.

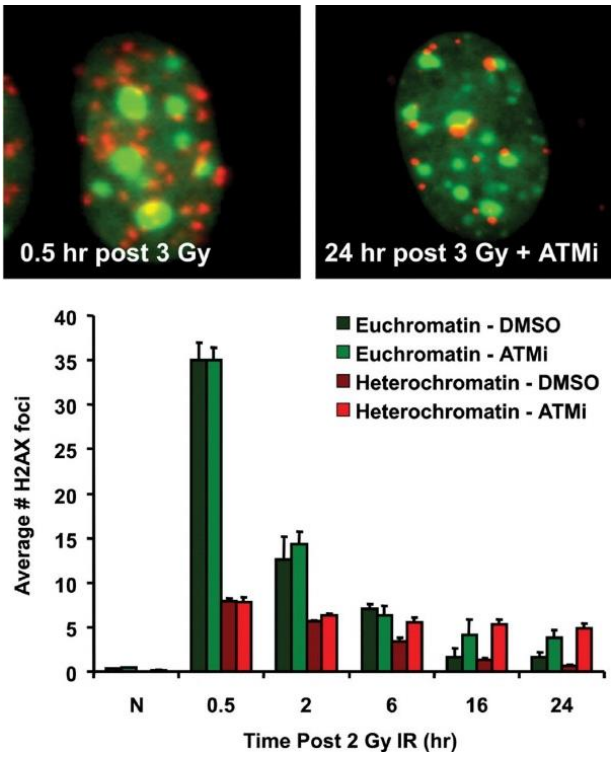

Figure 1.7 Heterochromatic breaks repair with slower kinetics. A) Model for the repair of fast and slow component. The Majority of X-ray induced DSBs breaks are repaired with fast kinetics and are associated with low complexity chromatin. Repair of DSBs in high complexity chromatin is associated with slower kinetics. Figure adapted from: Goodarzi, Jeggo and Lobrich, 2010. B) Inhibition of ATM kinase leads to persistent H2AX foci (red) associated with periphery of chromocenters (green) in murine cells. Figure adapted from: Goodarzi, Noon and Jeggo, 2009.

Another protein that has been previously implicated in the repair of slow repairing breaks is Artemis endonuclease (Woodbine *et al.*, 2010). More recently it has been proposed that in the G0/1 stage of the cell cycle c-NHEJ repairs breaks with biphasic kinetics, which depend on a need for resection prior to end ligation (Löbrich and Jeggo, 2017). It has been demonstrated that Artemis–mediated repair of slow component DSBs in G1 requires resection and microhomology-mediated end joining in order to repair those breaks. The majority of the breaks repaired using this process have been shown to result in deletions and half of the translocations that arise following the damage repair depends on this pathway (Biehs *et al.*, 2017). This suggests the possibility that these late repairing breaks are highly complex, and therefore, require extended periods of time to be resolved, rather than the delay in repair being due to increased chromatin compaction.

1.4 ACTIVATION OF THE DDR IN RESPONSE TO DSBS

1.4.1 Phosphatidylinositol-3-kinase (PIKK) family

DDR signalling is initiated and regulated by the PIKK family of three related kinases: ataxia telangiectasia mutated (ATM), ATM- and Rad3-related (ATR), and DNA-dependent protein kinase (DNA-PK). All PIKK family members have a similar domain organisation and common structural features containing N-terminal HEAT (huntington, elongation factor 3, protein phosphatase 2 and TOR1) repeats, the FAT (FRAP-ATM-TRRAP) domain, the catalytic kinase domain, PIKK regulatory and FAT motif (FAT-C) at the C-terminus (**Figure 1.8**) (Blackford and Jackson, 2017).

All three kinases have been shown to have a preference for phosphorylation of serine or threonine residues followed by glutamine (S/T-Q) (Chen *et al.*, 1991; Kim *et al.*, 1999). Although, all three kinases can be activated in response to DNA damage, ATM and DNA-PK primarily respond to DSBs, while ATR is activated by single strand regions of DNA and is the major player during replication stress (Stiff *et al.*, 2004; Saldivar, Cortez and Cimprich, 2017).

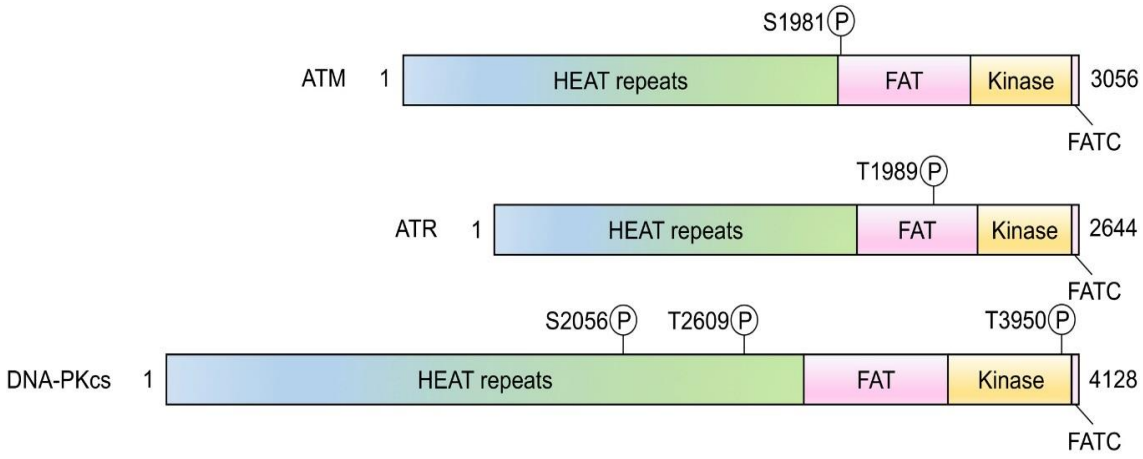

Figure 1.8 Structural organisation of PIKK family members: ATM, ATR and DNA-PK. Coloured boxes denote specific protein domains, while numbers represent specific amino acids. An encircled letter P indicates major phosphorylation sites. Figure adapted from Blackford and Jackson, 2017.

The sensing of DNA damage is crucial for human health and consequently cells deficient in any of the PIKK kinases show repair defects and increased genomic instability, which may lead to cancer or other diseases. ATR is essential for survival and its absence in mice leads to chromosome fragmentation and embryonic lethality (Brown and Baltimore, 2000). Hypomorphic mutations in ATR lead to Seckel syndrome which is characterised by intrauterine growth retardation, dwarfism, microcephaly and mental retardation (O'Driscoll *et al.*, 2003; Ogi *et al.*, 2012).

Although $ATM^{-/-}$ patients are viable, they display several abnormalities. Hypomorphic mutations in DNA-PK result in aberrant V(D)J recombination and consequently severe combined immunodeficiency (SCID), as well as profound neurological defects (Beamish *et al.*, 2000; van der Burg *et al.*, 2009; Woodbine *et al.*, 2013). ATM deficiency results in the disorder, A-T (ataxia telangiectasia) characterised by dilated blood vessels (telangiectasia) and progressive neurological deterioration, leading to a lack of movement coordination, as well as gait abnormality (ataxia). A-T patients also present with immunodeficiency and susceptibility to malignancies, particularly lymphoid tumors (McKinnon, 2004; Tubbs and Sleckman, 2014). Cells lacking both ATM and DNA-PK, are severely radiosensitive and show increased genomic instability further underscoring their importance in response to DSB-inducing insults.

1.4.1.1 Detection of DSBs and activation of ATM kinase

DNA DSBs are potentially one of the most deleterious genotoxic lesions, therefore they must be rapidly detected and repaired to ensure cell survival. ATM is a central DDR kinase, important for the maintenance of genomic integrity. In the absence of genotoxic stress, ATM exists in the form of inactive dimers , and requires a DSB for activation.

In response to genotoxic stress, DSBs are thought to be initially recognised by the MRN (Mre11-Rad50-Nbs1) complex, which binds to lesion and tethers the DNA ends, providing a platform for ATM binding. It is believed that Nbs1 recruits inactive ATM kinase dimers, resulting in auto-phosphorylation at residue S1981 and subsequent dissociation of active ATM monomers (**Figure 1.9**)

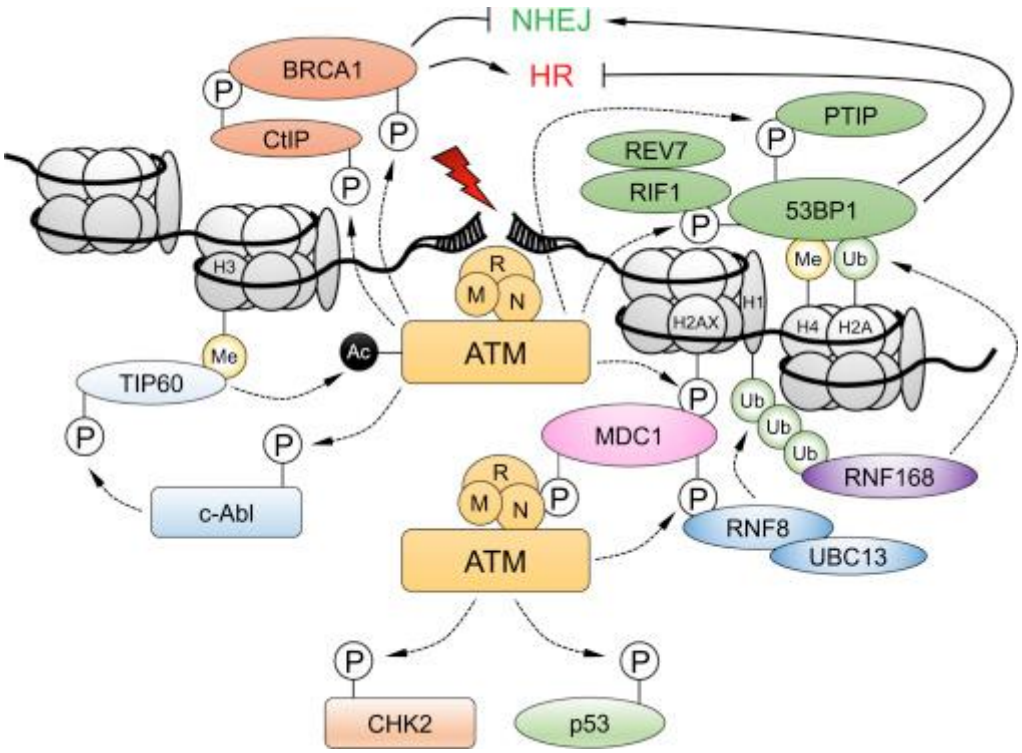

Figure 1.9 DNA DSB-dependent activation of ATM signalling cascade. MRN complex binds to DNA at DSB and subsequently recruits and activates ATM kinase. This initiates a cascade of phosphorylation and acetylation events, which sustain ATM signalling. c-Abl and TIP60 acetylate ATM, which than phosphorylates H2AX and MDC1. This subsequently leads to activation of a phosphorylation-ubiquitination cascade mediated by ubiquitin ligases RNF8 and RNF168 and consequently results in recruitment and spreading of 53BP1. ATM phosphorylates 53BP1, which then recruits its effectors, RIF1 and PTIP, which promote repair via NHEJ. NHEJ is counteracted by BRCA1 and CtIP, also ATM substrates, to promote repair via HR. P = phosphorylation, Ac = acetylation, Me = methylation, Ub = ubiquitination. Figure adapted from Blackford and Jackson, 2017.

(Falck, Coates and Jackson, 2005). However, other phosphorylation sites on ATM have been also proposed to play a role in its activation, including S367 and S1893 (Kozlov *et al.*, 2006). Once activated, ATM phosphorylates a plethora of other DDR proteins, resulting in activation of the DNA damage signalling cascade.

ATM-dependent signalling in response to DSBs has been shown to influence a multitude of signal transduction pathways affecting the repair of damage, cell-cycle arrest and apoptosis, as well as metabolism, bioenergetics, transcription and protein turnover (Shiloh, 2006).

1.4.2 Phosphorylation of the H2AX variant in response to DSB and amplification of the DDR

As already mentioned, one of the best described histone modifications occurring in response to DSBs is phosphorylation of the histone variant H2AX on serine 139 (H2A serine 129 in yeast). This residue is embedded within an SQE motif at the C-terminal tail of H2AX, which is a consensus sequence for phosphorylation by the PIKK kinases: ATM, ATR and DNA-PK.

Immunofluorescence studies demonstrated that γH2AX can be rapidly detected within a few minutes following DSB induction. Via an orchestrated assembly process, γH2AX recruits DDR proteins, which can then influence the nature of DSB repair and DDR signalling. It has been demonstrated that following H2AX phosphorylation, mediator of DNA damage checkpoint protein 1 (MDC1) gets recruited to DSBs and binds γH2AX directly via its C-terminal BRCT domain (Stucki *et al.*, 2005).

Direct interaction of MDC1 with γH2AX and ATM tethers it to the site of damage. This leads to the accumulation of ATM via a positive feedback loop facilitating further phosphorylation of H2AX along the broken chromosome, thus allowing the assembly of additional DDR factors on the chromatin (Lou *et al.*, 2006).

Chromatin immunoprecipitation (ChIP) based studies have demonstrated that H2AX phosphorylation can spread up to 1 Mbp away from each end of the

break. However it is depleted across 1-2 Kbp regions flanking the break (Shroff *et al.*, 2004a; Savic *et al.*, 2009b; Iacovoni *et al.*, 2010b). γH2AX domains form distinct nuclear foci, which are visible using immunofluorescence microscopy and are thought to represent DSB repair factories (Rogakou *et al.*, 1999a). They have been shown to co-localise with a plethora of other factors necessary for the repair of the break. As a result, γH2AX foci are one of the most common markers used for the detection of DSBs and immunofluorescence-based studies often use co-localisation with γH2AX, as a proof of protein recruitment to the site of a DSB.

It is worth mentioning at this point that H2AX-deficient cells show only a minor repair defect, with around 85% of the breaks being repaired following damage induction (Riballo *et al.*, 2004). However it is currently unknown whether accuracy of DNA repair under these circumstances is affected. Nonetheless, numerous studies have demonstrated H2AX phosphorylation aids recruitment and retention of several important DDR players. Consequently, cells deficient in the histone variant H2AX show radiosensitivity, increased genomic stability and cancer predisposition, mainly to leukaemia (Bassing *et al.*, 2003; Celeste *et al.*, 2003; Turinetto and Giachino, 2015).

1.4.3 RNF8/RNF168 signalling and ubiquitination of H2A(X)

Upon recruitment to DSBs, ATM phosphorylates MDC1 on a TQxF motif, which then serves as a binding platform for the recruitment of the E3 ubiquitin ligase, RING finger protein 8 (RNF8) via its forkhead-associated domain (FHA) (Kolas *et al.*, 2007). At the site of damage, RNF8 co-operates with UBC13, which is the E2 conjugating enzyme known to specifically catalyse the formation of K63 linked ubiquitin chains (Hofmann and Pickart, 1999; Kolas *et al.*, 2007; Mailand *et al.*, 2007; Michael S.Y. Huen *et al.*, 2007). It has been recently demonstrated that the major substrate for K63 ubiquitination at the site of DSBs is the linker histone H1. RNF8-dependent ubiquitination of H1 in response to DSBs is a critical priming step, which provides a high affinity binding platform for recruitment of another E3 ubiquitin ligase, RNF168. Accordingly,

downregulation of histone H1 or RNF8, leads to impaired RNF168 recruitment and a repair defect (Thorslund *et al.*, 2015b).

Ubiquitination of histone H2A variants on lysine 13/15 by RNF168 has been previously reported to be induced in response to DNA DSBs (Doil *et al.*, 2009b; Gatti *et al.*, 2012; Mattiroli, J. H. A. Vissers, *et al.*, 2012; Hu *et al.*, 2017). Deposition of this mark on the nucleosomes local to DSBs creates an essential platform for the recruitment, binding and retention of repair proteins, most prominently 53BP1 (**Figure 1.10**) (Doil *et al.*, 2009b; Fradet-Turcotte *et al.*, 2013; Hu *et al.*, 2017). Consequently, cells lacking RNF168 fail to recruit 53BP1 to the sites of breaks and display significant radiosensitivity (Doil *et al.*, 2009b; Stewart *et al.*, 2009; Devgan *et al.*, 2011; Bohgaki *et al.*, 2013; Pietrucha *et al.*, 2017).The protein turnover of RNF168 and the extent of RNF168-induced chromatin ubiquitination are tightly regulated in response to DNA damage by two E3 ubiquitin ligases, TRIP12 and UBR5. Consistently, if those are depleted, RNF168 hyper-accumulates at DSBs, leading to massive spreading of 53BP1 and BRCA1. It has been reported that RNF168 becomes a limiting factor in response to increasing amounts of IR, becoming saturated at ~20-40 DSBs, consequently leading to impaired formation of 53BP1 at higher IR doses (Gudjonsson *et al.*, 2012b). Recently, it has been demonstrated that efficient formation of 53BP1 foci is required for RAD51 recruitment and HR, and failure to do so, leads to hyper resection of DNA around the break and in G2 phase repair via the highly mutagenic RAD52-mediated single-strand annealing pathway (Ochs *et al.*, 2016).

1.4.4 Activation of cell cycle checkpoint control

In response to DNA damaging agents, such as IR, specific signalling pathways are activated in order to halt cell cycle progression. Arrest of the cell cycle is an important component of the DDR. By allowing additional time for DNA repair, the process serves to maintain genome stability and helps prevent cancer development. The main regulators of checkpoint arrest are activated by the kinases ATR and ATM, which upon activation phosphorylate the transducer

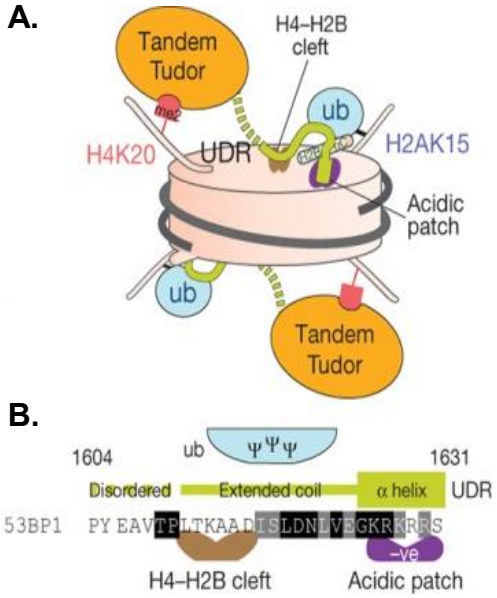

Figure 1.10 RNF168 ubiquitination-dependent recruitment of 53BP1. A) Model for the ubiquitin-dependent recognition of nucleosome by 53BP1. B) The amino acid sequence of 53BP1 ubiquitin recognition motif. Figure adapted from: Wilson *et al*., 2016.

its stabilisation and accumulation in the nucleus (Haupt *et al.*, 1997; Caspari, 2000).

The actions of p53 are achieved via transcriptional reprogramming (**Figure 1.11**), which leads to the activation of various genes involved in growth proteins, checkpoint kinase 1 and 2 (CHK1 and CHK2) respectively, and together with ATM they phosphorylate several residues on the tumour suppressor p53, which results in its dissociation from MDM2 (mouse double minute 2 homolog), inhibition, most prominently, the cyclin-dependent kinase inhibitor p21, which halts replication and promotes G1 phase checkpoint activation (Giono and Manfredi, 2006). Furthermore, p53 can also promote G2/M arrest through repression of CDC25C, a phosphatase that promotes mitosis (Clair and Manfredi, 2006).

In some circumstances, p53 may induce senescence, which is a permanent cell cycle arrest via transcriptional activation of the retinoblastoma (RB) tumour suppressor (Campisi and d'Adda di Fagagna, 2007). Additionally, p53 may also promote death via activation of pro-apoptotic genes, such as Bax, PUMA or Bcl-2 (Haupt *et al.*, 2003; Bieging, Mello and Attardi, 2014).

The p53-mediated stress response is exerted by the activation and repression of gene transcription, therefore is not surprising that p53 has also been shown to associate with chromatin remodelling complexes, suggesting p53-mediated DDR also leads to DNA damage-induced changes (Murphy *et al.*, 1999; Juan *et al.*, 2000; Espinosa and Emerson, 2001; Lagger *et al.*, 2003; Pfister *et al.*, 2015).

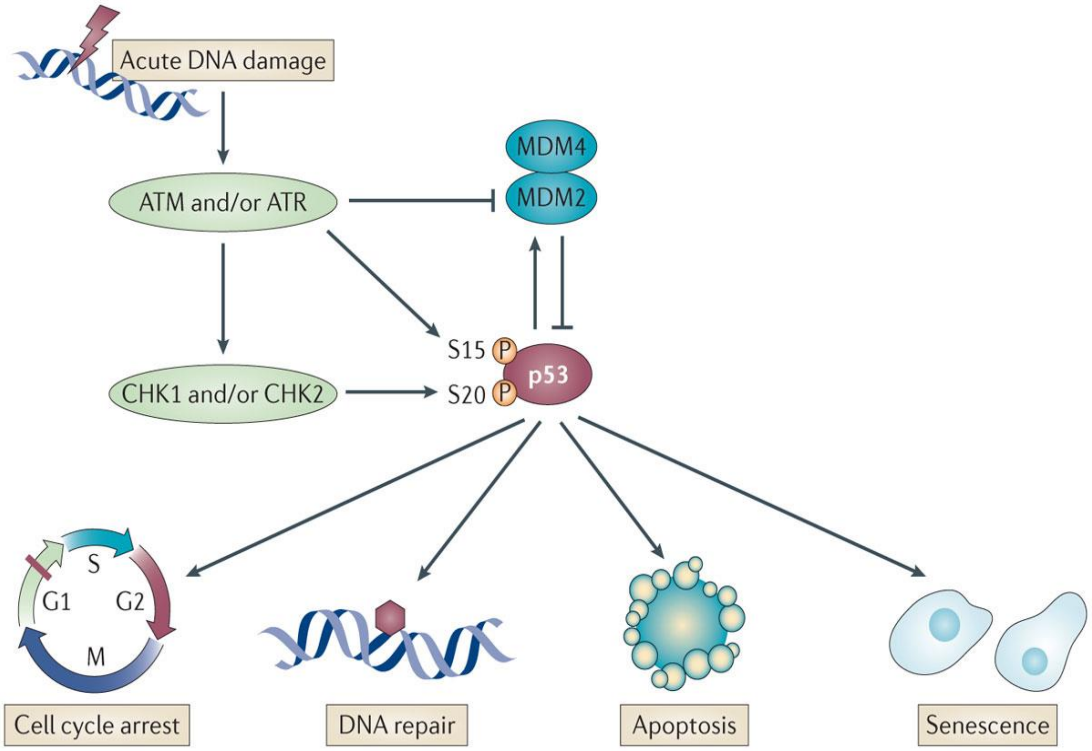

Figure 1.11 DNA damage induced activation of p53 signalling. Following acute DNA damage ATR/ATM and CHK1/2 phosphorylate p53 on serine residues 15 and 20, respectively. These phosphorylation events prevent p53 interaction with MDM2/4, and leading to its stabilisation. Additionally, these phosphorylation events allow for interaction with several transcriptional cofactors essential for activation of DNA damage-dependent cellular responses, such as cell cycle arrest, DNA repair, apoptosis and senescence. Figure adapted from: Bieging, Mello and Attardi, 2014

1.5 REPAIR OF DNA DSBS

Failure to accurately repair DNA DSBs leads to increased genomic instability, and therefore contributes to the development of cancer, neurodegeneration, accelerated aging and immunodeficiency (Hoeijmakers, 2009; O'Driscoll, 2012; Madabhushi, Pan and Tsai, 2014). Cells have evolved several pathways to repair DSBs, depending on the cell cycle phase and the availability of the cellular repair components.

1.5.1 Homologous recombination (HR)

In late S phase or G2, when a sister chromatid is available, cells may choose to repair some of the breaks via homology directed pathways (**Figure 1.12**). During this process, a 3' overhang single stranded DNA generated by 5'-3' resection of the ends of DSBs provides a substrate for assembly of RAD51 filaments. The 5'-3' resection is initiated by the MRN complex and CtIP, and serves as a critical step for the choice of the repair pathway (Symington and Gautier, 2011). Resection is a critical step in HR, and consequently failure to regulate this step leads to increased DNA damage sensitivity, genomic instability and cancer predisposition (Stracker *et al.*, 2004; Wu and Lee, 2006; Sartori *et al.*, 2007; Huertas and Jackson, 2009). In the following step, nucleoprotein filament formation enables invasion of single stranded DNA into the sister chromatid, which serves as a primer for repair synthesis by DNA polymerases using the intact sister homologue as a template, which is followed by ligation by DNA ligase I. This repair process leads to the formation of DNA crossovers, also referred to as Holliday junctions, which are than resolved to produce two intact DNA molecules (Matos and West, 2014).

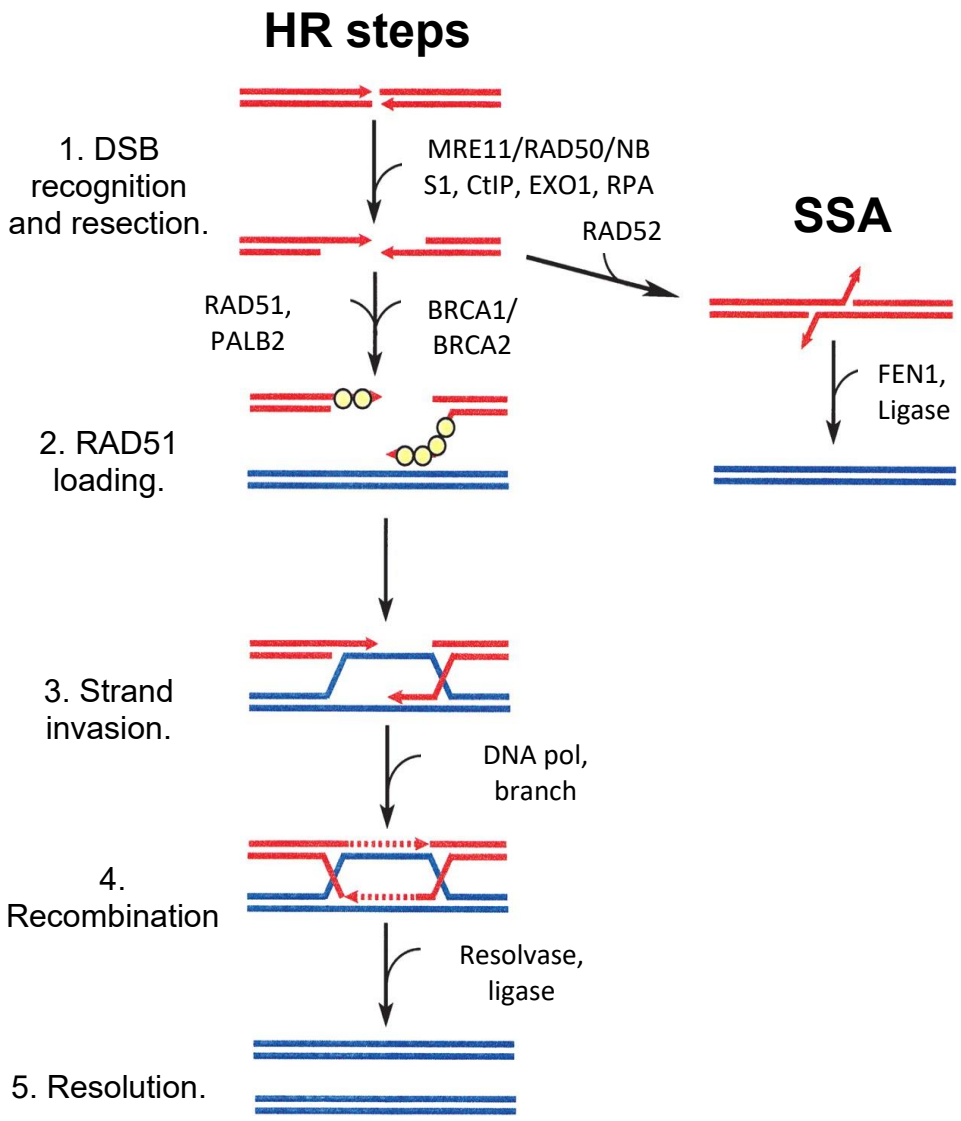

Figure 1.12 Major protein factors involved in HR. During HR repair**,** DSBs are recognised by the MRN complex, which activates ATM kinase leading to initiation of DSB repair. CtIP and EXO1 nucleases resect DNA from 5' to 3', resulting in the formation of ssDNA that is subsequently coated with RPA protein. Next, BRCA1/2 and PALB2 protein complex facilitates loading of RAD51, which then replaces RPA coated ssDNA. RAD51 nucleoprotein performs homology mediated search and mediates strand invasion. Damaged DNA is restored by branched migration, DNA synthesis, resolution and ligation. Alternatively, the repair may occur via the SSA pathway. Here, extensive regions of DNA are resected, revealing homologous repeats that are then annealed together. ssDNA flaps are removed by FEN1, leading to large deletions of genetic information. Red = DNA pre-repair; blue = DNA synthetized post-damage.

1.5.2 Classical NHEJ (c-NHEJ)

In all of the stages of the cell cycle, but particularly in G0/1 phase, when a sister homologue is not available, the majority of DSBs will be repaired via the classical NHEJ pathway, which essentially leads to ligation of the broken ends.

Repair by c-NHEJ can be divided into four major steps (**Figure 1.13**). Following break induction, broken DNA ends are recognised by the Ku70/80 heterodimer, which loads onto double-stranded DNA forming a ring-like structure around naked ends (Walker, Corpina and Goldberg, 2001). This complex protects DNA naked ends and acts as a scaffold to recruit the PI3K kinase, DNA-PKcs, which then forms a complex with Ku, creating a bridge between the DNA ends (DeFazio *et al.*, 2002). Recruitment of DNA-PK leads to phosphorylation of several substrates in proximity of the DSBs, including itself, which is necessary for the subsequent recruitment of NHEJ factors. Although *in vitro* and *in vivo* studies have identified several substrates for DNA-PK phosphorylation, such as H2AX, Ku70/80, XRCC4, XLF, Artemis and DNA ligase IV, these phosphorylation sites do not appear to be strictly required for NHEJ (Lee *et al.*, 2004; Wang *et al.*, 2004; Douglas *et al.*, 2005; Drouet *et al.*, 2005; Goodarzi *et al.*, 2006; YU *et al.*, 2008; Sharma *et al.*, 2016).

Genotoxins, such as IR, induce chemical modifications in the proximity or at the termini of DSBs, which often need processing to produce 3'-hydroxyl and 5'-phosphate groups at the opposing ends that are required for direct ligation of broken DNA (Povirk, 2012).

Several factors, for example Artemis, polynucleotide kinase 3'-phosphatase protein (PNKP), AP-endonuclease 1 (APE1) and tyrosyl-DNA phosphodiesterase (TDP1), which have a range of enzymatic activities, have been shown to be required for this end-processing. This procedure may however result in the formation of gaps that then need to be repaired by polymerases, which synthesise the missing DNA fragment (Deriano and Roth, 2013).

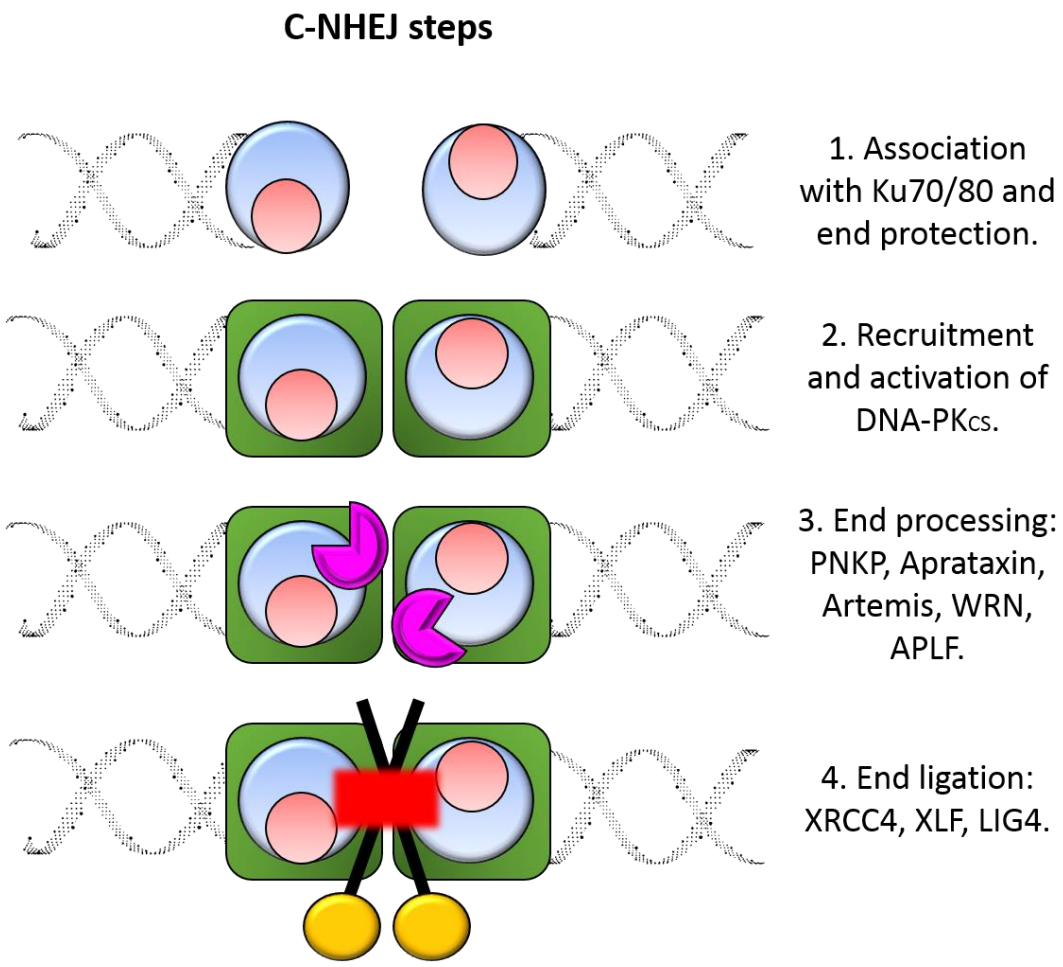

Figure 1.13 Major steps and protein factors involved in c-NHEJ. Classical NHEJ is initiated by loading of Ku70/80 heterodimer (blue and red circles) on the broken DNA ends, forming a cradle that harbours DNA molecules, aligns the ends and prevents degradation Once in place, Ku recruits the catalytic subunit of DNA-PK (green) to form the holoenzyme capable of phosphorylating several downstream NHEJ factors and regulating their interactions with Ku. Since NHEJ requires two blunt ends to join together, some terminal processing (magenta) may be required. For example, overhanging ends may be trimmed via action of nucleases, such as Artemis or/and correct 5' end chemistry may be restored by PNKP. Finally, once compatible ends are in place, XRCC4/XLF/LIG4 ligation complex is recruited to seal DNA ends together (yellow/red/black). For more detail description see the main text.

The retention of NHEJ factors depends on adaptor proteins, such as Aprataxin and PNK-like factor (APLF), paralog of XRCC4 and XLF (PAXX), and modulator of retroviral infection (MRI), whose function is redundant for NHEJ. They were proposed to form large multimeric, filament-like complexes around the break to promote the retention of NHEJ factors. Cells lacking one or more of these factors show mild defects in the repair of DSBs and radiosensitivity and increased genomic instability (Fenton *et al.*, 2013; Liu *et al.*, 2017; Hung *et al.*, 2018).

Once end-processing is complete, ligation is carried out by a complex composed of LigIV, XRCC4 and XRCC4-like factor (XLF), which are recruited to the break via interaction with the Ku70/80 heterodimer. This complex has been shown to be critical for NHEJ and consequently, cells lacking either LigIV or XRCC4 display embryonic lethality. Although cells lacking XLF can still recruit XRCC4 and LigIV to the break, $XLF^{-/-}$ patients display immunodeficiency and microcephaly. The core components of c-NHEJ are Ku70/80, DNA-PKcs, XRCC4, LigIV and XLF are essential for the efficient and timely repair of DSBs, and alterations in this pathway lead to a range of pathogenic phenotypes in humans (Pierce and Jasin, 2001).

1.5.3 Auxiliary pathways

Under certain circumstances, alternative pathways to NHEJ are used in the cell. Typically, these involve extensive resection of the DNA ends to expose regions of sequence homology, leading to their annealing and thus stabilisation of the broken ends (Ceccaldi, Rondinelli and D'Andrea, 2016).

Two main auxiliary pathways capable of resolving DSBs are alternative NHEJ (alt-NHEJ) and single strand annealing (SSA), and both require micro-homology usage to facilitate repair. SSA annealing is mediated by RAD52 rather than RAD51 and is used alternatively to HR during late S and G2 phases. On the other hand, alt-NHEJ can be potentially used throughout the cell cycle, at least in mouse cells (Simsek *et al.*, 2011; Iliakis, Murmann and Soni, 2015).

Interestingly, it has been recently demonstrated that exposure to high doses of IR (that lead to induction of more than 40-60 DSBs), may result in the depletion of some of the DDR factors and consequently a switch from the accurate to the more mutagenic repair pathways. In particular, RNF168 protein levels and turnover have been shown to be highly regulated throughout the cell cycle and at the site of DSBs. Consequently, at increasing amounts of DSBs, RNF168 gets diluted between more and more breaks. Since RNF168 is required for the recruitment of 53BP1 to DSBs, 53BP1 foci do not form efficiently at high IR doses (Gudjonsson *et al.*, 2012b; Ochs *et al.*, 2016).

Recently it has been demonstrated that 53BP1 is required for the formation of RAD51 filaments and subsequent repair via HR. Failure to recruit sufficient amount of 53BP1 to DSBs has been shown to result in extensive resection of DNA ends and repair via RAD52-directed SSA, consequently leading to large deletions (**Figure 1.12**) (Ochs *et al.*, 2016).

RNF168 is known to deposit the ubiquitin mark on lysine 15 of histone H2A variants, and this ubiquitination has been shown to be important for the recruitment of 53BP1 to DSBs. However, due to the lack of a specific and commercially available antibody, it is still to be confirmed whether it is limited ubiquitination of H2A variants by RNF168 or its other function that leads to the switch to the more mutagenic repair.

1.6 THE CURRENT METHODS TO STUDY DNA DAMAGE-ASSOCIATED HISTONE PTMS

1.6.1 Introduction

The two most common approaches used to investigate protein levels involve antibody-based and mass spectrometry-based (MS-based) proteomic approaches. Antibody-based proteomics relies on the specific binding affinity of antibody and its target to detect and quantify proteins of interest. Antibodies are used in applications such as chromatin immunoprecipitation (ChIP), immunofluorescence (IF) and immunoblotting (IB). However, specificity and reproducibility of antibodies is a common and well recognised issue that challenges the quality and the strength of experimental results (Bordeaux *et al.*, 2010; Bock *et al.*, 2011; Bradbury and Plückthun, 2015; Bradbury and Plückthun, 2015; Buck, 2015). Indeed, recent initiatives to address the quality of commercially available antibodies to histone PTMs revealed that at least 25% of those failed to specifically recognise their intended target (Egelhofer *et al.*, 2011). Furthermore, the recognition of histone PTMs by antibodies can be also influenced by batch-to-batch variations, as well as pattern of the neighbouring PTMs, which may introduce a specific bias to the study (**Figure 1.14**) (Fuchs *et al.*, 2011; Rothbart *et al.*, 2015). Therefore, the quality and specificity of anti-histone PTMs antibodies should be carefully assessed prior to experimental application, which may result in high cost and additional workload.

Once specific antibody has been found and validated, additional difficulties may arise in regards to the specific application they are used in. For instance, IF approaches identify DSB-associated changes based on the direct co-localisation of specific histone marks with damage foci, such as γH2AX or 53BP1 (Facchino *et al.*, 2010; Miller *et al.*, 2010a; Liu *et al.*, 2013; Gong *et al.*, 2017). While spatial co-localisation can reveal valuable information about size, number and sub-nuclear localisation of the damage focus, this method is very low throughput due to the limited number of fluorophores.

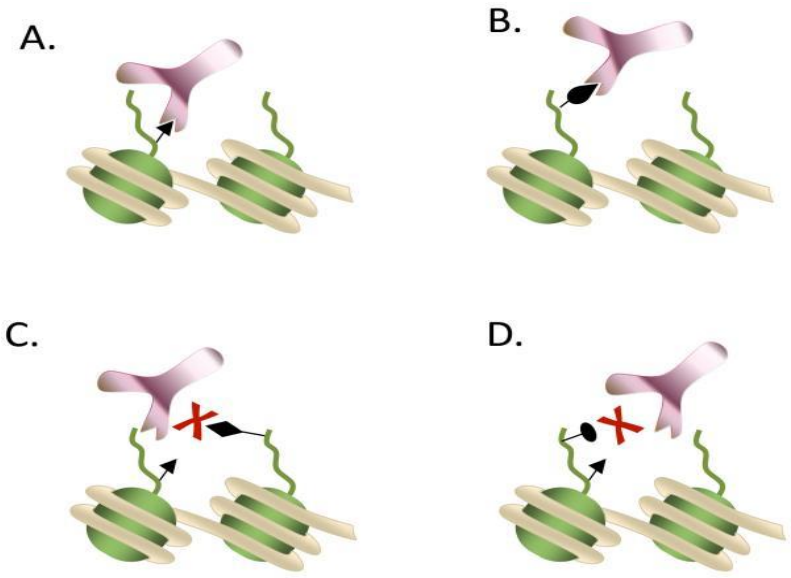

Figure 1.14 Examples of the basis for epitope steric hindrance during the antibody recognition. Cartoon representing an antibody A) recognition of the epitope without the interference, (B) cross-reacting with non-intended epitope, (C) not-recognising the epitope in the context of neighbouring PTM, and (D) not recognising the epitope due to obstruction by distantly located PTM. Figure adapted from: Önder *et al.*, 2015

Furthermore, the concept of co-localisation is also limited by the resolution power of the microscope used for the particular experiment, which means that often co-localisation may be concluded, while there may in fact be separation that is too small to be detected, consequently, making this approach vulnerable to human bias (Dunn, Kamocka and McDonald, 2011).

This problem also applies to ChIP-based approaches, since they also rely on the specificity of the antibodies. Another issue with ChIP-based approaches is the fact that they require a prior knowledge of the genomic locus containing the DNA break. To achieve that, restriction nucleases, such as I-SceI, HO and AsiSI are transfected into cells to induce the break in a sequence specific manner, resulting in a cycle of cutting and repair events. Since, the genomic region containing the DSB is known, they allow direct analysis of chromatin surrounding it, using chromatin immunoprecipitation (ChIP) based techniques. Due to the accessibility issues, most of these nucleases are known to cut mainly in the open chromatin regions. However, it is currently unknown, whether this process of continuous DNA cutting may affect the surrounding chromatin structure.

Although antibodies can be very sensitive in detecting histone PTMs, they are not ideal for discovery-type experiments, since they require prior knowledge of the type and location of modification. In addition to that, antibody-based studies can typically analyse only one PTM at a time, making this method low throughput and not suitable for the study of the combinatorial effects of PTMs.

In recent years MS-based proteomics has become the tool of choice for analysis of histone PTMs (Plazas-Mayorca*et al.*, 2010; Qi *et al.*, 2010; Sweet *et al.*, 2010; Martinez-Garcia *et al.*, 2011; Wu *et al.*, 2011; Zheng *et al.*, 2012, 2014; Maile *et al.*, 2015). Several MS-based assays have been developed for simultaneous monitoring of multiple histone PTMs in single experiments, therefore making this approach high throughput, as well as allowing for the examination of the combinatorial effects of multiple PTMs (Karch *et al.*, 2013). Since previous knowledge of the modification is not a requirement, MS-based analysis can also allow discovery of previously unknown marks, however the sensitivity of the detection of low abundance marks will be limited.

In this thesis I have combined the antibody-based and MS-based proteomic strategies to quantify histone PTMs associated with the nucleosomes containing histone γH2AX.

1.6.2 Overview of biological mass spectrometry workflow

Mass spectrometry proteomics is an analytical technique used to identify peptides and proteins within a mixture by measuring the mass-to-charge ratio (m/z) of ionised particles generated from this mixture. Commonly in MS-based proteomics, proteins are digested enzymatically to smaller fragments with proteases, such as trypsin or Arg-C (**Figure 1.15 A**). The peptides from complex mixtures are typically separated by liquid chromatography prior to the introduction into the mass spectrometer, where they get further fragmented into smaller pieces, known as 'fragment ions'.

The basic components of a mass spectrometer include an ion source, a mass analyser and a detector (**Figure 1.15 B**). After the samples are loaded onto a mass spectrometer they are vaporised and ionised by the ion source, where they acquire a charge that allows these molecules to accelerate them through the remaining parts of the system. In the mass analyser ions are subjected to the electric or magnetic field, which deflects the path of individual ions based on their m/z, leading to their separation. Additionally, mass analysers can be also used to perform a more targeted type of analysis, where only specific ions of interests are selected for further analysis. Once successfully selected by the mass analyser, ions reach the detector. For an electron multiplier detector, once ions hit the detector plate, a cascade of electrons is emitted leading to amplification of the signal, greatly improving sensitivity of detection. The whole process occurs in a vacuum.

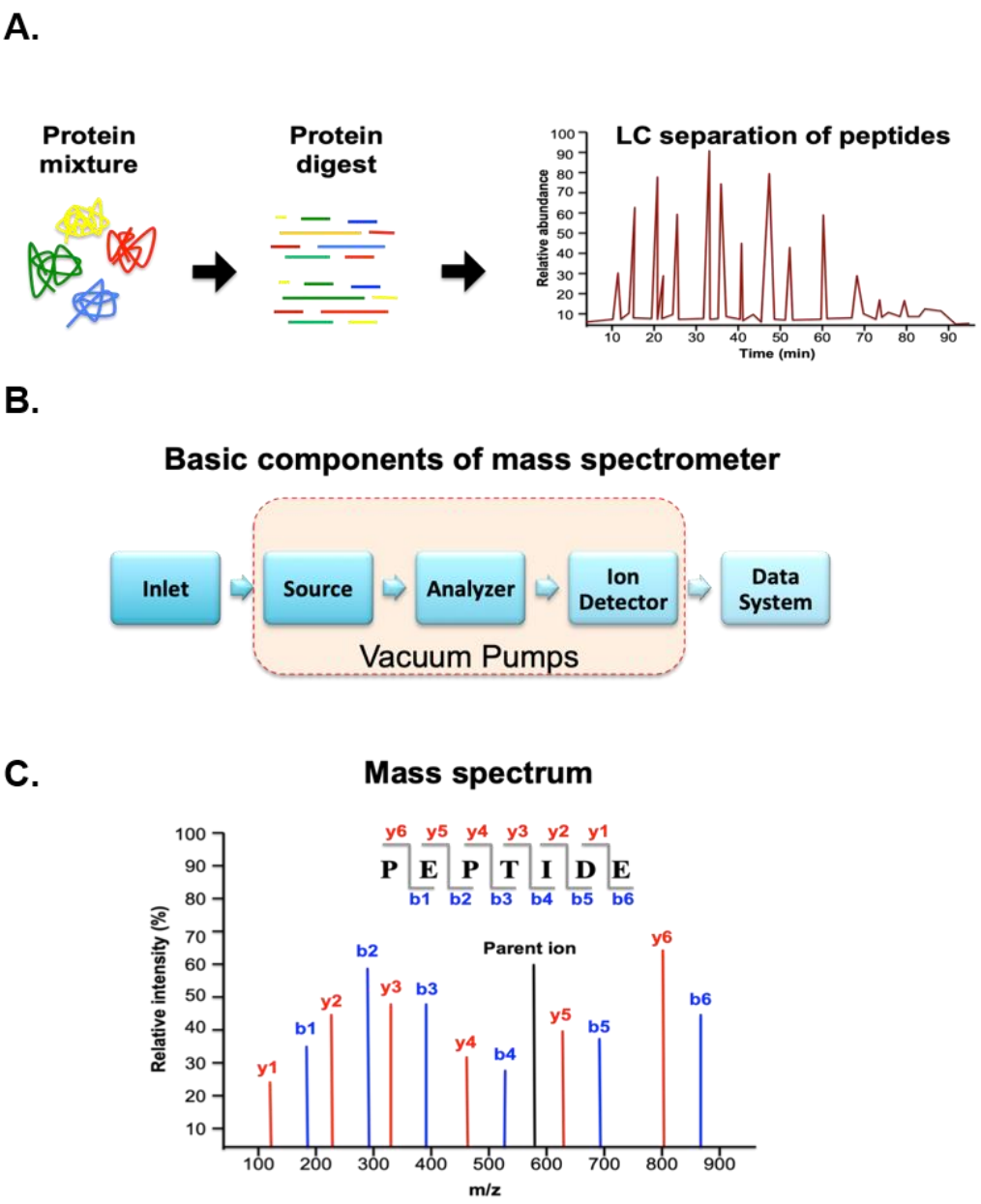

Figure 1.15. **Basic principles of protein 'bottom-up' liquid chromatography (LC)-coupled mass spectrometry workflow.** A) Protein mixture is enzymatically digested and peptides are separated on the LC column prior to MS analysis. B) Basic components of a mass spectrometer. LC-separated peptides enter the source to become ionised prior the entry to a mass analyser, where they become separated according to their m/z. Ionised peptides are detected in an ion detector and the intensities of the ions are recorded in the data system. C) Hypothetical mass spectrometry output from a hybrid mass spectrometry instrument. Relative intensities of 'PEPTIDE' parent and fragment ions ('b' and 'y') recorded on the spectrum.

study incorporates two detectors: a linear ion trap and an Orbitrap. In this setup specific ions can be selected and fragmented in the ion trap analyser and passed A variety of mass analysers has been developed that apply different principles and have different characteristics. The LTQ-Orbitrap-XL instrument used in this

to the Orbitrap, where their m/z ratio is determined at high resolution. In this study, collision induced dissociation (CID) was used to fragment the ions. This type of fragmentation induces fragmentation along the peptide bond in between carboxyl and amino groups of neighbouring amino acids, producing mainly ‘b’ (extend from amino-terminus of peptide) and ‘y’ (extend from carboxy-terminus) ions. The readout from a mass spectrometer of m/z values and their intensities is referred to as a ‘mass spectrum’ (**Figure 1.15 C**).

MS-proteomic technology can be utilised for data dependent acquisition (DDA) to perform discovery-based experiments (shotgun proteomics). In a typical shotgun-type of experiment the MS instrument generates a full scan mass spectra of precursor ions (MS1) to determine their mass to charge ratio (m/z), and then acquires MS/MS (MS2) spectra of the most intense peptides. Since in the DDA mode only the most abundant proteins/peptides are fragmented, this method has limited sensitivity.

MS-proteomic experiments can also be hypothesis driven (targeted proteomics). In contrast to shotgun-type of experiment, the MS instrument is programmed to analyse pre-defined set of peptides. Essentially, in targeted analysis, precursor ions of the peptides of interest are filtered based on their m/z, which are then fragmented to generate specific fragment/product ions that can be detected and quantified. Each specific precursor/product ion pair is referred to as a “transition”. This method allows for the characterisation of lower abundance peptides.

Targeted MS technologies, such as selected reaction monitoring (SRM), parallel reaction monitoring (PRM) and pseudo SRM (pSRM), allow highly reproducible detection and quantification of the specific set of peptides. These approaches differ depending on the instrument used. SRM experiments are conducted on a triple quadrupole MS, PRM analysis is conducted typically on Q Exactive

instruments, while pSRM assays are conducted exclusively on LTQ linear ion trap or LTQ-Orbitrap. pSRM records all the products of selected precursor ions, while in SRM only selected transitions are measured. Targeted MS approaches can be used for absolute and relative quantification of peptides of interest. Furthermore, these methods may involve the use of labelling (chemical or metabolic stable isotope labelling) or may be performed label-free (e.g. using internal peptides for standardisation).

Next I will describe the particular steps of an MS-based proteomic workflow in more detail.

1.6.3 Enzymatic digestion of proteins

Enzymatic digestion of proteins involves cleavage of the peptide bonds at specific amino acid residues along a polypeptide chain, yielding a range of smaller peptides that can be analysed by mass spectrometry. Multiple proteases are available for this purpose (**Table 1.3**). It is a very common technique and it is utilised in a variety of applications, such as determination of the peptide/protein sequence or PTM analysis.

Trypsin is the most widely used in bottom-up MS approaches and is considered the gold standard in proteomics (Switzar, Giera and Niessen, 2013). It cleaves peptide bonds C-terminal to basic residues lysine and arginine (K and R), unless they post-translationally modified by more than one methylation (K, R), acetylation and ubiquitination (K), or followed by proline residue (Olsen, Ong and Mann, 2004; Ong, Mittler and Mann, 2004; Baeza *et al.*, 2014). On average, trypsin digest creates ~14 residues long peptides that carry at least two positive charges, making it highly suitable for MS analysis (Switzar, Giera and Niessen, 2013).

Multiple protocols have been developed for trypsin digestion of samples in-solution and in-gel. They usually involve protein denaturation, reduction of di-sulphide bridges and subsequent alkylation of cysteine residues, with the inclusion of several steps that aid unfolding of the proteins and allow trypsin

access to K and R residues. The process is terminated by acidification of the sample, which prevents trypsin activity.

Protease	Family	Cleavage site
ArgC	Cysteine protease	C-terminal of R
AspN	Metalloprotease	N-terminal of D
Chymotrypsin	Serine protease	C-terminal of F, Y, L, W and M
GluC	Serine protease	C-terminal of D
LysargiNase	Metalloprotease	N-terminal of R and K
LysC	Serine protease	C-terminal of K
LysN	Metalloprotease	N-terminal of K
Pepsin	Aspartic protease	C-terminal of Y, F and W
Trypsin	Serine protease	C-terminal of R and K
WaLP and MaLP	Serine protease	C-terminal of aliphatic amino acids

Table 1.3. Example of proteases commonly used in proteomics workflows.

1.6.4 High performance liquid chromatography coupled to MS (HPLC-MS)

One of the ways by which MS samples can be introduced to the instrument is via direct infusion. This method however has several limitations, since the majority of MS instruments cannot perform separation of the components of the complex mixture and multiple peptides may have the same molecular mass and fragmentation pattern, potentially leading to increased experimental error. Therefore, combining MS with another separation technique is commonly used to achieve higher accuracy and reduced experimental error. Liquid chromatography is an analytical technique that leads to separation of the individual components of complex mixture based on their chemical properties (**Figure 1.16**) and it is an important step in proteomic workflow for achieving high signal to noise data and subsequently increased quantitative capabilities.

Reverse phase HPLC column packed with C18 material, which was used in this thesis, separates peptides in a biological mixture based on their properties. Depending on the properties of the peptides, the time of elution from the column will vary, with hydrophilic peptides eluting at earlier times and the more hydrophobic peptides being retained on a column for longer. The elution of peptides is experimentally manipulated by applying a concentration gradient of an organic solvent over time (from low to high concentration).

Attempts to simultaneously quantify large amounts of transitions in a single targeted MS run may lead to extended duty cycle of experiment and adversely affect quantitative performance of the assay. Therefore, only a limited number of peptides can be measured at one time. Retention time (RT) scheduling is often used to overcome this issue. In this approach, the retention times on the column for the peptides of interest are usually established empirically or with the use of bioinformatics prediction tools (Escher *et al.*, 2012; Gallien *et al.*, 2012). However, several variables may affect the stability of the RTs, preventing the acquisition of a quantitative data making it an important limitation to this method.

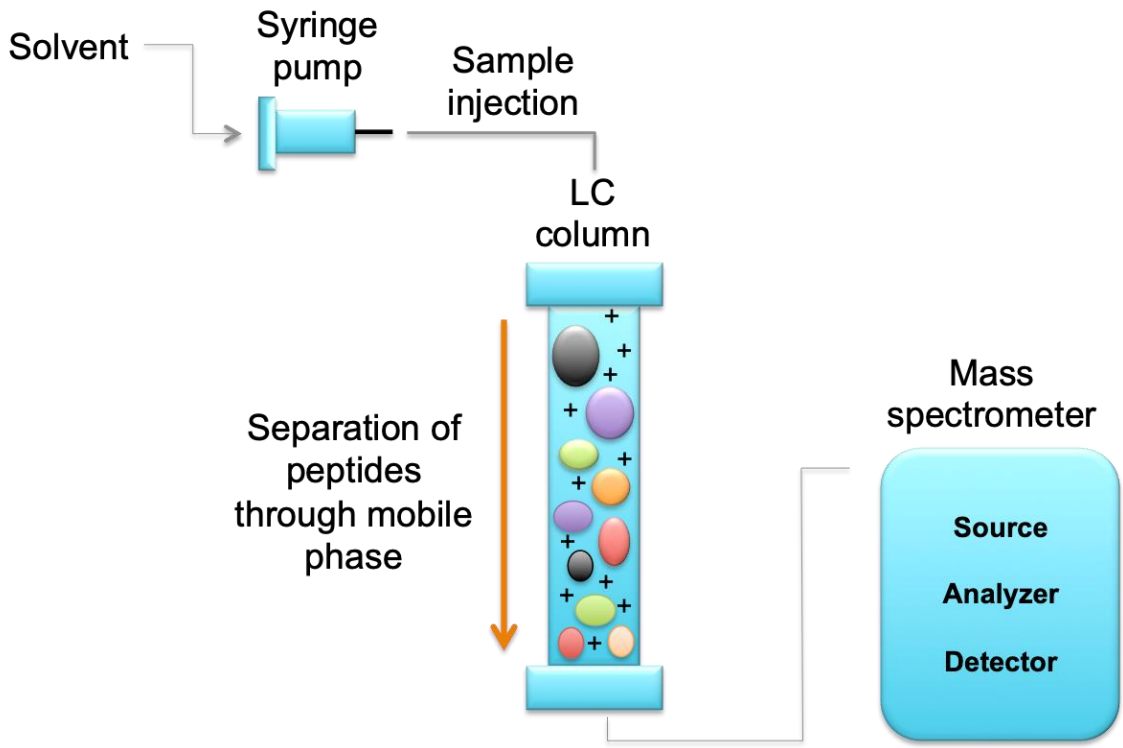

Figure 1.16. General LC-MS workflow. Following proteolytic digestion, proteins from complex biological samples are converted into peptides, which are then injected onto LC-column, where they are separated according to their chemical properties. As the samples are eluted from the LC column they are ionised prior to entry to a mass spectrometer.

1.6.5 Electrospray ionisation (ESI)

In order to measure m/z, the analyte must first be ionised. Broadly, ionisation techniques are divided into ‘hard’ and ‘soft’ ionisation methods. ‘Hard’ ionisation leads to extensive fragmentation of the molecule, producing multiple fragment ions, while ‘soft’ ionisation methods produce molecular ions, which are derived from neutral molecules by loss or gain of electrons. The two soft ionisation techniques most commonly used in proteomics are matrix-assisted laser desorption ionisation (MALDI) and electrospray ionisation (ESI), the latter was used in this thesis.

In ESI, a strong electric field is applied to the liquid sample passing through a capillary tube. This leads to the accumulation of charged molecular species at the end of the capillary tube, causing formation of highly charged droplets. A voltage applied to the capillary tube is causing the liquid analyte to leave the tube as a cone-shaped spray, with the ions accumulated on the surface of droplets (**Figure 1.17**).

In the case of protein and peptide samples, ions mainly carry positive charge, due to additives such as formic acid that are added to the solvents as proton donors. Passing through heated capillary before entering mass analyser desorbs the solutes. The differential pressure between the ionisation step, which occurs under atmospheric pressure, and downstream steps, which occur under the vacuum, facilitates the entry of the ions into the mass analyser.

Due to its ability to produce multiply charged ions, ESI is well suited for the study of biological molecules, such as proteins/peptides. Commonly, peptides carry single (+1), double (+2) or triple (+3) charge, depending on the size and the number of basic residues. As the most commonly protease used in MS-based proteomics is trypsin, which leaves basic lysine or arginine residue at the C-terminus, the majority of the peptides carry a +1 or +2 charge.

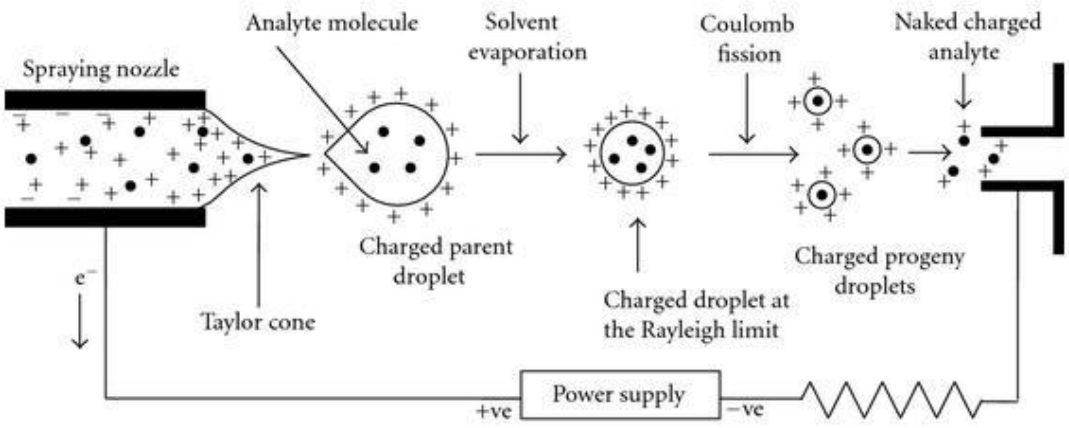

Figure 1.17 Schematic representation of ESI. Within ESI source, a continuous stream of solubilised sample is passed through spraying nozzle. Electrical energy is used to transfer the ions from solution into gaseous phase, which occurs in three steps. Firstly, charged parental droplets are dispersed via fine spray, which is followed by solvent evaporation. The droplets shrink until it reaches the point, when surface tension can no longer sustain the charge (the Rayleigh limit), resulting in “Coulombic explosion”, splitting the droplets apart, to produce smaller charged progeny droplets that can repeat the process, as well as naked charged analyte molecules. Adapted from Banerjee and Mazumdar, 2012.

1.6.6 Tandem mass spectrometry (MS/MS)

Mass analysers typically used in proteomic studies are time-of-flight, quadrupole, ion trap and Orbitrap (**Table 1.4**). The performance of those analysers is assessed by three criteria: 1) upper mass limit, 2) transmission and 3) resolution. The upper mass limit refers to the maximum m/z ratio that can be measured. Transmission is a ratio between the number of ions reaching the detector to the number of ions produced in the ion source. The resolution refers to the instruments ability to produce distinguishable signals from ions with small mass differences. Additional important aspects are dynamic range, analysis speed and fragmentation capabilities.

LTQ-Orbitrap XL mass spectrometer used in this study contains two mass analysers: linear ion trap and Orbitrap. A key advantage of this instrument is its ability to perform multiple stages of MS/MS fragmentation, allowing the yield of large amounts of structural information. The linear ion trap mass analyser is capable of isolating, storing and fragmenting ions. It works by confining ions radially with the use of quadrupole rods, while a static electrical potential on the ends of the electrodes serves to confine the ions axially. The combination of axial and radial trapping results in the ions arranging themselves in a linear string. The application of a dynamic field to the trapped ions leads to specific m/z values being isolated or activated for fragmentation. The advantages of linear ion traps are high sensitivity and high sequencing speed. However, in comparison to high resolution mass analysers, such as Orbitrap, their mass accuracy, mass resolution and linear dynamic range are relatively low. In hybrid MS instruments, linear ion traps are most frequently used for fragmentation due to their fast cycle times, resulting in the smaller number of ions required for MS/MS in that device.

Orbitrap mass analysers employ electrostatic fields to trap and measure ions. The Orbitrap cell is composed of a central spindle-like shaped electrode within an outer barrel-like shaped electrode insulated by a ceramic ring, which allows it to act as both, analyser and detector. The electrostatic field applied on ions inside the Orbitrap causes them to orbit around the central electrode with axial oscillations along the z-axis.

Mass analyzer	Resolution units	Mass accuracy	Sensitivity	Dynamic range	MS scan rate
Time-of-flight	15000	<5 ppm	Attomole	Low	Fast
Quadruple	2000	100 ppm	Attomole	High	Moderate
Ion trap	4000	100 - 300 ppm	Femtomole	Low	Moderate to fast
Orbitrap	15000	< 2 ppm	Femtomole	High	Slow

Table 1.4. Comparison of the features and specifications of the mass analysers commonly used in proteomics.

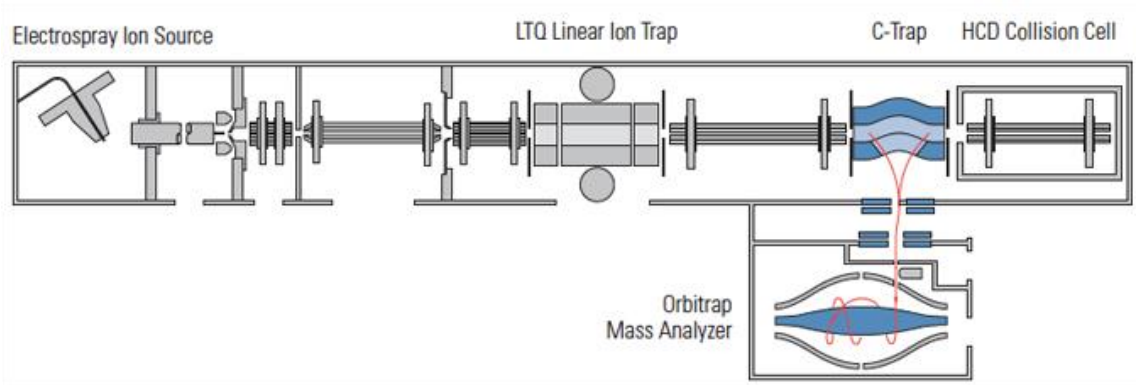

Figure 1.18 Schematic layout of the LTQ Orbitrap XL mass spectrometer. Ions created in the ESI source are trapped in the LTQ XL, axially ejected and collected in a C-shaped ion trap (C-Trap), then passed into the Orbitrap mass analyser, where they are captured by rapidly increasing voltage on the centre electrode of the Orbitrap. Trapped ions undertake circular trajectories around centre electrode and their axial oscillations. Depending on their m/z values, ions oscillate at different frequencies, allowing their separation. Figure adapted from http://planetorbitrap.com/ltq-orbitrap-xl.

Ions with different m/z values oscillate at different frequencies, allowing their separation. The mass spectra of the ions are acquired using image current detection by measuring the oscillation frequencies induced by ions on the outer electrode. Due to their superior high mass accuracies (1-2 parts per million (ppm)) and high resolution (150000 resolution units) Orbitrap analysers are commonly used when high resolution measurements are required. In addition, sub-fentomole sensitivity, large dynamic and m/z ranges make it particularly suitable for the studies of highly complex biological samples.

1.6.7 Mass spectrometry (MS) for the study of histone PTMs

Although antibodies can be very sensitive in detecting histone PTMs, they are not ideal for discovery-type of experiments, since they require prior knowledge of the type and location of modification. In addition to that, antibody-based studies can typically analyse only one PTM at a time, making this method low throughput and not suitable for the study of the combinatorial effects of PTMs.

In the recent years MS-based proteomics has become the tool of choice for analysis of histone PTMs (Plazas-Mayorca *et al.*, 2010; Qi *et al.*, 2010; Sweet *et al.*, 2010; Martinez-Garcia *et al.*, 2011; Wu *et al.*, 2011; Zheng *et al.*, 2012, 2014; Maile *et al.*, 2015). Several MS-based assays have been developed for simultaneous monitoring of multiple histone PTMs in single experiments, therefore making this approach high throughput, as well as allowing for the examination of the combinatorial effects of multiple PTMs (Karch *et al.*, 2013). Since previous knowledge of the modification is not a requirement, MS-based analysis can also allow discovery of previously unknown marks, however the sensitivity of the detection of low abundance marks may be limited.

By convention, MS-based strategies are divided into three main groups known as top-down, middle-down and bottom-up (**Figure 1.19**). All of these approaches have been previously applied to the studies of histone modifications,

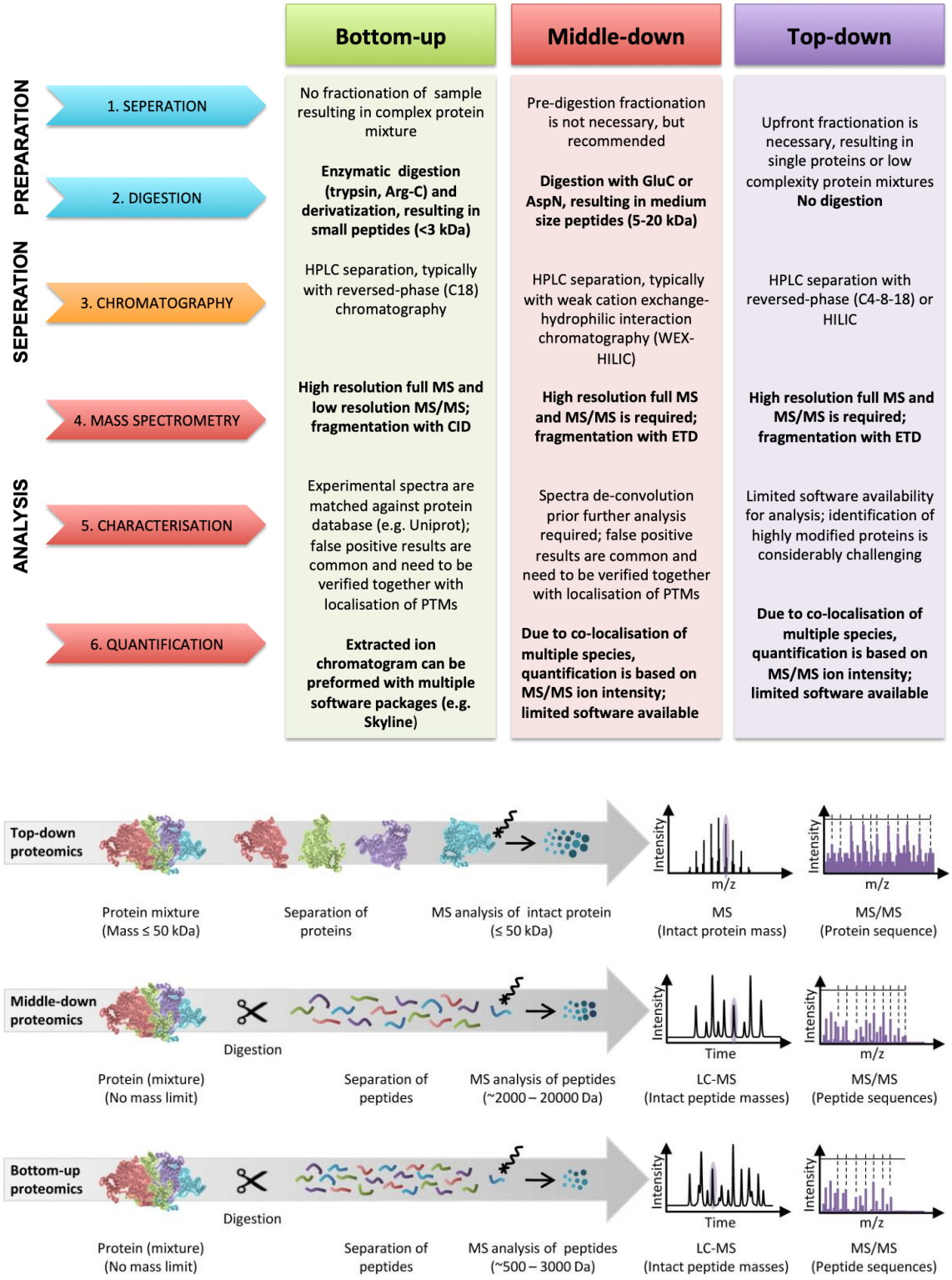

Figure 1.19 Summary of the key steps involved in bottom-up, middle-down and top-down MS strategies. Bottom panel figure is adapted from Switzar, Giera and Niessen, 2013.

and have several advantages and disadvantages depending on the application context. For instance, in top-down approach intact histone proteins are analysed, allowing investigation of combinatorial effects of PTMs. However, technically this approach is very challenging for several reasons: 1) MS/MS spectra are difficult to obtain due to poor ionisation efficiency of high molecular weight species, therefore require a large amount of starting material; 2) the separation of histones containing different combinations of the same number and type of PTMs is currently impossible; 3) the generated data is highly complex and computationally challenging to deconvolution.

In contrast to top-down MS strategy, both bottom-up and middle down approach use enzymes to digest proteins to smaller fragments. Most commonly used proteases cleave after basic or acidic residues. An analysis of the histone PTMs using proteolytic digest is not straightforward, since their sequence is highly enriched in lysine and arginine residues; predominantly at the N-terminal tails, where the majority of known PTMs are deposited. For instance, trypsin cleaves after basic residues, resulting in the small peptides that are difficult to be retained on the reverse phase chromatography column, thus are challenging for MS analysis. In contrast, digestion with proteases which cleave after acidic residues, for instance Glu-C, produces large, multiply charged peptides that are notoriously difficult for interpretation.

Several methods have been developed to overcome this issue. For example, Arg-C enzyme can be used to produce suitable length peptides, as it cuts principally after arginine residue (McKittrick *et al.*, 2004). However, Arg-C digestion was found to lack reliability (Garcia *et al.*, 2007). Alternatively, chemical derivatisation of unmodified lysines by adding a propionyl group prior to tryptic digestion can be used. This chemical derivatisation restricts action of trypsin to arginine residues and produces Arg-C-like peptides, but with increased reliability compared to Arg-C digest, making this method well suited for quantitative studies of histone PTMs (Garcia *et al.*, 2007). Due to relatively short length of the peptides produced in this way, MS spectra are less complex, when compared with top-down and middle-up approaches, and therefore easier

to interpret. In addition to that, propionic group increases hydrophobicity of the peptides, thus improving their retention on the chromatography column, and therefore, MS detection. For these reasons, a bottom-up approach using Arg-C-like tryptic digestion following propionylation of unmodified lysines, has been selected as the most suitable for this study.

However, several aspects needs to be considered, when using this method. Firstly, this derivatisation is not suitable in studies of naturally occurring histone propionylation (Sidoli *et al.*, 2015). Additionally, propionic anhydride derivatisation was found to lead to partial alkylation of the hydroxyl groups on the serine, tyrosine and threonine residues, while ammonium bicarbonate, a buffering agent commonly used in proteomic workflows, was found to compete with hydroxyl groups for propionylation (Liao *et al.*, 2013; Meert *et al.*, 2015). These side reactions may therefore lead to several analytical issues, leading to reduced accuracy of results, reproducibility and sensitivity of MS analysis.

More recently, it has been shown that some of these side reactions may be improved. For example, switching from ammonium bicarbonate to triethylammonium bicarbonate improves propionylation efficiency, but leads to increase in side reactions, due to reactivity of anhydride towards hydroxyl groups, which can be overcome by using an excess of hydroxyl amine to quench the reaction, or even reverse overpropionylation of unwanted residues (Meert *et al.*, 2016).

1.7 THE IMPORTANCE OF RESEARCH INTO THE CHROMATIN RESPONSE TO DNA DAMAGE AND THE AIMS OF THE PROJECT

The dramatic changes in histone PTMs associated with the repair of DNA lesions, as well as the loss of nucleosomes that potentially carry important epigenetic instructions, gives rise to the question of whether this information is re-established, and if so, how. It could be speculated that failure to faithfully recover from this kind of trauma can potentially lead to the loss or gain of the epigenetic memory, which, in turn, can have severe consequences for the

fitness of the organism. For instance, it was previously demonstrated that induction of DNA DSBs can lead to transcriptional silencing in the proximity of the break, which is usually reversible (Shanbhag *et al.*, 2010). However, there is a possibility that at a subset of these breaks, marks that are associated with transcriptional silencing persist, leaving a message that is propagated through subsequent cell divisions (Cuozzo *et al.*, 2007). This can be especially dangerous if the silenced region, for example, encodes a tumor suppressor gene.

To further underscore the importance of chromatin structure and the associated marks, it is worth noting that the enzymes involved in chromatin remodeling complexes are often mutated in cancers (Kandoth *et al.*, 2013), although their exact role is still to be elucidated. Therefore, insight into mechanisms involved in the dynamics of histone PTMs and histone exchange in response to genotoxic stress will be an important milestone in the understanding of the development of disease. Once acquired, this knowledge can be further used to screen and analyze cell lines from e.g. cancer patients. This knowledge could allow us to design therapies that specifically target pathways involved in disease states.

The central aim of my thesis was to enhance our understanding of the role of chromatin in the response to DNA DSBs. My specific target was to unravel the landscape of histone PTMs involved in the DDR and DSB repair. I have established a novel chromatin immunoprecipitation coupled with mass spectrometry method (ChIP/MS) for recovery of the nucleosomes from the sites of DNA damage and quantification of associated histone PTMs. I have used this procedure to gain further insight into the PTMs that arise in the DSB vicinity.

2 CHAPTER TWO: MATERIALS AND METHODS

2.1 CELL CULTURE AND STABLE ISOTOPE LABELLING WITH AMINO ACIDS IN CELL CULTURE (SILAC)

The cell lines used in this thesis were grown in the media described in the **Table 2.1** and were passaged every 3-4 days. For biotinylation experiments, the cell media was substituted with dialyzed serum (PAN Biotech). All of the cell lines were grown in 37^0C humidified atmosphere containing 5% CO_2.

For the biotinylation system, to induce damage cells were treated with the indicated concentration of Neocarzinostatin (NCS) (N9162, Sigma). Biotinylation was induced with 50 µM biotin (B4639, Sigma) for 5 min.

Cell line	Tissue of origin	Complete growth media	Complete SILAC growth media
HEK293	Human embryonic kidney cells	DMEM (GIBCO), 10% FCS (PAN Biotech), 2 mM L-Glutamine (GIBCO), 100 IU penicillin/streptomycin (Corning)	DMEM (cat.#0420, Atheneas) supplemented with 15% dialyzed serum (PAN Biotech) light lysine, arginine, leucine, and methionine provided with MEM by supplier. 1 h prior IR treatment media was switched to one supplemented with heavy methionine (L-Methionine-methyl-13C,d3; Sigma)
1BR.3 hTERT	Human skin fibroblast cells, transformed	MEM (GIBCO), 15% FCS (PAN Biotech), 2 mM L-Glutamine (GIBCO), 100 IU penicillin/streptomycin (Corning)	MEM (cat.#0424, Atheneas) supplemented with 15% dialyzed serum (PAN Biotech) light lysine, arginine, leucine and methionine provided with MEM by supplier . 1 h prior IR treatment media was switched to one supplemented with heavy methionine (L-Methionine-methyl-13C,d3; Sigma)
AT-1BR.3 hTERT	Human skin fibroblast cells derived from ATM patient, transformed	MEM (GIBCO), 15% FCS (PAN Biotech), 2 mM L-Glutamine (GIBCO), 100 IU penicillin/streptomycin (Corning)	MEM (cat.#0424, Atheneas) supplemented with 15% dialyzed serum (PAN Biotech) light lysine, arginine, leucine and methionine provided with MEM by supplier. 1 h prior IR treatment media was switched to one supplemented with heavy methionine (L-Methionine-methyl-13C,d3; Sigma)
A549	Human lung adenocarcinoma epithelial cells	DMEM (GIBCO), 10% FCS (PAN Biotech), 2 mM L-Glutamine (GIBCO), 100 IU penicillin/streptomycin (Corning)	NA
U2OS	Human bone osteosarcoma epithelial cells	DMEM (GIBCO), 10% FCS (PAN Biotech), 2 mM L-Glutamine (GIBCO), 100 IU penicillin/streptomycin (Corning)	NA

Table 2.1 The cell lines and growth media used in the thesis. DMEM = Dulbecco's Modified Eagle Medium; MEM = Minimum Essential Medium Eagle; SILAC = stable isotope labelling of amino acids in culture.

2.1.1 Plasmids and transfections

Plasmids pcDNA3.1(+) BirA-6xHis-GFP and pcDNA3.1(+) BAP-6xHis-H3.1 were previously described in (Kulyyassov *et al.*, 2011). To PCR RNF168 and 53BP1 the following primers were used: 5'AAAACTCGAGGCCACCATGGCTCTACCCAAAGACG3'/5'AAAGCGGCCGCTTACTTTGT3' and 5'AAAACTCGAGATGGACCCTACTGGAAGTC3'/5'AAAGCGGCCGCTTAGTGAGAAACATAATCGTGTTTATATT3' respectively. To make BirA-6xHis-RNF168/53BP1, the GFP in pcDNA3.1(+) BirA-6xHis-GFP was replaced with the wild type cDNA sequence of RNF168 and 53BP1 (kind gifts from C. Lukas and P. Jeggo respectively).

3xFLAG-BAP-H4 was constructed by cloning the fragment (5'-GCTAGCCTTAAGGCCACCATGGAATTCCTCGAGGACTACAAAGACGACGATGACAAGGATTATAAGGACGATGATGACAAGGACTACAAGGATGATGACGACAAGGCCATCGATGGCCTGAACGACATCTTCGAGGCCCAGAAGATCGAGGGCGAGTTCGgatcCTCTGGCAGAGGCAAAGGcGGAAAGGGCCTGGGAAAGGGCGGAGCCAAGCGGCACAGAAAGGTGCTGCGGGACAACATCCAGGGCATCACCAAGCCCGCCATCAGACGGCTGGCTAGAAGAGGCGGCGTGAAGAGAATCAGCGGCCTGATCTACGAAGAGACACGGGGCGTGCTGAAGGTGTTCCTGGAAAACGTGATCCGGGACGCCGTGACCTACACCGAGCACGCCAAGAGAAAGACCGTGACCGCCATGGACGTGGTGTACGCCCTGAAGAGACAGGGCAGAACCCTGTACGGCTTCGGCGGCTAACTCGAG-3'), synthesized by Eurofins Genomics, into the *Nhe*I/*Xho*I sites of the pcDNA3.1 vector. All the plasmid sequences were confirmed by Sanger sequencing. Transfections into cell lines were performed with Jet-PEI reagent (PolyPlus) according to manufacturer recommendations.

2.1.2 Generation of stable cell lines

To generate stable cell lines expressing 3xFLAG-BAP-H4 or BAP-tagged H3.1 plasmids were cut with *Bst*Z17I and *Sca*I, respectively, and transfected into U2OS cells with Jet-PEI (PolyPlus) transfection reagent according to

manufacturer recommendations. After 48 h successfully transfected cells were selected with 0.6 mg/ml of G418. Cells expressing BAP-tagged H3.1 were kept as polyclonal culture, while in the case of cells expressing BAP-tagged H4 monoclonal colonies were selected for further experiments. Positive transfectants were maintained thereafter in media containing 0.2 mg/ml of G418.

2.2 INDUCTION OF DNA DAMAGE

Where indicated in the results chapters, cells were damaged using X-rays. For this treatment, cells were grown to 90% confluence (HEK293) or G1-arrested by growing to confluence (1BR.3 hTERT and AT-1BR hTERT) and exposed to IR using an AGO HS X-Ray System at 250 kV potential and 500 mGy/min dose rate. Cells were collected at indicated time points by trypsinisation, washed in PBS, pelleted, snap-frozen in liquid nitrogen and stored at -80^{0}C.
For IR dose-response experiments, HEK293 cells were trypsinised and pelleted at 780 rcf for 2 min and re-suspended in complete DMEM. Exposure to gamma-rays was carried out using cesium-137 source (6 Gy/min). Cells were allowed to recover for 30 min, then pelleted, washed in PBS and snap-frozen in liquid nitrogen pellets were stored in -80^{0}C.

2.3 PREPARATION OF SAMPLES FOR MASS SPECTROMETRY ANALYSIS

Preparation of samples for MS involved several stages. These are described in detail in this section and include the following steps: 1) Isolation of nuclei; 2) Extraction of mono-nucleosomes; 3) Chemical derivatization (step used in the indicated experiments) and proteolytic digestion. The list of reagents and buffers used in this section is described in **Tables 2.2** and **2.3**.

Reagent name	Manufacturer	Product code
Propionic anhydride	Acros Organics	#131522500
Hydroxylamine	Sigma	#467804
TEAB (triethylammonium)	Sigma	T7408
Ammonium bicarbonate	Sigma	#09830
Anhydrous methanol	Acros Organics	#364391000
Trypsin	Promega	V511A
γH2AX antibody	Abcam	ab81299, LOT: GR297741-12
Protein G Dynabeads	Invitrogen	#10004D
Streptavidin Dynabeads	Invitrogen	#65001
AEBSF	Thermo Scientific	#78431
Leupeptin	Thermo Scientific	#78435
Pepstatin A	Thermo Scientific	#78436
Sodium butyrate	Acros Organics	#263191000
Sodium fluoride	Sigma	S7920
N-Ethylmaleimide	Thermo Scientific	#23030
MNase	Worthington	LS004798
2-Chloroacetamide	Sigma	C0267
λ-phosphatase	New England Biosciences	P0753S

Table 2.2 List of key reagents used during MS samples preparation.

Buffer	Components	Comment
Protease and epigenetic inhibitors	0.5 mM AEBSF (Thermo Scientific, #78431)	serine proteases inhibitor
	1 mM PMSF (Thermo Scientific, #36978)	serine proteases inhibitor
	21 µM leupeptin (Thermo Scientific, #78435)	serine and cysteine protease inhibitor
	2.9 µM pepstatin A (Thermo Scientific, #78436)	aspartic acid protease inhibitor
	10 mM sodium butyrate	HDAC inhibitor
	5 mM sodium fluoride	phosphatase inhibitor
	20 mM N-ethylmaleimide (Thermo Scientific, #23030)	DUB inhibitor
NIB-250	15 mM Tris-HCl pH 7.5	
	60 mM KCl	
	5 mM MgCl2	
	1 mM CaCl2	
	250 Sucrose	
	0.3 % NP-40 (IGEPAL CA-630)	detergent added for nuclear isolation step, but not wash step
	Protease and epigenetic inhibitors	added freshly
MNase digestion buffer	250 mM sucrose	nuclei cushion
	50 mM Tris-HCl	
	1 U/70 µg MNase (Worthington, LS004798)	
MNase quenching solution	10 mM EDTA	
IP wash buffer	500 mM NaCl	
	50 mM Tris-HCl	
	1 % NP-40	
	1 % Triton	
2xLaemlli buffer	4 % SDS	
	20 % glycerol	
	120 mM Tris-HCl pH 6.8	
	0.02 % bromophenol blue	
	5 % beta-mercaptoethanol	added freshly
Running buffer	25 mM Tris base	
	190 mM glycine	
	0.1 % SDS	
Transfer buffer	25 mM Tris base	
	190 mM glycine	
	10% methanol	added freshly

Table 2.3 Table of buffers and their components used in the Proteomic Methods section.

2.3.1 γH2AX-ChIP

Step 1: Nuclear isolation

Cell pellets were thawed on ice and re-suspended in 10 volumes of NIB-250 (Nuclear Isolation Buffer) described in **Table 2.3** containing 0.3% NP-40 and freshly added protease inhibitors (**Table 2.3**). Cells were incubated on ice for 5 min and the nuclei were pelleted at 500 rcf, 4^0C for 5 min. Nuclear pellets were washed in NIB-250 (without NP-40 and N-Ethylmaleimide) and pelleted as above.

Step 2: Chromatin extraction with Micrococcal nuclease digestion and λ-phosphatase treatment

Nuclei were re-suspended in the MNase buffer supplemented with protease and epigenetic inhibitors at DNA concentration 2 μg/μl and equilibrated to 37^0C for 10 mins. To follow, 1 U of Worthington MNase/70 μg of DNA was added and nuclei were incubated for 10 min (unless indicated otherwise) at 37^0C, 800 rpm (ThermoShaker). The reaction was quenched with 10 mM EDTA final concentration, nuclei were pelleted for 10 min, 9300 x g in the table top centrifuge at 4^0C and the supernatant was collected. To test antibody specificity, where indicated, protein phosphorylation was removed prior to immunoprecipitation. To do that, MNase extracts were treated with λ-Phosphatase (**Table 2.2**) according to manufacturer instructions.

Step 3: Analysis of DNA sizes following MNase digestion

Following MNase digest, the DNA size distribution was analysed with a Bioanalyzer (Agilent) DNA high-sensitive chip according to manufacturer instructions or by agarose gel electrophoresis. For the gel analysis samples were incubated with 2% SDS at 75^oC for 30 minutes, vortexing occasionally. For MNase time-course experiment (Fig. 3.2 A), equal amounts of digest corresponding to each time-point were loaded, and for the time-course after DNA damage induction (Fig. 3.2 B), 1μg of DNA per sample was loaded onto a

1.5% agarose gel. The DNA was resolved at 50 Volts, for 1 hour at 4°C, and stained with 0.5 μg/ml ethidium bromide.

Step 4: γH2AX IP

γH2AX-containing nucleosomes were immunoprecipitated with rabbit monoclonal antibody (ab81299, LOT: GR297741-12)). 0.5-1 mg of MNase digest was re-suspended to 0.5 mg/ml of final protein concentration. After addition of antibody (8 μg of antibody per mg of MNase digest after 10 Gy of X-rays; proportionally adjusted to different conditions), samples were incubated at 4^0C overnight, with rotation. 200 μg of Protein G Dynabeads (Invitrogen) per 1 μg of γH2AX antibody were added and incubated for 1 h. The samples were placed on a magnetic rack and the unbound flow-through was removed. The beads were washed 3 x 5 min at room temperature with IP wash buffer (500mM NaCl, 50 mM Tris-HCl, 1% NP-40, 1% Triton) with gentle shaking. Immunoprecipitated proteins were eluted twice (10 min shaking at room temperature) with 100 ng/μl synthetic phosphopeptide (ATQASphosQEY; synthetized by JPT) dissolved in double distilled water. Eluates were stored at -20^0C.

Step 5:

1. **In-solution Trypsin digestion for analysis of H2AX S139 phosphorylation**

Samples were thawed on ice. 50% of the γH2AX eluate (IP from 0.5 mg of MNase digest) and 5 μg of input sample per condition were adjusted to 10 μl volume and 50 mM ammonium bicarbonate. 0.25 μg of trypsin (Promega) was added per sample and incubated over night at 37°C. On the following day, samples were speedvac concentrated and acidified to 0.1 % TFA final concentration and 20 μl final volume. Samples were stored at -20^0C.

2. **In-solution Histone Derivatization and Trypsin digestion**

Samples were thawed on ice. 50% of the γH2AX eluate (IP from 0.5 mg of MNase digest) and 2 μg of input sample per condition were adjusted to 10 μl

volume and 100 mM TEAB. 1 μl of 1% propionic anhydride in acetonitrile was added to each sample and incubated for 2 min at room temperature. Reaction was quenched with 1 μl of 80 mM hydroxylamine (Sigma) for 20 min. If necessary, pH was adjusted to around 8 and 0.25 μg of trypsin (Promega) was added per sample and incubated over night at 37°C. On the following day, samples were subjected to a second round of derivatisation (as above), speedvac concentrated to 10 μl volume, acidified to 0.1 % TFA final concentration and 20 μl final volume. Samples were stored at -20^{0}C.

2.3.2 Streptavidin pull-down of biotinylated nucleosomes

Step 1: Nuclear isolation, **Step 2: Chromatin extraction** and **Step 3: Analysis of DNA sizes following MNase digestion** were performed as described in **Section 2.3.1.**

Step 4: Streptavidin pull-down of nucleosomes containing biotinylated histone H4.

Biotinylated nucleosomes were pulled-down using streptavidin coupled Dynabeads (Invitrogen). 100 μg of beads were used per 1 mg of MNase extract, incubated on the rotating wheel overnight at 4^{0}C. The beads were washed 3 x 5 min at room temperature with IP wash buffer (500mM NaCl, 50 mM Tris-HCl, 1% NP-40, 1% Triton) with gentle shaking. Precipitated proteins were eluted with 4% SDS buffer for 5 min at 95^{0}C. Eluates were stored at -20^{0}C.

Step 5: In-gel trypsin digestion for analysis of H2AX S139 phosphorylation and associated proteins

Samples were run into resolving 15% SDS-PAGE gel, stained with coomassie and the bands were cut out. Samples were de-stained (50% acetonitrile, 50 mM ammonium bicarbonate) for 3 x 5 min shaking and speedvac dried for 5min; reduced (10 mM DTT, 50 mM ammonium bicarbonate) at 50^{0}C for 45 min and alkylated (50 mM chloroacetamide, 50 mM ammonium bicarbonate) at room

temperature, for 45 min, in the dark. Samples were washed twice (50% acetonitrile, 50 mM ammonium bicarbonate), speedvac dried for 5 min and re-hydrated (12.5 ng/μl trypsin, 50 mM ammonium bicarbonate) for 10 min on ice. Excess trypsin was removed, gels were covered with 50 mM ammonium bicarbonate and incubated over night at 37^0C. Gel pieces dehydrated with 100% acetonitrile, peptides were collected. Samples were speedvac concentrated to remove acetonitrile and re-suspended in 0.1% TFA final concentration

2.3.3 Western Blotting

Samples were boiled in 2x Laemmli buffer (**Table 2.3**) and separated in either homemade SDS-PAGE (5% stacking/15% resolving acrylamide gel) or 4-20% gradient gels (Bio-Rad). Samples were resolved with 150 V in running buffer (**Table 2.3**). Proteins were transferred to nitrocellulose in a pre-chilled wet buffer (**Table 2.3**) for 60 minutes at 400 mA. Membranes were blocked in 5% BSA in 0.2% TBST buffer (20 mM Tris-HCl, 150 mM NaCl and 0.2 (v/v) Tween-20). Primary incubations were carried out at dilutions specified in the section 2.9, in 5% BSA in 0.2% TBST at 4ºC overnight. This was followed by three 10 minutes washes in 0.2% TBST at room temperature and 1 hour incubation in secondary HRP-linked antibody (dilutions in subchapter) and subsequently washed further three times in 0.2% TBST. Proteins were then detected with the chemiluminescent ECL western blotting reagent and exposed onto hyperfilm (Amersham Biosciences/GE Healthcare, Bucks, UK).

2.3.4 Silver staining

Following protein separation with SDS-PAGE as described above, gel membranes were incubated in fixing solution (50% ethanol and 10% acetic acid) for 30 min. Membranes were then hydrated for 15 min in 1:10 dilution of fixing solution (5% ethanol and 1% acetic acid and washed three times in water for 5 min per cycle prior incubation with 200 mg/L solution of sodium thiosulphate for 1 minute. Membranes were then rinsed three times with water and incubated for 20 minutes in the staining solution (2 mg/mL $AgNO_3$, 0.0277% formaldehyde).

After incubation membrane was rinsed in water three times. Finally, the membranes were placed in developing solution (60 mg/mL sodium carbonate, 0.0185% formaldehyde and 4 pg/mL sodium thiosulphate) untill protein bands were visible. The reaction was quenched with 5% acetic acid. Targeted mass spectrometry analysis

2.3.5 Nano-LC/MS

Peptide samples were analysed by nano-LC–MS (ThermoFisher U3000 nanoLC and Orbitrap XL mass spectrometer). Peptides were loaded onto a C18 trapping cartridge (Pepmap100 C18; 0.3 × 5 mm i.d.; 5 µm particle size) for 5 min at a flow-rate of 5 µL/min in 0.1% TFA loading buffer. Peptides were separated on an analytical column (PepMap100; 25 cm × 75 µm; 5 µm particle size) by a gradient from 1 to 45% ACN over 50 min, in the presence of 0.1% FA, at a flow rate of 0.3 µL/min.

Nanospray was from a New Objective emitter with 10 µm tip (FS360-20-10-N-20). Pseudo-SRM was carried out in the linear ion trap of an Orbitrap XL, with a precursor isolation window of 2 *m*/*z*, an ion-trap fill time of maximum 50 ms and an LTQ target ion count of 1E4. A high-resolution precursor scan was carried out in the Orbitrap (5E5 target). Total cycle time was <2 s, enabling at least 10 points across eluting peptide peaks for quantitation.

2.3.6 Pseudo-SRM creation and analysis

Skyline v3.1 (MacCoss Lab, University of Washington) was used for both development of pseudo-SRM methods and for data analysis. Peptide sequences for proteins of interest were obtained from Uniprot and entered into Skyline. Predicted b and y ions were surveyed on the instrument. To distinguish between different isobaric masses at least three transitions were selected that were unique to each peptide. Integration boundaries for all the peaks were inspected manually and edited if necessary to fully integrate the peak. At least two peak widths of elution time (one on either side of the peak) outside the peak were allowed to understand the surrounding noise and potential interference. Due to change in the retention times during MS runs, occasionally the

quantitative peak area would be reduced, in which case, these peaks would be removed from further quantitation. **Appendix Table 1** contains the list of targeted peptides, their m/z and transitions used for quantification.

2.3.7 Statistical analysis

LC-pseudoSRM raw mass spectra were imported to and processed using Skyline v.3.1. Statistical bioinformatics analysis was performed with Microsoft Excel 2013 and GraphPad Prism v.7.04 computing software. Relative abundance of each targeted peptide at a given time-point was calculated. For each peptide in a group, all transitions were summarized and the proportion of that peptide relative to all differentially modified peptides in the group was calculated and expressed as percentage value. All p-values are from two-tailed, paired t-tests. Error bars represent the standard error of the mean, unless indicated differently.

2.3.8 Data dependent acquisition and sample analysis

Database search was performed using Mascot Ver.2.3.2. Data were searched against the human Swiss-Prot database. Peptides were matched using trypsin as digestion enzyme. Peptide mass tolerance was set to 5 ppm and fragment mass tolerance was set to 0.5 Da. A maximum of two missed cleavages was allowed. Carbamidomethylation of cysteines was set as fixed modification. Oxidation of methionine, mono-, di- and trimethylation of lysine, as well as acetylation and Gly-Gly lysine were set as variable modifications.

2.4 FLUORESCENCE-ACTIVATED CELL SORTING (FACS) ANALYSIS OF CELL CYCLE STAGES

For cell cycle analysis, cells were fixed with cold ethanol 70%, washed with PBS and re-suspended in PBS containing propidium iodide (PI, Sigma, 5 ug/ml) and RNAse A (Sigma, 50 ug/ml) overnight at 4 °C. Samples were run on a FACS-accuri (Beckton Dickinson) and data analysed with the BD accuri software. Briefly, single cells were gated, first on their size (FLH) and their granularity (SSC) to exclude debris, and then on the linearity between FLH-H

and FLH-A signal to exclude doublets. PI signal (correlating with DNA content) was read on the FL2 detector.

2.5 IMMUNO-FLUORESCENCE (IF)

The cells were grown on 96-well plates (Corning CoStar) and treated as indicated. They were fixed with 4% formaldehyde for 15 min, permeabilised with 0.3% Triton for 10 min, washed with PBS, incubated with primary antibodies for 1h, washed 3 times with PBS (5 min), incubated with secondary antibodies for 30 min and washed twice in PBS (5 min), then incubated in DAPI (1:20,000) for 7 min and replaced with PBS. Images were acquired with the ScanR system (Olympus).

2.6 ANTIBODIES

The antibodies and their dilutions employed in this study are listed in **Table 2.4**. For IF antibodies were diluted in 1% BSA in PBS, while for IB they were diluted in 5% milk, or in the case of streptavidin, in 5% BSA.

Antibody	Specie and clone specificity	Product code	Manufacturer	IF dilution	WB dilution
γH2AX	mouse monoclonal	JBW301	Millipore	1:1000	1:500
53BP1	rabbit polyclonal	H300-272A	Bethyl	1:1000	NA
FLAG (clone M2)	mouse monoclonal	F3165	Sigma	1:500	1:1000
polyHis (clone HIS-1)	mouse monoclonal	H1029	Sigma	1:1000	1:3000
Histone H3	rabbit polyclonal	ab8898	Abcam	1:1000	1:1000
Histone H4	rabbit polyclonal	ab10158	Abcam	NA	1:1000
H3K9me3	rabbit polyclonal	07-442	Millipore	NA	1:1000
α-Tubulin	rat monoclonal	ab6160	Abcam	NA	1:5000
ATM S1981phos	rabbit monoclonal	ab81292	Abcam	NA	1:1000
p53 S15phos	rabbit polyclonal	9284	Cell Signalling Technologies		1:1000
anti-mouse HRP IgG	goat	7076S	Cell Signalling Technologies	NA	1:10000
anti-rabbit HRP IgG	goat	7074S	Cell Signalling Technologies	NA	1:10000
anti-rat-HRP	goat	ab97057	Abcam	NA	1:10000
Biotin detection					
Streptavidin-AlexaFluor568	NA	S11226	Invitrogen	NA	1:500
Streptavidin-HRP	NA	RPN1231	GE Healthcare	1:3000	NA

Table 2.4 Table of antibodies used in this thesis. NA = not available

3 CHAPTER THREE: DEVELOPMENT OF A NOVEL MASS SPECTROMETRY METHOD FOR QUANTIFICATION OF HISTONE POST-TRANSLATIONAL MODIFICATION AT THE SITES OF DNA DSBS

3.1 INTRODUCTION

In recent years several histone post-translational modifications (PTMs) have been shown to play an important role in regulating the DDR and repair processes in eukaryotic cells. Numerous histone PTMs have been reported to change, either increasing or decreasing, at the sites of DNA DSBs. Furthermore, several histone modifiers have been shown to be recruited to the sites of DNA DSBs, but for many of them their exact role in the process of repair still remains obscure.

In order to understand the mechanism underlying the chromatin response to DNA damage and how failure in this process can lead to disease states, it is crucial to identify the spatio-temporal landscape of histone PTMs and histone turnover that is associated with the repair of the break. Methods traditionally adapted to study histone PTMs involve use of techniques, such as immuno-fluorescence and chromatin immuno-precipitation. These techniques rely on the use of antibodies specifically raised to given modifications. Although these are very powerful methods, the downside is that they require knowledge of the modification of interest in advance. Moreover, some antibodies can have poor specificity resulting from cross-reactivity with similar modifications set in the same sequence context (Bock *et al.*, 2014). Due to the nature of histones being heavily post-translationally modified, there is also the risk that specific modifications may not be detected as a result of epitope occlusion by the neighboring mark (Cheung, 2004).

Recently, mass spectrometry (MS) based proteomics has emerged as a powerful tool to study protein PTMs. This method enables the discovery of novel histone modifications, as well as the sensitive detection and quantification of low abundance marks. We have developed a targeted mass spectrometry approach to quantify histone PTMs on the nucleosomes containing γH2AX. This MS approach allows simultaneous quantification of numerous PTMs, including those for which specific antibodies are not available (e.g. H2AK15 ubiquitination). In this study, we enrich chromatin close to DSBs using γH2AX antibody, enabling sensitive detection of local changes in histone PTMs.

3.2 AIMS OF THIS CHAPTER

To quantify dynamic changes in histone PTMs at the nucleosomes local to DSBs, I aimed to develop a mass spectrometry-based method for enrichment, detection and quantification of these marks. To achieve this, we designed and optimised chromatin immuno-precipitation of mono-nucleosomes containing histone γH2AX, followed by targeted mass spectrometry (γH2AX-ChIP/MS). This chapter describes the development and validation of a novel method for the enrichment and quantification of histone marks associated with DNA DSBs.

3.3 EXPERIMENTAL DESIGN

To sensitively detect and quantify histone PTMs associated with DNA DSBs, a γH2AX-ChIP/MS method was designed. Briefly, cells were damaged IR and collected after the indicated recovery times (**Fig.3.1 A**). To enrich for nuclear proteins, the nuclei were isolated and chromatin solubilised using MNase treatment to yield mainly a mono-nucleosomal preparation (**Fig.3.1 B**). Nucleosomes from the sites of DNA damage were then recovered by γH2AX chromatin immuno-precipitation (**Fig.3.1 C**).

Since histone proteins are very rich in lysine and arginine residues, simple trypsin digestion would result in the production of multiple peptides too small to be retained on the chromatography column. To overcome this issue, γH2AX precipitates, as well as the starting material, were derivatized with propionic anhydride in two rounds, separated by a trypsin digestion step (**Fig.3.1 D**). The first round of derivatization served to propionylate unmodified and mono-methylated lysine residues, which consequently resulted in an Arg-C-like digestion by trypsin. The second round served to propionylate the N-termini of the peptides, for improved chromatographic retention of hydrophilic peptides. Since all of the lysine residues are thus blocked either by endogenous modifications or an added propionyl group, this approach generates a highly reproducible set of peptides of equal length. Furthermore, propionylation of the lysine residues and N-termini of the peptides neutralises their charge, leading to

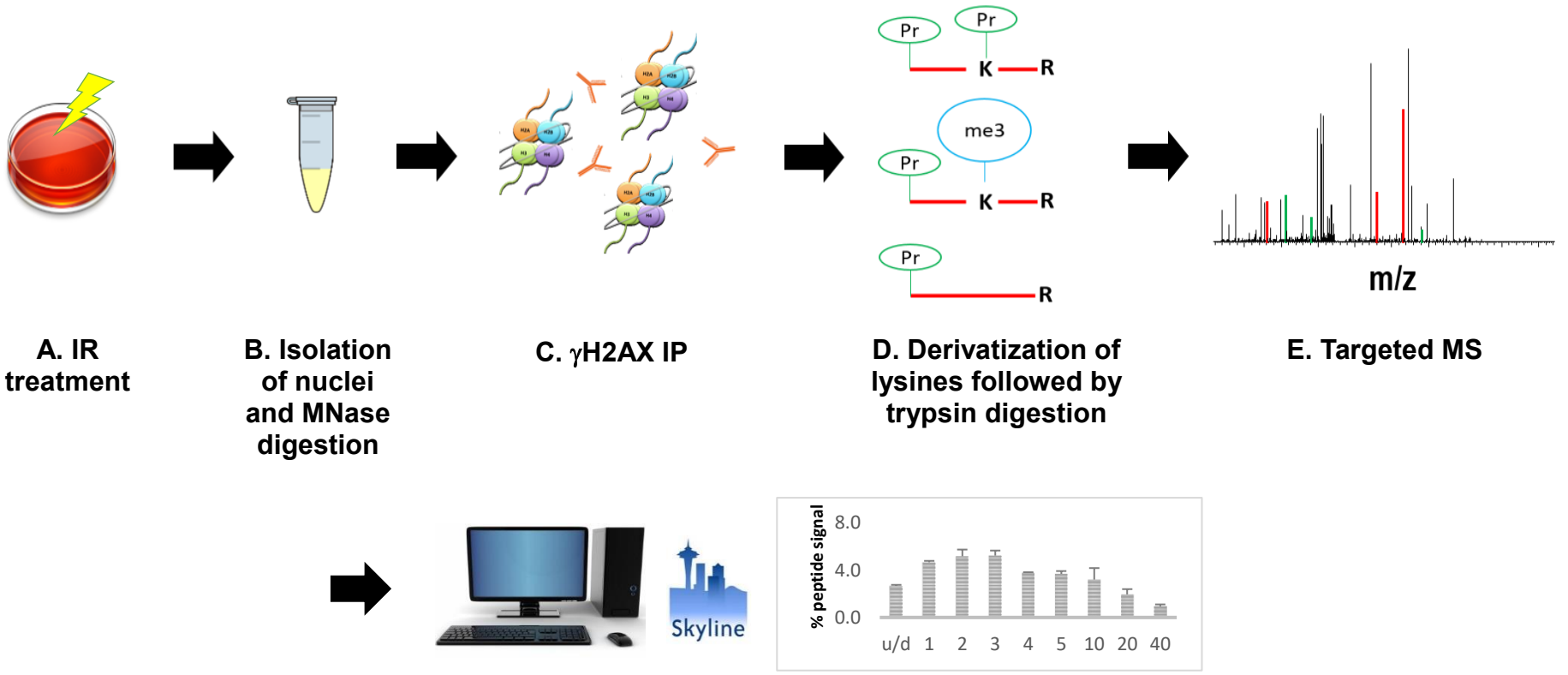

Figure 3.1 Schematic workflow of the experimental approach to study histone PTMs associated with the sites of DNA damage.

a decrease in their hydrophilicity and consequent improved retention on the nanoLC column (Garcia *et al.*, 2007b).

The samples prepared in this way were then analysed with LC-MS/MS using a pseudo-SRM approach (**Fig.3.1 E**). The resulting data was then analysed using Skyline software (**Fig.3.1 F**). The relative abundance of a modified peptide was obtained by integrating the area under the specific peak and division by the total area of all modified and unmodified forms.

3.4 VALIDATION OF THE γH2AX-CHIP/MS APPROACH

3.4.1 Micrococcal Nuclease treatment for mono-nucleosomal preparation of the chromatin

Previously, our laboratory conducted a mass spectrometry analysis and quantification of the levels of histone H2A variants in three different cell lines (U2OS, HeLa and LCL), showing that H2AX constitutes between 2 and 5% of the thirteen H2A family members quantified (Hatimy *et al.*, 2015b). Each nucleosome contains two H2A histones. Assuming a random distribution, this would suggest that on average only one in ten to twenty five nucleosomes would contain the H2AX variant. Therefore, in order to be able to maximise the ability of the γH2AX antibody to specifically enrich for γH2AX-containing nucleosomes, the chromatin must be extensively digested using micrococcal nuclease, which is known to digest DNA between nucleosomes, to yield a predominantly mono-nucleosomal preparation.

To develop a method for the production of a mono-nucleosomal preparation, I have determined the time that is required for complete digestion of inter-nucleosomal DNA. This revealed that after 9-12 minutes of MNase treatment most of the DNA fragments were between 100-200 base pairs, which is consistent with a mainly mono-nucleosomal preparation (**Fig. 3.2 A**). Longer treatment resulted in complete digestion of the nucleosomal DNA

A.

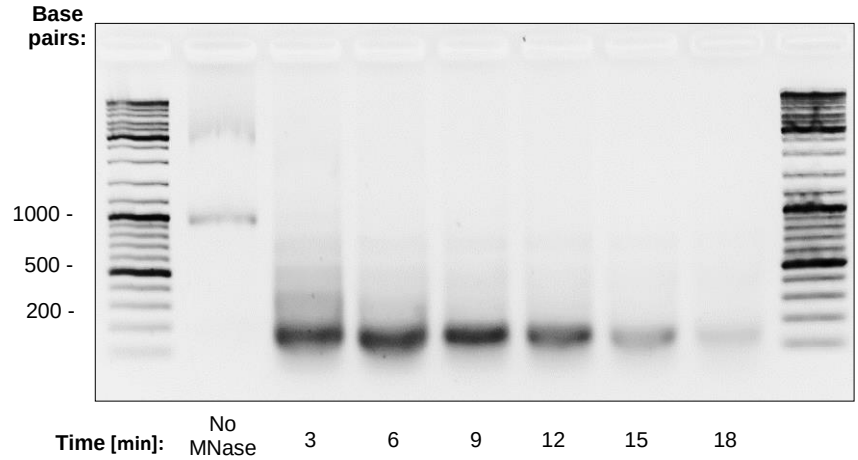
Base pairs:
1000 -
500 -
200 -
Time [min]:
No MNase
3
6
9
12
15
18

B.

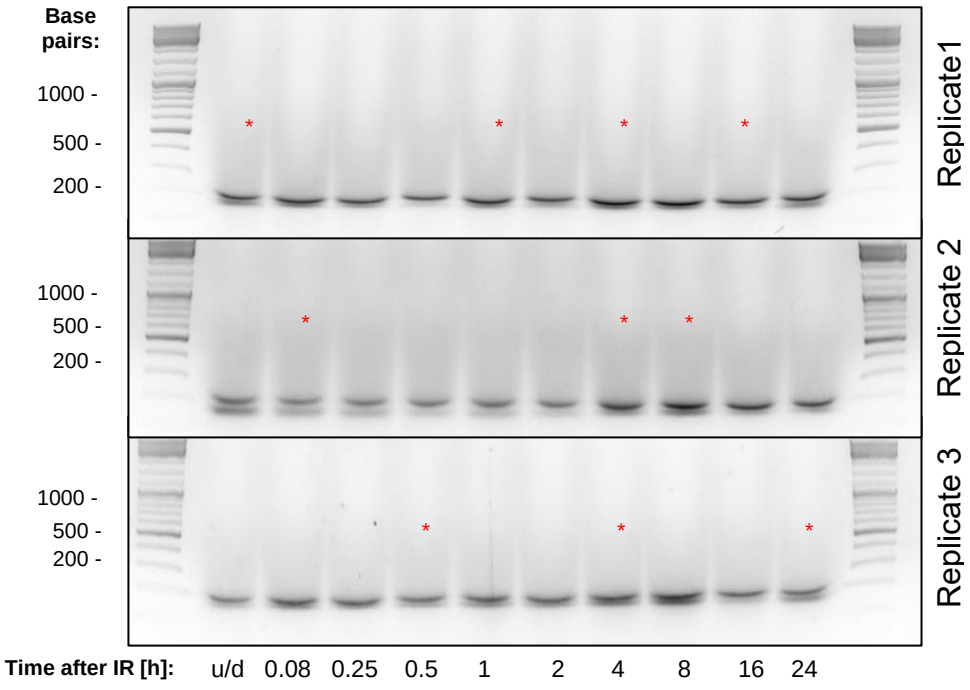
Base pairs:
1000 -
500 -
200 -
Replicate1
Replicate 2
Replicate 3
Time after IR [h]:
u/d
0.08
0.25
0.5
1
2
4
8
16
24

C.

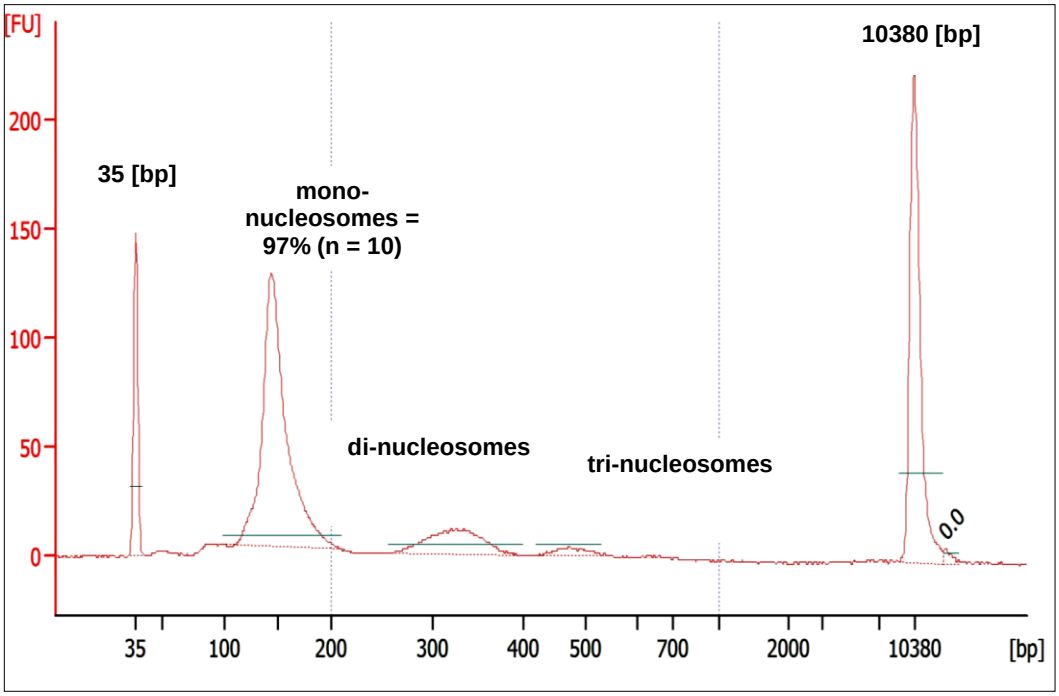
[FU]
200
150
100
50
0
35 [bp]
mono-
nucleosomes =
97% (n = 10)
di-nucleosomes
tri-nucleosomes
10380 [bp]
0.0
35
100
200
300
400
500
700
2000
10380
[bp]

D.

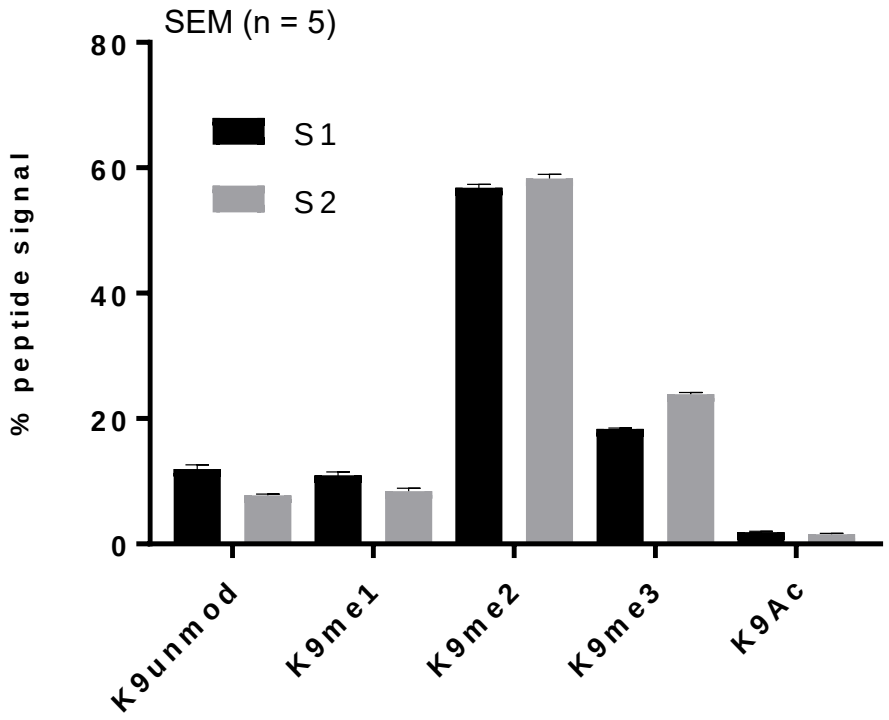
SEM (n = 5)
S1
S2
% peptide signal
80
60
40
20
0
K9unmod
K9me1
K9me2
K9me3
K9Ac

Figure 3.2 MNase treatment for extraction of mono-nucleosomes. A) MNase treatment time course. Nuclei of HEK293 cells were isolated and treated with MNase for the indicated times. Extracted DNA was run on a 1.5% agarose gel and visualised with ethidium bromide. B) HEK293 cells were treated with 3 Gy x-rays and collected at the indicated time-points. Nuclei were isolated and the chromatin was extracted following 10 minutes of MNase treatment. The extent of digestion was verified by DNA gel electrophoresis (B) and Bioanalyzer analysis (C). Red stars indicate samples that were randomly selected for Bioanalyzer analysis. C) A representative Bioanylazer trace. Lower and upper markers peak at 35 bp and 10380 bp, respectively. FU = fluorescence units. D) MS analysis and quantification of histone H3 K9 modifications. MNase extracted (S1) and remaining pellet (S2) samples were run into SDS gel and prepared as in Methods section. H3 K9 modifications were quantified relative to each other. Error bars represent standard error of the mean from 5 biological replicates.

To follow this, HEK293 cells were treated with 3 Gy of X-rays and collected at the indicated time-points (**Fig. 3.2 B**). The mono-nucleosomes were extracted using a 10 minute MNase treatment. The extent of DNA digestion was confirmed by agarose gel analysis (**Fig. 3.2 B**). Since some smearing suggestive of higher DNA molecular sizes was observed, a selection of randomly picked samples was further analysed (**Fig. 3.2 B** – denoted with red stars) using a Bioanalyzer microfluidic capillary separation spectrophotometer (**Fig. 3.2 C**). This was done to precisely quantify the average size of DNA fragments. It was calculated that MNase extracts consisted on average of 97% mono-nucleosomes (Appendix Table 2).

In addition, I tested whether MNase digestion showed any bias towards specific types of chromatin. To this end, we quantified epigenetic marks on histone H3 lysine9 (H3K9). H3 K9 di- and trimethylated are known markers of heterochromatin, while unmodified, monomethylated and acetylated versions are known to be present in more open and transcriptionally active chromatin (euchromatin) (Rea *et al.*, 2000; Nakayama, 2001; Barski *et al.*, 2007). This analysis confirmed that MNase digests both types of chromatin (**Fig. 3.2 D**).

3.4.2 Antibody titration

The specificity of the antibody used for the immunoprecipitation of γH2AX-containing nucleosomes was tested. Firstly, titration of the antibody was performed to determine the amount required to achieve complete depletion of γH2AX (**Fig. 3.3 A**). To this end, a range of antibody concentrations linearly increasing from 1-8 μg per mg of MNase extract were tested. This showed that between 4 and 8 μg/mg of antibody was sufficient to deplete the majority of γH2AX in HEK293 cells exposed to 10 Gy X-rays. Furthermore, increasing amounts of histone H4 were co-immunoprecipitated in a manner dependent upon the amount of γH2AX. Moreover, γH2AX-IP in a λ-phosphatase treated sample was also performed. λ-phosphatase treatment led to removal of the

majority of the histone H2AX S139 phospho-group, which consistently resulted in a low level of co-immunoprecipitated histone H4 (**Fig.3.3 A**). Collectively, these experiments suggested that co-immunoprecipitation of H4 using γH2AX antibody, depends predominantly on the presence of γH2AX.

3.4.3 Phospho-peptide elution

Immuno-precipitated samples are commonly eluted from the beads with SDS-containing buffer, which is incompatible with mass-spectrometry analysis. Therefore, prior to mass spectrometry the samples are cleaned-up by electrophoresis through a SDS-PAGE gel to remove detergent. However, the extraction of the protein sample from the gel often leads to significant loss of the material. This is an even greater problem when attempting to immuno-precipitate low abundance proteins, and consequently requires cell culture experiments to be conducted on a large scale, which is laborious and expensive. Furthermore, SDS-buffer also elutes the antibody chains, as well as other non-specific factors that bind to the isolation matrix, which may also interfere with the mass spectrometry analysis. Therefore, to avoid the above, elution by competition was tested. To do that, we designed and purchased a synthetic peptide containing phosphorylated H2AX S139 and its surrounding amino acid residues (ATQA(pS)QEY, Peptide Protein Research Ltd.). This proved to be as effective in elution of γH2AX as SDS buffer (**Fig. 3.3 B**), while avoiding the problem of contamination by antibody chains (**Fig. 3.3 C**). In addition, since there is no requirement for detergent removal via gel electrophoresis clean-up, this method leads to enhanced recovery of protein, as well as increased specificity, since only direct antibody binding proteins are eluted.

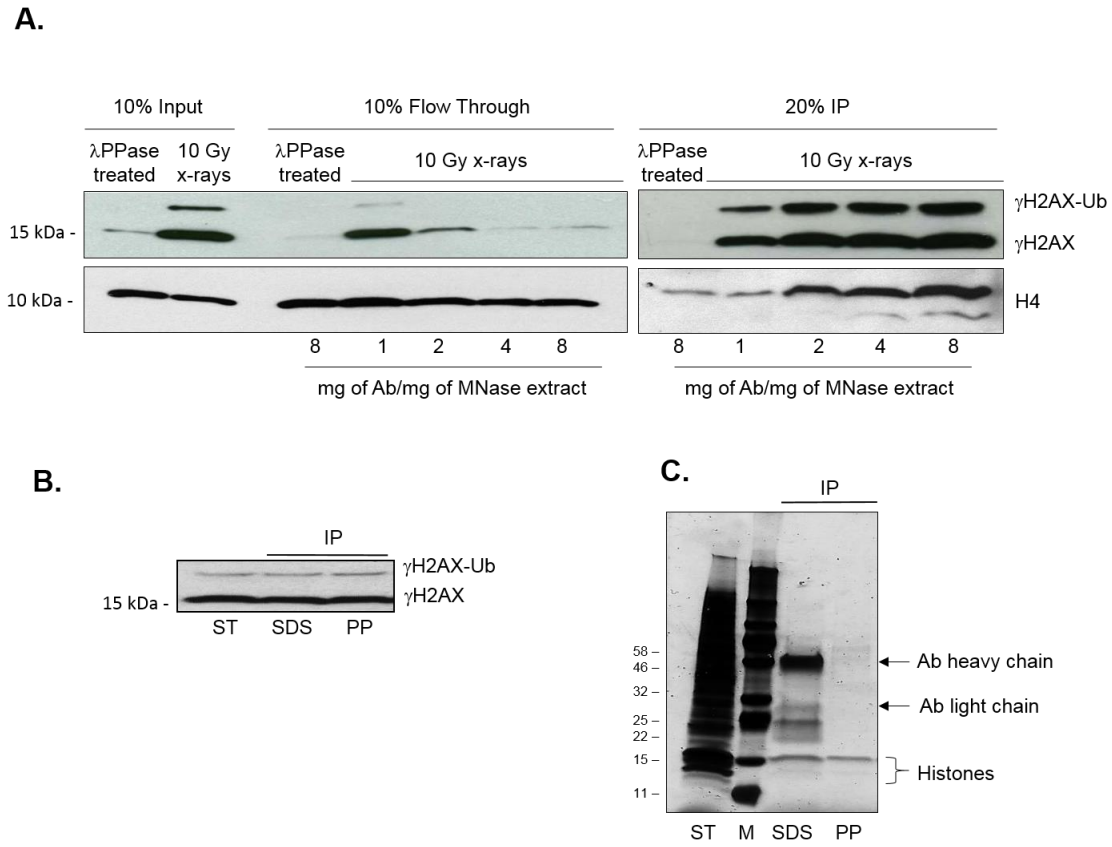

Figure 3.3 Optimisation of γH2AX IP. A) Antibody titration. HEK293 cells were treated either with 10 Gy x-rays to induce H2AX S139 phosphorylation or λPPase to remove phosphate group from proteins. Increasing amount of antibody was added to 200 µg of MNase extracts at the concentrations indicated on the figure. 10% of the input and flow through, and 20% of IP were loaded on the 15% SDS-PAGE gel. Input and Flow Through, and IP blots were acquired at different exposure times for both antibodies. B and C) Phospho-peptide elution. HEK293 cells were damaged with 10 Gy X-rays. γH2AX IP was performed and the immuno-precipitates were eluted with 4% SDS buffer (SDS) or increasing concentrations of phospho-peptide (PP) (ATQA(pS)QEY). 5% of input and 8% of IP samples were run on 4-20% of SDS-PAGE gel and probed for γH2AX (B) or silver stained (C). IP = immunoprecipitate; ST = input; M = protein marker; PP = phosphopeptide;

3.4.4 Recovery of nucleosomes from the site of DNA damage

Using an approach previously developed in our laboratory (Hatimy *et al.*, 2015b), we quantified the abundance of H2AX relative to other H2A variants in the IP and input samples, comparing the H2AX-specific peptide GKTGGKAR with the major form of this peptide, GKQGGKAR, (present in 11 H2A variants) and GKQGGKVR (present in H2AJ) (**Figure 3.4**).

Next, the ability to recover nucleosomes from the sites of DNA damage using this approach was tested. To achieve this, I first confirmed that IR treatment was able to prompt phosphorylation of histone H2AX. As expected, induction of γH2AX was observed as quickly as 5 min following treatment with 3 Gy X-rays and returned close to its background levels by 24 hours (**Fig. 3.5 A**).

We observed that in HEK293 cells, of all H2A variants measured, H2AX on average represents 4% of the total, while in the γH2AX -IP samples around 50-60% of total H2A was H2AX (**Figure 3.5 B**). Although we were able to detect the GKQGGKVR peptide, we removed it from further quantification due to its low abundance (< 0.5% - data not shown). Since the MNase digestion yields mainly mono-nucleosomes, this result suggests that the majority of histone H2AX is deposited in nucleosomes asymmetrically, being associated with another H2A variant.

Moreover, I was able to detect and quantify the ratio of phosphorylated H2AX S139 to unmodified H2AX S139 in both IP and input samples. This showed that on average more than 80% of histone H2AX is phosphorylated on S139 (**Fig. 3.4 C and D**). Collectively, this analysis shows that nucleosomes containing a well-known marker of DNA damage are recovered using this approach.

Human H2As

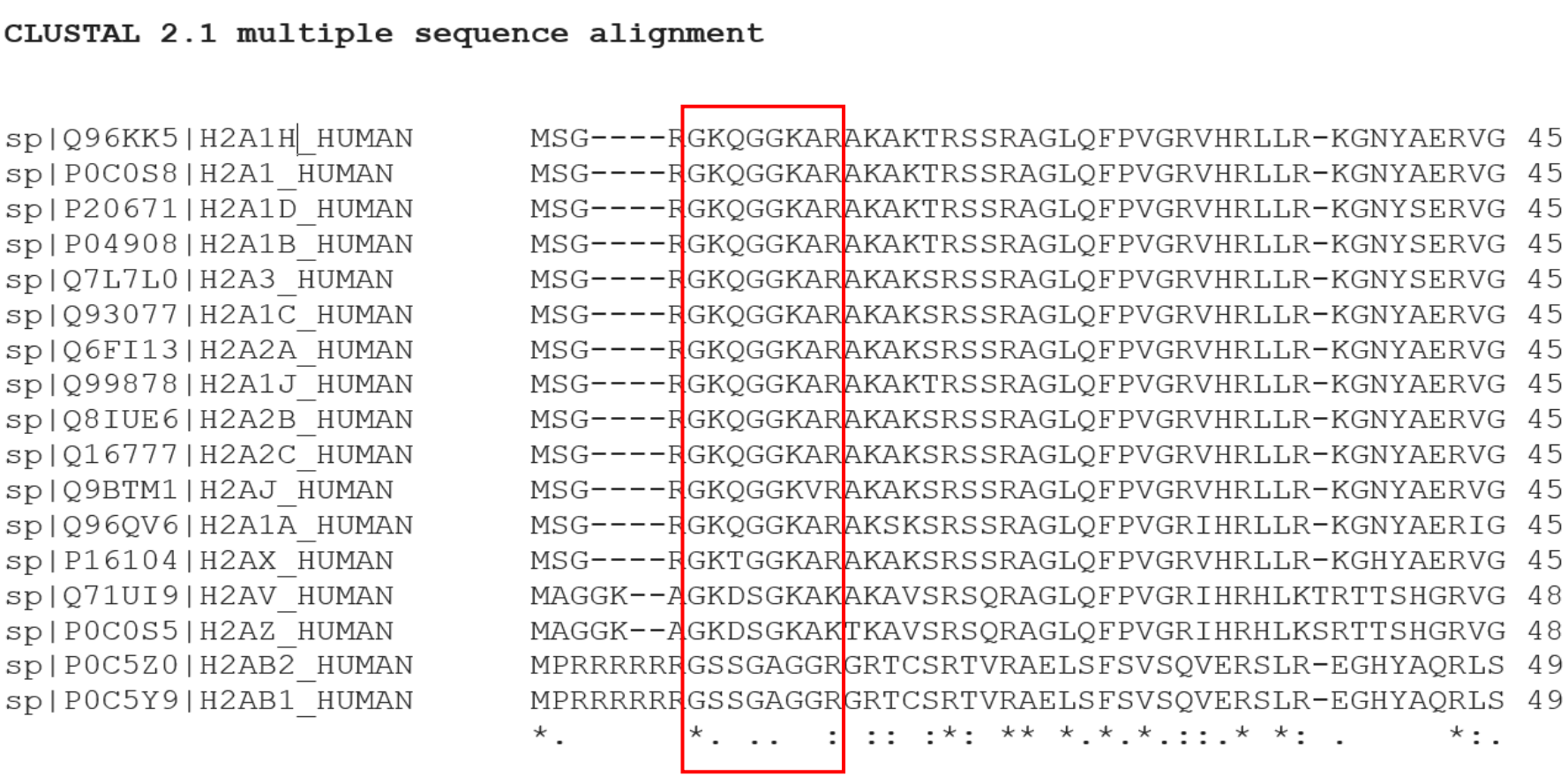

Figure 3.4 Sequence alignment of the N-terminal portion of histone H2A variants using Clustal programme. H2A peptide containing amino acids [5-12] is unique in H2AX.

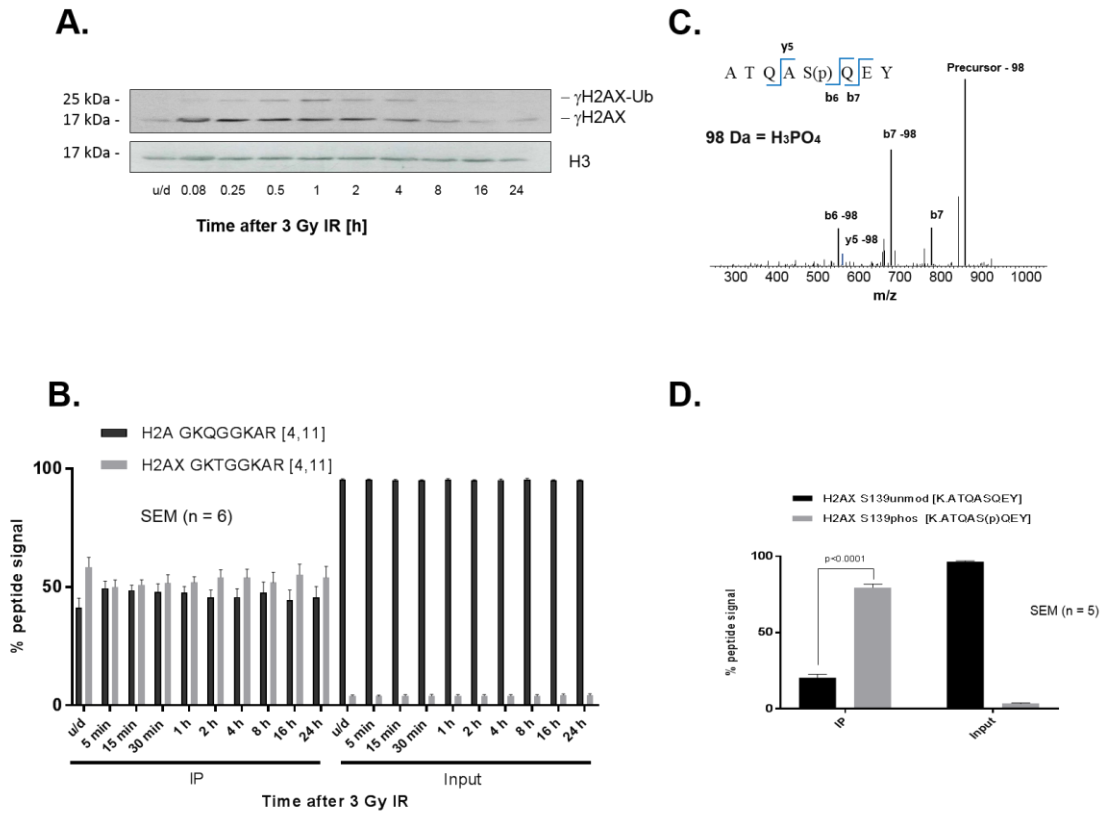

Figure 3.5 Recovery of nucleosomes from the sites of DNA damage. A) Western blot analysis of the time-dependent DNA damage induction in HEK293 cells following treatment with 3 Gy of X-rays. To monitor DNA damage response, γH2AX marker was used; upper band represents mono-ubiquitinated histone γH2AX (γH2AX-Ub). B) Quantification of the abundance of histone H2A variants in the input and γH2AX IP samples. Error bars represent three biological replicates. C) MS/MS fragmentation of singly charged ATQASQEY S139phos precursor. D) Quantification of the ratio of phosphorylated to unphosphorylated H2AX S139. Error bars represent the average of six independent replicates.

3.5 SELECTION AND OPTIMISATION OF PSEUDO-SRM PARAMETERS OF TARGETED PEPTIDES

Targeted proteomics assays are characterised and assessed based on several performance metrics and features. These include peptide stability over time, reproducibility, limit of detection (LOD) and limit of quantification.

3.5.1 Stability

Stability was assessed based on the ability to detect a given peptide over time. During the initial MS runs, we observed significant time- and concentration-dependent effects on the detection of some of the more hydrophobic, late eluting peptides (**Fig. 3.6** – top panel). Since adsorption of the peptides to the solid surfaces is an acknowledged concern in quantitative proteomics (Hoofnagle *et al.*, 2016), we considered that this issue may also be an underling problem responsible for run-to-run variation that we consistently observed. To overcome this problem, previous reports suggested that addition of carrier proteins, detergents (Lawless, Hopkins and Anwer, 1998; Song *et al.*, 2002) or organic solvent (Stejskal, Potěšil and Zdráhal, 2013) to the samples could serve to minimise peptide loss. Furthermore, it was reported that the loss of peptide intensity by adsorption to the vial is more extensive for low-concentration samples due to limited binding capacity of the wetted solid surface area (John *et al.*, 2004). Indeed, we found that increasing the concentration of the samples in combination with 24 hours pre-run incubation in the auto-sampler at $4^{O}C$ significantly improved the recovery of troublesome peptides, yielding more reproducible results (**Fig. 3.6** – bottom panel).

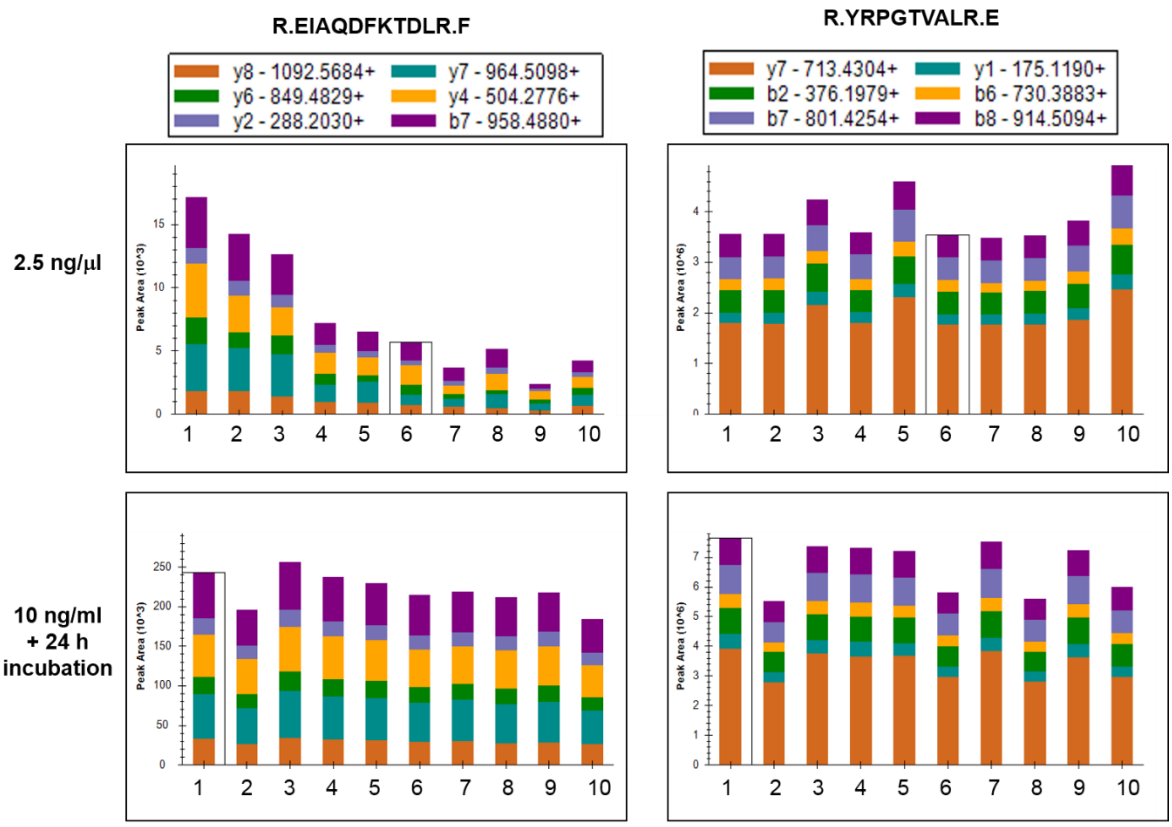

Figure 3.6 The effect of the sample concentration on peptide quantification. A single MNase extracted chromatin sample was diluted to a final concentration of 2.5 or 10 ng/µl. The 10 ng/µl sample was also incubated for 24h in the auto sampler pre-run. Each concentration was aliquoted into 10 vials and injected on the chromatography column at equal volumes. Figure was extracted from Skyline and shows calculated peak area for concentration of affected H3 K79me1 peptide (R.EIAQDFKTDLR.F) and unaffected H4 peptide (R.YRPGTVALR.E).

3.5.2 Reproducibility

Reproducibility refers to the observed run-to-run variation in quantification associated with a specific peptide. To measure that, digested input samples were diluted to a final concentration of 10 ng/μl, while γH2AX IP samples were diluted to 1% of IP sample/μl. These were then incubated in the auto-sampler at $4^{O}C$ for 24 hours to reduce the time-dependent effect on the peptide quantification. Each sample was then analysed in 20 technical replicates and the coefficient of variation (%CV, the standard of deviation divided by the mean) was calculated for each peptide (19 replicates for IP samples, since one had to be discarded due to a technical issue). CV calculations allow estimates of the level of change we would have detected (above assay noise) (**Appendix Table 2**).

The %CV for the majority of the peptides fell between 0.1-15%. As the H3 K79me1 peptide was highly irreproducible (CV >69%), it was discarded from further analysis. The signal to noise ratio for H3 K9acK14un peptide was very low (below the limit of detection).

3.5.3 Peptide linear dynamic range

The linear dynamic range, the lower limits of detection and upper limit of quantification for the assayed peptides were determined. Since we expected that there may be differences in the complexity of the matrix between the input and IP samples, a response curve was generated for both, the input (linearly increasing from 0.8 – 100 ng) and IP (linearly increasing from 0.1 – 12.5 % of IP) samples. The R^2 and slope for each targeted peptide was determined and is indicated on the graph **Fig. 3.7** (full data is available in **Appendix Figure 1**).

A.

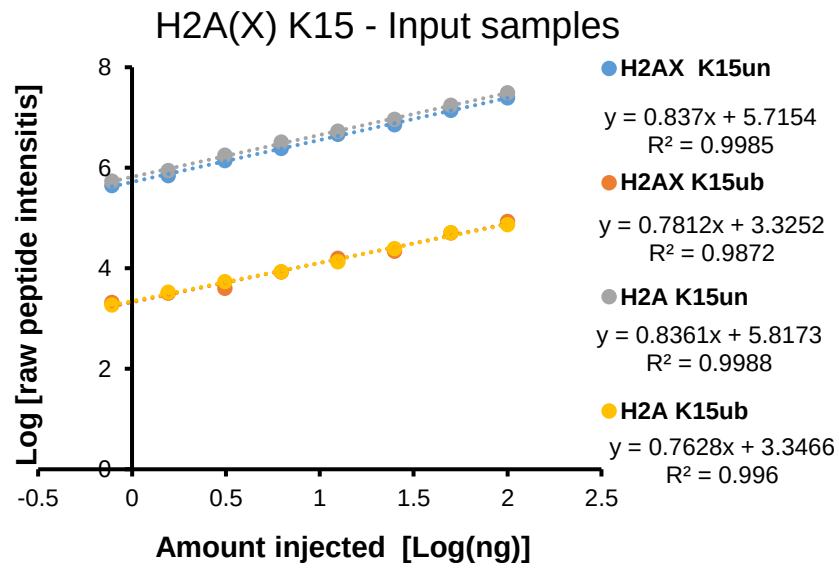

B.

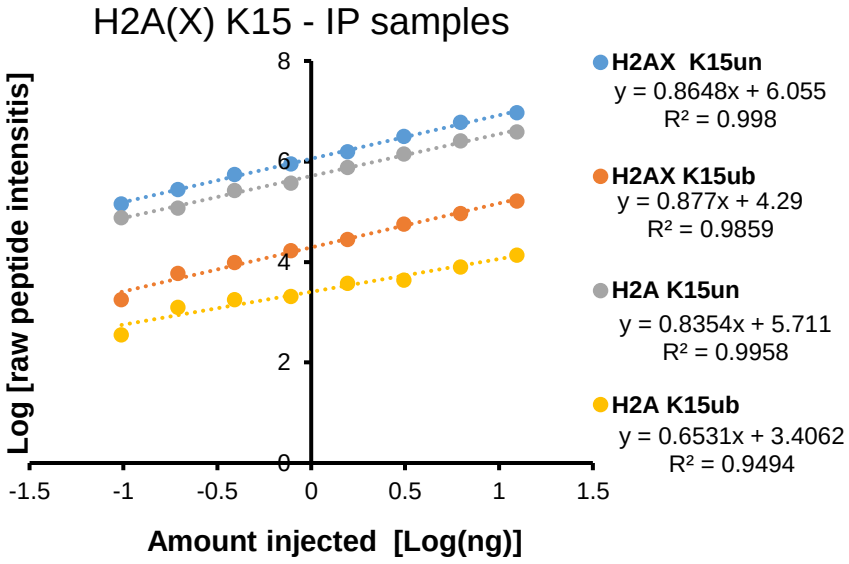

Figure 3.7 Example of peptide response curve. A) The input samples linearly increasing from 0.8 – 100 ng and B) IP samples linearly increasing from 0.1 – 12.5 % of IP samples were injected into chromatography column and analysed by mass spectrometry. The raw intensities for each peptide were plotted on the double-Log10 scale. R^2 and slope of the linear trendline for each peptide was displayed on the graph.

The response curve allowed us to determine the lowest amount of sample required for confident detection of all of the desired peptides (i.e. the signal was distinct from the noise). Based on that we observed that the majority of the peptides could be detected even at the lowest injection amounts used, however, to be able to detect and quantify all of the desired peptides in a single run, the lowest possible loading would be around 20 ng for input sample and 3% of IP (based on IP from starting amount of 0.5 mg of MNase extract after 3 Gy of IR).

Furthermore, the upper limit of quantification for this study was determined. It has been observed that the majority of the targeted peptides displayed linearity across all tested concentrations. However, for a small subset of peptides the signal intensity departed from linearity at 60 ng of injection (**Fig. 3.8**). Consequently, in future experiments we allowed some space for the error and injected 35 ng of input and 5% of IP sample per run.

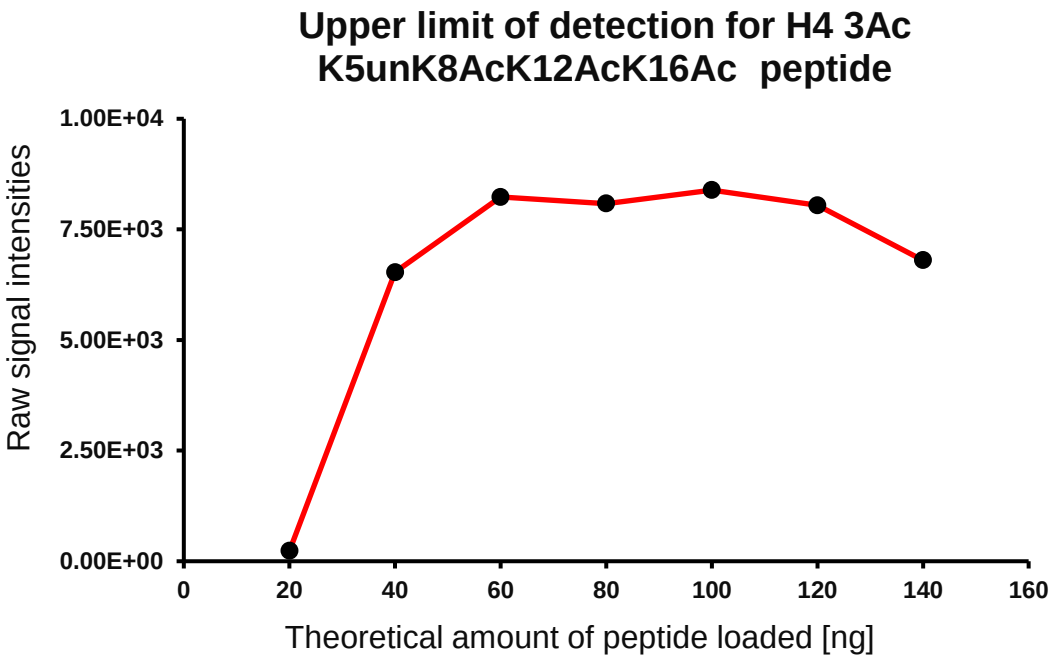

Figure 3.8 Measurement of upper limit of quantification. H4 3Ac K5unK8AcK12AcK16Ac peptide becomes saturated at higher concentrations of input sample (>60 ng).

3.6 DISCUSSION

Here I have presented the development and optimisation of a novel γH2AX-ChIP/MS approach for investigation of post-translational modifications on nucleosomes associated with histone H2AX phosphorylated on S139, a known marker for DNA damage.

To this end, I have shown that this method enables the specific enrichment of γH2AX-containing nucleosomes, as evidenced by the fact that at least 50% of the histone H2A forms in the γH2AX-IP sample is H2AX (**Fig. 3.5 B**). If one assumes a random distribution of histone H2AX throughout the genome, this result is expected since MNase extraction of chromatin used as a starting material for this IP predominantly consists of mono-nucleosomes (**Fig. 3.2 A-C**). In addition to that, at least 80% of H2AX in the IP samples is phosphorylated on S139 (**Fig. 3.5 C** and **D**), further confirming the specificity of the γH2AX antibody used in this study.

Additionally, I have demonstrated that competitive elution of the γH2AX-precipitate with the antigen-phosphopeptide used for production of this antibody, improves the stringency of this protocol. I have shown that phosphopeptide elution is as effective as SDS at recovering γH2AX (F**ig. 3.3 B**), while avoiding contamination with antibody chains (**Fig. 3.3 C**). Another advantage of this method of elution is the avoidance of the gel clean-up stage, which is a cause of significant loss of material.

With the use of the targeted mass spectrometry method we were able to detect over 60 histone peptides in a single MS run. These included histone variants and differentially modified histone peptides. The ideal conditions for stability of majority of the peptides were determined and the coefficient of variation was measured for each peptide in the input and IP matrices (**Fig. 3.6**., **Appendix Figure 1 and Appendix Table 3**). Moreover, the lower limit of detection, as well as upper limit of quantification have been measured for each peptide and based on that ideal loading, the amounts for input and IP samples were determined.

In a typical SRM experiment where one tries to measure the abundance of the protein, usually only a few of the best behaving peptides are measured (i.e. peptides with good stability, low %CV and large dynamic range). Since we are measuring specific PTM-containing peptides, we do not have the luxury of choosing the best behaving peptides. This leads to decreased sensitivity of the assay, specifically in the case of the peptides with larger %CV. Therefore; in other words, we cannot exclude the possibility that there may be some changes in peptide abundance that we were not able to detect.

In conclusion, I have validated and optimised a novel high throughput and multiplex method for detection and quantification of histone post-translational modifications and histone variants associated with DNA damage. Subsequently, this method was used to measure both temporal and IR dose-associated chromatin changes (Chapter 4). Furthermore, I have used this method to investigate the chromatin context associated with late repairing breaks in ATM-inhibited cells (Chapter 5).

4 CHAPTER FOUR: QUANTIFICATION OF HISTONE POST-TRANSLATIONAL MODIFICATIONS ASSOCIATED WITH DNA DSBs

4.1 INTRODUCTION

Phosphorylation of H2AX on serine 139 is the most commonly used marker of DNA DSBs (see introduction for more details). This modification has been shown to spread up to 1 Mbp away from the site of damage (Rogakou *et al.*, 1998a, 1999b; Savic *et al.*, 2009b; Iacovoni *et al.*, 2010b). It has been proposed that chromatin presents a barrier to repair of DSBs, and in the past years there have been multiple studies reporting DNA damage induced changes in histone acetylation, ubiquitination and methylation (see Introduction and **Table 1.1**).

In the previous chapter, I have presented a method for enrichment of nucleosomes containing γH2AX. Here I combined this method with a pulse-chase strategy to quantify co-occurring histone modifications. Furthermore, I have used an IR-dose response approach to look for factors that might become limiting at high doses.

4.2 H2A(X) K15 UBIQUITINATION MARKS NUCLEOSOMES SURROUNDING DNA DSBS

4.2.1 Assay design for detection of H2A(X) K15 ubiquitination

Dynamic spatiotemporal alterations in chromatin modifications local to DSBs have been reported to play a crucial role in the regulation of the cellular response associated with a repair process. As mentioned in the introduction, previous studies suggest a crucial role for RNF168 induced ubiquitination in the repair of DSBs. Due to lack of a specific assay to directly detect damage-induced H2A(X) K15 ubiquitination, this modification has not previously been quantified and more indirect approaches have been used to investigate its role in response to genotoxic stress. These included mutational studies and

the use of the FK2 antibody, which is known to detect DSB induced ubiquitin foci (Huen *et al.*, 2007; Doil *et al.*, 2009b; Gatti *et al.*, 2012; Mattiroli, Vissers, *et al.*, 2012; Fradet-Turcotte *et al.*, 2013).

The N-terminal portion of H2A containing the K13/15 ubiquitination sites (amino acids 12-17) is largely conserved between all variants (**Figure 4.1**). We targeted the two most common variants of the peptide encompassing these sites: AKAKTR, present in five variants, and AKAKSR, the version present in eight variants including H2AX (from now on referred to as H2A and H2AX-like, respectively). Although, H2A(X) K13Ub was detectable and did not co-elute with K15Ub, the signal was low and close to the background. Therefore, for further study we focused on K15Ub. To develop a sensitive SRM assay for detection of H2A ubiquitination by MS, we employed synthetic peptides containing a K15 Gly-Gly modification, identical to that generated by trypsin digestion of ubiquitinated lysine residues. Following derivatization and digestion, the peptides were detected by the pseudo-SRM assay (**Figure 4.2**).

4.2.2 Quantification of temporal changes in H2A K15 ubiquitination

We combined γH2AX-ChIP/MS with a time-course strategy to quantify temporal changes in H2A(X) K15 ubiquitination. In agreement with previously published studies, we detected an increase in K15 ubiquitination following damage induction (**Figure 4.3**). Globally, the rise in the K15Ub mark was observed by 5-15 minutes following 3 Gy X-rays, reaching a peak around 0.5-1 hour, and staying relatively stable up to 4-8 hours, when it slowly decreased (**Figure 4.3 A and B**). At 24 hours following damage induction, K15 ubiquitination remained above the background level, suggesting that not all DSB have undergone repair.

Consistent with RNF168 being recruited to damage foci, we observed a marked accumulation of this mark in γH2AX-IP samples over input samples (**Figure 4.3 C and D**). Interestingly, the dynamics of the ubiquitin deposition on K15 differed between H2A and H2AX-like peptide. Both, globally and

locally, an increase in H2AX-like K15Ub was observed within 5 minutes after damage, whereas the same level of ubiquitination on the H2A peptide was reached at

Human H2As

```
CLUSTAL 2.1 multiple sequence alignment


sp|Q96KK5|H2A1H_HUMAN      MSG----RGKQGGKARAKAKTRSSRAGLQFPVGRVHRLLR-KGNYAERVG 45
sp|P0C0S8|H2A1_HUMAN       MSG----RGKQGGKARAKAKTRSSRAGLQFPVGRVHRLLR-KGNYAERVG 45
sp|P20671|H2A1D_HUMAN      MSG----RGKQGGKARAKAKTRSSRAGLQFPVGRVHRLLR-KGNYSERVG 45
sp|P04908|H2A1B_HUMAN      MSG----RGKQGGKARAKAKTRSSRAGLQFPVGRVHRLLR-KGNYSERVG 45
sp|Q7L7L0|H2A3_HUMAN       MSG----RGKQGGKARAKAKSRSSRAGLQFPVGRVHRLLR-KGNYSERVG 45
sp|Q93077|H2A1C_HUMAN      MSG----RGKQGGKARAKAKSRSSRAGLQFPVGRVHRLLR-KGNYAERVG 45
sp|Q6FI13|H2A2A_HUMAN      MSG----RGKQGGKARAKAKSRSSRAGLQFPVGRVHRLLR-KGNYAERVG 45
sp|Q99878|H2A1J_HUMAN      MSG----RGKQGGKARAKAKTRSSRAGLQFPVGRVHRLLR-KGNYAERVG 45
sp|Q8IUE6|H2A2B_HUMAN      MSG----RGKQGGKARAKAKSRSSRAGLQFPVGRVHRLLR-KGNYAERVG 45
sp|Q16777|H2A2C_HUMAN      MSG----RGKQGGKARAKAKSRSSRAGLQFPVGRVHRLLR-KGNYAERVG 45
sp|Q9BTM1|H2AJ_HUMAN       MSG----RGKQGGKVRAKAKSRSSRAGLQFPVGRVHRLLR-KGNYAERVG 45
sp|Q96QV6|H2A1A_HUMAN      MSG----RGKQGGKARAKSKSRSSRAGLQFPVGRIHRLLR-KGNYAERIG 45
sp|P16104|H2AX_HUMAN       MSG----RGKTGGKARAKAKSRSSRAGLQFPVGRVHRLLR-KGHYAERVG 45
sp|Q71UI9|H2AV_HUMAN       MAGGK--AGKDSGKAKAKAVSRSQRAGLQFPVGRIHRHLKTRTTSHGRVG 48
sp|P0C0S5|H2AZ_HUMAN       MAGGK--AGKDSGKAKTKAVSRSQRAGLQFPVGRIHRHLKSRTTSHGRVG 48
sp|P0C5Z0|H2AB2_HUMAN      MPRRRRRRGSSGAGGRGRTCSRTVRAELSFSVSQVERSLR-EGHYAQRLS 49
sp|P0C5Y9|H2AB1_HUMAN      MPRRRRRRGSSGAGGRGRTCSRTVRAELSFSVSQVERSLR-EGHYAQRLS 49
                           *.      *. ..  : :: :*: ** *.*.*.::.* *: .     *:.
```

Figure 4.1 Sequence alignment of the N-terminal portion of histone H2A variants using Clustal programme. K13/15 ubiquitination sites are largely conserved between different variants (red box).

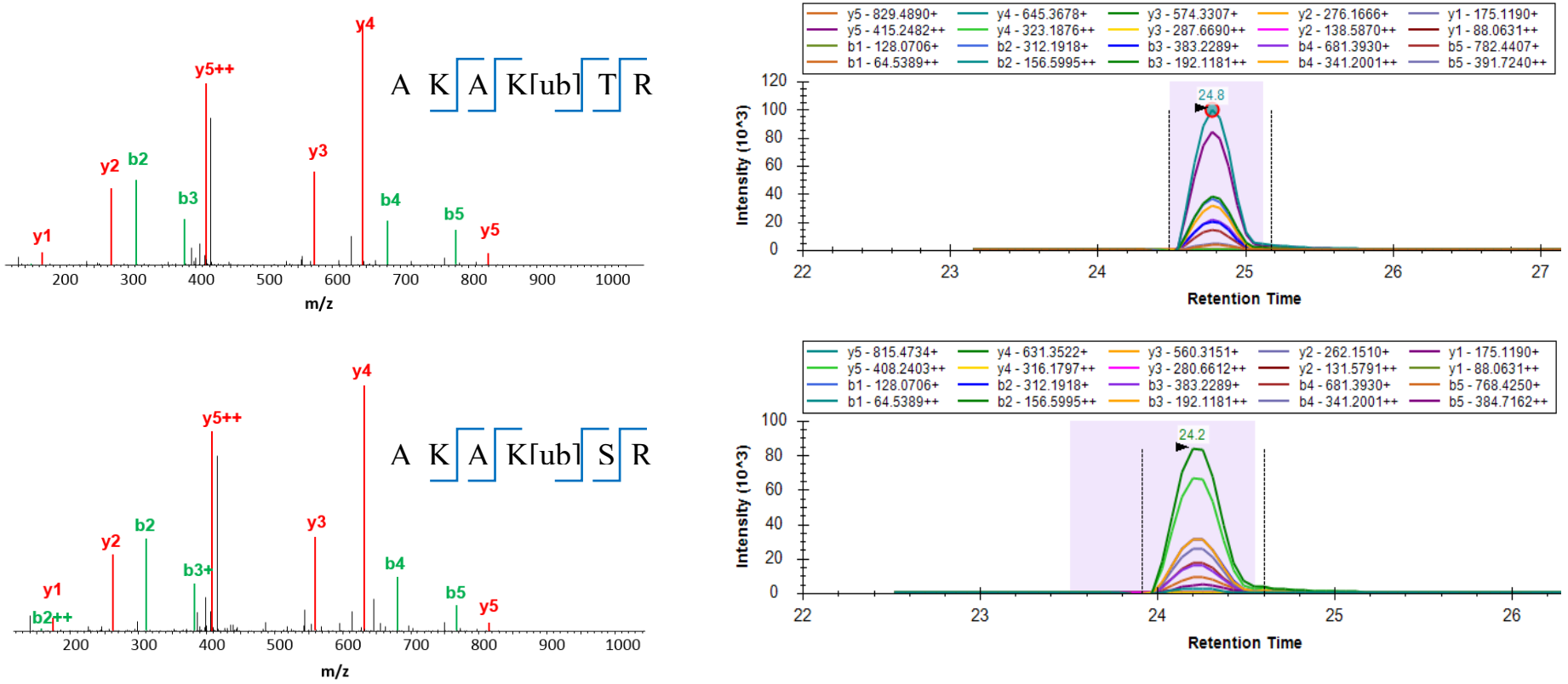

Figure 4.2 H2A(X) K15Ub synthetic peptide for the development of sensitive pSRM. 50 fmol of each of derivatized peptides were injected and analysed by pSRM assay. MS/MS fragmentation of doubly charged H2A K15ub (top panel) and H2AX-like K15ub (bottom panel) synthetic peptides. Extracted fragment ion mass spectra shown on left panel. Red and green bars represent y- and b-ions, respectively. Right panel shows extracted ion chromatograms with detected fragment ions displayed in the boxes above respective chromatograms.

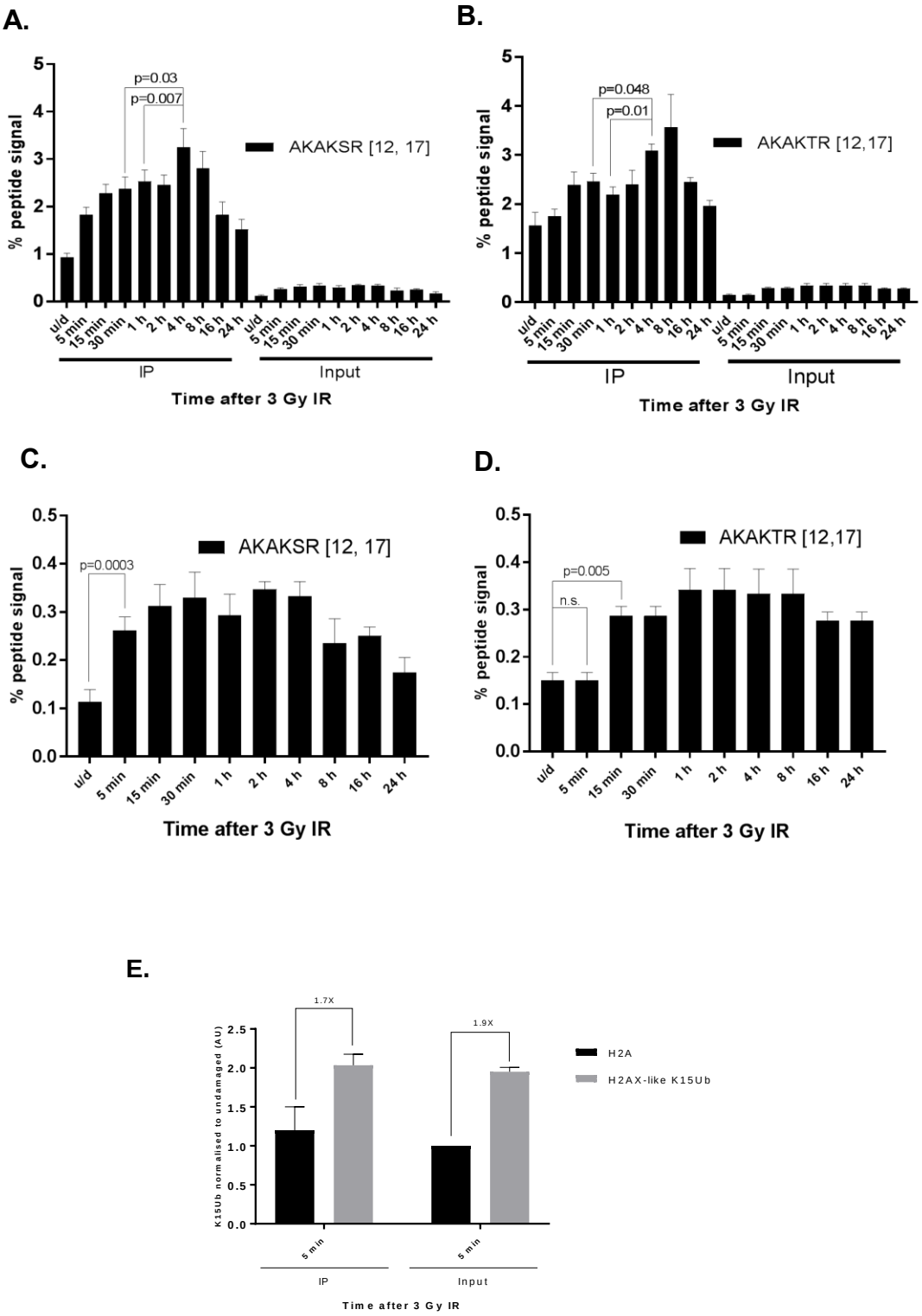
A.
B.
C.
D.
E.
% peptide signal
AKAKSR [12, 17]
AKAKTR [12,17]
p=0.03
p=0.007
p=0.048
p=0.01
p=0.0003
p=0.005
n.s.
u/d
5 min
15 min
30 min
1 h
2 h
4 h
8 h
16 h
24 h
IP
Input
Time after 3 Gy IR
K15Ub normalised to undamaged (AU)
1.7X
1.9X
H2A
H2AX-like K15Ub

Figure 4.3 Ionising radiation induced ubiquitination of H2A(X) K15 is enriched at γH2AX nucleosomes. A) HEK293 cells were damaged with 3 Gy X-rays and collected at the indicated time points. H2A(X) peptide spanning amino acid residues 12-17 containing ubiquitinated or unmodified lysine 15 were targeted for MS analysis. Percentage of H2A(X) K15 ubiquitinated relative to unmodified was quantified for all time points, both in the γH2AX-IP and input samples (A and B). Quantification of H2A K15 ubiquitination in the input samples was magnified in (C and D). E) Fold enrichment of K15 ubiquitination on the H2A- and H2AX-like peptide calculated relative to undamaged at 5 min post IR in IP and Input samples, showing the faster rate of ubiquitin deposition on H2AX-like K15 peptide. Error bars represent standard error of the mean in six biological replicates.

15 minutes, suggesting that deposition of ubiquitin on H2AX-like peptide was nearly twice as fast as on the H2A peptide (**Figure 4.3 E**). At the local level, we could detect several fold higher levels of H2A(X) K15 ubiquitination. Even in the undamaged sample, this mark was on average 11- and 6-fold higher compared with the undamaged input sample (**Figure 4.3 A and B** respectively). This result is not surprising, since these experiment were conducted in asynchronous cells, and it is well known that during S-phase, replication stress arises with activation of DNA repair pathways (Técher *et al.*, 2017). However, the local dynamics of K15Ub on the γH2AX nucleosomes were different from the global dynamics. Whereas globally K15Ub peaked between 0.5-1 hours after damage, locally the peak was reached between 4-8 hours following damage induction, where it was over 20-fold higher relative to the undamaged input sample. In contrast, γH2AX peaked by 0.5-1 hour (**Figure 3.5 A**).

4.2.3 H2A K15 ubiquitination decreases in response to increasing doses of IR

As mentioned in the introduction, previous studies have shown that 53BP1 foci are dependent on RNF168 and that they do not display a linear increase with dose, potentially due to limited RNF168. To examine whether this dependency might be due to an impaired ability to create H2A(X) K15 ubiquitination at high doses, we exposed HEK293 cells to increasing doses of IR, allowed them to recover for 30 minutes and analysed the samples as previously. As expected, western blot analysis showed a linear increase in the γH2AX damage mark with increasing IR dose (**Fig. 4.4 A**). In contrast, K15 ubiquitination per immunoprecipitated γH2AX nucleosome increased up to 3 Gy IR and decreased at higher doses (**Fig. 4.4 B**).

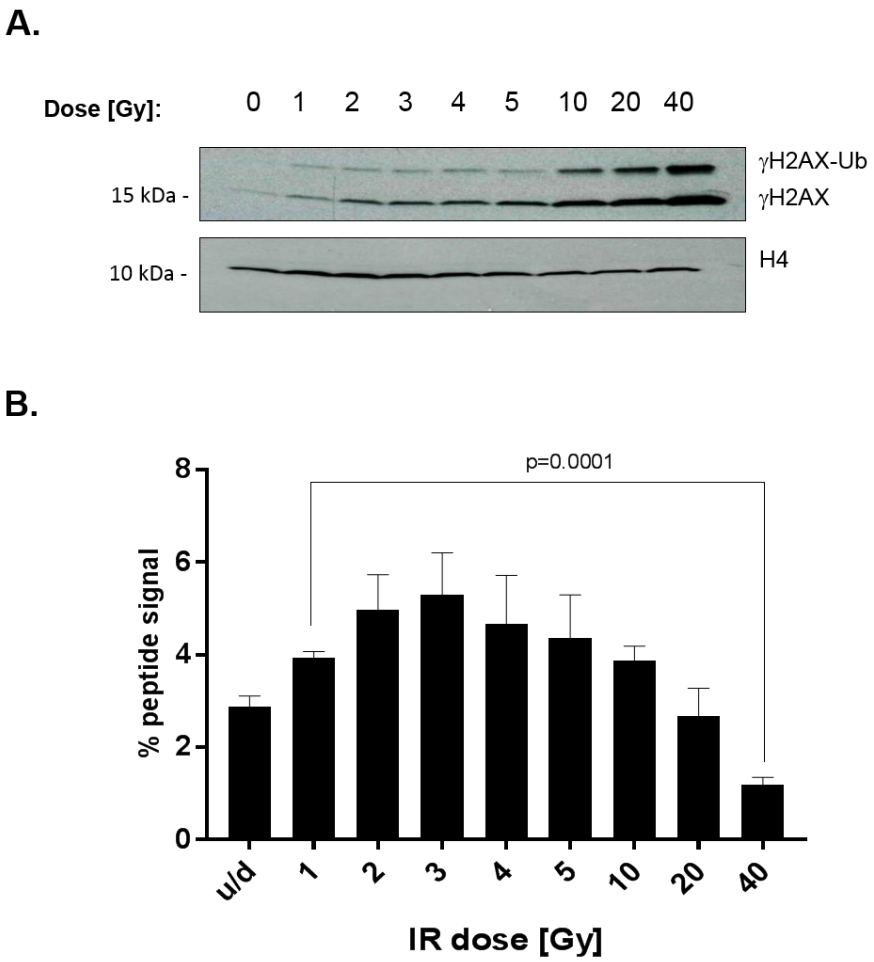

Figure 4.4 Histone H2A K15 ubiquitination is a limiting factor in response to DNA damage. A) Western blot analysis of γH2AX response to increasing doses of ionizing radiation. HEK293 cell were damaged with the indicated dose, allowed to recover for 30 minutes and collected. MNase extracted chromatin was run on SDS-PAGE gel and probed for γH2AX and histone H4. B) γH2AX-containing nucleosomes were immunoprecipitated and H2A K15 ubiquitination was quantified. Each biological replicate was run in technical duplicate. Error bars represent SEM (n = 3).

4.3 HISTONE H3 MODIFICATIONS DO NOT CHANGE IN RESPONSE TO IR

4.3.1 H3K9 and K14 modifications

Modifications on histone H3 lysine 9 (H3K9) are involved in the epigenetic regulation of cellular identity. For instance, the acetylated form of H3 K9 is found at the transcription start sites of genes and is associated with the activation of gene expression (Karmodiya *et al.*, 2012), while H3 K9me2/3 are found in condensed, transcriptionally silenced chromatin regions (Jacobson *et al.*, 2000; Lachner *et al.*, 2001; Peters *et al.*, 2002; Hathaway *et al.*, 2012).

As mentioned in the introduction H3K9me3-marked chromatin has been reported to be refractory to repair. It has been proposed that its condensed structure makes it more difficult for the repair machinery to access it, therefore a chromatin relaxation step is required prior to this process (Goodarzi *et al.*, 2008).

Furthermore, several studies have suggested that changes in H3K9 acetylation and methylation also may be involved in the DDR. For instance, it has been shown that failure to down regulate H3K9 acetylation in response to DNA damage leads to increased radiosensitivity and impaired recruitment of ATM (Meyer *et al.*, 2016b). However, somewhat contradictory observations have been reported in the literature regarding H3 K9me2/3, which were demonstrated to increase, decrease and remain unchanged at the sites of DNA DSBs (Falk *et al.*, 2007; Young, McDonald and Hendzel, 2013; Ayrapetov *et al.*, 2014a; Jiang *et al.*, 2015; Wu *et al.*, 2015).

We further explored the role of the modifications on this residue in the DDR. In our assay we were able to detect unmodified, mono-, di-, trimethylated and acetylated versions of an H3K9 peptide in combination with unmodified or acetylated K14, which gave us a total of 10 differentially modified peptides (**Figure 4.5**). We combined γH2AX-ChIP/MS with a time-course strategy to quantify temporal and IR-dose dependent changes in H3K9 modifications.

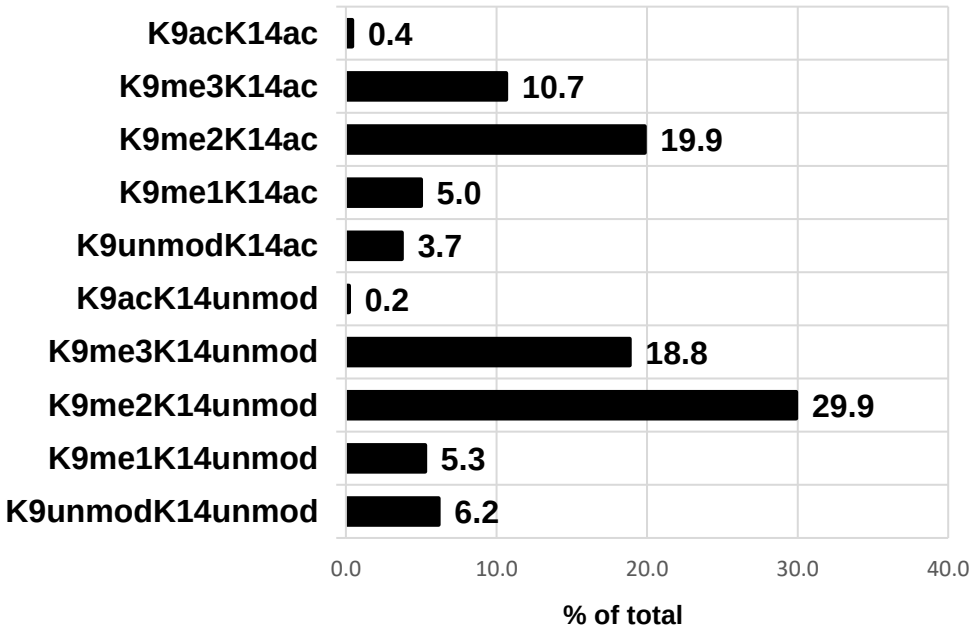

Figure 4.5 Quantification of H3 K9K14 modifications. Chromatin was extracted with MNase from untreated HEK293 cells. The ratio of 10 differentially modified H3 peptides containing lysine 9 and lysine 14 were quantified and expressed as a percentage of total (average of n = 20). The data is not corrected for ionisation efficiency.

Figure 4.5 Quantification of H3 K9K14 modifications. Chromatin was extracted with MNase from untreated HEK293 cells. The ratio of 10 differentially modified H3 peptides containing lysine 9 and lysine 14 were quantified and expressed as a percentage of total (average of n = 20). The data is not corrected for ionisation efficiency.

We found that in γH2AX nucleosomes none of the targeted methylations significantly changed (**Figure 4.6**). A slight decrease in K9 acetylation was observed, however a one-way ANOVA test did not show that change to be significant.

H3 peptide encompassing K9 contains another lysine residue (K14), which is known to be either unmodified or acetylated. We also monitored this mark over 24 h after IR, but no significant changes in the acetylation state of this residue were observed (data not shown).

Next, we considered the possibility that we were not able to detect new methylation at the site of the break due to low sensitivity of the method used. To test this hypothesis we combined γH2AX-ChIP/MS method with heavy methyl SILAC labelling to analyse the turnover of methylation following damage induction. To do that HEK293 cells were cultured in media containing light methionine, then switched to the heavy methionine media 1 h prior to damage induction with 3Gy X-rays (**Figure 4.7**). The cells were collected at several time points and prepared as previously. γH2AX IP and Input samples were then analysed using the pseudo-SRM method, targeting all of the potential combinations of H3K9 peptide.

As the heavy label gets incorporated, peaks corresponding to new H3K9me3 intermediate state precursor ions can be progressively observed on the spectrum. Analysis of the cells grown in the light media only, shows precursor ions that correspond to H3K9me3 containing three light, thus three "old" methyl groups (K9me3:0) (**Figure 4.7 B** – top panel). Upon the switch to the heavy media, new intermediates can be observed; for example K9me3:2, refers to H3K9 trimethylated, with two heavy or "new" methyl groups (**Figure 4.7 B**). Quantification of H3K9me3 turnover rate showed no large difference in the methylation between γH2AX and Input samples (**Figure 4.7 C**). However, this result should be confirmed with additional biological replicates.

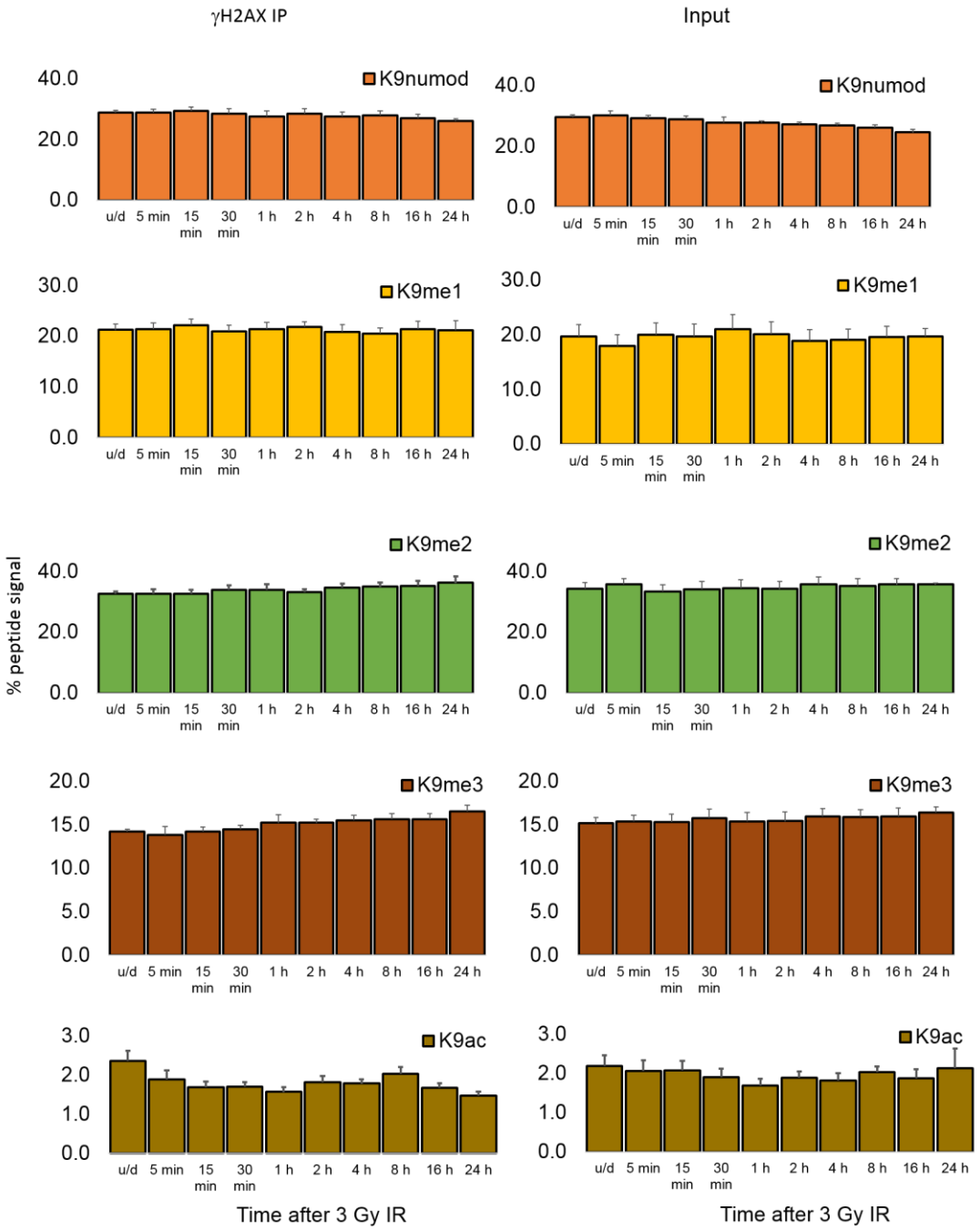
γH2AX IP
Input
K9numod
K9me1
K9me2
K9me3
K9ac
% peptide signal
u/d
5 min
15 min
30 min
1 h
2 h
4 h
8 h
16 h
24 h
Time after 3 Gy IR

Figure 4.6 Histone H3 K9 methylation is not significantly affected by ionising radiation. Quantification of histone H3K9 modifications following IR in γH2AX (left panel) and Input (right panel) samples. HEK293 cells were treated with 3 Gy IR and collected at the indicated time points. Histone H3 peptides (R.KSTGGKAPR.K [amino acids 9 - 17]), either unmodified, mono-, di-, tri-methylated or acetylated on lysine 9, and unmodified or acetylated on lysine 14 were targeted for MS analysis. Relative abundance of each peptide was quantified for each time point. Each biological replicate was run in technical duplicate. Error bars represent standard error of the mean in six biological replicates.

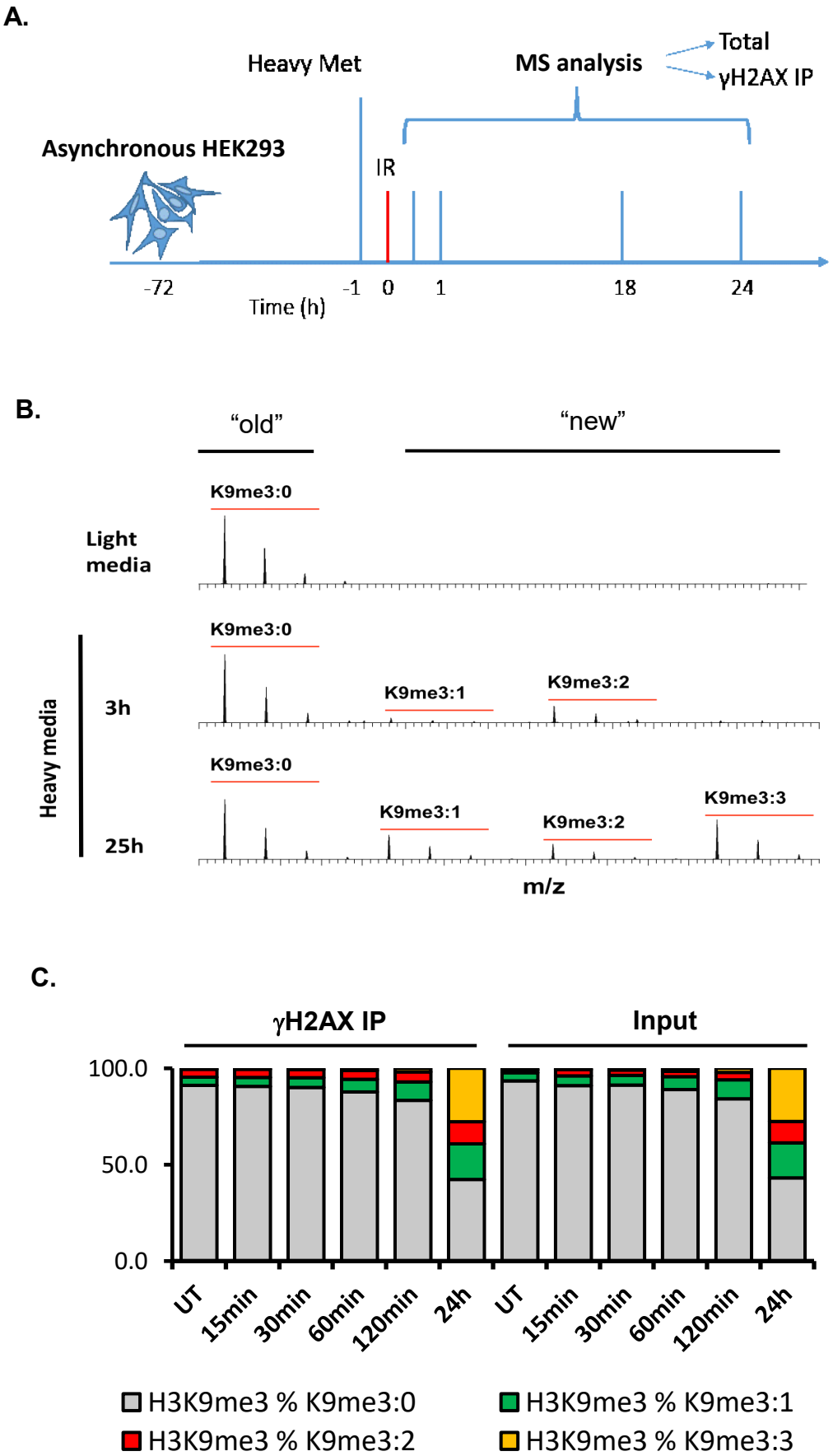
A.
Heavy Met
MS analysis
Total
γH2AX IP
Asynchronous HEK293
IR
-72
-1
0
1
18
24
Time (h)
B.
"old"
"new"
K9me3:0
Light media
K9me3:0
K9me3:1
K9me3:2
Heavy media
3h
K9me3:0
K9me3:1
K9me3:2
K9me3:3
25h
m/z
C.
γH2AX IP
Input
100.0
50.0
0.0
UT
15min
30min
60min
120min
24h
UT
15min
30min
60min
120min
24h
H3K9me3 % K9me3:0
H3K9me3 % K9me3:1
H3K9me3 % K9me3:2
H3K9me3 % K9me3:3

Figure 4.7 Heavy methyl SILAC labelling to study turnover of histone H3 K9 methylation in response to DNA damage. A) Strategy for using heavy methyl-SILAC labeling to study dynamics of histone methylation. HEK293 cells were switched from light to heavy methionine-labeled medium to allow for incorporation of the heavy methyl group on histones 1 h prior to 3 Gy X-rays. B) Extracted mass spectrum, showing time-dependent incorporation of heavy label to histone H3K9me3. C) Quantification of H3K9me3 turnover following 3 Gy X-rays. The experiment was run in technical duplicates.

4.3.2 Other histone H3 modifications

Several modifications on histone H3 have been previously reported to be involved in the DDR (see Introduction). Using our γH2AX-ChIP/MS approach we were able to monitor the dynamics of methylation and acetylation on the several H3 residues. These included: K4, K9, K14, K18, K23, K27, K36 and K79. We found no significant changes in the methylation and/or acetylation of any of these residues suggesting that majority of the epigenetic marks on this histone remain stable in response to DNA damage.

4.4 QUANTIFICATION OF H4 N-TERMINAL MODIFICATIONS IN RESPONSE TO IR

The amino acid sequence of histone H4 is the most conserved component of the core nucleosome. In human cells, there is a single histone H4 encoded by 14 genes. The N-terminal tail of histone H4 has been reported to be highly modified by acetylation, methylation and phosphorylation in order to regulate cellular processes, such as transcription, replication, checkpoint activation and DNA repair.

The modification of several H4 N-terminal residues have been previously described to change in response to DSBs. Using our γH2AX-ChIP/MS method we were able to detect and quantify modifications on peptides containing lysine residues 5, 8, 12 and 16 (amino acids 4-17) and lysine 20 (amino acids 20-23).

4.4.1 H4 K5, 8, 12 and 16

Acetylation and deacetylation of the N-terminal lysine residues of H4 were previously implicated in the DDR (Bird *et al.*, 2002; Tamburini and Tyler,

2005; Murr *et al.*, 2006; Miller *et al.*, 2010; Sharma *et al.*, 2010b; Krishnan *et al.*, 2011; Krishnan *et al.*, 2011; Hsiao and Mizzen, 2013; Tang *et al.*, 2013). Furthermore, HDAC inhibitors were shown to sensitise cells to DNA damage, suggesting an important role for the regulation of histone acetylation during the DDR (Groselj *et al.*, 2013).

Using our targeted mass spectrometry approach, we were able to detect and quantify the abundance of ten differentially modified H4 N-terminal peptides containing lysine residues K5, 8, 12 and 16 (H4 K5-16). This analysis showed that in HEK293 cells the peptide containing these residues is predominantly unmodified or acetylated on K16, representing approximately 46% and 41% of all H4 K5-16 modifications respectively (**Figure 4.8 A**). Two other readily detectible forms were peptides acetylated on K12 and 16, and peptides acetylated on K5, representing being 4.5% of all modified versions we were able to detect.

Next, we quantified the changes in acetylation on each of the lysine residues in the K5-16 peptide. Quantification of the ratio of acetylated versus unmodified K16 showed that this residue is not significantly affected by DNA damage, either globally or at the γH2AX nucleosomes, as judged by one-way ANOVA test. However, we saw a small, but significant decrease in the global levels of K5 and 8 acetylation (**Figure 4.8 B and C**).

4.4.2 H4K20 modifications

Constitutive and abundant di-methylation of the histone H4K20 is involved in the recruitment and retention of 53BP1 at the site of DSBs upon damage induction (Botuyan *et al.*, 2006b). Mono- and tri-methylation of H4K20 were previously reported to increase at the sites of DSBs (Pei *et al.*, 2011). However, using γH2AX-ChIP/MS, I found no significant changes in the methylation of this residue, as judged by t-test (**Figure 4.9**).

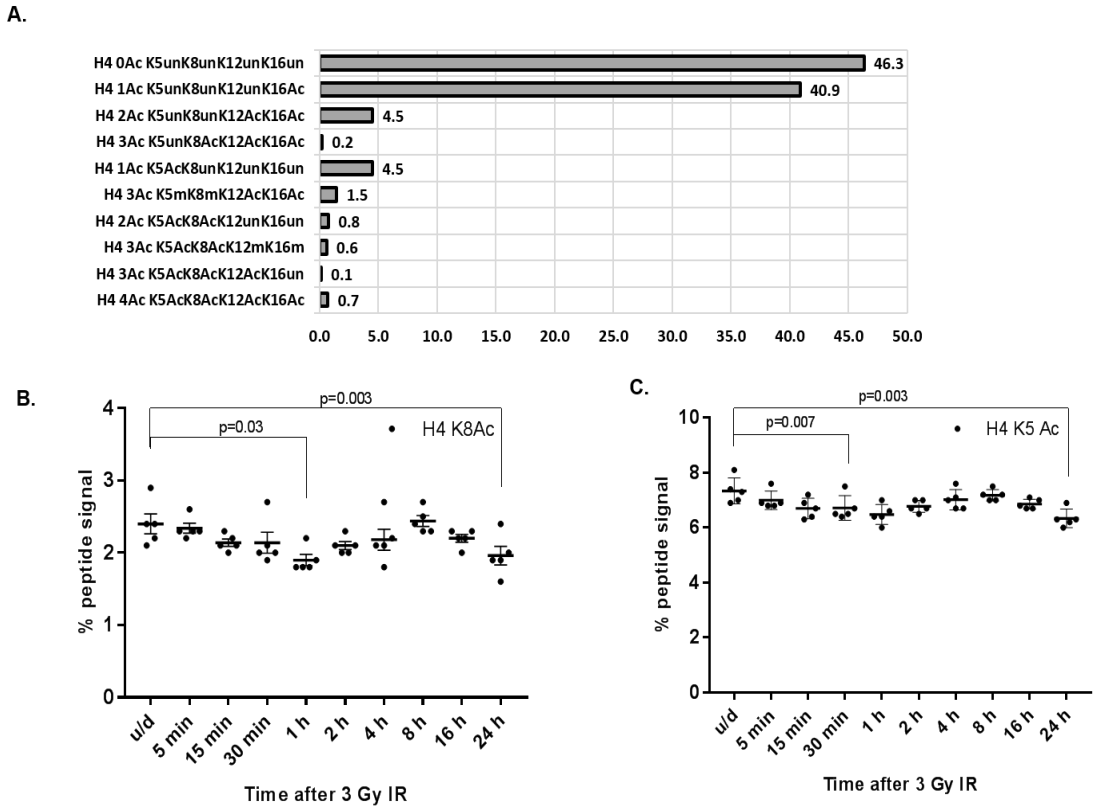

Figure 4.8 IR-induced global decrease in H4 K5/8 acetylation. A) Distribution of H4 K5-16 modifications in HEK293 cells. The Chromatin was extracted with MNase from untreated HEK293 cells. The ratio of 10 differentially modified H4 peptides containing lysine 5 to lysine 16 were quantified and expressed as a percentage of the total (average of n = 20 technical replicates). The data is not corrected for ionisation efficiency. Un = unmodified, Ac = acetylated, m = one of two lysine residues in a single peptide demarked with "m" (maybe) is modified. B) Temporal quantification of global acetylation on the histone H4 K5 in response to 3 Gy X-ray. C) Temporal quantification of global acetylation on the histone H4 K8 in response to 3 Gy X-ray. Error bars show SEM (n = 5). P value was determined using a *t* test (two-tailed, paired).


γH2AX IP
Input
% peptide signal
K20numod
K20me1
K20me2
K20me3
IP_u/d
IP_5min
IP_15min
IP_30min
IP_1h
IP_2h
IP_4h
IP_8h
IP_16h
IP_24h
Input_u/d
Input_5min
Input_15min
Input_30min
Input_1h
Input_2h
Input_4h
Input_8h
Input_16h
Input_24h

Figure 4.9 Histone H4 K20 methylation is not significantly affected by ionising radiation. Quantification of histone H4K20 modifications following IR in γH2AX (left panel) and Input (right panel) samples. HEK293 cells were treated with 3 Gy IR and collected at the indicated time points. Histone H3 peptides (R.KVLR.D [amino acid residues 20 - 23]), either unmodified, mono-, di-, tri-methylated on lysine 20 were targeted for MS analysis. Relative abundance of each peptide was quantified for each time point. Each biological replicate was run in technical duplicate. Error bars represent standard error of the mean in three biological replicates.

4.5 DISCUSSION

In this study, we used a novel ChIP-MS approach to quantify histone PTMs at γH2AX-containing mono-nucleosomes following IR. We found that the majority of the histone marks examined were unaffected by DNA damage, both globally and at γH2AX-containing nucleosomes. However, at this stage we cannot exclude the possibility that these marks show either transient changes or changes at a subset of DSBs. In considering this, it has to be appreciated that our procedure assesses the average change at multiple DSBs throughout the genome, in contrast to procedures using a site specific DSB. Our procedure may, therefore, lack sensitivity for the detection of subtle changes arising in a sub-class of DSBs. Additionally, by enriching for γH2AX nucleosomes, which are depleted in close proximity to the break (1-2 Kbp) (Shroff *et al.*, 2004b; Savic *et al.*, 2009c; Iacovoni *et al.*, 2010a), it is likely that we fail to detect PTMs that arise in non-γH2AX containing regions.

We observed a small, but significant bimodal decrease in global acetylation of H4 K5 and K8. Although the precise role of this deacetylation remains unclear, histone deacetylases (HDACs) have been reported to contribute to checkpoint arrest and p53-dependent transcriptional reprograming after DNA damage (Ho *et al.*, 2005). Our findings are supportive of a role for histone deacetylation raising the possibility that HDACs contribute to the regulation of specific genes for the execution of these responses.

The main modification we observed at the site of damage is ubiquitination of H2A(X) K15. This study allowed us to describe two important additional features for this damage induced PTM that may have potential functional relevance. Firstly, we found that ubiquitin is deposited initially at H2AX-like K15-containing peptides, while the ubiquitination of the other H2A variants proceeds with slower kinetics, suggesting that the H2AX-like peptide is a preferred substrate for RNF168. Secondly, we show that, in contrast to H2AX S139 phosphorylation, H2A(X) K15Ub is non-linear with dose. Even at 3 Gy, we do not observe the expected linear increase in signal, and at higher IR doses we see a decrease in ubiquitination per γH2AX, and therefore by implication a decrease in ubiquitination per DSB. Other studies have shown that 53BP1 is not recruited

with linear kinetics, with the ubiquitin ligase, RNF168, being proposed to be the limiting factor, i.e. RNF168 levels stay constant following damage induction, therefore, it becomes diluted between increasing number of DSBs (Gudjonsson *et al.*, 2012a). A 1 Gy X-ray treatment is expected to induce on average 20-40 γH2AX foci per cell by 30 minutes after treatment, decreasing to 5-10 foci at 4 hours as a result of the DDR (Bauerschmidt *et al.*, 2010). Given a linear increase in DSBs with increasing X-ray dose (Löbrich, Rydberg and Cooper, 1995) we would expect to generate 60-120 DSBs at 30 minutes after 3 Gy IR, reducing to 15-30 DSBs at 4 hours. Our findings, therefore, suggest that ubiquitination may become limiting between 40 and 60 DSBs per cell. Another feature we observed was an increase in ubiquitination between 4-8 hours post 3 Gy irradiation (Gudjonsson *et al.*, 2012a). Although this could be explained by slow deposition of this mark, we favour the explanation that there could be increased availability of RNF168 at later time points as repair occurs and the number of γH2AX foci diminish, in other words at earlier times RNF168 is saturated but becomes available as repair ensues. Such an explanation is consistent with, and might even be expected from, the restricted availability of RNF168 after 3 Gy. These estimates based on the non-linear behaviour of H2A(X)K15 ubiquitination are consistent with other estimates based on analysis of 53BP1 recruitment to DSBs, which is dependent on the ubiquitin mark (Ochs *et al.*, 2016). Ochs *et al*, (2016) showed that in S/G2 phase robust 53BP1 accumulation is required for RAD51 filament formation and faithful repair via HR, while insufficient 53BP1 accumulation was shown to redirect the repair towards mutagenic RAD52-dependent SSA. Here, I have showed that H2A(X) K15Ub, a binding platform necessary for 53BP1 recruitment to DSBs, decreases in response to high doses of IR, suggesting this ubiquitination is necessary for faithful repair of DSBs (**Figure 4.10**). These observations have an important implication when considering high dose exposures such as the doses received during radiotherapy and will be discussed later.

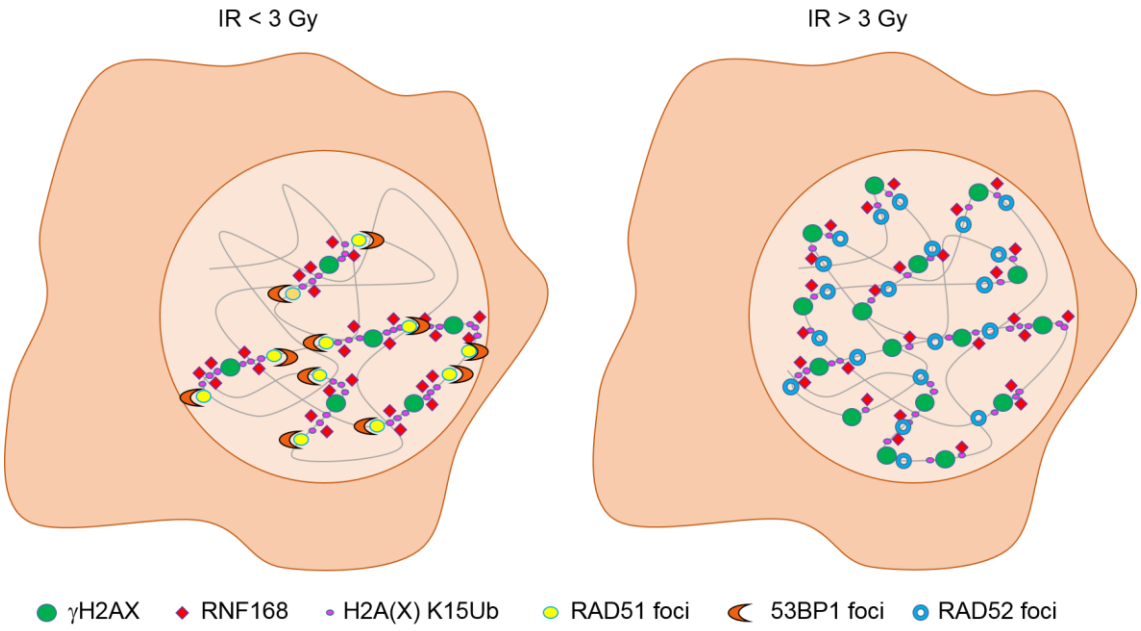

Figure 4.10 Schematic representation of the proposed effect of high IR doses on H2A(X) K15 ubiquitination. Following DNA damage induction with IR in S/G2 phase, RNF168 is recruited to the DSB marked with γH2AX (green), where it ubiquitinates histones H2A(X) K15. Below 3 Gy of IR sufficient amount of H2A(X) K15 ubiquitination takes place, leading to recruitment of 53BP1 and RAD51 to the sites of DSBs, which are then repaired by HR. As the IR doses increase above 3 Gy, limited amounts of RNF168 dilute between multiple breaks, leading to insufficient H2A(X) K15 ubiquitination, and thus decreased 53BP1 recruitment, causing a switch from RAD51-dependent HR to RAD52-dependent SSA.

5 CHAPTER FIVE: CHARACTERISATION OF THE CHROMATIN ASSOCIATED WITH LATE REPAIRING DNA DSBS IN ATM DEFICIENT CELLS

5.1 INTRODUCTION

γH2AX is the most commonly used DSB marker. It is understood that chromatin presents a barrier to the repair of DSBs, and numerous histone acetylation, ubiquitination and methylation events have been reported to be associated with DSB signalling and repair (discussed in the Introduction).

H2AX S139p is predominantly carried out by ATM kinase, but in its absence DNA-PK can also phosphorylate H2AX (Stiff *et al.*, 2004). However, ATM is required for the repair of a subset (15-20%) of IR-induced breaks, representing those repaired with slower kinetics (Riballo *et al.*, 2004). Significantly, there is evidence that these DSB co-localise with heterochromatic regions (Goodarzi *et al.*, 2008).

As discussed in the Introduction, KAP1 is a well-known heterochromatin building factor. Upon DSB induction, KAP1 is phosphorylated on S248 throughout the nucleus to promote global relaxation of chromatin (Goodarzi *et al.*, 2008). Phosphorylated KAP1 was also shown to form foci that co-localise with γH2AX at heterochromatic lesions at late repairing time-points (Riballo *et al.*, 2004). Cells lacking MDC1, RNF8 and RNF168, fail to form 53BP1 foci, leading to inefficient accumulation of Mre11-NBS1 and ATM, which leads to a failure in the formation of KAP1 S248phos foci (Riballo *et al.*, 2004). Consequently, this results in a repair defect at slow component, heterochromatin-associated breaks.

KAP1 is also a known silencing factor and was observed to associate with a variety of proteins involved in transcription regulation, such as histone acetylases and deacetylases, as well as histone and DNA methyltransferases (Cheng, Kuo and Ann, 2014). In the cell, KAP1 has been shown to localise to discrete compartments within the nucleus, including pericentric and centromeric heterochromatin, euchromatin, but was also found in the cytoplasm, implicating its function in diverse cellular activities (Ryan *et al.*, 1999; Matsuda *et al.*, 2001; Yang *et al.*, 2013). Interestingly, it has been also demonstrated that KAP1, as well as other compacting factors, such as SUV39h1 and HP1, are recruited to

DSBs to promote chromatin condensation shortly following damage induction (Ayrapetov *et al.*, 2014).

5.2 AIMS OF THIS CHAPTER

Given the observation that chromatin compacting factors are recruited to the sites of DNA damage, we asked the question whether the repair-defective, ATM-dependent DSBs originate in the heterochromatin or do they become heterochromatinised as a consequence of DDR.

To investigate heterochromatin associated DSBs in mammalian cells, previous studies took advantage of murine cells, in which heterochromatin can be easily observed as large, DAPI-dense chromocenters (Goodarzi *et al.*, 2008). The weakness of this approach is that it is indirect and simply relies on the co-localisation between the damage markers and DAPI-stained chromocenters. Furthermore, it does not permit differentiation between pre-existing and new, damaged-induced, chromatin modifications. Importantly, heterochromatin organisation is different in murine cells, i.e. in murine cells heterochromatin organises to large structures known as chromocenters, while in human cells heterochromatin is spread throughout the nucleus (Jones, 1970; Pardue and Gall, 1970; Ou *et al.*, 2017), and therefore the same repair mechanism may not be applicable to human cells.

In this thesis I have presented a novel method for the enrichment and quantification of the nucleosomes containing γH2AX in order to detect co-occurring histone modifications. Here, I further employ a label-switch strategy to immunoprecipitate persistent γH2AX chromatin in ATM inhibited (ATMi) or A-T cells, previously demonstrated to be enriched in heterochromatic regions of the genome (Goodarzi *et al*., 2008). I use heavy methyl SILAC labelling to distinguish between pre-existing and new methylation on histone H3K9. Here I present the analysis of the relative enrichment of heterochromatin modifications in these slow-repairing foci.

5.3 APPROACH TO STUDY HISTONE METHYLATION AT LATE REPAIRING DSBS USING HEAVY METHYL SILAC LABELLING

Heavy methyl SILAC labelling was used in the past to distinguish pre-existing and new methyl marks on histones (Zee *et al.*, 2010; Cao, Zee and Garcia, 2013). I have combined the γH2AX-ChIP/MS method described in Chapter 3 with SILAC labelling using light and heavy methionine to study the origin of the heterochromatin associated with the slow repair component in ATM deficient cells. The basic principles of this method are depicted in the **Figure 5.1 A.** The cells were arrested in the G0/1 phase of the cell cycle by contact inhibition. Three days after the cells reached 100% confluence, cell growth media containing light methionine was switched to media containing heavy methionine and allowed 1 h for its incorporation (described in more detail in the Introduction). Following damage induction, cells were collected at the indicated time-points. The Input and γH2AX-IPed samples were analysed using LC-MS.

5.3.1 G0/1 cell cycle arrest

To reduce background γH2AX related to replication stress, cells were arrested in the G0/1 stage of the cell cycle by contact inhibition. Fluorescence activated cell sorting (FACS) analysis was used to examine the cell cycle profile (see Method and Materials). This showed that growing cells to full confluence is sufficient to inhibit cell cycle progression and yield a population with predominantly G0/G1 phase cells and undetectable levels of S phase cells (**Figure 5.2**).

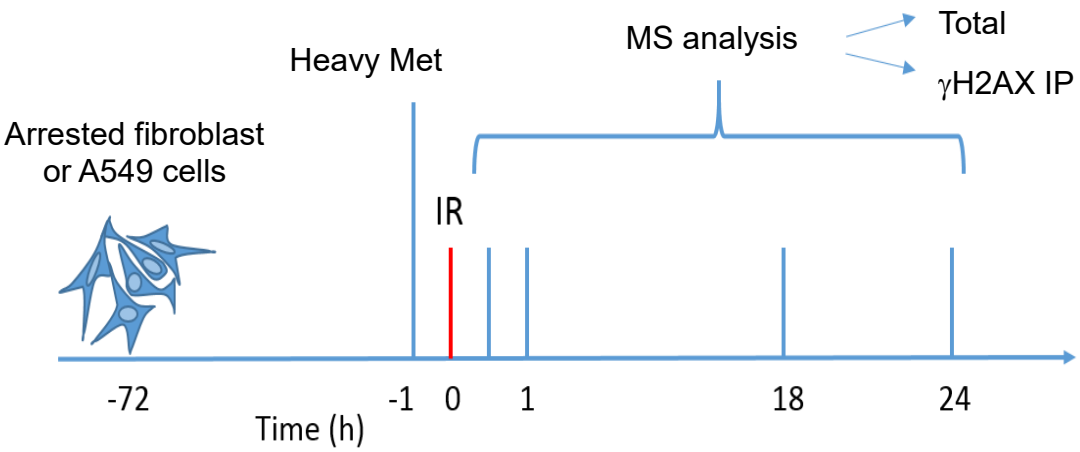

Figure 5.1. Strategy for the approach to study DSB-associated H3K9 methylation. 72 h after cells reach confluency and 1 h prior to IR, the cell media was switched from light to heavy methionine to allow time for incorporation into cells. Following IR, cells were collected at the indicated time-points.

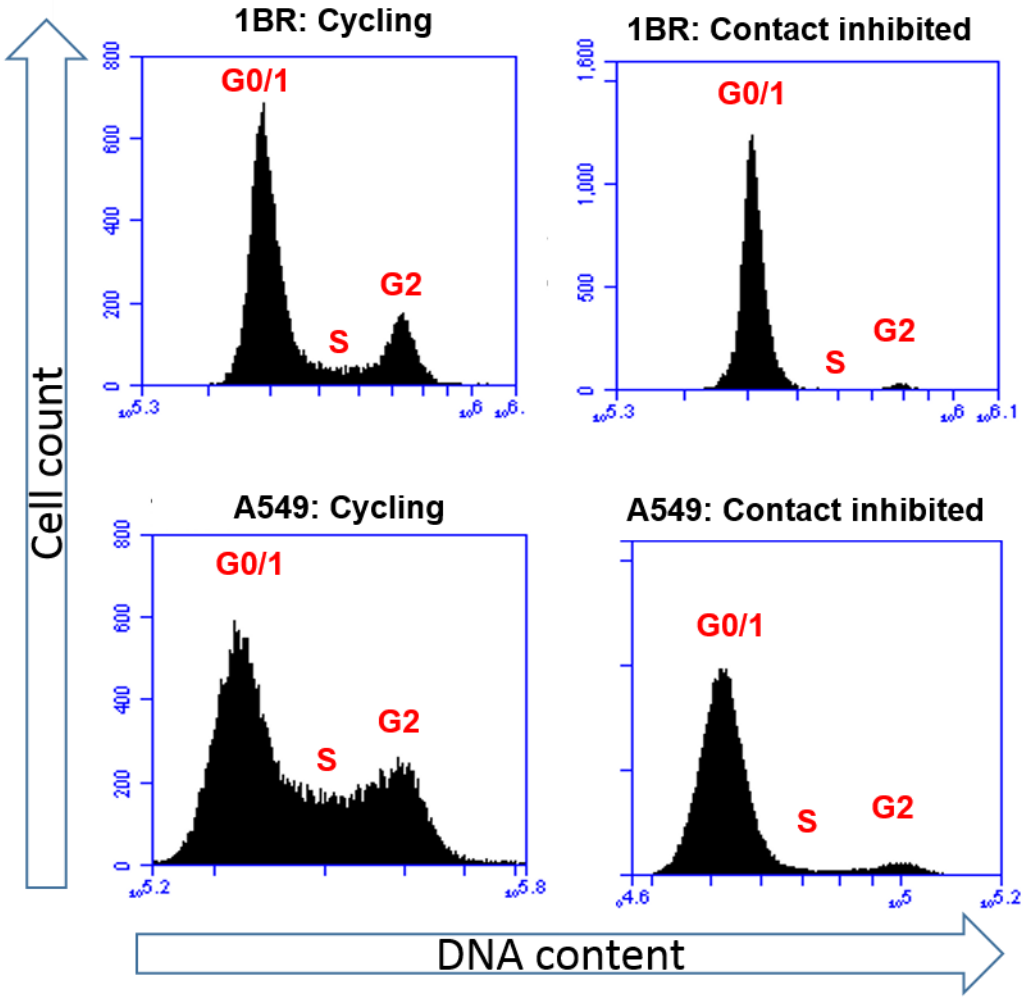

Figure 5.2. Contact inhibition of cells in G0/1 cell cycle phase. The FACS profile of cycling and contact inhibited 1BR (top panel) and A549 (bottom panel) cells.

5.3.2 ATM inhibition results in a defect in the slow repair component

To confirm the repair defect related to ATM deficiency, first, I established that KU55933 (ATM inhibiting drug, ATMi) treatment is able to prevent ATM activation (Hickson *et al.*, 2004). Upon IR treatment, ATM is known to undergo auto-phosphorylation on S1981 and to phosphorylate p53 on S15, which are often used as markers of ATM activity**. Figure 5.3** shows that ATMi treatment prior to IR prevents the phosphorylation of these residues, consistent with inactivation of ATM kinase function. Moreover, consistent with previous reports, inactivation of ATM resulted in a repair defect at 24 h post IR, as judged by increased number of γH2AX foci, as compared to wild type (wt) cells (**Figure 5.4 A and B**).

Similarly, I wanted to confirm that the repair defect also occurs in the A549 cells upon ATMi inhibition. These cells are much smaller in size and grow faster than fibroblasts, resulting in a much higher yield in a shorter period of time. Furthermore, A549 cells can be also arrested by contact inhibition (**Figure 5.2**).

Upon ATM inhibition we observed a decrease in H2AX phosphorylation as judged by Western Blot analysis (**Figure 5.5 A**). Therefore, to determine whether ATM inhibition leads to the same repair defect of the late repair component as observed in 1BR3 cells, I enumerated IR induced γH2AX that co-localised with 53BP1 foci and observed the anticipated repair defect (**Figure 5.5 B and C**). The reason behind enumerating co-localised foci was due to the fact that ATM inhibition leads to decreased phosphorylation of H2AX, and therefore, smaller and more difficult to detect foci. Unfortunately, due to technical issues with the chromatography, which led to loss of the data for multiple peptides, this experiment was not fit for quantification, and due to the time limitation A549 experiments were not continued.

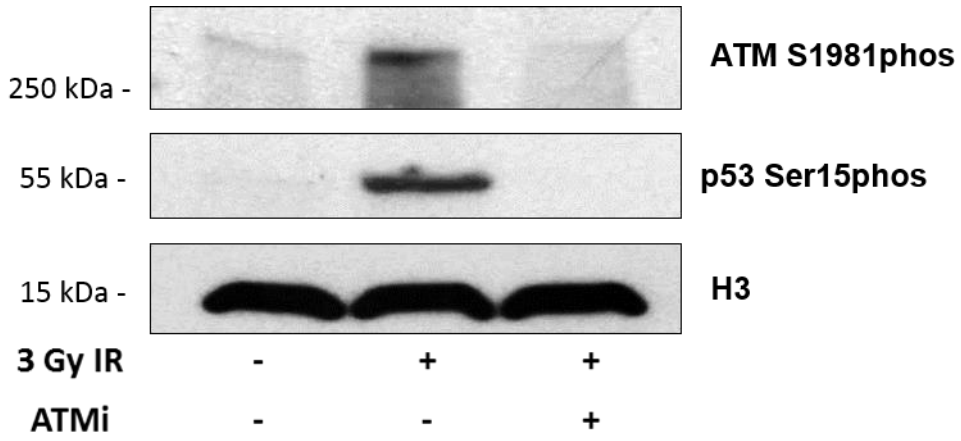

Figure 5.3. KU55933 treatment inhibits ATM activity. Western blot analysis showing that ATMi treatment prevents ATM activation following IR. A549 cells were treated with 10 µM of KU55933 for 1h, damaged with 3 Gy of X-rays and allowed 1 h recovery time prior to collection. ATM autophosphoryation was monitored using phospho-specific antibodies to the ATM autophosphoryation site, S1981 and phosphorylation of p53 was monitored using p53 Ser 15-phosphorylation specific antibodies.

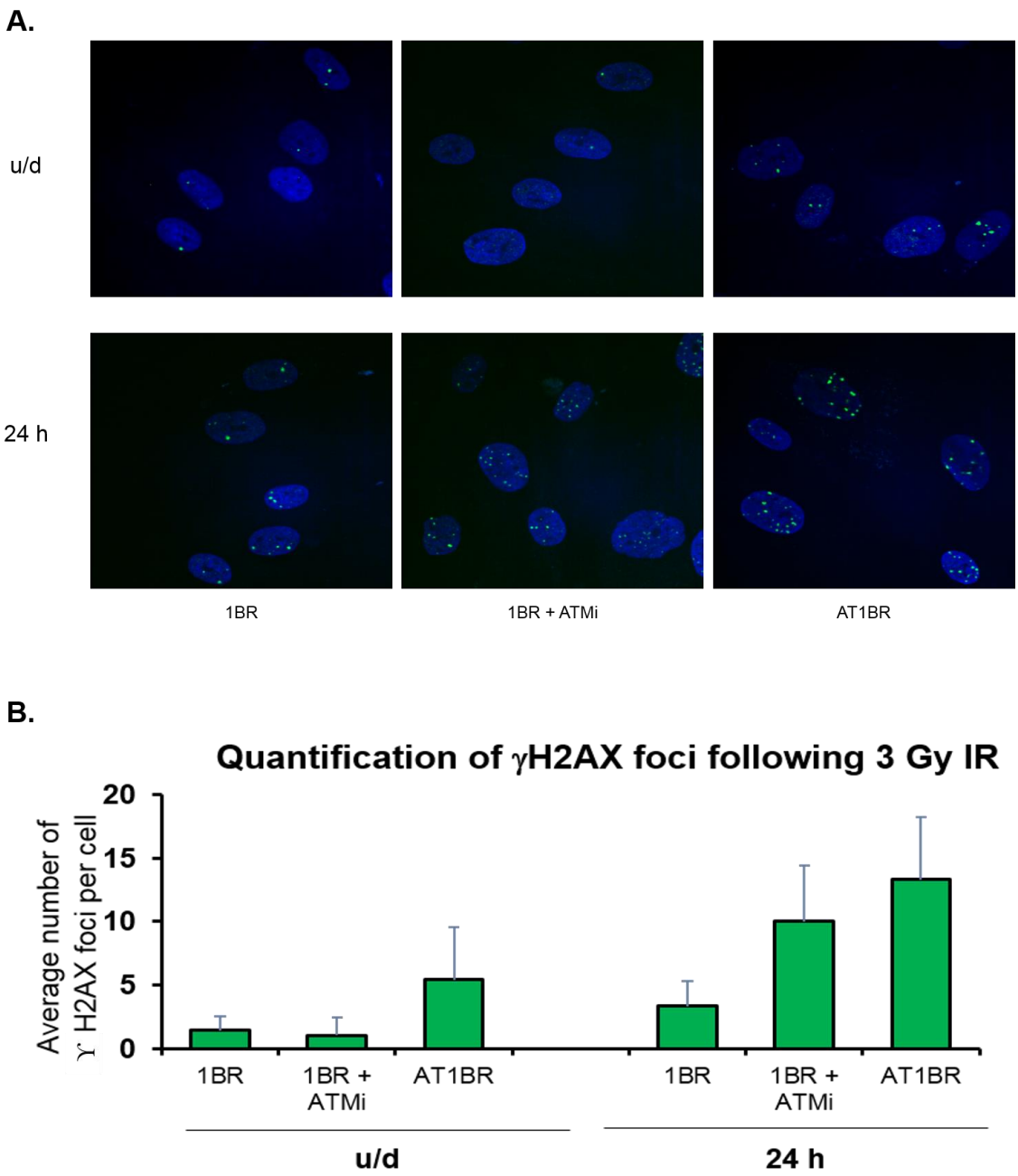

Figure 5.4. AT patient derived and ATMi treated cells show a repair defect 24 h following IR. A) 1BR -/+ ATMi and AT1BR fibroblast cells, undamaged or treated with 3 Gy X-rays, were immunostained for γH2AX (green). The nucleus was stained with DAPI (blue). B) Quantification of γH2AX foci from (A). The average of 50 cells/condition were counted. Error bars represent 1 SD. u/d = undamaged, 24 h = 24 h post-IR

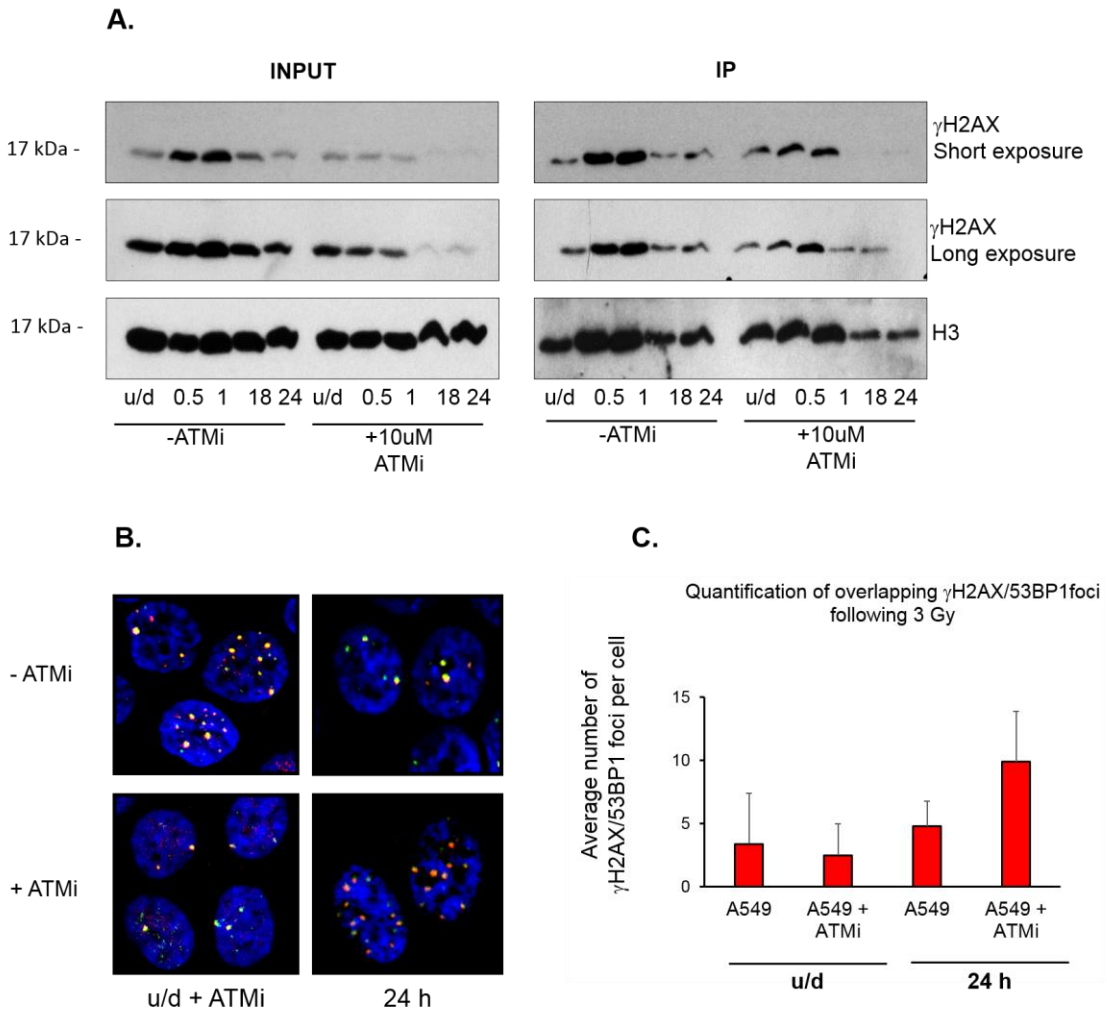

Figure 5.5. ATMi treatment of A549 cells results in a DSB repair defect. A) Western blot analysis of γH2AX following 3 Gy of X-ray treatment in A549 cells -/+ ATMi pre-treatment. B) ATMi treated A549 cells show repair defect 24 h post-IR. IF analysis of γH2AX (green) and 53BP1 (red) foci following ATMi treatment. The nucleus was stained blue with DAPI. C) Quantification of γH2AX/53BP1 overlapping foci. Average of 100 cells per condition was counted. Error bars represent 1 standard deviation.

5.4 QUANTIFICATION OF PRE-EXISTING AND NEW H3K9 METHYL MARKS ASSOCIATED WITH THE γH2AX-NUCLEOSOMES IN THE WILD TYPE AND ATM DEFICIENT FIBROBLAST

As previously discussed, heterochromatin-associated H3K9me3 marks have been shown to be enriched at late repairing DSBs. To quantify whether these late repairing breaks originate from pre-existing heterochromatin or become heterochromatinised as a consequence of the DDR, I have used heavy methyl SILAC labelling as described above. Surprisingly, quantification of H3K9me3 in the γH2AX immunoprecipitated samples revealed that there was no enrichment of these marks at the 24 h time-point relative to 1 h either in the control or ATM inhibited/mutated cells.

Furthermore, I quantified the turnover of H3K9 methylation on the γH2AX nucleosomes associated with the late repairing breaks. As discussed in the Introduction, di- and tri-methylation of this residue was previously reported to increase at DSBs (Ayrapetov *et al.*, 2014c). However, we did not observe any significant difference in the turnover of H3K9me2 at the γH2AX nucleosomes relative to the global turnover of these marks (**Appendix Figure 2 A**). A small increase in new tri-methylation, created from pre-existing mono- and di-methylation was observed at γH2AX nucleosomes at 24 h in the 1BR and AT1BR cells, however this was not statistically significant (**Appendix Figure 2 B**). The signal from fully new tri-methyl H3K9 (all heavy label) was too close to the background to be reliably quantified (**Appendix Figure 3**).

Larger amounts of the sample should be loaded for MS analysis to improve the quantification of these peptides. This, however, could not be readily achieved with 1BR.3 cells. This is due to the fact that these cells are much larger than HEK293 or A549 cells. Based on the cell count, I have calculated on one 15 cm^2 plate one can grow on average ~$4x10^7$ HEK293 cells, while only ~$5x10^6$ of 1BR.3 can fit into the same space. Additionally, ATM inhibition leads to decreased phosphorylation of H2AX. Therefore, substantial upscaling of the cell culture would be required to grow sufficient a amount of 1BR.3 cells to perform these experiments, significantly increasing the costs and labour time.

5.5 DISCUSSION

A previous study proposed a model whereby H3K9me3 marked heterochromatin poses a barrier to DSB repair processes and that this barrier is removed in an ATM-dependent manner for the repair to proceed (Goodarzi *et al.*, 2008). However, *de novo* histone H3K9 methylation has been also shown to occur during the response to DNA DSBs (Ayrapetov *et al.*, 2014a). This suggested to us an alternative possibility that H3K9me3 marks associated with the late repairing breaks may be a consequence of DDR signalling, rather than pre-existing heterochromatin.

To test that, I combined the γH2AX-ChIP/MS method described in Chapter 3 with heavy methyl SILAC labelling to differentiate between pre-existing and new H3K9 methyl marks. Surprisingly, quantification of H3K9me3 on γH2AX-nucleosomes showed no difference in the proportion of this mark in the late relative to early time points following IR in 1BR wt, AT1BR and ATMi treated 1BR. I was not able to consolidate the previous findings from Goodarzi *et al.*, (2008), which raises the concern about the use of the DAPI-stained chromocenters co-localisation method as a read-out for heterochromatic DSBs. This may be due to resolution microscope constraints, i.e. the co-localisation between chromocenters and γH2AX foci maybe the effect of a poor spatial resolution, rather than actual co-localisation. If correct, these data suggests that ATM-dependent late repairing breaks do not originate from heterochromatin and the issue underlying the requirement for ATM to repair those breaks is still to be determined. Another possibility is that those γH2AX regions, although originated somewhere else in the genome, somehow became associated with the chromocenters following IR. However, to strengthen this conclusion, these experiments need to be repeated.

Furthermore, we did not observe significant differences in the rate of methylation at the site of γH2AX-nucleosomes as compared to the global turnover rate for this mark, suggesting that this modification does not change on the γH2AX nucleosomes or the change is too small to be sensitively detected by this method. However, because the γH2AX domains are very large, I may fail to

detect any changes in a smaller region at a defined distance from the DSB. Thus, I cannot exclude the possibility that this modification may occur at smaller, specific sub-domains of γH2AX.

Another possibility may be that this modification changes in the proximity of the break where the nucleosomes are depleted of γH2AX, and since this system relies on the γH2AX mark for the enrichment of DSB-associated nucleosomes, we would not be able to enrich for them using this method.

An important constraint for this study was the limited yield of γH2AX nucleosomes obtained from fibroblast cells and the extensive amount of time to grow large enough cultures for γH2AX IP. In comparison to HEK293 cell, which were used for γH2AX IP in the previous chapters, fibroblast cells are much larger and slower growing. This means that the cost of these experiments was prohibitively large, especially if I aimed to load higher levels of samples. Therefore, I have also optimised the conditions for performing these experiments in A549 cells, which are faster growing and have a potential of yielding higher amounts of sample. However time constraints stopped me pursuing further experiments.

The nature of the late repairing DSBs remains an important unanswered question and the method I have used to investigate it has the potential of addressing it further. The initial data is thought-provoking and with further improvement in the yield of γH2AX IP sample this method could be used to investigate other chromatin marks associated with those breaks.

6 CHAPTER SIX: DEVELOPMENT OF A SYSTEM FOR *IN VIVO* BIOTINYLATION OF DSB-ASSOCIATED NUCLEOSOMES

6.1 INTRODUCTION

In vivo proximity biotin labeling of proteins mediated by the *E. coli* derived biotin ligase enzyme, BirA, was previously described by several groups, who have used it to identify protein complexes, protein-protein interactions and to label sites of UV induced DNA damage (Fernández-Suárez, Chen and Ting, 2008; Kulyyassov *et al.*, 2011; Lau and Cheung, 2013; Ma *et al.*, 2013; Shoaib *et al.*, 2013). In this system, one of the proteins of interest is fused with the BirA biotin ligase, while the other is fused with a biotin acceptor peptide (BAP) containing a lysine residue in a sequence-specific context, which is amenable to biotinylation by BirA in a proximity-dependent manner. It has been shown in previous studies that BirA is not able to biotinylate endogenous proteins in mammalian cells; conversely mammalian biotin ligases do not recognize BAP (de Boer *et al.*, 2003; Chen *et al.*, 2005; Howarth *et al.*, 2005).

The aim of this chapter was to establish an antibody-free system that allowed us to specifically label and pull-down chromatin from the site of DNA damage.

6.2 EXPERIMENTAL APPROACH FOR IN VIVO BIOTIN LABELLING OF THE NUCLEOSOMES IN PROXIMITY OF DSBS.

A schematic representation of the system to allow biotinylation in vivo is presented in **Figure 6.1 A**. Briefly, upon DNA damage induction and addition of biotin to the cell media, the BirA-tagged DDR protein becomes recruited to the site of DNA damage, where it can promote the biotinylation of BAP-tagged histones. Biotinylated nucleosomes can be than detected and pulled-down using streptavidin.

To test the system, two DDR proteins known to be recruited to the site of breaks, RNF168 and 53BP1 were tagged with the BirA biotin ligase (**Figure 6.1 B**). Since histone H4 has a only single isoform, which is incorporated in all nucleosomes

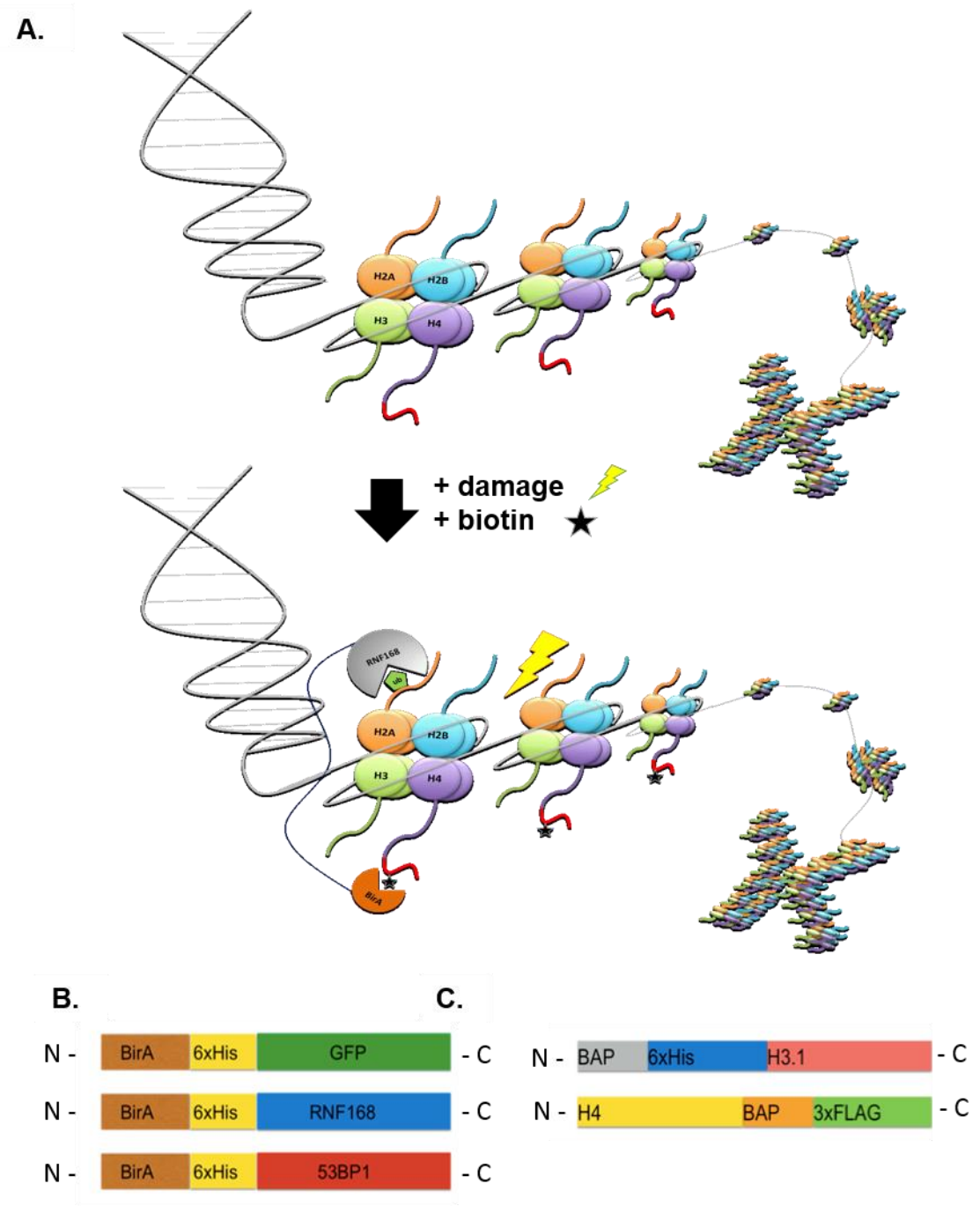

Figure 6.1. Schematic representation of biotinylation system. A) Briefly, upon DNA damage induction DDR proteins tagged with BirA will be recruited to nucleosomes around the break containing BAP-tagged histones. Lysine residue within BAP sequence will be biotinylated by proximal BirA tagged to DDR protein. B) Schematic representation of BirA-tagged constructs. C) Schematic representation of BAP-tagged constructs. BAP = biotin acceptor peptide.

throughout the genome, we decided to fuse this histone with the BAP sequence (**Figure 6.1 A**).

A previously described BirA-GFP and BAP-H3.1 pair were also used to test the method (Kulyyassov *et al.*, 2011). Upon transient co-expression of BirA-GFP and BAP-H3.1 in U2OS cells we observed a pan-nuclear pattern of biotin staining, consistent with the nuclear localisation of histone H3, suggesting specific biotinylation of the BAP-tag (**Figure 6.2**).

6.3 GENERATION OF CELL LINES STABLY EXPRESSING BAP-TAGGED HISTONE H4

The vectors for expression of BirA-RNF168, BirA-53BP1 and 3xFLAG-BAP-H4 and the method for the generation of the U2OS 3xFLAG-BAP-H4 stable cell line are described in the Methods and Materials section 2.1.1 and 2.1.2. The expression of recombinant H4 was confirmed and quantified using immunofluorescence screening of selected single clones (**Figure 6.3 A and B**). Since Clone 6 showed the most uniform expression, it was selected for further experiments. The expected molecular weight of 3xFLAG-BAP-H4 protein of 17 kDa was calculated using ProtParam tool (Walker, 2005), and confirmed by immunoblotting all cell lysates made from Clone 6 (**Figure 6.3 C**).

6.4 BIRA-RNF168 LABELS NUCLEOSOMES AT THE SITE OF DSB WITH BIOTIN

To follow, I have verified BirA-tagged DDR proteins are recruited to the sites of DSBs. To do that, U2OS 3xFLAG-BAP-H4 cells were transiently transfected with BirA-6xHis-RNF168 or BirA-6xHis-53BP1 vectors and cultured to grow 24 h allowing for expression of the recombinant proteins. DNA DSBs were induced with 50 ng/ml neocarzinostatin (NCS), with 1 h recovery time prior to fixation with formaldehyde.

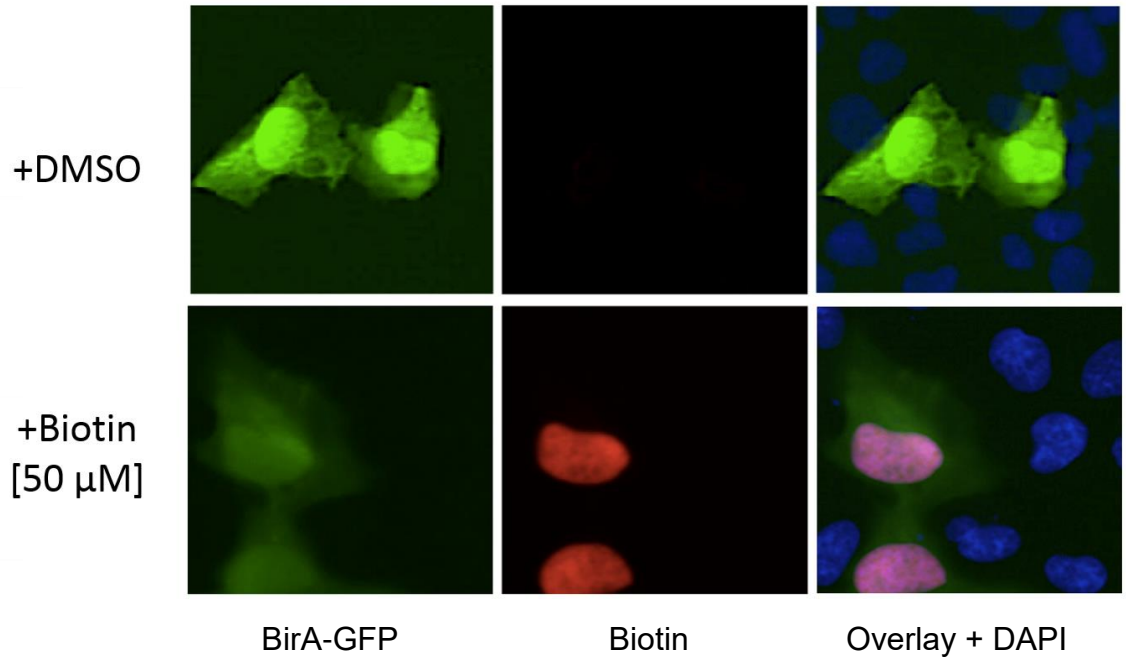

Figure 6.2. Test of the two-component biotinylation system. U2OS cells were transiently transfected with BirA-GFP and BAP-H3 expression plasmids. After 24 h, 50 µM biotin was introduced to the cell media for 5 min prior to fixation and visualisation.

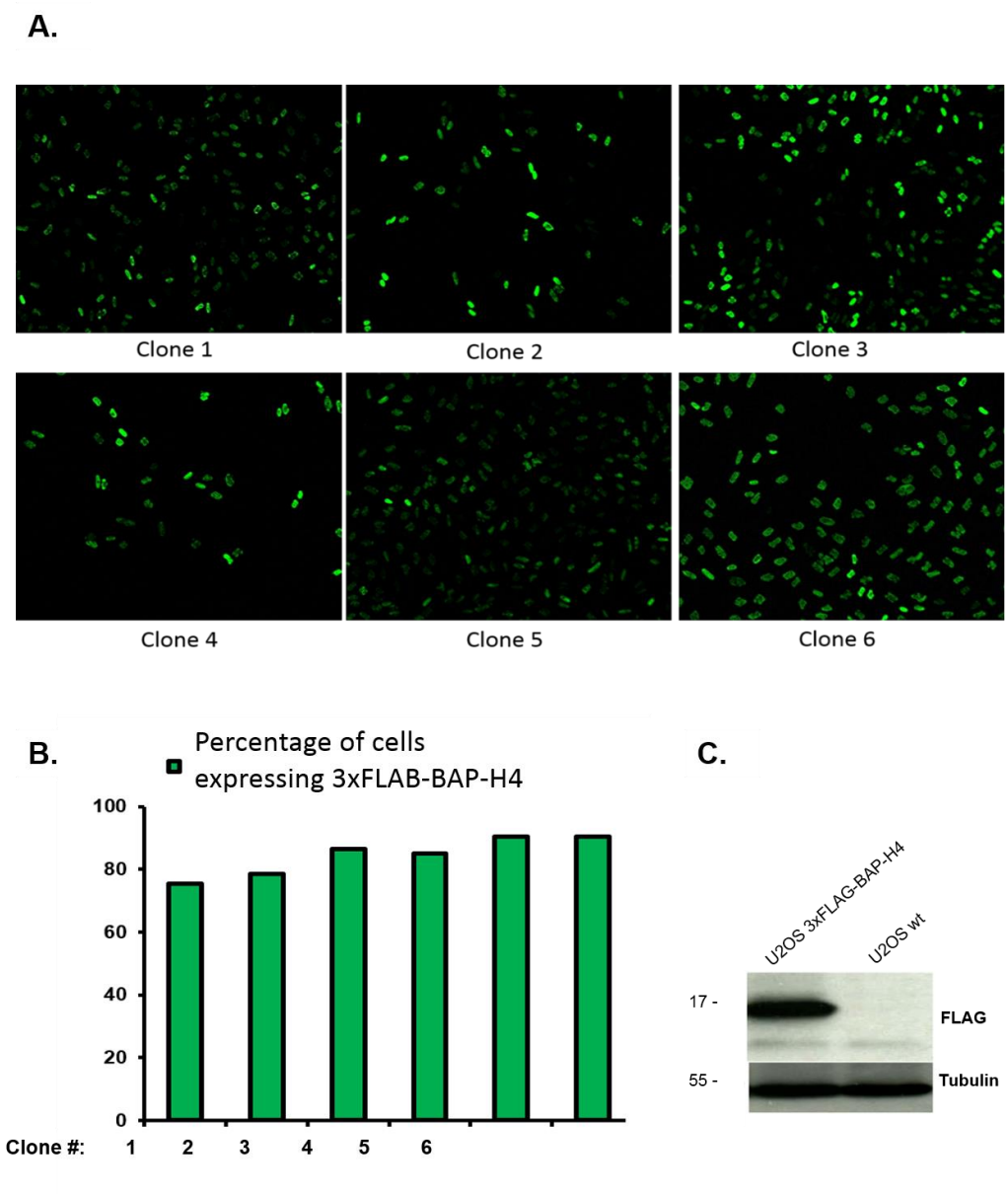

Figure 6.3. Generation of U2OS 3xFLAG-BAP-H4. A) Representative images of six U2OS clones stably expressing H4-BAP-3xFLAG construct. The cells were stained using α-FLAG antibody. Images were obtained on ScanR microscope (Olympus), 20X magnification B) Quantification of the percentage of cells expressing the 3xFLAG-BAP-H4 construct in each clone. C) Western Blot analysis of the expression of 3xFLAG-BAP-H4 construct.

Nuclear localisation of the recombinant proteins was confirmed by immunofluorescence. Furthermore, BirA-tagged proteins were recruited to the site of DNA damage, as assessed by co-localisation of the DSB marker, γH2AX, and the His-tag (**Figure 6.4**).

Due to the low transfection efficiency of the BirA-53BP1 construct, further experiments were continued using BirA-RNF168.

6.5 BirA-RNF168 BIOTINYLATES NUCLEOSOMES AT THE SITE OF DSBs

To test whether BirA-tagged RNF168 was able to induce biotinylation at the site of DSBs, U2OS 3xFLAG-BAP-H4 cells were transiently transfected with the BirA-RNF168 construct as previously described. DSBs were introduced using 50 ng/µl neocarzinostatin (NCS) treatment, followed by 1h recovery time and then 5 min treatment with biotin prior to fixation with formaldehyde.

We observed a nuclear pattern of biotinylation upon addition of biotin to the media in the U2OS 3xFLAG-BAP-H4 cells transfected with the BirA-constructs but not in the U2OS wt cells (**Figure 6.5**). Importantly, biotin foci in the cells transfected with BirA-RNF168 co-localised with 53BP1 foci, suggesting specific biotinylation of BAP tagged histones around DSBs.

Biotinylated nucleosomes were then pulled-down with streptavidin coated magnetic beads and analysed by immunoblotting. Upon DNA damage induction and biotin treatment, the samples showed enrichment in components of the nucleosome, such as H3 and H4, and importantly γH2AX, suggesting that we are indeed enriching for DSB-associated chromatin (**Figure 6.6**). However, some background biotinylation was also observed. This is due to the fact that biotin is an essential vitamin, therefore, cannot be completely depleted from the growth media, consequently DSBs caused by endogenous cellular activities also get biotinylated upon BirA-RNF168 recruitment.

Next, I attempted to identify the proteins associated with nucleosomes biotinylated by BirA-RNF168 in response to damage. To do that, HEK293 cells

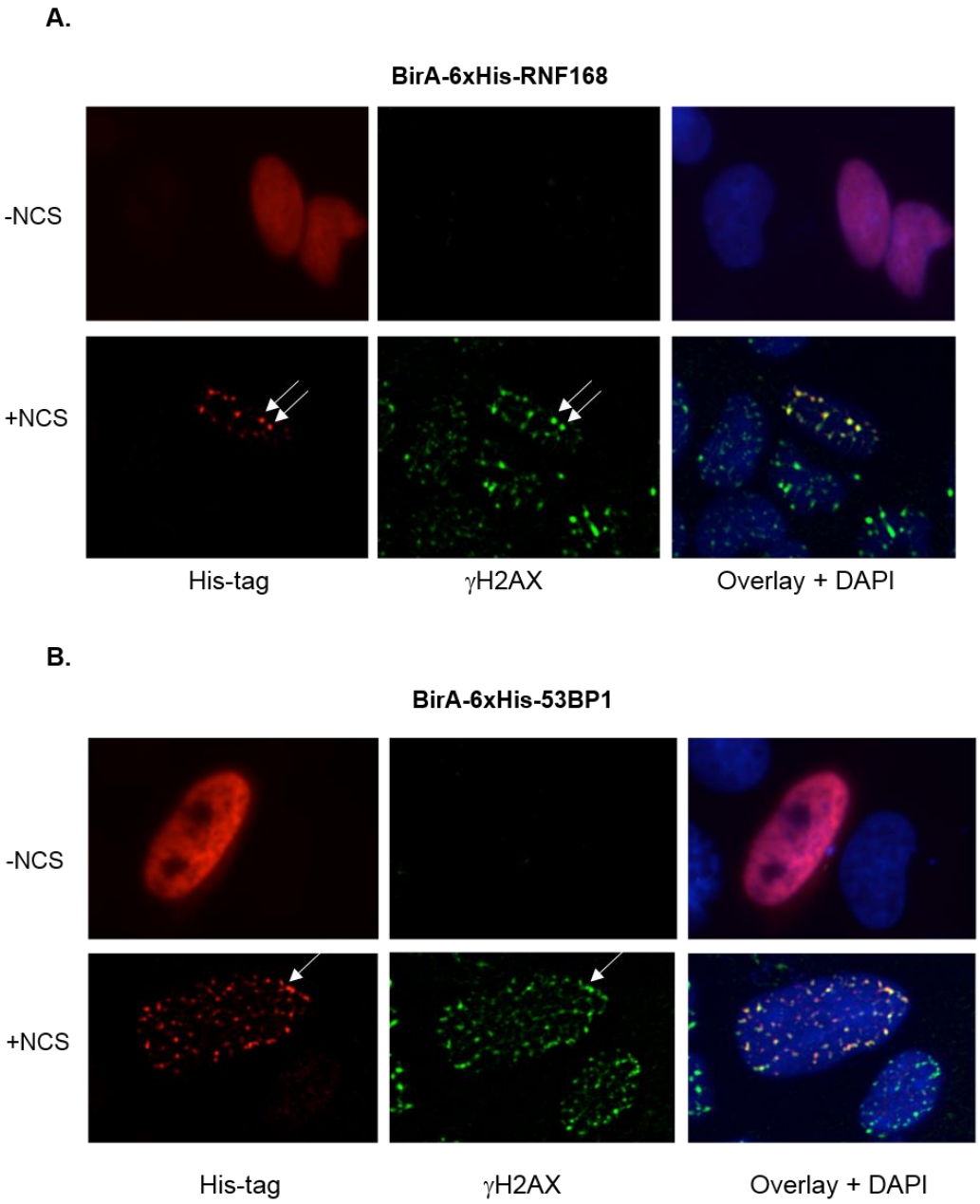

Figure 6.4. Test of BirA-constructs. A and B) Cells were transfected with BirA-tagged DNA damage proteins and damaged with 100 ng/µl of NCS. After 30 min recovery time, cells were fixed. Immunofluorescence analysis shows that both of BirA-tagged constructs localize to the nucleus and are recruited to DNA damage-dependent γH2AX foci. White arrows show examples of co-localising foci. NCS = neocarzinostatin.

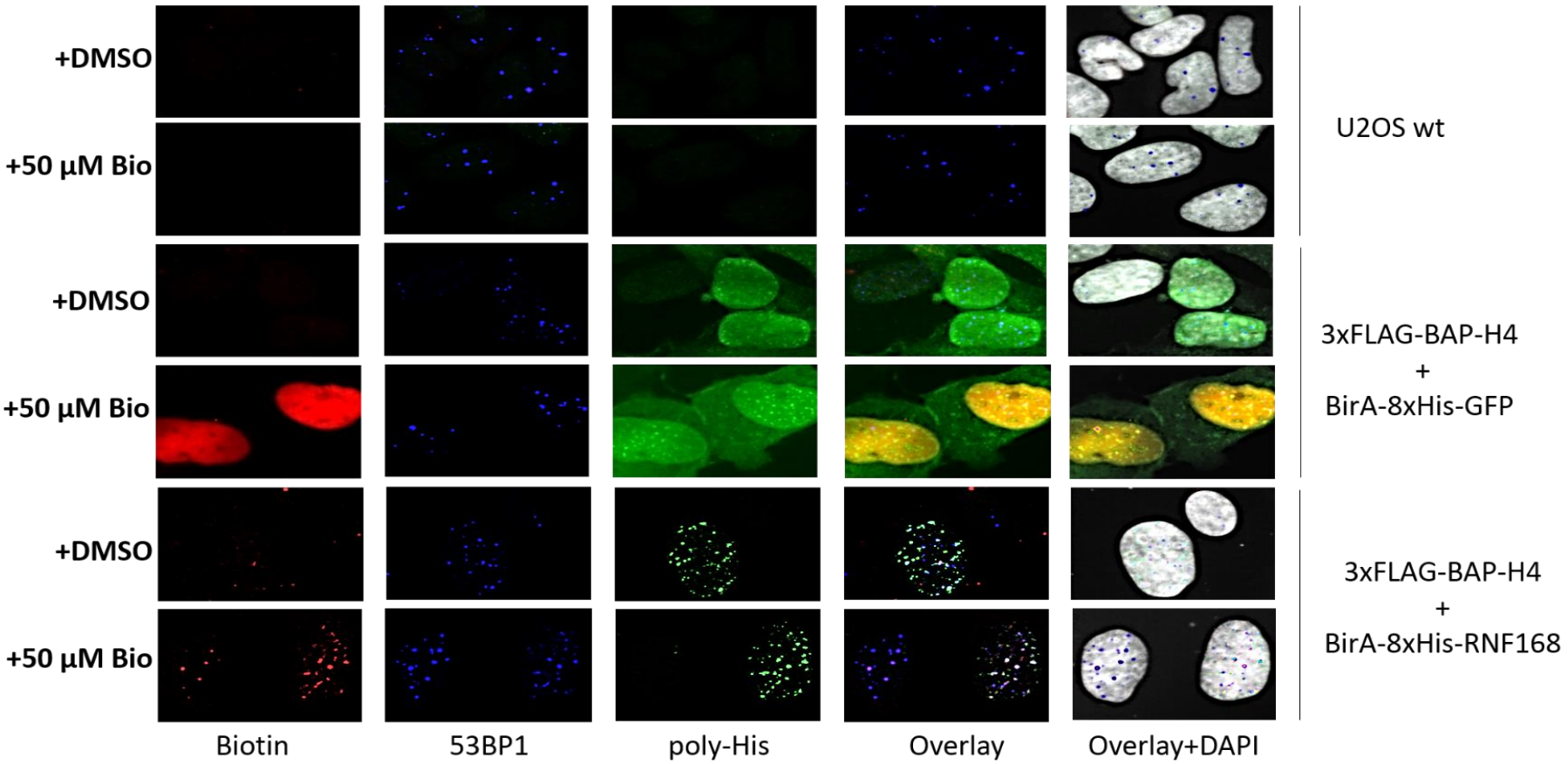

Figure 6.5. BirA-RNF 168 biotinylates the chromatin specifically at the site of DSB. Biotinylation at the site of damage does not occur in wild type U2OS cells (top panel). U2OS cells stably expressing the 3xFLAG-BAP-H4 construct were transiently transfected with BirA-8xHis-GFP (middle panel) or BirA-8xHis-RNF168 (bottom panel). Biotinylation at the site of DSBs depends on RNF168.

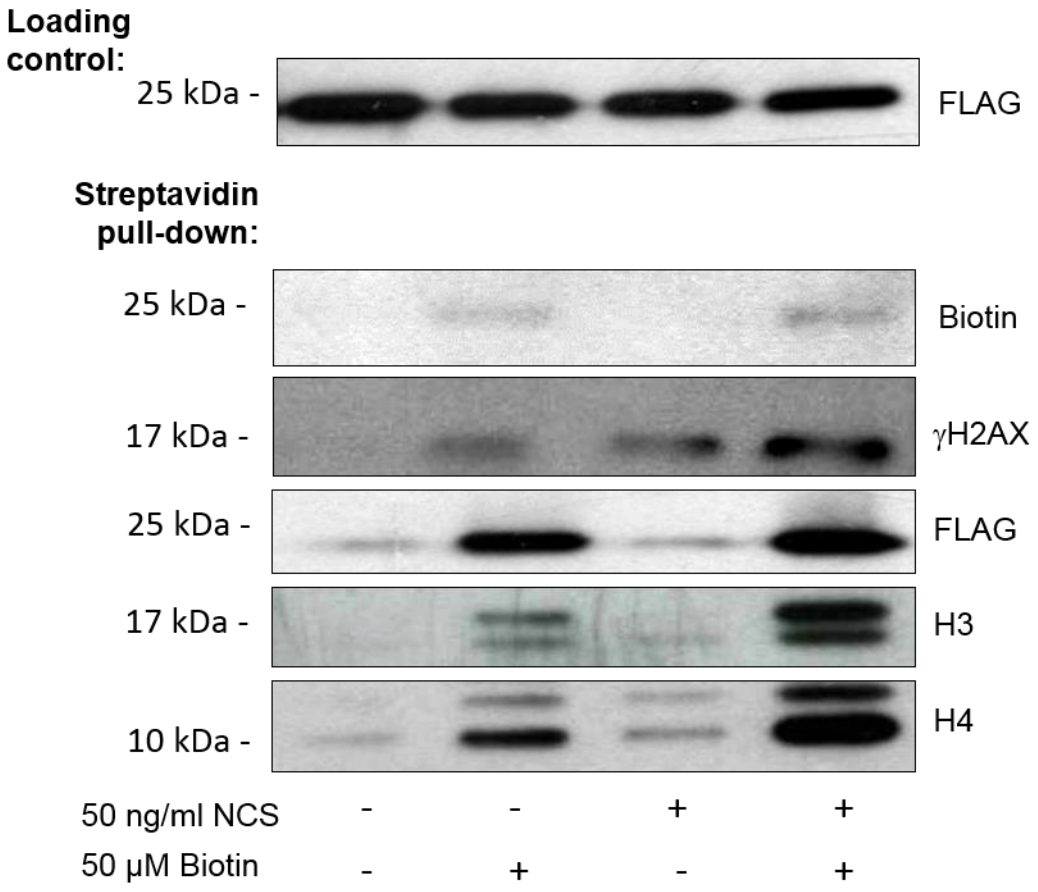

Figure 6.6 Biotinylated nucleosomes are enriched in the γH2AX variant marker of DSB. 3xFLAG-BAP-H4 U2OS cells were transiently transfected with BirA-RNF168 and incubated for 48h. Cells were damaged, or not, with NCS and treated, or not, with biotin for 5min. Biotinylated nucleosomes were pulled-down with streptavidin-coated magnetic beads. Expected size of the recombinant 3xFLAG-BAP-H4 is 23.4 kDa.

were transiently transfected with 3xFLAG-BAP-H4 and with or without BirA-RNF168. Cells were damaged with 5 Gy X-rays and allowed 1 h recovery time. Prior to collection, biotin was introduced to the cell media for 5 min. A streptavidin pull-down was performed and the samples obtained in this way were run on the SDS-PAGE gel, stained with coomassie blue (**Figure 6.7**). Pulled-down samples were analysed using a DDA MS approach (full list of identified proteins and the peptide scores are in the **Appendix Table 4**). Consistent with the idea that we are pulling-down nucleosomes from the site of DNA damage, we identified several components of the nucleosome, as well as known DDR-associated proteins (**Appendix Table 4**), indicative of pull-down of DSB-associated chromatin.

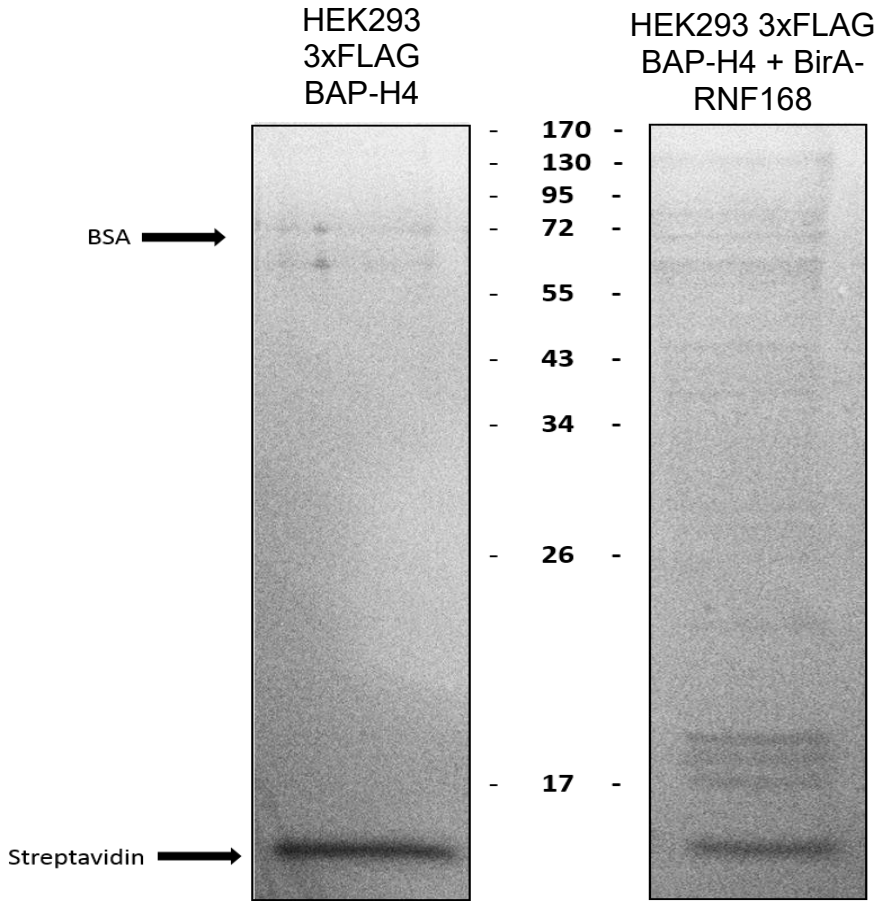

Figure 6.7 MS analysis of streptavidin pull-down of biotinylated nucleosomes. Coomassie staining of streptavidin pull-down form HEK293 cell transfected with 3xFLAG-BAP-H4 -/+ BirA-RNF168. Marker in the middle corresponds to protein molecular mass in kDa.

6.6 DISCUSSION

Here I have presented as a proof-of-principle, a two-component system for the labelling of DNA damage associated nucleosomes. I have shown BirA-biotin ligase tagged RNF168 and 53BP1 are recruited to the sites of γH2AX foci, where they induce biotinylation of BAP-tagged histone H4 in a proximity-dependent manner (**Figure 6.4 and Figure 6.5**). Streptavidin has been used to pull-down biotinylated nucleosomes, and consistent with the idea that these nucleosomes are located at the site of DNA damage, they were enriched for γH2AX (**Figure 6.6**), as well as other previously described DDR factors, such as RNF168 or DNA-PK (**Figure 6.7**).

During this work, stable cell lines expressing the biotin acceptor peptide fused to H4 (HEK293 and U2OS 3xFLAG-BAP-H4) were produced (**Figure 6.6**). Since biotin is an essential vitamin and the cells would be unable to grow healthily without it, BirA-tagged components were transiently transfected to avoid continuous biotinylation in response to endogenous DSBs. This system therefore relies on a high transfection efficiency. However, we found that the transfection efficiency varied from experiment to experiment (data not shown). Therefore, in future it would be necessary to optimise this process in order to be able to produce reproducible data.

The particular strength of this method is that it does not rely on the use of antibodies. In contrast to the S139phos mark on histone H2AX, which is removed once repair has been completed, it has been previously shown that the biotin label is stable for at least 24 h, suggesting the possibility that tracking of the breaks that have been already repaired would be possible, and potentially with tracking continued to a daughter cell. This would be particularly useful in addressing questions about DNA damage inflicted epigenetic scaring, or in other words, can DDR modify chromatin in the way that indicates recent repair events.

As mentioned in the introduction, γH2AX is depleted in the immediate proximity of the break (1-2 kbp), therefore, it is not possible to map histone

modifications associated with those nucleosomes using the γH2AX-ChIP method described in the Chapter 3. By fusing BirA to different DDR and repair proteins, such as Ku70/80 or XRCC4, which are known to be recruited only very close to the DNA break, it would be theoretically possible to biotin label and hence identify the DSB-proximal nucleosomes and track them over time.

7 CHAPTER SEVEN: DISCUSSION

7.1 UNDERSTANDING OF MOLECULAR PATHWAYS INVOLVED IN DDR IS CLINICALLY RELEVANT

On a daily basis we are exposed to factors that either directly or indirectly are able to induce DNA DSBs. A failure to repair them can be very detrimental to human health, which is illustrated by the range of pathologies associated with deficiencies in factors involved in repair or signalling processes. Some of the outcomes of improper repair include gene mutations, which may consequently lead to cancer development, or may cause cell death, which may be highly impacting if a given cell is a stem cell or post-mitotic neuron, as this may contribute to premature aging and neurodegeneration, respectively.

DSB-inducing sources are commonly used in diagnostic medical devices, such as X-rays and computed tomography. Importantly, DNA damage-inducing therapies, such as radiation therapy (RT) or chemotherapeutic drugs, for example etoposide, are the most common cancer treatments. During these treatments healthy tissue, as well as cancer are exposed to the DNA damaging agents.

In developed countries, more than half of patients with cancer receive RT at some stage of disease management (Begg, Stewart and Vens, 2011). A small percentage of those patients (~5%) develop severe normal tissue toxicity, the mechanism of which is still not exactly clear, but is thought to be linked to an intrinsic inability to resolve IR-induced DSBs (Nahas and Gatti, 2009). Importantly, based on the response of this small subgroup, RT doses for all the patients are decreased. Therefore a better understanding of the basis for this radiosensitivity would permit the development of predictive tests, which would identify these patients and allow dose escalation for well responding patients.

RT induces intricate molecular responses in cells, which may repair the break (accurately or inaccurately) or prevent propagation of the damage by inducting cellular senesce or apoptosis. Since the DNA repair machinery is often compromised in cancer cells, they are frequently more susceptible to

the toxic effects of DSBs, leading to cell death and tumour shrinkage. As opposed to cancer cells, healthy tissue has been shown to be more efficient in accurately repairing DNA damage. However, repair capacity has been shown to be dependent on the damage dose, as well as age, gender and genetic background. While highly successful, RT has been shown to significantly increase the risk of development of secondary malignancies. Even exposure to very low doses of IR has been shown to be associated with increase in cancer risk and the higher the accumulated dose, the greater risk of the cancer development (Mole, 1990; Leuraud *et al.*, 2015).

The faithful repair of DNA damage in healthy tissue is crucial to genomic integrity. Significant collective effort is going into the elucidating steps and factors involved in the repair and DDR. Improved understanding of molecular responses underlying these pathways is essential to promote the design of improved cancer therapies, and to advance the efficacy of RT.

7.2 REQUIREMENT FOR A NEW METHOD TO EXAMINE THE CHROMATIN RESPONSE TO DSBS

The discovery of DNA damage induced phosphorylation of the histone variant H2AX gave rise to a new area of research interest in the field of the DDR and repair, bringing about the realisation that chromatin plays an integral role in mediating these processes. Since that initial discovery, multiple reports have implicated a plethora of histone residues in the cellular response to DSBs, suggesting that dramatic remodelling of the chromatin is an essential part of the repair process (Hunt *et al.*, 2013). However, conflicting reports can be found for many of these marks.

One possible explanation for these discrepancies could be the use of antibodies. Owing to the nature of histone proteins being heavily modified, antibodies to histone modifications have often been shown to struggle with the recognition of their intended target, potentially due to epitope obstruction or to the antibody being biased to recognise the epitope only within a specific

PTM pattern. Additionally, the low throughput capabilities of antibody-based approaches constitute a major issue when studying multiple modifications simultaneously. This prompted us to develop a new method for investigation of histone modifications at the site of DNA damage, which I have presented in this thesis.

7.3 IR DOES NOT INDUCE SIGNIFICANT CHANGES IN THE MAJORITY OF PTMS ON HISTONE H3 AND H4

In Chapter 3 I have presented a novel method to study DSB associated histone PTMs. In this approach, a highly specific antibody to γH2AX was used to recover nucleosomes flanking DSBs induced with IR. Using a targeted MS method, I was able to sensitively detect and quantify multiple histone peptides in a single run to gain insight into the temporal, as well as dose-dependent, dynamics of histone PTMs associated with IR-induced γH2AX-nucleosomes. I was able to show that the majority of the associated histone PTMs remain stable over the large γH2AX domains.

Interestingly, these results corroborate those found with recent ChIP studies, where it was found that γH2AX is the major histone PTM changing over large (up to 1 Mbp) regions flanking the breaks (Clouaire *et al.*, 2018). However, they found few changes happening over smaller regions, suggesting our γH2AX-ChIP/MS is perhaps not sensitive enough to detect them.

However, while this method has the advantage that it provides an average view over multiple DSBs, a disadvantage is that I cannot exclude the possibility that some of these changes may occur at a specific subset of breaks, or at regions much smaller than γH2AX, i.e. if DNA damage induces the changes in the PTMs that do not spread as extensively as γH2AX, there is a possibility that we would not be able to sensitively detect those changes. Similarly, since γH2AX is depleted near the site of break, the PTMs in these regions cannot be quantified using γH2AX-ChIP. In addition to that, we

cannot also exclude the possibility that some of the chromatin changes may occur in larger domains devoid of γH2AX. To address that, an *in vivo* biotinylation system presented in Chapter 6 could theoretically be used to also pull down non-γH2AX nucleosomes associated with DSBs. Additionally, by tagging DDR and repair proteins with BirA known to be recruited only near the sites of breaks (e.g. Ku70/80 or XRCC4), we could label the nucleosomes directly flanking the break, permitting us to analyse these regions. In the future, this method could be also combined with cross-linking to identify novel histone PTMs and components of the repair complexes.

7.4 H2A(X) K15Ub AS THE MAJOR PTM INDUCED ON γH2AX-NUCLEOSOMES IN RESPONSE TO IR AND ITS CLINICAL SIGNIFICANCE

The main modification we observed on the γH2AX-nucleosomes was ubiquitination of H2A(X) K15. The increase in the K15Ub mark was several fold higher on the γH2AX-nucleosomes compared to the global level of this mark, suggesting that this mark is specifically induced at the site of damage. I found that H2AX-like K15 was ubiquitinated faster than H2A K15. Importantly, I showed that the ubiquitination response is non-linear with respect to dose since it gets saturated following exposure to doses as low as in the range 2-3 Gy, and the amount of H2A(X) K15Ub diminishes per γH2AX with increasing doses of IR.

These observations have an important implication when considering high dose exposures such as the doses received during radiotherapy. It has been observed that at high IR doses, damaged cells struggle to recruit 53BP1, resulting in a switch from error-free RAD51-dependent homology-dependent repair to the more mutagenic RAD52-dependent SSA pathway, suggesting that 53BP1 is required for RAD51 foci formation and HR (Ochs *et al.*, 2016). However, 53BP1, the recruitment of which requires H2AK15Ub, is also required to promote c-NHEJ, potentially affecting the fidelity of DSB re-

joining. Dose fractionation during RT is known to enhance the normal tissue response to radiation and, in cellular studies, dose splitting or low dose rate radiation is also known to enhance survival (Bedford and Cornforth, 1987). In these cellular studies using G0/G1 cells where only c-NHEJ takes place, the number of chromosomal translocations closely parallels survival and dose splitting diminishes translocation events and enhances survival. C-NHEJ proteins are abundant and re-joining occurs efficiently even at high doses (Bedford and Cornforth, 1987; Cornforth and Bedford, 1987). This raises the possibility that chromatin changes (including PTMs) at the DSB site function to prevent translocations and that at higher doses a critical factor becomes limiting. Our findings raise the possibility that H2AK15Ub could be the PTM that is limiting at higher doses. Interestingly, standard RT protocols deliver daily fractions of 2 Gy, a dose which appears to lie in the linear dose response range for H2AK15Ub.

7.5 ATM-DEPENDENT LATE REPAIRING BREAKS ARE NOT ENRICHED IN H3K9ME3 MARKS IN HUMAN CELLS

Whilst the majority of IR induced DSBs are repaired within the first 2 h after damage induction, there is a subset of slow repairing DSBs, which requires ATM kinase activity. Previous studies in murine cells showed that these ATM-dependent breaks are associated with heterochromatin (Goodarzi *et al.*, 2008). It was suggested that heterochromatin poses a barrier to the repair process and that it needs to be de-condensed to allow efficient recruitment of the repair machinery and subsequent repair. It has been also shown that chromatin compaction occurs shortly after damage induction (Ayrapetov *et al.*, 2014). Therefore we have questioned whether the ATM-dependent, late repairing breaks really originate in heterochromatin, or whether they could become heterochromatinised as a result of the DDR.

Surprisingly, my preliminary data indicates that in human cells these late repairing breaks are not associated with heterochromatin *per se*. This

assumption is based on the fact that I did not observe enrichment in H3K9me2/3 at the late, as compared to early, repairing breaks. Furthermore, using the heavy methyl SILAC labelling method to monitor the turnover of the methylation of H3K9 residue, I found no significant difference between methylation at DSBs as compared to the global rate of turnover of this mark.

DSBs within other chromatin types have also been proposed to require ATM function for their repair. Recent reports suggest that DSBs in regions of active transcription marked by H3K36me3 also show delayed repair kinetics, raising a possibility that they may also contribute to the slow DSB repair component (Aymard *et al.*, 2017). Interestingly, the antibody used to detect H3K9me3 in both, Goodarzi *et al.* (2008) and Ayrapetov *et al.*, (2014), has been shown to cross-react with other tri-methylated histone residues, including H3K4me3, H3K36me3 and H4K20me3 (The Histone Antibody Specificity Database, (Rothbart *et al.*, 2015). This raises the possibility that the apparent increase in H3K9me3 at the site of a DSB may, in fact, be an artefact of the antibody used.

ATM has also been shown to be required for the repair of breaks with ends blocked by covalent links and hairpin structures (Barlow *et al.*, 1997; Bredemeyer *et al.*, 2006; Álvarez-Quilón *et al.*, 2014; Katyal *et al.*, 2014). This suggests that difficult to repair break ends may also require ATM-dependent damage response, further contributing to the list of break-types requiring ATM.

Due to time constraints, at this stage I was not able to determine whether other types of chromatin, such as facultative heterochromatin or transcriptionally active chromatin are associated with those breaks. Therefore, the question of whether specific types of chromatin may require ATM for the repair of DSBs still remains open and additional work is clearly required to understand its role in repair. The γH2AX-ChIP/MS method developed in this thesis still has a potential to address at least some of these questions.

7.6 SUMMARY

In summary, I have developed and optimised novel methods for the enrichment, detection and quantification of histone post-translational marks associated with DSBs. I have used a γH2AX-ChIP/MS approach to demonstrate that H2AK15Ub is the major histone mark changing at DSBs. I have characterised the changes in H2AK15Ub and showed that it does not arise linearly with dose but becomes saturated at high doses. This could be explained by recent findings reporting that the ubiquitin ligase, RNF168, which deposits K15Ub becomes saturated at higher doses. Furthermore, I have discussed clinically relevant implications of this finding. Additionally, I have used this method to quantify histone H3K9 modifications in ATM deficient cells. The preliminary data from these experiments was contrary to what is currently believed, that ATM-dependent late repairing DSBs are not enriched in heterochromatin marks in human cells.

8 REFERENCES

Adam, S., Polo, S. E. and Almouzni, G. (2013) 'Transcription recovery after DNA damage requires chromatin priming by the H3.3 histone chaperone HIRA.', *Cell*, 155(1), pp. 94–106. doi: 10.1016/j.cell.2013.08.029.

Alatwi, H. E. and Downs, J. A. (2015) 'Removal of H2A.Z by INO80 promotes homologous recombination.', *EMBO reports*. EMBO Press, 16(8), pp. 986–94. doi: 10.15252/embr.201540330.

Álvarez-Quilón, A., Serrano-Benítez, A., Ariel Lieberman, J., Quintero, C., Sánchez-Gutiérrez, D., Escudero, L. M. and Cortés-Ledesma, F. (2014) 'ATM specifically mediates repair of double-strand breaks with blocked DNA ends', *Nature Communications*. Nature Publishing Group, 5(1), p. 3347. doi: 10.1038/ncomms4347.

Aymard, F., Aguirrebengoa, M., Guillou, E., Javierre, B. M., Bugler, B., Arnould, C., Rocher, V., Iacovoni, J. S., Biernacka, A., Skrzypczak, M., Ginalski, K., Rowicka, M., Fraser, P. and Legube, G. (2017) 'Genome-wide mapping of long-range contacts unveils clustering of DNA double-strand breaks at damaged active genes', *Nature Structural & Molecular Biology*. Nature Publishing Group, 24(4), pp. 353–361. doi: 10.1038/nsmb.3387.

Aymard, F., Bugler, B., Schmidt, C. K., Guillou, E., Caron, P., Briois, S., Iacovoni, J. S., Daburon, V., Miller, K. M., Jackson, S. P. and Legube, G. (2014) 'Transcriptionally active chromatin recruits homologous recombination at DNA double-strand breaks.', *Nature structural & molecular biology*. Nature Publishing Group, a division of Macmillan Publishers Limited. All Rights Reserved., 21(4), pp. 366–74. doi: 10.1038/nsmb.2796.

Ayoub, N., Jeyasekharan, A. D., Bernal, J. A. and Venkitaraman, A. R. (2008) 'HP1-β mobilization promotes chromatin changes that initiate the DNA

damage response', *Nature*. Nature Publishing Group, 453(7195), pp. 682–686. doi: 10.1038/nature06875.

Ayrapetov, M. K., Gursoy-Yuzugullu, O., Xu, C., Xu, Y. and Price, B. D. (2014a) 'DNA double-strand breaks promote methylation of histone H3 on lysine 9 and transient formation of repressive chromatin.', *Proceedings of the National Academy of Sciences of the United States of America*. National Academy of Sciences, 111(25), pp. 9169–74. doi: 10.1073/pnas.1403565111.

Ayrapetov, M. K., Gursoy-Yuzugullu, O., Xu, C., Xu, Y. and Price, B. D. (2014b) 'DNA double-strand breaks promote methylation of histone H3 on lysine 9 and transient formation of repressive chromatin.', *Proceedings of the National Academy of Sciences of the United States of America*, 111(25), pp. 9169–74. doi: 10.1073/pnas.1403565111.

Ayrapetov, M. K., Gursoy-Yuzugullu, O., Xu, C., Xu, Y. and Price, B. D. (2014c) 'DNA double-strand breaks promote methylation of histone H3 on lysine 9 and transient formation of repressive chromatin.', *Proceedings of the National Academy of Sciences of the United States of America*, 111(25), pp. 9169–74. doi: 10.1073/pnas.1403565111.

Babu, A. and Verma, R. S. (1987) 'Chromosome structure: euchromatin and heterochromatin.', *International review of cytology*, 108, pp. 1–60. Available at: http://www.ncbi.nlm.nih.gov/pubmed/2822591 (Accessed: 4 September 2018).

Baeza, J., Dowell, J. A., Smallegan, M. J., Fan, J., Amador-Noguez, D., Khan, Z. and Denu, J. M. (2014) 'Stoichiometry of Site-specific Lysine Acetylation in an Entire Proteome', *Journal of Biological Chemistry*, 289(31), pp. 21326–21338. doi: 10.1074/jbc.M114.581843.

Banerjee, S. and Mazumdar, S. (2012) 'Electrospray Ionization Mass Spectrometry: A Technique to Access the Information beyond the Molecular Weight of the Analyte', *International Journal of Analytical Chemistry*. Hindawi, 2012, pp. 1–40. doi: 10.1155/2012/282574.

Bannister, A. J. and Kouzarides, T. (2011) 'Regulation of chromatin by histone modifications', *Cell Research*. Nature Publishing Group, 21(3), pp.

381–395. doi: 10.1038/cr.2011.22.

Barlow, C., Liyanage, M., Moens, P. B., Deng, C.-X., Ried, T. and Wynshaw-Boris, A. (1997) ‘Partial rescue of the prophase I defects of Atm-deficient mice by p53 and p21 null alleles’, *Nature Genetics*. Nature Publishing Group, 17(4), pp. 462–466. doi: 10.1038/ng1297-462.

Barski, A., Cuddapah, S., Cui, K., Roh, T.-Y., Schones, D. E., Wang, Z., Wei, G., Chepelev, I. and Zhao, K. (2007) ‘High-Resolution Profiling of Histone Methylations in the Human Genome’, *Cell*, 129(4), pp. 823–837. doi: 10.1016/j.cell.2007.05.009.

Bassing, C. H., Suh, H., Ferguson, D. O., Chua, K. F., Manis, J., Eckersdorff, M., Gleason, M., Bronson, R., Lee, C. and Alt, F. W. (2003) ‘Histone H2AX: a dosage-dependent suppressor of oncogenic translocations and tumors.’, *Cell*, 114(3), pp. 359–70. Available at: http://www.ncbi.nlm.nih.gov/pubmed/12914700 (Accessed: 11 June 2018).

Bauerschmidt, C., Arrichiello, C., Burdak-Rothkamm, S., Woodcock, M., Hill, M. A., Stevens, D. L. and Rothkamm, K. (2010) ‘Cohesin promotes the repair of ionizing radiation-induced DNA double-strand breaks in replicated chromatin.’, *Nucleic acids research*. Oxford University Press, 38(2), pp. 477–87. doi: 10.1093/nar/gkp976.

Beamish, H. J., Jessberger, R., Riballo, E., Priestley, A., Blunt, T., Kysela, B. and Jeggo, P. A. (2000) ‘The C-terminal conserved domain of DNA-PKcs, missing in the SCID mouse, is required for kinase activity.’, *Nucleic acids research*. Oxford University Press, 28(7), pp. 1506–13. Available at: http://www.ncbi.nlm.nih.gov/pubmed/10710416 (Accessed: 5 September 2018).

Bedford, J. S. and Cornforth, M. N. (1987) ‘Relationship between the recovery from sublethal X-ray damage and the rejoining of chromosome breaks in normal human fibroblasts.’, *Radiation research*, 111(3), pp. 406–23. Available at: http://www.ncbi.nlm.nih.gov/pubmed/3659276 (Accessed: 21 July 2018).

Bedford, M. T. and Clarke, S. G. (2009) ‘Protein Arginine Methylation in

Mammals: Who, What, and Why', *Molecular Cell*, 33(1), pp. 1–13. doi: 10.1016/j.molcel.2008.12.013.

Begg, A. C., Stewart, F. A. and Vens, C. (2011) 'Strategies to improve radiotherapy with targeted drugs', *Nature Reviews Cancer*, 11(4), pp. 239–253. doi: 10.1038/nrc3007.

Behjati, S., Tarpey, P. S., Presneau, N., Scheipl, S., Pillay, N., Van Loo, P., Wedge, D. C., Cooke, S. L., Gundem, G., Davies, H., Nik-Zainal, S., Martin, S., McLaren, S., Goody, V., Robinson, B., Butler, A., Teague, J. W., Halai, D., Khatri, B., Myklebost, O., Baumhoer, D., Jundt, G., Hamoudi, R., Tirabosco, R., Amary, M. F., Futreal, P. A., Stratton, M. R., Campbell, P. J. and Flanagan, A. M. (2013) 'Distinct H3F3A and H3F3B driver mutations define chondroblastoma and giant cell tumor of bone', *Nature Genetics*, 45(12), pp. 1479–1482. doi: 10.1038/ng.2814.

Bernier, J., Hall, E. J. and Giaccia, A. (2004) 'Radiation oncology: a century of achievements', *Nature Reviews Cancer*. Nature Publishing Group, 4(9), pp. 737–747. doi: 10.1038/nrc1451.

Bieging, K. T., Mello, S. S. and Attardi, L. D. (2014) 'Unravelling mechanisms of p53-mediated tumour suppression', *Nature Reviews Cancer*, 14(5), pp. 359–370. doi: 10.1038/nrc3711.

Biehs, R., Steinlage, M., Barton, O., Juhász, S., Künzel, J., Spies, J., Shibata, A., Jeggo, P. A. and Löbrich, M. (2017) 'DNA Double-Strand Break Resection Occurs during Non-homologous End Joining in G1 but Is Distinct from Resection during Homologous Recombination', *Molecular Cell*, 65(4), p. 671–684.e5. doi: 10.1016/j.molcel.2016.12.016.

Bird, A. W., Yu, D. Y., Pray-Grant, M. G., Qiu, Q., Harmon, K. E., Megee, P. C., Grant, P. A., Smith, M. M. and Christman, M. F. (2002) 'Acetylation of histone H4 by Esa1 is required for DNA double-strand break repair', *Nature*, 419(6905), pp. 411–415. doi: 10.1038/nature01035.

Blackford, A. N. and Jackson, S. P. (2017) 'ATM, ATR, and DNA-PK: The Trinity at the Heart of the DNA Damage Response.', *Molecular cell*. Elsevier, 66(6), pp. 801–817. doi: 10.1016/j.molcel.2017.05.015.

Bock, I., Dhayalan, A., Kudithipudi, S., Brandt, O., Rathert, P. and Jeltsch, A. (2014) 'Detailed specificity analysis of antibodies binding to modified histone tails with peptide arrays', *Epigenetics*. Taylor & Francis, 6(2), pp. 256–263. doi: 10.4161/epi.6.2.13837.

de Boer, E., Rodriguez, P., Bonte, E., Krijgsveld, J., Katsantoni, E., Heck, A., Grosveld, F. and Strouboulis, J. (2003) 'Efficient biotinylation and single-step purification of tagged transcription factors in mammalian cells and transgenic mice.', *Proceedings of the National Academy of Sciences of the United States of America*, 100(13), pp. 7480–5. doi: 10.1073/pnas.1332608100.

Bohgaki, M., Bohgaki, T., El Ghamrasni, S., Srikumar, T., Maire, G., Panier, S., Fradet-Turcotte, A., Stewart, G. S., Raught, B., Hakem, A. and Hakem, R. (2013) 'RNF168 ubiquitylates 53BP1 and controls its response to DNA double-strand breaks.', *Proceedings of the National Academy of Sciences of the United States of America*. National Academy of Sciences, 110(52), pp. 20982–7. doi: 10.1073/pnas.1320302111.

Botuyan, M. V., Lee, J., Ward, I. M., Kim, J.-E., Thompson, J. R., Chen, J. and Mer, G. (2006a) 'Structural Basis for the Methylation State-Specific Recognition of Histone H4-K20 by 53BP1 and Crb2 in DNA Repair', *Cell*, 127(7), pp. 1361–1373. doi: 10.1016/j.cell.2006.10.043.

Botuyan, M. V., Lee, J., Ward, I. M., Kim, J.-E., Thompson, J. R., Chen, J. and Mer, G. (2006b) 'Structural Basis for the Methylation State-Specific Recognition of Histone H4-K20 by 53BP1 and Crb2 in DNA Repair', *Cell*, 127(7), pp. 1361–1373. doi: 10.1016/j.cell.2006.10.043.

Bredemeyer, A. L., Sharma, G. G., Huang, C.-Y., Helmink, B. A., Walker, L. M., Khor, K. C., Nuskey, B., Sullivan, K. E., Pandita, T. K., Bassing, C. H. and Sleckman, B. P. (2006) 'ATM stabilizes DNA double-strand-break complexes during V(D)J recombination', *Nature*. Nature Publishing Group, 442(7101), pp. 466–470. doi: 10.1038/nature04866.

Brown, E. J. and Baltimore, D. (2000) 'ATR disruption leads to chromosomal fragmentation and early embryonic lethality.', *Genes & development*. Cold Spring Harbor Laboratory Press, 14(4), pp. 397–402. Available at:

http://www.ncbi.nlm.nih.gov/pubmed/10691732 (Accessed: 5 September 2018).

Brown, L. C., Mutter, R. W. and Halyard, M. Y. (2015) 'Benefits, risks, and safety of external beam radiation therapy for breast cancer.', *International journal of women's health*. Dove Press, 7, pp. 449–58. doi: 10.2147/IJWH.S55552.

Brustel, J., Kozik, Z., Gromak, N., Savic, V. and Sweet, S. M. M. (2018) 'Large XPF-dependent deletions following misrepair of a DNA double strand break are prevented by the RNA:DNA helicase Senataxin', *Scientific Reports*, 8(1), p. 3850. doi: 10.1038/s41598-018-21806-y.

van der Burg, M., Ijspeert, H., Verkaik, N. S., Turul, T., Wiegant, W. W., Morotomi-Yano, K., Mari, P.-O., Tezcan, I., Chen, D. J., Zdzienicka, M. Z., van Dongen, J. J. M. and van Gent, D. C. (2009) 'A DNA-PKcs mutation in a radiosensitive T-B- SCID patient inhibits Artemis activation and nonhomologous end-joining.', *The Journal of clinical investigation*. American Society for Clinical Investigation, 119(1), pp. 91–8. doi: 10.1172/JCI37141.

Campisi, J. and d'Adda di Fagagna, F. (2007) 'Cellular senescence: when bad things happen to good cells', *Nature Reviews Molecular Cell Biology*. Nature Publishing Group, 8(9), pp. 729–740. doi: 10.1038/nrm2233.

Cao, J. and Yan, Q. (2012) 'Histone ubiquitination and deubiquitination in transcription, DNA damage response, and cancer.', *Frontiers in oncology*. Frontiers Media SA, 2, p. 26. doi: 10.3389/fonc.2012.00026.

Cao, X.-J., Zee, B. M. and Garcia, B. A. (2013) 'Heavy methyl-SILAC labeling coupled with liquid chromatography and high-resolution mass spectrometry to study the dynamics of site-specific histone methylation.', *Methods in molecular biology (Clifton, N.J.)*. NIH Public Access, 977, pp. 299–313. doi: 10.1007/978-1-62703-284-1_24.

Caspari, T. (2000) 'How to activate p53.', *Current biology : CB*. Elsevier, 10(8), pp. R315-7. doi: 10.1016/S0960-9822(00)00439-5.

Ceccaldi, R., Rondinelli, B. and D'Andrea, A. D. (2016) 'Repair Pathway

Choices and Consequences at the Double-Strand Break.', *Trends in cell biology*. NIH Public Access, 26(1), pp. 52–64. doi: 10.1016/j.tcb.2015.07.009.

Celeste, A., Difilippantonio, S., Difilippantonio, M. J., Fernandez-Capetillo, O., Pilch, D. R., Sedelnikova, O. A., Eckhaus, M., Ried, T., Bonner, W. M. and Nussenzweig, A. (2003) 'H2AX haploinsufficiency modifies genomic stability and tumor susceptibility.', *Cell*, 114(3), pp. 371–383. Available at: http://www.ncbi.nlm.nih.gov/pubmed/12914701 (Accessed: 11 June 2018).

Chen, I., Howarth, M., Lin, W. and Ting, A. Y. (2005) 'Site-specific labeling of cell surface proteins with biophysical probes using biotin ligase.', *Nature methods*, 2(2), pp. 99–104. doi: 10.1038/nmeth735.

Chen, Y. R., Lees-Miller, S. P., Tegtmeyer, P. and Anderson, C. W. (1991) 'The human DNA-activated protein kinase phosphorylates simian virus 40 T antigen at amino- and carboxy-terminal sites.', *Journal of virology*, 65(10), pp. 5131–40. Available at: http://www.ncbi.nlm.nih.gov/pubmed/1654434 (Accessed: 4 September 2018).

Cheng, C.-T., Kuo, C.-Y. and Ann, D. K. (2014) 'KAPtain in charge of multiple missions: Emerging roles of KAP1', *World Journal of Biological Chemistry*. Baishideng Publishing Group Inc., 5(3), p. 308. doi: 10.4331/wjbc.v5.i3.308.

Cheung, P. (2004) 'Generation and characterization of antibodies directed against di-modified histones, and comments on antibody and epitope recognition.', *Methods in enzymology*, 376, pp. 221–34. doi: 10.1016/S0076-6879(03)76015-7.

Chiu, L.-Y., Gong, F. and Miller, K. M. (2017) 'Bromodomain proteins: repairing DNA damage within chromatin.', *Philosophical transactions of the Royal Society of London. Series B, Biological sciences*. The Royal Society, 372(1731), p. 20160286. doi: 10.1098/rstb.2016.0286.

Clair, S. St. and Manfredi, J. J. (2006) 'The Dual Specificity Phosphatase Cdc25C is a Direct Target for Transcriptional Repression by the Tumor Suppressor p53', *Cell Cycle*, 5(7), pp. 709–713. doi: 10.4161/cc.5.7.2628.

Clouaire, T., Rocher, V., Lashgari, A., Arnould, C., Aguirrebengoa, M., Biernacka, A., Skrzypczak, M., Aymard, F., Fongang, B., Dojer, N., Iacovoni, J. S., Rowicka, M., Ginalski, K., Côté, J. and Legube, G. (2018) 'Comprehensive Mapping of Histone Modifications at DNA Double-Strand Breaks Deciphers Repair Pathway Chromatin Signatures', *Molecular Cell*. Elsevier, 0(0). doi: 10.1016/J.MOLCEL.2018.08.020.

Cornforth, M. N. and Bedford, J. S. (1987) 'A quantitative comparison of potentially lethal damage repair and the rejoining of interphase chromosome breaks in low passage normal human fibroblasts.', *Radiation research*, 111(3), pp. 385–405. Available at: http://www.ncbi.nlm.nih.gov/pubmed/3659275 (Accessed: 21 July 2018).

Cristini, A., Park, J.-H., Capranico, G., Legube, G., Favre, G., Sordet, O., W., G., K., S., R.H., M. and J.H., H. (2016) 'DNA-PK triggers histone ubiquitination and signaling in response to DNA double-strand breaks produced during the repair of transcription-blocking topoisomerase I lesions', *Nucleic Acids Research*. Oxford University Press, 44(3), pp. 1161–1178. doi: 10.1093/nar/gkv1196.

Cuozzo, C., Porcellini, A., Angrisano, T., Morano, A., Lee, B., Di Pardo, A., Messina, S., Iuliano, R., Fusco, A., Santillo, M. R., Muller, M. T., Chiariotti, L., Gottesman, M. E. and Avvedimento, E. V (2007) 'DNA damage, homology-directed repair, and DNA methylation.', *PLoS genetics*, 3(7), p. e110. doi: 10.1371/journal.pgen.0030110.

DeFazio, L. G., Stansel, R. M., Griffith, J. D. and Chu, G. (2002) 'Synapsis of DNA ends by DNA-dependent protein kinase', *The EMBO Journal*, 21(12), pp. 3192–3200. doi: 10.1093/emboj/cdf299.

Deriano, L. and Roth, D. B. (2013) 'Modernizing the Nonhomologous End-Joining Repertoire: Alternative and Classical NHEJ Share the Stage', *Annual Review of Genetics*, 47(1), pp. 433–455. doi: 10.1146/annurev-genet-110711-155540.

Devgan, S. S., Sanal, O., Doil, C., Nakamura, K., Nahas, S. A., Pettijohn, K., Bartek, J., Lukas, C., Lukas, J. and Gatti, R. A. (2011) 'Homozygous

deficiency of ubiquitin-ligase ring-finger protein RNF168 mimics the radiosensitivity syndrome of ataxia-telangiectasia.', *Cell death and differentiation*. Nature Publishing Group, 18(9), pp. 1500–6. doi: 10.1038/cdd.2011.18.

Dikic, I., Wakatsuki, S. and Walters, K. J. (2009) 'Ubiquitin-binding domains — from structures to functions', *Nature Reviews Molecular Cell Biology*. Nature Publishing Group, 10(10), pp. 659–671. doi: 10.1038/nrm2767.

Doil, C., Mailand, N., Bekker-Jensen, S., Menard, P., Larsen, D. H., Pepperkok, R., Ellenberg, J., Panier, S., Durocher, D., Bartek, J., Lukas, J. and Lukas, C. (2009a) 'RNF168 Binds and Amplifies Ubiquitin Conjugates on Damaged Chromosomes to Allow Accumulation of Repair Proteins', *Cell*, 136(3), pp. 435–446. doi: 10.1016/j.cell.2008.12.041.

Doil, C., Mailand, N., Bekker-Jensen, S., Menard, P., Larsen, D. H., Pepperkok, R., Ellenberg, J., Panier, S., Durocher, D., Bartek, J., Lukas, J. and Lukas, C. (2009b) 'RNF168 Binds and Amplifies Ubiquitin Conjugates on Damaged Chromosomes to Allow Accumulation of Repair Proteins', *Cell*. Cell Press, 136(3), pp. 435–446. doi: 10.1016/J.CELL.2008.12.041.

Douglas, P., Gupta, S., Morrice, N., Meek, K. and Lees-Miller, S. P. (2005) 'DNA-PK-dependent phosphorylation of Ku70/80 is not required for non-homologous end joining', *DNA Repair*, 4(9), pp. 1006–1018. doi: 10.1016/j.dnarep.2005.05.003.

Drouet, J., Delteil, C., Lefrançois, J., Concannon, P., Salles, B. and Calsou, P. (2005) 'DNA-dependent protein kinase and XRCC4-DNA ligase IV mobilization in the cell in response to DNA double strand breaks.', *The Journal of biological chemistry*. American Society for Biochemistry and Molecular Biology, 280(8), pp. 7060–9. doi: 10.1074/jbc.M410746200.

Dudley, D. D., Chaudhuri, J., Bassing, C. H. and Alt, F. W. (2005) 'Mechanism and Control of V(D)J Recombination versus Class Switch Recombination: Similarities and Differences', in *Advances in immunology*, pp. 43–112. doi: 10.1016/S0065-2776(04)86002-4.

Dunne-Daly, C. F. (1999) 'Principles of radiotherapy and radiobiology.',

Seminars in oncology nursing, 15(4), pp. 250–9. Available at: http://www.ncbi.nlm.nih.gov/pubmed/10588029 (Accessed: 25 August 2018).

Escher, C., Reiter, L., MacLean, B., Ossola, R., Herzog, F., Chilton, J., MacCoss, M. J. and Rinner, O. (2012) 'Using iRT, a normalized retention time for more targeted measurement of peptides', *PROTEOMICS*. John Wiley & Sons, Ltd, 12(8), pp. 1111–1121. doi: 10.1002/pmic.201100463.

Espada, L. and Ermolaeva, M. A. (2016) 'DNA Damage as a Critical Factor of Stem Cell Aging and Organ Homeostasis', *Current Stem Cell Reports*. Springer International Publishing, 2(3), pp. 290–298. doi: 10.1007/s40778-016-0052-6.

Espinosa, J. M. and Emerson, B. M. (2001) 'Transcriptional regulation by p53 through intrinsic DNA/chromatin binding and site-directed cofactor recruitment.', *Molecular cell*, 8(1), pp. 57–69. Available at: http://www.ncbi.nlm.nih.gov/pubmed/11511360 (Accessed: 9 September 2018).

Falck, J., Coates, J. and Jackson, S. P. (2005) 'Conserved modes of recruitment of ATM, ATR and DNA-PKcs to sites of DNA damage', *Nature*, 434(7033), pp. 605–611. doi: 10.1038/nature03442.

Falk, M., Lukasova, E., Gabrielova, B., Ondrej, V. and Kozubek, S. (2007) 'Chromatin dynamics during DSB repair', *Biochimica et Biophysica Acta (BBA) - Molecular Cell Research*. Elsevier, 1773(10), pp. 1534–1545. doi: 10.1016/J.BBAMCR.2007.07.002.

Fenton, A. L., Shirodkar, P., Macrae, C. J., Meng, L. and Koch, C. A. (2013) 'The PARP3- and ATM-dependent phosphorylation of APLF facilitates DNA double-strand break repair', *Nucleic Acids Research*. Oxford University Press, 41(7), pp. 4080–4092. doi: 10.1093/nar/gkt134.

Fernández-Suárez, M., Chen, T. S. and Ting, A. Y. (2008) 'Protein-protein interaction detection in vitro and in cells by proximity biotinylation.', *Journal of the American Chemical Society*. American Chemical Society, 130(29), pp. 9251–3. doi: 10.1021/ja801445p.

Fnu, S., Williamson, E. A., De Haro, L. P., Brenneman, M., Wray, J., Shaheen, M., Radhakrishnan, K., Lee, S.-H., Nickoloff, J. A. and Hromas, R. (2011) 'Methylation of histone H3 lysine 36 enhances DNA repair by nonhomologous end-joining', *Proceedings of the National Academy of Sciences*, 108(2), pp. 540–545. doi: 10.1073/pnas.1013571108.

Fnu, S., Williamson, E. A., De Haro, L. P., Brenneman, M., Wray, J., Shaheen, M., Radhakrishnan, K., Lee, S.-H., Nickoloff, J. A. and Hromas, R. (2011) 'Methylation of histone H3 lysine 36 enhances DNA repair by nonhomologous end-joining.', *Proceedings of the National Academy of Sciences of the United States of America*. National Academy of Sciences, 108(2), pp. 540–5. doi: 10.1073/pnas.1013571108.

Fradet-Turcotte, A., Canny, M. D., Escribano-Díaz, C., Orthwein, A., Leung, C. C. Y., Huang, H., Landry, M.-C., Kitevski-LeBlanc, J., Noordermeer, S. M., Sicheri, F. and Durocher, D. (2013) '53BP1 is a reader of the DNA-damage-induced H2A Lys 15 ubiquitin mark.', *Nature*. PMC Canada manuscript submission, 499(7456), pp. 50–4. doi: 10.1038/nature12318.

Fuks, F. (2005) 'DNA methylation and histone modifications: teaming up to silence genes', *Current Opinion in Genetics & Development*, 15(5), pp. 490–495. doi: 10.1016/j.gde.2005.08.002.

Gallien, S., Peterman, S., Kiyonami, R., Souady, J., Duriez, E., Schoen, A. and Domon, B. (2012) 'Highly multiplexed targeted proteomics using precise control of peptide retention time', *PROTEOMICS*, 12(8), pp. 1122–1133. doi: 10.1002/pmic.201100533.

Garcia, B. A., Mollah, S., Ueberheide, B. M., Busby, S. A., Muratore, T. L., Shabanowitz, J. and Hunt, D. F. (2007a) 'Chemical derivatization of histones for facilitated analysis by mass spectrometry.', *Nature protocols*. NIH Public Access, 2(4), pp. 933–8. doi: 10.1038/nprot.2007.106.

Garcia, B. A., Mollah, S., Ueberheide, B. M., Busby, S. A., Muratore, T. L., Shabanowitz, J. and Hunt, D. F. (2007b) 'Chemical derivatization of histones for facilitated analysis by mass spectrometry.', *Nature protocols*. NIH Public Access, 2(4), pp. 933–8. doi: 10.1038/nprot.2007.106.

Gatti, M., Pinato, S., Maspero, E., Soffientini, P., Polo, S. and Penengo, L. (2012) ‘A novel ubiquitin mark at the N-terminal tail of histone H2As targeted by RNF168 ubiquitin ligase.’, *Cell cycle (Georgetown, Tex.)*. Taylor & Francis, 11(13), pp. 2538–44. doi: 10.4161/cc.20919.

Giono, L. E. and Manfredi, J. J. (2006) ‘The p53 tumor suppressor participates in multiple cell cycle checkpoints’, *Journal of Cellular Physiology*, 209(1), pp. 13–20. doi: 10.1002/jcp.20689.

Gómez-Herreros, F., Zagnoli-Vieira, G., Ntai, I., Martínez-Macías, M. I., Anderson, R. M., Herrero-Ruíz, A. and Caldecott, K. W. (2017) ‘TDP2 suppresses chromosomal translocations induced by DNA topoisomerase II during gene transcription’, *Nature Communications*. Nature Publishing Group, 8(1), p. 233. doi: 10.1038/s41467-017-00307-y.

Gong, F., Clouaire, T., Aguirrebengoa, M., Legube, G. and Miller, K. M. (2017) ‘Histone demethylase KDM5A regulates the ZMYND8-NuRD chromatin remodeler to promote DNA repair.’, *The Journal of cell biology*. Rockefeller University Press, 216(7), pp. 1959–1974. doi: 10.1083/jcb.201611135.

Goodarzi, A. A., Jeggo, P. and Lobrich, M. (2010) ‘The influence of heterochromatin on DNA double strand break repair: Getting the strong, silent type to relax.’, *DNA repair*, 9(12), pp. 1273–82. doi: 10.1016/j.dnarep.2010.09.013.

Goodarzi, A. A., Noon, A. T., Deckbar, D., Ziv, Y., Shiloh, Y., Löbrich, M. and Jeggo, P. A. (2008a) ‘ATM Signaling Facilitates Repair of DNA Double-Strand Breaks Associated with Heterochromatin’, *Molecular Cell*, 31(2), pp. 167–177. doi: 10.1016/j.molcel.2008.05.017.

Goodarzi, A. A., Noon, A. T., Deckbar, D., Ziv, Y., Shiloh, Y., Löbrich, M. and Jeggo, P. A. (2008b) ‘ATM Signaling Facilitates Repair of DNA Double-Strand Breaks Associated with Heterochromatin’, *Molecular Cell*, 31(2), pp. 167–177. doi: 10.1016/j.molcel.2008.05.017.

Goodarzi, A. A., Noon, A. T., Deckbar, D., Ziv, Y., Shiloh, Y., Löbrich, M. and Jeggo, P. A. (2008) ‘ATM signaling facilitates repair of DNA double-strand

breaks associated with heterochromatin.', *Molecular cell*, 31(2), pp. 167–77. doi: 10.1016/j.molcel.2008.05.017.

Goodarzi, A. A., Noon, A. T. and Jeggo, P. A. (2009) 'The impact of heterochromatin on DSB repair.', *Biochemical Society transactions*. Portland Press Limited, 37(Pt 3), pp. 569–76. doi: 10.1042/BST0370569.

Goodarzi, A. A., Yu, Y., Riballo, E., Douglas, P., Walker, S. A., Ye, R., Härer, C., Marchetti, C., Morrice, N., Jeggo, P. A. and Lees-Miller, S. P. (2006) 'DNA-PK autophosphorylation facilitates Artemis endonuclease activity.', *The EMBO journal*. European Molecular Biology Organization, 25(16), pp. 3880–9. doi: 10.1038/sj.emboj.7601255.

Green, C. M. and Almouzni, G. (2003) 'Local action of the chromatin assembly factor CAF-1 at sites of nucleotide excision repair in vivo.', *The EMBO journal*. European Molecular Biology Organization, 22(19), pp. 5163–74. doi: 10.1093/emboj/cdg478.

Greer, E. L. and Shi, Y. (2012) 'Histone methylation: a dynamic mark in health, disease and inheritance', *Nature Reviews Genetics*. Nature Publishing Group, 13(5), pp. 343–357. doi: 10.1038/nrg3173.

Groh, M., Albulescu, L. O., Cristini, A. and Gromak, N. (2017) 'Senataxin: Genome Guardian at the Interface of Transcription and Neurodegeneration', *Journal of Molecular Biology*, 429(21), pp. 3181–3195. doi: 10.1016/j.jmb.2016.10.021.

Groselj, B., Sharma, N. L., Hamdy, F. C., Kerr, M. and Kiltie, A. E. (2013) 'Histone deacetylase inhibitors as radiosensitisers: effects on DNA damage signalling and repair', *British Journal of Cancer*, 108(4), pp. 748–754. doi: 10.1038/bjc.2013.21.

Gudjonsson, T., Altmeyer, M., Savic, V., Toledo, L., Dinant, C., Grøfte, M., Bartkova, J., Poulsen, M., Oka, Y., Bekker-Jensen, S., Mailand, N., Neumann, B., Heriche, J.-K., Shearer, R., Saunders, D., Bartek, J., Lukas, J. and Lukas, C. (2012a) 'TRIP12 and UBR5 Suppress Spreading of Chromatin Ubiquitylation at Damaged Chromosomes', *Cell*. Cell Press, 150(4), pp. 697–709. doi: 10.1016/J.CELL.2012.06.039.

Gudjonsson, T., Altmeyer, M., Savic, V., Toledo, L., Dinant, C., Grøfte, M., Bartkova, J., Poulsen, M., Oka, Y., Bekker-Jensen, S., Mailand, N., Neumann, B., Heriche, J.-K., Shearer, R., Saunders, D., Bartek, J., Lukas, J. and Lukas, C. (2012b) 'TRIP12 and UBR5 suppress spreading of chromatin ubiquitylation at damaged chromosomes.', *Cell*, 150(4), pp. 697–709. doi: 10.1016/j.cell.2012.06.039.

Gupta, A., Sharma, G. G., Young, C. S. H., Agarwal, M., Smith, E. R., Paull, T. T., Lucchesi, J. C., Khanna, K. K., Ludwig, T. and Pandita, T. K. (2005) 'Involvement of Human MOF in ATM Function', *Molecular and Cellular Biology*, 25(12), pp. 5292–5305. doi: 10.1128/MCB.25.12.5292-5305.2005.

Gupta, R. A., Shah, N., Wang, K. C., Kim, J., Horlings, H. M., Wong, D. J., Tsai, M.-C., Hung, T., Argani, P., Rinn, J. L., Wang, Y., Brzoska, P., Kong, B., Li, R., West, R. B., van de Vijver, M. J., Sukumar, S. and Chang, H. Y. (2010) 'Long non-coding RNA HOTAIR reprograms chromatin state to promote cancer metastasis', *Nature*, 464(7291), pp. 1071–1076. doi: 10.1038/nature08975.

Gursoy-Yuzugullu, O., Ayrapetov, M. K. and Price, B. D. (2015) 'Histone chaperone Anp32e removes H2A.Z from DNA double-strand breaks and promotes nucleosome reorganization and DNA repair', *Proceedings of the National Academy of Sciences*, 112(24), pp. 7507–7512. doi: 10.1073/pnas.1504868112.

Haber, D. A. and Fearon, E. R. (1998) 'The promise of cancer genetics.', *Lancet (London, England)*. Elsevier, 351 Suppl 2, p. SII1-8. doi: 10.1016/S0140-6736(98)90326-9.

Hathaway, N. A., Bell, O., Hodges, C., Miller, E. L., Neel, D. S. and Crabtree, G. R. (2012) 'Dynamics and Memory of Heterochromatin in Living Cells', *Cell*, 149(7), pp. 1447–1460. doi: 10.1016/j.cell.2012.03.052.

Hatimy, A. A., Browne, M. J. G., Flaus, A. and Sweet, S. M. M. (2015a) 'Histone H2AX Y142 phosphorylation is a low abundance modification', *International Journal of Mass Spectrometry*. Elsevier, 391, pp. 139–145. doi: 10.1016/J.IJMS.2015.07.028.

Hatimy, A. A., Browne, M. J. G., Flaus, A. and Sweet, S. M. M. (2015b) ‘Histone H2AX Y142 phosphorylation is a low abundance modification’, *International Journal of Mass Spectrometry*. Elsevier, 391, pp. 139–145. doi: 10.1016/J.IJMS.2015.07.028.

Haupt, S., Berger, M., Goldberg, Z. and Haupt, Y. (2003) ‘Apoptosis - the p53 network.’, *Journal of cell science*. The Company of Biologists Ltd, 116(Pt 20), pp. 4077–85. doi: 10.1242/jcs.00739.

Haupt, Y., Maya, R., Kazaz, A. and Oren, M. (1997) ‘Mdm2 promotes the rapid degradation of p53’, *Nature*, 387(6630), pp. 296–299. doi: 10.1038/387296a0.

Hickey, B. E., James, M. L., Lehman, M., Hider, P. N., Jeffery, M., Francis, D. P. and See, A. M. (2016) ‘Hypofractionated radiation therapy for early breast cancer’, *Cochrane Database of Systematic Reviews*, 7, p. CD003860. doi: 10.1002/14651858.CD003860.pub4.

Hickson, I., Zhao, Y., Richardson, C. J., Green, S. J., Martin, N. M. B., Orr, A. I., Reaper, P. M., Jackson, S. P., Curtin, N. J. and Smith, G. C. M. (2004) ‘Identification and Characterization of a Novel and Specific Inhibitor of the Ataxia-Telangiectasia Mutated Kinase ATM’, *Cancer Research*, 64(24), pp. 9152–9159. doi: 10.1158/0008-5472.CAN-04-2727.

Ho, J. S. L., Ma, W., Mao, D. Y. L. and Benchimol, S. (2005) ‘p53-Dependent transcriptional repression of c-myc is required for G1 cell cycle arrest.’, *Molecular and cellular biology*. American Society for Microbiology (ASM), 25(17), pp. 7423–31. doi: 10.1128/MCB.25.17.7423-7431.2005.

Hoeijmakers, J. H. J. (2009) ‘DNA Damage, Aging, and Cancer’, *New England Journal of Medicine*. Massachusetts Medical Society , 361(15), pp. 1475–1485. doi: 10.1056/NEJMra0804615.

Hoeijmakers, J. H. J. (2009) ‘DNA damage, aging, and cancer.’, *New England Journal of Medicine*, 361(15), pp. 1475–85. Available at: http://www.ncbi.nlm.nih.gov/pubmed/19812404.

Hofmann, R. M. and Pickart, C. M. (1999) ‘Noncanonical MMS2-encoded

ubiquitin-conjugating enzyme functions in assembly of novel polyubiquitin chains for DNA repair.', *Cell*, 96(5), pp. 645–53. Available at: http://www.ncbi.nlm.nih.gov/pubmed/10089880 (Accessed: 7 August 2018).

Hoofnagle, A. N., Whiteaker, J. R., Carr, S. A., Kuhn, E., Liu, T., Massoni, S. A., Thomas, S. N., Townsend, R. R., Zimmerman, L. J., Boja, E., Chen, J., Crimmins, D. L., Davies, S. R., Gao, Y., Hiltke, T. R., Ketchum, K. A., Kinsinger, C. R., Mesri, M., Meyer, M. R., Qian, W.-J., Schoenherr, R. M., Scott, M. G., Shi, T., Whiteley, G. R., Wrobel, J. A., Wu, C., Ackermann, B. L., Aebersold, R., Barnidge, D. R., Bunk, D. M., Clarke, N., Fishman, J. B., Grant, R. P., Kusebauch, U., Kushnir, M. M., Lowenthal, M. S., Moritz, R. L., Neubert, H., Patterson, S. D., Rockwood, A. L., Rogers, J., Singh, R. J., Van Eyk, J. E., Wong, S. H., Zhang, S., Chan, D. W., Chen, X., Ellis, M. J., Liebler, D. C., Rodland, K. D., Rodriguez, H., Smith, R. D., Zhang, Z., Zhang, H. and Paulovich, A. G. (2016) 'Recommendations for the Generation, Quantification, Storage, and Handling of Peptides Used for Mass Spectrometry-Based Assays.', *Clinical chemistry*. NIH Public Access, 62(1), pp. 48–69. doi: 10.1373/clinchem.2015.250563.

Horton, J. R., Upadhyay, A. K., Qi, H. H., Zhang, X., Shi, Y. and Cheng, X. (2010) 'Enzymatic and structural insights for substrate specificity of a family of jumonji histone lysine demethylases', *Nature Structural & Molecular Biology*. Nature Publishing Group, 17(1), pp. 38–43. doi: 10.1038/nsmb.1753.

Howarth, M., Takao, K., Hayashi, Y. and Ting, A. Y. (2005) 'Targeting quantum dots to surface proteins in living cells with biotin ligase.', *Proceedings of the National Academy of Sciences of the United States of America*, 102(21), pp. 7583–8. doi: 10.1073/pnas.0503125102.

Hsiao, K.-Y. and Mizzen, C. A. (2013) 'Histone H4 deacetylation facilitates 53BP1 DNA damage signaling and double-strand break repair', *Journal of Molecular Cell Biology*, 5(3), pp. 157–165. doi: 10.1093/jmcb/mjs066.

Hsiao, K. and Mizzen, C. A. (2013) 'Histone H 4 deacetylation facilitates 53 BP 1 DNA damage signaling and double-strand break repair', 4(0), pp. 1–9.

Hu, Q., Botuyan, M. V., Cui, G., Zhao, D. and Mer, G. (2017) 'Mechanisms of

Ubiquitin-Nucleosome Recognition and Regulation of 53BP1 Chromatin Recruitment by RNF168/169 and RAD18', *Molecular Cell*. Cell Press, 66(4), p. 473–487.e9. doi: 10.1016/J.MOLCEL.2017.04.009.

Huen, M. S. Y., Grant, R., Manke, I., Minn, K., Yu, X., Yaffe, M. B. and Chen, J. (2007) 'RNF8 Transduces the DNA-Damage Signal via Histone Ubiquitylation and Checkpoint Protein Assembly', *Cell*. Cell Press, 131(5), pp. 901–914. doi: 10.1016/J.CELL.2007.09.041.

Huen, M. S. Y., Grant, R., Manke, I., Minn, K., Yu, X., Yaffe, M. B. and Chen, J. (2007) 'RNF8 transduces the DNA-damage signal via histone ubiquitylation and checkpoint protein assembly.', *Cell*. NIH Public Access, 131(5), pp. 901–14. doi: 10.1016/j.cell.2007.09.041.

Huertas, P. and Jackson, S. P. (2009) 'Human CtIP Mediates Cell Cycle Control of DNA End Resection and Double Strand Break Repair', *Journal of Biological Chemistry*, 284(14), pp. 9558–9565. doi: 10.1074/jbc.M808906200.

Hung, P. J., Johnson, B., Chen, B.-R., Byrum, A. K., Bredemeyer, A. L., Yewdell, W. T., Johnson, T. E., Lee, B. J., Deivasigamani, S., Hindi, I., Amatya, P., Gross, M. L., Paull, T. T., Pisapia, D. J., Chaudhuri, J., Petrini, J. J. H., Mosammaparast, N., Amarasinghe, G. K., Zha, S., Tyler, J. K. and Sleckman, B. P. (2018) 'MRI Is a DNA Damage Response Adaptor during Classical Non-homologous End Joining.', *Molecular cell*. Elsevier, 71(2), p. 332–342.e8. doi: 10.1016/j.molcel.2018.06.018.

Hunt, C. R., Ramnarain, D., Horikoshi, N., Iyengar, P., Pandita, R. K., Shay, J. W. and Pandita, T. K. (2013) 'Histone modifications and DNA double-strand break repair after exposure to ionizing radiations.', *Radiation research*. NIH Public Access, 179(4), pp. 383–92. doi: 10.1667/RR3308.2.

Huyen, Y., Zgheib, O., DiTullio Jr, R. A., Gorgoulis, V. G., Zacharatos, P., Petty, T. J., Sheston, E. A., Mellert, H. S., Stavridi, E. S. and Halazonetis, T. D. (2004) 'Methylated lysine 79 of histone H3 targets 53BP1 to DNA double-strand breaks', *Nature*. Nature Publishing Group, 432(7015), pp. 406–411. doi: 10.1038/nature03114.

Huynh, J. L. and Casaccia, P. (2013) 'Epigenetic mechanisms in multiple

sclerosis: implications for pathogenesis and treatment.', *The Lancet. Neurology*. Elsevier, 12(2), pp. 195–206. doi: 10.1016/S1474-4422(12)70309-5.

Hwang, J. K., Alt, F. W. and Yeap, L.-S. (2015) 'Related Mechanisms of Antibody Somatic Hypermutation and Class Switch Recombination', in *Mobile DNA III*. American Society of Microbiology, pp. 325–348. doi: 10.1128/microbiolspec.MDNA3-0037-2014.

Hyun, K., Jeon, J., Park, K. and Kim, J. (2017) 'Writing, erasing and reading histone lysine methylations', *Experimental & Molecular Medicine*. Nature Publishing Group, 49(4), pp. e324–e324. doi: 10.1038/emm.2017.11.

Iacovoni, J. S., Caron, P., Lassadi, I., Nicolas, E., Massip, L., Trouche, D. and Legube, G. (2010a) 'High-resolution profiling of gammaH2AX around DNA double strand breaks in the mammalian genome.', *The EMBO journal*. European Molecular Biology Organization, 29(8), pp. 1446–57. doi: 10.1038/emboj.2010.38.

Iacovoni, J. S., Caron, P., Lassadi, I., Nicolas, E., Massip, L., Trouche, D. and Legube, G. (2010b) 'High-resolution profiling of γH2AX around DNA double strand breaks in the mammalian genome', *The EMBO Journal*, 29(8), pp. 1446–1457. doi: 10.1038/emboj.2010.38.

Ikura, M., Furuya, K., Matsuda, S., Matsuda, R., Shima, H., Adachi, J., Matsuda, T., Shiraki, T. and Ikura, T. (2015) 'Acetylation of Histone H2AX at Lys 5 by the TIP60 Histone Acetyltransferase Complex Is Essential for the Dynamic Binding of NBS1 to Damaged Chromatin.', *Molecular and cellular biology*. American Society for Microbiology Journals, 35(24), pp. 4147–57. doi: 10.1128/MCB.00757-15.

Iliakis, G., Murmann, T. and Soni, A. (2015) 'Alternative end-joining repair pathways are the ultimate backup for abrogated classical non-homologous end-joining and homologous recombination repair: Implications for the formation of chromosome translocations', *Mutation Research/Genetic Toxicology and Environmental Mutagenesis*, 793, pp. 166–175. doi: 10.1016/j.mrgentox.2015.07.001.

Jackson, S. P. and Bartek, J. (2009) ‘The DNA-damage response in human biology and disease.’, *Nature*, 461(7267), pp. 1071–8. doi: 10.1038/nature08467.

Jacobson, R. H., Ladurner, A. G., King, D. S., Tjian, R. and Grewal, S. I. S. (2000) ‘Structure and function of a human TAFII250 double bromodomain module.’, *Science (New York, N.Y.)*. American Association for the Advancement of Science, 288(5470), pp. 1422–5. doi: 10.1126/science.288.5470.1422.

Jang, S. M., Kauzlaric, A., Quivy, J.-P., Pontis, J., Rauwel, B., Coluccio, A., Offner, S., Duc, J., Turelli, P., Almouzni, G. and Trono, D. (2018) ‘KAP1 facilitates reinstatement of heterochromatin after DNA replication’, *Nucleic Acids Research*. doi: 10.1093/nar/gky580.

Jeggo, P. A., Pearl, L. H. and Carr, A. M. (2016) ‘DNA repair, genome stability and cancer: a historical perspective’, *Nature Reviews Cancer*. Nature Publishing Group, 16(1), pp. 35–42. doi: 10.1038/nrc.2015.4.

Jiang, X., Xu, Y. and Price, B. D. (2010) ‘Acetylation of H2AX on lysine 36 plays a key role in the DNA double-strand break repair pathway.’, *FEBS letters*. NIH Public Access, 584(13), pp. 2926–30. doi: 10.1016/j.febslet.2010.05.017.

Jiang, Y., Qian, X., Shen, J., Wang, Y., Li, X., Liu, R., Xia, Y., Chen, Q., Peng, G., Lin, S.-Y. and Lu, Z. (2015) ‘Local generation of fumarate promotes DNA repair through inhibition of histone H3 demethylation.’, *Nature cell biology*. NIH Public Access, 17(9), pp. 1158–68. doi: 10.1038/ncb3209.

John, H., Walden, M., Schafer, S., Genz, S. and Forssmann, W.-G. (2004) ‘Analytical procedures for quantification of peptides in pharmaceutical research by liquid chromatography?mass spectrometry’, *Analytical and Bioanalytical Chemistry*. Springer-Verlag, 378(4), pp. 883–897. doi: 10.1007/s00216-003-2298-y.

JONES, K. W. (1970) ‘Chromosomal and Nuclear Location of Mouse Satellite DNA in Individual Cells’, *Nature*. Nature Publishing Group, 225(5236), pp. 912–915. doi: 10.1038/225912a0.

Juan, L. J., Shia, W. J., Chen, M. H., Yang, W. M., Seto, E., Lin, Y. S. and Wu, C. W. (2000) 'Histone deacetylases specifically down-regulate p53-dependent gene activation.', *The Journal of biological chemistry*. American Society for Biochemistry and Molecular Biology, 275(27), pp. 20436–43. doi: 10.1074/jbc.M000202200.

Jung, D. and Alt, F. W. (2004) 'Unraveling V(D)J recombination; insights into gene regulation.', *Cell*, 116(2), pp. 299–311. Available at: http://www.ncbi.nlm.nih.gov/pubmed/14744439 (Accessed: 21 September 2018).

Kakarougkas, A., Ismail, A., Klement, K., Goodarzi, A. A., Conrad, S., Freire, R., Shibata, A., Lobrich, M. and Jeggo, P. A. (2013) 'Opposing roles for 53BP1 during homologous recombination', *Nucleic Acids Research*, 41(21), pp. 9719–9731. doi: 10.1093/nar/gkt729.

Kandoth, C., McLellan, M. D., Vandin, F., Ye, K., Niu, B., Lu, C., Xie, M., Zhang, Q., McMichael, J. F., Wyczalkowski, M. A., Leiserson, M. D. M., Miller, C. A., Welch, J. S., Walter, M. J., Wendl, M. C., Ley, T. J., Wilson, R. K., Raphael, B. J. and Ding, L. (2013) 'Mutational landscape and significance across 12 major cancer types.', *Nature*. Nature Publishing Group, a division of Macmillan Publishers Limited. All Rights Reserved., 502(7471), pp. 333–9. doi: 10.1038/nature12634.

Karch, K. R., DeNizio, J. E., Black, B. E. and Garcia, B. A. (2013) 'Identification and interrogation of combinatorial histone modifications', *Frontiers in Genetics*. Frontiers, 4, p. 264. doi: 10.3389/fgene.2013.00264.

Karmodiya, K., Krebs, A. R., Oulad-Abdelghani, M., Kimura, H. and Tora, L. (2012) 'H3K9 and H3K14 acetylation co-occur at many gene regulatory elements, while H3K14ac marks a subset of inactive inducible promoters in mouse embryonic stem cells.', *BMC genomics*. BioMed Central, 13, p. 424. doi: 10.1186/1471-2164-13-424.

Katan-Khaykovich, Y. and Struhl, K. (2005) 'Heterochromatin formation involves changes in histone modifications over multiple cell generations.', *The EMBO journal*. European Molecular Biology Organization, 24(12), pp.

2138–49. doi: 10.1038/sj.emboj.7600692.

Katyal, S., Lee, Y., Nitiss, K. C., Downing, S. M., Li, Y., Shimada, M., Zhao, J., Russell, H. R., Petrini, J. H. J., Nitiss, J. L. and McKinnon, P. J. (2014) 'Aberrant topoisomerase-1 DNA lesions are pathogenic in neurodegenerative genome instability syndromes', *Nature Neuroscience*. Nature Research, 17(6), pp. 813–821. doi: 10.1038/nn.3715.

Khurana, S., Kruhlak, M. J., Kim, J., Tran, A. D., Liu, J., Nyswaner, K., Shi, L., Jailwala, P., Sung, M.-H., Hakim, O. and Oberdoerffer, P. (2014) 'A Macrohistone Variant Links Dynamic Chromatin Compaction to BRCA1-Dependent Genome Maintenance', *Cell Reports*, 8(4), pp. 1049–1062. doi: 10.1016/j.celrep.2014.07.024.

Kim, J., Guermah, M., McGinty, R. K., Lee, J.-S., Tang, Z., Milne, T. A., Shilatifard, A., Muir, T. W. and Roeder, R. G. (2009) 'RAD6-Mediated Transcription-Coupled H2B Ubiquitylation Directly Stimulates H3K4 Methylation in Human Cells', *Cell*, 137(3), pp. 459–471. doi: 10.1016/j.cell.2009.02.027.

Kim, S. T., Lim, D. S., Canman, C. E. and Kastan, M. B. (1999) 'Substrate specificities and identification of putative substrates of ATM kinase family members.', *The Journal of biological chemistry*, 274(53), pp. 37538–43. Available at: http://www.ncbi.nlm.nih.gov/pubmed/10608806 (Accessed: 4 September 2018).

Kolas, N. K., Chapman, J. R., Nakada, S., Ylanko, J., Chahwan, R., Sweeney, F. D., Panier, S., Mendez, M., Wildenhain, J., Thomson, T. M., Pelletier, L., Jackson, S. P. and Durocher, D. (2007) 'Orchestration of the DNA-damage response by the RNF8 ubiquitin ligase.', *Science (New York, N.Y.)*. American Association for the Advancement of Science, 318(5856), pp. 1637–40. doi: 10.1126/science.1150034.

Kouzarides, T. (2007) 'Chromatin modifications and their function.', *Cell*, 128(4), pp. 693–705. doi: 10.1016/j.cell.2007.02.005.

Koyama, M. and Kurumizaka, H. (2018) 'Structural diversity of the nucleosome', *The Journal of Biochemistry*. Oxford University Press, 163(2),

pp. 85–95. doi: 10.1093/jb/mvx081.

Kozlov, S. V, Graham, M. E., Peng, C., Chen, P., Robinson, P. J. and Lavin, M. F. (2006) 'Involvement of novel autophosphorylation sites in ATM activation', *The EMBO Journal*, 25(15), pp. 3504–3514. doi: 10.1038/sj.emboj.7601231.

Krishnan, V., Chow, M. Z. Y., Wang, Z., Zhang, L., Liu, B., Liu, X. and Zhou, Z. (2011) 'Histone H4 lysine 16 hypoacetylation is associated with defective DNA repair and premature senescence in Zmpste24-deficient mice', *Proceedings of the National Academy of Sciences*, 108(30), pp. 12325–12330. doi: 10.1073/pnas.1102789108.

Krishnan, V., Chow, M. Z. Y., Wang, Z., Zhang, L., Liu, B., Liu, X. and Zhou, Z. (2011) 'Histone H4 lysine 16 hypoacetylation is associated with defective DNA repair and premature senescence in Zmpste24-deficient mice.', *Proceedings of the National Academy of Sciences of the United States of America*, 108(30), pp. 12325–30. doi: 10.1073/pnas.1102789108.

Krogan, N. J., Dover, J., Wood, A., Schneider, J., Heidt, J., Boateng, M. A., Dean, K., Ryan, O. W., Golshani, A., Johnston, M., Greenblatt, J. F. and Shilatifard, A. (2003) 'The Paf1 complex is required for histone H3 methylation by COMPASS and Dot1p: linking transcriptional elongation to histone methylation.', *Molecular cell*, 11(3), pp. 721–9. Available at: http://www.ncbi.nlm.nih.gov/pubmed/12667454 (Accessed: 30 August 2018).

Kulyyassov, A., Shoaib, M., Pichugin, A., Kannouche, P., Ramanculov, E., Lipinski, M. and Ogryzko, V. (2011) 'PUB-MS: a mass spectrometry-based method to monitor protein-protein proximity in vivo.', *Journal of proteome research*, 10(10), pp. 4416–27. doi: 10.1021/pr200189p.

Kwon, S. H. and Workman, J. L. (2011) 'The changing faces of HP1: From heterochromatin formation and gene silencing to euchromatic gene expression', *BioEssays*, 33(4), pp. 280–289. doi: 10.1002/bies.201000138.

Lachner, M., O'Carroll, D., Rea, S., Mechtler, K. and Jenuwein, T. (2001) 'Methylation of histone H3 lysine 9 creates a binding site for HP1 proteins', *Nature*. Nature Publishing Group, 410(6824), pp. 116–120. doi:

10.1038/35065132.

Lagger, G., Doetzlhofer, A., Schuettengruber, B., Haidweger, E., Simboeck, E., Tischler, J., Chiocca, S., Suske, G., Rotheneder, H., Wintersberger, E. and Seiser, C. (2003) 'The tumor suppressor p53 and histone deacetylase 1 are antagonistic regulators of the cyclin-dependent kinase inhibitor p21/WAF1/CIP1 gene.', *Molecular and cellular biology*. American Society for Microbiology Journals, 23(8), pp. 2669–79. doi: 10.1128/MCB.23.8.2669-2679.2003.

Lau, P. N. I. and Cheung, P. (2013) 'Elucidating combinatorial histone modifications and crosstalks by coupling histone-modifying enzyme with biotin ligase activity.', *Nucleic acids research*, 41(3), p. e49. doi: 10.1093/nar/gks1247.

Lawless, M. K., Hopkins, S. and Anwer, M. K. (1998) 'Quantitation of a 36-amino-acid peptide inhibitor of HIV-1 membrane fusion in animal and human plasma using high-performance liquid chromatography and fluorescence detection', *Journal of Chromatography B: Biomedical Sciences and Applications*. Elsevier, 707(1–2), pp. 213–217. doi: 10.1016/S0378-4347(97)00609-9.

Lawrence, M., Daujat, S. and Schneider, R. (2016) 'Lateral Thinking: How Histone Modifications Regulate Gene Expression', *Trends in Genetics*, 32(1), pp. 42–56. doi: 10.1016/j.tig.2015.10.007.

Lee, K.-J., Jovanovic, M., Udayakumar, D., Bladen, C. L. and Dynan, W. S. (2004) 'Identification of DNA-PKcs phosphorylation sites in XRCC4 and effects of mutations at these sites on DNA end joining in a cell-free system', *DNA Repair*, 3(3), pp. 267–276. doi: 10.1016/j.dnarep.2003.11.005.

Leuraud, K., Richardson, D. B., Cardis, E., Daniels, R. D., Gillies, M., O'Hagan, J. A., Hamra, G. B., Haylock, R., Laurier, D., Moissonnier, M., Schubauer-Berigan, M. K., Thierry-Chef, I. and Kesminiene, A. (2015) 'Ionising radiation and risk of death from leukaemia and lymphoma in radiation-monitored workers (INWORKS): an international cohort study', *The Lancet Haematology*, 2(7), pp. e276–e281. doi: 10.1016/S2352-

3026(15)00094-0.

Liao, R., Wu, H., Deng, H., Yu, Y., Hu, M., Zhai, H., Yang, P., Zhou, S. and Yi, W. (2013) 'Specific and Efficient N-Propionylation of Histones with Propionic Acid *N* -Hydroxysuccinimide Ester for Histone Marks Characterization by LC-MS', *Analytical Chemistry*. American Chemical Society, 85(4), pp. 2253–2259. doi: 10.1021/ac303171h.

Liu, X., Shao, Z., Jiang, W., Lee, B. J. and Zha, S. (2017) 'PAXX promotes KU accumulation at DNA breaks and is essential for end-joining in XLF-deficient mice', *Nature Communications*. Nature Publishing Group, 8, p. 13816. doi: 10.1038/ncomms13816.

Löbrich, M. and Jeggo, P. (2017) 'A Process of Resection-Dependent Nonhomologous End Joining Involving the Goddess Artemis.', *Trends in biochemical sciences*. Elsevier, 42(9), pp. 690–701. doi: 10.1016/j.tibs.2017.06.011.

Löbrich, M., Rydberg, B. and Cooper, P. K. (1995) 'Repair of x-ray-induced DNA double-strand breaks in specific Not I restriction fragments in human fibroblasts: joining of correct and incorrect ends.', *Proceedings of the National Academy of Sciences of the United States of America*. National Academy of Sciences, 92(26), pp. 12050–4. Available at: http://www.ncbi.nlm.nih.gov/pubmed/8618842 (Accessed: 6 June 2018).

Lomax, M. E., Folkes, L. K. and O'Neill, P. (2013) 'Biological Consequences of Radiation-induced DNA Damage: Relevance to Radiotherapy', *Clinical Oncology*, 25(10), pp. 578–585. doi: 10.1016/j.clon.2013.06.007.

Lou, Z., Minter-Dykhouse, K., Franco, S., Gostissa, M., Rivera, M. A., Celeste, A., Manis, J. P., Van Deursen, J., Nussenzweig, A., Paull, T. T., Alt, F. W. and Chen, J. (2006) 'MDC1 maintains genomic stability by participating in the amplification of ATM-dependent DNA damage signals', *Molecular Cell*. Cell Press, 21(2), pp. 187–200. doi: 10.1016/j.molcel.2005.11.025.

Luger, K., Mäder, A. W., Richmond, R. K., Sargent, D. F. and Richmond, T. J. (1997) 'Crystal structure of the nucleosome core particle at 2.8 A resolution.', *Nature*, 389(6648), pp. 251–60. doi: 10.1038/38444.

Lukas, J., Lukas, C. and Bartek, J. (2011) ‘More than just a focus: The chromatin response to DNA damage and its role in genome integrity maintenance.’, *Nature cell biology*. Nature Publishing Group, 13(10), pp. 1161–9. doi: 10.1038/ncb2344.

Ma, T., Chen, Y., Zhang, F., Yang, C.-Y., Wang, S. and Yu, X. (2013) ‘RNF111-dependent neddylation activates DNA damage-induced ubiquitination.’, *Molecular cell*. Elsevier Inc., 49(5), pp. 897–907. doi: 10.1016/j.molcel.2013.01.006.

Madabhushi, R., Pan, L. and Tsai, L.-H. (2014) ‘DNA damage and its links to neurodegeneration.’, *Neuron*. Elsevier, 83(2), pp. 266–282. doi: 10.1016/j.neuron.2014.06.034.

Mailand, N., Bekker-Jensen, S., Faustrup, H., Melander, F., Bartek, J., Lukas, C. and Lukas, J. (2007) ‘RNF8 Ubiquitylates Histones at DNA Double-Strand Breaks and Promotes Assembly of Repair Proteins’, *Cell*. Cell Press, 131(5), pp. 887–900. doi: 10.1016/J.CELL.2007.09.040.

Maile, T. M., Izrael-Tomasevic, A., Cheung, T., Guler, G. D., Tindell, C., Masselot, A., Liang, J., Zhao, F., Trojer, P., Classon, M. and Arnott, D. (2015) ‘Mass spectrometric quantification of histone post-translational modifications by a hybrid chemical labeling method.’, *Molecular & cellular proteomics : MCP*. American Society for Biochemistry and Molecular Biology, 14(4), pp. 1148–58. doi: 10.1074/mcp.O114.046573.

Mariño-Ramírez, L., Kann, M. G., Shoemaker, B. A. and Landsman, D. (2005) ‘Histone structure and nucleosome stability.’, *Expert review of proteomics*. NIH Public Access, 2(5), pp. 719–29. doi: 10.1586/14789450.2.5.719.

Martinez-Garcia, E., Popovic, R., Min, D.-J., Sweet, S. M. M., Thomas, P. M., Zamdborg, L., Heffner, A., Will, C., Lamy, L., Staudt, L. M., Levens, D. L., Kelleher, N. L. and Licht, J. D. (2011) ‘The MMSET histone methyl transferase switches global histone methylation and alters gene expression in t(4;14) multiple myeloma cells’, *Blood*, 117(1), pp. 211–220. doi: 10.1182/blood-2010-07-298349.

Matos, J. and West, S. C. (2014) ‘Holliday junction resolution: Regulation in

space and time', *DNA Repair*, 19, pp. 176–181. doi: 10.1016/j.dnarep.2014.03.013.

Matsuda, E., Agata, Y., Sugai, M., Katakai, T., Gonda, H. and Shimizu, A. (2001) 'Targeting of Krüppel-associated box-containing zinc finger proteins to centromeric heterochromatin. Implication for the gene silencing mechanisms.', *The Journal of biological chemistry*. American Society for Biochemistry and Molecular Biology, 276(17), pp. 14222–9. doi: 10.1074/jbc.M010663200.

Mattiroli, F., Vissers, J. H. A., van Dijk, W. J., Ikpa, P., Citterio, E., Vermeulen, W., Marteijn, J. A. and Sixma, T. K. (2012) 'RNF168 Ubiquitinates K13-15 on H2A/H2AX to Drive DNA Damage Signaling', *Cell*. Cell Press, 150(6), pp. 1182–1195. doi: 10.1016/J.CELL.2012.08.005.

Mattiroli, F., Vissers, J. H. a, van Dijk, W. J., Ikpa, P., Citterio, E., Vermeulen, W., Marteijn, J. a and Sixma, T. K. (2012) 'RNF168 ubiquitinates K13-15 on H2A/H2AX to drive DNA damage signaling.', *Cell*. Elsevier Inc., 150(6), pp. 1182–95. doi: 10.1016/j.cell.2012.08.005.

Maze, I., Noh, K.-M., Soshnev, A. A. and Allis, C. D. (2014) 'Every amino acid matters: essential contributions of histone variants to mammalian development and disease', *Nature Reviews Genetics*. Nature Publishing Group, 15(4), pp. 259–271. doi: 10.1038/nrg3673.

McGinty, R. K. and Tan, S. (2015) 'Nucleosome Structure and Function', *Chemical Reviews*. American Chemical Society, 115(6), pp. 2255–2273. doi: 10.1021/cr500373h.

McKinnon, P. J. (2004) 'ATM and ataxia telangiectasia.', *EMBO reports*. European Molecular Biology Organization, 5(8), pp. 772–6. doi: 10.1038/sj.embor.7400210.

McKinnon, P. J. (2017) 'Genome integrity and disease prevention in the nervous system.', *Genes & development*. Cold Spring Harbor Laboratory Press, 31(12), pp. 1180–1194. doi: 10.1101/gad.301325.117.

McKittrick, E., Gafken, P. R., Ahmad, K. and Henikoff, S. (2004) 'Histone

H3.3 is enriched in covalent modifications associated with active chromatin.', *Proceedings of the National Academy of Sciences of the United States of America*. National Academy of Sciences, 101(6), pp. 1525–30. doi: 10.1073/pnas.0308092100.

Meert, P., Dierickx, S., Govaert, E., De Clerck, L., Willems, S., Dhaenens, M. and Deforce, D. (2016) 'Tackling aspecific side reactions during histone propionylation: The promise of reversing overpropionylation.', *Proteomics*. Wiley-Blackwell, 16(14), pp. 1970–4. doi: 10.1002/pmic.201600045.

Meert, P., Govaert, E., Scheerlinck, E., Dhaenens, M. and Deforce, D. (2015) 'Pitfalls in histone propionylation during bottom-up mass spectrometry analysis', *PROTEOMICS*. John Wiley & Sons, Ltd, 15(17), pp. 2966–2971. doi: 10.1002/pmic.201400569.

Mehrotra, P. V., Ahel, D., Ryan, D. P., Weston, R., Wiechens, N., Kraehenbuehl, R., Owen-Hughes, T. and Ahel, I. (2011) 'DNA repair factor APLF is a histone chaperone.', *Molecular cell*, 41(1), pp. 46–55. doi: 10.1016/j.molcel.2010.12.008.

Meyer, B., Fabbrizi, M. R., Raj, S., Zobel, C. L., Hallahan, D. E. and Sharma, G. G. (2016a) 'Histone H3 Lysine 9 Acetylation Obstructs ATM Activation and Promotes Ionizing Radiation Sensitivity in Normal Stem Cells.', *Stem cell reports*. Elsevier, 7(6), pp. 1013–1022. doi: 10.1016/j.stemcr.2016.11.004.

Meyer, B., Fabbrizi, M. R., Raj, S., Zobel, C. L., Hallahan, D. E. and Sharma, G. G. (2016b) 'Histone H3 Lysine 9 Acetylation Obstructs ATM Activation and Promotes Ionizing Radiation Sensitivity in Normal Stem Cells.', *Stem cell reports*. Elsevier, 7(6), pp. 1013–1022. doi: 10.1016/j.stemcr.2016.11.004.

Miller, K. M., Tjeertes, J. V, Coates, J., Legube, G., Polo, S. E., Britton, S. and Jackson, S. P. (2010) 'Human HDAC1 and HDAC2 function in the DNA-damage response to promote DNA nonhomologous end-joining', *Nature Structural & Molecular Biology*, 17(99), pp. 1144–1151. doi: 10.1038/nsmb.1899.

Mischo, H. E., Gómez-González, B., Grzechnik, P., Rondón, A. G., Wei, W., Steinmetz, L., Aguilera, A. and Proudfoot, N. J. (2011) 'Yeast Sen1 Helicase

Protects the Genome from Transcription-Associated Instability', *Molecular Cell*, 41(1), pp. 21–32. doi: 10.1016/j.molcel.2010.12.007.

Mole, R. H. (1990) 'Childhood cancer after prenatal exposure to diagnostic X-ray examinations in Britain.', *British journal of cancer*, 62(1), pp. 152–68. Available at: http://www.ncbi.nlm.nih.gov/pubmed/2202420 (Accessed: 3 October 2018).

Mosammaparast, N., Kim, H., Laurent, B., Zhao, Y., Lim, H. J., Majid, M. C., Dango, S., Luo, Y., Hempel, K., Sowa, M. E., Gygi, S. P., Steen, H., Harper, J. W., Yankner, B. and Shi, Y. (2013) 'The histone demethylase LSD1/KDM1A promotes the DNA damage response', *The Journal of Cell Biology*, 203(3), pp. 457–470. doi: 10.1083/jcb.201302092.

Murphy, M., Ahn, J., Walker, K. K., Hoffman, W. H., Evans, R. M., Levine, A. J. and George, D. L. (1999) 'Transcriptional repression by wild-type p53 utilizes histone deacetylases, mediated by interaction with mSin3a.', *Genes & development*. Cold Spring Harbor Laboratory Press, 13(19), pp. 2490–501. Available at: http://www.ncbi.nlm.nih.gov/pubmed/10521394 (Accessed: 9 September 2018).

Murr, R., Loizou, J. I., Yang, Y.-G., Cuenin, C., Li, H., Wang, Z.-Q. and Herceg, Z. (2006) 'Histone acetylation by Trrap-Tip60 modulates loading of repair proteins and repair of DNA double-strand breaks.', *Nature cell biology*, 8(1), pp. 91–9. doi: 10.1038/ncb1343.

Nahas, S. A. and Gatti, R. A. (2009) 'DNA double strand break repair defects, primary immunodeficiency disorders, and "radiosensitivity"'. doi: 10.1097/ACI.0b013e328332be17.

Nakayama, J. -i. (2001) 'Role of Histone H3 Lysine 9 Methylation in Epigenetic Control of Heterochromatin Assembly', *Science*, 292(5514), pp. 110–113. doi: 10.1126/science.1060118.

Nitiss, J. L. (2009) 'DNA topoisomerase II and its growing repertoire of biological functions.', *Nature reviews. Cancer*. NIH Public Access, 9(5), pp. 327–37. doi: 10.1038/nrc2608.

Nitiss, J. L. (2009) ‘Targeting DNA topoisomerase II in cancer chemotherapy’, *Nature Reviews Cancer*, 9(5), pp. 338–350. doi: 10.1038/nrc2607.

Noon, A. T., Shibata, A., Rief, N., Löbrich, M., Stewart, G. S., Jeggo, P. A. and Goodarzi, A. A. (2010) ‘53BP1-dependent robust localized KAP-1 phosphorylation is essential for heterochromatic DNA double-strand break repair’, *Nature Cell Biology*, 12(2), pp. 177–184. doi: 10.1038/ncb2017.

O’Driscoll, M. (2012) ‘Diseases associated with defective responses to DNA damage.’, *Cold Spring Harbor perspectives in biology*. Cold Spring Harbor Laboratory Press, 4(12). doi: 10.1101/cshperspect.a012773.

O’Driscoll, M., Ruiz-Perez, V. L., Woods, C. G., Jeggo, P. A. and Goodship, J. A. (2003) ‘A splicing mutation affecting expression of ataxia–telangiectasia and Rad3–related protein (ATR) results in Seckel syndrome’, *Nature Genetics*, 33(4), pp. 497–501. doi: 10.1038/ng1129.

Ochs, F., Somyajit, K., Altmeyer, M., Rask, M.-B., Lukas, J. and Lukas, C. (2016) ‘53BP1 fosters fidelity of homology-directed DNA repair’, *Nature Structural & Molecular Biology*. Nature Publishing Group, 23(8), pp. 714–721. doi: 10.1038/nsmb.3251.

Ogawa, Y., Sun, B. K. and Lee, J. T. (2008) ‘Intersection of the RNA Interference and X-Inactivation Pathways’, *Science*, 320(5881), pp. 1336–1341. doi: 10.1126/science.1157676.

Ogi, T., Walker, S., Stiff, T., Hobson, E., Limsirichaikul, S., Carpenter, G., Prescott, K., Suri, M., Byrd, P. J., Matsuse, M., Mitsutake, N., Nakazawa, Y., Vasudevan, P., Barrow, M., Stewart, G. S., Taylor, A. M. R., O’Driscoll, M. and Jeggo, P. A. (2012) ‘Identification of the first ATRIP-deficient patient and novel mutations in ATR define a clinical spectrum for ATR-ATRIP Seckel Syndrome.’, *PLoS genetics*. Public Library of Science, 8(11), p. e1002945. doi: 10.1371/journal.pgen.1002945.

Ogiwara, H., Ui, A., Otsuka, A., Satoh, H., Yokomi, I., Nakajima, S., Yasui, A., Yokota, J. and Kohno, T. (2011) ‘Histone acetylation by CBP and p300 at double-strand break sites facilitates SWI/SNF chromatin remodeling and the recruitment of non-homologous end joining factors’, *Oncogene*. Nature

Publishing Group, 30(18), pp. 2135–2146. doi: 10.1038/onc.2010.592.

Olsen, J. V, Ong, S.-E. and Mann, M. (2004) 'Trypsin cleaves exclusively C-terminal to arginine and lysine residues.', *Molecular & cellular proteomics : MCP*. American Society for Biochemistry and Molecular Biology, 3(6), pp. 608–14. doi: 10.1074/mcp.T400003-MCP200.

Önder, Ö., Sidoli, S., Carroll, M. and Garcia, B. A. (2015) 'Progress in epigenetic histone modification analysis by mass spectrometry for clinical investigations.', *Expert review of proteomics*. NIH Public Access, 12(5), pp. 499–517. doi: 10.1586/14789450.2015.1084231.

Ong, S.-E., Mittler, G. and Mann, M. (2004) 'Identifying and quantifying in vivo methylation sites by heavy methyl SILAC', *Nature Methods*. Nature Publishing Group, 1(2), pp. 119–126. doi: 10.1038/nmeth715.

Ordu, O., Lusser, A. and Dekker, N. H. (2016) 'Recent insights from in vitro single-molecule studies into nucleosome structure and dynamics', *Biophysical Reviews*. Springer Berlin Heidelberg, 8(S1), pp. 33–49. doi: 10.1007/s12551-016-0212-z.

Orphanides, G. and Reinberg, D. (2000) 'RNA polymerase II elongation through chromatin', *Nature*, 407(6803), pp. 471–476. doi: 10.1038/35035000.

Osamor, V., Chinedu, S., Azuh, D., Iweala, E. and Ogunlana, O. (2016) 'The interplay of post-translational modification and gene therapy', *Drug Design, Development and Therapy*. Dove Press, 10, p. 861. doi: 10.2147/DDDT.S80496.

Ou, H. D., Phan, S., Deerinck, T. J., Thor, A., Ellisman, M. H. and O'Shea, C. C. (2017a) 'ChromEMT: Visualizing 3D chromatin structure and compaction in interphase and mitotic cells.', *Science (New York, N.Y.)*. American Association for the Advancement of Science, 357(6349), p. eaag0025. doi: 10.1126/science.aag0025.

Ou, H. D., Phan, S., Deerinck, T. J., Thor, A., Ellisman, M. H. and O'Shea, C. C. (2017b) 'ChromEMT: Visualizing 3D chromatin structure and compaction in interphase and mitotic cells.', *Science (New York, N.Y.)*. American

Association for the Advancement of Science, 357(6349), p. eaag0025. doi: 10.1126/science.aag0025.

Pardue, M. L. and Gall, J. G. (1970) ‘Chromosomal localization of mouse satellite DNA.’, *Science (New York, N.Y.)*, 168(3937), pp. 1356–8. Available at: http://www.ncbi.nlm.nih.gov/pubmed/5462793 (Accessed: 8 October 2018).

Parthun, M. R. (2007) ‘Hat1: the emerging cellular roles of a type B histone acetyltransferase’, *Oncogene*. Nature Publishing Group, 26(37), pp. 5319–5328. doi: 10.1038/sj.onc.1210602.

Pearl, L. H., Schierz, A. C., Ward, S. E., Al-Lazikani, B. and Pearl, F. M. G. (2015) ‘Therapeutic opportunities within the DNA damage response’, *Nature Reviews Cancer*. Nature Publishing Group, 15(3), pp. 166–180. doi: 10.1038/nrc3891.

Pei, H., Zhang, L., Luo, K., Qin, Y., Chesi, M., Fei, F., Bergsagel, P. L., Wang, L., You, Z. and Lou, Z. (2011) ‘MMSET regulates histone H4K20 methylation and 53BP1 accumulation at DNA damage sites’, *Nature*, 470(7332), pp. 124–128. doi: 10.1038/nature09658.

Pellegrino, S., Michelena, J., Teloni, F., Imhof, R. and Altmeyer, M. (2017) ‘Replication-Coupled Dilution of H4K20me2 Guides 53BP1 to Pre-replicative Chromatin.’, *Cell reports*. Europe PMC Funders, 19(9), pp. 1819–1831. doi: 10.1016/j.celrep.2017.05.016.

Pesavento, J. J., Yang, H., Kelleher, N. L. and Mizzen, C. A. (2008) ‘Certain and Progressive Methylation of Histone H4 at Lysine 20 during the Cell Cycle’, *Molecular and Cellular Biology*, 28(1), pp. 468–486. doi: 10.1128/MCB.01517-07.

Peters, A. H. F. M., Mermoud, J. E., O’Carroll, D., Pagani, M., Schweizer, D., Brockdorff, N. and Jenuwein, T. (2002) ‘Histone H3 lysine 9 methylation is an epigenetic imprint of facultative heterochromatin’, *Nature Genetics*. Nature Publishing Group, 30(1), pp. 77–80. doi: 10.1038/ng789.

Pfister, N. T., Fomin, V., Regunath, K., Zhou, J. Y., Zhou, W., Silwal-Pandit,

L., Freed-Pastor, W. A., Laptenko, O., Neo, S. P., Bargonetti, J., Hoque, M., Tian, B., Gunaratne, J., Engebraaten, O., Manley, J. L., Børresen-Dale, A.-L., Neilsen, P. M. and Prives, C. (2015) 'Mutant p53 cooperates with the SWI/SNF chromatin remodeling complex to regulate VEGFR2 in breast cancer cells.', *Genes & development*. Cold Spring Harbor Laboratory Press, 29(12), pp. 1298–315. doi: 10.1101/gad.263202.115.

Pfister, S. X., Ahrabi, S., Zalmas, L.-P., Sarkar, S., Aymard, F., Bachrati, C. Z., Helleday, T., Legube, G., La Thangue, N. B., Porter, A. C. G. and Humphrey, T. C. (2014) 'SETD2-Dependent Histone H3K36 Trimethylation Is Required for Homologous Recombination Repair and Genome Stability', *Cell Reports*, 7(6), pp. 2006–2018. doi: 10.1016/j.celrep.2014.05.026.

Pierce, A. J. and Jasin, M. (2001) 'NHEJ Deficiency and Disease', *Molecular Cell*. Cell Press, 8(6), pp. 1160–1161. doi: 10.1016/S1097-2765(01)00424-5.

Pietrucha, B., Heropolitańska-Pliszka, E., Geffers, R., Enßen, J., Wieland, B., Bogdanova, N. V. and Dörk, T. (2017) 'Clinical and Biological Manifestation of RNF168 Deficiency in Two Polish Siblings.', *Frontiers in immunology*. Frontiers Media SA, 8, p. 1683. doi: 10.3389/fimmu.2017.01683.

Pinato, S., Scandiuzzi, C., Arnaudo, N., Citterio, E., Gaudino, G. and Penengo, L. (2009) 'RNF168, a new RING finger, MIU-containing protein that modifies chromatin by ubiquitination of histones H2A and H2AX', *BMC Molecular Biology*, 10(1), p. 55. doi: 10.1186/1471-2199-10-55.

Plazas-Mayorca, M. D., Bloom, J. S., Zeissler, U., Leroy, G., Young, N. L., DiMaggio, P. A., Krugylak, L., Schneider, R. and Garcia, B. A. (2010) 'Quantitative proteomics reveals direct and indirect alterations in the histone code following methyltransferase knockdown', *Molecular BioSystems*, 6(9), p. 1719. doi: 10.1039/c003307c.

Pollard, J. M. and Gatti, R. A. (2009) 'Clinical radiation sensitivity with DNA repair disorders: an overview.', *International journal of radiation oncology, biology, physics*. NIH Public Access, 74(5), pp. 1323–31. doi: 10.1016/j.ijrobp.2009.02.057.

Polo, S. E. and Almouzni, G. (2015) 'Chromatin dynamics after DNA damage:

The legacy of the access–repair–restore model', *DNA Repair*, 36, pp. 114–121. doi: 10.1016/j.dnarep.2015.09.014.

Pommier, Y., Barcelo, J. M., Rao, V. A., Sordet, O., Jobson, A. G., Thibaut, L., Miao, Z.-H., Seiler, J. A., Zhang, H., Marchand, C., Agama, K., Nitiss, J. L. and Redon, C. (2006) 'Repair of topoisomerase I-mediated DNA damage.', *Progress in nucleic acid research and molecular biology*. NIH Public Access, 81, pp. 179–229. doi: 10.1016/S0079-6603(06)81005-6.

Pommier, Y., Sun, Y., Huang, S. N. and Nitiss, J. L. (2016) 'Roles of eukaryotic topoisomerases in transcription, replication and genomic stability', *Nature Reviews Molecular Cell Biology*, 17(11), pp. 703–721. doi: 10.1038/nrm.2016.111.

Povirk, L. F. (2012) 'Processing of Damaged DNA Ends for Double-Strand Break Repair in Mammalian Cells', *ISRN Molecular Biology*, 2012, pp. 1–16. doi: 10.5402/2012/345805.

Qi, H. H., Sarkissian, M., Hu, G.-Q., Wang, Z., Bhattacharjee, A., Gordon, D. B., Gonzales, M., Lan, F., Ongusaha, P. P., Huarte, M., Yaghi, N. K., Lim, H., Garcia, B. A., Brizuela, L., Zhao, K., Roberts, T. M. and Shi, Y. (2010) 'Histone H4K20/H3K9 demethylase PHF8 regulates zebrafish brain and craniofacial development', *Nature*, 466(7305), pp. 503–507. doi: 10.1038/nature09261.

Rea, S., Eisenhaber, F., O'Carroll, D., Strahl, B. D., Sun, Z.-W., Schmid, M., Opravil, S., Mechtler, K., Ponting, C. P., Allis, C. D. and Jenuwein, T. (2000) 'Regulation of chromatin structure by site-specific histone H3 methyltransferases', *Nature*, 406(6796), pp. 593–599. doi: 10.1038/35020506.

Reinhardt, H. C. and Yaffe, M. B. (2013) 'Phospho-Ser/Thr-binding domains: navigating the cell cycle and DNA damage response', *Nature Reviews Molecular Cell Biology*. Nature Publishing Group, 14(9), pp. 563–580. doi: 10.1038/nrm3640.

Riballo, E., Kühne, M., Rief, N., Doherty, A., Smith, G. C. M., Recio, M.-J., Reis, C., Dahm, K., Fricke, A., Krempler, A., Parker, A. R., Jackson, S. P.,

Gennery, A., Jeggo, P. A. and Löbrich, M. (2004) ‘A pathway of double-strand break rejoining dependent upon ATM, Artemis, and proteins locating to gamma-H2AX foci.’, *Molecular cell*, 16(5), pp. 715–24. doi: 10.1016/j.molcel.2004.10.029.

Rinn, J. L., Kertesz, M., Wang, J. K., Squazzo, S. L., Xu, X., Brugmann, S. A., Goodnough, L. H., Helms, J. A., Farnham, P. J., Segal, E. and Chang, H. Y. (2007) ‘Functional Demarcation of Active and Silent Chromatin Domains in Human HOX Loci by Noncoding RNAs’, *Cell*, 129(7), pp. 1311–1323. doi: 10.1016/j.cell.2007.05.022.

Rogakou, E. P., Boon, C., Redon, C. and Bonner, W. M. (1999a) ‘Megabase chromatin domains involved in DNA double-strand breaks in vivo.’, *The Journal of cell biology*, 146(5), pp. 905–16. Available at: http://www.ncbi.nlm.nih.gov/pubmed/10477747 (Accessed: 15 January 2018).

Rogakou, E. P., Boon, C., Redon, C. and Bonner, W. M. (1999b) ‘Megabase chromatin domains involved in DNA double-strand breaks in vivo.’, *The Journal of cell biology*, 146(5), pp. 905–16. Available at: http://www.ncbi.nlm.nih.gov/pubmed/10477747 (Accessed: 1 June 2018).

Rogakou, E. P., Pilch, D. R., Orr, A. H., Ivanova, V. S. and Bonner, W. M. (1998a) ‘DNA double-stranded breaks induce histone H2AX phosphorylation on serine 139.’, *The Journal of biological chemistry*, 273(10), pp. 5858–68. Available at: http://www.ncbi.nlm.nih.gov/pubmed/9488723 (Accessed: 1 June 2018).

Rogakou, E. P., Pilch, D. R., Orr, A. H., Ivanova, V. S. and Bonner, W. M. (1998b) ‘DNA double-stranded breaks induce histone H2AX phosphorylation on serine 139.’, *The Journal of biological chemistry*, 273(10), pp. 5858–68. Available at: http://www.ncbi.nlm.nih.gov/pubmed/9488723 (Accessed: 15 January 2018).

Rogers, P. B., Plowman, P. N., Harris, S. J. and Arlett, C. F. (2000) ‘Four radiation hypersensitivity cases and their implications for clinical radiotherapy.’, *Radiotherapy and oncology : journal of the European Society for Therapeutic Radiology and Oncology*. Elsevier, 57(2), pp. 143–54. doi:

10.1016/S0167-8140(00)00249-8.

Rothbart, S. B., Dickson, B. M., Raab, J. R., Grzybowski, A. T., Krajewski, K., Guo, A. H., Shanle, E. K., Josefowicz, S. Z., Fuchs, S. M., Allis, C. D., Magnuson, T. R., Ruthenburg, A. J. and Strahl, B. D. (2015) 'An Interactive Database for the Assessment of Histone Antibody Specificity.', *Molecular cell*. NIH Public Access, 59(3), pp. 502–11. doi: 10.1016/j.molcel.2015.06.022.

Ryan, R. F., Schultz, D. C., Ayyanathan, K., Singh, P. B., Friedman, J. R., Fredericks, W. J. and Rauscher, F. J. (1999) 'KAP-1 corepressor protein interacts and colocalizes with heterochromatic and euchromatic HP1 proteins: a potential role for Krüppel-associated box-zinc finger proteins in heterochromatin-mediated gene silencing.', *Molecular and cellular biology*, 19(6), pp. 4366–78. Available at: http://www.ncbi.nlm.nih.gov/pubmed/10330177 (Accessed: 17 September 2018).

Saksouk, N., Simboeck, E. and Déjardin, J. (2015) 'Constitutive heterochromatin formation and transcription in mammals', *Epigenetics & Chromatin*, 8(1), p. 3. doi: 10.1186/1756-8935-8-3.

Saldivar, J. C., Cortez, D. and Cimprich, K. A. (2017) 'The essential kinase ATR: ensuring faithful duplication of a challenging genome', *Nature Reviews Molecular Cell Biology*. Nature Publishing Group, 18(10), pp. 622–636. doi: 10.1038/nrm.2017.67.

Sartori, A. A., Lukas, C., Coates, J., Mistrik, M., Fu, S., Bartek, J., Baer, R., Lukas, J. and Jackson, S. P. (2007) 'Human CtIP promotes DNA end resection', *Nature*, 450(7169), pp. 509–514. doi: 10.1038/nature06337.

Savic, V., Yin, B., Maas, N. L., Bredemeyer, A. L., Carpenter, A. C., Helmink, B. A., Yang-Iott, K. S., Sleckman, B. P. and Bassing, C. H. (2009a) 'Formation of Dynamic γ-H2AX Domains along Broken DNA Strands Is Distinctly Regulated by ATM and MDC1 and Dependent upon H2AX Densities in Chromatin', *Molecular Cell*, 34(3), pp. 298–310. doi: 10.1016/j.molcel.2009.04.012.

Savic, V., Yin, B., Maas, N. L., Bredemeyer, A. L., Carpenter, A. C., Helmink,

B. A., Yang-Iott, K. S., Sleckman, B. P. and Bassing, C. H. (2009b) ‘Formation of Dynamic γ-H2AX Domains along Broken DNA Strands Is Distinctly Regulated by ATM and MDC1 and Dependent upon H2AX Densities in Chromatin’, *Molecular Cell*. Cell Press, 34(3), pp. 298–310. doi: 10.1016/J.MOLCEL.2009.04.012.

Savic, V., Yin, B., Maas, N. L., Bredemeyer, A. L., Carpenter, A. C., Helmink, B. A., Yang-Iott, K. S., Sleckman, B. P. and Bassing, C. H. (2009c) ‘Formation of Dynamic γ-H2AX Domains along Broken DNA Strands Is Distinctly Regulated by ATM and MDC1 and Dependent upon H2AX Densities in Chromatin’, *Molecular Cell*. Cell Press, 34(3), pp. 298–310. doi: 10.1016/J.MOLCEL.2009.04.012.

Schwartzentruber, J., Korshunov, A., Liu, X.-Y., Jones, D. T. W., Pfaff, E., Jacob, K., Sturm, D., Fontebasso, A. M., Quang, D.-A. K., Tönjes, M., Hovestadt, V., Albrecht, S., Kool, M., Nantel, A., Konermann, C., Lindroth, A., Jäger, N., Rausch, T., Ryzhova, M., Korbel, J. O., Hielscher, T., Hauser, P., Garami, M., Klekner, A., Bognar, L., Ebinger, M., Schuhmann, M. U., Scheurlen, W., Pekrun, A., Frühwald, M. C., Roggendorf, W., Kramm, C., Dürken, M., Atkinson, J., Lepage, P., Montpetit, A., Zakrzewska, M., Zakrzewski, K., Liberski, P. P., Dong, Z., Siegel, P., Kulozik, A. E., Zapatka, M., Guha, A., Malkin, D., Felsberg, J., Reifenberger, G., von Deimling, A., Ichimura, K., Collins, V. P., Witt, H., Milde, T., Witt, O., Zhang, C., Castelo-Branco, P., Lichter, P., Faury, D., Tabori, U., Plass, C., Majewski, J., Pfister, S. M. and Jabado, N. (2012) ‘Driver mutations in histone H3.3 and chromatin remodelling genes in paediatric glioblastoma’, *Nature*, 482(7384), pp. 226–231. doi: 10.1038/nature10833.

Schwer, B., Wei, P.-C., Chang, A. N., Kao, J., Du, Z., Meyers, R. M. and Alt, F. W. (2016) ‘Transcription-associated processes cause DNA double-strand breaks and translocations in neural stem/progenitor cells.’, *Proceedings of the National Academy of Sciences of the United States of America*. National Academy of Sciences, 113(8), pp. 2258–63. doi: 10.1073/pnas.1525564113.

Shanbhag, N. M., Rafalska-Metcalf, I. U., Balane-Bolivar, C., Janicki, S. M. and Greenberg, R. A. (2010) ‘ATM-dependent chromatin changes silence

transcription in cis to DNA double-strand breaks.', *Cell*. NIH Public Access, 141(6), pp. 970–81. doi: 10.1016/j.cell.2010.04.038.

Sharma, G. G., So, S., Gupta, A., Kumar, R., Cayrou, C., Avvakumov, N., Bhadra, U., Pandita, R. K., Porteus, M. H., Chen, D. J., Cote, J. and Pandita, T. K. (2010a) 'MOF and Histone H4 Acetylation at Lysine 16 Are Critical for DNA Damage Response and Double-Strand Break Repair', *Molecular and Cellular Biology*, 30(14), pp. 3582–3595. doi: 10.1128/MCB.01476-09.

Sharma, G. G., So, S., Gupta, A., Kumar, R., Cayrou, C., Avvakumov, N., Bhadra, U., Pandita, R. K., Porteus, M. H., Chen, D. J., Cote, J. and Pandita, T. K. (2010b) 'MOF and Histone H4 Acetylation at Lysine 16 Are Critical for DNA Damage Response and Double-Strand Break Repair', *Molecular and Cellular Biology*, 30(14), pp. 3582–3595. doi: 10.1128/MCB.01476-09.

Sharma, M. K., Imamichi, S., Fukuchi, M., Samarth, R. M., Tomita, M. and Matsumoto, Y. (2016) '*In cellulo* phosphorylation of XRCC4 Ser320 by DNA-PK induced by DNA damage', *Journal of Radiation Research*, 57(2), pp. 115–120. doi: 10.1093/jrr/rrv086.

Shiloh, Y. (2006) 'The ATM-mediated DNA-damage response: taking shape.', *Trends in biochemical sciences*. Elsevier, 31(7), pp. 402–10. doi: 10.1016/j.tibs.2006.05.004.

Shoaib, M., Kulyyassov, A., Robin, C., Winczura, K., Tarlykov, P., Despas, E., Kannouche, P., Ramanculov, E., Lipinski, M. and Ogryzko, V. (2013) 'PUB-NChIP--"in vivo biotinylation" approach to study chromatin in proximity to a protein of interest.', *Genome research*, 23(2), pp. 331–40. doi: 10.1101/gr.134874.111.

Shroff, R., Arbel-Eden, A., Pilch, D., Ira, G., Bonner, W. M., Petrini, J. H., Haber, J. E. and Lichten, M. (2004a) 'Distribution and Dynamics of Chromatin Modification Induced by a Defined DNA Double-Strand Break', *Current Biology*, 14(19), pp. 1703–1711. doi: 10.1016/j.cub.2004.09.047.

Shroff, R., Arbel-Eden, A., Pilch, D., Ira, G., Bonner, W. M., Petrini, J. H., Haber, J. E. and Lichten, M. (2004b) 'Distribution and Dynamics of Chromatin Modification Induced by a Defined DNA Double-Strand Break',

Current Biology. Cell Press, 14(19), pp. 1703–1711. doi: 10.1016/J.CUB.2004.09.047.

Sidoli, S., Yuan, Z.-F., Lin, S., Karch, K., Wang, X., Bhanu, N., Arnaudo, A. M., Britton, L.-M., Cao, X.-J., Gonzales-Cope, M., Han, Y., Liu, S., Molden, R. C., Wein, S., Afjehi-Sadat, L. and Garcia, B. A. (2015) 'Drawbacks in the use of unconventional hydrophobic anhydrides for histone derivatization in bottom-up proteomics PTM analysis.', *Proteomics*. NIH Public Access, 15(9), pp. 1459–69. doi: 10.1002/pmic.201400483.

Simsek, D., Brunet, E., Wong, S. Y.-W., Katyal, S., Gao, Y., McKinnon, P. J., Lou, J., Zhang, L., Li, J., Rebar, E. J., Gregory, P. D., Holmes, M. C. and Jasin, M. (2011) 'DNA Ligase III Promotes Alternative Nonhomologous End-Joining during Chromosomal Translocation Formation', *PLoS Genetics*. Edited by J. E. Haber, 7(6), p. e1002080. doi: 10.1371/journal.pgen.1002080.

Skourti-Stathaki, K., Proudfoot, N. J. and Gromak, N. (2011) 'Human Senataxin Resolves RNA/DNA Hybrids Formed at Transcriptional Pause Sites to Promote Xrn2-Dependent Termination', *Molecular Cell*, 42(6), pp. 794–805. doi: 10.1016/j.molcel.2011.04.026.

Smerdon, M. J. and Conconi, A. (1999) 'Modulation of DNA damage and DNA repair in chromatin.', *Progress in nucleic acid research and molecular biology*, 62, pp. 227–55. Available at: http://www.ncbi.nlm.nih.gov/pubmed/9932456 (Accessed: 31 August 2018).

Sollier, J., Stork, C. T., García-Rubio, M. L., Paulsen, R. D., Aguilera, A. and Cimprich, K. A. (2014) 'Transcription-Coupled Nucleotide Excision Repair Factors Promote R-Loop-Induced Genome Instability', *Molecular Cell*, 56(6), pp. 777–785. doi: 10.1016/j.molcel.2014.10.020.

Song, K.-H., An, H.-M., Kim, H.-J., Ahn, S.-H., Chung, S.-J. and Shim, C.-K. (2002) 'Simple liquid chromatography–electrospray ionization mass spectrometry method for the routine determination of salmon calcitonin in serum', *Journal of Chromatography B*. Elsevier, 775(2), pp. 247–255. doi: 10.1016/S1570-0232(02)00316-1.

Stejskal, K., Potěšil, D. and Zdráhal, Z. (2013) 'Suppression of Peptide

Sample Losses in Autosampler Vials', *Journal of Proteome Research*. American Chemical Society, 12(6), pp. 3057–3062. doi: 10.1021/pr400183v.

Stewart, G. S., Panier, S., Townsend, K., Al-Hakim, A. K., Kolas, N. K., Miller, E. S., Nakada, S., Ylanko, J., Olivarius, S., Mendez, M., Oldreive, C., Wildenhain, J., Tagliaferro, A., Pelletier, L., Taubenheim, N., Durandy, A., Byrd, P. J., Stankovic, T., Taylor, A. M. R. and Durocher, D. (2009) 'The RIDDLE Syndrome Protein Mediates a Ubiquitin-Dependent Signaling Cascade at Sites of DNA Damage', *Cell*, 136(3), pp. 420–434. doi: 10.1016/j.cell.2008.12.042.

Stiff, T., O'Driscoll, M., Rief, N., Iwabuchi, K., Löbrich, M. and Jeggo, P. A. (2004) 'ATM and DNA-PK function redundantly to phosphorylate H2AX after exposure to ionizing radiation.', *Cancer research*, 64(7), pp. 2390–6. Available at: http://www.ncbi.nlm.nih.gov/pubmed/15059890 (Accessed: 15 January 2018).

Stork, C. T., Bocek, M., Crossley, M. P., Sollier, J., Sanz, L. A., Chédin, F., Swigut, T. and Cimprich, K. A. (2016) 'Co-transcriptional R-loops are the main cause of estrogen-induced DNA damage', *eLife*, 5. doi: 10.7554/eLife.17548.

Stracker, T. H., Theunissen, J.-W. F., Morales, M. and Petrini, J. H. J. (2004) 'The Mre11 complex and the metabolism of chromosome breaks: the importance of communicating and holding things together', *DNA Repair*, 3(8–9), pp. 845–854. doi: 10.1016/j.dnarep.2004.03.014.

Strahl, B. D. and Allis, C. D. (2000) 'The language of covalent histone modifications', *Nature*, 403(6765), pp. 41–45. doi: 10.1038/47412.

Stucki, M., Clapperton, J. A., Mohammad, D., Yaffe, M. B., Smerdon, S. J. and Jackson, S. P. (2005) 'MDC1 directly binds phosphorylated histone H2AX to regulate cellular responses to DNA double-strand breaks.', *Cell*. Elsevier, 123(7), pp. 1213–26. doi: 10.1016/j.cell.2005.09.038.

Sun, Y., Jiang, X., Xu, Y., Ayrapetov, M. K., Moreau, L. A., Whetstine, J. R. and Price, B. D. (2009) 'Histone H3 methylation links DNA damage detection to activation of the tumour suppressor Tip60', *Nature Cell Biology*, 11(11), pp.

1376–1382. doi: 10.1038/ncb1982.

Sweet, S. M. M., Li, M., Thomas, P. M., Durbin, K. R. and Kelleher, N. L. (2010) ‘Kinetics of Re-establishing H3K79 Methylation Marks in Global Human Chromatin’, *Journal of Biological Chemistry*, 285(43), pp. 32778–32786. doi: 10.1074/jbc.M110.145094.

Switzar, L., Giera, M. and Niessen, W. M. A. (2013) ‘Protein Digestion: An Overview of the Available Techniques and Recent Developments’, *Journal of Proteome Research*. American Chemical Society, 12(3), pp. 1067–1077. doi: 10.1021/pr301201x.

Symington, L. S. and Gautier, J. (2011) ‘Double-Strand Break End Resection and Repair Pathway Choice’, *Annual Review of Genetics*, 45(1), pp. 247–271. doi: 10.1146/annurev-genet-110410-132435.

Tamburini, B. A. and Tyler, J. K. (2005) ‘Localized histone acetylation and deacetylation triggered by the homologous recombination pathway of double-strand DNA repair.’, *Molecular and cellular biology*, 25(12), pp. 4903–13. doi: 10.1128/MCB.25.12.4903-4913.2005.

Tang, J., Cho, N. W., Cui, G., Manion, E. M., Shanbhag, N. M., Botuyan, M. V., Mer, G. and Greenberg, R. A. (2013) ‘Acetylation limits 53BP1 association with damaged chromatin to promote homologous recombination.’, *Nature structural & molecular biology*, 20(3), pp. 317–25. doi: 10.1038/nsmb.2499.

Técher, H., Koundrioukoff, S., Nicolas, A. and Debatisse, M. (2017) ‘The impact of replication stress on replication dynamics and DNA damage in vertebrate cells’, *Nature Reviews Genetics*. Nature Publishing Group, 18(9), pp. 535–550. doi: 10.1038/nrg.2017.46.

Tessadori, F., Giltay, J. C., Hurst, J. A., Massink, M. P., Duran, K., Vos, H. R., van Es, R. M., Scott, R. H., van Gassen, K. L. I., Bakkers, J., van Haaften, G. and van Haaften, G. (2017) ‘Germline mutations affecting the histone H4 core cause a developmental syndrome by altering DNA damage response and cell cycle control’, *Nature Genetics*, 49(11), pp. 1642–1646. doi: 10.1038/ng.3956.

Thorslund, T., Ripplinger, A., Hoffmann, S., Wild, T., Uckelmann, M., Villumsen, B., Narita, T., Sixma, T. K., Choudhary, C., Bekker-Jensen, S. and Mailand, N. (2015a) 'Histone H1 couples initiation and amplification of ubiquitin signalling after DNA damage', *Nature*, 527(7578), pp. 389–393. doi: 10.1038/nature15401.

Thorslund, T., Ripplinger, A., Hoffmann, S., Wild, T., Uckelmann, M., Villumsen, B., Narita, T., Sixma, T. K., Choudhary, C., Bekker-Jensen, S. and Mailand, N. (2015b) 'Histone H1 couples initiation and amplification of ubiquitin signalling after DNA damage', *Nature*. Nature Publishing Group, 527(7578), pp. 389–393. doi: 10.1038/nature15401.

Tjeertes, J. V, Miller, K. M. and Jackson, S. P. (2009) 'Screen for DNA-damage-responsive histone modifications identifies H3K9Ac and H3K56Ac in human cells', *The EMBO Journal*, 28(13), pp. 1878–1889. doi: 10.1038/emboj.2009.119.

Trojer, P. and Reinberg, D. (2007) 'Facultative Heterochromatin: Is There a Distinctive Molecular Signature?', *Molecular Cell*. Cell Press, 28(1), pp. 1–13. doi: 10.1016/J.MOLCEL.2007.09.011.

Tubbs, A. T. and Sleckman, B. P. (2014) 'ATM deficiency: revealing the pathways to cancer.', *Cell cycle (Georgetown, Tex.)*. Taylor & Francis, 13(19), p. 2992. doi: 10.4161/15384101.2014.959849.

Turinetto, V. and Giachino, C. (2015) 'Multiple facets of histone variant H2AX: a DNA double-strand-break marker with several biological functions', *Nucleic Acids Research*. Oxford University Press, 43(5), pp. 2489–2498. doi: 10.1093/nar/gkv061.

Tuzon, C. T., Spektor, T., Kong, X., Congdon, L. M., Wu, S., Schotta, G., Yokomori, K. and Rice, J. C. (2014) 'Concerted Activities of Distinct H4K20 Methyltransferases at DNA Double-Strand Breaks Regulate 53BP1 Nucleation and NHEJ-Directed Repair', *Cell Reports*, 8(2), pp. 430–438. doi: 10.1016/j.celrep.2014.06.013.

Verdel, A. (2004) 'RNAi-Mediated Targeting of Heterochromatin by the RITS Complex', *Science*, 303(5658), pp. 672–676. doi: 10.1126/science.1093686.

Walker, J. M. (ed.) (2005) *The Proteomics Protocols Handbook*. Totowa, NJ: Humana Press. doi: 10.1385/1592598900.

Walker, J. R., Corpina, R. A. and Goldberg, J. (2001) 'Structure of the Ku heterodimer bound to DNA and its implications for double-strand break repair', *Nature*, 412(6847), pp. 607–614. doi: 10.1038/35088000.

Wang, Y.-G., Nnakwe, C., Lane, W. S., Modesti, M. and Frank, K. M. (2004) 'Phosphorylation and regulation of DNA ligase IV stability by DNA-dependent protein kinase.', *The Journal of biological chemistry*. American Society for Biochemistry and Molecular Biology, 279(36), pp. 37282–90. doi: 10.1074/jbc.M401217200.

Wei, P.-C., Chang, A. N., Kao, J., Du, Z., Meyers, R. M., Alt, F. W. and Schwer, B. (2016) 'Long Neural Genes Harbor Recurrent DNA Break Clusters in Neural Stem/Progenitor Cells', *Cell*, 164(4), pp. 644–655. doi: 10.1016/j.cell.2015.12.039.

Wei, S., Li, C., Yin, Z., Wen, J., Meng, H., Xue, L. and Wang, J. (2018) 'Histone methylation in DNA repair and clinical practice: new findings during the past 5-years', *Journal of Cancer*, 9(12), pp. 2072–2081. doi: 10.7150/jca.23427.

Wilson, M. D., Benlekbir, S., Fradet-Turcotte, A., Sherker, A., Julien, J.-P., McEwan, A., Noordermeer, S. M., Sicheri, F., Rubinstein, J. L. and Durocher, D. (2016) 'The structural basis of modified nucleosome recognition by 53BP1', *Nature*. Nature Publishing Group, 536(7614), pp. 100–103. doi: 10.1038/nature18951.

Woo, C. J., Kharchenko, P. V., Daheron, L., Park, P. J. and Kingston, R. E. (2010) 'A Region of the Human HOXD Cluster that Confers Polycomb-Group Responsiveness', *Cell*, 140(1), pp. 99–110. doi: 10.1016/j.cell.2009.12.022.

Woodbine, L., Gennery, A. R. and Jeggo, P. A. (2014) 'The clinical impact of deficiency in DNA non-homologous end-joining', *DNA Repair*, 16, pp. 84–96. doi: 10.1016/j.dnarep.2014.02.011.

Woodbine, L., Grigoriadou, S., Goodarzi, A. A., Riballo, E., Tape, C., Oliver,

A. W., van Zelm, M. C., Buckland, M. S., Davies, E. G., Pearl, L. H. and Jeggo, P. A. (2010) 'An Artemis polymorphic variant reduces Artemis activity and confers cellular radiosensitivity.', *DNA repair*, 9(9), pp. 1003–10. doi: 10.1016/j.dnarep.2010.07.001.

Woodbine, L., Neal, J. A., Sasi, N.-K., Shimada, M., Deem, K., Coleman, H., Dobyns, W. B., Ogi, T., Meek, K., Davies, E. G. and Jeggo, P. A. (2013) 'PRKDC mutations in a SCID patient with profound neurological abnormalities.', *The Journal of clinical investigation*. American Society for Clinical Investigation, 123(7), pp. 2969–80. doi: 10.1172/JCI67349.

Woodcock, C. L. and Ghosh, R. P. (2010) 'Chromatin higher-order structure and dynamics.', *Cold Spring Harbor perspectives in biology*. Cold Spring Harbor Laboratory Press, 2(5), p. a000596. doi: 10.1101/cshperspect.a000596.

Wu, G., Broniscer, A., McEachron, T. A., Lu, C., Paugh, B. S., Becksfort, J., Qu, C., Ding, L., Huether, R., Parker, M., Zhang, J., Gajjar, A., Dyer, M. A., Mullighan, C. G., Gilbertson, R. J., Mardis, E. R., Wilson, R. K., Downing, J. R., Ellison, D. W., Zhang, J., Baker, S. J. and St. Jude Children's Research Hospital–Washington University Pediatric Cancer Genome Project (2012) 'Somatic histone H3 alterations in pediatric diffuse intrinsic pontine gliomas and non-brainstem glioblastomas', *Nature Genetics*, 44(3), pp. 251–253. doi: 10.1038/ng.1102.

Wu, G. and Lee, W.-H. (2006) 'CtIP, a Multivalent Adaptor Connecting Transcriptional Regulation, Checkpoint Control and Tumor Suppression', *Cell Cycle*, 5(15), pp. 1592–1596. doi: 10.4161/cc.5.15.3127.

Wu, L., Zee, B. M., Wang, Y., Garcia, B. A. and Dou, Y. (2011) 'The RING Finger Protein MSL2 in the MOF Complex Is an E3 Ubiquitin Ligase for H2B K34 and Is Involved in Crosstalk with H3 K4 and K79 Methylation', *Molecular Cell*, 43(1), pp. 132–144. doi: 10.1016/j.molcel.2011.05.015.

Wu, W., Nishikawa, H., Fukuda, T., Vittal, V., Asano, M., Miyoshi, Y., Klevit, R. E. and Ohta, T. (2015) 'Interaction of BARD1 and HP1 Is Required for BRCA1 Retention at Sites of DNA Damage.', *Cancer research*. NIH Public

Access, 75(7), pp. 1311–21. doi: 10.1158/0008-5472.CAN-14-2796.

Xie, A., Odate, S., Chandramouly, G. and Scully, R. (2010) 'H2AX post-translational modifications in the ionizing radiation response and homologous recombination.', *Cell cycle (Georgetown, Tex.)*. Taylor & Francis, 9(17), pp. 3602–10. doi: 10.4161/cc.9.17.12884.

Xu, Y., Ayrapetov, M. K., Xu, C., Gursoy-Yuzugullu, O., Hu, Y. and Price, B. D. (2012) 'Histone H2A.Z controls a critical chromatin remodeling step required for DNA double-strand break repair.', *Molecular cell*, 48(5), pp. 723–33. doi: 10.1016/j.molcel.2012.09.026.

Yan, Q., Dutt, S., Xu, R., Graves, K., Juszczynski, P., Manis, J. P. and Shipp, M. A. (2009) 'BBAP Monoubiquitylates Histone H4 at Lysine 91 and Selectively Modulates the DNA Damage Response', *Molecular Cell*, 36(1), pp. 110–120. doi: 10.1016/j.molcel.2009.08.019.

Yan, Q., Dutt, S., Xu, R., Graves, K., Juszczynski, P., Manis, J. P. and Shipp, M. A. (2009) 'BBAP monoubiquitylates histone H4 at lysine 91 and selectively modulates the DNA damage response.', *Molecular cell*. NIH Public Access, 36(1), pp. 110–20. doi: 10.1016/j.molcel.2009.08.019.

Yan, Q., Xu, R., Zhu, L., Cheng, X., Wang, Z., Manis, J. and Shipp, M. A. (2013) 'BAL1 and Its Partner E3 Ligase, BBAP, Link Poly(ADP-Ribose) Activation, Ubiquitylation, and Double-Strand DNA Repair Independent of ATM, MDC1, and RNF8', *Molecular and Cellular Biology*, 33(4), pp. 845–857. doi: 10.1128/MCB.00990-12.

Yang, Y., Fiskus, W., Yong, B., Atadja, P., Takahashi, Y., Pandita, T. K., Wang, H.-G. and Bhalla, K. N. (2013) 'Acetylated hsp70 and KAP1-mediated Vps34 SUMOylation is required for autophagosome creation in autophagy.', *Proceedings of the National Academy of Sciences of the United States of America*. National Academy of Sciences, 110(17), pp. 6841–6. doi: 10.1073/pnas.1217692110.

Yarnold, J. (2018) 'Changes in radiotherapy fractionation—breast cancer', *The British Journal of Radiology*. The British Institute of Radiology., p. 20170849. doi: 10.1259/bjr.20170849.

Young, L. C., McDonald, D. W. and Hendzel, M. J. (2013) ‘Kdm4b histone demethylase is a DNA damage response protein and confers a survival advantage following γ-irradiation.’, *The Journal of biological chemistry*. American Society for Biochemistry and Molecular Biology, 288(29), pp. 21376–88. doi: 10.1074/jbc.M113.491514.

YU, Y., MAHANEY, B., YANO, K., YE, R., FANG, S., DOUGLAS, P., CHEN, D. and LEESMILLER, S. (2008) ‘DNA-PK and ATM phosphorylation sites in XLF/Cernunnos are not required for repair of DNA double strand breaks’, *DNA Repair*, 7(10), pp. 1680–1692. doi: 10.1016/j.dnarep.2008.06.015.

Yüce, Ö. and West, S. C. (2013) ‘Senataxin, defective in the neurodegenerative disorder ataxia with oculomotor apraxia 2, lies at the interface of transcription and the DNA damage response.’, *Molecular and cellular biology*. American Society for Microbiology (ASM), 33(2), pp. 406–17. doi: 10.1128/MCB.01195-12.

Zee, B. M., Levin, R. S., Xu, B., LeRoy, G., Wingreen, N. S. and Garcia, B. A. (2010) ‘*In Vivo* Residue-specific Histone Methylation Dynamics’, *Journal of Biological Chemistry*, 285(5), pp. 3341–3350. doi: 10.1074/jbc.M109.063784.

Zhang, Y. and Reinberg, D. (2001) ‘Transcription regulation by histone methylation: interplay between different covalent modifications of the core histone tails.’, *Genes & development*. Cold Spring Harbor Laboratory Press, 15(18), pp. 2343–60. doi: 10.1101/gad.927301.

Zheng, Y., Sweet, S. M. M., Popovic, R., Martinez-Garcia, E., Tipton, J. D., Thomas, P. M., Licht, J. D. and Kelleher, N. L. (2012) ‘Total kinetic analysis reveals how combinatorial methylation patterns are established on lysines 27 and 36 of histone H3’, *Proceedings of the National Academy of Sciences*, 109(34), pp. 13549–13554. doi: 10.1073/pnas.1205707109.

Zheng, Y., Tipton, J. D., Thomas, P. M., Kelleher, N. L. and Sweet, S. M. M. (2014) ‘Site-specific human histone H3 methylation stability: fast K4me3 turnover’, *PROTEOMICS*, 14(19), pp. 2190–2199. doi: 10.1002/pmic.201400060.

9 APPENDIX

Protein Gene	Peptide Modified Sequence	Precursor m/z	Precursor Charge	Fragment Ion	Peptide Abbreviated Name
HIST2H3A	T[+56]K[+42]QTAR	401.7427	2	precursor	K4me3
HIST2H3A	T[+56]K[+42]QTAR	401.7427	2	precursor [M+1]	K4me3
HIST2H3A	T[+56]K[+42]QTAR	401.7427	2	precursor [M+2]	K4me3
HIST2H3A	T[+56]K[+42]QTAR	401.7427	2	y4	K4me3
HIST2H3A	T[+56]K[+42]QTAR	401.7427	2	y1	K4me3
HIST2H3A	T[+56]K[+42]QTAR	401.7427	2	b1	K4me3
HIST2H3A	T[+56]K[+42]QTAR	401.7427	2	b3	K4me3

HIST2H3A	T[+56]K[+42]QTAR	401.7427	2	b4	K4me3
HIST2H3A	T[+56]K[+42]QTAR	401.7427	2	b5	K4me3
HIST2H3A	T[+56]K[+28]QTAR	394.7348	2	precursor	K4me2
HIST2H3A	T[+56]K[+28]QTAR	394.7348	2	precursor [M+1]	K4me2
HIST2H3A	T[+56]K[+28]QTAR	394.7348	2	precursor [M+2]	K4me2
HIST2H3A	T[+56]K[+28]QTAR	394.7348	2	y4	K4me2
HIST2H3A	T[+56]K[+28]QTAR	394.7348	2	y1	K4me2
HIST2H3A	T[+56]K[+28]QTAR	394.7348	2	b1	K4me2
HIST2H3A	T[+56]K[+28]QTAR	394.7348	2	b3	K4me2
HIST2H3A	T[+56]K[+28]QTAR	394.7348	2	b4	K4me2
HIST2H3A	T[+56]K[+28]QTAR	394.7348	2	b5	K4me2
HIST2H3A	T[+56]K[+56]QTAR	816.4573	1	precursor	K4me0
HIST2H3A	T[+56]K[+56]QTAR	816.4573	1	precursor [M+1]	K4me0
HIST2H3A	T[+56]K[+56]QTAR	816.4573	1	precursor [M+2]	K4me0
HIST2H3A	T[+56]K[+56]QTAR	816.4573	1	y5	K4me0
HIST2H3A	T[+56]K[+56]QTAR	816.4573	1	y3	K4me0
HIST2H3A	T[+56]K[+56]QTAR	816.4573	1	y2	K4me0
HIST2H3A	T[+56]K[+56]QTAR	816.4573	1	b2	K4me0
HIST2H3A	T[+56]K[+56]QTAR	816.4573	1	b2 -18	K4me0
HIST2H3A	T[+56]K[+56]QTAR	816.4573	1	b3 -18	K4me0
HIST2H3A	T[+56]K[+56]QTAR	816.4573	1	b4	K4me0
HIST2H3A	T[+56]K[+56]QTAR	816.4573	1	b4 -18	K4me0
HIST2H3A	T[+56]K[+56]QTAR	816.4573	1	b5	K4me0
HIST2H3A	T[+56]K[+56]QTAR	816.4573	1	b5 -18	K4me0
HIST2H3A	T[+56]K[+70]QTAR	830.4730	1	precursor	K4me1
HIST2H3A	T[+56]K[+70]QTAR	830.4730	1	precursor [M+1]	K4me1
HIST2H3A	T[+56]K[+70]QTAR	830.4730	1	precursor [M+2]	K4me1
HIST2H3A	T[+56]K[+70]QTAR	830.4730	1	y3	K4me1
HIST2H3A	T[+56]K[+70]QTAR	830.4730	1	y2	K4me1
HIST2H3A	T[+56]K[+70]QTAR	830.4730	1	b2	K4me1
HIST2H3A	T[+56]K[+70]QTAR	830.4730	1	b2 -18	K4me1
HIST2H3A	T[+56]K[+70]QTAR	830.4730	1	b3 -18	K4me1
HIST2H3A	T[+56]K[+70]QTAR	830.4730	1	b4	K4me1
HIST2H3A	T[+56]K[+70]QTAR	830.4730	1	b4 -18	K4me1
HIST2H3A	T[+56]K[+70]QTAR	830.4730	1	b5 -18	K4me1
HIST2H3A	K[+112.1]STGGK[+42]APR	528.2958	2	precursor	K9unmodK14Ac
HIST2H3A	K[+112.1]STGGK[+42]APR	528.2958	2	precursor [M+1]	K9unmodK14Ac

HIST2H3A	K[+112.1]STGGK[+42]APR	528.29583	2	precursor [M+2]	K9unmodK14Ac
HIST2H3A	K[+112.1]STGGK[+42]APR	528.29583	2	y8	K9unmodK14Ac
HIST2H3A	K[+112.1]STGGK[+42]APR	528.29583	2	y7	K9unmodK14Ac
HIST2H3A	K[+112.1]STGGK[+42]APR	528.29583	2	y6	K9unmodK14Ac
HIST2H3A	K[+112.1]STGGK[+42]APR	528.29583	2	y5	K9unmodK14Ac
HIST2H3A	K[+112.1]STGGK[+42]APR	528.29583	2	b1	K9unmodK14Ac
HIST2H3A	K[+112.1]STGGK[+42]APR	528.29583	2	b2	K9unmodK14Ac
HIST2H3A	K[+112.1]STGGK[+42]APR	528.29583	2	b3	K9unmodK14Ac
HIST2H3A	K[+112.1]STGGK[+42]APR	528.29583	2	b4	K9unmodK14Ac
HIST2H3A	K[+112.1]STGGK[+56]APR	535.30366	2	precursor	K9unmodK14unmod
HIST2H3A	K[+112.1]STGGK[+56]APR	535.30366	2	precursor [M+1]	K9unmodK14unmod
HIST2H3A	K[+112.1]STGGK[+56]APR	535.30366	2	precursor [M+2]	K9unmodK14unmod
HIST2H3A	K[+112.1]STGGK[+56]APR	535.30366	2	y8	K9unmodK14unmod
HIST2H3A	K[+112.1]STGGK[+56]APR	535.30366	2	y7	K9unmodK14unmod
HIST2H3A	K[+112.1]STGGK[+56]APR	535.30366	2	y6	K9unmodK14unmod
HIST2H3A	K[+112.1]STGGK[+56]APR	535.30366	2	y5	K9unmodK14unmod
HIST2H3A	K[+112.1]STGGK[+56]APR	535.30366	2	y3	K9unmodK14unmod
HIST2H3A	K[+112.1]STGGK[+56]APR	535.30366	2	y2	K9unmodK14unmod
HIST2H3A	K[+112.1]STGGK[+56]APR	535.30366	2	b1	K9unmodK14unmod
HIST2H3A	K[+112.1]STGGK[+56]APR	535.30366	2	b2	K9unmodK14unmod
HIST2H3A	K[+112.1]STGGK[+56]APR	535.30366	2	b6	K9unmodK14unmod
HIST2H3A	K[+112.1]STGGK[+56]APR	535.30366	2	b7	K9unmodK14unmod
HIST2H3A	K[+126.1]STGGK[+42]APR	535.30366	2	precursor	K9me1K14Ac
HIST2H3A	K[+126.1]STGGK[+42]APR	535.30366	2	precursor [M+1]	K9me1K14Ac
HIST2H3A	K[+126.1]STGGK[+42]APR	535.30366	2	precursor [M+2]	K9me1K14Ac
HIST2H3A	K[+126.1]STGGK[+42]APR	535.30366	2	y8	K9me1K14Ac
HIST2H3A	K[+126.1]STGGK[+42]APR	535.30366	2	y7	K9me1K14Ac
HIST2H3A	K[+126.1]STGGK[+42]APR	535.30366	2	y6	K9me1K14Ac
HIST2H3A	K[+126.1]STGGK[+42]APR	535.30366	2	y5	K9me1K14Ac
HIST2H3A	K[+126.1]STGGK[+42]APR	535.30366	2	y3	K9me1K14Ac
HIST2H3A	K[+126.1]STGGK[+42]APR	535.30366	2	y2	K9me1K14Ac
HIST2H3A	K[+126.1]STGGK[+42]APR	535.30366	2	b1	K9me1K14Ac
HIST2H3A	K[+126.1]STGGK[+42]APR	535.30366	2	b2	K9me1K14Ac
HIST2H3A	K[+126.1]STGGK[+42]APR	535.30366	2	b6	K9me1K14Ac
HIST2H3A	K[+126.1]STGGK[+42]APR	535.30366	2	b7	K9me1K14Ac
HIST2H3A	K[+126.1]STGGK[+56]APR	542.31148	2	precursor	K9me1K14unmod
HIST2H3A	K[+126.1]STGGK[+56]APR	542.3114	2	precursor	K9me1K14unmod

		8		[M+1]	
HIST2H3A	K[+126.1]STGGK[+56]APR	542.3114 8	2	precursor [M+2]	K9me1K14unmod
HIST2H3A	K[+126.1]STGGK[+56]APR	542.3114 8	2	y8	K9me1K14unmod
HIST2H3A	K[+126.1]STGGK[+56]APR	542.3114 8	2	y7	K9me1K14unmod
HIST2H3A	K[+126.1]STGGK[+56]APR	542.3114 8	2	y6	K9me1K14unmod
HIST2H3A	K[+126.1]STGGK[+56]APR	542.3114 8	2	y5	K9me1K14unmod
HIST2H3A	K[+126.1]STGGK[+56]APR	542.3114 8	2	y3	K9me1K14unmod
HIST2H3A	K[+126.1]STGGK[+56]APR	542.3114 8	2	y2	K9me1K14unmod
HIST2H3A	K[+126.1]STGGK[+56]APR	542.3114 8	2	b1	K9me1K14unmod
HIST2H3A	K[+126.1]STGGK[+56]APR	542.3114 8	2	b2	K9me1K14unmod
HIST2H3A	K[+126.1]STGGK[+56]APR	542.3114 8	2	b6	K9me1K14unmod
HIST2H3A	K[+126.1]STGGK[+56]APR	542.3114 8	2	b7	K9me1K14unmod
HIST2H3A	K[+84.1]STGGK[+42]APR	514.2983 7	2	precursor	K9me2K14Ac
HIST2H3A	K[+84.1]STGGK[+42]APR	514.2983 7	2	precursor [M+1]	K9me2K14Ac
HIST2H3A	K[+84.1]STGGK[+42]APR	514.2983 7	2	precursor [M+2]	K9me2K14Ac
HIST2H3A	K[+84.1]STGGK[+42]APR	514.2983 7	2	y8	K9me2K14Ac
HIST2H3A	K[+84.1]STGGK[+42]APR	514.2983 7	2	y7	K9me2K14Ac
HIST2H3A	K[+84.1]STGGK[+42]APR	514.2983 7	2	y6	K9me2K14Ac
HIST2H3A	K[+84.1]STGGK[+42]APR	514.2983 7	2	y5	K9me2K14Ac
HIST2H3A	K[+84.1]STGGK[+42]APR	514.2983 7	2	y3	K9me2K14Ac
HIST2H3A	K[+84.1]STGGK[+42]APR	514.2983 7	2	y2	K9me2K14Ac
HIST2H3A	K[+84.1]STGGK[+42]APR	514.2983 7	2	b1	K9me2K14Ac
HIST2H3A	K[+84.1]STGGK[+42]APR	514.2983 7	2	b2	K9me2K14Ac
HIST2H3A	K[+84.1]STGGK[+42]APR	514.2983 7	2	b6	K9me2K14Ac
HIST2H3A	K[+84.1]STGGK[+42]APR	514.2983 7	2	b7	K9me2K14Ac
HIST2H3A	K[+84.1]STGGK[+42]APR	514.2983 7	2	b8	K9me2K14Ac
HIST2H3A	K[+84.1]STGGK[+56]APR	521.3062	2	precursor	K9me2K14unmod
HIST2H3A	K[+84.1]STGGK[+56]APR	521.3062	2	precursor [M+1]	K9me2K14unmod
HIST2H3A	K[+84.1]STGGK[+56]APR	521.3062	2	precursor [M+2]	K9me2K14unmod
HIST2H3A	K[+84.1]STGGK[+56]APR	521.3062	2	y8	K9me2K14unmod
HIST2H3A	K[+84.1]STGGK[+56]APR	521.3062	2	y7	K9me2K14unmod
HIST2H3A	K[+84.1]STGGK[+56]APR	521.3062	2	y6	K9me2K14unmod
HIST2H3A	K[+84.1]STGGK[+56]APR	521.3062	2	y5	K9me2K14unmod
HIST2H3A	K[+84.1]STGGK[+56]APR	521.3062	2	y3	K9me2K14unmod
HIST2H3A	K[+84.1]STGGK[+56]APR	521.3062	2	y2	K9me2K14unmod
HIST2H3A	K[+84.1]STGGK[+56]APR	521.3062	2	b1	K9me2K14unmod
HIST2H3A	K[+84.1]STGGK[+56]APR	521.3062	2	b2	K9me2K14unmod
HIST2H3A	K[+84.1]STGGK[+56]APR	521.3062	2	b6	K9me2K14unmod
HIST2H3A	K[+84.1]STGGK[+56]APR	521.3062	2	b7	K9me2K14unmod

HIST2H3A	K[+84.1]STGGK[+56]APR	521.3062	2	b8	K9me2K14unmod
HIST2H3A	K[+98]STGGK[+42]APR	521.2880 1	2	precursor	K9AcK14Ac
HIST2H3A	K[+98]STGGK[+42]APR	521.2880 1	2	precursor [M+1]	K9AcK14Ac
HIST2H3A	K[+98]STGGK[+42]APR	521.2880 1	2	precursor [M+2]	K9AcK14Ac
HIST2H3A	K[+98]STGGK[+42]APR	521.2880 1	2	y8	K9AcK14Ac
HIST2H3A	K[+98]STGGK[+42]APR	521.2880 1	2	y7	K9AcK14Ac
HIST2H3A	K[+98]STGGK[+42]APR	521.2880 1	2	y6	K9AcK14Ac
HIST2H3A	K[+98]STGGK[+42]APR	521.2880 1	2	y5	K9AcK14Ac
HIST2H3A	K[+98]STGGK[+42]APR	521.2880 1	2	y4	K9AcK14Ac
HIST2H3A	K[+98]STGGK[+42]APR	521.2880 1	2	y2	K9AcK14Ac
HIST2H3A	K[+98]STGGK[+42]APR	521.2880 1	2	b1	K9AcK14Ac
HIST2H3A	K[+98]STGGK[+42]APR	521.2880 1	2	b2	K9AcK14Ac
HIST2H3A	K[+98]STGGK[+42]APR	521.2880 1	2	b6	K9AcK14Ac
HIST2H3A	K[+98]STGGK[+42]APR	521.2880 1	2	b7	K9AcK14Ac
HIST2H3A	K[+98]STGGK[+42]APR	521.2880 1	2	b8	K9AcK14Ac
HIST2H3A	K[+98]STGGK[+56]APR	528.2958 3	2	precursor	K9AcK14unmod
HIST2H3A	K[+98]STGGK[+56]APR	528.2958 3	2	precursor [M+1]	K9AcK14unmod
HIST2H3A	K[+98]STGGK[+56]APR	528.2958 3	2	precursor [M+2]	K9AcK14unmod
HIST2H3A	K[+98]STGGK[+56]APR	528.2958 3	2	y8	K9AcK14unmod
HIST2H3A	K[+98]STGGK[+56]APR	528.2958 3	2	y7	K9AcK14unmod
HIST2H3A	K[+98]STGGK[+56]APR	528.2958 3	2	y6	K9AcK14unmod
HIST2H3A	K[+98]STGGK[+56]APR	528.2958 3	2	y5	K9AcK14unmod
HIST2H3A	K[+98]STGGK[+56]APR	528.2958 3	2	b1	K9AcK14unmod
HIST2H3A	K[+98]STGGK[+56]APR	528.2958 3	2	b2	K9AcK14unmod
HIST2H3A	K[+98]STGGK[+56]APR	528.2958 3	2	b3	K9AcK14unmod
HIST2H3A	K[+98]STGGK[+56]APR	528.2958 3	2	b4	K9AcK14unmod
HIST2H3A	K[+98.1]STGGK[+42]APR	521.3062	2	precursor	K9me3K14Ac
HIST2H3A	K[+98.1]STGGK[+42]APR	521.3062	2	precursor [M+1]	K9me3K14Ac
HIST2H3A	K[+98.1]STGGK[+42]APR	521.3062	2	precursor [M+2]	K9me3K14Ac
HIST2H3A	K[+98.1]STGGK[+42]APR	521.3062	2	y8	K9me3K14Ac
HIST2H3A	K[+98.1]STGGK[+42]APR	521.3062	2	y7	K9me3K14Ac
HIST2H3A	K[+98.1]STGGK[+42]APR	521.3062	2	y6	K9me3K14Ac
HIST2H3A	K[+98.1]STGGK[+42]APR	521.3062	2	y5	K9me3K14Ac
HIST2H3A	K[+98.1]STGGK[+42]APR	521.3062	2	y3	K9me3K14Ac
HIST2H3A	K[+98.1]STGGK[+42]APR	521.3062	2	y2	K9me3K14Ac
HIST2H3A	K[+98.1]STGGK[+42]APR	521.3062	2	b2	K9me3K14Ac
HIST2H3A	K[+98.1]STGGK[+42]APR	521.3062	2	b6	K9me3K14Ac
HIST2H3A	K[+98.1]STGGK[+42]APR	521.3062	2	b7	K9me3K14Ac
HIST2H3A	K[+98.1]STGGK[+42]APR	521.3062	2	b8	K9me3K14Ac

HIST2H3A	K[+98.1]STGGK[+56]APR	528.31402	2	precursor	K9me3K14unmod
HIST2H3A	K[+98.1]STGGK[+56]APR	528.31402	2	precursor [M+1]	K9me3K14unmod
HIST2H3A	K[+98.1]STGGK[+56]APR	528.31402	2	precursor [M+2]	K9me3K14unmod
HIST2H3A	K[+98.1]STGGK[+56]APR	528.31402	2	y8	K9me3K14unmod
HIST2H3A	K[+98.1]STGGK[+56]APR	528.31402	2	y7	K9me3K14unmod
HIST2H3A	K[+98.1]STGGK[+56]APR	528.31402	2	y6	K9me3K14unmod
HIST2H3A	K[+98.1]STGGK[+56]APR	528.31402	2	y5	K9me3K14unmod
HIST2H3A	K[+98.1]STGGK[+56]APR	528.31402	2	y3	K9me3K14unmod
HIST2H3A	K[+98.1]STGGK[+56]APR	528.31402	2	y2	K9me3K14unmod
HIST2H3A	K[+98.1]STGGK[+56]APR	528.31402	2	b2	K9me3K14unmod
HIST2H3A	K[+98.1]STGGK[+56]APR	528.31402	2	b4	K9me3K14unmod
HIST2H3A	K[+98.1]STGGK[+56]APR	528.31402	2	b6	K9me3K14unmod
HIST2H3A	K[+98.1]STGGK[+56]APR	528.31402	2	b7	K9me3K14unmod
HIST2H3A	K[+98.1]STGGK[+56]APR	528.31402	2	b8	K9me3K14unmod
HIST2H3A	K[+112.1]QLATK[+42]AAR	570.84041	2	precursor	K18unmodK23Ac
HIST2H3A	K[+112.1]QLATK[+42]AAR	570.84041	2	precursor [M+1]	K18unmodK23Ac
HIST2H3A	K[+112.1]QLATK[+42]AAR	570.84041	2	precursor [M+2]	K18unmodK23Ac
HIST2H3A	K[+112.1]QLATK[+42]AAR	570.84041	2	y8	K18unmodK23Ac
HIST2H3A	K[+112.1]QLATK[+42]AAR	570.84041	2	y7	K18unmodK23Ac
HIST2H3A	K[+112.1]QLATK[+42]AAR	570.84041	2	y6	K18unmodK23Ac
HIST2H3A	K[+112.1]QLATK[+42]AAR	570.84041	2	y5	K18unmodK23Ac
HIST2H3A	K[+112.1]QLATK[+42]AAR	570.84041	2	b1	K18unmodK23Ac
HIST2H3A	K[+112.1]QLATK[+42]AAR	570.84041	2	b3	K18unmodK23Ac
HIST2H3A	K[+112.1]QLATK[+56]AAR	577.84823	2	precursor	K18unmodK23unmod
HIST2H3A	K[+112.1]QLATK[+56]AAR	577.84823	2	precursor [M+1]	K18unmodK23unmod
HIST2H3A	K[+112.1]QLATK[+56]AAR	577.84823	2	precursor [M+2]	K18unmodK23unmod
HIST2H3A	K[+112.1]QLATK[+56]AAR	577.84823	2	y8	K18unmodK23unmod
HIST2H3A	K[+112.1]QLATK[+56]AAR	577.84823	2	y6	K18unmodK23unmod
HIST2H3A	K[+112.1]QLATK[+56]AAR	577.84823	2	y5	K18unmodK23unmod
HIST2H3A	K[+112.1]QLATK[+56]AAR	577.84823	2	b1	K18unmodK23unmod
HIST2H3A	K[+112.1]QLATK[+56]AAR	577.84823	2	b3	K18unmodK23unmod
HIST2H3A	K[+126.1]QLATK[+42]AAR	577.84823	2	precursor	K18me1K23Ac
HIST2H3A	K[+126.1]QLATK[+42]AAR	577.84823	2	precursor [M+1]	K18me1K23Ac
HIST2H3A	K[+126.1]QLATK[+42]AAR	577.84823	2	precursor [M+2]	K18me1K23Ac
HIST2H3A	K[+126.1]QLATK[+42]AAR	577.84823	2	y8	K18me1K23Ac
HIST2H3A	K[+126.1]QLATK[+42]AAR	577.84823	2	y6	K18me1K23Ac
HIST2H3A	K[+126.1]QLATK[+42]AAR	577.8482	2	y5	K18me1K23Ac

		3			
HIST2H3A	K[+126.1]QLATK[+42]AAR	577.8482 3	2	b1	K18me1K23Ac
HIST2H3A	K[+126.1]QLATK[+42]AAR	577.8482 3	2	b3	K18me1K23Ac
HIST2H3A	K[+126.1]QLATK[+56]AAR	584.8560 6	2	precursor	Precursor K18me1K23un
HIST2H3A	K[+126.1]QLATK[+56]AAR	584.8560 6	2	precursor [M+1]	Precursor K18me1K23un
HIST2H3A	K[+126.1]QLATK[+56]AAR	584.8560 6	2	precursor [M+2]	Precursor K18me1K23un
HIST2H3A	K[+126.1]QLATK[+56]AAR	584.8560 6	2	y8	Precursor K18me1K23un
HIST2H3A	K[+126.1]QLATK[+56]AAR	584.8560 6	2	y6	Precursor K18me1K23un
HIST2H3A	K[+126.1]QLATK[+56]AAR	584.8560 6	2	y5	Precursor K18me1K23un
HIST2H3A	K[+126.1]QLATK[+56]AAR	584.8560 6	2	b1	Precursor K18me1K23un
HIST2H3A	K[+126.1]QLATK[+56]AAR	584.8560 6	2	b3	Precursor K18me1K23un
HIST2H3A	K[+98]QLATK[+42]AAR	563.8325 8	2	precursor	Precursor K18AcK23Ac
HIST2H3A	K[+98]QLATK[+42]AAR	563.8325 8	2	precursor [M+1]	Precursor K18AcK23Ac
HIST2H3A	K[+98]QLATK[+42]AAR	563.8325 8	2	precursor [M+2]	Precursor K18AcK23Ac
HIST2H3A	K[+98]QLATK[+42]AAR	563.8325 8	2	y8	Precursor K18AcK23Ac
HIST2H3A	K[+98]QLATK[+42]AAR	563.8325 8	2	y6	Precursor K18AcK23Ac
HIST2H3A	K[+98]QLATK[+42]AAR	563.8325 8	2	y5	Precursor K18AcK23Ac
HIST2H3A	K[+98]QLATK[+42]AAR	563.8325 8	2	b1	Precursor K18AcK23Ac
HIST2H3A	K[+98]QLATK[+42]AAR	563.8325 8	2	b3	Precursor K18AcK23Ac
HIST2H3A	K[+98]QLATK[+56]AAR	570.8404 1	2	precursor	K18AcK23unmod
HIST2H3A	K[+98]QLATK[+56]AAR	570.8404 1	2	precursor [M+1]	K18AcK23unmod
HIST2H3A	K[+98]QLATK[+56]AAR	570.8404 1	2	precursor [M+2]	K18AcK23unmod
HIST2H3A	K[+98]QLATK[+56]AAR	570.8404 1	2	y8	K18AcK23unmod
HIST2H3A	K[+98]QLATK[+56]AAR	570.8404 1	2	y6	K18AcK23unmod
HIST2H3A	K[+98]QLATK[+56]AAR	570.8404 1	2	y5	K18AcK23unmod
HIST2H3A	K[+98]QLATK[+56]AAR	570.8404 1	2	b1	K18AcK23unmod
HIST2H3A	K[+98]QLATK[+56]AAR	570.8404 1	2	b3	K18AcK23unmod
HIST2H3A	K[+112.1]SAPATGGVK[+28]K[+56]PHR	543.9860 2	3	precursor	k27unmodK36me2
HIST2H3A	K[+112.1]SAPATGGVK[+28]K[+56]PHR	543.9860 2	3	precursor [M+1]	k27unmodK36me2
HIST2H3A	K[+112.1]SAPATGGVK[+28]K[+56]PHR	543.9860 2	3	precursor [M+2]	k27unmodK36me2
HIST2H3A	K[+112.1]SAPATGGVK[+28]K[+56]PHR	543.9860 2	3	y13	k27unmodK36me2
HIST2H3A	K[+112.1]SAPATGGVK[+28]K[+56]PHR	543.9860 2	3	y12	k27unmodK36me2
HIST2H3A	K[+112.1]SAPATGGVK[+28]K[+56]PHR	543.9860 2	3	y11	k27unmodK36me2
HIST2H3A	K[+112.1]SAPATGGVK[+28]K[+56]PHR	543.9860 2	3	b1	k27unmodK36me2
HIST2H3A	K[+112.1]SAPATGGVK[+42]K[+56]PHR	548.6579	3	precursor	K27unmodK36me3
HIST2H3A	K[+112.1]SAPATGGVK[+42]K[+56]PHR	548.6579	3	precursor [M+1]	K27unmodK36me3
HIST2H3A	K[+112.1]SAPATGGVK[+42]K[+56]PHR	548.6579	3	precursor [M+2]	K27unmodK36me3

HIST2H3A	K[+112.1]SAPATGGVK[+42]K[+56]PHR	548.6579	3	y13	K27unmodK36me3
HIST2H3A	K[+112.1]SAPATGGVK[+42]K[+56]PHR	548.6579	3	y12	K27unmodK36me3
HIST2H3A	K[+112.1]SAPATGGVK[+42]K[+56]PHR	548.6579	3	y11	K27unmodK36me3
HIST2H3A	K[+112.1]SAPATGGVK[+42]K[+56]PHR	548.6579	3	b1	K27unmodK36me3
HIST2H3A	K[+112.1]SAPATGGVK[+56]K[+56]PHR	829.47285	2	precursor	K27unmodK36unmod
HIST2H3A	K[+112.1]SAPATGGVK[+56]K[+56]PHR	829.47285	2	precursor [M+1]	K27unmodK36unmod
HIST2H3A	K[+112.1]SAPATGGVK[+56]K[+56]PHR	829.47285	2	precursor [M+2]	K27unmodK36unmod
HIST2H3A	K[+112.1]SAPATGGVK[+56]K[+56]PHR	829.47285	2	y13	K27unmodK36unmod
HIST2H3A	K[+112.1]SAPATGGVK[+56]K[+56]PHR	829.47285	2	y11	K27unmodK36unmod
HIST2H3A	K[+112.1]SAPATGGVK[+56]K[+56]PHR	829.47285	2	y9	K27unmodK36unmod
HIST2H3A	K[+112.1]SAPATGGVK[+56]K[+56]PHR	829.47285	2	y8	K27unmodK36unmod
HIST2H3A	K[+112.1]SAPATGGVK[+56]K[+56]PHR	829.47285	2	y5	K27unmodK36unmod
HIST2H3A	K[+112.1]SAPATGGVK[+56]K[+56]PHR	829.47285	2	y4	K27unmodK36unmod
HIST2H3A	K[+112.1]SAPATGGVK[+56]K[+56]PHR	829.47285	2	y3	K27unmodK36unmod
HIST2H3A	K[+112.1]SAPATGGVK[+70]K[+56]PHR	836.48067	2	precursor	K27unmodK36me1
HIST2H3A	K[+112.1]SAPATGGVK[+70]K[+56]PHR	836.48067	2	precursor [M+1]	K27unmodK36me1
HIST2H3A	K[+112.1]SAPATGGVK[+70]K[+56]PHR	836.48067	2	precursor [M+2]	K27unmodK36me1
HIST2H3A	K[+112.1]SAPATGGVK[+70]K[+56]PHR	836.48067	2	y13	K27unmodK36me1
HIST2H3A	K[+112.1]SAPATGGVK[+70]K[+56]PHR	836.48067	2	y11	K27unmodK36me1
HIST2H3A	K[+112.1]SAPATGGVK[+70]K[+56]PHR	836.48067	2	y8	K27unmodK36me1
HIST2H3A	K[+112.1]SAPATGGVK[+70]K[+56]PHR	836.48067	2	y5	K27unmodK36me1
HIST2H3A	K[+112.1]SAPATGGVK[+70]K[+56]PHR	836.48067	2	y13	K27unmodK36me1
HIST2H3A	K[+112.1]SAPATGGVK[+70]K[+56]PHR	836.48067	2	y11	K27unmodK36me1
HIST2H3A	K[+126.1]SAPATGGVK[+28]K[+56]PHR	548.6579	3	precursor	K27me1K36me2
HIST2H3A	K[+126.1]SAPATGGVK[+28]K[+56]PHR	548.6579	3	precursor [M+1]	K27me1K36me2
HIST2H3A	K[+126.1]SAPATGGVK[+28]K[+56]PHR	548.6579	3	precursor [M+2]	K27me1K36me2
HIST2H3A	K[+126.1]SAPATGGVK[+28]K[+56]PHR	548.6579	3	y13	K27me1K36me2
HIST2H3A	K[+126.1]SAPATGGVK[+28]K[+56]PHR	548.6579	3	y12	K27me1K36me2
HIST2H3A	K[+126.1]SAPATGGVK[+28]K[+56]PHR	548.6579	3	y11	K27me1K36me2
HIST2H3A	K[+126.1]SAPATGGVK[+28]K[+56]PHR	548.6579	3	b1	K27me1K36me2
HIST2H3A	K[+126.1]SAPATGGVK[+28]K[+56]PHR	548.6579	3	b2	K27me1K36me2
HIST2H3A	K[+126.1]SAPATGGVK[+42]K[+56]PHR	553.32978	3	precursor	K27me1K36me3
HIST2H3A	K[+126.1]SAPATGGVK[+42]K[+56]PHR	553.32978	3	precursor [M+1]	K27me1K36me3
HIST2H3A	K[+126.1]SAPATGGVK[+42]K[+56]PHR	553.32978	3	precursor [M+2]	K27me1K36me3
HIST2H3A	K[+126.1]SAPATGGVK[+42]K[+56]PHR	553.32978	3	y13	K27me1K36me3
HIST2H3A	K[+126.1]SAPATGGVK[+42]K[+56]PHR	553.32978	3	y12	K27me1K36me3
HIST2H3A	K[+126.1]SAPATGGVK[+42]K[+	553.3297	3	y11	K27me1K36me3

	56]PHR	8			
HIST2H3A	K[+126.1]SAPATGGVK[+42]K[+56]PHR	553.32978	3	y10	K27me1K36me3
HIST2H3A	K[+126.1]SAPATGGVK[+42]K[+56]PHR	553.32978	3	b1	K27me1K36me3
HIST2H3A	K[+126.1]SAPATGGVK[+42]K[+56]PHR	553.32978	3	b2	K27me1K36me3
HIST2H3A	K[+126.1]SAPATGGVK[+56]K[+56]PHR	836.48067	2	precursor	K27me1K36unmod
HIST2H3A	K[+126.1]SAPATGGVK[+56]K[+56]PHR	836.48067	2	precursor [M+1]	K27me1K36unmod
HIST2H3A	K[+126.1]SAPATGGVK[+56]K[+56]PHR	836.48067	2	precursor [M+2]	K27me1K36unmod
HIST2H3A	K[+126.1]SAPATGGVK[+56]K[+56]PHR	836.48067	2	y13	K27me1K36unmod
HIST2H3A	K[+126.1]SAPATGGVK[+56]K[+56]PHR	836.48067	2	y11	K27me1K36unmod
HIST2H3A	K[+126.1]SAPATGGVK[+56]K[+56]PHR	836.48067	2	y9	K27me1K36unmod
HIST2H3A	K[+126.1]SAPATGGVK[+56]K[+56]PHR	836.48067	2	y8	K27me1K36unmod
HIST2H3A	K[+126.1]SAPATGGVK[+56]K[+56]PHR	836.48067	2	y5	K27me1K36unmod
HIST2H3A	K[+126.1]SAPATGGVK[+56]K[+56]PHR	836.48067	2	y3	K27me1K36unmod
HIST2H3A	K[+126.1]SAPATGGVK[+56]K[+56]PHR	836.48067	2	y13	K27me1K36unmod
HIST2H3A	K[+126.1]SAPATGGVK[+56]K[+56]PHR	836.48067	2	y11	K27me1K36unmod
HIST2H3A	K[+126.1]SAPATGGVK[+70]K[+56]PHR	843.4885	2	precursor	K27me1K36me1
HIST2H3A	K[+126.1]SAPATGGVK[+70]K[+56]PHR	843.4885	2	precursor [M+1]	K27me1K36me1
HIST2H3A	K[+126.1]SAPATGGVK[+70]K[+56]PHR	843.4885	2	precursor [M+2]	K27me1K36me1
HIST2H3A	K[+126.1]SAPATGGVK[+70]K[+56]PHR	843.4885	2	y13	K27me1K36me1
HIST2H3A	K[+126.1]SAPATGGVK[+70]K[+56]PHR	843.4885	2	y11	K27me1K36me1
HIST2H3A	K[+126.1]SAPATGGVK[+70]K[+56]PHR	843.4885	2	y9	K27me1K36me1
HIST2H3A	K[+126.1]SAPATGGVK[+70]K[+56]PHR	843.4885	2	y8	K27me1K36me1
HIST2H3A	K[+126.1]SAPATGGVK[+70]K[+56]PHR	843.4885	2	y5	K27me1K36me1
HIST2H3A	K[+126.1]SAPATGGVK[+70]K[+56]PHR	843.4885	2	y4	K27me1K36me1
HIST2H3A	K[+126.1]SAPATGGVK[+70]K[+56]PHR	843.4885	2	y3	K27me1K36me1
HIST2H3A	K[+126.1]SAPATGGVK[+70]K[+56]PHR	843.4885	2	y13	K27me1K36me1
HIST2H3A	K[+126.1]SAPATGGVK[+70]K[+56]PHR	843.4885	2	y11	K27me1K36me1
HIST2H3A	K[+84.1]SAPATGGVK[+28]K[+56]PHR	534.65438	3	precursor	K27me2K36me2
HIST2H3A	K[+84.1]SAPATGGVK[+28]K[+56]PHR	534.65438	3	precursor [M+1]	K27me2K36me2
HIST2H3A	K[+84.1]SAPATGGVK[+28]K[+56]PHR	534.65438	3	precursor [M+2]	K27me2K36me2
HIST2H3A	K[+84.1]SAPATGGVK[+28]K[+56]PHR	534.65438	3	y3	K27me2K36me2
HIST2H3A	K[+84.1]SAPATGGVK[+28]K[+56]PHR	534.65438	3	y13	K27me2K36me2
HIST2H3A	K[+84.1]SAPATGGVK[+28]K[+56]PHR	534.65438	3	y11	K27me2K36me2
HIST2H3A	K[+84.1]SAPATGGVK[+28]K[+56]PHR	534.65438	3	b4	K27me2K36me2
HIST2H3A	K[+84.1]SAPATGGVK[+28]K[+56]PHR	534.65438	3	b10	K27me2K36me2
HIST2H3A	K[+84.1]SAPATGGVK[+28]K[+56]PHR	534.65438	3	b11	K27me2K36me2
HIST2H3A	K[+84.1]SAPATGGVK[+28]K[+56]PHR	534.65438	3	b13	K27me2K36me2

HIST2H3A	K[+84.1]SAPATGGVK[+42]K[+56]PHR	539.32626	3	precursor	K27me2K36me3
HIST2H3A	K[+84.1]SAPATGGVK[+42]K[+56]PHR	539.32626	3	precursor [M+1]	K27me2K36me3
HIST2H3A	K[+84.1]SAPATGGVK[+42]K[+56]PHR	539.32626	3	precursor [M+2]	K27me2K36me3
HIST2H3A	K[+84.1]SAPATGGVK[+42]K[+56]PHR	539.32626	3	y13	K27me2K36me3
HIST2H3A	K[+84.1]SAPATGGVK[+42]K[+56]PHR	539.32626	3	y11	K27me2K36me3
HIST2H3A	K[+84.1]SAPATGGVK[+42]K[+56]PHR	539.32626	3	b1	K27me2K36me3
HIST2H3A	K[+84.1]SAPATGGVK[+42]K[+56]PHR	539.32626	3	b3	K27me2K36me3
HIST2H3A	K[+84.1]SAPATGGVK[+42]K[+56]PHR	539.32626	3	b4	K27me2K36me3
HIST2H3A	K[+84.1]SAPATGGVK[+56]K[+56]PHR	543.98602	3	precursor	K27me2K36unmod
HIST2H3A	K[+84.1]SAPATGGVK[+56]K[+56]PHR	543.98602	3	precursor [M+1]	K27me2K36unmod
HIST2H3A	K[+84.1]SAPATGGVK[+56]K[+56]PHR	543.98602	3	precursor [M+2]	K27me2K36unmod
HIST2H3A	K[+84.1]SAPATGGVK[+56]K[+56]PHR	543.98602	3	y5	K27me2K36unmod
HIST2H3A	K[+84.1]SAPATGGVK[+56]K[+56]PHR	543.98602	3	y4	K27me2K36unmod
HIST2H3A	K[+84.1]SAPATGGVK[+56]K[+56]PHR	543.98602	3	y3	K27me2K36unmod
HIST2H3A	K[+84.1]SAPATGGVK[+56]K[+56]PHR	543.98602	3	b3	K27me2K36unmod
HIST2H3A	K[+84.1]SAPATGGVK[+56]K[+56]PHR	543.98602	3	b8	K27me2K36unmod
HIST2H3A	K[+84.1]SAPATGGVK[+56]K[+56]PHR	543.98602	3	b9	K27me2K36unmod
HIST2H3A	K[+84.1]SAPATGGVK[+56]K[+56]PHR	543.98602	3	b10	K27me2K36unmod
HIST2H3A	K[+84.1]SAPATGGVK[+70]K[+56]PHR	548.6579	3	precursor	K27me2K36me1
HIST2H3A	K[+84.1]SAPATGGVK[+70]K[+56]PHR	548.6579	3	precursor [M+1]	K27me2K36me1
HIST2H3A	K[+84.1]SAPATGGVK[+70]K[+56]PHR	548.6579	3	precursor [M+2]	K27me2K36me1
HIST2H3A	K[+84.1]SAPATGGVK[+70]K[+56]PHR	548.6579	3	y5	K27me2K36me1
HIST2H3A	K[+84.1]SAPATGGVK[+70]K[+56]PHR	548.6579	3	y4	K27me2K36me1
HIST2H3A	K[+84.1]SAPATGGVK[+70]K[+56]PHR	548.6579	3	y3	K27me2K36me1
HIST2H3A	K[+84.1]SAPATGGVK[+70]K[+56]PHR	548.6579	3	b3	K27me2K36me1
HIST2H3A	K[+84.1]SAPATGGVK[+70]K[+56]PHR	548.6579	3	b8	K27me2K36me1
HIST2H3A	K[+84.1]SAPATGGVK[+70]K[+56]PHR	548.6579	3	b9	K27me2K36me1
HIST2H3A	K[+84.1]SAPATGGVK[+70]K[+56]PHR	548.6579	3	b10	K27me2K36me1
HIST2H3A	K[+84.1]SAPATGGVK[+70]K[+56]PHR	548.6579	3	b11	K27me2K36me1
HIST2H3A	K[+98.1]SAPATGGVK[+28]K[+56]PHR	539.32626	3	precursor	K27me3K36me2
HIST2H3A	K[+98.1]SAPATGGVK[+28]K[+56]PHR	539.32626	3	precursor [M+1]	K27me3K36me2
HIST2H3A	K[+98.1]SAPATGGVK[+28]K[+56]PHR	539.32626	3	precursor [M+2]	K27me3K36me2
HIST2H3A	K[+98.1]SAPATGGVK[+28]K[+56]PHR	539.32626	3	y5	K27me3K36me2
HIST2H3A	K[+98.1]SAPATGGVK[+28]K[+56]PHR	539.32626	3	y11	K27me3K36me2
HIST2H3A	K[+98.1]SAPATGGVK[+28]K[+56]PHR	539.32626	3	b3	K27me3K36me2
HIST2H3A	K[+98.1]SAPATGGVK[+28]K[+56]PHR	539.32626	3	b4	K27me3K36me2
HIST2H3A	K[+98.1]SAPATGGVK[+28]K[+5	539.3262	3	b5	K27me3K36me2

	6]PHR	6			
HIST2H3A	K[+98.1]SAPATGGVK[+28]K[+56]PHR	539.32626	3	b8	K27me3K36me2
HIST2H3A	K[+98.1]SAPATGGVK[+28]K[+56]PHR	539.32626	3	b9	K27me3K36me2
HIST2H3A	K[+98.1]SAPATGGVK[+56]K[+56]PHR	548.6579	3	precursor	K27me3K36unmod
HIST2H3A	K[+98.1]SAPATGGVK[+56]K[+56]PHR	548.6579	3	precursor [M+1]	K27me3K36unmod
HIST2H3A	K[+98.1]SAPATGGVK[+56]K[+56]PHR	548.6579	3	precursor [M+2]	K27me3K36unmod
HIST2H3A	K[+98.1]SAPATGGVK[+56]K[+56]PHR	548.6579	3	y5	K27me3K36unmod
HIST2H3A	K[+98.1]SAPATGGVK[+56]K[+56]PHR	548.6579	3	y4	K27me3K36unmod
HIST2H3A	K[+98.1]SAPATGGVK[+56]K[+56]PHR	548.6579	3	y3	K27me3K36unmod
HIST2H3A	K[+98.1]SAPATGGVK[+56]K[+56]PHR	548.6579	3	y8	K27me3K36unmod
HIST2H3A	K[+98.1]SAPATGGVK[+56]K[+56]PHR	548.6579	3	b3	K27me3K36unmod
HIST2H3A	K[+98.1]SAPATGGVK[+56]K[+56]PHR	548.6579	3	b5	K27me3K36unmod
HIST2H3A	K[+98.1]SAPATGGVK[+56]K[+56]PHR	548.6579	3	b6	K27me3K36unmod
HIST2H3A	K[+98.1]SAPATGGVK[+56]K[+56]PHR	548.6579	3	b8	K27me3K36unmod
HIST2H3A	K[+98.1]SAPATGGVK[+56]K[+56]PHR	548.6579	3	b11	K27me3K36unmod
HIST2H3A	K[+98.1]SAPATGGVK[+56]K[+56]PHR	548.6579	3	b12	K27me3K36unmod
HIST2H3A	K[+98.1]SAPATGGVK[+56]K[+56]PHR	548.6579	3	b13	K27me3K36unmod
HIST2H3A	K[+98.1]SAPATGGVK[+70]K[+56]PHR	553.32978	3	precursor	K27me3K36me1
HIST2H3A	K[+98.1]SAPATGGVK[+70]K[+56]PHR	553.32978	3	precursor [M+1]	K27me3K36me1
HIST2H3A	K[+98.1]SAPATGGVK[+70]K[+56]PHR	553.32978	3	precursor [M+2]	K27me3K36me1
HIST2H3A	K[+98.1]SAPATGGVK[+70]K[+56]PHR	553.32978	3	y8	K27me3K36me1
HIST2H3A	K[+98.1]SAPATGGVK[+70]K[+56]PHR	553.32978	3	y7	K27me3K36me1
HIST2H3A	K[+98.1]SAPATGGVK[+70]K[+56]PHR	553.32978	3	y5	K27me3K36me1
HIST2H3A	K[+98.1]SAPATGGVK[+70]K[+56]PHR	553.32978	3	y4	K27me3K36me1
HIST2H3A	K[+98.1]SAPATGGVK[+70]K[+56]PHR	553.32978	3	y3	K27me3K36me1
HIST2H3A	K[+98.1]SAPATGGVK[+70]K[+56]PHR	553.32978	3	b3	K27me3K36me1
HIST2H3A	K[+98.1]SAPATGGVK[+70]K[+56]PHR	553.32978	3	b6	K27me3K36me1
HIST2H3A	K[+98.1]SAPATGGVK[+70]K[+56]PHR	553.32978	3	b9	K27me3K36me1
HIST2H3A	K[+98.1]SAPATGGVK[+70]K[+56]PHR	553.32978	3	b10	K27me3K36me1
HIST2H3A	K[+98.1]SAPATGGVK[+70]K[+56]PHR	553.32978	3	b8	K27me3K36me1
HIST2H3A	K[+98.1]SAPATGGVK[+70]K[+56]PHR	553.32978	3	b9	K27me3K36me1
HIST2H3A	EIAQDFK[+56]TDLR	696.3619	2	precursor	control K79unmod missed2ndprop unmod
HIST2H3A	EIAQDFK[+56]TDLR	696.3619	2	precursor [M+1]	control K79unmod missed2ndprop unmod
HIST2H3A	EIAQDFK[+56]TDLR	696.3619	2	precursor [M+2]	control K79unmod missed2ndprop unmod
HIST2H3A	EIAQDFK[+56]TDLR	696.3619	2	y9	control K79unmod missed2ndprop unmod
HIST2H3A	EIAQDFK[+56]TDLR	696.3619	2	y7	control K79unmod missed2ndprop unmod
HIST2H3A	EIAQDFK[+56]TDLR	696.3619	2	y6	control K79unmod missed2ndprop unmod

HIST2H3A	EIAQDFK[+56]TDLR	696.3619	2	y4	control K79unmod missed2ndprop unmod
HIST2H3A	EIAQDFK[+56]TDLR	696.3619	2	y2	control K79unmod missed2ndprop unmod
HIST2H3A	EIAQDFK[+56]TDLR	696.3619	2	b5	control K79unmod missed2ndprop unmod
HIST2H3A	E[+56]IAQDFK[+28]TDLR	710.37755	2	precursor	K79me2
HIST2H3A	E[+56]IAQDFK[+28]TDLR	710.37755	2	precursor [M+1]	K79me2
HIST2H3A	E[+56]IAQDFK[+28]TDLR	710.37755	2	precursor [M+2]	K79me2
HIST2H3A	E[+56]IAQDFK[+28]TDLR	710.37755	2	y9	K79me2
HIST2H3A	E[+56]IAQDFK[+28]TDLR	710.37755	2	y7	K79me2
HIST2H3A	E[+56]IAQDFK[+28]TDLR	710.37755	2	y6	K79me2
HIST2H3A	E[+56]IAQDFK[+28]TDLR	710.37755	2	y2	K79me2
HIST2H3A	E[+56]IAQDFK[+28]TDLR	710.37755	2	b7	K79me2
HIST2H3A	E[+56]IAQDFK[+28]TDLR	710.37755	2	b9	K79me2
HIST2H3A	E[+56]IAQDFK[+56]TDLR	724.37501	2	precursor	K79unmod
HIST2H3A	E[+56]IAQDFK[+56]TDLR	724.37501	2	precursor [M+1]	K79unmod
HIST2H3A	E[+56]IAQDFK[+56]TDLR	724.37501	2	precursor [M+2]	K79unmod
HIST2H3A	E[+56]IAQDFK[+56]TDLR	724.37501	2	y8	K79unmod
HIST2H3A	E[+56]IAQDFK[+56]TDLR	724.37501	2	y7	K79unmod
HIST2H3A	E[+56]IAQDFK[+56]TDLR	724.37501	2	y6	K79unmod
HIST2H3A	E[+56]IAQDFK[+56]TDLR	724.37501	2	y5	K79unmod
HIST2H3A	E[+56]IAQDFK[+56]TDLR	724.37501	2	y4	K79unmod
HIST2H3A	E[+56]IAQDFK[+56]TDLR	724.37501	2	b7	K79unmod
HIST2H3A	E[+56]IAQDFK[+70]TDLR	731.38283	2	precursor	K79me1
HIST2H3A	E[+56]IAQDFK[+70]TDLR	731.38283	2	precursor [M+1]	K79me1
HIST2H3A	E[+56]IAQDFK[+70]TDLR	731.38283	2	precursor [M+2]	K79me1
HIST2H3A	E[+56]IAQDFK[+70]TDLR	731.38283	2	y8	K79me1
HIST2H3A	E[+56]IAQDFK[+70]TDLR	731.38283	2	y7	K79me1
HIST2H3A	E[+56]IAQDFK[+70]TDLR	731.38283	2	y6	K79me1
HIST2H3A	E[+56]IAQDFK[+70]TDLR	731.38283	2	y4	K79me1
HIST2H3A	E[+56]IAQDFK[+70]TDLR	731.38283	2	y2	K79me1
HIST2H3A	E[+56]IAQDFK[+70]TDLR	731.38283	2	b7	K79me1
HIST1H2AB H2AFM; HIST1H2AE H2AFA	G[+56]K[+56]QGGK[+56]AR	485.27744	2	precursor	GK-H2A control 4-11
HIST1H2AB H2AFM; HIST1H2AE H2AFA	G[+56]K[+56]QGGK[+56]AR	485.27744	2	precursor [M+1]	GK-H2A control 4-11
HIST1H2AB H2AFM; HIST1H2AE H2AFA	G[+56]K[+56]QGGK[+56]AR	485.27744	2	precursor [M+2]	GK-H2A control 4-11
HIST1H2AB H2AFM; HIST1H2AE H2AFA	G[+56]K[+56]QGGK[+56]AR	485.27744	2	b2	GK-H2A control 4-11
HIST1H2AB H2AFM; HIST1H2AE H2AFA	G[+56]K[+56]QGGK[+56]AR	485.27744	2	b3	GK-H2A control 4-11
HIST1H2AB H2AFM; HIST1H2AE H2AFA	G[+56]K[+56]QGGK[+56]AR	485.27744	2	b5	GK-H2A control 4-11
HIST1H2AB H2AFM;	G[+56]K[+56]QGGK[+56]AR	485.2774	2	b6	GK-H2A control 4-11

HIST1H2AE H2AFA		4			
HIST1H2AB H2AFM; HIST1H2AE H2AFA	G[+56]K[+56]QGGK[+56]AR	485.27744	2	b7	GK-H2A control 4-11
HIST1H2AB H2AFM; HIST1H2AE H2AFA	G[+56]K[+56]QGGK[+56]AR	485.27744	2	y6	GK-H2A control 4-11
HIST1H2AB H2AFM; HIST1H2AE H2AFA	G[+56]K[+56]QGGK[+56]AR	485.27744	2	y5	GK-H2A control 4-11
HIST1H2AB H2AFM; HIST1H2AE H2AFA	G[+56]K[+56]QGGK[+56]AR	485.27744	2	y3	GK-H2A control 4-11
HIST1H2AB H2AFM; HIST1H2AE H2AFA	G[+56]K[+56]QGGK[+56]AR	485.27744	2	y2	GK-H2A control 4-11
HIST1H2AB H2AFM; HIST1H2AE H2AFA	G[+56]K[+56]QGGK[+56]AR	485.27744	2	y1	GK-H2A control 4-11
HIST1H2AB H2AFM; HIST1H2AE H2AFA	A[+56]K[+56]AK[+56]TR	421.75835	2	precursor	H2A K13unK15un
HIST1H2AB H2AFM; HIST1H2AE H2AFA	A[+56]K[+56]AK[+56]TR	421.75835	2	precursor [M+1]	H2A K13unK15un
HIST1H2AB H2AFM; HIST1H2AE H2AFA	A[+56]K[+56]AK[+56]TR	421.75835	2	precursor [M+2]	H2A K13unK15un
HIST1H2AB H2AFM; HIST1H2AE H2AFA	A[+56]K[+56]AK[+56]TR	421.75835	2	b2	H2A K13unK15un
HIST1H2AB H2AFM; HIST1H2AE H2AFA	A[+56]K[+56]AK[+56]TR	421.75835	2	b3	H2A K13unK15un
HIST1H2AB H2AFM; HIST1H2AE H2AFA	A[+56]K[+56]AK[+56]TR	421.75835	2	b4	H2A K13unK15un
HIST1H2AB H2AFM; HIST1H2AE H2AFA	A[+56]K[+56]AK[+56]TR	421.75835	2	b5	H2A K13unK15un
HIST1H2AB H2AFM; HIST1H2AE H2AFA	A[+56]K[+56]AK[+56]TR	421.75835	2	y5	H2A K13unK15un
HIST1H2AB H2AFM; HIST1H2AE H2AFA	A[+56]K[+56]AK[+56]TR	421.75835	2	y4	H2A K13unK15un
HIST1H2AB H2AFM; HIST1H2AE H2AFA	A[+56]K[+56]AK[+56]TR	421.75835	2	y3	H2A K13unK15un
HIST1H2AB H2AFM; HIST1H2AE H2AFA	A[+56]K[+56]AK[+56]TR	421.75835	2	y2	H2A K13unK15un
HIST1H2AB H2AFM; HIST1H2AE H2AFA	A[+56]K[+56]AK[+56]TR	421.75835	2	y1	H2A K13unK15un
HIST1H2AB H2AFM; HIST1H2AE H2AFA	A[+56]K[+56]AK[+170.1]TR	478.77982	2	precursor	H2A K13unK15ub
HIST1H2AB H2AFM; HIST1H2AE H2AFA	A[+56]K[+56]AK[+170.1]TR	478.77982	2	precursor [M+1]	H2A K13unK15ub
HIST1H2AB H2AFM; HIST1H2AE H2AFA	A[+56]K[+56]AK[+170.1]TR	478.77982	2	precursor [M+2]	H2A K13unK15ub
HIST1H2AB H2AFM; HIST1H2AE H2AFA	A[+56]K[+56]AK[+170.1]TR	478.77982	2	b2	H2A K13unK15ub
HIST1H2AB H2AFM; HIST1H2AE H2AFA	A[+56]K[+56]AK[+170.1]TR	478.77982	2	b4	H2A K13unK15ub
HIST1H2AB H2AFM; HIST1H2AE H2AFA	A[+56]K[+56]AK[+170.1]TR	478.77982	2	b5	H2A K13unK15ub
HIST1H2AB H2AFM; HIST1H2AE H2AFA	A[+56]K[+56]AK[+170.1]TR	478.77982	2	y5	H2A K13unK15ub
HIST1H2AB H2AFM; HIST1H2AE H2AFA	A[+56]K[+56]AK[+170.1]TR	478.77982	2	y4	H2A K13unK15ub
HIST1H2AB H2AFM; HIST1H2AE H2AFA	A[+56]K[+56]AK[+170.1]TR	478.77982	2	y3	H2A K13unK15ub
HIST1H2AB H2AFM; HIST1H2AE H2AFA	A[+56]K[+56]AK[+170.1]TR	478.77982	2	y2	H2A K13unK15ub
HIST1H2AB H2AFM; HIST1H2AE H2AFA	K[+112.1]GNYSER	483.23798	2	precursor	KGNYSER
HIST1H2AB H2AFM; HIST1H2AE H2AFA	K[+112.1]GNYSER	483.23798	2	precursor [M+1]	KGNYSER
HIST1H2AB H2AFM; HIST1H2AE H2AFA	K[+112.1]GNYSER	483.23798	2	precursor [M+2]	KGNYSER
HIST1H2AB H2AFM; HIST1H2AE H2AFA	K[+112.1]GNYSER	483.23798	2	b1	KGNYSER
HIST1H2AB H2AFM; HIST1H2AE H2AFA	K[+112.1]GNYSER	483.23798	2	b2	KGNYSER
HIST1H2AB H2AFM; HIST1H2AE H2AFA	K[+112.1]GNYSER	483.23798	2	b3	KGNYSER
HIST1H2AB H2AFM; HIST1H2AE H2AFA	K[+112.1]GNYSER	483.23798	2	b4	KGNYSER
HIST1H2AB H2AFM; HIST1H2AE H2AFA	K[+112.1]GNYSER	483.23798	2	b5	KGNYSER

HIST1H2AB H2AFM; HIST1H2AE H2AFA	K[+112.1]GNYSER	483.23798	2	b6	KGNYSER
HIST1H2AB H2AFM; HIST1H2AE H2AFA	K[+112.1]GNYSER	483.23798	2	y6	KGNYSER
HIST1H2AB H2AFM; HIST1H2AE H2AFA	K[+112.1]GNYSER	483.23798	2	y5	KGNYSER
HIST1H2AB H2AFM; HIST1H2AE H2AFA	K[+112.1]GNYSER	483.23798	2	y4	KGNYSER
HIST1H2AB H2AFM; HIST1H2AE H2AFA	K[+112.1]GNYSER	483.23798	2	y3	KGNYSER
HIST1H2AB H2AFM; HIST1H2AE H2AFA	K[+112.1]GNYSER	483.23798	2	y2	KGNYSER
HIST1H2AB H2AFM; HIST1H2AE H2AFA	K[+112.1]GNYSER	483.23798	2	y1	KGNYSER
H2AFX	G[+56]K[+56]TGGK[+56]AR	471.77199	2	precursor	GK-H2AX control 4-11
H2AFX	G[+56]K[+56]TGGK[+56]AR	471.77199	2	precursor [M+1]	GK-H2AX control 4-11
H2AFX	G[+56]K[+56]TGGK[+56]AR	471.77199	2	precursor [M+2]	GK-H2AX control 4-11
H2AFX	G[+56]K[+56]TGGK[+56]AR	471.77199	2	b2	GK-H2AX control 4-11
H2AFX	G[+56]K[+56]TGGK[+56]AR	471.77199	2	b3	GK-H2AX control 4-11
H2AFX	G[+56]K[+56]TGGK[+56]AR	471.77199	2	b5	GK-H2AX control 4-11
H2AFX	G[+56]K[+56]TGGK[+56]AR	471.77199	2	b6	GK-H2AX control 4-11
H2AFX	G[+56]K[+56]TGGK[+56]AR	471.77199	2	b7	GK-H2AX control 4-11
H2AFX	G[+56]K[+56]TGGK[+56]AR	471.77199	2	y6	GK-H2AX control 4-11
H2AFX	G[+56]K[+56]TGGK[+56]AR	471.77199	2	y5	GK-H2AX control 4-11
H2AFX	G[+56]K[+56]TGGK[+56]AR	471.77199	2	y4	GK-H2AX control 4-11
H2AFX	G[+56]K[+56]TGGK[+56]AR	471.77199	2	y3	GK-H2AX control 4-11
H2AFX	G[+56]K[+56]TGGK[+56]AR	471.77199	2	y2	GK-H2AX control 4-11
H2AFX	A[+56]K[+56]AK[+56]SR	414.75053	2	precursor	H2AX K13unK15un
H2AFX	A[+56]K[+56]AK[+56]SR	414.75053	2	precursor [M+1]	H2AX K13unK15un
H2AFX	A[+56]K[+56]AK[+56]SR	414.75053	2	precursor [M+2]	H2AX K13unK15un
H2AFX	A[+56]K[+56]AK[+56]SR	414.75053	2	b2	H2AX K13unK15un
H2AFX	A[+56]K[+56]AK[+56]SR	414.75053	2	b3	H2AX K13unK15un
H2AFX	A[+56]K[+56]AK[+56]SR	414.75053	2	b4	H2AX K13unK15un
H2AFX	A[+56]K[+56]AK[+56]SR	414.75053	2	b5	H2AX K13unK15un
H2AFX	A[+56]K[+56]AK[+56]SR	414.75053	2	y5	H2AX K13unK15un
H2AFX	A[+56]K[+56]AK[+56]SR	414.75053	2	y4	H2AX K13unK15un
H2AFX	A[+56]K[+56]AK[+56]SR	414.75053	2	y3	H2AX K13unK15un
H2AFX	A[+56]K[+56]AK[+56]SR	414.75053	2	y2	H2AX K13unK15un
H2AFX	A[+56]K[+56]AK[+56]SR	414.75053	2	y1	H2AX K13unK15un
H2AFX	A[+56]K[+56]AK[+170.1]SR	471.77199	2	precursor	H2AX K13unK15ub
H2AFX	A[+56]K[+56]AK[+170.1]SR	471.77199	2	precursor [M+1]	H2AX K13unK15ub
H2AFX	A[+56]K[+56]AK[+170.1]SR	471.77199	2	precursor [M+2]	H2AX K13unK15ub
H2AFX	A[+56]K[+56]AK[+170.1]SR	471.77199	2	y4	H2AX K13unK15ub
H2AFX	A[+56]K[+56]AK[+170.1]SR	471.7719	2	y3	H2AX K13unK15ub

		9			
H2AFX	A[+56]K[+56]AK[+170.1]SR	471.77199	2	y2	H2AX K13unK15ub
H2AFX	A[+56]K[+56]AK[+170.1]SR	471.77199	2	b4	H2AX K13unK15ub
H2AFX	K[+112.1]GHYAER	486.74852	2	precursor	KGHYAER H2AX only
H2AFX	K[+112.1]GHYAER	486.74852	2	precursor [M+1]	KGHYAER H2AX only
H2AFX	K[+112.1]GHYAER	486.74852	2	precursor [M+2]	KGHYAER H2AX only
H2AFX	K[+112.1]GHYAER	486.74852	2	b1	KGHYAER H2AX only
H2AFX	K[+112.1]GHYAER	486.74852	2	b3	KGHYAER H2AX only
H2AFX	K[+112.1]GHYAER	486.74852	2	b4	KGHYAER H2AX only
H2AFX	K[+112.1]GHYAER	486.74852	2	b5	KGHYAER H2AX only
H2AFX	K[+112.1]GHYAER	486.74852	2	b6	KGHYAER H2AX only
H2AFX	K[+112.1]GHYAER	486.74852	2	y6	KGHYAER H2AX only
H2AFX	K[+112.1]GHYAER	486.74852	2	y5	KGHYAER H2AX only
H2AFX	K[+112.1]GHYAER	486.74852	2	y4	KGHYAER H2AX only
H2AFX	K[+112.1]GHYAER	486.74852	2	y3	KGHYAER H2AX only
H2AFX	K[+112.1]GHYAER	486.74852	2	y2	KGHYAER H2AX only
H2AFX	K[+98]GHYAER	479.74069	2	precursor	Acetylated version
H2AFX	K[+98]GHYAER	479.74069	2	precursor [M+1]	Acetylated version
H2AFX	K[+98]GHYAER	479.74069	2	precursor [M+2]	Acetylated version
H2AFX	K[+98]GHYAER	479.74069	2	b1	Acetylated version
H2AFX	K[+98]GHYAER	479.74069	2	b2	Acetylated version
H2AFX	K[+98]GHYAER	479.74069	2	b3	Acetylated version
H2AFX	K[+98]GHYAER	479.74069	2	b4	Acetylated version
H2AFX	K[+98]GHYAER	479.74069	2	b5	Acetylated version
H2AFX	K[+98]GHYAER	479.74069	2	b6	Acetylated version
H2AFX	K[+98]GHYAER	479.74069	2	y6	Acetylated version
H2AFX	K[+98]GHYAER	479.74069	2	y5	Acetylated version
H2AFX	K[+98]GHYAER	479.74069	2	y4	Acetylated version
H2AFX	K[+98]GHYAER	479.74069	2	y3	Acetylated version
H2AFX	K[+98]GHYAER	479.74069	2	y2	Acetylated version
H2AFX	K[+98]GHYAER	479.74069	2	y1	Acetylated version
H2AFX	H[+56]LQLAIR	453.77962	2	precursor	2nd strongest H2A pep
H2AFX	H[+56]LQLAIR	453.77962	2	precursor [M+1]	2nd strongest H2A pep
H2AFX	H[+56]LQLAIR	453.77962	2	precursor [M+2]	2nd strongest H2A pep
H2AFX	H[+56]LQLAIR	453.77962	2	b1	2nd strongest H2A pep
H2AFX	H[+56]LQLAIR	453.77962	2	b2	2nd strongest H2A pep
H2AFX	H[+56]LQLAIR	453.77962	2	b3	2nd strongest H2A pep

H2AFX	H[+56]LQLAIR	453.77962	2	b4	2nd strongest H2A pep
H2AFX	H[+56]LQLAIR	453.77962	2	b5	2nd strongest H2A pep
H2AFX	H[+56]LQLAIR	453.77962	2	b6	2nd strongest H2A pep
H2AFX	H[+56]LQLAIR	453.77962	2	y6	2nd strongest H2A pep
H2AFX	H[+56]LQLAIR	453.77962	2	y5	2nd strongest H2A pep
H2AFX	H[+56]LQLAIR	453.77962	2	y4	2nd strongest H2A pep
H2AFX	H[+56]LQLAIR	453.77962	2	y3	2nd strongest H2A pep
H2AFX	H[+56]LQLAIR	453.77962	2	y2	2nd strongest H2A pep
H2AFX	H[+56]LQLAIR	453.77962	2	y1	2nd strongest H2A pep
H2AFJ	G[+56]K[+56]QGGK[+56]VR	499.29309	2	precursor	GK-H2AJ control 4-11
H2AFJ	G[+56]K[+56]QGGK[+56]VR	499.29309	2	precursor [M+1]	GK-H2AJ control 4-11
H2AFJ	G[+56]K[+56]QGGK[+56]VR	499.29309	2	precursor [M+2]	GK-H2AJ control 4-11
H2AFJ	G[+56]K[+56]QGGK[+56]VR	499.29309	2	b2	GK-H2AJ control 4-11
H2AFJ	G[+56]K[+56]QGGK[+56]VR	499.29309	2	b3	GK-H2AJ control 4-11
H2AFJ	G[+56]K[+56]QGGK[+56]VR	499.29309	2	b4	GK-H2AJ control 4-11
H2AFJ	G[+56]K[+56]QGGK[+56]VR	499.29309	2	b5	GK-H2AJ control 4-11
H2AFJ	G[+56]K[+56]QGGK[+56]VR	499.29309	2	b6	GK-H2AJ control 4-11
H2AFJ	G[+56]K[+56]QGGK[+56]VR	499.29309	2	b7	GK-H2AJ control 4-11
H2AFJ	G[+56]K[+56]QGGK[+56]VR	499.29309	2	y7	GK-H2AJ control 4-11
H2AFJ	G[+56]K[+56]QGGK[+56]VR	499.29309	2	y6	GK-H2AJ control 4-11
H2AFJ	G[+56]K[+56]QGGK[+56]VR	499.29309	2	y5	GK-H2AJ control 4-11
H2AFJ	K[+112.1]GNYAER	475.24052	2	precursor	KGNYAER
H2AFJ	K[+112.1]GNYAER	475.24052	2	precursor [M+1]	KGNYAER
H2AFJ	K[+112.1]GNYAER	475.24052	2	precursor [M+2]	KGNYAER
H2AFJ	K[+112.1]GNYAER	475.24052	2	b1	KGNYAER
H2AFJ	K[+112.1]GNYAER	475.24052	2	b2	KGNYAER
H2AFJ	K[+112.1]GNYAER	475.24052	2	b3	KGNYAER
H2AFJ	K[+112.1]GNYAER	475.24052	2	b4	KGNYAER
H2AFJ	K[+112.1]GNYAER	475.24052	2	b5	KGNYAER
H2AFJ	K[+112.1]GNYAER	475.24052	2	b6	KGNYAER
H2AFJ	K[+112.1]GNYAER	475.24052	2	y6	KGNYAER
H2AFJ	K[+112.1]GNYAER	475.24052	2	y5	KGNYAER
H2AFJ	K[+112.1]GNYAER	475.24052	2	y4	KGNYAER
H2AFJ	K[+112.1]GNYAER	475.24052	2	y3	KGNYAER
H2AFJ	K[+112.1]GNYAER	475.24052	2	y2	KGNYAER
H2AFJ	K[+112.1]GNYAER	475.24052	2	y1	KGNYAER
H2AFZ	H[+56]LK[+56]SR	376.7243	2	precursor	H2AZ

		1			
H2AFZ	H[+56]LK[+56]SR	376.7243 1	2	precursor [M+1]	H2AZ
H2AFZ	H[+56]LK[+56]SR	376.7243 1	2	precursor [M+2]	H2AZ
H2AFZ	H[+56]LK[+56]SR	376.7243 1	2	y4	H2AZ
H2AFZ	H[+56]LK[+56]SR	376.7243 1	2	y3	H2AZ
H2AFZ	H[+56]LK[+56]SR	376.7243 1	2	b4	H2AZ
HIST1H4A	G[+56]K[+42]GGK[+42]GLGK[+42]GGAK[+42]R	747.9229 9	2	precursor	H4 4Ac K5AcK8AcK12AcK16Ac
HIST1H4A	G[+56]K[+42]GGK[+42]GLGK[+42]GGAK[+42]R	747.9229 9	2	precursor [M+1]	H4 4Ac K5AcK8AcK12AcK16Ac
HIST1H4A	G[+56]K[+42]GGK[+42]GLGK[+42]GGAK[+42]R	747.9229 9	2	precursor [M+2]	H4 4Ac K5AcK8AcK12AcK16Ac
HIST1H4A	G[+56]K[+42]GGK[+42]GLGK[+42]GGAK[+42]R	747.9229 9	2	y9	H4 4Ac K5AcK8AcK12AcK16Ac
HIST1H4A	G[+56]K[+42]GGK[+42]GLGK[+42]GGAK[+42]R	747.9229 9	2	y8	H4 4Ac K5AcK8AcK12AcK16Ac
HIST1H4A	G[+56]K[+42]GGK[+42]GLGK[+42]GGAK[+42]R	747.9229 9	2	y5	H4 4Ac K5AcK8AcK12AcK16Ac
HIST1H4A	G[+56]K[+42]GGK[+42]GLGK[+42]GGAK[+42]R	747.9229 9	2	y4	H4 4Ac K5AcK8AcK12AcK16Ac
HIST1H4A	G[+56]K[+42]GGK[+42]GLGK[+42]GGAK[+42]R	747.9229 9	2	b5	H4 4Ac K5AcK8AcK12AcK16Ac
HIST1H4A	G[+56]K[+42]GGK[+42]GLGK[+42]GGAK[+42]R	747.9229 9	2	b6	H4 4Ac K5AcK8AcK12AcK16Ac
HIST1H4A	G[+56]K[+42]GGK[+42]GLGK[+42]GGAK[+42]R	747.9229 9	2	b8	H4 4Ac K5AcK8AcK12AcK16Ac
HIST1H4A	G[+56]K[+42]GGK[+42]GLGK[+42]GGAK[+42]R	747.9229 9	2	b9	H4 4Ac K5AcK8AcK12AcK16Ac
HIST1H4A	G[+56]K[+42]GGK[+42]GLGK[+42]GGAK[+42]R	747.9229 9	2	b10	H4 4Ac K5AcK8AcK12AcK16Ac
HIST1H4A	G[+56]K[+42]GGK[+42]GLGK[+42]GGAK[+42]R	747.9229 9	2	b12	H4 4Ac K5AcK8AcK12AcK16Ac
HIST1H4A	G[+56]K[+42]GGK[+42]GLGK[+42]GGAK[+42]R	747.9229 9	2	b13	H4 4Ac K5AcK8AcK12AcK16Ac
HIST1H4A	G[+56]K[+42]GGK[+42]GLGK[+42]GGAK[+56]R	754.9308 1	2	precursor	H4 3Ac K5AcK8AcK12AcK16un
HIST1H4A	G[+56]K[+42]GGK[+42]GLGK[+42]GGAK[+56]R	754.9308 1	2	precursor [M+1]	H4 3Ac K5AcK8AcK12AcK16un
HIST1H4A	G[+56]K[+42]GGK[+42]GLGK[+42]GGAK[+56]R	754.9308 1	2	precursor [M+2]	H4 3Ac K5AcK8AcK12AcK16un
HIST1H4A	G[+56]K[+42]GGK[+42]GLGK[+42]GGAK[+56]R	754.9308 1	2	y5	H4 3Ac K5AcK8AcK12AcK16un
HIST1H4A	G[+56]K[+42]GGK[+42]GLGK[+42]GGAK[+56]R	754.9308 1	2	y4	H4 3Ac K5AcK8AcK12AcK16un
HIST1H4A	G[+56]K[+42]GGK[+42]GLGK[+42]GGAK[+56]R	754.9308 1	2	y3	H4 3Ac K5AcK8AcK12AcK16un
HIST1H4A	G[+56]K[+42]GGK[+42]GLGK[+42]GGAK[+56]R	754.9308 1	2	b9	H4 3Ac K5AcK8AcK12AcK16un
HIST1H4A	G[+56]K[+42]GGK[+42]GLGK[+42]GGAK[+56]R	754.9308 1	2	b10	H4 3Ac K5AcK8AcK12AcK16un
HIST1H4A	G[+56]K[+42]GGK[+42]GLGK[+42]GGAK[+56]R	754.9308 1	2	b12	H4 3Ac K5AcK8AcK12AcK16un
HIST1H4A	G[+56]K[+42]GGK[+42]GLGK[+56]GGAK[+42]R	754.9308 1	2	precursor	H4 3Ac K5AcK8AcK12mK16m
HIST1H4A	G[+56]K[+42]GGK[+42]GLGK[+56]GGAK[+42]R	754.9308 1	2	precursor [M+1]	H4 3Ac K5AcK8AcK12mK16m
HIST1H4A	G[+56]K[+42]GGK[+42]GLGK[+56]GGAK[+42]R	754.9308 1	2	precursor [M+2]	H4 3Ac K5AcK8AcK12mK16m
HIST1H4A	G[+56]K[+42]GGK[+42]GLGK[+56]GGAK[+42]R	754.9308 1	2	y9	H4 3Ac K5AcK8AcK12mK16m
HIST1H4A	G[+56]K[+42]GGK[+42]GLGK[+56]GGAK[+42]R	754.9308 1	2	y8	H4 3Ac K5AcK8AcK12mK16m
HIST1H4A	G[+56]K[+42]GGK[+42]GLGK[+56]GGAK[+42]R	754.9308 1	2	y7	H4 3Ac K5AcK8AcK12mK16m
HIST1H4A	G[+56]K[+42]GGK[+42]GLGK[+56]GGAK[+42]R	754.9308 1	2	y6	H4 3Ac K5AcK8AcK12mK16m
HIST1H4A	G[+56]K[+42]GGK[+42]GLGK[+56]GGAK[+42]R	754.9308 1	2	b5	H4 3Ac K5AcK8AcK12mK16m

HIST1H4A	G[+56]K[+42]GGK[+42]GLGK[+56]GGAK[+42]R	754.93081	2	b6	H4 3Ac K5AcK8AcK12mK16m
HIST1H4A	G[+56]K[+42]GGK[+42]GLGK[+56]GGAK[+42]R	754.93081	2	b8	H4 3Ac K5AcK8AcK12mK16m
HIST1H4A	G[+56]K[+42]GGK[+42]GLGK[+56]GGAK[+56]R	761.93864	2	precursor	H4 2Ac K5AcK8AcK12unK16un
HIST1H4A	G[+56]K[+42]GGK[+42]GLGK[+56]GGAK[+56]R	761.93864	2	precursor [M+1]	H4 2Ac K5AcK8AcK12unK16un
HIST1H4A	G[+56]K[+42]GGK[+42]GLGK[+56]GGAK[+56]R	761.93864	2	precursor [M+2]	H4 2Ac K5AcK8AcK12unK16un
HIST1H4A	G[+56]K[+42]GGK[+42]GLGK[+56]GGAK[+56]R	761.93864	2	y12	H4 2Ac K5AcK8AcK12unK16un
HIST1H4A	G[+56]K[+42]GGK[+42]GLGK[+56]GGAK[+56]R	761.93864	2	y9	H4 2Ac K5AcK8AcK12unK16un
HIST1H4A	G[+56]K[+42]GGK[+42]GLGK[+56]GGAK[+56]R	761.93864	2	y7	H4 2Ac K5AcK8AcK12unK16un
HIST1H4A	G[+56]K[+42]GGK[+42]GLGK[+56]GGAK[+56]R	761.93864	2	y5	H4 2Ac K5AcK8AcK12unK16un
HIST1H4A	G[+56]K[+42]GGK[+42]GLGK[+56]GGAK[+56]R	761.93864	2	y4	H4 2Ac K5AcK8AcK12unK16un
HIST1H4A	G[+56]K[+42]GGK[+42]GLGK[+56]GGAK[+56]R	761.93864	2	y3	H4 2Ac K5AcK8AcK12unK16un
HIST1H4A	G[+56]K[+42]GGK[+42]GLGK[+56]GGAK[+56]R	761.93864	2	y2	H4 2Ac K5AcK8AcK12unK16un
HIST1H4A	G[+56]K[+42]GGK[+42]GLGK[+56]GGAK[+56]R	761.93864	2	b3	H4 2Ac K5AcK8AcK12unK16un
HIST1H4A	G[+56]K[+42]GGK[+42]GLGK[+56]GGAK[+56]R	761.93864	2	b4	H4 2Ac K5AcK8AcK12unK16un
HIST1H4A	G[+56]K[+42]GGK[+42]GLGK[+56]GGAK[+56]R	761.93864	2	b6	H4 2Ac K5AcK8AcK12unK16un
HIST1H4A	G[+56]K[+42]GGK[+42]GLGK[+56]GGAK[+56]R	761.93864	2	b9	H4 2Ac K5AcK8AcK12unK16un
HIST1H4A	G[+56]K[+42]GGK[+42]GLGK[+56]GGAK[+56]R	761.93864	2	b10	H4 2Ac K5AcK8AcK12unK16un
HIST1H4A	G[+56]K[+42]GGK[+42]GLGK[+56]GGAK[+56]R	761.93864	2	b11	H4 2Ac K5AcK8AcK12unK16un
HIST1H4A	G[+56]K[+42]GGK[+42]GLGK[+56]GGAK[+56]R	761.93864	2	b12	H4 2Ac K5AcK8AcK12unK16un
HIST1H4A	G[+56]K[+42]GGK[+56]GLGK[+42]GGAK[+42]R	754.93081	2	precursor	H4 3Ac K5mK8mK12AcK16Ac
HIST1H4A	G[+56]K[+42]GGK[+56]GLGK[+42]GGAK[+42]R	754.93081	2	precursor [M+1]	H4 3Ac K5mK8mK12AcK16Ac
HIST1H4A	G[+56]K[+42]GGK[+56]GLGK[+42]GGAK[+42]R	754.93081	2	precursor [M+2]	H4 3Ac K5mK8mK12AcK16Ac
HIST1H4A	G[+56]K[+42]GGK[+56]GLGK[+42]GGAK[+42]R	754.93081	2	y9	H4 3Ac K5mK8mK12AcK16Ac
HIST1H4A	G[+56]K[+42]GGK[+56]GLGK[+42]GGAK[+42]R	754.93081	2	y8	H4 3Ac K5mK8mK12AcK16Ac
HIST1H4A	G[+56]K[+42]GGK[+56]GLGK[+42]GGAK[+42]R	754.93081	2	y7	H4 3Ac K5mK8mK12AcK16Ac
HIST1H4A	G[+56]K[+42]GGK[+56]GLGK[+42]GGAK[+42]R	754.93081	2	y6	H4 3Ac K5mK8mK12AcK16Ac
HIST1H4A	G[+56]K[+42]GGK[+56]GLGK[+42]GGAK[+42]R	754.93081	2	b5	H4 3Ac K5mK8mK12AcK16Ac
HIST1H4A	G[+56]K[+42]GGK[+56]GLGK[+42]GGAK[+42]R	754.93081	2	b6	H4 3Ac K5mK8mK12AcK16Ac
HIST1H4A	G[+56]K[+42]GGK[+56]GLGK[+42]GGAK[+42]R	754.93081	2	b8	H4 3Ac K5mK8mK12AcK16Ac
HIST1H4A	G[+56]K[+42]GGK[+56]GLGK[+56]GGAK[+56]R	768.94646	2	precursor	H4 1Ac K5AcK8unK12unK16un
HIST1H4A	G[+56]K[+42]GGK[+56]GLGK[+56]GGAK[+56]R	768.94646	2	precursor [M+1]	H4 1Ac K5AcK8unK12unK16un
HIST1H4A	G[+56]K[+42]GGK[+56]GLGK[+56]GGAK[+56]R	768.94646	2	precursor [M+2]	H4 1Ac K5AcK8unK12unK16un
HIST1H4A	G[+56]K[+42]GGK[+56]GLGK[+56]GGAK[+56]R	768.94646	2	y12	H4 1Ac K5AcK8unK12unK16un
HIST1H4A	G[+56]K[+42]GGK[+56]GLGK[+56]GGAK[+56]R	768.94646	2	y9	H4 1Ac K5AcK8unK12unK16un
HIST1H4A	G[+56]K[+42]GGK[+56]GLGK[+56]GGAK[+56]R	768.94646	2	y7	H4 1Ac K5AcK8unK12unK16un
HIST1H4A	G[+56]K[+42]GGK[+56]GLGK[+56]GGAK[+56]R	768.94646	2	y6	H4 1Ac K5AcK8unK12unK16un
HIST1H4A	G[+56]K[+42]GGK[+56]GLGK[+	768.9464	2	y5	H4 1Ac

	56]GGAK[+56]R	6			K5AcK8unK12unK16un
HIST1H4A	G[+56]K[+42]GGK[+56]GLGK[+56]GGAK[+56]R	768.94646	2	y4	H4 1Ac K5AcK8unK12unK16un
HIST1H4A	G[+56]K[+42]GGK[+56]GLGK[+56]GGAK[+56]R	768.94646	2	y2	H4 1Ac K5AcK8unK12unK16un
HIST1H4A	G[+56]K[+42]GGK[+56]GLGK[+56]GGAK[+56]R	768.94646	2	b3	H4 1Ac K5AcK8unK12unK16un
HIST1H4A	G[+56]K[+42]GGK[+56]GLGK[+56]GGAK[+56]R	768.94646	2	b4	H4 1Ac K5AcK8unK12unK16un
HIST1H4A	G[+56]K[+42]GGK[+56]GLGK[+56]GGAK[+56]R	768.94646	2	b5	H4 1Ac K5AcK8unK12unK16un
HIST1H4A	G[+56]K[+42]GGK[+56]GLGK[+56]GGAK[+56]R	768.94646	2	b6	H4 1Ac K5AcK8unK12unK16un
HIST1H4A	G[+56]K[+42]GGK[+56]GLGK[+56]GGAK[+56]R	768.94646	2	b8	H4 1Ac K5AcK8unK12unK16un
HIST1H4A	G[+56]K[+42]GGK[+56]GLGK[+56]GGAK[+56]R	768.94646	2	b9	H4 1Ac K5AcK8unK12unK16un
HIST1H4A	G[+56]K[+42]GGK[+56]GLGK[+56]GGAK[+56]R	768.94646	2	b10	H4 1Ac K5AcK8unK12unK16un
HIST1H4A	G[+56]K[+42]GGK[+56]GLGK[+56]GGAK[+56]R	768.94646	2	b11	H4 1Ac K5AcK8unK12unK16un
HIST1H4A	G[+56]K[+42]GGK[+56]GLGK[+56]GGAK[+56]R	768.94646	2	b12	H4 1Ac K5AcK8unK12unK16un
HIST1H4A	G[+56]K[+56]GGK[+42]GLGK[+42]GGAK[+42]R	754.93081	2	precursor	H4 3Ac K5unK8AcK12AcK16Ac
HIST1H4A	G[+56]K[+56]GGK[+42]GLGK[+42]GGAK[+42]R	754.93081	2	precursor [M+1]	H4 3Ac K5unK8AcK12AcK16Ac
HIST1H4A	G[+56]K[+56]GGK[+42]GLGK[+42]GGAK[+42]R	754.93081	2	precursor [M+2]	H4 3Ac K5unK8AcK12AcK16Ac
HIST1H4A	G[+56]K[+56]GGK[+42]GLGK[+42]GGAK[+42]R	754.93081	2	y12	H4 3Ac K5unK8AcK12AcK16Ac
HIST1H4A	G[+56]K[+56]GGK[+42]GLGK[+42]GGAK[+42]R	754.93081	2	y11	H4 3Ac K5unK8AcK12AcK16Ac
HIST1H4A	G[+56]K[+56]GGK[+42]GLGK[+42]GGAK[+42]R	754.93081	2	y10	H4 3Ac K5unK8AcK12AcK16Ac
HIST1H4A	G[+56]K[+56]GGK[+42]GLGK[+42]GGAK[+42]R	754.93081	2	b2	H4 3Ac K5unK8AcK12AcK16Ac
HIST1H4A	G[+56]K[+56]GGK[+42]GLGK[+42]GGAK[+42]R	754.93081	2	b3	H4 3Ac K5unK8AcK12AcK16Ac
HIST1H4A	G[+56]K[+56]GGK[+42]GLGK[+42]GGAK[+42]R	754.93081	2	b4	H4 3Ac K5unK8AcK12AcK16Ac
HIST1H4A	G[+56]K[+56]GGK[+56]GLGK[+42]GGAK[+42]R	761.93864	2	precursor	H4 2Ac K5unK8unK12AcK16Ac
HIST1H4A	G[+56]K[+56]GGK[+56]GLGK[+42]GGAK[+42]R	761.93864	2	precursor [M+1]	H4 2Ac K5unK8unK12AcK16Ac
HIST1H4A	G[+56]K[+56]GGK[+56]GLGK[+42]GGAK[+42]R	761.93864	2	precursor [M+2]	H4 2Ac K5unK8unK12AcK16Ac
HIST1H4A	G[+56]K[+56]GGK[+56]GLGK[+42]GGAK[+42]R	761.93864	2	y12	H4 2Ac K5unK8unK12AcK16Ac
HIST1H4A	G[+56]K[+56]GGK[+56]GLGK[+42]GGAK[+42]R	761.93864	2	y9	H4 2Ac K5unK8unK12AcK16Ac
HIST1H4A	G[+56]K[+56]GGK[+56]GLGK[+42]GGAK[+42]R	761.93864	2	y6	H4 2Ac K5unK8unK12AcK16Ac
HIST1H4A	G[+56]K[+56]GGK[+56]GLGK[+42]GGAK[+42]R	761.93864	2	y5	H4 2Ac K5unK8unK12AcK16Ac
HIST1H4A	G[+56]K[+56]GGK[+56]GLGK[+42]GGAK[+42]R	761.93864	2	y4	H4 2Ac K5unK8unK12AcK16Ac
HIST1H4A	G[+56]K[+56]GGK[+56]GLGK[+42]GGAK[+42]R	761.93864	2	y2	H4 2Ac K5unK8unK12AcK16Ac
HIST1H4A	G[+56]K[+56]GGK[+56]GLGK[+42]GGAK[+42]R	761.93864	2	b5	H4 2Ac K5unK8unK12AcK16Ac
HIST1H4A	G[+56]K[+56]GGK[+56]GLGK[+42]GGAK[+42]R	761.93864	2	b6	H4 2Ac K5unK8unK12AcK16Ac
HIST1H4A	G[+56]K[+56]GGK[+56]GLGK[+42]GGAK[+42]R	761.93864	2	b9	H4 2Ac K5unK8unK12AcK16Ac
HIST1H4A	G[+56]K[+56]GGK[+56]GLGK[+42]GGAK[+42]R	761.93864	2	b10	H4 2Ac K5unK8unK12AcK16Ac
HIST1H4A	G[+56]K[+56]GGK[+56]GLGK[+42]GGAK[+42]R	761.93864	2	b12	H4 2Ac K5unK8unK12AcK16Ac
HIST1H4A	G[+56]K[+56]GGK[+56]GLGK[+42]GGAK[+42]R	761.93864	2	b13	H4 2Ac K5unK8unK12AcK16Ac
HIST1H4A	G[+56]K[+56]GGK[+56]GLGK[+56]GGAK[+42]R	768.94646	2	precursor	H4 1Ac K5unK8unK12unK16Ac

HIST1H4A	G[+56]K[+56]GGK[+56]GLGK[+56]GGAK[+42]R	768.94646	2	precursor [M+1]	H4 1Ac K5unK8unK12unK16Ac
HIST1H4A	G[+56]K[+56]GGK[+56]GLGK[+56]GGAK[+42]R	768.94646	2	precursor [M+2]	H4 1Ac K5unK8unK12unK16Ac
HIST1H4A	G[+56]K[+56]GGK[+56]GLGK[+56]GGAK[+42]R	768.94646	2	y12	H4 1Ac K5unK8unK12unK16Ac
HIST1H4A	G[+56]K[+56]GGK[+56]GLGK[+56]GGAK[+42]R	768.94646	2	y9	H4 1Ac K5unK8unK12unK16Ac
HIST1H4A	G[+56]K[+56]GGK[+56]GLGK[+56]GGAK[+42]R	768.94646	2	y8	H4 1Ac K5unK8unK12unK16Ac
HIST1H4A	G[+56]K[+56]GGK[+56]GLGK[+56]GGAK[+42]R	768.94646	2	y7	H4 1Ac K5unK8unK12unK16Ac
HIST1H4A	G[+56]K[+56]GGK[+56]GLGK[+56]GGAK[+42]R	768.94646	2	y6	H4 1Ac K5unK8unK12unK16Ac
HIST1H4A	G[+56]K[+56]GGK[+56]GLGK[+56]GGAK[+42]R	768.94646	2	y5	H4 1Ac K5unK8unK12unK16Ac
HIST1H4A	G[+56]K[+56]GGK[+56]GLGK[+56]GGAK[+42]R	768.94646	2	y4	H4 1Ac K5unK8unK12unK16Ac
HIST1H4A	G[+56]K[+56]GGK[+56]GLGK[+56]GGAK[+42]R	768.94646	2	y2	H4 1Ac K5unK8unK12unK16Ac
HIST1H4A	G[+56]K[+56]GGK[+56]GLGK[+56]GGAK[+42]R	768.94646	2	b3	H4 1Ac K5unK8unK12unK16Ac
HIST1H4A	G[+56]K[+56]GGK[+56]GLGK[+56]GGAK[+42]R	768.94646	2	b4	H4 1Ac K5unK8unK12unK16Ac
HIST1H4A	G[+56]K[+56]GGK[+56]GLGK[+56]GGAK[+42]R	768.94646	2	b5	H4 1Ac K5unK8unK12unK16Ac
HIST1H4A	G[+56]K[+56]GGK[+56]GLGK[+56]GGAK[+42]R	768.94646	2	b6	H4 1Ac K5unK8unK12unK16Ac
HIST1H4A	G[+56]K[+56]GGK[+56]GLGK[+56]GGAK[+42]R	768.94646	2	b8	H4 1Ac K5unK8unK12unK16Ac
HIST1H4A	G[+56]K[+56]GGK[+56]GLGK[+56]GGAK[+42]R	768.94646	2	b9	H4 1Ac K5unK8unK12unK16Ac
HIST1H4A	G[+56]K[+56]GGK[+56]GLGK[+56]GGAK[+42]R	768.94646	2	b10	H4 1Ac K5unK8unK12unK16Ac
HIST1H4A	G[+56]K[+56]GGK[+56]GLGK[+56]GGAK[+42]R	768.94646	2	b12	H4 1Ac K5unK8unK12unK16Ac
HIST1H4A	G[+56]K[+56]GGK[+56]GLGK[+56]GGAK[+42]R	768.94646	2	b13	H4 1Ac K5unK8unK12unK16Ac
HIST1H4A	G[+56]K[+56]GGK[+56]GLGK[+56]GGAK[+56]R	775.95429	2	precursor	H4 0Ac K5unK8unK12unK16un
HIST1H4A	G[+56]K[+56]GGK[+56]GLGK[+56]GGAK[+56]R	775.95429	2	precursor [M+1]	H4 0Ac K5unK8unK12unK16un
HIST1H4A	G[+56]K[+56]GGK[+56]GLGK[+56]GGAK[+56]R	775.95429	2	precursor [M+2]	H4 0Ac K5unK8unK12unK16un
HIST1H4A	G[+56]K[+56]GGK[+56]GLGK[+56]GGAK[+56]R	775.95429	2	y9	H4 0Ac K5unK8unK12unK16un
HIST1H4A	G[+56]K[+56]GGK[+56]GLGK[+56]GGAK[+56]R	775.95429	2	y8	H4 0Ac K5unK8unK12unK16un
HIST1H4A	G[+56]K[+56]GGK[+56]GLGK[+56]GGAK[+56]R	775.95429	2	y6	H4 0Ac K5unK8unK12unK16un
HIST1H4A	G[+56]K[+56]GGK[+56]GLGK[+56]GGAK[+56]R	775.95429	2	y5	H4 0Ac K5unK8unK12unK16un
HIST1H4A	G[+56]K[+56]GGK[+56]GLGK[+56]GGAK[+56]R	775.95429	2	y4	H4 0Ac K5unK8unK12unK16un
HIST1H4A	G[+56]K[+56]GGK[+56]GLGK[+56]GGAK[+56]R	775.95429	2	b5	H4 0Ac K5unK8unK12unK16un
HIST1H4A	G[+56]K[+56]GGK[+56]GLGK[+56]GGAK[+56]R	775.95429	2	b6	H4 0Ac K5unK8unK12unK16un
HIST1H4A	G[+56]K[+56]GGK[+56]GLGK[+56]GGAK[+56]R	775.95429	2	b8	H4 0Ac K5unK8unK12unK16un
HIST1H4A	G[+56]K[+56]GGK[+56]GLGK[+56]GGAK[+56]R	775.95429	2	b9	H4 0Ac K5unK8unK12unK16un
HIST1H4A	G[+56]K[+56]GGK[+56]GLGK[+56]GGAK[+56]R	775.95429	2	b12	H4 0Ac K5unK8unK12unK16un
HIST1H4A	G[+56]K[+56]GGK[+56]GLGK[+56]GGAK[+56]R	775.95429	2	b13	H4 0Ac K5unK8unK12unK16un
HIST1H4A	K[+112.1]VLR	627.41882	1	precursor	H4K20unmod
HIST1H4A	K[+112.1]VLR	627.41882	1	precursor [M+1]	H4K20unmod
HIST1H4A	K[+112.1]VLR	627.41882	1	precursor [M+2]	H4K20unmod
HIST1H4A	K[+112.1]VLR	627.4188	1	y3	H4K20unmod

		2			
HIST1H4A	K[+112.1]VLR	627.41882	1	y2	H4K20unmod
HIST1H4A	K[+112.1]VLR	627.41882	1	b1	H4K20unmod
HIST1H4A	K[+112.1]VLR	627.41882	1	b2	H4K20unmod
HIST1H4A	K[+112.1]VLR	627.41882	1	b3	H4K20unmod
HIST1H4A	K[+126.1]VLR	641.43447	1	precursor	H4K20me1
HIST1H4A	K[+126.1]VLR	641.43447	1	precursor [M+1]	H4K20me1
HIST1H4A	K[+126.1]VLR	641.43447	1	precursor [M+2]	H4K20me1
HIST1H4A	K[+126.1]VLR	641.43447	1	y3	H4K20me1
HIST1H4A	K[+126.1]VLR	641.43447	1	y2	H4K20me1
HIST1H4A	K[+126.1]VLR	641.43447	1	b1	H4K20me1
HIST1H4A	K[+126.1]VLR	641.43447	1	b2	H4K20me1
HIST1H4A	K[+126.1]VLR	641.43447	1	b3	H4K20me1
HIST1H4A	K[+84.1]VLR	300.21559	2	precursor	H4K20me2
HIST1H4A	K[+84.1]VLR	300.21559	2	precursor [M+1]	H4K20me2
HIST1H4A	K[+84.1]VLR	300.21559	2	precursor [M+2]	H4K20me2
HIST1H4A	K[+84.1]VLR	300.21559	2	y3	H4K20me2
HIST1H4A	K[+84.1]VLR	300.21559	2	y1	H4K20me2
HIST1H4A	K[+84.1]VLR	300.21559	2	b1	H4K20me2
HIST1H4A	K[+84.1]VLR	300.21559	2	b2	H4K20me2
HIST1H4A	K[+84.1]VLR	300.21559	2	b3	H4K20me2
HIST1H4A	K[+98.1]VLR	307.22342	2	precursor	H4K20me3
HIST1H4A	K[+98.1]VLR	307.22342	2	precursor [M+1]	H4K20me3
HIST1H4A	K[+98.1]VLR	307.22342	2	precursor [M+2]	H4K20me3
HIST1H4A	K[+98.1]VLR	307.22342	2	y3	H4K20me3
HIST1H4A	K[+98.1]VLR	307.22342	2	y1	H4K20me3
HIST1H4A	K[+98.1]VLR	307.22342	2	b1	H4K20me3
HIST1H4A	K[+98.1]VLR	307.22342	2	b2	H4K20me3
HIST1H4A	K[+98.1]VLR	307.22342	2	b3	H4K20me3
HIST1H4A	D[+56]AVTYTEHAK[+56]R	701.8517	2	precursor	H4 control 68-78
HIST1H4A	D[+56]AVTYTEHAK[+56]R	701.8517	2	precursor [M+1]	H4 control 68-78
HIST1H4A	D[+56]AVTYTEHAK[+56]R	701.8517	2	precursor [M+2]	H4 control 68-78
HIST1H4A	D[+56]AVTYTEHAK[+56]R	701.8517	2	y8	H4 control 68-78
HIST1H4A	D[+56]AVTYTEHAK[+56]R	701.8517	2	y7	H4 control 68-78
HIST1H4A	D[+56]AVTYTEHAK[+56]R	701.8517	2	y6	H4 control 68-78
HIST1H4A	D[+56]AVTYTEHAK[+56]R	701.8517	2	y4	H4 control 68-78
HIST1H4A	D[+56]AVTYTEHAK[+56]R	701.8517	2	y3	H4 control 68-78
HIST1H4A	D[+56]AVTYTEHAK[+56]R	701.8517	2	b3	H4 control 68-78

HIST1H4A	D[+56]AVTYTEHAK[+56]R	701.8517	2	b4	H4 control 68-78
HIST1H4A	D[+56]AVTYTEHAK[+56]R	701.8517	2	b9	H4 control 68-78
HIST1H4A	D[+56]AVTYTEHAK[+56]R	701.8517	2	b10	H4 control 68-78

Appendix Table 1. List of the targeted peptides.

	DNA size	**DNA concentration [pg/ml]**	**% of mono-nucleosomes**
Sample 1	Mono-nucleosomal	232.13	94.4
	Poly-nucleosomal	13.84	
Sample 2	Mono-nucleosomal	92.06	96.5
	Poly-nucleosomal	3.33	
Sample 3	Mono-nucleosomal	307.29	99.0
	Poly-nucleosomal	3.15	
Sample 4	Mono-nucleosomal	223.19	98.1
	Poly-nucleosomal	4.35	
Sample 5	Mono-nucleosomal	196.59	96.7
	Poly-nucleosomal	6.75	

Sample 6	Mono-nucleosomal	241.79	97.3
	Poly-nucleosomal	6.75	
Sample 7	Mono-nucleosomal	271.14	98.6
	Poly-nucleosomal	3.72	
Sample 8	Mono-nucleosomal	227.96	96.1
	Poly-nucleosomal	9.32	
Sample 9	Mono-nucleosomal	396.49	97.9
	Poly-nucleosomal	8.49	
Sample 10	Mono-nucleosomal	355.93	96.5
	Poly-nucleosomal	12.8	

Appendix Table 2. Quantification of the nucleosomal DNA size. MNase extracted chromatin samples indicated with the red stars on Figure 3.2 B were examined by Bioanalyzer analysis to verify the extent of digestion. For each Bioanylazer trace, the area under the peak corresponding to mono- and poly-nucleosomal DNA sizes was calculated. The percentage of mono-nucleosomal DNA was calculated relative to the total amount of DNA of all sizes present in each sample.

		Input	IP
Histone	Peptide name	%CV	%CV
H3	H3 K4unmod	2.2	15
	H3 K4me1	16.8	17
	H3 K4me2	21.7	28
	H3 K4me3	28.8	N/D
	H3 K9unmodK14unmod	8.8	7.7
	H3 K9me1K14unmod	10	7.7
	H3 K9me2K14unmod	2.6	3.5
	H3 K9me3K14unmod	4.6	4.5
	H3 K9acK14unmod	13.1	26.2
	H3 K9unmodK14ac	11	11

	H3 K9me1K14ac	9.9	5.7
	H3 K9me2K14ac	3.3	4.3
	H3 K9me3K14ac	4.2	3.7
	H3 K9acK14ac	18.6	19.1
	H3 K27unmodK36unmod	9.1	8
	H3 K27unmodK36me1	14.5	14.9
	H3 K27unmodK36me2	8.6	10
	H3 K27unmodK36me3	10.8	14.4
	H3 K27me1K36unmod	13.3	11.6
	H3 K27me1K36me1	10.7	14.3
	H3 K27me1K36me2	11.3	8.1
	H3 K27me1K36me3	11.9	10.1
	H3 K27me2K36unmod	7.8	4.7
	H3 K27me2K36me1	10	5.7
	H3 K27me2K36me2	7.2	14.2
	H3 K27me2K36me3	9.4	18.6
	H3 K27me3K36unmod	8.6	7
	H3 K27me3K36me1	7.4	6.5
	H3 K27me3K36me2	9.2	N/D
	H3 K79unmod	1	24.6
	H3 K79me1	69.3	76.8
	H3 K79me2	10	56.6
H4	H4 K5AcK8AcK12AcK16Ac	8.4	13.8
	H4 K5AcK8AcK12AcK16un	14.4	33.4
	H4 K5AcK8AcK12mK16m	5.8	15.9

	H4 K5AcK8AcK12unK16un	9.3	17.3
	H4 K5mK8mK12AcK16Ac	7.6	9.1
	H4 K5AcK8unK12unK16un	7.4	4.5
	H4 K5unK8AcK12AcK16Ac	11	27.1
	H4 K5unK8unK12AcK16Ac	16.9	3.4
	H4 K5unK8unK12unK16Ac	5.8	2
	H4 K5unK8unK12unK16un	5.7	2.6
	H4 K20un	9.7	6.5
	H4 K20me1	7.4	7.4
	H4 K20me2	2.7	2.3
	H4 K20me3	16.8	5.8
H2A type 1-B/E	Amino acids 4-11	0.5	5.8
	Amino acids 36-42	8.2	10.3
	H2A K13unK15un	0.4	1
	H2A K13unK15ub	29.1	23
H2AX	Amino acids 4-11	8.8	4.2
	Amino acids 36-42	9.9	7
	H2AX-like K13unK15un	0.1	0.5
	H2AX-like K13unK15ub	17.1	13
H2AJ	Amino acids 4-11	14.7	N/D
	Amino acids 36-42	3.8	7.4

Appendix Table 3. Table showing %CV for each of the targeted peptides for the input and IP samples.

UniProt accession	m/z	Peptide score	Peptide p-value	Peptide sequence
O00422|SAP18_HUMAN	719.8445	37.18	0.0028	KGTDDSMTLQSQK
O00422|SAP18_HUMAN	719.8453	63.88	6.40E-06	KGTDDSMTLQSQK
O00422|SAP18_HUMAN	719.8436	64.42	5.20E-06	KGTDDSMTLQSQK
O00422|SAP18_HUMAN	719.8441	66.56	3.10E-06	KGTDDSMTLQSQK
O00567|NOP56_HUMAN	654.8839	38.82	0.005	LIAHAGSLTNLAK
O00571|DDX3X_HUMAN	762.8958	43.85	0.002	VGNLGLATSFFNER
O00571|DDX3X_HUMAN	762.8923	43.76	0.0019	VGNLGLATSFFNER
O00571|DDX3X_HUMAN	762.8908	46.22	0.00095	VGNLGLATSFFNER
O00571|DDX3X_HUMAN	762.8926	49.26	0.00051	VGNLGLATSFFNER
O00571|DDX3X_HUMAN	762.8948	57.44	7.20E-05	VGNLGLATSFFNER
O14514|BAI1_HUMAN	453.7074	34.54	0.0021	DCGGGLQTR

O14514|BAI1_HUMAN	453.7081	36.21	0.0015	DCGGGLQTR
O14979|HNRDL_HUMAN	735.3752	39.46	0.0037	MFIGGLSWDTSKK
O14979|HNRDL_HUMAN	735.3765	44.29	0.0013	MFIGGLSWDTSKK
O14979|HNRDL_HUMAN	735.3741	50.95	0.00026	MFIGGLSWDTSKK
O14979|HNRDL_HUMAN	735.3737	52.99	0.00015	MFIGGLSWDTSKK
O43143|DHX15_HUMAN	707.8666	44.03	0.0016	YGVIILDEAHER
O43143|DHX15_HUMAN	707.8689	49.77	0.00046	YGVIILDEAHER
O43143|DHX15_HUMAN	707.869	53.5	0.00019	YGVIILDEAHER
O43390|HNRPR_HUMAN	649.7922	30.39	0.0036	DYAFVHFEDR
O43390|HNRPR_HUMAN	647.6684	43.68	0.0029	VTEGLVDVILYHQPDDK
O43390|HNRPR_HUMAN	649.7925	31.7	0.0027	DYAFVHFEDR
O43390|HNRPR_HUMAN	669.3481	42.41	0.0024	TKENILEEFSK
O43390|HNRPR_HUMAN	631.303	39.45	0.0017	LMMDPLSGQNR
O43390|HNRPR_HUMAN	1254.123	46.94	0.0015	YGGPPPDSVYSGVQPGIGTEVFVGK
O43390|HNRPR_HUMAN	770.3795	43.2	0.0013	LKDYAFVHFEDR
O43390|HNRPR_HUMAN	669.3479	45.21	0.0012	TKENILEEFSK
O43390|HNRPR_HUMAN	669.3491	47.26	0.00084	TKENILEEFSK
O43390|HNRPR_HUMAN	669.348	47.08	0.00079	TKENILEEFSK
O43390|HNRPR_HUMAN	631.3025	44.28	0.00064	LMMDPLSGQNR
O43390|HNRPR_HUMAN	669.348	48.34	0.00059	TKENILEEFSK
O43390|HNRPR_HUMAN	770.3806	47.08	0.00053	LKDYAFVHFEDR
O43390|HNRPR_HUMAN	1348.644	49.89	0.00046	VWGNVVTVEWADPVEEPDPEVMAK
O43390|HNRPR_HUMAN	879.8892	42.01	0.00036	STAYEDYYYHPPPR
O43390|HNRPR_HUMAN	1254.121	53.01	0.00034	YGGPPPDSVYSGVQPGIGTEVFVGK
O43390|HNRPR_HUMAN	879.8894	42.24	0.00034	STAYEDYYYHPPPR
O43390|HNRPR_HUMAN	879.8904	42.65	0.0003	STAYEDYYYHPPPR
O43390|HNRPR_HUMAN	647.6694	54.37	0.00024	VTEGLVDVILYHQPDDK
O43390|HNRPR_	647.6	54.55	0.00023	VTEGLVDVILYHQPDDK

HUMAN	671			
O43390|HNRPR_HUMAN	730.8947	55.92	0.00022	NLATTVTEEILEK
O43390|HNRPR_HUMAN	649.7924	44.11	0.00016	DYAFVHFEDR
O43390|HNRPR_HUMAN	649.7918	43	0.00016	DYAFVHFEDR
O43390|HNRPR_HUMAN	1254.123	57.12	0.00014	YGGPPPDSVYSGVQPGIGTEVFVGK
O43390|HNRPR_HUMAN	879.8903	46.78	0.00012	STAYEDYYYHPPPR
O43390|HNRPR_HUMAN	730.8938	58.81	0.00011	NLATTVTEEILEK
O43390|HNRPR_HUMAN	1254.123	58.24	0.00011	YGGPPPDSVYSGVQPGIGTEVFVGK
O43390|HNRPR_HUMAN	649.7918	46.08	7.80E-05	DYAFVHFEDR
O43390|HNRPR_HUMAN	1254.123	59.83	7.50E-05	YGGPPPDSVYSGVQPGIGTEVFVGK
O43390|HNRPR_HUMAN	805.4003	56.73	7.20E-05	DLYEDELVPLFEK
O43390|HNRPR_HUMAN	1254.124	61.58	5.00E-05	YGGPPPDSVYSGVQPGIGTEVFVGK
O43390|HNRPR_HUMAN	770.3812	57.65	4.60E-05	LKDYAFVHFEDR
O43390|HNRPR_HUMAN	669.3488	60.02	4.50E-05	TKENILEEFSK
O43390|HNRPR_HUMAN	649.7908	49.98	4.40E-05	DYAFVHFEDR
O43390|HNRPR_HUMAN	669.3486	60.39	4.20E-05	TKENILEEFSK
O43390|HNRPR_HUMAN	730.8943	63.89	3.40E-05	NLATTVTEEILEK
O43390|HNRPR_HUMAN	805.4047	59.92	3.40E-05	DLYEDELVPLFEK
O43390|HNRPR_HUMAN	879.8891	53.41	2.50E-05	STAYEDYYYHPPPR
O43390|HNRPR_HUMAN	1348.647	63.35	2.20E-05	VWGNVVTVEWADPVEEPDPEVMAK
O43390|HNRPR_HUMAN	971.0034	65.95	2.00E-05	VTEGLVDVILYHQPDDK
O43390|HNRPR_HUMAN	971.0009	66.22	1.80E-05	VTEGLVDVILYHQPDDK
O43390|HNRPR_HUMAN	879.8898	55.31	1.70E-05	STAYEDYYYHPPPR
O43390|HNRPR_HUMAN	730.894	69.16	1.00E-05	NLATTVTEEILEK
O43390|HNRPR_HUMAN	879.8906	57.92	9.80E-06	STAYEDYYYHPPPR
O43390|HNRPR_HUMAN	730.8936	69.58	9.10E-06	NLATTVTEEILEK
O43390|HNRPR_HUMAN	805.4049	65.85	8.80E-06	DLYEDELVPLFEK
O43390|HNRPR_HUMAN	879.8886	60.53	4.70E-06	STAYEDYYYHPPPR

O43390|HNRPR_HUMAN	879.888	60.36	4.60E-06	STAYEDYYYHPPPR
O43390|HNRPR_HUMAN	805.4039	69.35	4.50E-06	DLYEDELVPLFEK
O43390|HNRPR_HUMAN	879.8898	61.78	3.80E-06	STAYEDYYYHPPPR
O43390|HNRPR_HUMAN	879.8918	62.23	3.70E-06	STAYEDYYYHPPPR
O43390|HNRPR_HUMAN	1254.125	73.27	3.50E-06	YGGPPPDSVYSGVQPGIGTEVFVGK
O43390|HNRPR_HUMAN	770.3829	70.71	2.80E-06	LKDYAFVHFEDR
O43390|HNRPR_HUMAN	879.8889	66.08	1.40E-06	STAYEDYYYHPPPR
O43390|HNRPR_HUMAN	879.8881	67.56	8.80E-07	STAYEDYYYHPPPR
O43390|HNRPR_HUMAN	770.3811	75.14	8.20E-07	LKDYAFVHFEDR
O43390|HNRPR_HUMAN	730.894	81.88	5.40E-07	NLATTVTEEILEK
O43390|HNRPR_HUMAN	879.8882	69.71	5.40E-07	STAYEDYYYHPPPR
O43390|HNRPR_HUMAN	730.8928	84.79	2.50E-07	NLATTVTEEILEK
O43390|HNRPR_HUMAN	1254.124	88.44	1.00E-07	YGGPPPDSVYSGVQPGIGTEVFVGK
O60506|HNRPQ_HUMAN	1283.627	40.58	0.0047	YGGPPPDSVYSGQQPSVGTEIFVGK
O60506|HNRPQ_HUMAN	630.8233	41.44	0.0034	LMMDPLTGLNR
O60506|HNRPQ_HUMAN	630.8242	42.66	0.0024	LMMDPLTGLNR
O60506|HNRPQ_HUMAN	814.7565	46.48	0.0023	VAEKLDEIYVAGLVAHSDLDER
O60506|HNRPQ_HUMAN	529.7724	39.7	0.002	LYNNHEIR
O60506|HNRPQ_HUMAN	529.77	40.78	0.0018	LYNNHEIR
O60506|HNRPQ_HUMAN	737.3911	46.43	0.0017	NLANTVTEEILEK
O60506|HNRPQ_HUMAN	971.991	46.18	0.0013	VTEGLTDVILYHQPDDK
O60506|HNRPQ_HUMAN	1283.626	46.41	0.0012	YGGPPPDSVYSGQQPSVGTEIFVGK
O60506|HNRPQ_HUMAN	1283.624	47.91	0.00083	YGGPPPDSVYSGQQPSVGTEIFVGK
O60506|HNRPQ_HUMAN	814.7521	52.6	0.0005	VAEKLDEIYVAGLVAHSDLDER
O60506|HNRPQ_HUMAN	1283.623	50.06	0.00049	YGGPPPDSVYSGQQPSVGTEIFVGK
O60506|HNRPQ_HUMAN	797.4039	49.61	0.00046	DLFEDELVPLFEK
O60506|HNRPQ_HUMAN	1283.626	51.59	0.00037	YGGPPPDSVYSGQQPSVGTEIFVGK
O60506|HNRPQ_	797.4	51.86	0.00027	DLFEDELVPLFEK

HUMAN	036			
O60506|HNRPQ_HUMAN	737.3916	54.58	0.00026	NLANTVTEEILEK
O60506|HNRPQ_HUMAN	971.9896	52.61	0.00026	VTEGLTDVILYHQPDDK
O60506|HNRPQ_HUMAN	797.4024	52.96	0.00023	DLFEDELVPLFEK
O60506|HNRPQ_HUMAN	630.825	53.94	0.00021	LMMDPLTGLNR
O60506|HNRPQ_HUMAN	797.4044	53.8	0.00021	DLFEDELVPLFEK
O60506|HNRPQ_HUMAN	737.3912	55.63	0.0002	NLANTVTEEILEK
O60506|HNRPQ_HUMAN	737.3906	56.36	0.00018	NLANTVTEEILEK
O60506|HNRPQ_HUMAN	737.3901	56.33	0.00016	NLANTVTEEILEK
O60506|HNRPQ_HUMAN	797.4039	56.56	9.30E-05	DLFEDELVPLFEK
O60506|HNRPQ_HUMAN	737.3919	59.52	8.20E-05	NLANTVTEEILEK
O60506|HNRPQ_HUMAN	971.9904	59.01	6.70E-05	VTEGLTDVILYHQPDDK
O60506|HNRPQ_HUMAN	529.7701	56.03	5.20E-05	LYNNHEIR
O60506|HNRPQ_HUMAN	737.3911	62.13	4.50E-05	NLANTVTEEILEK
O60506|HNRPQ_HUMAN	737.3906	63.7	3.20E-05	NLANTVTEEILEK
O60506|HNRPQ_HUMAN	630.8242	62.06	2.80E-05	LMMDPLTGLNR
O60506|HNRPQ_HUMAN	1283.625	63.21	2.50E-05	YGGPPPDSVYSGQQPSVGTEIFVGK
O60506|HNRPQ_HUMAN	797.4039	62.4	2.40E-05	DLFEDELVPLFEK
O60506|HNRPQ_HUMAN	737.3923	65.78	1.90E-05	NLANTVTEEILEK
O60506|HNRPQ_HUMAN	630.8252	65.24	1.40E-05	LMMDPLTGLNR
O60506|HNRPQ_HUMAN	797.4023	65.36	1.30E-05	DLFEDELVPLFEK
O60506|HNRPQ_HUMAN	797.4022	64.98	1.30E-05	DLFEDELVPLFEK
O60506|HNRPQ_HUMAN	797.4035	69.4	4.60E-06	DLFEDELVPLFEK
O60506|HNRPQ_HUMAN	797.4031	70.29	3.80E-06	DLFEDELVPLFEK
O60506|HNRPQ_HUMAN	797.4033	79.67	4.40E-07	DLFEDELVPLFEK
O60506|HNRPQ_HUMAN	1327.624	94.92	1.00E-08	VWGNVGTVEWADPIEDPDPEVMAK
O60832|DKC1_HUMAN	1055.121	42.26	0.0034	ALETLTGALFQRPPLIAAVK
O60832|DKC1_HUMAN	1055.123	44.53	0.0015	ALETLTGALFQRPPLIAAVK

O60832|DKC1_HUMAN	1055.121	50.72	0.00049	ALETLTGALFQRPPLIAAVK
O60832|DKC1_HUMAN	657.3785	57.94	0.00013	LDTSQWPLLLK
O60832|DKC1_HUMAN	1055.125	61.88	2.80E-05	ALETLTGALFQRPPLIAAVK
O75367|H2AY_HUMAN	908.4879	45.33	0.0029	NGPLEVAGAAVSAGHGLPAK
O75367|H2AY_HUMAN	804.4047	42.04	0.0028	AISSYFVSTMSSSIK
O75367|H2AY_HUMAN	908.4855	49.67	0.0011	NGPLEVAGAAVSAGHGLPAK
O75367|H2AY_HUMAN	993.5695	49.46	0.001	GVTIASGGVLPNIHPELLAK
O75367|H2AY_HUMAN	993.5687	51.77	0.0006	GVTIASGGVLPNIHPELLAK
O75367|H2AY_HUMAN	993.5698	55.62	0.00025	GVTIASGGVLPNIHPELLAK
O75367|H2AY_HUMAN	1064.012	51.58	0.00023	AASADSTTEGTPADGFTVLSTK
O75367|H2AY_HUMAN	908.4863	58.11	0.00014	NGPLEVAGAAVSAGHGLPAK
O75367|H2AY_HUMAN	993.5679	60.73	7.50E-05	GVTIASGGVLPNIHPELLAK
O75367|H2AY_HUMAN	993.5701	61.13	6.20E-05	GVTIASGGVLPNIHPELLAK
O75367|H2AY_HUMAN	1064.005	58.14	4.50E-05	AASADSTTEGTPADGFTVLSTK
O75367|H2AY_HUMAN	1064.007	58.53	4.20E-05	AASADSTTEGTPADGFTVLSTK
O75367|H2AY_HUMAN	1064.007	59.17	3.80E-05	AASADSTTEGTPADGFTVLSTK
O75367|H2AY_HUMAN	908.486	65.48	2.90E-05	NGPLEVAGAAVSAGHGLPAK
O75367|H2AY_HUMAN	993.5698	65.4	2.70E-05	GVTIASGGVLPNIHPELLAK
O75367|H2AY_HUMAN	667.9031	61.77	2.70E-05	GKLEAIITPPPAK
O75367|H2AY_HUMAN	1064.008	60.74	2.60E-05	AASADSTTEGTPADGFTVLSTK
O75367|H2AY_HUMAN	993.571	66.1	1.70E-05	GVTIASGGVLPNIHPELLAK
O75367|H2AY_HUMAN	1064.006	62.7	1.60E-05	AASADSTTEGTPADGFTVLSTK
O75367|H2AY_HUMAN	1064.006	63.13	1.50E-05	AASADSTTEGTPADGFTVLSTK
O75367|H2AY_HUMAN	1064.004	62.65	1.50E-05	AASADSTTEGTPADGFTVLSTK
O75367|H2AY_HUMAN	993.5707	67.36	1.40E-05	GVTIASGGVLPNIHPELLAK
O75367|H2AY_HUMAN	1064.005	63.29	1.40E-05	AASADSTTEGTPADGFTVLSTK
O75367|H2AY_HUMAN	908.4877	68.83	1.30E-05	NGPLEVAGAAVSAGHGLPAK
O75367|H2AY_H	908.4	69.14	1.20E-05	NGPLEVAGAAVSAGHGLPAK

UMAN	872			
O75367|H2AY_HUMAN	993.5687	69.08	1.10E-05	GVTIASGGVLPNIHPELLAK
O75367|H2AY_HUMAN	1064.007	64.82	9.70E-06	AASADSTTEGTPADGFTVLSTK
O75367|H2AY_HUMAN	1064.005	64.84	9.60E-06	AASADSTTEGTPADGFTVLSTK
O75367|H2AY_HUMAN	993.5692	69.65	8.90E-06	GVTIASGGVLPNIHPELLAK
O75367|H2AY_HUMAN	908.4873	72.97	5.10E-06	NGPLEVAGAAVSAGHGLPAK
O75367|H2AY_HUMAN	993.571	71.25	5.10E-06	GVTIASGGVLPNIHPELLAK
O75367|H2AY_HUMAN	1064.006	67.79	5.10E-06	AASADSTTEGTPADGFTVLSTK
O75367|H2AY_HUMAN	993.569	72.36	4.80E-06	GVTIASGGVLPNIHPELLAK
O75367|H2AY_HUMAN	993.5703	72.65	4.40E-06	GVTIASGGVLPNIHPELLAK
O75367|H2AY_HUMAN	1064.006	68.49	4.40E-06	AASADSTTEGTPADGFTVLSTK
O75367|H2AY_HUMAN	908.4868	74.57	3.60E-06	NGPLEVAGAAVSAGHGLPAK
O75367|H2AY_HUMAN	993.5699	75.07	2.90E-06	GVTIASGGVLPNIHPELLAK
O75367|H2AY_HUMAN	993.5705	75.69	2.20E-06	GVTIASGGVLPNIHPELLAK
O75367|H2AY_HUMAN	908.4861	77.5	1.80E-06	NGPLEVAGAAVSAGHGLPAK
O75367|H2AY_HUMAN	908.4869	77.45	1.80E-06	NGPLEVAGAAVSAGHGLPAK
O75367|H2AY_HUMAN	667.905	72.94	1.70E-06	GKLEAIITPPPAK
O75367|H2AY_HUMAN	908.4882	77.31	1.60E-06	NGPLEVAGAAVSAGHGLPAK
O75367|H2AY_HUMAN	1064.008	72.9	1.60E-06	AASADSTTEGTPADGFTVLSTK
O75367|H2AY_HUMAN	1064.007	72.93	1.50E-06	AASADSTTEGTPADGFTVLSTK
O75367|H2AY_HUMAN	993.5696	80.93	7.20E-07	GVTIASGGVLPNIHPELLAK
O75367|H2AY_HUMAN	908.4855	86.32	2.40E-07	NGPLEVAGAAVSAGHGLPAK
O75367|H2AY_HUMAN	908.4885	91.06	7.50E-08	NGPLEVAGAAVSAGHGLPAK
O75367|H2AY_HUMAN	908.4876	92.18	6.00E-08	NGPLEVAGAAVSAGHGLPAK
O75367|H2AY_HUMAN	908.4887	96.05	2.30E-08	NGPLEVAGAAVSAGHGLPAK
O75367|H2AY_HUMAN	908.486	98.76	1.30E-08	NGPLEVAGAAVSAGHGLPAK
O75367|H2AY_HUMAN	908.4863	98.89	1.10E-08	NGPLEVAGAAVSAGHGLPAK
O75367|H2AY_HUMAN	908.4877	109.74	1.10E-09	NGPLEVAGAAVSAGHGLPAK

O75367|H2AY_HUMAN	908.487	117.03	2.00E-10	NGPLEVAGAAVSAGHGLPAK
O75475|PSIP1_HUMAN	794.3837	37.64	0.003	KDEEGQKEEDKPR
O75475|PSIP1_HUMAN	625.8403	43.59	0.0024	DFKPGDLIFAK
O75475|PSIP1_HUMAN	625.8398	44.48	0.002	DFKPGDLIFAK
O75475|PSIP1_HUMAN	880.9297	62.09	2.20E-05	KGFNEGLWEIDNNPK
O75533|SF3B1_HUMAN	606.3033	38.66	0.0026	THEDIEAQIR
O75533|SF3B1_HUMAN	918.9893	59.14	9.80E-05	SLVEIIEHGLVDEQQK
O75533|SF3B1_HUMAN	918.9867	59.58	9.20E-05	SLVEIIEHGLVDEQQK
O95777|LSM8_HUMAN	1258.107	96.08	1.10E-08	GDNVAVIGEIDEETDSALDLGNIR
O95777|LSM8_HUMAN	1258.109	102.22	2.80E-09	GDNVAVIGEIDEETDSALDLGNIR
P02533|K1C14_HUMAN	681.351	66.08	1.30E-05	EVATNSELVQSGK
P02533|K1C14_HUMAN	681.3472	67.47	8.90E-06	EVATNSELVQSGK
P02545|LMNA_HUMAN	591.8082	40.69	0.0023	TLEGELHDLR
P02545|LMNA_HUMAN	594.3209	44.6	0.0022	LRDLEDSLAR
P02545|LMNA_HUMAN	594.3223	45.52	0.0021	LRDLEDSLAR
P02545|LMNA_HUMAN	594.3201	45.21	0.0021	LRDLEDSLAR
P02545|LMNA_HUMAN	803.4106	44.19	0.002	VAVEEVDEEGKFVR
P02545|LMNA_HUMAN	622.3638	49.02	0.0013	LKDLEALLNSK
P02545|LMNA_HUMAN	622.3663	49.79	0.0011	LKDLEALLNSK
P02545|LMNA_HUMAN	1183.078	47.64	0.0011	ASASGSGAQVGGPISSGSSASSVTVTR
P02545|LMNA_HUMAN	947.4645	46.1	0.0011	MQQQLDEYQELLDIK
P02545|LMNA_HUMAN	594.3216	48.01	0.001	LRDLEDSLAR
P02545|LMNA_HUMAN	622.365	52.6	0.0005	LKDLEALLNSK
P02545|LMNA_HUMAN	803.4063	51.87	0.00034	VAVEEVDEEGKFVR
P02545|LMNA_HUMAN	622.3641	56.69	0.00024	LKDLEALLNSK
P02545|LMNA_HUMAN	594.3209	54.36	0.00024	LRDLEDSLAR
P02545|LMNA_HUMAN	594.321	54.27	0.00024	LRDLEDSLAR
P02545|LMNA_H	622.3	56.91	0.00021	LKDLEALLNSK

UMAN	639			
P02545|LMNA_HUMAN	622.3635	59.59	0.00011	LKDLEALLNSK
P02545|LMNA_HUMAN	594.3206	58.22	9.80E-05	LRDLEDSLAR
P02545|LMNA_HUMAN	803.4061	57.27	9.40E-05	VAVEEVDEEGKFVR
P02545|LMNA_HUMAN	783.8805	54.04	8.60E-05	SVGGSGGGSFGDNLVTR
P02545|LMNA_HUMAN	622.3642	61.89	7.10E-05	LKDLEALLNSK
P02545|LMNA_HUMAN	947.4647	66.04	1.10E-05	MQQQLDEYQELLDIK
P02545|LMNA_HUMAN	876.9324	66.68	7.90E-06	NSNLVGAAHEELQQSR
P02545|LMNA_HUMAN	876.9337	69.54	3.80E-06	NSNLVGAAHEELQQSR
P02545|LMNA_HUMAN	876.9351	71.45	2.80E-06	NSNLVGAAHEELQQSR
P02545|LMNA_HUMAN	947.4636	73.26	1.80E-06	MQQQLDEYQELLDIK
P02545|LMNA_HUMAN	947.4682	74.83	1.60E-06	MQQQLDEYQELLDIK
P02545|LMNA_HUMAN	947.4638	74.52	1.40E-06	MQQQLDEYQELLDIK
P02545|LMNA_HUMAN	876.9328	74.41	1.40E-06	NSNLVGAAHEELQQSR
P02545|LMNA_HUMAN	876.9338	75.48	9.90E-07	NSNLVGAAHEELQQSR
P02545|LMNA_HUMAN	947.4669	77.34	8.60E-07	MQQQLDEYQELLDIK
P02545|LMNA_HUMAN	947.4623	77.03	7.70E-07	MQQQLDEYQELLDIK
P02545|LMNA_HUMAN	947.4659	79.14	5.40E-07	MQQQLDEYQELLDIK
P02545|LMNA_HUMAN	876.9341	81.57	2.60E-07	NSNLVGAAHEELQQSR
P02545|LMNA_HUMAN	876.9319	82.22	2.20E-07	NSNLVGAAHEELQQSR
P02545|LMNA_HUMAN	876.9335	82.79	2.00E-07	NSNLVGAAHEELQQSR
P02545|LMNA_HUMAN	947.4653	83.71	1.90E-07	MQQQLDEYQELLDIK
P02545|LMNA_HUMAN	876.9323	82.78	1.90E-07	NSNLVGAAHEELQQSR
P02545|LMNA_HUMAN	947.4626	84.76	1.30E-07	MQQQLDEYQELLDIK
P02545|LMNA_HUMAN	947.4647	85.56	1.20E-07	MQQQLDEYQELLDIK
P02545|LMNA_HUMAN	947.4633	85.2	1.20E-07	MQQQLDEYQELLDIK
P02545|LMNA_HUMAN	876.9317	85.12	1.00E-07	NSNLVGAAHEELQQSR
P02545|LMNA_HUMAN	876.9318	87.37	6.60E-08	NSNLVGAAHEELQQSR

P02545|LMNA_HUMAN	876.9335	93.72	1.60E-08	NSNLVGAAHEELQQSR
P02545|LMNA_HUMAN	947.4642	102.83	2.30E-09	MQQQLDEYQELLDIK
P02545|LMNA_HUMAN	876.9343	104.21	1.40E-09	NSNLVGAAHEELQQSR
P02768|ALBU_HUMAN	464.2487	38.44	0.0032	YLYEIAR
P02768|ALBU_HUMAN	464.2487	38.63	0.0031	YLYEIAR
P02768|ALBU_HUMAN	464.2493	40.1	0.0022	YLYEIAR
P02768|ALBU_HUMAN	464.249	40.07	0.0022	YLYEIAR
P02768|ALBU_HUMAN	464.2486	40.46	0.002	YLYEIAR
P02768|ALBU_HUMAN	464.2487	42.28	0.0013	YLYEIAR
P02768|ALBU_HUMAN	464.2488	42.24	0.0013	YLYEIAR
P02768|ALBU_HUMAN	571.8588	48.55	0.0011	KQTALVELVK
P02768|ALBU_HUMAN	464.2486	43.23	0.0011	YLYEIAR
P02768|ALBU_HUMAN	571.8584	49.79	0.00089	KQTALVELVK
P02768|ALBU_HUMAN	571.8587	50.24	0.00078	KQTALVELVK
P02768|ALBU_HUMAN	756.4235	50.51	0.00065	VPQVSTPTLVEVSR
P02768|ALBU_HUMAN	571.8585	51.5	0.0006	KQTALVELVK
P02768|ALBU_HUMAN	571.8584	51.46	0.0006	KQTALVELVK
P02768|ALBU_HUMAN	571.8589	51.2	0.00058	KQTALVELVK
P02768|ALBU_HUMAN	756.423	51.33	0.00051	VPQVSTPTLVEVSR
P02768|ALBU_HUMAN	756.423	51.98	0.00044	VPQVSTPTLVEVSR
P02768|ALBU_HUMAN	571.858	54.8	0.00028	KQTALVELVK
P02768|ALBU_HUMAN	820.47	58.83	0.00011	KVPQVSTPTLVEVSR
P02768|ALBU_HUMAN	756.4238	58.98	9.40E-05	VPQVSTPTLVEVSR
P02768|ALBU_HUMAN	820.4711	62.28	4.50E-05	KVPQVSTPTLVEVSR
P02768|ALBU_HUMAN	571.8593	63.45	3.50E-05	KQTALVELVK
P02768|ALBU_HUMAN	820.4691	67.67	1.60E-05	KVPQVSTPTLVEVSR
P02768|ALBU_HUMAN	756.4225	67.61	1.20E-05	VPQVSTPTLVEVSR
P02768|ALBU_HU	756.4	71.13	5.00E-06	VPQVSTPTLVEVSR

MAN	244			
P02768|ALBU_HUMAN	820.4698	73.35	3.80E-06	KVPQVSTPTLVEVSR
P02768|ALBU_HUMAN	820.4705	73.76	3.70E-06	KVPQVSTPTLVEVSR
P02768|ALBU_HUMAN	820.4702	76.5	1.80E-06	KVPQVSTPTLVEVSR
P02768|ALBU_HUMAN	820.4702	79.91	8.20E-07	KVPQVSTPTLVEVSR
P02768|ALBU_HUMAN	820.4699	80.15	7.90E-07	KVPQVSTPTLVEVSR
P02768|ALBU_HUMAN	756.4229	82.23	4.10E-07	VPQVSTPTLVEVSR
P02768|ALBU_HUMAN	820.4696	87.95	1.50E-07	KVPQVSTPTLVEVSR
P02768|ALBU_HUMAN	820.4705	90.59	7.70E-08	KVPQVSTPTLVEVSR
P02768|ALBU_HUMAN	820.4706	93.44	4.00E-08	KVPQVSTPTLVEVSR
P02768|ALBU_HUMAN	820.4698	93.24	3.90E-08	KVPQVSTPTLVEVSR
P02768|ALBU_HUMAN	820.47	93.27	3.80E-08	KVPQVSTPTLVEVSR
P02768|ALBU_HUMAN	820.4699	93.55	3.60E-08	KVPQVSTPTLVEVSR
P02768|ALBU_HUMAN	820.4708	97.8	1.50E-08	KVPQVSTPTLVEVSR
P02768|ALBU_HUMAN	820.4704	98	1.30E-08	KVPQVSTPTLVEVSR
P04083|ANXA1_HUMAN	851.9457	53.45	0.00036	GLGTDEDTLIEILASR
P04083|ANXA1_HUMAN	775.9111	57.16	0.00013	GTDVNVFNTILTTR
P04083|ANXA1_HUMAN	631.8044	54.1	6.70E-05	TPAQFDADELR
P04083|ANXA1_HUMAN	775.9113	70.85	5.40E-06	GTDVNVFNTILTTR
P04264|K2C1_HUMAN	697.3667	41.95	0.0035	TNAENEFVTIKK
P04264|K2C1_HUMAN	533.2625	37.08	0.0033	AQYEDIAQK
P04264|K2C1_HUMAN	533.2624	38.28	0.0025	AQYEDIAQK
P04264|K2C1_HUMAN	697.3693	44.04	0.0022	TNAENEFVTIKK
P04264|K2C1_HUMAN	537.2994	46.94	0.002	LRSEIDNVK
P04264|K2C1_HUMAN	697.3684	44.65	0.0018	TNAENEFVTIKK
P04264|K2C1_HUMAN	800.4167	45.54	0.0017	NKLNDLEDALQQAK
P04264|K2C1_HUMAN	563.2734	39.07	0.0017	AEAESLYQSK
P04264|K2C1_HUMAN	800.4173	46.17	0.0016	NKLNDLEDALQQAK

P04264|K2C1_HUMAN	697.3688	46.03	0.0014	TNAENEFVTIKK
P04264|K2C1_HUMAN	876.4151	42.76	0.0013	GSGGGSSGGSIGGRGSSSGGVK
P04264|K2C1_HUMAN	834.4209	48.4	0.0012	SKAEAESLYQSKYEELQITAGR
P04264|K2C1_HUMAN	633.3207	46.75	0.00063	TNAENEFVTIK
P04264|K2C1_HUMAN	1104.772	32.14	0.00061	GSYGSGGSSYGSGGGSYGSGGGGGGHGSYGSGSSSGGYR
P04264|K2C1_HUMAN	633.3207	47.15	0.00056	TNAENEFVTIK
P04264|K2C1_HUMAN	533.2628	44.77	0.00056	AQYEDIAQK
P04264|K2C1_HUMAN	533.2636	45.53	0.00052	AQYEDIAQK
P04264|K2C1_HUMAN	971.4996	51.56	0.00047	LNDLEDALQQAKEDLAR
P04264|K2C1_HUMAN	829.3976	45.97	0.00044	SGGGFSSGSAGIINYQR
P04264|K2C1_HUMAN	533.2622	45.83	0.00044	AQYEDIAQK
P04264|K2C1_HUMAN	546.7527	43.02	0.0004	GSGGGSSGGSIGGR
P04264|K2C1_HUMAN	800.418	52.68	0.00031	NKLNDLEDALQQAK
P04264|K2C1_HUMAN	533.2623	47.47	0.0003	AQYEDIAQK
P04264|K2C1_HUMAN	670.8365	49.14	0.00029	SKAEAESLYQSK
P04264|K2C1_HUMAN	633.3209	51.23	0.00024	TNAENEFVTIK
P04264|K2C1_HUMAN	697.3671	54.1	0.00022	TNAENEFVTIKK
P04264|K2C1_HUMAN	633.3207	51.24	0.00022	TNAENEFVTIK
P04264|K2C1_HUMAN	563.2741	48.38	0.00022	AEAESLYQSK
P04264|K2C1_HUMAN	800.4167	55.08	0.00019	NKLNDLEDALQQAK
P04264|K2C1_HUMAN	533.2642	50.4	0.00018	AQYEDIAQK
P04264|K2C1_HUMAN	738.3771	55.15	0.00016	WELLQQVDTSTR
P04264|K2C1_HUMAN	563.2729	49.59	0.00015	AEAESLYQSK
P04264|K2C1_HUMAN	738.3767	55.86	0.00014	WELLQQVDTSTR
P04264|K2C1_HUMAN	670.8365	52.41	0.00014	SKAEAESLYQSK
P04264|K2C1_HUMAN	533.2627	51.49	0.00012	AQYEDIAQK
P04264|K2C1_HUMAN	834.4206	58.46	0.00011	SKAEAESLYQSKYEELQITAGR
P04264|K2C1_HU	692.3	53.26	0.00011	SLNNQFASFIDK

MAN	469			
P04264|K2C1_HUMAN	546.7538	49.34	0.00011	GSGGGSSGGSIGGR
P04264|K2C1_HUMAN	800.4216	57.56	9.70E-05	NKLNDLEDALQQAK
P04264|K2C1_HUMAN	670.8365	54.27	9.00E-05	SKAEAESLYQSK
P04264|K2C1_HUMAN	697.3672	58.11	8.80E-05	TNAENEFVTIKK
P04264|K2C1_HUMAN	738.3763	58.13	8.10E-05	WELLQQVDTSTR
P04264|K2C1_HUMAN	651.8591	60.79	7.90E-05	SLDLDSIIAEVK
P04264|K2C1_HUMAN	1192.476	41.89	6.50E-05	GGGGGGYGSGGSSYGSGGGSYGSGGGGGGGR
P04264|K2C1_HUMAN	738.3757	58.44	6.40E-05	WELLQQVDTSTR
P04264|K2C1_HUMAN	670.836	56.11	6.20E-05	SKAEAESLYQSK
P04264|K2C1_HUMAN	563.2727	53.91	5.80E-05	AEAESLYQSK
P04264|K2C1_HUMAN	670.8363	56.45	5.70E-05	SKAEAESLYQSK
P04264|K2C1_HUMAN	633.3212	57.71	5.60E-05	TNAENEFVTIK
P04264|K2C1_HUMAN	633.3209	57.53	5.50E-05	TNAENEFVTIK
P04264|K2C1_HUMAN	651.8603	62.51	5.30E-05	SLDLDSIIAEVK
P04264|K2C1_HUMAN	670.8373	57.13	5.20E-05	SKAEAESLYQSK
P04264|K2C1_HUMAN	563.2726	54.51	5.00E-05	AEAESLYQSK
P04264|K2C1_HUMAN	563.2729	54.76	4.70E-05	AEAESLYQSK
P04264|K2C1_HUMAN	738.3759	60.13	4.30E-05	WELLQQVDTSTR
P04264|K2C1_HUMAN	563.2747	54.91	4.30E-05	AEAESLYQSK
P04264|K2C1_HUMAN	697.367	61.88	3.70E-05	TNAENEFVTIKK
P04264|K2C1_HUMAN	800.4168	62.27	3.60E-05	NKLNDLEDALQQAK
P04264|K2C1_HUMAN	738.3773	61.8	3.50E-05	WELLQQVDTSTR
P04264|K2C1_HUMAN	670.8362	58.8	3.30E-05	SKAEAESLYQSK
P04264|K2C1_HUMAN	651.8589	65.28	2.80E-05	SLDLDSIIAEVK
P04264|K2C1_HUMAN	692.3466	60.11	2.70E-05	SLNNQFASFIDK
P04264|K2C1_HUMAN	679.3504	61.52	2.50E-05	LNDLEDALQQAK
P04264|K2C1_HUMAN	670.837	60.15	2.30E-05	SKAEAESLYQSK

P04264|K2C1_HUMAN	692.3459	60.93	2.20E-05	SLNNQFASFIDK
P04264|K2C1_HUMAN	670.837	60.4	2.20E-05	SKAEAESLYQSK
P04264|K2C1_HUMAN	829.3989	59.38	2.20E-05	SGGGFSSGSAGIINYQR
P04264|K2C1_HUMAN	829.3969	59.05	2.20E-05	SGGGFSSGSAGIINYQR
P04264|K2C1_HUMAN	800.4173	65.14	2.10E-05	NKLNDLEDALQQAK
P04264|K2C1_HUMAN	697.3669	64.44	2.00E-05	TNAENEFVTIKK
P04264|K2C1_HUMAN	670.8359	61.16	2.00E-05	SKAEAESLYQSK
P04264|K2C1_HUMAN	738.3762	64.38	1.90E-05	WELLQQVDTSTR
P04264|K2C1_HUMAN	800.418	65.36	1.70E-05	NKLNDLEDALQQAK
P04264|K2C1_HUMAN	651.8602	66.65	1.60E-05	SLDLDSIIAEVK
P04264|K2C1_HUMAN	697.3677	64.99	1.60E-05	TNAENEFVTIKK
P04264|K2C1_HUMAN	738.376	64.43	1.60E-05	WELLQQVDTSTR
P04264|K2C1_HUMAN	670.8364	62.65	1.40E-05	SKAEAESLYQSK
P04264|K2C1_HUMAN	697.3678	66.25	1.20E-05	TNAENEFVTIKK
P04264|K2C1_HUMAN	679.349	65.77	1.10E-05	LNDLEDALQQAK
P04264|K2C1_HUMAN	692.3455	64.27	1.00E-05	SLNNQFASFIDK
P04264|K2C1_HUMAN	692.3469	63.91	9.90E-06	SLNNQFASFIDK
P04264|K2C1_HUMAN	692.3466	64.72	9.20E-06	SLNNQFASFIDK
P04264|K2C1_HUMAN	692.3463	64.71	9.20E-06	SLNNQFASFIDK
P04264|K2C1_HUMAN	738.3757	67.01	8.90E-06	WELLQQVDTSTR
P04264|K2C1_HUMAN	692.3462	65.42	7.90E-06	SLNNQFASFIDK
P04264|K2C1_HUMAN	692.3469	65.11	7.50E-06	SLNNQFASFIDK
P04264|K2C1_HUMAN	800.4183	69.38	6.60E-06	NKLNDLEDALQQAK
P04264|K2C1_HUMAN	738.3759	68.36	6.50E-06	WELLQQVDTSTR
P04264|K2C1_HUMAN	697.3674	69.61	6.30E-06	TNAENEFVTIKK
P04264|K2C1_HUMAN	563.2735	63.82	5.80E-06	AEAESLYQSK
P04264|K2C1_HUMAN	738.3763	70.08	5.20E-06	WELLQQVDTSTR
P04264|K2C1_HUMAN	738.3	70.15	5.10E-06	WELLQQVDTSTR

MAN	763			
P04264|K2C1_HUMAN	829.3985	66.68	4.50E-06	SGGGFSSGSAGIINYQR
P04264|K2C1_HUMAN	738.3754	70.09	4.40E-06	WELLQQVDTSTR
P04264|K2C1_HUMAN	829.4012	66.87	4.30E-06	SGGGFSSGSAGIINYQR
P04264|K2C1_HUMAN	670.8361	68.02	4.00E-06	SKAEAESLYQSK
P04264|K2C1_HUMAN	692.3467	67.98	3.90E-06	SLNNQFASFIDK
P04264|K2C1_HUMAN	692.3464	68.67	3.70E-06	SLNNQFASFIDK
P04264|K2C1_HUMAN	679.3486	70.19	3.60E-06	LNDLEDALQQAK
P04264|K2C1_HUMAN	650.7664	54.38	3.60E-06	NMQDMVEDYR
P04264|K2C1_HUMAN	692.3472	68.85	3.50E-06	SLNNQFASFIDK
P04264|K2C1_HUMAN	692.3462	69.1	3.40E-06	SLNNQFASFIDK
P04264|K2C1_HUMAN	692.3469	68.85	3.20E-06	SLNNQFASFIDK
P04264|K2C1_HUMAN	651.8606	75.35	2.80E-06	SLDLDSIIAEVK
P04264|K2C1_HUMAN	697.3668	72.82	2.80E-06	TNAENEFVTIKK
P04264|K2C1_HUMAN	650.7693	57.08	2.80E-06	NMQDMVEDYR
P04264|K2C1_HUMAN	651.8597	74.87	2.60E-06	SLDLDSIIAEVK
P04264|K2C1_HUMAN	650.7679	57.31	2.40E-06	NMQDMVEDYR
P04264|K2C1_HUMAN	697.3676	73.61	2.20E-06	TNAENEFVTIKK
P04264|K2C1_HUMAN	829.3986	70.3	1.90E-06	SGGGFSSGSAGIINYQR
P04264|K2C1_HUMAN	829.3981	70.7	1.80E-06	SGGGFSSGSAGIINYQR
P04264|K2C1_HUMAN	829.3985	70.62	1.80E-06	SGGGFSSGSAGIINYQR
P04264|K2C1_HUMAN	651.8586	77.37	1.70E-06	SLDLDSIIAEVK
P04264|K2C1_HUMAN	679.3498	73.32	1.70E-06	LNDLEDALQQAK
P04264|K2C1_HUMAN	738.3757	74.65	1.50E-06	WELLQQVDTSTR
P04264|K2C1_HUMAN	670.8363	72.57	1.40E-06	SKAEAESLYQSK
P04264|K2C1_HUMAN	651.8602	78.11	1.20E-06	SLDLDSIIAEVK
P04264|K2C1_HUMAN	692.3468	73.48	1.10E-06	SLNNQFASFIDK
P04264|K2C1_HUMAN	670.84	74.27	1.00E-06	SKAEAESLYQSK

P04264|K2C1_HUMAN	651.859	79.85	9.80E-07	SLDLDSIIAEVK
P04264|K2C1_HUMAN	738.3754	76.65	9.60E-07	WELLQQVDTSTR
P04264|K2C1_HUMAN	679.349	76.54	9.00E-07	LNDLEDALQQAK
P04264|K2C1_HUMAN	738.3751	77.09	8.80E-07	WELLQQVDTSTR
P04264|K2C1_HUMAN	679.3487	76.71	8.00E-07	LNDLEDALQQAK
P04264|K2C1_HUMAN	651.8591	81.01	7.60E-07	SLDLDSIIAEVK
P04264|K2C1_HUMAN	651.8594	81.14	7.40E-07	SLDLDSIIAEVK
P04264|K2C1_HUMAN	563.273	72.92	7.20E-07	AEAESLYQSK
P04264|K2C1_HUMAN	670.8367	75.09	6.60E-07	SKAEAESLYQSK
P04264|K2C1_HUMAN	650.7669	62.26	6.20E-07	NMQDMVEDYR
P04264|K2C1_HUMAN	651.8601	81.2	5.80E-07	SLDLDSIIAEVK
P04264|K2C1_HUMAN	650.767	62.64	5.70E-07	NMQDMVEDYR
P04264|K2C1_HUMAN	829.3992	75.33	5.30E-07	SGGGFSSGSAGIINYQR
P04264|K2C1_HUMAN	679.3491	79.83	4.20E-07	LNDLEDALQQAK
P04264|K2C1_HUMAN	692.3463	78.3	4.10E-07	SLNNQFASFIDK
P04264|K2C1_HUMAN	692.347	78.41	4.00E-07	SLNNQFASFIDK
P04264|K2C1_HUMAN	1192.477	64.02	4.00E-07	GGGGGGYGSGGSSYGSGGGSYGSGGGGGGGR
P04264|K2C1_HUMAN	679.3492	80.21	3.90E-07	LNDLEDALQQAK
P04264|K2C1_HUMAN	651.8592	83.99	3.80E-07	SLDLDSIIAEVK
P04264|K2C1_HUMAN	858.9272	80.82	3.80E-07	QISNLQQSISDAEQR
P04264|K2C1_HUMAN	651.8589	84.15	3.70E-07	SLDLDSIIAEVK
P04264|K2C1_HUMAN	692.3467	78.4	3.50E-07	SLNNQFASFIDK
P04264|K2C1_HUMAN	858.9272	81.22	3.40E-07	QISNLQQSISDAEQR
P04264|K2C1_HUMAN	546.7534	73.82	3.40E-07	GSGGGSSGGSIGGR
P04264|K2C1_HUMAN	546.7532	74.01	3.30E-07	GSGGGSSGGSIGGR
P04264|K2C1_HUMAN	858.9266	80.98	3.20E-07	QISNLQQSISDAEQR
P04264|K2C1_HUMAN	546.7529	74.6	2.80E-07	GSGGGSSGGSIGGR
P04264|K2C1_HU	679.3	81.7	2.60E-07	LNDLEDALQQAK

MAN	496			
P04264|K2C1_HUMAN	858.9276	85.43	1.40E-07	QISNLQQSISDAEQR
P04264|K2C1_HUMAN	633.3203	84.68	1.10E-07	TNAENEFVTIK
P04264|K2C1_HUMAN	858.9278	88.1	7.70E-08	QISNLQQSISDAEQR
P04264|K2C1_HUMAN	858.9277	89.97	5.00E-08	QISNLQQSISDAEQR
P04264|K2C1_HUMAN	679.3503	89.89	3.70E-08	LNDLEDALQQAK
P04264|K2C1_HUMAN	651.8594	95.93	2.40E-08	SLDLDSIIAEVK
P04264|K2C1_HUMAN	1192.475	76.36	2.30E-08	GGGGGGYGSGGSSYGSGGGSYGSGGGGGGGR
P04264|K2C1_HUMAN	1192.477	77.77	1.70E-08	GGGGGGYGSGGSSYGSGGGSYGSGGGGGGGR
P04264|K2C1_HUMAN	858.9264	95.14	1.30E-08	QISNLQQSISDAEQR
P04264|K2C1_HUMAN	858.9274	98.5	6.90E-09	QISNLQQSISDAEQR
P04264|K2C1_HUMAN	1192.477	85.34	2.90E-09	GGGGGGYGSGGSSYGSGGGSYGSGGGGGGGR
P04264|K2C1_HUMAN	546.7531	94.89	2.70E-09	GSGGGSSGGSIGGR
P04264|K2C1_HUMAN	858.9274	104.06	1.90E-09	QISNLQQSISDAEQR
P04264|K2C1_HUMAN	858.9271	104.14	1.80E-09	QISNLQQSISDAEQR
P04264|K2C1_HUMAN	1192.478	88.1	1.50E-09	GGGGGGYGSGGSSYGSGGGSYGSGGGGGGGR
P04264|K2C1_HUMAN	858.9274	107.1	9.60E-10	QISNLQQSISDAEQR
P04264|K2C1_HUMAN	1192.477	95.08	3.10E-10	GGGGGGYGSGGSSYGSGGGSYGSGGGGGGGR
P04264|K2C1_HUMAN	858.9274	113.44	2.20E-10	QISNLQQSISDAEQR
P04264|K2C1_HUMAN	1192.478	99.37	1.20E-10	GGGGGGYGSGGSSYGSGGGSYGSGGGGGGGR
P04264|K2C1_HUMAN	1192.476	101.27	7.50E-11	GGGGGGYGSGGSSYGSGGGSYGSGGGGGGGR
P04264|K2C1_HUMAN	1192.477	105.36	2.90E-11	GGGGGGYGSGGSSYGSGGGSYGSGGGGGGGR
P04264|K2C1_HUMAN	1192.476	105.58	2.80E-11	GGGGGGYGSGGSSYGSGGGSYGSGGGGGGGR
P04264|K2C1_HUMAN	1192.476	106.72	2.10E-11	GGGGGGYGSGGSSYGSGGGSYGSGGGGGGGR
P04264|K2C1_HUMAN	1192.485	119.13	1.20E-12	GGGGGGYGSGGSSYGSGGGSYGSGGGGGGGR
P05386|RLA1_HUMAN	851.9482	46.91	0.0016	AAGVNVEPFWPGLFAK
P05386|RLA1_HUMAN	851.9485	51.06	0.00065	AAGVNVEPFWPGLFAK
P05386|RLA1_HUMAN	851.9483	50.92	0.00064	AAGVNVEPFWPGLFAK

P05386|RLA1_HUMAN	851.9498	50.85	0.00063	AAGVNVEPFWPGLFAK
P05386|RLA1_HUMAN	851.9479	52.23	0.00047	AAGVNVEPFWPGLFAK
P05386|RLA1_HUMAN	851.9544	54.1	0.00034	AAGVNVEPFWPGLFAK
P05386|RLA1_HUMAN	851.949	54.14	0.00033	AAGVNVEPFWPGLFAK
P05386|RLA1_HUMAN	851.9479	54	0.00031	AAGVNVEPFWPGLFAK
P05386|RLA1_HUMAN	851.9528	58.67	0.00012	AAGVNVEPFWPGLFAK
P05386|RLA1_HUMAN	851.9484	58.71	0.00011	AAGVNVEPFWPGLFAK
P05387|RLA2_HUMAN	886.9525	41.12	0.0043	ILDSVGIEADDDRLNK
P05387|RLA2_HUMAN	1387.716	44.65	0.0036	LASVPAGGAVAVSAAPGSAAPAAGSAPAAAEEK
P05387|RLA2_HUMAN	886.9529	49.08	0.00071	ILDSVGIEADDDRLNK
P05387|RLA2_HUMAN	886.9532	52.29	0.00035	ILDSVGIEADDDRLNK
P05387|RLA2_HUMAN	1387.714	57.14	0.0002	LASVPAGGAVAVSAAPGSAAPAAGSAPAAAEEK
P05387|RLA2_HUMAN	1387.713	64.51	3.70E-05	LASVPAGGAVAVSAAPGSAAPAAGSAPAAAEEK
P05387|RLA2_HUMAN	1387.717	65.07	3.40E-05	LASVPAGGAVAVSAAPGSAAPAAGSAPAAAEEK
P05387|RLA2_HUMAN	1387.715	66.86	2.20E-05	LASVPAGGAVAVSAAPGSAAPAAGSAPAAAEEK
P05387|RLA2_HUMAN	1387.717	68.04	1.70E-05	LASVPAGGAVAVSAAPGSAAPAAGSAPAAAEEK
P05387|RLA2_HUMAN	1387.713	70.63	9.20E-06	LASVPAGGAVAVSAAPGSAAPAAGSAPAAAEEK
P05387|RLA2_HUMAN	1387.718	70.67	8.80E-06	LASVPAGGAVAVSAAPGSAAPAAGSAPAAAEEK
P05388|RLA0_HUMAN	1376.732	78.59	1.50E-06	AFLADPSAFVAAAPVAAATTAAPAAAAAPAK
P05388|RLA0_HUMAN	1376.734	80.61	1.00E-06	AFLADPSAFVAAAPVAAATTAAPAAAAAPAK
P05388|RLA0_HUMAN	1376.737	88	1.70E-07	AFLADPSAFVAAAPVAAATTAAPAAAAAPAK
P05388|RLA0_HUMAN	1376.735	88.84	1.40E-07	AFLADPSAFVAAAPVAAATTAAPAAAAAPAK
P05388|RLA0_HUMAN	1376.734	96.47	2.50E-08	AFLADPSAFVAAAPVAAATTAAPAAAAAPAK
P05388|RLA0_HUMAN	1376.738	98.48	1.60E-08	AFLADPSAFVAAAPVAAATTAAPAAAAAPAK
P05388|RLA0_HUMAN	1376.733	110.26	1.10E-09	AFLADPSAFVAAAPVAAATTAAPAAAAAPAK
P05787|K2C8_HUMAN	710.3768	41.84	0.0045	LEGLTDEINFLR
P05787|K2C8_HUMAN	710.381	45.63	0.002	LEGLTDEINFLR
P05787|K2C8_HU	710.3	53.8	0.00027	LEGLTDEINFLR

MAN	763			
P05787|K2C8_HUMAN	710.3759	69.9	7.10E-06	LEGLTDEINFLR
P06748|NPM_HUMAN	784.8672	34.23	0.0048	VDNDENEHQLSLR
P06748|NPM_HUMAN	715.6743	38.58	0.0034	DELHIVEAEAMNYEGSPIK
P06748|NPM_HUMAN	466.2389	41.94	0.0023	GPSSVEDIK
P06748|NPM_HUMAN	512.2475	38.15	0.002	ADKDYHFK
P06748|NPM_HUMAN	910.425	43.35	0.0019	MTDQEAIQDLWQWR
P06748|NPM_HUMAN	523.58	39.29	0.0014	VDNDENEHQLSLR
P06748|NPM_HUMAN	1114.109	49.02	0.0013	MSVQPTVSLGGFEITPPVVLR
P06748|NPM_HUMAN	523.58	39.61	0.0013	VDNDENEHQLSLR
P06748|NPM_HUMAN	910.4233	45.74	0.0011	MTDQEAIQDLWQWR
P06748|NPM_HUMAN	512.2469	39.88	0.0011	ADKDYHFK
P06748|NPM_HUMAN	512.2471	39.51	0.001	ADKDYHFK
P06748|NPM_HUMAN	466.2388	45.6	0.00099	GPSSVEDIK
P06748|NPM_HUMAN	512.2473	39.63	0.00098	ADKDYHFK
P06748|NPM_HUMAN	466.2381	45.31	0.00094	GPSSVEDIK
P06748|NPM_HUMAN	466.2383	45.36	0.00093	GPSSVEDIK
P06748|NPM_HUMAN	512.2474	39.82	0.00093	ADKDYHFK
P06748|NPM_HUMAN	512.2477	41.36	0.00092	ADKDYHFK
P06748|NPM_HUMAN	466.2386	46.56	0.00079	GPSSVEDIK
P06748|NPM_HUMAN	512.2468	41.37	0.00077	ADKDYHFK
P06748|NPM_HUMAN	1114.108	51.61	0.00075	MSVQPTVSLGGFEITPPVVLR
P06748|NPM_HUMAN	784.869	42.8	0.00074	VDNDENEHQLSLR
P06748|NPM_HUMAN	910.4234	47.57	0.00068	MTDQEAIQDLWQWR
P06748|NPM_HUMAN	910.4266	46.12	0.00067	MTDQEAIQDLWQWR
P06748|NPM_HUMAN	512.247	41.44	0.00066	ADKDYHFK
P06748|NPM_HUMAN	977.1558	51.73	0.00058	TVSLGAGAKDELHIVEAEAMNYEGSPIK
P06748|NPM_HUMAN	1114.109	52.73	0.00055	MSVQPTVSLGGFEITPPVVLR

P06748|NPM_HUMAN	466.2385	47.81	0.00054	GPSSVEDIK
P06748|NPM_HUMAN	1114.107	52.84	0.00052	MSVQPTVSLGGFEITPPVVLR
P06748|NPM_HUMAN	466.2382	48.01	0.00051	GPSSVEDIK
P06748|NPM_HUMAN	1114.113	53.85	0.00044	MSVQPTVSLGGFEITPPVVLR
P06748|NPM_HUMAN	1465.231	52.98	0.00044	TVSLGAGAKDELHIVEAEAMNYEGSPIK
P06748|NPM_HUMAN	910.4232	49.58	0.00044	MTDQEAIQDLWQWR
P06748|NPM_HUMAN	910.4225	49.95	0.0004	MTDQEAIQDLWQWR
P06748|NPM_HUMAN	910.4235	50.24	0.00037	MTDQEAIQDLWQWR
P06748|NPM_HUMAN	715.6748	48.25	0.00037	DELHIVEAEAMNYEGSPIK
P06748|NPM_HUMAN	466.2387	50.25	0.00034	GPSSVEDIK
P06748|NPM_HUMAN	1114.113	55.53	0.00029	MSVQPTVSLGGFEITPPVVLR
P06748|NPM_HUMAN	1114.109	55.45	0.00029	MSVQPTVSLGGFEITPPVVLR
P06748|NPM_HUMAN	715.675	50.54	0.00023	DELHIVEAEAMNYEGSPIK
P06748|NPM_HUMAN	466.2389	52.17	0.00022	GPSSVEDIK
P06748|NPM_HUMAN	715.6746	50.59	0.00022	DELHIVEAEAMNYEGSPIK
P06748|NPM_HUMAN	910.4217	51.07	0.0002	MTDQEAIQDLWQWR
P06748|NPM_HUMAN	715.6749	51.76	0.00017	DELHIVEAEAMNYEGSPIK
P06748|NPM_HUMAN	715.6765	52.79	0.00016	DELHIVEAEAMNYEGSPIK
P06748|NPM_HUMAN	1114.113	58.85	0.00014	MSVQPTVSLGGFEITPPVVLR
P06748|NPM_HUMAN	715.6746	54.77	8.50E-05	DELHIVEAEAMNYEGSPIK
P06748|NPM_HUMAN	1465.228	60.38	7.60E-05	TVSLGAGAKDELHIVEAEAMNYEGSPIK
P06748|NPM_HUMAN	784.8671	52.8	6.60E-05	VDNDENEHQLSLR
P06748|NPM_HUMAN	910.4229	57.93	6.40E-05	MTDQEAIQDLWQWR
P06748|NPM_HUMAN	1465.231	61.66	5.80E-05	TVSLGAGAKDELHIVEAEAMNYEGSPIK
P06748|NPM_HUMAN	910.4238	58.89	5.20E-05	MTDQEAIQDLWQWR
P06748|NPM_HUMAN	1114.108	63.51	4.80E-05	MSVQPTVSLGGFEITPPVVLR
P06748|NPM_HUMAN	1287.104	57.82	4.00E-05	ADKDYHFKVDNDENEHQLSLR
P06748|NPM_HU	910.4	60.61	3.50E-05	MTDQEAIQDLWQWR

MAN	228			
P06748|NPM_HUMAN	858.4042	58.2	3.50E-05	ADKDYHFKVDNDENEHQLSLR
P06748|NPM_HUMAN	1465.231	64.73	2.90E-05	TVSLGAGAKDELHIVEAEAMNYEGSPIK
P06748|NPM_HUMAN	977.1582	65.14	2.70E-05	TVSLGAGAKDELHIVEAEAMNYEGSPIK
P06748|NPM_HUMAN	910.4227	61.84	2.60E-05	MTDQEAIQDLWQWR
P06748|NPM_HUMAN	910.4227	62.03	2.50E-05	MTDQEAIQDLWQWR
P06748|NPM_HUMAN	858.4035	60.22	2.10E-05	ADKDYHFKVDNDENEHQLSLR
P06748|NPM_HUMAN	1465.227	67.79	1.40E-05	TVSLGAGAKDELHIVEAEAMNYEGSPIK
P06748|NPM_HUMAN	784.8679	59.2	1.30E-05	VDNDENEHQLSLR
P06748|NPM_HUMAN	977.1565	69.91	8.70E-06	TVSLGAGAKDELHIVEAEAMNYEGSPIK
P06748|NPM_HUMAN	784.8674	61.11	8.60E-06	VDNDENEHQLSLR
P06748|NPM_HUMAN	1465.231	70.4	7.90E-06	TVSLGAGAKDELHIVEAEAMNYEGSPIK
P06748|NPM_HUMAN	1114.111	71.26	7.60E-06	MSVQPTVSLGGFEITPPVVLR
P06748|NPM_HUMAN	1465.231	70.63	7.50E-06	TVSLGAGAKDELHIVEAEAMNYEGSPIK
P06748|NPM_HUMAN	858.4036	64.82	7.40E-06	ADKDYHFKVDNDENEHQLSLR
P06748|NPM_HUMAN	1465.231	71.01	6.90E-06	TVSLGAGAKDELHIVEAEAMNYEGSPIK
P06748|NPM_HUMAN	977.1576	74.52	3.20E-06	TVSLGAGAKDELHIVEAEAMNYEGSPIK
P06748|NPM_HUMAN	784.8677	65.74	2.90E-06	VDNDENEHQLSLR
P06748|NPM_HUMAN	1114.109	76.61	2.20E-06	MSVQPTVSLGGFEITPPVVLR
P06748|NPM_HUMAN	1465.228	75.82	2.20E-06	TVSLGAGAKDELHIVEAEAMNYEGSPIK
P06748|NPM_HUMAN	1287.104	72.19	1.50E-06	ADKDYHFKVDNDENEHQLSLR
P06748|NPM_HUMAN	784.8675	69.82	1.20E-06	VDNDENEHQLSLR
P06748|NPM_HUMAN	784.8674	70.31	1.00E-06	VDNDENEHQLSLR
P06748|NPM_HUMAN	858.4031	73.63	9.60E-07	ADKDYHFKVDNDENEHQLSLR
P06748|NPM_HUMAN	1073.01	74.94	9.40E-07	DELHIVEAEAMNYEGSPIK
P06748|NPM_HUMAN	784.8669	71.59	9.30E-07	VDNDENEHQLSLR
P06748|NPM_HUMAN	784.8678	70.67	9.30E-07	VDNDENEHQLSLR
P06748|NPM_HUMAN	1114.111	81.29	7.60E-07	MSVQPTVSLGGFEITPPVVLR

P06748|NPM_HUMAN	1465.227	80.7	6.90E-07	TVSLGAGAKDELHIVEAEAMNYEGSPIK
P06748|NPM_HUMAN	1287.099	75.75	5.50E-07	ADKDYHFKVDNDENEHQLSLR
P06748|NPM_HUMAN	977.1559	82.87	4.40E-07	TVSLGAGAKDELHIVEAEAMNYEGSPIK
P06748|NPM_HUMAN	858.4026	77.79	3.60E-07	ADKDYHFKVDNDENEHQLSLR
P06748|NPM_HUMAN	977.1546	84.24	3.10E-07	TVSLGAGAKDELHIVEAEAMNYEGSPIK
P06748|NPM_HUMAN	1073.01	80.23	2.70E-07	DELHIVEAEAMNYEGSPIK
P06748|NPM_HUMAN	784.8682	76.6	2.40E-07	VDNDENEHQLSLR
P06748|NPM_HUMAN	1073.01	80.94	2.30E-07	DELHIVEAEAMNYEGSPIK
P06748|NPM_HUMAN	858.4042	80.11	2.30E-07	ADKDYHFKVDNDENEHQLSLR
P06748|NPM_HUMAN	1073.011	81.27	2.20E-07	DELHIVEAEAMNYEGSPIK
P06748|NPM_HUMAN	1073.009	81.49	2.00E-07	DELHIVEAEAMNYEGSPIK
P06748|NPM_HUMAN	1114.109	87.72	1.70E-07	MSVQPTVSLGGFEITPPVVLR
P06748|NPM_HUMAN	977.1553	88.07	1.40E-07	TVSLGAGAKDELHIVEAEAMNYEGSPIK
P06748|NPM_HUMAN	977.156	88.49	1.20E-07	TVSLGAGAKDELHIVEAEAMNYEGSPIK
P06748|NPM_HUMAN	1114.109	89.74	1.10E-07	MSVQPTVSLGGFEITPPVVLR
P06748|NPM_HUMAN	977.1542	89.25	9.80E-08	TVSLGAGAKDELHIVEAEAMNYEGSPIK
P06748|NPM_HUMAN	977.1554	90.03	8.50E-08	TVSLGAGAKDELHIVEAEAMNYEGSPIK
P06748|NPM_HUMAN	1073.011	86.62	6.50E-08	DELHIVEAEAMNYEGSPIK
P06748|NPM_HUMAN	977.1552	92.43	4.90E-08	TVSLGAGAKDELHIVEAEAMNYEGSPIK
P06748|NPM_HUMAN	1287.102	86.71	4.90E-08	ADKDYHFKVDNDENEHQLSLR
P06748|NPM_HUMAN	1073.009	87.4	4.60E-08	DELHIVEAEAMNYEGSPIK
P06748|NPM_HUMAN	977.1577	93.14	4.40E-08	TVSLGAGAKDELHIVEAEAMNYEGSPIK
P06748|NPM_HUMAN	1114.11	94.78	3.40E-08	MSVQPTVSLGGFEITPPVVLR
P06748|NPM_HUMAN	977.1547	93.86	3.40E-08	TVSLGAGAKDELHIVEAEAMNYEGSPIK
P06748|NPM_HUMAN	1114.109	95.12	3.10E-08	MSVQPTVSLGGFEITPPVVLR
P06748|NPM_HUMAN	977.155	95.14	2.60E-08	TVSLGAGAKDELHIVEAEAMNYEGSPIK
P06748|NPM_HUMAN	1114.109	100.12	1.00E-08	MSVQPTVSLGGFEITPPVVLR
P06748|NPM_HU	1114.	100.16	9.90E-09	MSVQPTVSLGGFEITPPVVLR

MAN	109			
P06748|NPM_HUMAN	1287.102	94.77	7.50E-09	ADKDYHFKVDNDENEHQLSLR
P06748|NPM_HUMAN	1073.01	96.07	7.20E-09	DELHIVEAEAMNYEGSPIK
P06748|NPM_HUMAN	977.1563	100.9	7.10E-09	TVSLGAGAKDELHIVEAEAMNYEGSPIK
P06748|NPM_HUMAN	1114.109	105.41	3.00E-09	MSVQPTVSLGGFEITPPVVLR
P06748|NPM_HUMAN	1114.109	105.57	2.80E-09	MSVQPTVSLGGFEITPPVVLR
P06748|NPM_HUMAN	1073.01	101.16	2.30E-09	DELHIVEAEAMNYEGSPIK
P06748|NPM_HUMAN	1287.1	107.01	4.20E-10	ADKDYHFKVDNDENEHQLSLR
P06748|NPM_HUMAN	1416.186	179.05	1.20E-18	LAADEDDDDDEEDDDEDDDDDDFDDEEAEEKAPVKK
P06748|NPM_HUMAN	1416.185	181.25	7.50E-19	LAADEDDDDDEEDDDEDDDDDDFDDEEAEEKAPVKK
P06748|NPM_HUMAN	1373.486	199.25	2.60E-20	LAADEDDDDDEEDDDEDDDDDDFDDEEAEEKAPVK
P06748|NPM_HUMAN	1373.486	202.59	1.20E-20	LAADEDDDDDEEDDDEDDDDDDFDDEEAEEKAPVK
P07355|ANXA2_HUMAN	970.4828	40.25	0.0043	TDLEKDIISDTSGDFRK
P07355|ANXA2_HUMAN	647.3234	40.87	0.004	TDLEKDIISDTSGDFRK
P07355|ANXA2_HUMAN	970.4795	40.58	0.0037	TDLEKDIISDTSGDFRK
P07355|ANXA2_HUMAN	922.9525	39.98	0.0037	LSLEGDHSTPPSAYGSVK
P07355|ANXA2_HUMAN	647.3232	41.69	0.0031	TDLEKDIISDTSGDFRK
P07355|ANXA2_HUMAN	647.3228	41.92	0.0029	TDLEKDIISDTSGDFRK
P07355|ANXA2_HUMAN	794.8868	38.83	0.0029	SYSPYDMLESIRK
P07355|ANXA2_HUMAN	794.8859	39.63	0.0026	SYSPYDMLESIRK
P07355|ANXA2_HUMAN	922.9523	41.49	0.0025	LSLEGDHSTPPSAYGSVK
P07355|ANXA2_HUMAN	906.435	41.18	0.002	TDLEKDIISDTSGDFR
P07355|ANXA2_HUMAN	922.9526	42.71	0.0019	LSLEGDHSTPPSAYGSVK
P07355|ANXA2_HUMAN	922.9526	42.66	0.0019	LSLEGDHSTPPSAYGSVK
P07355|ANXA2_HUMAN	922.9525	43.79	0.0015	LSLEGDHSTPPSAYGSVK
P07355|ANXA2_HUMAN	677.3331	41.56	0.0015	DIISDTSGDFRK
P07355|ANXA2_HUMAN	906.4346	42.73	0.0013	TDLEKDIISDTSGDFR
P07355|ANXA2_HUMAN	611.7982	43.96	0.00084	TPAQYDASELK

P07355|ANXA2_HUMAN	647.3226	47.3	0.00083	TDLEKDIISDTSGDFRK
P07355|ANXA2_HUMAN	922.9521	46.33	0.00081	LSLEGDHSTPPSAYGSVK
P07355|ANXA2_HUMAN	922.9525	47.24	0.00069	LSLEGDHSTPPSAYGSVK
P07355|ANXA2_HUMAN	1078.032	48.77	0.00068	AYTNFDAERDALNIETAIK
P07355|ANXA2_HUMAN	1078.033	49.35	0.00067	AYTNFDAERDALNIETAIK
P07355|ANXA2_HUMAN	611.7985	45.76	0.00059	TPAQYDASELK
P07355|ANXA2_HUMAN	611.7994	45.69	0.00053	TPAQYDASELK
P07355|ANXA2_HUMAN	906.4368	47.42	0.00049	TDLEKDIISDTSGDFR
P07355|ANXA2_HUMAN	611.7993	46.2	0.00048	TPAQYDASELK
P07355|ANXA2_HUMAN	922.9515	49.66	0.00038	LSLEGDHSTPPSAYGSVK
P07355|ANXA2_HUMAN	970.486	51.59	0.00034	TDLEKDIISDTSGDFRK
P07355|ANXA2_HUMAN	922.9506	50.05	0.00031	LSLEGDHSTPPSAYGSVK
P07355|ANXA2_HUMAN	906.4389	50.02	0.00031	TDLEKDIISDTSGDFR
P07355|ANXA2_HUMAN	906.4348	49.95	0.00026	TDLEKDIISDTSGDFR
P07355|ANXA2_HUMAN	906.4343	50.31	0.00023	TDLEKDIISDTSGDFR
P07355|ANXA2_HUMAN	730.8381	45.51	0.00022	SYSPYDMLESIR
P07355|ANXA2_HUMAN	922.9534	52.26	0.00021	LSLEGDHSTPPSAYGSVK
P07355|ANXA2_HUMAN	922.9531	52.57	0.0002	LSLEGDHSTPPSAYGSVK
P07355|ANXA2_HUMAN	906.4353	51.13	0.0002	TDLEKDIISDTSGDFR
P07355|ANXA2_HUMAN	906.4339	51.82	0.00017	TDLEKDIISDTSGDFR
P07355|ANXA2_HUMAN	922.9518	55.02	0.00011	LSLEGDHSTPPSAYGSVK
P07355|ANXA2_HUMAN	730.8372	48.48	0.00011	SYSPYDMLESIR
P07355|ANXA2_HUMAN	622.8148	53.7	9.20E-05	TNQELQEINR
P07355|ANXA2_HUMAN	622.814	52.96	9.00E-05	TNQELQEINR
P07355|ANXA2_HUMAN	611.7991	53.88	8.70E-05	TPAQYDASELK
P07355|ANXA2_HUMAN	611.7989	53.86	8.70E-05	TPAQYDASELK
P07355|ANXA2_HUMAN	647.322	57.06	8.20E-05	TDLEKDIISDTSGDFRK
P07355|ANXA2_H	622.8	53.65	7.70E-05	TNQELQEINR

UMAN	134			
P07355|ANXA2_HUMAN	622.8143	56.21	5.70E-05	TNQELQEINR
P07355|ANXA2_HUMAN	611.7993	55.5	5.70E-05	TPAQYDASELK
P07355|ANXA2_HUMAN	771.9252	63	5.10E-05	GVDEVTIVNILTNR
P07355|ANXA2_HUMAN	730.8378	52.46	5.00E-05	SYSPYDMLESIR
P07355|ANXA2_HUMAN	622.8141	57.1	4.60E-05	TNQELQEINR
P07355|ANXA2_HUMAN	622.8122	57.52	4.50E-05	TNQELQEINR
P07355|ANXA2_HUMAN	622.8157	57.81	4.20E-05	TNQELQEINR
P07355|ANXA2_HUMAN	730.8375	53.44	3.50E-05	SYSPYDMLESIR
P07355|ANXA2_HUMAN	622.8137	57.71	3.00E-05	TNQELQEINR
P07355|ANXA2_HUMAN	622.8133	58.82	2.40E-05	TNQELQEINR
P07355|ANXA2_HUMAN	647.3235	63.24	2.30E-05	TDLEKDIISDTSGDFRK
P07355|ANXA2_HUMAN	730.8374	55.55	2.10E-05	SYSPYDMLESIR
P07355|ANXA2_HUMAN	906.4339	61.05	2.00E-05	TDLEKDIISDTSGDFR
P07355|ANXA2_HUMAN	771.9258	67.4	1.80E-05	GVDEVTIVNILTNR
P07355|ANXA2_HUMAN	611.7996	62.16	1.20E-05	TPAQYDASELK
P07355|ANXA2_HUMAN	622.814	61.88	1.20E-05	TNQELQEINR
P07355|ANXA2_HUMAN	1032.993	64.28	1.10E-05	RAEDGSVIDYELIDQDAR
P07355|ANXA2_HUMAN	1032.994	63.87	1.10E-05	RAEDGSVIDYELIDQDAR
P07355|ANXA2_HUMAN	622.8135	62.05	1.10E-05	TNQELQEINR
P07355|ANXA2_HUMAN	1032.993	65.24	8.60E-06	RAEDGSVIDYELIDQDAR
P07355|ANXA2_HUMAN	730.838	60.74	6.50E-06	SYSPYDMLESIR
P07355|ANXA2_HUMAN	1032.996	67.14	6.40E-06	RAEDGSVIDYELIDQDAR
P07355|ANXA2_HUMAN	622.8121	66.63	5.30E-06	TNQELQEINR
P07355|ANXA2_HUMAN	1032.992	68.16	4.10E-06	RAEDGSVIDYELIDQDAR
P07355|ANXA2_HUMAN	730.8376	63.74	3.70E-06	SYSPYDMLESIR
P07355|ANXA2_HUMAN	771.9254	74.77	3.40E-06	GVDEVTIVNILTNR
P07355|ANXA2_HUMAN	1032.994	71.32	2.00E-06	RAEDGSVIDYELIDQDAR

P07355|ANXA2_HUMAN	771.9249	77.61	1.80E-06	GVDEVTIVNILTNR
P07355|ANXA2_HUMAN	771.9263	78.58	1.30E-06	GVDEVTIVNILTNR
P07355|ANXA2_HUMAN	771.926	80.03	1.00E-06	GVDEVTIVNILTNR
P07355|ANXA2_HUMAN	771.9258	80.21	9.70E-07	GVDEVTIVNILTNR
P07355|ANXA2_HUMAN	771.9265	80.15	9.50E-07	GVDEVTIVNILTNR
P07355|ANXA2_HUMAN	1032.995	75.4	8.50E-07	RAEDGSVIDYELIDQDAR
P07355|ANXA2_HUMAN	1032.997	76.5	7.30E-07	RAEDGSVIDYELIDQDAR
P07355|ANXA2_HUMAN	1032.993	77.31	5.50E-07	RAEDGSVIDYELIDQDAR
P07355|ANXA2_HUMAN	1032.992	77.18	5.30E-07	RAEDGSVIDYELIDQDAR
P07355|ANXA2_HUMAN	1032.994	84.7	9.40E-08	RAEDGSVIDYELIDQDAR
P07355|ANXA2_HUMAN	1032.995	88.45	4.10E-08	RAEDGSVIDYELIDQDAR
P07355|ANXA2_HUMAN	1032.996	90.6	2.90E-08	RAEDGSVIDYELIDQDAR
P07910|HNRPC_HUMAN	614.8646	43.33	0.005	LKGDDLQAIKK
P07910|HNRPC_HUMAN	777.3484	32.26	0.0035	NDKSEEEQSSSSVK
P07910|HNRPC_HUMAN	777.3504	34.13	0.0028	NDKSEEEQSSSSVK
P07910|HNRPC_HUMAN	777.3524	35.31	0.0026	NDKSEEEQSSSSVK
P07910|HNRPC_HUMAN	777.3519	35.02	0.0025	NDKSEEEQSSSSVK
P07910|HNRPC_HUMAN	614.8659	46.57	0.0023	LKGDDLQAIKK
P07910|HNRPC_HUMAN	494.2762	46.36	0.0023	GDDLQAIKK
P07910|HNRPC_HUMAN	614.8649	46.97	0.0019	LKGDDLQAIKK
P07910|HNRPC_HUMAN	614.8643	48.33	0.0016	LKGDDLQAIKK
P07910|HNRPC_HUMAN	614.8649	48.68	0.0013	LKGDDLQAIKK
P07910|HNRPC_HUMAN	614.8646	49.95	0.0011	LKGDDLQAIKK
P07910|HNRPC_HUMAN	665.3303	47.34	0.00042	GFAFVQYVNER
P07910|HNRPC_HUMAN	777.3484	43.11	0.00029	NDKSEEEQSSSSVK
P07910|HNRPC_HUMAN	777.3482	44.82	0.00019	NDKSEEEQSSSSVK
P07910|HNRPC_HUMAN	841.9601	61.57	5.60E-05	MIAGQVLDINLAAEPK
P07910|HNRPC_H	1145.	60.39	1.20E-05	SAAEMYGSVTEHPSPSPLLSSSFDLDYDFQR

UMAN	185			
P07910|HNRPC_HUMAN	665.3303	64.25	8.50E-06	GFAFVQYVNER
P07910|HNRPC_HUMAN	665.3308	63.53	8.00E-06	GFAFVQYVNER
P07910|HNRPC_HUMAN	777.3483	58.69	7.70E-06	NDKSEEEQSSSSVK
P07910|HNRPC_HUMAN	665.3313	64.29	7.60E-06	GFAFVQYVNER
P07910|HNRPC_HUMAN	665.3313	64.66	6.90E-06	GFAFVQYVNER
P07910|HNRPC_HUMAN	665.3312	63.93	6.90E-06	GFAFVQYVNER
P07910|HNRPC_HUMAN	777.3479	60.41	4.80E-06	NDKSEEEQSSSSVK
P07910|HNRPC_HUMAN	665.33	67.4	4.10E-06	GFAFVQYVNER
P07910|HNRPC_HUMAN	777.3461	59.61	4.10E-06	NDKSEEEQSSSSVK
P07910|HNRPC_HUMAN	665.3302	67.5	4.00E-06	GFAFVQYVNER
P07910|HNRPC_HUMAN	841.962	73.06	3.70E-06	MIAGQVLDINLAAEPK
P07910|HNRPC_HUMAN	777.3482	64.16	2.20E-06	NDKSEEEQSSSSVK
P07910|HNRPC_HUMAN	777.3474	65.05	1.70E-06	NDKSEEEQSSSSVK
P07910|HNRPC_HUMAN	777.348	65.45	1.50E-06	NDKSEEEQSSSSVK
P07910|HNRPC_HUMAN	777.3477	67	1.00E-06	NDKSEEEQSSSSVK
P07910|HNRPC_HUMAN	665.3303	75.05	6.40E-07	GFAFVQYVNER
P07910|HNRPC_HUMAN	841.9614	89.04	1.10E-07	MIAGQVLDINLAAEPK
P07910|HNRPC_HUMAN	841.9586	90.32	6.80E-08	MIAGQVLDINLAAEPK
P07910|HNRPC_HUMAN	841.9593	92.29	4.80E-08	MIAGQVLDINLAAEPK
P07910|HNRPC_HUMAN	841.9596	93.72	3.40E-08	MIAGQVLDINLAAEPK
P07910|HNRPC_HUMAN	841.9595	95.68	2.10E-08	MIAGQVLDINLAAEPK
P07910|HNRPC_HUMAN	841.9583	96.48	1.60E-08	MIAGQVLDINLAAEPK
P07910|HNRPC_HUMAN	841.9618	98.13	1.20E-08	MIAGQVLDINLAAEPK
P07910|HNRPC_HUMAN	841.9589	100.48	7.10E-09	MIAGQVLDINLAAEPK
P07910|HNRPC_HUMAN	841.9593	100.96	6.50E-09	MIAGQVLDINLAAEPK
P07910|HNRPC_HUMAN	841.9603	103.83	3.10E-09	MIAGQVLDINLAAEPK
P07910|HNRPC_HUMAN	841.9598	104.43	2.90E-09	MIAGQVLDINLAAEPK

P07910|HNRPC_HUMAN	841.9609	106.92	1.80E-09	MIAGQVLDINLAAEPK
P07910|HNRPC_HUMAN	841.9601	107.04	1.60E-09	MIAGQVLDINLAAEPK
P07910|HNRPC_HUMAN	841.959	107.61	1.40E-09	MIAGQVLDINLAAEPK
P07910|HNRPC_HUMAN	841.9598	107.49	1.40E-09	MIAGQVLDINLAAEPK
P07910|HNRPC_HUMAN	841.9586	107.56	1.20E-09	MIAGQVLDINLAAEPK
P07910|HNRPC_HUMAN	841.9593	110.8	6.80E-10	MIAGQVLDINLAAEPK
P07910|HNRPC_HUMAN	841.9579	110.8	6.50E-10	MIAGQVLDINLAAEPK
P07910|HNRPC_HUMAN	841.9581	110.75	6.50E-10	MIAGQVLDINLAAEPK
P07910|HNRPC_HUMAN	841.9584	113.18	3.40E-10	MIAGQVLDINLAAEPK
P07910|HNRPC_HUMAN	841.9587	114.32	2.90E-10	MIAGQVLDINLAAEPK
P07910|HNRPC_HUMAN	841.9584	118.12	1.10E-10	MIAGQVLDINLAAEPK
P07910|HNRPC_HUMAN	841.9591	121.11	6.30E-11	MIAGQVLDINLAAEPK
P07910|HNRPC_HUMAN	841.9591	124.72	2.70E-11	MIAGQVLDINLAAEPK
P08133|ANXA6_HUMAN	859.42	40	0.0034	SLHQAIEGDTSGDFLK
P08133|ANXA6_HUMAN	536.8021	44.54	0.0032	SEIDLLNIR
P08133|ANXA6_HUMAN	859.42	40.66	0.0029	SLHQAIEGDTSGDFLK
P08133|ANXA6_HUMAN	844.4084	38.84	0.0029	GTVRPANDFNPDADAK
P08133|ANXA6_HUMAN	536.8018	45.63	0.0025	SEIDLLNIR
P08133|ANXA6_HUMAN	859.42	42.16	0.0021	SLHQAIEGDTSGDFLK
P08133|ANXA6_HUMAN	842.0509	36.89	0.0021	GSIHDFPGFDPNQDAEALYTAMK
P08133|ANXA6_HUMAN	590.3062	46.33	0.0015	GLGTDEDTIIDIITHR
P08133|ANXA6_HUMAN	859.42	44.48	0.0012	SLHQAIEGDTSGDFLK
P08133|ANXA6_HUMAN	873.4193	45.57	0.00065	DLEADIIGDTSGHFQK
P08133|ANXA6_HUMAN	842.0514	42.95	0.0005	GSIHDFPGFDPNQDAEALYTAMK
P08133|ANXA6_HUMAN	811.374	44.71	0.00037	SLEDALSSDTSGHFR
P08133|ANXA6_HUMAN	536.8018	57.23	0.00017	SEIDLLNIR
P08133|ANXA6_HUMAN	546.2759	52.67	0.00014	SELDMLDIR
P08133|ANXA6_H	536.8	59.89	9.30E-05	SEIDLLNIR

UMAN	016			
P08133|ANXA6_HUMAN	842.0496	50.43	8.00E-05	GSIHDFPGFDPNQDAEALYTAMK
P08133|ANXA6_HUMAN	873.4187	55.38	6.70E-05	DLEADIIGDTSGHFQK
P08133|ANXA6_HUMAN	884.9559	61.42	4.60E-05	GLGTDEDTIIDIITHR
P08133|ANXA6_HUMAN	884.9549	60.93	4.50E-05	GLGTDEDTIIDIITHR
P08133|ANXA6_HUMAN	842.0527	54.72	3.70E-05	GSIHDFPGFDPNQDAEALYTAMK
P08133|ANXA6_HUMAN	842.051	54.7	3.30E-05	GSIHDFPGFDPNQDAEALYTAMK
P08133|ANXA6_HUMAN	873.418	58.45	3.10E-05	DLEADIIGDTSGHFQK
P08133|ANXA6_HUMAN	811.3729	57.2	2.00E-05	SLEDALSSDTSGHFR
P08133|ANXA6_HUMAN	873.4194	61.59	1.60E-05	DLEADIIGDTSGHFQK
P08133|ANXA6_HUMAN	811.3723	58.21	1.50E-05	SLEDALSSDTSGHFR
P08133|ANXA6_HUMAN	873.4185	62.33	1.30E-05	DLEADIIGDTSGHFQK
P08133|ANXA6_HUMAN	873.4178	62.9	1.00E-05	DLEADIIGDTSGHFQK
P08133|ANXA6_HUMAN	873.4174	63.83	8.70E-06	DLEADIIGDTSGHFQK
P08133|ANXA6_HUMAN	884.9541	69.44	6.70E-06	GLGTDEDTIIDIITHR
P08133|ANXA6_HUMAN	873.4177	65.12	6.50E-06	DLEADIIGDTSGHFQK
P08133|ANXA6_HUMAN	811.3724	62.2	6.00E-06	SLEDALSSDTSGHFR
P08133|ANXA6_HUMAN	884.9547	75.85	1.50E-06	GLGTDEDTIIDIITHR
P08133|ANXA6_HUMAN	873.4188	75.28	6.90E-07	DLEADIIGDTSGHFQK
P08133|ANXA6_HUMAN	861.4572	80.86	6.20E-07	GFGSDKEAILDIITSR
P08133|ANXA6_HUMAN	861.456	80.83	6.00E-07	GFGSDKEAILDIITSR
P08133|ANXA6_HUMAN	861.453	82.45	4.40E-07	GFGSDKEAILDIITSR
P08133|ANXA6_HUMAN	861.456	85.37	2.10E-07	GFGSDKEAILDIITSR
P08133|ANXA6_HUMAN	811.3759	76.93	2.10E-07	SLEDALSSDTSGHFR
P08133|ANXA6_HUMAN	811.3736	77.48	1.70E-07	SLEDALSSDTSGHFR
P08133|ANXA6_HUMAN	861.4568	89.28	8.40E-08	GFGSDKEAILDIITSR
P08133|ANXA6_HUMAN	861.4548	97.91	1.20E-08	GFGSDKEAILDIITSR
P08133|ANXA6_HUMAN	861.4553	102.42	4.50E-09	GFGSDKEAILDIITSR

P08579|RU2B_HUMAN	973.9493	69.7	1.50E-06	HDIAFVEFENDGQAGAAR
P08579|RU2B_HUMAN	973.9543	81.35	1.50E-07	HDIAFVEFENDGQAGAAR
P08621|RU17_HUMAN	630.3311	41.32	0.0047	RQQEVETELK
P08621|RU17_HUMAN	619.3301	39.41	0.0038	EFEVYGPIKR
P08621|RU17_HUMAN	630.3323	42.59	0.0037	RQQEVETELK
P08621|RU17_HUMAN	641.3561	41.03	0.0033	DPIPYLPPLEK
P08621|RU17_HUMAN	619.3306	39.6	0.0032	EFEVYGPIKR
P08621|RU17_HUMAN	921.8959	29.7	0.0026	MWDPHNDPNAQGDAFK
P08621|RU17_HUMAN	619.3306	40.58	0.0025	EFEVYGPIKR
P08621|RU17_HUMAN	619.3308	41.99	0.0018	EFEVYGPIKR
P08621|RU17_HUMAN	630.333	53.13	0.00032	RQQEVETELK
P08621|RU17_HUMAN	707.322	46.34	0.00018	GYAFIEYEHER
P08621|RU17_HUMAN	707.3233	53.76	2.70E-05	GYAFIEYEHER
P08621|RU17_HUMAN	707.3239	54.83	2.30E-05	GYAFIEYEHER
P08621|RU17_HUMAN	707.3233	54.87	2.10E-05	GYAFIEYEHER
P08621|RU17_HUMAN	707.3218	57.18	1.40E-05	GYAFIEYEHER
P08621|RU17_HUMAN	707.323	57.38	1.20E-05	GYAFIEYEHER
P08621|RU17_HUMAN	707.3225	60.72	6.60E-06	GYAFIEYEHER
P08670|VIME_HUMAN	918.9023	32.58	0.0046	DGQVINETSQHHDDLE
P08670|VIME_HUMAN	834.924	41.03	0.0039	ETNLDSLPLVDTHSK
P08670|VIME_HUMAN	918.9012	33.23	0.0039	DGQVINETSQHHDDLE
P08670|VIME_HUMAN	918.9016	33.57	0.0036	DGQVINETSQHHDDLE
P08670|VIME_HUMAN	834.9238	42.17	0.003	ETNLDSLPLVDTHSK
P08670|VIME_HUMAN	918.9019	34.62	0.0029	DGQVINETSQHHDDLE
P08670|VIME_HUMAN	785.9485	46.97	0.0017	ISLPLPNFSSLNLR
P08670|VIME_HUMAN	834.9233	44.89	0.0014	ETNLDSLPLVDTHSK
P08670|VIME_HUMAN	834.9232	44.8	0.0014	ETNLDSLPLVDTHSK
P08670|VIME_HU	918.9	38.34	0.0012	DGQVINETSQHHDDLE

MAN	006			
P08670|VIME_HUMAN	627.7847	38.01	0.0012	LGDLYEEEMR
P08670|VIME_HUMAN	834.9236	46.16	0.0011	ETNLDSLPLVDTHSK
P08670|VIME_HUMAN	834.9232	46.23	0.001	ETNLDSLPLVDTHSK
P08670|VIME_HUMAN	918.9017	39.43	0.00094	DGQVINETSQHHDDLE
P08670|VIME_HUMAN	714.8571	44.3	0.00092	SLYASSPGGVYATR
P08670|VIME_HUMAN	714.8582	46.16	0.00058	SLYASSPGGVYATR
P08670|VIME_HUMAN	714.8582	46.24	0.00057	SLYASSPGGVYATR
P08670|VIME_HUMAN	714.8575	45.86	0.00056	SLYASSPGGVYATR
P08670|VIME_HUMAN	627.7846	41.61	0.00053	LGDLYEEEMR
P08670|VIME_HUMAN	785.9485	52.47	0.00049	ISLPLPNFSSLNLR
P08670|VIME_HUMAN	918.9003	42.14	0.00049	DGQVINETSQHHDDLE
P08670|VIME_HUMAN	714.8591	47.22	0.00047	SLYASSPGGVYATR
P08670|VIME_HUMAN	627.7856	41.65	0.00047	LGDLYEEEMR
P08670|VIME_HUMAN	627.7856	41.71	0.00046	LGDLYEEEMR
P08670|VIME_HUMAN	714.8587	48.34	0.00036	SLYASSPGGVYATR
P08670|VIME_HUMAN	918.8997	44.27	0.0003	DGQVINETSQHHDDLE
P08670|VIME_HUMAN	785.9496	55.15	0.00029	ISLPLPNFSSLNLR
P08670|VIME_HUMAN	918.9015	44.5	0.00029	DGQVINETSQHHDDLE
P08670|VIME_HUMAN	918.9006	44.8	0.00027	DGQVINETSQHHDDLE
P08670|VIME_HUMAN	785.9478	57.01	0.00019	ISLPLPNFSSLNLR
P08670|VIME_HUMAN	585.3582	54.66	0.00018	ILLAELEQLK
P08670|VIME_HUMAN	785.9498	59.05	0.00012	ISLPLPNFSSLNLR
P08670|VIME_HUMAN	785.9497	59.47	0.00011	ISLPLPNFSSLNLR
P08670|VIME_HUMAN	918.9011	48.69	0.00011	DGQVINETSQHHDDLE
P08670|VIME_HUMAN	714.86	54.67	0.0001	SLYASSPGGVYATR
P08670|VIME_HUMAN	585.358	57.16	9.90E-05	ILLAELEQLK
P08670|VIME_HUMAN	627.7853	48.73	9.80E-05	LGDLYEEEMR

P08670|VIME_HUMAN	627.785	48.85	9.60E-05	LGDLYEEEMR
P08670|VIME_HUMAN	627.7857	49.16	8.30E-05	LGDLYEEEMR
P08670|VIME_HUMAN	918.9012	50.35	7.50E-05	DGQVINETSQHHDDLE
P08670|VIME_HUMAN	585.358	58.48	7.30E-05	ILLAELEQLK
P08670|VIME_HUMAN	867.9083	55.1	6.30E-05	LQDEIQNMKEEMAR
P08670|VIME_HUMAN	585.3597	59.94	4.90E-05	ILLAELEQLK
P08670|VIME_HUMAN	714.8572	56.99	4.90E-05	SLYASSPGGVYATR
P08670|VIME_HUMAN	585.3589	60.07	4.80E-05	ILLAELEQLK
P08670|VIME_HUMAN	714.8583	57.26	4.50E-05	SLYASSPGGVYATR
P08670|VIME_HUMAN	785.9496	65.8	2.40E-05	ISLPLPNFSSLNLR
P08670|VIME_HUMAN	585.3597	64.56	1.70E-05	ILLAELEQLK
P08670|VIME_HUMAN	918.9009	57.32	1.50E-05	DGQVINETSQHHDDLE
P08670|VIME_HUMAN	627.7853	57.63	1.30E-05	LGDLYEEEMR
P08670|VIME_HUMAN	785.9493	69.76	1.00E-05	ISLPLPNFSSLNLR
P08670|VIME_HUMAN	867.9106	63.87	9.60E-06	LQDEIQNMKEEMAR
P08670|VIME_HUMAN	867.9088	68.11	3.20E-06	LQDEIQNMKEEMAR
P08670|VIME_HUMAN	1093.984	63.72	2.60E-06	EMEENFAVEAANYQDTIGR
P08670|VIME_HUMAN	585.3593	72.98	2.40E-06	ILLAELEQLK
P08670|VIME_HUMAN	918.9045	65.37	2.40E-06	DGQVINETSQHHDDLE
P08670|VIME_HUMAN	867.9071	70.22	2.00E-06	LQDEIQNMKEEMAR
P08670|VIME_HUMAN	867.9093	71.95	1.80E-06	LQDEIQNMKEEMAR
P08670|VIME_HUMAN	785.949	78.43	1.40E-06	ISLPLPNFSSLNLR
P08670|VIME_HUMAN	867.9079	72.77	1.10E-06	LQDEIQNMKEEMAR
P08670|VIME_HUMAN	785.9495	79.83	1.00E-06	ISLPLPNFSSLNLR
P08670|VIME_HUMAN	1093.985	69.08	9.10E-07	EMEENFAVEAANYQDTIGR
P08670|VIME_HUMAN	767.4274	80.35	6.90E-07	KVESLQEEIAFLK
P08670|VIME_HUMAN	785.949	83.49	4.40E-07	ISLPLPNFSSLNLR
P08670|VIME_HUMAN	1063.	82.91	3.50E-07	LLQDSVDFSLADAINTEFK

MAN	538			
P08670|VIME_HUMAN	767.4285	85.02	2.50E-07	KVESLQEEIAFLK
P08670|VIME_HUMAN	1093.983	74.01	2.40E-07	EMEENFAVEAANYQDTIGR
P08670|VIME_HUMAN	767.4286	88.36	1.20E-07	KVESLQEEIAFLK
P08670|VIME_HUMAN	767.4276	88.32	1.10E-07	KVESLQEEIAFLK
P08670|VIME_HUMAN	767.4269	89.64	8.30E-08	KVESLQEEIAFLK
P08670|VIME_HUMAN	1093.985	79.97	7.50E-08	EMEENFAVEAANYQDTIGR
P08670|VIME_HUMAN	867.9069	84.41	7.00E-08	LQDEIQNMKEEMAR
P08670|VIME_HUMAN	767.4282	90.72	6.70E-08	KVESLQEEIAFLK
P08670|VIME_HUMAN	867.9084	84.97	6.60E-08	LQDEIQNMKEEMAR
P08670|VIME_HUMAN	1093.985	81.28	5.50E-08	EMEENFAVEAANYQDTIGR
P08670|VIME_HUMAN	767.4282	91.82	5.20E-08	KVESLQEEIAFLK
P08670|VIME_HUMAN	867.9091	88.57	3.80E-08	LQDEIQNMKEEMAR
P08670|VIME_HUMAN	1093.984	82.61	3.50E-08	EMEENFAVEAANYQDTIGR
P08670|VIME_HUMAN	767.4279	94.36	2.80E-08	KVESLQEEIAFLK
P08670|VIME_HUMAN	867.9086	93.02	1.00E-08	LQDEIQNMKEEMAR
P08670|VIME_HUMAN	767.4284	105.84	2.10E-09	KVESLQEEIAFLK
P08670|VIME_HUMAN	1093.984	95.76	2.00E-09	EMEENFAVEAANYQDTIGR
P08670|VIME_HUMAN	1063.538	106.15	1.70E-09	LLQDSVDFSLADAINTEFK
P08670|VIME_HUMAN	767.428	110.59	6.90E-10	KVESLQEEIAFLK
P08670|VIME_HUMAN	1093.983	101.59	4.20E-10	EMEENFAVEAANYQDTIGR
P08670|VIME_HUMAN	1063.538	121.72	4.60E-11	LLQDSVDFSLADAINTEFK
P08758|ANXA5_HUMAN	852.9518	42.03	0.005	GLGTDEESILTLLTSR
P08758|ANXA5_HUMAN	637.824	39.35	0.0033	NFATSLYSMIK
P08758|ANXA5_HUMAN	553.7937	41.32	0.003	SEIDLFNIR
P08758|ANXA5_HUMAN	637.8256	42.51	0.0023	NFATSLYSMIK
P08758|ANXA5_HUMAN	701.8734	45.73	0.0021	KNFATSLYSMIK
P08758|ANXA5_HUMAN	637.8231	43.14	0.0021	NFATSLYSMIK

P08758|ANXA5_HUMAN	637.824	42.01	0.0019	NFATSLYSMIK
P08758|ANXA5_HUMAN	670.8082	38.7	0.001	GTVTDFPGFDER
P08758|ANXA5_HUMAN	701.8716	48.31	0.00099	KNFATSLYSMIK
P08758|ANXA5_HUMAN	670.8079	39.58	0.00084	GTVTDFPGFDER
P08758|ANXA5_HUMAN	723.8857	52.77	0.0004	DLLDDLKSELTGK
P08758|ANXA5_HUMAN	723.8865	54.44	0.00027	DLLDDLKSELTGK
P08758|ANXA5_HUMAN	723.8863	54.95	0.00024	DLLDDLKSELTGK
P08758|ANXA5_HUMAN	578.2888	50.18	0.0002	GAGTDDHTLIR
P08758|ANXA5_HUMAN	578.2892	50.19	0.00017	GAGTDDHTLIR
P08758|ANXA5_HUMAN	723.8858	57.2	0.00014	DLLDDLKSELTGK
P08758|ANXA5_HUMAN	723.8861	59.07	9.30E-05	DLLDDLKSELTGK
P08758|ANXA5_HUMAN	723.8856	59.19	9.00E-05	DLLDDLKSELTGK
P08758|ANXA5_HUMAN	723.8865	59.52	8.40E-05	DLLDDLKSELTGK
P08758|ANXA5_HUMAN	578.2896	54.23	6.50E-05	GAGTDDHTLIR
P08758|ANXA5_HUMAN	807.4553	62.48	6.00E-05	ETSGNLEQLLLAVVK
P08758|ANXA5_HUMAN	670.8069	50.38	5.90E-05	GTVTDFPGFDER
P08758|ANXA5_HUMAN	670.8076	50.26	5.40E-05	GTVTDFPGFDER
P08758|ANXA5_HUMAN	670.8081	52.44	4.30E-05	GTVTDFPGFDER
P08758|ANXA5_HUMAN	578.2892	56.73	3.70E-05	GAGTDDHTLIR
P08758|ANXA5_HUMAN	670.8082	54.09	3.00E-05	GTVTDFPGFDER
P08758|ANXA5_HUMAN	807.4556	65.71	2.90E-05	ETSGNLEQLLLAVVK
P08758|ANXA5_HUMAN	807.4572	64.9	2.90E-05	ETSGNLEQLLLAVVK
P08758|ANXA5_HUMAN	807.4577	65.39	2.80E-05	ETSGNLEQLLLAVVK
P08758|ANXA5_HUMAN	867.4409	64.98	2.40E-05	SIPAYLAETLYYAMK
P08758|ANXA5_HUMAN	807.4555	67.13	2.10E-05	ETSGNLEQLLLAVVK
P08758|ANXA5_HUMAN	670.8084	55.78	2.10E-05	GTVTDFPGFDER
P08758|ANXA5_HUMAN	807.4573	66.67	1.90E-05	ETSGNLEQLLLAVVK
P08758|ANXA5_H	807.4	67.9	1.60E-05	ETSGNLEQLLLAVVK

UMAN	579			
P08758|ANXA5_HUMAN	723.886	68.78	9.90E-06	DLLDDLKSELTGK
P08758|ANXA5_HUMAN	1329.624	64.78	9.20E-06	DPDAGIDEAQVEQDAQALFQAGELK
P08758|ANXA5_HUMAN	807.4569	70.19	8.40E-06	ETSGNLEQLLLAVVK
P08758|ANXA5_HUMAN	670.8079	62.35	4.50E-06	GTVTDFPGFDER
P08758|ANXA5_HUMAN	578.2892	66.69	3.70E-06	GAGTDDHTLIR
P08758|ANXA5_HUMAN	807.4575	74.53	3.40E-06	ETSGNLEQLLLAVVK
P08758|ANXA5_HUMAN	807.4576	75.45	2.70E-06	ETSGNLEQLLLAVVK
P08758|ANXA5_HUMAN	852.952	98.01	1.30E-08	GLGTDEESILTLLTSR
P08758|ANXA5_HUMAN	852.9515	98.44	1.20E-08	GLGTDEESILTLLTSR
P08758|ANXA5_HUMAN	852.9517	98.43	1.20E-08	GLGTDEESILTLLTSR
P08758|ANXA5_HUMAN	852.9519	102.39	4.60E-09	GLGTDEESILTLLTSR
P08758|ANXA5_HUMAN	1329.63	98.7	4.40E-09	DPDAGIDEAQVEQDAQALFQAGELK
P08758|ANXA5_HUMAN	1444.62	93.79	1.10E-09	QVYEEEYGSSLEDDVVGDTSGYYQR
P08758|ANXA5_HUMAN	1444.616	93.3	1.10E-09	QVYEEEYGSSLEDDVVGDTSGYYQR
P08758|ANXA5_HUMAN	1444.619	96.28	5.70E-10	QVYEEEYGSSLEDDVVGDTSGYYQR
P08758|ANXA5_HUMAN	1444.62	99.9	2.70E-10	QVYEEEYGSSLEDDVVGDTSGYYQR
P08758|ANXA5_HUMAN	1329.625	110.56	2.40E-10	DPDAGIDEAQVEQDAQALFQAGELK
P08758|ANXA5_HUMAN	852.9517	116.6	1.80E-10	GLGTDEESILTLLTSR
P08758|ANXA5_HUMAN	852.9518	116.56	1.80E-10	GLGTDEESILTLLTSR
P08758|ANXA5_HUMAN	852.9524	116.49	1.80E-10	GLGTDEESILTLLTSR
P08758|ANXA5_HUMAN	852.9522	116.59	1.70E-10	GLGTDEESILTLLTSR
P08758|ANXA5_HUMAN	1444.62	105.89	6.70E-11	QVYEEEYGSSLEDDVVGDTSGYYQR
P08758|ANXA5_HUMAN	1444.619	110.38	2.10E-11	QVYEEEYGSSLEDDVVGDTSGYYQR
P08758|ANXA5_HUMAN	1329.627	122.71	1.60E-11	DPDAGIDEAQVEQDAQALFQAGELK
P08758|ANXA5_HUMAN	1444.625	122.64	1.60E-12	QVYEEEYGSSLEDDVVGDTSGYYQR
P08865|RSSA_HUMAN	849.9307	63.65	1.70E-05	FTPGTFTNQIQAAFR
P08865|RSSA_HUMAN	870.9788	68.94	1.00E-05	AIVAIENPADVSVISSR

P08865|RSSA_HUMAN	849.9324	66.52	1.00E-05	FTPGTFTNQIQAAFR
P08865|RSSA_HUMAN	849.9302	66.59	8.90E-06	FTPGTFTNQIQAAFR
P08865|RSSA_HUMAN	849.931	67.76	7.00E-06	FTPGTFTNQIQAAFR
P08865|RSSA_HUMAN	849.9313	72.6	2.40E-06	FTPGTFTNQIQAAFR
P08865|RSSA_HUMAN	849.9322	74.5	1.40E-06	FTPGTFTNQIQAAFR
P08865|RSSA_HUMAN	870.9777	80.58	6.60E-07	AIVAIENPADVSVISSR
P08865|RSSA_HUMAN	849.9294	78.48	6.50E-07	FTPGTFTNQIQAAFR
P08865|RSSA_HUMAN	849.931	78.7	5.60E-07	FTPGTFTNQIQAAFR
P08865|RSSA_HUMAN	849.9305	79.05	5.10E-07	FTPGTFTNQIQAAFR
P08865|RSSA_HUMAN	849.9316	91.01	3.60E-08	FTPGTFTNQIQAAFR
P08865|RSSA_HUMAN	849.9321	91.15	3.10E-08	FTPGTFTNQIQAAFR
P09012|SNRPA_HUMAN	802.3705	32.81	0.0042	SMQGFPFYDKPMR
P09012|SNRPA_HUMAN	1364.203	44.49	0.0036	AVQGGGATPVVGAVQGPVPGMPPMTQAPR
P09012|SNRPA_HUMAN	802.3733	35.75	0.0033	SMQGFPFYDKPMR
P09012|SNRPA_HUMAN	1364.207	46.42	0.0024	AVQGGGATPVVGAVQGPVPGMPPMTQAPR
P09012|SNRPA_HUMAN	802.3702	44.52	0.00029	SMQGFPFYDKPMR
P09012|SNRPA_HUMAN	994.9737	95.04	8.40E-09	HDIAFVEFDNEVQAGAAR
P09234|RU1C_HUMAN	739.3523	35.96	0.0048	WMEEQAQSLIDK
P09234|RU1C_HUMAN	739.3513	54.68	5.70E-05	WMEEQAQSLIDK
P09651|ROA1_HUMAN	543.5961	36.31	0.0047	SSGPYGGGGQYFAKPR
P09651|ROA1_HUMAN	650.3292	38.53	0.0034	SESPKEPEQLR
P09651|ROA1_HUMAN	543.5961	38.21	0.003	SSGPYGGGGQYFAKPR
P09651|ROA1_HUMAN	543.5969	42.33	0.0011	SSGPYGGGGQYFAKPR
P09651|ROA1_HUMAN	837.4073	47.28	0.00087	GFGFVTYATVEEVDAAMNARPHK
P09651|ROA1_HUMAN	837.4062	51.06	0.00033	GFGFVTYATVEEVDAAMNARPHK
P09651|ROA1_HUMAN	1255.613	52.38	0.00032	GFGFVTYATVEEVDAAMNARPHK
P09651|ROA1_HUMAN	837.406	51.92	0.00028	GFGFVTYATVEEVDAAMNARPHK
P09651|ROA1_HU	837.4	53.85	0.00019	GFGFVTYATVEEVDAAMNARPHK

MAN	066			
P09651|ROA1_HUMAN	543.5969	51.48	0.00013	SSGPYGGGGQYFAKPR
P09651|ROA1_HUMAN	814.8937	60.28	2.00E-05	SSGPYGGGGQYFAKPR
P09651|ROA1_HUMAN	814.8933	60.2	2.00E-05	SSGPYGGGGQYFAKPR
P09651|ROA1_HUMAN	543.5966	62.66	9.70E-06	SSGPYGGGGQYFAKPR
P09651|ROA1_HUMAN	1255.607	71.91	2.90E-06	GFGFVTYATVEEVDAAMNARPHK
P09651|ROA1_HUMAN	814.8926	68.96	2.50E-06	SSGPYGGGGQYFAKPR
P09651|ROA1_HUMAN	847.8505	58.76	2.30E-06	NQGGYGGSSSSSSYGSGR
P09651|ROA1_HUMAN	847.8496	59.9	1.70E-06	NQGGYGGSSSSSSYGSGR
P09651|ROA1_HUMAN	814.8923	71.72	1.40E-06	SSGPYGGGGQYFAKPR
P09651|ROA1_HUMAN	847.8504	60.95	1.40E-06	NQGGYGGSSSSSSYGSGR
P09651|ROA1_HUMAN	814.8926	71.85	1.30E-06	SSGPYGGGGQYFAKPR
P09651|ROA1_HUMAN	847.8506	61.37	1.30E-06	NQGGYGGSSSSSSYGSGR
P09651|ROA1_HUMAN	814.8914	75.31	5.20E-07	SSGPYGGGGQYFAKPR
P09651|ROA1_HUMAN	847.8519	67.09	3.30E-07	NQGGYGGSSSSSSYGSGR
P09651|ROA1_HUMAN	847.8569	71.31	2.00E-07	NQGGYGGSSSSSSYGSGR
P09651|ROA1_HUMAN	814.8915	81.08	1.40E-07	SSGPYGGGGQYFAKPR
P09651|ROA1_HUMAN	847.8527	71.27	1.40E-07	NQGGYGGSSSSSSYGSGR
P09651|ROA1_HUMAN	814.8934	83.52	9.30E-08	SSGPYGGGGQYFAKPR
P09651|ROA1_HUMAN	847.8513	75.1	5.10E-08	NQGGYGGSSSSSSYGSGR
P09651|ROA1_HUMAN	814.8983	88.47	3.00E-08	SSGPYGGGGQYFAKPR
P09651|ROA1_HUMAN	814.8928	89.38	2.20E-08	SSGPYGGGGQYFAKPR
P09651|ROA1_HUMAN	814.8922	94.85	6.70E-09	SSGPYGGGGQYFAKPR
P09651|ROA1_HUMAN	814.8929	96.73	4.00E-09	SSGPYGGGGQYFAKPR
P09651|ROA1_HUMAN	814.8915	97.07	3.60E-09	SSGPYGGGGQYFAKPR
P09651|ROA1_HUMAN	814.8925	100.15	2.00E-09	SSGPYGGGGQYFAKPR
P09651|ROA1_HUMAN	814.8926	99.98	1.90E-09	SSGPYGGGGQYFAKPR
P09651|ROA1_HUMAN	847.8511	93.45	7.50E-10	NQGGYGGSSSSSSYGSGR

P09651|ROA1_HUMAN	814.8921	107.43	3.70E-10	SSGPYGGGGQYFAKPR
P09651|ROA1_HUMAN	814.8922	107.76	3.40E-10	SSGPYGGGGQYFAKPR
P09651|ROA1_HUMAN	814.8917	107.84	2.90E-10	SSGPYGGGGQYFAKPR
P09651|ROA1_HUMAN	847.8511	101.27	1.20E-10	NQGGYGGSSSSSSYGSGR
P09651|ROA1_HUMAN	847.8515	102.32	9.70E-11	NQGGYGGSSSSSSYGSGR
P09651|ROA1_HUMAN	847.8519	105.55	4.70E-11	NQGGYGGSSSSSSYGSGR
P09651|ROA1_HUMAN	814.8915	116.51	4.00E-11	SSGPYGGGGQYFAKPR
P09651|ROA1_HUMAN	814.8925	119	2.60E-11	SSGPYGGGGQYFAKPR
P09651|ROA1_HUMAN	847.8518	111.31	1.30E-11	NQGGYGGSSSSSSYGSGR
P09651|ROA1_HUMAN	814.8915	127.8	3.00E-12	SSGPYGGGGQYFAKPR
P09651|ROA1_HUMAN	847.8517	118.39	2.50E-12	NQGGYGGSSSSSSYGSGR
P09651|ROA1_HUMAN	847.8509	118.54	2.30E-12	NQGGYGGSSSSSSYGSGR
P09651|ROA1_HUMAN	847.8514	131.48	1.20E-13	NQGGYGGSSSSSSYGSGR
P09661|RU2A_HUMAN	1403.196	53.38	0.00038	IPVIENLGATLDQFDAIDFSDNEIR
P09661|RU2A_HUMAN	1403.201	67.83	1.50E-05	IPVIENLGATLDQFDAIDFSDNEIR
P09661|RU2A_HUMAN	1403.197	72.05	5.10E-06	IPVIENLGATLDQFDAIDFSDNEIR
P09874|PARP1_HUMAN	747.9143	46.12	0.0016	KPPLLNNADSVQAK
P09874|PARP1_HUMAN	747.9184	46.67	0.0013	KPPLLNNADSVQAK
P09874|PARP1_HUMAN	750.3568	58.66	1.90E-05	HPDVEVDGFSELR
P09874|PARP1_HUMAN	750.3583	61.67	1.10E-05	HPDVEVDGFSELR
P09874|PARP1_HUMAN	750.3613	74.1	6.30E-07	HPDVEVDGFSELR
P0C0S5|H2AZ_HUMAN	559.7817	37.62	0.0047	GDEELDSLIK
P0C0S5|H2AZ_HUMAN	559.7802	39.79	0.0029	GDEELDSLIK
P0C0S5|H2AZ_HUMAN	559.7803	40.39	0.0026	GDEELDSLIK
P0C0S5|H2AZ_HUMAN	559.7806	42.12	0.0017	GDEELDSLIK
P0C0S5|H2AZ_HUMAN	559.7809	43.13	0.0013	GDEELDSLIK
P0C0S5|H2AZ_HUMAN	559.7805	43.86	0.0012	GDEELDSLIK
P0C0S5|H2AZ_HU	559.7	43.86	0.0011	GDEELDSLIK

MAN	809			
P0C0S5|H2AZ_HUMAN	559.7808	53.92	0.00011	GDEELDSLIK
P0DMV8|HS71A_HUMAN	829.9285	47.74	0.001	NQVALNPQNTVFDAK
P0DMV8|HS71A_HUMAN	829.9283	48.49	0.00084	NQVALNPQNTVFDAK
P0DMV8|HS71A_HUMAN	829.9305	54.33	0.00028	NQVALNPQNTVFDAK
P0DMV8|HS71A_HUMAN	829.9272	53.03	0.00028	NQVALNPQNTVFDAK
P0DMV8|HS71A_HUMAN	829.9272	59.21	6.70E-05	NQVALNPQNTVFDAK
P0DMV8|HS71A_HUMAN	829.9289	60.76	4.60E-05	NQVALNPQNTVFDAK
P0DMV8|HS71A_HUMAN	829.9282	65.41	1.70E-05	NQVALNPQNTVFDAK
P10412|H14_HUMAN	422.7469	44.91	0.004	KATGAATPK
P10412|H14_HUMAN	392.7362	39.28	0.0032	KPAAAAGAK
P10412|H14_HUMAN	392.7365	40.29	0.0025	KPAAAAGAK
P10412|H14_HUMAN	392.7362	41.48	0.0019	KPAAAAGAK
P10412|H14_HUMAN	392.7364	42.11	0.0017	KPAAAAGAK
P11142|HSP7C_HUMAN	705.8364	35.34	0.0041	RFDDAVVQSDMK
P11142|HSP7C_HUMAN	741.4056	44.8	0.0023	SQIHDIVLVGGSTR
P11142|HSP7C_HUMAN	825.3973	42.76	0.0013	NQVAMNPTNTVFDAK
P11142|HSP7C_HUMAN	741.4055	47.97	0.0011	SQIHDIVLVGGSTR
P11142|HSP7C_HUMAN	741.4049	51.89	0.00044	SQIHDIVLVGGSTR
P11142|HSP7C_HUMAN	705.8374	45.46	0.00036	RFDDAVVQSDMK
P11142|HSP7C_HUMAN	825.3982	48.93	0.00027	NQVAMNPTNTVFDAK
P11142|HSP7C_HUMAN	705.8348	47.44	0.00025	RFDDAVVQSDMK
P11142|HSP7C_HUMAN	825.3976	51.82	0.00016	NQVAMNPTNTVFDAK
P11142|HSP7C_HUMAN	741.4044	57.33	0.00013	SQIHDIVLVGGSTR
P11142|HSP7C_HUMAN	825.4016	55	8.80E-05	NQVAMNPTNTVFDAK
P11142|HSP7C_HUMAN	741.4042	59.13	8.40E-05	SQIHDIVLVGGSTR
P11142|HSP7C_HUMAN	741.405	59.25	8.20E-05	SQIHDIVLVGGSTR
P11142|HSP7C_HUMAN	741.4059	59.18	8.00E-05	SQIHDIVLVGGSTR

P11142|HSP7C_HUMAN	741.4058	60.03	6.60E-05	SQIHDIVLVGGSTR
P11142|HSP7C_HUMAN	1387.665	61.67	3.00E-05	QTQTFTTYSDNQPGVLIQVYEGER
P11142|HSP7C_HUMAN	825.3996	60.71	2.40E-05	NQVAMNPTNTVFDAK
P11142|HSP7C_HUMAN	825.4013	64.41	1.10E-05	NQVAMNPTNTVFDAK
P11142|HSP7C_HUMAN	1387.667	67.41	8.30E-06	QTQTFTTYSDNQPGVLIQVYEGER
P11142|HSP7C_HUMAN	705.8352	62.63	7.70E-06	RFDDAVVQSDMK
P11142|HSP7C_HUMAN	825.3989	89.55	2.80E-08	NQVAMNPTNTVFDAK
P11387|TOP1_HUMAN	877.4599	46.22	0.0016	GPVFAPPYEPLPENVK
P11388|TOP2A_HUMAN	963.9973	41.72	0.0049	VTIDPENNLISIWNNGK
P11388|TOP2A_HUMAN	835.8987	42.48	0.001	YSGPEDDAAISLAFSK
P11388|TOP2A_HUMAN	835.897	51.71	0.00012	YSGPEDDAAISLAFSK
P13645|K1C10_HUMAN	747.3698	37.88	0.0048	SQYEQLAEQNRK
P13645|K1C10_HUMAN	583.2939	37.2	0.0045	LENEIQTYR
P13645|K1C10_HUMAN	583.2939	37.95	0.0038	LENEIQTYR
P13645|K1C10_HUMAN	559.7565	31.04	0.0037	HGNSHQGEPR
P13645|K1C10_HUMAN	650.7993	31.83	0.0033	NHEEEMKDLR
P13645|K1C10_HUMAN	617.841	43.02	0.003	LKYENEVALR
P13645|K1C10_HUMAN	583.2932	40.15	0.0029	LENEIQTYR
P13645|K1C10_HUMAN	583.2937	39.31	0.0028	LENEIQTYR
P13645|K1C10_HUMAN	747.3707	41.28	0.0022	SQYEQLAEQNRK
P13645|K1C10_HUMAN	583.2945	40.44	0.002	LENEIQTYR
P13645|K1C10_HUMAN	899.0072	46.22	0.0019	NVQALEIELQSQLALK
P13645|K1C10_HUMAN	747.3679	42.4	0.0017	SQYEQLAEQNRK
P13645|K1C10_HUMAN	559.7576	34.8	0.0016	HGNSHQGEPR
P13645|K1C10_HUMAN	747.3693	43.93	0.0013	SQYEQLAEQNRK
P13645|K1C10_HUMAN	747.3691	43.64	0.0013	SQYEQLAEQNRK
P13645|K1C10_HUMAN	617.8408	47.27	0.0012	LKYENEVALR
P13645|K1C10_H	617.8	47.22	0.001	LKYENEVALR

UMAN	413			
P13645|K1C10_HUMAN	717.8881	48.93	0.00084	IRLENEIQTYR
P13645|K1C10_HUMAN	899.0093	49.44	0.00079	NVQALEIELQSQLALK
P13645|K1C10_HUMAN	516.3004	49.03	0.00076	VLDELTLTK
P13645|K1C10_HUMAN	516.3007	49.38	0.00068	VLDELTLTK
P13645|K1C10_HUMAN	747.3703	47.23	0.00056	SQYEQLAEQNRK
P13645|K1C10_HUMAN	747.3698	47.33	0.00055	SQYEQLAEQNRK
P13645|K1C10_HUMAN	747.37	47.59	0.00052	SQYEQLAEQNRK
P13645|K1C10_HUMAN	617.8422	51.44	0.00048	LKYENEVALR
P13645|K1C10_HUMAN	717.8854	52.36	0.00044	IRLENEIQTYR
P13645|K1C10_HUMAN	717.8873	53.03	0.00032	IRLENEIQTYR
P13645|K1C10_HUMAN	747.3683	49.95	0.0003	SQYEQLAEQNRK
P13645|K1C10_HUMAN	717.8865	54.75	0.00026	IRLENEIQTYR
P13645|K1C10_HUMAN	747.3693	50.75	0.00026	SQYEQLAEQNRK
P13645|K1C10_HUMAN	516.3005	54.07	0.00023	VLDELTLTK
P13645|K1C10_HUMAN	583.2939	50.58	0.00021	LENEIQTYR
P13645|K1C10_HUMAN	583.2934	50.69	0.00019	LENEIQTYR
P13645|K1C10_HUMAN	854.3864	47.18	0.00016	GSLGGGFSSGGFSGGSFSR
P13645|K1C10_HUMAN	516.3015	56.78	0.00015	VLDELTLTK
P13645|K1C10_HUMAN	691.3248	49.32	0.00013	ALEESNYELEGK
P13645|K1C10_HUMAN	747.3698	54.49	0.00011	SQYEQLAEQNRK
P13645|K1C10_HUMAN	717.8854	58.84	9.80E-05	IRLENEIQTYR
P13645|K1C10_HUMAN	516.301	58.61	9.70E-05	VLDELTLTK
P13645|K1C10_HUMAN	747.369	54.58	9.50E-05	SQYEQLAEQNRK
P13645|K1C10_HUMAN	717.8873	58.96	8.30E-05	IRLENEIQTYR
P13645|K1C10_HUMAN	717.8862	61.09	6.00E-05	IRLENEIQTYR
P13645|K1C10_HUMAN	717.8863	61.11	5.90E-05	IRLENEIQTYR
P13645|K1C10_HUMAN	717.8872	60.67	5.80E-05	IRLENEIQTYR

P13645|K1C10_HUMAN	717.8868	61.03	4.70E-05	IRLENEIQTYR
P13645|K1C10_HUMAN	998.9866	59.77	3.90E-05	ELTTEIDNNIEQISSYK
P13645|K1C10_HUMAN	717.8866	61.63	3.80E-05	IRLENEIQTYR
P13645|K1C10_HUMAN	516.3007	62.25	3.50E-05	VLDELTLTK
P13645|K1C10_HUMAN	717.8865	63.73	3.30E-05	IRLENEIQTYR
P13645|K1C10_HUMAN	717.8869	63.58	2.60E-05	IRLENEIQTYR
P13645|K1C10_HUMAN	717.8867	66.08	1.40E-05	IRLENEIQTYR
P13645|K1C10_HUMAN	683.3211	60.73	8.40E-06	SQYEQLAEQNR
P13645|K1C10_HUMAN	899.0112	71.1	6.70E-06	NVQALEIELQSQLALK
P13645|K1C10_HUMAN	691.3261	62.67	6.00E-06	ALEESNYELEGK
P13645|K1C10_HUMAN	899.0078	73.29	4.00E-06	NVQALEIELQSQLALK
P13645|K1C10_HUMAN	854.3855	70.09	8.80E-07	GSLGGGFSSGGFSGGSFSR
P13645|K1C10_HUMAN	854.3869	69.87	7.80E-07	GSLGGGFSSGGFSGGSFSR
P13645|K1C10_HUMAN	998.9867	77.49	6.50E-07	ELTTEIDNNIEQISSYK
P13645|K1C10_HUMAN	683.3211	73.07	4.90E-07	SQYEQLAEQNR
P13645|K1C10_HUMAN	899.0067	82.78	4.80E-07	NVQALEIELQSQLALK
P13645|K1C10_HUMAN	683.3208	73.6	4.80E-07	SQYEQLAEQNR
P13645|K1C10_HUMAN	683.3199	73.16	4.80E-07	SQYEQLAEQNR
P13645|K1C10_HUMAN	998.9868	79.67	4.00E-07	ELTTEIDNNIEQISSYK
P13645|K1C10_HUMAN	899.01	84.3	2.70E-07	NVQALEIELQSQLALK
P13645|K1C10_HUMAN	998.9872	82.78	2.00E-07	ELTTEIDNNIEQISSYK
P13645|K1C10_HUMAN	998.9862	82.81	1.80E-07	ELTTEIDNNIEQISSYK
P13645|K1C10_HUMAN	695.8416	82.72	1.70E-07	QSLEASLAETEGR
P13645|K1C10_HUMAN	683.3209	78.12	1.70E-07	SQYEQLAEQNR
P13645|K1C10_HUMAN	695.8408	82.72	1.50E-07	QSLEASLAETEGR
P13645|K1C10_HUMAN	683.3218	78.16	1.50E-07	SQYEQLAEQNR
P13645|K1C10_HUMAN	854.3879	78.82	1.10E-07	GSLGGGFSSGGFSGGSFSR
P13645|K1C10_H	899.0	88.75	9.60E-08	NVQALEIELQSQLALK

UMAN	095			
P13645|K1C10_HUMAN	691.3269	81.63	8.00E-08	ALEESNYELEGK
P13645|K1C10_HUMAN	691.3259	82.09	6.70E-08	ALEESNYELEGK
P13645|K1C10_HUMAN	691.3258	82.55	6.30E-08	ALEESNYELEGK
P13645|K1C10_HUMAN	691.3264	82.2	5.90E-08	ALEESNYELEGK
P13645|K1C10_HUMAN	691.3264	82.39	5.60E-08	ALEESNYELEGK
P13645|K1C10_HUMAN	998.9881	90.13	3.40E-08	ELTTEIDNNIEQISSYK
P13645|K1C10_HUMAN	854.3876	84.2	3.40E-08	GSLGGGFSSGGFSGGSFSR
P13645|K1C10_HUMAN	998.9866	91.07	2.90E-08	ELTTEIDNNIEQISSYK
P13645|K1C10_HUMAN	691.3262	87.53	2.00E-08	ALEESNYELEGK
P13645|K1C10_HUMAN	691.326	87.35	2.00E-08	ALEESNYELEGK
P13645|K1C10_HUMAN	691.3264	86.92	2.00E-08	ALEESNYELEGK
P13645|K1C10_HUMAN	998.9862	95.46	9.60E-09	ELTTEIDNNIEQISSYK
P13645|K1C10_HUMAN	695.8412	96.26	7.20E-09	QSLEASLAETEGR
P13645|K1C10_HUMAN	854.3882	90.52	7.10E-09	GSLGGGFSSGGFSGGSFSR
P13645|K1C10_HUMAN	998.9874	99.18	4.50E-09	ELTTEIDNNIEQISSYK
P13645|K1C10_HUMAN	998.9865	99.16	4.40E-09	ELTTEIDNNIEQISSYK
P13645|K1C10_HUMAN	998.9863	99.16	4.10E-09	ELTTEIDNNIEQISSYK
P13645|K1C10_HUMAN	695.8412	101.07	2.40E-09	QSLEASLAETEGR
P13645|K1C10_HUMAN	695.8416	101.6	2.20E-09	QSLEASLAETEGR
P13645|K1C10_HUMAN	854.3864	96.01	2.10E-09	GSLGGGFSSGGFSGGSFSR
P13645|K1C10_HUMAN	854.3875	96.17	2.00E-09	GSLGGGFSSGGFSGGSFSR
P13645|K1C10_HUMAN	695.8427	101.66	1.90E-09	QSLEASLAETEGR
P13645|K1C10_HUMAN	695.8408	101.65	1.90E-09	QSLEASLAETEGR
P13645|K1C10_HUMAN	854.3871	96.24	1.90E-09	GSLGGGFSSGGFSGGSFSR
P13645|K1C10_HUMAN	854.388	97.29	1.60E-09	GSLGGGFSSGGFSGGSFSR
P13645|K1C10_HUMAN	854.3871	97.74	1.40E-09	GSLGGGFSSGGFSGGSFSR
P13645|K1C10_HUMAN	854.3872	97.52	1.40E-09	GSLGGGFSSGGFSGGSFSR

P13645|K1C10_HUMAN	854.3864	105.6	2.30E-10	GSLGGGFSSGGFSGGSFSR
P13645|K1C10_HUMAN	854.3865	115.97	2.20E-11	GSLGGGFSSGGFSGGSFSR
P13645|K1C10_HUMAN	854.3873	115.91	2.10E-11	GSLGGGFSSGGFSGGSFSR
P13645|K1C10_HUMAN	854.387	120.47	6.80E-12	GSLGGGFSSGGFSGGSFSR
P13647|K2C5_HUMAN	597.79	41.92	0.00097	YEELQQTAGR
P13647|K2C5_HUMAN	597.789	47.74	0.00023	YEELQQTAGR
P13647|K2C5_HUMAN	597.7896	55.37	3.90E-05	YEELQQTAGR
P14678|RSMB_HUMAN	519.8592	36.48	0.0018	RVLGLVLLR
P14678|RSMB_HUMAN	519.8591	37.05	0.0016	RVLGLVLLR
P14678|RSMB_HUMAN	519.8586	36.94	0.0016	RVLGLVLLR
P14678|RSMB_HUMAN	519.8591	39.84	0.00084	RVLGLVLLR
P14678|RSMB_HUMAN	777.8925	46.34	0.00081	GENLVSMTVEGPPPK
P14678|RSMB_HUMAN	777.893	46.86	0.00069	GENLVSMTVEGPPPK
P14678|RSMB_HUMAN	777.8937	56.07	0.0001	GENLVSMTVEGPPPK
P14678|RSMB_HUMAN	1084.557	60.12	8.10E-05	GENLVSMTVEGPPPKDTGIAR
P14678|RSMB_HUMAN	519.859	50.95	6.50E-05	RVLGLVLLR
P14678|RSMB_HUMAN	777.892	58.02	5.90E-05	GENLVSMTVEGPPPK
P14678|RSMB_HUMAN	777.8933	58.58	5.60E-05	GENLVSMTVEGPPPK
P14678|RSMB_HUMAN	777.8951	58.44	5.60E-05	GENLVSMTVEGPPPK
P14678|RSMB_HUMAN	777.8925	58.69	4.70E-05	GENLVSMTVEGPPPK
P14678|RSMB_HUMAN	777.8934	59.7	4.40E-05	GENLVSMTVEGPPPK
P14678|RSMB_HUMAN	777.8933	67.08	7.90E-06	GENLVSMTVEGPPPK
P14678|RSMB_HUMAN	1084.55	96.71	1.60E-08	GENLVSMTVEGPPPKDTGIAR
P16403|H12_HUMAN	443.7702	45.53	0.0039	KPAAATVTK
P16403|H12_HUMAN	507.8173	49.25	0.0014	KPAAATVTKK
P16403|H12_HUMAN	507.8177	50.27	0.0011	KPAAATVTKK
P16403|H12_HUMAN	507.8174	52.31	0.00068	KPAAATVTKK
P17096|HMGA1_	853.4	52.05	0.0007	KQPPVSPGTALVGSQKEPSEVPTPK

HUMAN	634			
P17096|HMGA1_HUMAN	1118.997	40.74	0.00059	KLEKEEEEGISQESSEEEQ
P17096|HMGA1_HUMAN	1118.998	49.68	7.80E-05	KLEKEEEEGISQESSEEEQ
P17096|HMGA1_HUMAN	1118.999	51.1	5.70E-05	KLEKEEEEGISQESSEEEQ
P17096|HMGA1_HUMAN	1118.998	56.8	1.50E-05	KLEKEEEEGISQESSEEEQ
P17096|HMGA1_HUMAN	1118.998	61.03	5.60E-06	KLEKEEEEGISQESSEEEQ
P17096|HMGA1_HUMAN	1118.998	61.85	4.70E-06	KLEKEEEEGISQESSEEEQ
P17096|HMGA1_HUMAN	1118.998	64.79	2.40E-06	KLEKEEEEGISQESSEEEQ
P17096|HMGA1_HUMAN	1118.996	72.9	3.50E-07	KLEKEEEEGISQESSEEEQ
P17096|HMGA1_HUMAN	1118.996	80.73	5.80E-08	KLEKEEEEGISQESSEEEQ
P19338|NUCL_HUMAN	734.0126	36.85	0.0047	GLSEDTTEETLKESFDGSVR
P19338|NUCL_HUMAN	596.8112	40.04	0.004	IVTDRETGSSK
P19338|NUCL_HUMAN	782.713	40.68	0.0034	EAMEDGEIDGNKVTLDWAKPK
P19338|NUCL_HUMAN	529.3044	44.37	0.003	VTLDWAKPK
P19338|NUCL_HUMAN	734.0118	39	0.0029	GLSEDTTEETLKESFDGSVR
P19338|NUCL_HUMAN	469.2513	41.1	0.0026	TGISDVFAK
P19338|NUCL_HUMAN	469.2516	41.46	0.0024	TGISDVFAK
P19338|NUCL_HUMAN	856.7727	47.94	0.0015	QKVEGTEPTTAFNLFVGNLNFNK
P19338|NUCL_HUMAN	529.3038	47.39	0.0015	VTLDWAKPK
P19338|NUCL_HUMAN	596.8102	43.42	0.0012	IVTDRETGSSK
P19338|NUCL_HUMAN	406.7335	43.58	0.0011	LELQGPR
P19338|NUCL_HUMAN	529.305	49.19	0.001	VTLDWAKPK
P19338|NUCL_HUMAN	529.3035	49.01	0.001	VTLDWAKPK
P19338|NUCL_HUMAN	782.7121	45.84	0.001	EAMEDGEIDGNKVTLDWAKPK
P19338|NUCL_HUMAN	529.3031	49.31	0.00096	VTLDWAKPK
P19338|NUCL_HUMAN	782.7127	47.29	0.00067	EAMEDGEIDGNKVTLDWAKPK
P19338|NUCL_HUMAN	529.3036	50.95	0.00065	VTLDWAKPK
P19338|NUCL_HUMAN	529.304	51.79	0.00054	VTLDWAKPK

P19338|NUCL_HUMAN	782.7121	49.45	0.00044	EAMEDGEIDGNKVTLDWAKPK
P19338|NUCL_HUMAN	734.0121	47.24	0.00043	GLSEDTTEETLKESFDGSVR
P19338|NUCL_HUMAN	734.0133	47.3	0.00041	GLSEDTTEETLKESFDGSVR
P19338|NUCL_HUMAN	797.8738	45.72	0.00039	GYAFIEFASFEDAK
P19338|NUCL_HUMAN	1373.816	39.1	0.00032	KEDSDEEEDDDSEEDEEDDEDEDEDEDEIEPAAMK
P19338|NUCL_HUMAN	782.7119	52.53	0.00021	EAMEDGEIDGNKVTLDWAKPK
P19338|NUCL_HUMAN	734.0111	49.92	0.00021	GLSEDTTEETLKESFDGSVR
P19338|NUCL_HUMAN	782.7118	52.68	0.0002	EAMEDGEIDGNKVTLDWAKPK
P19338|NUCL_HUMAN	699.3231	47.69	0.00016	TEADAEKTFEEK
P19338|NUCL_HUMAN	782.7128	59	4.80E-05	EAMEDGEIDGNKVTLDWAKPK
P19338|NUCL_HUMAN	797.8721	54.52	4.20E-05	GYAFIEFASFEDAK
P19338|NUCL_HUMAN	699.3239	52.93	4.20E-05	TEADAEKTFEEK
P19338|NUCL_HUMAN	699.3236	54.05	3.70E-05	TEADAEKTFEEK
P19338|NUCL_HUMAN	1251.133	63.56	3.60E-05	TLVLSNLSYSATEETLQEVFEK
P19338|NUCL_HUMAN	699.3235	54.7	3.20E-05	TEADAEKTFEEK
P19338|NUCL_HUMAN	699.322	54.7	2.40E-05	TEADAEKTFEEK
P19338|NUCL_HUMAN	699.324	56.23	2.00E-05	TEADAEKTFEEK
P19338|NUCL_HUMAN	654.2725	48.79	1.30E-05	EAMEDGEIDGNK
P19338|NUCL_HUMAN	654.2735	48.72	1.30E-05	EAMEDGEIDGNK
P19338|NUCL_HUMAN	654.2722	49.13	1.20E-05	EAMEDGEIDGNK
P19338|NUCL_HUMAN	824.8695	64.82	1.80E-06	FGYVDFESAEDLEK
P19338|NUCL_HUMAN	824.8712	65.8	1.70E-06	FGYVDFESAEDLEK
P19338|NUCL_HUMAN	824.8707	66.24	1.50E-06	FGYVDFESAEDLEK
P19338|NUCL_HUMAN	781.3417	64.35	1.20E-06	GFGFVDFNSEEDAK
P19338|NUCL_HUMAN	781.3419	64.16	1.20E-06	GFGFVDFNSEEDAK
P19338|NUCL_HUMAN	797.8723	70.68	1.10E-06	GYAFIEFASFEDAK
P19338|NUCL_HUMAN	781.3414	64.31	9.80E-07	GFGFVDFNSEEDAK
P19338|NUCL_HU	996.4	78.35	8.90E-07	VTQDELKEVFEDAAEIR

MAN	973			
P19338|NUCL_HUMAN	781.342	66.21	7.70E-07	GFGFVDFNSEEDAK
P19338|NUCL_HUMAN	996.4972	79.21	7.30E-07	VTQDELKEVFEDAAEIR
P19338|NUCL_HUMAN	797.8715	72.85	6.30E-07	GYAFIEFASFEDAK
P19338|NUCL_HUMAN	781.3418	67.06	6.30E-07	GFGFVDFNSEEDAK
P19338|NUCL_HUMAN	797.8721	73.22	5.70E-07	GYAFIEFASFEDAK
P19338|NUCL_HUMAN	824.8696	70.08	5.30E-07	FGYVDFESAEDLEK
P19338|NUCL_HUMAN	1156.577	81.44	5.20E-07	VEGTEPTTAFNLFVGNLNFNK
P19338|NUCL_HUMAN	781.3419	68.34	4.60E-07	GFGFVDFNSEEDAK
P19338|NUCL_HUMAN	1251.131	82.6	4.40E-07	TLVLSNLSYSATEETLQEVFEK
P19338|NUCL_HUMAN	781.3411	67.91	4.40E-07	GFGFVDFNSEEDAK
P19338|NUCL_HUMAN	996.4982	81.4	3.80E-07	VTQDELKEVFEDAAEIR
P19338|NUCL_HUMAN	824.87	71.99	3.70E-07	FGYVDFESAEDLEK
P19338|NUCL_HUMAN	781.3412	68.69	3.70E-07	GFGFVDFNSEEDAK
P19338|NUCL_HUMAN	782.7131	80.5	3.50E-07	EAMEDGEIDGNKVTLDWAKPK
P19338|NUCL_HUMAN	797.8729	77.44	2.70E-07	GYAFIEFASFEDAK
P19338|NUCL_HUMAN	824.87	74.21	2.20E-07	FGYVDFESAEDLEK
P19338|NUCL_HUMAN	824.8709	74.88	2.10E-07	FGYVDFESAEDLEK
P19338|NUCL_HUMAN	797.8724	78.67	1.90E-07	GYAFIEFASFEDAK
P19338|NUCL_HUMAN	1156.577	86.22	1.70E-07	VEGTEPTTAFNLFVGNLNFNK
P19338|NUCL_HUMAN	996.4978	87.27	1.10E-07	VTQDELKEVFEDAAEIR
P19338|NUCL_HUMAN	797.8727	81.02	1.10E-07	GYAFIEFASFEDAK
P19338|NUCL_HUMAN	1100.515	83.62	9.90E-08	GLSEDTTEETLKESFDGSVR
P19338|NUCL_HUMAN	996.4977	87.95	9.40E-08	VTQDELKEVFEDAAEIR
P19338|NUCL_HUMAN	1156.576	89.61	8.30E-08	VEGTEPTTAFNLFVGNLNFNK
P19338|NUCL_HUMAN	996.4991	90.35	5.40E-08	VTQDELKEVFEDAAEIR
P19338|NUCL_HUMAN	797.8727	84.96	4.60E-08	GYAFIEFASFEDAK
P19338|NUCL_HUMAN	797.8718	84.61	4.30E-08	GYAFIEFASFEDAK

P19338|NUCL_HUMAN	824.8705	82.99	3.10E-08	FGYVDFESAEDLEK
P19338|NUCL_HUMAN	797.8738	87.59	2.50E-08	GYAFIEFASFEDAK
P19338|NUCL_HUMAN	996.498	95.09	1.80E-08	VTQDELKEVFEDAAEIR
P19338|NUCL_HUMAN	1100.515	91.26	1.70E-08	GLSEDTTEETLKESFDGSVR
P19338|NUCL_HUMAN	824.8712	85.81	1.70E-08	FGYVDFESAEDLEK
P19338|NUCL_HUMAN	1156.578	96.84	1.60E-08	VEGTEPTTAFNLFVGNLNFNK
P19338|NUCL_HUMAN	1100.515	91.61	1.60E-08	GLSEDTTEETLKESFDGSVR
P19338|NUCL_HUMAN	1156.576	97.19	1.50E-08	VEGTEPTTAFNLFVGNLNFNK
P19338|NUCL_HUMAN	1156.577	97.51	1.30E-08	VEGTEPTTAFNLFVGNLNFNK
P19338|NUCL_HUMAN	797.8733	91.25	1.10E-08	GYAFIEFASFEDAK
P19338|NUCL_HUMAN	797.8716	91.12	9.00E-09	GYAFIEFASFEDAK
P19338|NUCL_HUMAN	1251.134	99.87	8.60E-09	TLVLSNLSYSATEETLQEVFEK
P19338|NUCL_HUMAN	996.4987	99.5	6.10E-09	VTQDELKEVFEDAAEIR
P19338|NUCL_HUMAN	824.8709	90.34	5.90E-09	FGYVDFESAEDLEK
P19338|NUCL_HUMAN	1100.516	96.21	5.40E-09	GLSEDTTEETLKESFDGSVR
P19338|NUCL_HUMAN	1251.134	102.7	4.70E-09	TLVLSNLSYSATEETLQEVFEK
P19338|NUCL_HUMAN	1251.134	102.82	4.50E-09	TLVLSNLSYSATEETLQEVFEK
P19338|NUCL_HUMAN	1251.134	103.69	3.60E-09	TLVLSNLSYSATEETLQEVFEK
P19338|NUCL_HUMAN	1251.134	103.8	3.50E-09	TLVLSNLSYSATEETLQEVFEK
P19338|NUCL_HUMAN	1251.133	105.81	2.10E-09	TLVLSNLSYSATEETLQEVFEK
P19338|NUCL_HUMAN	1251.133	108.8	1.10E-09	TLVLSNLSYSATEETLQEVFEK
P19338|NUCL_HUMAN	1100.514	103.55	1.00E-09	GLSEDTTEETLKESFDGSVR
P19338|NUCL_HUMAN	1100.514	108.59	3.10E-10	GLSEDTTEETLKESFDGSVR
P19338|NUCL_HUMAN	996.4954	118.22	8.70E-11	VTQDELKEVFEDAAEIR
P19338|NUCL_HUMAN	1251.133	121.53	5.70E-11	TLVLSNLSYSATEETLQEVFEK
P19338|NUCL_HUMAN	1100.515	121.18	1.70E-11	GLSEDTTEETLKESFDGSVR
P19338|NUCL_HUMAN	1100.514	121.44	1.60E-11	GLSEDTTEETLKESFDGSVR
P20073|ANXA7_H	845.9	65.68	1.30E-05	GFGTDEQAIVDVVANR

UMAN	21			
P20073|ANXA7_HUMAN	845.9202	75.67	1.20E-06	GFGTDEQAIVDVVANR
P20073|ANXA7_HUMAN	845.9213	89.33	5.80E-08	GFGTDEQAIVDVVANR
P20700|LMNB1_HUMAN	723.8972	42	0.0049	IESLSSQLSNLQK
P20700|LMNB1_HUMAN	1054.502	44.73	0.001	DQMQQQLNDYEQLLDVK
P20700|LMNB1_HUMAN	723.8922	56.85	0.00016	IESLSSQLSNLQK
P20700|LMNB1_HUMAN	1137.857	82.93	8.10E-08	TTIPEEEEEEEEAAGVVVEEELFHQQGTPR
P20700|LMNB1_HUMAN	1137.859	84.87	5.60E-08	TTIPEEEEEEEEAAGVVVEEELFHQQGTPR
P22087|FBRL_HUMAN	536.2993	41.75	0.0029	NGGHFVISIK
P22087|FBRL_HUMAN	767.4296	46.75	0.0016	DHAVVVGVYRPPPK
P22087|FBRL_HUMAN	767.4271	47.52	0.0013	DHAVVVGVYRPPPK
P22087|FBRL_HUMAN	767.4291	49.93	0.00072	DHAVVVGVYRPPPK
P22087|FBRL_HUMAN	767.4295	50.45	0.00063	DHAVVVGVYRPPPK
P22087|FBRL_HUMAN	936.554	51.05	0.00046	LAAAILGGVDQIHIKPGAK
P22087|FBRL_HUMAN	767.4293	57.71	0.00012	DHAVVVGVYRPPPK
P22087|FBRL_HUMAN	767.4286	60.03	7.90E-05	DHAVVVGVYRPPPK
P22087|FBRL_HUMAN	767.428	60.73	6.60E-05	DHAVVVGVYRPPPK
P22087|FBRL_HUMAN	767.4284	62.58	4.40E-05	DHAVVVGVYRPPPK
P22087|FBRL_HUMAN	767.4296	63.23	3.50E-05	DHAVVVGVYRPPPK
P22087|FBRL_HUMAN	936.5557	66.12	1.40E-05	LAAAILGGVDQIHIKPGAK
P22087|FBRL_HUMAN	755.8702	63.73	9.50E-06	VSISEGDDKIEYR
P22087|FBRL_HUMAN	755.8714	64.6	8.70E-06	VSISEGDDKIEYR
P22087|FBRL_HUMAN	755.8716	64.74	8.20E-06	VSISEGDDKIEYR
P22087|FBRL_HUMAN	755.8725	67.17	4.60E-06	VSISEGDDKIEYR
P22087|FBRL_HUMAN	936.5584	76.71	9.80E-07	LAAAILGGVDQIHIKPGAK
P22087|FBRL_HUMAN	936.5546	80	6.00E-07	LAAAILGGVDQIHIKPGAK
P22087|FBRL_HUMAN	755.8722	76.15	5.80E-07	VSISEGDDKIEYR
P22087|FBRL_HUMAN	755.8729	78.13	4.10E-07	VSISEGDDKIEYR

P22087|FBRL_HUMAN	755.8712	77.76	4.00E-07	VSISEGDDKIEYR
P22087|FBRL_HUMAN	936.5535	83.6	2.70E-07	LAAAILGGVDQIHIKPGAK
P22087|FBRL_HUMAN	936.5555	89.48	6.50E-08	LAAAILGGVDQIHIKPGAK
P22087|FBRL_HUMAN	936.5542	95.95	1.40E-08	LAAAILGGVDQIHIKPGAK
P22087|FBRL_HUMAN	936.5559	97.91	9.50E-09	LAAAILGGVDQIHIKPGAK
P22626|ROA2_HUMAN	669.8522	39.13	0.005	EESGKPGAHVTVK
P22626|ROA2_HUMAN	544.2436	27.96	0.0047	NYYEQWGK
P22626|ROA2_HUMAN	627.3246	41.54	0.0046	LFVGGIKEDTEEHHLR
P22626|ROA2_HUMAN	544.2432	28.35	0.0045	NYYEQWGK
P22626|ROA2_HUMAN	627.3245	41.99	0.0041	LFVGGIKEDTEEHHLR
P22626|ROA2_HUMAN	431.2806	39.07	0.004	KLFVGGIK
P22626|ROA2_HUMAN	1139.08	43.31	0.0039	GFGFVTFDDHDPVDKIVLQK
P22626|ROA2_HUMAN	627.3255	42.12	0.0038	LFVGGIKEDTEEHHLR
P22626|ROA2_HUMAN	544.2443	28.91	0.0038	NYYEQWGK
P22626|ROA2_HUMAN	1098.978	30.75	0.0035	EDTEEHHLRDYFEEYGK
P22626|ROA2_HUMAN	1004.53	44.5	0.0033	KLFVGGIKEDTEEHHLR
P22626|ROA2_HUMAN	431.2802	39.92	0.0033	KLFVGGIK
P22626|ROA2_HUMAN	669.8521	41.15	0.0032	EESGKPGAHVTVK
P22626|ROA2_HUMAN	1110.538	41.04	0.0031	DYFEEYGKIDTIEIITDR
P22626|ROA2_HUMAN	544.2441	29.84	0.0031	NYYEQWGK
P22626|ROA2_HUMAN	689.32	35.63	0.003	GGGGNFGPGPGSNFR
P22626|ROA2_HUMAN	689.3163	35.2	0.0029	GGGGNFGPGPGSNFR
P22626|ROA2_HUMAN	670.0231	45.74	0.0025	KLFVGGIKEDTEEHHLR
P22626|ROA2_HUMAN	899.9611	44.03	0.0024	LFIGGLSFETTEESLR
P22626|ROA2_HUMAN	627.325	44.39	0.0023	LFVGGIKEDTEEHHLR
P22626|ROA2_HUMAN	669.8522	42.47	0.0023	EESGKPGAHVTVK
P22626|ROA2_HUMAN	759.7206	45.78	0.0022	GFGFVTFDDHDPVDKIVLQK
P22626|ROA2_HUMAN	899.9	44.8	0.0021	LFIGGLSFETTEESLR

MAN	631			
P22626|ROA2_HUMAN	1098.976	32.5	0.0021	EDTEEHHLRDYFEEYGK
P22626|ROA2_HUMAN	544.2433	31.51	0.0021	NYYEQWGK
P22626|ROA2_HUMAN	1004.534	46.51	0.002	KLFVGGIKEDTEEHHLR
P22626|ROA2_HUMAN	627.3247	45.07	0.002	LFVGGIKEDTEEHHLR
P22626|ROA2_HUMAN	1110.534	43.04	0.0019	DYFEEYGKIDTIEIITDR
P22626|ROA2_HUMAN	899.9642	45.98	0.0017	LFIGGLSFETTEESLR
P22626|ROA2_HUMAN	627.3243	45.71	0.0017	LFVGGIKEDTEEHHLR
P22626|ROA2_HUMAN	627.3244	46.17	0.0016	LFVGGIKEDTEEHHLR
P22626|ROA2_HUMAN	670.0228	47.8	0.0015	KLFVGGIKEDTEEHHLR
P22626|ROA2_HUMAN	689.3167	38.54	0.0015	GGGGNFGPGPGSNFR
P22626|ROA2_HUMAN	1098.974	34.12	0.0013	EDTEEHHLRDYFEEYGK
P22626|ROA2_HUMAN	1004.531	49.08	0.0012	KLFVGGIKEDTEEHHLR
P22626|ROA2_HUMAN	669.852	45.49	0.0012	EESGKPGAHVTVK
P22626|ROA2_HUMAN	1098.976	35.34	0.0011	EDTEEHHLRDYFEEYGK
P22626|ROA2_HUMAN	544.2437	34.12	0.0011	NYYEQWGK
P22626|ROA2_HUMAN	899.9614	48.13	0.00096	LFIGGLSFETTEESLR
P22626|ROA2_HUMAN	431.2807	46.66	0.0007	KLFVGGIK
P22626|ROA2_HUMAN	689.32	42.01	0.0007	GGGGNFGPGPGSNFR
P22626|ROA2_HUMAN	627.3254	49.85	0.00064	LFVGGIKEDTEEHHLR
P22626|ROA2_HUMAN	705.8457	44.97	0.00064	YHTINGHNAEVR
P22626|ROA2_HUMAN	707.5878	48.1	0.00053	GFGFVTFSSMAEVDAAMAARPHSIDGR
P22626|ROA2_HUMAN	705.8463	45.88	0.00053	YHTINGHNAEVR
P22626|ROA2_HUMAN	940.4836	51.14	0.00051	LFVGGIKEDTEEHHLR
P22626|ROA2_HUMAN	431.281	48.3	0.00051	KLFVGGIK
P22626|ROA2_HUMAN	1139.077	52.57	0.00049	GFGFVTFDDHDPVDKIVLQK
P22626|ROA2_HUMAN	1004.534	52.8	0.00048	KLFVGGIKEDTEEHHLR
P22626|ROA2_HUMAN	1004.532	52.42	0.00048	KLFVGGIKEDTEEHHLR

P22626|ROA2_HUMAN	689.3163	43.07	0.00047	GGGGNFGPGPGSNFR
P22626|ROA2_HUMAN	1110.539	49.44	0.00044	DYFEEYGKIDTIEIITDR
P22626|ROA2_HUMAN	431.2805	48.74	0.00044	KLFVGGIK
P22626|ROA2_HUMAN	689.3166	43.84	0.00043	GGGGNFGPGPGSNFR
P22626|ROA2_HUMAN	544.2437	38.47	0.00042	NYYEQWGK
P22626|ROA2_HUMAN	507.2239	38.13	0.00041	GGNFGFGDSR
P22626|ROA2_HUMAN	669.8522	50.19	0.00039	EESGKPGAHVTVK
P22626|ROA2_HUMAN	1095.453	35.37	0.00036	NMGGPYGGGNYGPGGSGGSGGYGGR
P22626|ROA2_HUMAN	899.9619	52.89	0.00031	LFIGGLSFETTEESLR
P22626|ROA2_HUMAN	705.8453	47.96	0.00031	YHTINGHNAEVR
P22626|ROA2_HUMAN	627.3246	53.46	0.0003	LFVGGIKEDTEEHHLR
P22626|ROA2_HUMAN	899.9618	53.41	0.00028	LFIGGLSFETTEESLR
P22626|ROA2_HUMAN	1098.98	41.73	0.00028	EDTEEHHLRDYFEEYGK
P22626|ROA2_HUMAN	940.4835	54.62	0.00023	LFVGGIKEDTEEHHLR
P22626|ROA2_HUMAN	627.3251	54.76	0.00022	LFVGGIKEDTEEHHLR
P22626|ROA2_HUMAN	1095.456	38.59	0.00022	NMGGPYGGGNYGPGGSGGSGGYGGR
P22626|ROA2_HUMAN	1110.536	52.72	0.0002	DYFEEYGKIDTIEIITDR
P22626|ROA2_HUMAN	705.8462	50	0.0002	YHTINGHNAEVR
P22626|ROA2_HUMAN	1110.534	52.96	0.00019	DYFEEYGKIDTIEIITDR
P22626|ROA2_HUMAN	1004.532	56.59	0.00018	KLFVGGIKEDTEEHHLR
P22626|ROA2_HUMAN	940.4844	55.78	0.00017	LFVGGIKEDTEEHHLR
P22626|ROA2_HUMAN	627.3253	55.77	0.00017	LFVGGIKEDTEEHHLR
P22626|ROA2_HUMAN	627.3248	56.14	0.00016	LFVGGIKEDTEEHHLR
P22626|ROA2_HUMAN	627.3251	56.43	0.00015	LFVGGIKEDTEEHHLR
P22626|ROA2_HUMAN	940.4847	56.54	0.00014	LFVGGIKEDTEEHHLR
P22626|ROA2_HUMAN	1139.077	58.33	0.00012	GFGFVTFDDHDPVDKIVLQK
P22626|ROA2_HUMAN	940.4842	57.15	0.00012	LFVGGIKEDTEEHHLR
P22626|ROA2_HUMAN	899.9	57.07	0.00012	LFIGGLSFETTEESLR

MAN	62			
P22626|ROA2_HUMAN	899.9644	57.72	0.00011	LFIGGLSFETTEESLR
P22626|ROA2_HUMAN	627.3254	57.52	0.00011	LFVGGIKEDTEEHHLR
P22626|ROA2_HUMAN	611.2789	46.6	0.00011	QEMQEVQSSR
P22626|ROA2_HUMAN	507.2236	43.73	0.00011	GGNFGFGDSR
P22626|ROA2_HUMAN	611.2781	47.53	9.30E-05	QEMQEVQSSR
P22626|ROA2_HUMAN	1004.531	59.82	9.20E-05	KLFVGGIKEDTEEHHLR
P22626|ROA2_HUMAN	617.9592	53.47	9.10E-05	RGFGFVTFDDHDPVDK
P22626|ROA2_HUMAN	1248.019	43.27	8.90E-05	GFGDGYNGYGGGPGGGNFGGSPGYGGGR
P22626|ROA2_HUMAN	1110.536	56.78	7.70E-05	DYFEEYGKIDTIEIITDR
P22626|ROA2_HUMAN	594.8251	61.37	6.90E-05	IDTIEIITDR
P22626|ROA2_HUMAN	1004.533	61.56	6.60E-05	KLFVGGIKEDTEEHHLR
P22626|ROA2_HUMAN	611.2778	49.34	6.40E-05	QEMQEVQSSR
P22626|ROA2_HUMAN	689.3165	52.28	5.70E-05	GGGGNFGPGPGSNFR
P22626|ROA2_HUMAN	1095.457	45.04	5.20E-05	NMGGPYGGGNYGPGGSGGSGGYGGR
P22626|ROA2_HUMAN	705.8462	56.23	4.90E-05	YHTINGHNAEVR
P22626|ROA2_HUMAN	899.9638	61.53	4.80E-05	LFIGGLSFETTEESLR
P22626|ROA2_HUMAN	1004.535	64.47	3.50E-05	KLFVGGIKEDTEEHHLR
P22626|ROA2_HUMAN	1004.533	64.23	3.30E-05	KLFVGGIKEDTEEHHLR
P22626|ROA2_HUMAN	899.9606	62.82	3.20E-05	LFIGGLSFETTEESLR
P22626|ROA2_HUMAN	1110.535	60.75	3.20E-05	DYFEEYGKIDTIEIITDR
P22626|ROA2_HUMAN	848.3832	53.11	3.20E-05	GFGFVTFDDHDPVDK
P22626|ROA2_HUMAN	899.9653	63.24	3.10E-05	LFIGGLSFETTEESLR
P22626|ROA2_HUMAN	705.8458	58.37	3.00E-05	YHTINGHNAEVR
P22626|ROA2_HUMAN	899.9622	63.12	2.90E-05	LFIGGLSFETTEESLR
P22626|ROA2_HUMAN	899.9644	63.64	2.80E-05	LFIGGLSFETTEESLR
P22626|ROA2_HUMAN	940.4854	63.56	2.80E-05	LFVGGIKEDTEEHHLR
P22626|ROA2_HUMAN	611.2786	52.51	2.80E-05	QEMQEVQSSR

P22626|ROA2_HUMAN	705.8463	58.79	2.70E-05	YHTINGHNAEVR
P22626|ROA2_HUMAN	940.484	63.99	2.60E-05	LFVGGIKEDTEEHHLR
P22626|ROA2_HUMAN	1110.543	62.63	2.60E-05	DYFEEYGKIDTIEIITDR
P22626|ROA2_HUMAN	594.8251	65.73	2.50E-05	IDTIEIITDR
P22626|ROA2_HUMAN	940.4836	64.32	2.50E-05	LFVGGIKEDTEEHHLR
P22626|ROA2_HUMAN	1004.532	65.56	2.40E-05	KLFVGGIKEDTEEHHLR
P22626|ROA2_HUMAN	899.9625	63.67	2.40E-05	LFIGGLSFETTEESLR
P22626|ROA2_HUMAN	940.4846	64.53	2.20E-05	LFVGGIKEDTEEHHLR
P22626|ROA2_HUMAN	899.9644	65.02	2.10E-05	LFIGGLSFETTEESLR
P22626|ROA2_HUMAN	940.4847	64.8	2.10E-05	LFVGGIKEDTEEHHLR
P22626|ROA2_HUMAN	940.4851	64.7	2.10E-05	LFVGGIKEDTEEHHLR
P22626|ROA2_HUMAN	1110.536	62.53	2.10E-05	DYFEEYGKIDTIEIITDR
P22626|ROA2_HUMAN	940.4835	65.1	2.00E-05	LFVGGIKEDTEEHHLR
P22626|ROA2_HUMAN	899.9668	65.94	1.80E-05	LFIGGLSFETTEESLR
P22626|ROA2_HUMAN	964.0098	66.83	1.70E-05	KLFIGGLSFETTEESLR
P22626|ROA2_HUMAN	1095.455	49.43	1.70E-05	NMGGPYGGGNYGPGGSGGSGGYGGR
P22626|ROA2_HUMAN	611.2791	55.94	1.60E-05	QEMQEVQSSR
P22626|ROA2_HUMAN	611.2776	55.93	1.50E-05	QEMQEVQSSR
P22626|ROA2_HUMAN	940.483	66.64	1.40E-05	LFVGGIKEDTEEHHLR
P22626|ROA2_HUMAN	899.9629	66.45	1.40E-05	LFIGGLSFETTEESLR
P22626|ROA2_HUMAN	940.4855	66.76	1.30E-05	LFVGGIKEDTEEHHLR
P22626|ROA2_HUMAN	611.2784	55.9	1.30E-05	QEMQEVQSSR
P22626|ROA2_HUMAN	594.8253	68.25	1.20E-05	IDTIEIITDR
P22626|ROA2_HUMAN	940.4834	67.35	1.20E-05	LFVGGIKEDTEEHHLR
P22626|ROA2_HUMAN	594.8249	69.53	1.10E-05	IDTIEIITDR
P22626|ROA2_HUMAN	1004.532	69.12	1.10E-05	KLFVGGIKEDTEEHHLR
P22626|ROA2_HUMAN	940.4851	67.84	1.00E-05	LFVGGIKEDTEEHHLR
P22626|ROA2_HUMAN	1004.	69.41	9.80E-06	KLFVGGIKEDTEEHHLR

MAN	532			
P22626|ROA2_HUMAN	899.9615	68.29	9.20E-06	LFIGGLSFETTEESLR
P22626|ROA2_HUMAN	940.4843	68.5	8.90E-06	LFVGGIKEDTEEHHLR
P22626|ROA2_HUMAN	705.8453	63.69	8.30E-06	YHTINGHNAEVR
P22626|ROA2_HUMAN	899.9613	68.97	7.90E-06	LFIGGLSFETTEESLR
P22626|ROA2_HUMAN	964.0117	70.75	7.50E-06	KLFIGGLSFETTEESLR
P22626|ROA2_HUMAN	940.4843	69.55	7.00E-06	LFVGGIKEDTEEHHLR
P22626|ROA2_HUMAN	964.01	70.56	6.90E-06	KLFIGGLSFETTEESLR
P22626|ROA2_HUMAN	899.9644	69.9	6.70E-06	LFIGGLSFETTEESLR
P22626|ROA2_HUMAN	1110.539	68.17	6.50E-06	DYFEEYGKIDTIEIITDR
P22626|ROA2_HUMAN	899.9639	70.55	6.30E-06	LFIGGLSFETTEESLR
P22626|ROA2_HUMAN	1004.533	71.98	5.90E-06	KLFVGGIKEDTEEHHLR
P22626|ROA2_HUMAN	1004.53	72.39	5.60E-06	KLFVGGIKEDTEEHHLR
P22626|ROA2_HUMAN	848.3842	61.86	5.40E-06	GFGFVTFDDHDPVDK
P22626|ROA2_HUMAN	611.2782	59.77	5.40E-06	QEMQEVQSSR
P22626|ROA2_HUMAN	899.9615	70.68	5.30E-06	LFIGGLSFETTEESLR
P22626|ROA2_HUMAN	940.4835	70.98	5.10E-06	LFVGGIKEDTEEHHLR
P22626|ROA2_HUMAN	899.9683	72.5	3.80E-06	LFIGGLSFETTEESLR
P22626|ROA2_HUMAN	964.0099	73.48	3.50E-06	KLFIGGLSFETTEESLR
P22626|ROA2_HUMAN	1004.532	74.55	3.40E-06	KLFVGGIKEDTEEHHLR
P22626|ROA2_HUMAN	899.9614	72.75	3.30E-06	LFIGGLSFETTEESLR
P22626|ROA2_HUMAN	848.384	63.98	3.30E-06	GFGFVTFDDHDPVDK
P22626|ROA2_HUMAN	594.825	75.88	2.50E-06	IDTIEIITDR
P22626|ROA2_HUMAN	594.825	76.01	2.40E-06	IDTIEIITDR
P22626|ROA2_HUMAN	899.9623	73.79	2.40E-06	LFIGGLSFETTEESLR
P22626|ROA2_HUMAN	940.4872	75.93	1.90E-06	LFVGGIKEDTEEHHLR
P22626|ROA2_HUMAN	899.9607	75.29	1.80E-06	LFIGGLSFETTEESLR
P22626|ROA2_HUMAN	848.3841	66.74	1.80E-06	GFGFVTFDDHDPVDK

P22626|ROA2_HUMAN	899.9615	75.95	1.60E-06	LFIGGLSFETTEESLR
P22626|ROA2_HUMAN	940.4852	76.22	1.50E-06	LFVGGIKEDTEEHHLR
P22626|ROA2_HUMAN	899.9619	76.19	1.50E-06	LFIGGLSFETTEESLR
P22626|ROA2_HUMAN	1110.537	74.01	1.50E-06	DYFEEYGKIDTIEIITDR
P22626|ROA2_HUMAN	940.4838	77	1.30E-06	LFVGGIKEDTEEHHLR
P22626|ROA2_HUMAN	1004.532	79.07	1.10E-06	KLFVGGIKEDTEEHHLR
P22626|ROA2_HUMAN	1110.537	75.29	1.10E-06	DYFEEYGKIDTIEIITDR
P22626|ROA2_HUMAN	899.9641	78.08	1.00E-06	LFIGGLSFETTEESLR
P22626|ROA2_HUMAN	899.9664	78.48	9.70E-07	LFIGGLSFETTEESLR
P22626|ROA2_HUMAN	899.963	78.36	9.10E-07	LFIGGLSFETTEESLR
P22626|ROA2_HUMAN	940.486	78.83	8.50E-07	LFVGGIKEDTEEHHLR
P22626|ROA2_HUMAN	1004.53	80.49	8.30E-07	KLFVGGIKEDTEEHHLR
P22626|ROA2_HUMAN	1004.53	80.38	8.00E-07	KLFVGGIKEDTEEHHLR
P22626|ROA2_HUMAN	899.9626	78.91	7.90E-07	LFIGGLSFETTEESLR
P22626|ROA2_HUMAN	899.9633	78.99	7.80E-07	LFIGGLSFETTEESLR
P22626|ROA2_HUMAN	899.9635	79.09	7.70E-07	LFIGGLSFETTEESLR
P22626|ROA2_HUMAN	899.9672	79.15	7.60E-07	LFIGGLSFETTEESLR
P22626|ROA2_HUMAN	594.8249	81.02	7.50E-07	IDTIEIITDR
P22626|ROA2_HUMAN	1095.455	63.01	7.50E-07	NMGGPYGGGNYGPGGSGGSGGYGGR
P22626|ROA2_HUMAN	940.485	79.33	7.40E-07	LFVGGIKEDTEEHHLR
P22626|ROA2_HUMAN	940.4855	79.5	7.10E-07	LFVGGIKEDTEEHHLR
P22626|ROA2_HUMAN	899.9618	79.46	6.90E-07	LFIGGLSFETTEESLR
P22626|ROA2_HUMAN	1004.531	81.67	6.60E-07	KLFVGGIKEDTEEHHLR
P22626|ROA2_HUMAN	848.384	71.46	5.90E-07	GFGFVTFDDHDPVDK
P22626|ROA2_HUMAN	940.4849	80.42	5.70E-07	LFVGGIKEDTEEHHLR
P22626|ROA2_HUMAN	964.0103	81.73	4.90E-07	KLFIGGLSFETTEESLR
P22626|ROA2_HUMAN	848.3842	73.41	3.80E-07	GFGFVTFDDHDPVDK
P22626|ROA2_HU	594.8	83.58	3.70E-07	IDTIEIITDR

MAN	243			
P22626|ROA2_HUMAN	1110.537	80.36	3.40E-07	DYFEEYGKIDTIEIITDR
P22626|ROA2_HUMAN	899.9628	82.92	3.10E-07	LFIGGLSFETTEESLR
P22626|ROA2_HUMAN	899.9618	83.18	2.90E-07	LFIGGLSFETTEESLR
P22626|ROA2_HUMAN	848.3831	73.71	2.90E-07	GFGFVTFDDHDPVDK
P22626|ROA2_HUMAN	594.8252	84.57	2.80E-07	IDTIEIITDR
P22626|ROA2_HUMAN	899.9623	83.18	2.70E-07	LFIGGLSFETTEESLR
P22626|ROA2_HUMAN	1004.534	84.92	2.60E-07	KLFVGGIKEDTEEHHLR
P22626|ROA2_HUMAN	899.9614	83.98	2.50E-07	LFIGGLSFETTEESLR
P22626|ROA2_HUMAN	1004.53	85.92	2.30E-07	KLFVGGIKEDTEEHHLR
P22626|ROA2_HUMAN	899.9621	84.24	2.30E-07	LFIGGLSFETTEESLR
P22626|ROA2_HUMAN	1110.537	82.23	2.30E-07	DYFEEYGKIDTIEIITDR
P22626|ROA2_HUMAN	964.0111	85.92	2.20E-07	KLFIGGLSFETTEESLR
P22626|ROA2_HUMAN	1095.455	68.24	2.20E-07	NMGGPYGGGNYGPGGSGGSGGYGGR
P22626|ROA2_HUMAN	899.9626	84.85	2.00E-07	LFIGGLSFETTEESLR
P22626|ROA2_HUMAN	899.9623	85.73	1.50E-07	LFIGGLSFETTEESLR
P22626|ROA2_HUMAN	940.487	87.78	1.20E-07	LFVGGIKEDTEEHHLR
P22626|ROA2_HUMAN	1004.536	89.78	9.30E-08	KLFVGGIKEDTEEHHLR
P22626|ROA2_HUMAN	1095.453	71.57	8.70E-08	NMGGPYGGGNYGPGGSGGSGGYGGR
P22626|ROA2_HUMAN	964.0097	90.05	7.50E-08	KLFIGGLSFETTEESLR
P22626|ROA2_HUMAN	964.0101	90.53	6.50E-08	KLFIGGLSFETTEESLR
P22626|ROA2_HUMAN	1004.533	92.35	5.50E-08	KLFVGGIKEDTEEHHLR
P22626|ROA2_HUMAN	964.0088	91.89	4.90E-08	KLFIGGLSFETTEESLR
P22626|ROA2_HUMAN	899.9626	91.06	4.80E-08	LFIGGLSFETTEESLR
P22626|ROA2_HUMAN	899.9624	92	3.60E-08	LFIGGLSFETTEESLR
P22626|ROA2_HUMAN	1110.538	90.88	3.20E-08	DYFEEYGKIDTIEIITDR
P22626|ROA2_HUMAN	899.9615	93.02	3.10E-08	LFIGGLSFETTEESLR
P22626|ROA2_HUMAN	848.3842	84.82	2.80E-08	GFGFVTFDDHDPVDK

P22626|ROA2_HUMAN	1095.454	77.41	2.50E-08	NMGGPYGGGNYGPGGSGGSGGYGGR
P22626|ROA2_HUMAN	899.9628	94.21	2.30E-08	LFIGGLSFETTEESLR
P22626|ROA2_HUMAN	940.4859	95.81	1.70E-08	LFVGGIKEDTEEHHLR
P22626|ROA2_HUMAN	899.9622	97.17	1.20E-08	LFIGGLSFETTEESLR
P22626|ROA2_HUMAN	899.9625	97.26	1.10E-08	LFIGGLSFETTEESLR
P22626|ROA2_HUMAN	899.9624	96.94	1.10E-08	LFIGGLSFETTEESLR
P22626|ROA2_HUMAN	1110.537	95.67	9.90E-09	DYFEEYGKIDTIEIITDR
P22626|ROA2_HUMAN	964.0109	101.24	5.30E-09	KLFIGGLSFETTEESLR
P22626|ROA2_HUMAN	899.9617	101.73	4.10E-09	LFIGGLSFETTEESLR
P22626|ROA2_HUMAN	940.4854	104.73	2.20E-09	LFVGGIKEDTEEHHLR
P22626|ROA2_HUMAN	1004.532	106.27	2.10E-09	KLFVGGIKEDTEEHHLR
P22626|ROA2_HUMAN	1110.537	106.26	8.80E-10	DYFEEYGKIDTIEIITDR
P22626|ROA2_HUMAN	1248.021	108.62	2.90E-11	GFGDGYNGYGGGPGGGNFGGSPGYGGGR
P22626|ROA2_HUMAN	1248.022	109.99	2.00E-11	GFGDGYNGYGGGPGGGNFGGSPGYGGGR
P22626|ROA2_HUMAN	1248.02	110.25	1.90E-11	GFGDGYNGYGGGPGGGNFGGSPGYGGGR
P22626|ROA2_HUMAN	1248.021	114.24	7.90E-12	GFGDGYNGYGGGPGGGNFGGSPGYGGGR
P22626|ROA2_HUMAN	1248.021	118	3.20E-12	GFGDGYNGYGGGPGGGNFGGSPGYGGGR
P22626|ROA2_HUMAN	1095.454	118.81	1.90E-12	NMGGPYGGGNYGPGGSGGSGGYGGR
P22626|ROA2_HUMAN	1095.455	123.07	7.40E-13	NMGGPYGGGNYGPGGSGGSGGYGGR
P22626|ROA2_HUMAN	1095.453	123.51	5.80E-13	NMGGPYGGGNYGPGGSGGSGGYGGR
P22626|ROA2_HUMAN	1095.455	124.5	5.30E-13	NMGGPYGGGNYGPGGSGGSGGYGGR
P22626|ROA2_HUMAN	1248.021	126.07	5.10E-13	GFGDGYNGYGGGPGGGNFGGSPGYGGGR
P22626|ROA2_HUMAN	1248.021	126.25	5.00E-13	GFGDGYNGYGGGPGGGNFGGSPGYGGGR
P22626|ROA2_HUMAN	1248.022	126.12	4.90E-13	GFGDGYNGYGGGPGGGNFGGSPGYGGGR
P22626|ROA2_HUMAN	1095.453	125.94	3.30E-13	NMGGPYGGGNYGPGGSGGSGGYGGR
P22626|ROA2_HUMAN	1095.454	127.62	2.20E-13	NMGGPYGGGNYGPGGSGGSGGYGGR
P22626|ROA2_HUMAN	1095.455	130.51	1.30E-13	NMGGPYGGGNYGPGGSGGSGGYGGR
P22626|ROA2_HUMAN	1095.	130.51	1.20E-13	NMGGPYGGGNYGPGGSGGSGGYGGR

MAN	454			
P23246|SFPQ_HUMAN	572.3147	41.14	0.0045	FATHAAALSVR
P23246|SFPQ_HUMAN	904.4588	42.43	0.0038	LFVGNLPADITEDEFK
P23246|SFPQ_HUMAN	572.3154	43.17	0.0028	FATHAAALSVR
P23246|SFPQ_HUMAN	1320.155	48.33	0.001	NLSPYVSNELLEEAFSQFGPIER
P23246|SFPQ_HUMAN	886.367	33.05	0.0005	MGGGGAMNMGDPYGSGGQK
P23246|SFPQ_HUMAN	572.3143	53.35	0.00033	FATHAAALSVR
P23246|SFPQ_HUMAN	572.3152	52.52	0.00033	FATHAAALSVR
P23246|SFPQ_HUMAN	626.8126	49.17	0.00022	YGEPGEVFINK
P23246|SFPQ_HUMAN	572.3154	55.44	0.00017	FATHAAALSVR
P23246|SFPQ_HUMAN	572.3149	58.54	8.20E-05	FATHAAALSVR
P23246|SFPQ_HUMAN	572.315	62.44	3.30E-05	FATHAAALSVR
P23246|SFPQ_HUMAN	1320.147	74.13	2.40E-06	NLSPYVSNELLEEAFSQFGPIER
P23246|SFPQ_HUMAN	1320.15	81.73	4.30E-07	NLSPYVSNELLEEAFSQFGPIER
P23246|SFPQ_HUMAN	1320.151	86.59	1.50E-07	NLSPYVSNELLEEAFSQFGPIER
P23246|SFPQ_HUMAN	1320.15	93.14	3.10E-08	NLSPYVSNELLEEAFSQFGPIER
P23246|SFPQ_HUMAN	1320.154	100.98	5.70E-09	NLSPYVSNELLEEAFSQFGPIER
P26599|PTBP1_HUMAN	496.274	38.13	0.0048	HQNVQLPR
P26599|PTBP1_HUMAN	496.2729	40.62	0.0036	HQNVQLPR
P26599|PTBP1_HUMAN	496.2735	44.85	0.0013	HQNVQLPR
P26599|PTBP1_HUMAN	496.2728	52.16	0.00025	HQNVQLPR
P26599|PTBP1_HUMAN	496.274	53.05	0.00015	HQNVQLPR
P26599|PTBP1_HUMAN	496.2735	54.9	0.00013	HQNVQLPR
P30050|RL12_HUMAN	833.9872	47.51	0.0012	QAQIEVVPSASALIIK
P31942|HNRH3_HUMAN	526.7762	37.23	0.0044	VHIDIGADGR
P31942|HNRH3_HUMAN	726.6704	37.59	0.0033	ATGEADVEFVTHEDAVAAMSK
P31942|HNRH3_HUMAN	526.7767	41.01	0.0018	VHIDIGADGR
P31942|HNRH3_HUMAN	636.3144	42.88	0.0011	STGEAFVQFASK

P31942|HNRH3_HUMAN	526.7765	44.2	0.00089	VHIDIGADGR
P31942|HNRH3_HUMAN	706.7971	30.77	0.00084	DGMDNQGGYGSVGR
P31942|HNRH3_HUMAN	670.3005	37.72	0.00076	HNGPNDASDGTVR
P31942|HNRH3_HUMAN	706.7952	37.86	0.00018	DGMDNQGGYGSVGR
P31942|HNRH3_HUMAN	706.7953	38.85	0.00014	DGMDNQGGYGSVGR
P31942|HNRH3_HUMAN	636.3138	53.2	9.60E-05	STGEAFVQFASK
P31942|HNRH3_HUMAN	706.7945	51.42	7.90E-06	DGMDNQGGYGSVGR
P31942|HNRH3_HUMAN	1261.572	82.76	6.70E-08	YIELFLNSTPGGGSGMGGSGMGGYGR
P35527|K1C9_HUMAN	530.7832	41.63	0.0049	TLLDIDNTR
P35527|K1C9_HUMAN	1131.54	40.71	0.0042	KDIENQYETQITQIEHEVSSSGQEVQSSAK
P35527|K1C9_HUMAN	926.4682	41.16	0.004	TLNDMRQEYEQLIAK
P35527|K1C9_HUMAN	1046.445	27.04	0.0038	GSRGGSGGSYGGGGSGGGYGGGSGSR
P35527|K1C9_HUMAN	530.7834	43.12	0.0036	TLLDIDNTR
P35527|K1C9_HUMAN	926.4668	42.04	0.0032	TLNDMRQEYEQLIAK
P35527|K1C9_HUMAN	530.7831	43.71	0.003	TLLDIDNTR
P35527|K1C9_HUMAN	926.4674	42.32	0.003	TLNDMRQEYEQLIAK
P35527|K1C9_HUMAN	926.4661	42.77	0.0026	TLNDMRQEYEQLIAK
P35527|K1C9_HUMAN	675.8451	41.32	0.0022	IGLGGRGGSGGSYGR
P35527|K1C9_HUMAN	926.4656	44.23	0.0019	TLNDMRQEYEQLIAK
P35527|K1C9_HUMAN	926.4634	44.86	0.0016	TLNDMRQEYEQLIAK
P35527|K1C9_HUMAN	919.4858	47.42	0.0014	HGVQELEIELQSQLSK
P35527|K1C9_HUMAN	919.4839	47.77	0.0013	HGVQELEIELQSQLSK
P35527|K1C9_HUMAN	926.4676	47.89	0.00085	TLNDMRQEYEQLIAK
P35527|K1C9_HUMAN	530.7834	50.37	0.00067	TLLDIDNTR
P35527|K1C9_HUMAN	533.2516	40.63	0.00067	STMQELNSR
P35527|K1C9_HUMAN	1088.84	45.35	0.00064	DIENQYETQITQIEHEVSSSGQEVQSSAK
P35527|K1C9_HUMAN	579.2978	46.03	0.00051	QGVDADINGLR
P35527|K1C9_HU	530.7	51.68	0.0005	TLLDIDNTR

MAN	835			
P35527|K1C9_HUMAN	919.4854	52.44	0.0004	HGVQELEIELQSQLSK
P35527|K1C9_HUMAN	1088.839	49.1	0.00027	DIENQYETQITQIEHEVSSSGQEVQSSAK
P35527|K1C9_HUMAN	530.7834	55.86	0.00019	TLLDIDNTR
P35527|K1C9_HUMAN	1255.57	48.58	0.00016	EIETYHNLLEGGQEDFESSGAGK
P35527|K1C9_HUMAN	579.2971	51.88	0.00013	QGVDADINGLR
P35527|K1C9_HUMAN	530.7832	57.76	0.00012	TLLDIDNTR
P35527|K1C9_HUMAN	1088.843	54.29	0.0001	DIENQYETQITQIEHEVSSSGQEVQSSAK
P35527|K1C9_HUMAN	926.4668	58.05	7.90E-05	TLNDMRQEYEQLIAK
P35527|K1C9_HUMAN	530.7836	59.88	7.50E-05	TLLDIDNTR
P35527|K1C9_HUMAN	618.2667	45.91	7.20E-05	FSSSSGYGGGSSR
P35527|K1C9_HUMAN	926.4675	59.24	6.20E-05	TLNDMRQEYEQLIAK
P35527|K1C9_HUMAN	616.8021	55.91	5.50E-05	SGGGGGGGLGSGGSIR
P35527|K1C9_HUMAN	533.2513	52.02	4.90E-05	STMQELNSR
P35527|K1C9_HUMAN	1075.102	43.66	4.30E-05	GGSGGSHGGGSGFGGESGGSYGGGEEASGSGGGYGGGSGK
P35527|K1C9_HUMAN	793.8845	57.25	4.20E-05	VQALEEANNDLENK
P35527|K1C9_HUMAN	579.2969	58.16	3.20E-05	QGVDADINGLR
P35527|K1C9_HUMAN	837.3819	54.94	3.20E-05	EIETYHNLLEGGQEDFESSGAGK
P35527|K1C9_HUMAN	579.2984	58.97	2.80E-05	QGVDADINGLR
P35527|K1C9_HUMAN	616.8	57.92	2.60E-05	SGGGGGGGLGSGGSIR
P35527|K1C9_HUMAN	579.2975	59.16	2.50E-05	QGVDADINGLR
P35527|K1C9_HUMAN	919.4861	65.58	1.90E-05	HGVQELEIELQSQLSK
P35527|K1C9_HUMAN	837.3831	58.36	1.70E-05	EIETYHNLLEGGQEDFESSGAGK
P35527|K1C9_HUMAN	919.4852	66.65	1.60E-05	HGVQELEIELQSQLSK
P35527|K1C9_HUMAN	919.4833	66.41	1.60E-05	HGVQELEIELQSQLSK
P35527|K1C9_HUMAN	1088.84	62.63	1.20E-05	DIENQYETQITQIEHEVSSSGQEVQSSAK
P35527|K1C9_HUMAN	616.8015	62.57	1.20E-05	SGGGGGGGLGSGGSIR
P35527|K1C9_HUMAN	1088.842	64.39	9.40E-06	DIENQYETQITQIEHEVSSSGQEVQSSAK

P35527|K1C9_HUMAN	579.2979	64.73	6.90E-06	QGVDADINGLR
P35527|K1C9_HUMAN	579.2974	65.33	6.00E-06	QGVDADINGLR
P35527|K1C9_HUMAN	919.4866	70.98	5.90E-06	HGVQELEIELQSQLSK
P35527|K1C9_HUMAN	579.2979	65.4	5.90E-06	QGVDADINGLR
P35527|K1C9_HUMAN	919.4853	71.38	5.50E-06	HGVQELEIELQSQLSK
P35527|K1C9_HUMAN	1075.099	52.71	5.40E-06	GGSGGSHGGGSGFGGESGGSYGGGEEASGSGGGYGGGSGK
P35527|K1C9_HUMAN	919.4825	71.78	4.90E-06	HGVQELEIELQSQLSK
P35527|K1C9_HUMAN	616.8015	67.44	4.30E-06	SGGGGGGGLGSGGSIR
P35527|K1C9_HUMAN	618.2668	58.72	3.80E-06	FSSSSGYGGGSSR
P35527|K1C9_HUMAN	1088.838	67.4	3.70E-06	DIENQYETQITQIEHEVSSSGQEVQSSAK
P35527|K1C9_HUMAN	793.8843	67.6	3.40E-06	VQALEEANNDLENK
P35527|K1C9_HUMAN	1255.565	64.39	3.20E-06	EIETYHNLLEGGQEDFESSGAGK
P35527|K1C9_HUMAN	618.2663	59.91	2.50E-06	FSSSSGYGGGSSR
P35527|K1C9_HUMAN	1088.841	70.15	2.30E-06	DIENQYETQITQIEHEVSSSGQEVQSSAK
P35527|K1C9_HUMAN	1255.567	66.6	2.00E-06	EIETYHNLLEGGQEDFESSGAGK
P35527|K1C9_HUMAN	1255.566	66.62	1.90E-06	EIETYHNLLEGGQEDFESSGAGK
P35527|K1C9_HUMAN	618.266	61.79	1.60E-06	FSSSSGYGGGSSR
P35527|K1C9_HUMAN	919.4862	79.35	8.70E-07	HGVQELEIELQSQLSK
P35527|K1C9_HUMAN	793.8837	74.56	7.10E-07	VQALEEANNDLENK
P35527|K1C9_HUMAN	1255.574	74.75	4.50E-07	EIETYHNLLEGGQEDFESSGAGK
P35527|K1C9_HUMAN	1088.839	77.45	3.90E-07	DIENQYETQITQIEHEVSSSGQEVQSSAK
P35527|K1C9_HUMAN	919.484	83.25	3.50E-07	HGVQELEIELQSQLSK
P35527|K1C9_HUMAN	919.4835	83.24	3.40E-07	HGVQELEIELQSQLSK
P35527|K1C9_HUMAN	618.2653	68.76	3.40E-07	FSSSSGYGGGSSR
P35527|K1C9_HUMAN	616.8019	78.85	3.10E-07	SGGGGGGGLGSGGSIR
P35527|K1C9_HUMAN	618.2664	68.94	3.10E-07	FSSSSGYGGGSSR
P35527|K1C9_HUMAN	1088.839	79.05	2.60E-07	DIENQYETQITQIEHEVSSSGQEVQSSAK
P35527|K1C9_HU	896.3	66	2.50E-07	GGSGGSYGGGGSGGGYGGGSGSR

MAN	632			
P35527|K1C9_HUMAN	919.4854	84.8	2.30E-07	HGVQELEIELQSQLSK
P35527|K1C9_HUMAN	793.8837	79.76	2.10E-07	VQALEEANNDLENK
P35527|K1C9_HUMAN	618.2662	70.7	2.10E-07	FSSSSGYGGGSSR
P35527|K1C9_HUMAN	616.8019	81.6	1.70E-07	SGGGGGGGLGSGGSIR
P35527|K1C9_HUMAN	793.8831	81.18	1.60E-07	VQALEEANNDLENK
P35527|K1C9_HUMAN	616.8024	81.12	1.60E-07	SGGGGGGGLGSGGSIR
P35527|K1C9_HUMAN	618.266	71.89	1.60E-07	FSSSSGYGGGSSR
P35527|K1C9_HUMAN	896.3656	69.29	1.20E-07	GGSGGSYGGGGSGGGYGGGSGSR
P35527|K1C9_HUMAN	793.8845	85.98	5.60E-08	VQALEEANNDLENK
P35527|K1C9_HUMAN	616.8012	88.09	3.30E-08	SGGGGGGGLGSGGSIR
P35527|K1C9_HUMAN	919.4877	94.3	2.90E-08	HGVQELEIELQSQLSK
P35527|K1C9_HUMAN	1255.565	85.42	2.60E-08	EIETYHNLLEGGQEDFESSGAGK
P35527|K1C9_HUMAN	896.3665	75.99	2.50E-08	GGSGGSYGGGGSGGGYGGGSGSR
P35527|K1C9_HUMAN	919.4836	95.07	2.20E-08	HGVQELEIELQSQLSK
P35527|K1C9_HUMAN	793.8847	89.99	2.20E-08	VQALEEANNDLENK
P35527|K1C9_HUMAN	793.8862	91.31	1.70E-08	VQALEEANNDLENK
P35527|K1C9_HUMAN	896.368	77.64	1.70E-08	GGSGGSYGGGGSGGGYGGGSGSR
P35527|K1C9_HUMAN	793.8839	92.84	1.10E-08	VQALEEANNDLENK
P35527|K1C9_HUMAN	896.3673	85.94	2.50E-09	GGSGGSYGGGGSGGGYGGGSGSR
P35527|K1C9_HUMAN	793.8841	101.64	1.40E-09	VQALEEANNDLENK
P35527|K1C9_HUMAN	896.3657	88.86	1.30E-09	GGSGGSYGGGGSGGGYGGGSGSR
P35527|K1C9_HUMAN	793.8848	102.15	1.20E-09	VQALEEANNDLENK
P35527|K1C9_HUMAN	793.8843	102.09	1.20E-09	VQALEEANNDLENK
P35527|K1C9_HUMAN	793.8842	102.06	1.20E-09	VQALEEANNDLENK
P35527|K1C9_HUMAN	793.8848	105.51	6.20E-10	VQALEEANNDLENK
P35527|K1C9_HUMAN	793.8844	105.68	5.30E-10	VQALEEANNDLENK
P35527|K1C9_HUMAN	896.3663	93.62	4.30E-10	GGSGGSYGGGGSGGGYGGGSGSR

P35527|K1C9_HUMAN	1353.081	98.95	3.20E-10	GGGGSFGYSYGGGSGGGFSASSLGGGFGGGSR
P35527|K1C9_HUMAN	896.3668	94.9	3.20E-10	GGSGGSYGGGGSGGGYGGGSGSR
P35527|K1C9_HUMAN	1353.08	99.08	2.90E-10	GGGGSFGYSYGGGSGGGFSASSLGGGFGGGSR
P35527|K1C9_HUMAN	896.3659	95.93	2.60E-10	GGSGGSYGGGGSGGGYGGGSGSR
P35527|K1C9_HUMAN	1353.082	100.9	2.40E-10	GGGGSFGYSYGGGSGGGFSASSLGGGFGGGSR
P35527|K1C9_HUMAN	1353.08	101	1.90E-10	GGGGSFGYSYGGGSGGGFSASSLGGGFGGGSR
P35527|K1C9_HUMAN	1353.082	103.64	1.20E-10	GGGGSFGYSYGGGSGGGFSASSLGGGFGGGSR
P35527|K1C9_HUMAN	896.3657	99.68	1.10E-10	GGSGGSYGGGGSGGGYGGGSGSR
P35527|K1C9_HUMAN	896.3671	99.97	1.00E-10	GGSGGSYGGGGSGGGYGGGSGSR
P35527|K1C9_HUMAN	1353.08	104.17	9.00E-11	GGGGSFGYSYGGGSGGGFSASSLGGGFGGGSR
P35527|K1C9_HUMAN	1353.08	104.23	8.90E-11	GGGGSFGYSYGGGSGGGFSASSLGGGFGGGSR
P35527|K1C9_HUMAN	1353.08	104.67	8.00E-11	GGGGSFGYSYGGGSGGGFSASSLGGGFGGGSR
P35527|K1C9_HUMAN	1353.081	107.88	3.90E-11	GGGGSFGYSYGGGSGGGFSASSLGGGFGGGSR
P35527|K1C9_HUMAN	1353.08	111.2	1.90E-11	GGGGSFGYSYGGGSGGGFSASSLGGGFGGGSR
P35527|K1C9_HUMAN	1353.08	114.72	7.90E-12	GGGGSFGYSYGGGSGGGFSASSLGGGFGGGSR
P35527|K1C9_HUMAN	1353.081	117.93	4.30E-12	GGGGSFGYSYGGGSGGGFSASSLGGGFGGGSR
P35527|K1C9_HUMAN	896.3654	117.73	1.70E-12	GGSGGSYGGGGSGGGYGGGSGSR
P35527|K1C9_HUMAN	896.3664	123.91	4.10E-13	GGSGGSYGGGGSGGGYGGGSGSR
P35637|FUS_HUMAN	1195.874	34.16	0.0043	HDSEQDNSDNNTIFVQGLGENVTIESVADYFK
P35637|FUS_HUMAN	831.4229	41.51	0.0041	LKGEATVSFDDPPSAK
P35637|FUS_HUMAN	831.423	42.17	0.0037	LKGEATVSFDDPPSAK
P35637|FUS_HUMAN	704.845	41.84	0.0015	TGQPMINLYTDR
P35637|FUS_HUMAN	831.4196	45.6	0.0014	LKGEATVSFDDPPSAK
P35637|FUS_HUMAN	1126.99	34.69	0.0012	APKPDGPGGGPGGSHMGGNYGDDR
P35637|FUS_HUMAN	912.4479	46.96	0.00076	TGQPMINLYTDRETGK
P35637|FUS_HUMAN	831.4205	51.34	0.00038	LKGEATVSFDDPPSAK
P35637|FUS_HUMAN	831.4186	51.65	0.00033	LKGEATVSFDDPPSAK
P35637|FUS_HU	831.4	55.01	0.00019	LKGEATVSFDDPPSAK

MAN	231			
P35637|FUS_HUMAN	947.9697	58.76	6.50E-05	AAIDWFDGKEFSGNPIK
P35637|FUS_HUMAN	947.9673	59.12	5.90E-05	AAIDWFDGKEFSGNPIK
P35637|FUS_HUMAN	831.422	59.65	5.40E-05	LKGEATVSFDDPPSAK
P35637|FUS_HUMAN	947.9667	63.49	1.90E-05	AAIDWFDGKEFSGNPIK
P35637|FUS_HUMAN	831.4199	65.45	1.30E-05	LKGEATVSFDDPPSAK
P35637|FUS_HUMAN	947.9662	69.65	4.70E-06	AAIDWFDGKEFSGNPIK
P35637|FUS_HUMAN	947.9677	70.5	4.20E-06	AAIDWFDGKEFSGNPIK
P35637|FUS_HUMAN	947.9678	80.59	4.10E-07	AAIDWFDGKEFSGNPIK
P35637|FUS_HUMAN	947.9676	81.98	2.90E-07	AAIDWFDGKEFSGNPIK
P35637|FUS_HUMAN	1126.987	71.34	2.90E-07	APKPDGPGGGPGGSHMGGNYGDDR
P35659|DEK_HUMAN	678.8301	35.65	0.0041	NVGQFSGFPFEK
P35659|DEK_HUMAN	581.8154	41.69	0.0032	LTMQVSSLQR
P35659|DEK_HUMAN	581.8151	41.68	0.0031	LTMQVSSLQR
P35659|DEK_HUMAN	678.8297	38.92	0.0018	NVGQFSGFPFEK
P35659|DEK_HUMAN	678.83	39.51	0.0017	NVGQFSGFPFEK
P35659|DEK_HUMAN	831.882	38.94	0.0014	VYENYPTYDLTER
P35659|DEK_HUMAN	831.8849	40.32	0.0011	VYENYPTYDLTER
P35659|DEK_HUMAN	678.8306	42.64	0.00069	NVGQFSGFPFEK
P35659|DEK_HUMAN	831.8842	42.56	0.00066	VYENYPTYDLTER
P35659|DEK_HUMAN	678.8309	43.03	0.00057	NVGQFSGFPFEK
P35659|DEK_HUMAN	709.8802	52.78	0.00039	LLASANLEEVTMK
P35659|DEK_HUMAN	678.8304	45.4	0.00037	NVGQFSGFPFEK
P35659|DEK_HUMAN	678.8304	45.99	0.00032	NVGQFSGFPFEK
P35659|DEK_HUMAN	678.8303	48.51	0.00018	NVGQFSGFPFEK
P35659|DEK_HUMAN	709.8813	63.37	3.40E-05	LLASANLEEVTMK
P35659|DEK_HUMAN	678.8315	58.96	1.80E-05	NVGQFSGFPFEK
P35908|K22E_HUMAN	464.5636	37.43	0.0045	SKEEAEALYHSK

P35908|K22E_HUMAN	464.5635	38.07	0.0039	SKEEAEALYHSK
P35908|K22E_HUMAN	752.6841	37.26	0.0036	TSQNSELNNMQDLVEDYKK
P35908|K22E_HUMAN	599.2775	33.35	0.0034	GGSISGGGYGSGGGK
P35908|K22E_HUMAN	519.2646	38.38	0.0032	YLDGLTAER
P35908|K22E_HUMAN	497.7862	39.77	0.0031	LQGEIAHVK
P35908|K22E_HUMAN	597.8093	40.2	0.0029	KYEDEINKR
P35908|K22E_HUMAN	1364.696	45.01	0.0027	FGGFGGPGGVGGLGGPGGFGPGGYPGGIHEVSVNQSLLQPLNVK
P35908|K22E_HUMAN	597.8084	41.35	0.0025	KYEDEINKR
P35908|K22E_HUMAN	871.3797	31.47	0.0023	GGSGGGGSISGGGYGSGGGSGGR
P35908|K22E_HUMAN	668.8563	44.85	0.0019	TAAENDFVTLKK
P35908|K22E_HUMAN	752.6843	40.65	0.0017	TSQNSELNNMQDLVEDYKK
P35908|K22E_HUMAN	519.2642	41.63	0.0016	YLDGLTAER
P35908|K22E_HUMAN	752.6859	41.59	0.0016	TSQNSELNNMQDLVEDYKK
P35908|K22E_HUMAN	871.3793	33.01	0.0016	GGSGGGGSISGGGYGSGGGSGGR
P35908|K22E_HUMAN	597.309	44.86	0.0014	YEELQVTVGR
P35908|K22E_HUMAN	519.2646	41.92	0.0014	YLDGLTAER
P35908|K22E_HUMAN	1364.694	48.09	0.0013	FGGFGGPGGVGGLGGPGGFGPGGYPGGIHEVSVNQSLLQPLNVK
P35908|K22E_HUMAN	597.8082	43.96	0.0012	KYEDEINKR
P35908|K22E_HUMAN	730.9	48.97	0.0011	VDLLNQEIEFLK
P35908|K22E_HUMAN	665.32	41.73	0.001	NVQDAIADAEQR
P35908|K22E_HUMAN	597.8082	45.29	0.00091	KYEDEINKR
P35908|K22E_HUMAN	660.7925	36.3	0.00084	HGGGGGGFGGGGFGSR
P35908|K22E_HUMAN	597.3094	46.62	0.0008	YEELQVTVGR
P35908|K22E_HUMAN	597.8092	46.17	0.00074	KYEDEINKR
P35908|K22E_HUMAN	599.2773	40.08	0.00068	GGSISGGGYGSGGGK
P35908|K22E_HUMAN	597.3087	48.71	0.00057	YEELQVTVGR
P35908|K22E_HUMAN	870.8577	34.78	0.00048	GSSSGGGYSSGSSSYGSGGR
P35908|K22E_HU	519.2	48.02	0.00035	YLDGLTAER

MAN	648			
P35908|K22E_HUMAN	597.8082	49.83	0.00032	KYEDEINKR
P35908|K22E_HUMAN	519.2645	48.67	0.0003	YLDGLTAER
P35908|K22E_HUMAN	919.96	52.25	0.00029	SISISVAGGGGGFGAAGGFGGR
P35908|K22E_HUMAN	871.3743	37.74	0.00027	GGSGGGGSISGGGYGSGGGSGGR
P35908|K22E_HUMAN	519.2656	49.23	0.00026	YLDGLTAER
P35908|K22E_HUMAN	871.3755	38.8	0.00026	GGSGGGGSISGGGYGSGGGSGGR
P35908|K22E_HUMAN	597.3107	51.75	0.00024	YEELQVTVGR
P35908|K22E_HUMAN	871.3785	42.48	0.00017	GGSGGGGSISGGGYGSGGGSGGR
P35908|K22E_HUMAN	597.808	53.2	0.00015	KYEDEINKR
P35908|K22E_HUMAN	597.3089	55.47	0.00012	YEELQVTVGR
P35908|K22E_HUMAN	696.3442	54.19	0.00011	SKEEAEALYHSK
P35908|K22E_HUMAN	871.3774	43.68	0.00011	GGSGGGGSISGGGYGSGGGSGGR
P35908|K22E_HUMAN	665.32	51.9	9.80E-05	NVQDAIADAEQR
P35908|K22E_HUMAN	871.3738	44.19	5.70E-05	GGSGGGGSISGGGYGSGGGSGGR
P35908|K22E_HUMAN	870.8546	42.9	5.10E-05	GSSSGGGYSSGSSSYGSGGR
P35908|K22E_HUMAN	519.2643	56.94	4.70E-05	YLDGLTAER
P35908|K22E_HUMAN	696.342	59.29	3.60E-05	SKEEAEALYHSK
P35908|K22E_HUMAN	870.8555	44.71	3.40E-05	GSSSGGGYSSGSSSYGSGGR
P35908|K22E_HUMAN	730.9	66.11	2.20E-05	VDLLNQEIEFLK
P35908|K22E_HUMAN	604.8096	61.77	2.20E-05	TAAENDFVTLK
P35908|K22E_HUMAN	696.3427	61.47	2.20E-05	SKEEAEALYHSK
P35908|K22E_HUMAN	871.3762	50.32	2.20E-05	GGSGGGGSISGGGYGSGGGSGGR
P35908|K22E_HUMAN	919.9604	63.5	2.10E-05	SISISVAGGGGGFGAAGGFGGR
P35908|K22E_HUMAN	730.9	66.49	2.00E-05	VDLLNQEIEFLK
P35908|K22E_HUMAN	870.856	47	2.00E-05	GSSSGGGYSSGSSSYGSGGR
P35908|K22E_HUMAN	696.3437	61.86	1.90E-05	SKEEAEALYHSK
P35908|K22E_HUMAN	871.3756	50.55	1.90E-05	GGSGGGGSISGGGYGSGGGSGGR

P35908|K22E_HUMAN	696.3422	62.91	1.50E-05	SKEEAEALYHSK
P35908|K22E_HUMAN	730.9	68.79	1.20E-05	VDLLNQEIEFLK
P35908|K22E_HUMAN	730.9	68.65	1.20E-05	VDLLNQEIEFLK
P35908|K22E_HUMAN	519.2642	63.07	1.10E-05	YLDGLTAER
P35908|K22E_HUMAN	871.3756	54.9	7.10E-06	GGSGGGGSISGGGYGSGGGSGGR
P35908|K22E_HUMAN	696.343	67.63	5.40E-06	SKEEAEALYHSK
P35908|K22E_HUMAN	696.3431	67.91	5.10E-06	SKEEAEALYHSK
P35908|K22E_HUMAN	627.8049	65.11	5.10E-06	GFSSGSAVVSGGSR
P35908|K22E_HUMAN	696.3406	66.89	5.00E-06	SKEEAEALYHSK
P35908|K22E_HUMAN	627.8064	66.23	4.10E-06	GFSSGSAVVSGGSR
P35908|K22E_HUMAN	660.7948	61.29	3.90E-06	HGGGGGGFGGGGFGSR
P35908|K22E_HUMAN	660.7953	61.77	3.60E-06	HGGGGGGFGGGGFGSR
P35908|K22E_HUMAN	604.8095	70.16	3.30E-06	TAAENDFVTLK
P35908|K22E_HUMAN	665.3218	66.01	3.30E-06	NVQDAIADAEQR
P35908|K22E_HUMAN	660.7955	62.61	3.00E-06	HGGGGGGFGGGGFGSR
P35908|K22E_HUMAN	730.9014	74.98	2.60E-06	VDLLNQEIEFLK
P35908|K22E_HUMAN	696.3436	71.43	2.10E-06	SKEEAEALYHSK
P35908|K22E_HUMAN	871.3767	60.57	2.10E-06	GGSGGGGSISGGGYGSGGGSGGR
P35908|K22E_HUMAN	665.32	68.81	2.00E-06	NVQDAIADAEQR
P35908|K22E_HUMAN	597.3098	72.28	1.90E-06	YEELQVTVGR
P35908|K22E_HUMAN	696.3419	71.98	1.90E-06	SKEEAEALYHSK
P35908|K22E_HUMAN	730.9016	77.58	1.60E-06	VDLLNQEIEFLK
P35908|K22E_HUMAN	730.9013	77.29	1.50E-06	VDLLNQEIEFLK
P35908|K22E_HUMAN	730.9013	77.68	1.40E-06	VDLLNQEIEFLK
P35908|K22E_HUMAN	696.3435	73.97	1.20E-06	SKEEAEALYHSK
P35908|K22E_HUMAN	665.3217	70.44	1.20E-06	NVQDAIADAEQR
P35908|K22E_HUMAN	696.342	75.63	8.00E-07	SKEEAEALYHSK
P35908|K22E_HU	730.9	80.53	7.30E-07	VDLLNQEIEFLK

MAN	014			
P35908|K22E_HUMAN	696.3403	75.39	6.90E-07	SKEEAEALYHSK
P35908|K22E_HUMAN	604.8094	77.25	6.40E-07	TAAENDFVTLK
P35908|K22E_HUMAN	627.8053	73.36	6.30E-07	GFSSGSAVVSGGSR
P35908|K22E_HUMAN	660.7949	69.69	5.70E-07	HGGGGGGFGGGGFGSR
P35908|K22E_HUMAN	660.7953	70.28	5.10E-07	HGGGGGGFGGGGFGSR
P35908|K22E_HUMAN	870.8552	63.45	4.50E-07	GSSSGGGYSSGSSSYGSGGR
P35908|K22E_HUMAN	919.9571	80.32	4.10E-07	SISISVAGGGGGFGAAGGFGGR
P35908|K22E_HUMAN	730.9	84.04	3.50E-07	VDLLNQEIEFLK
P35908|K22E_HUMAN	660.7943	69.88	3.50E-07	HGGGGGGFGGGGFGSR
P35908|K22E_HUMAN	627.8058	77.11	2.60E-07	GFSSGSAVVSGGSR
P35908|K22E_HUMAN	604.81	81.8	2.00E-07	TAAENDFVTLK
P35908|K22E_HUMAN	660.7949	75.12	1.60E-07	HGGGGGGFGGGGFGSR
P35908|K22E_HUMAN	1200.01	70.44	1.40E-07	GGGFGGGSSFGGGSGFSGGGFGGGGFGGGR
P35908|K22E_HUMAN	627.8061	80.08	1.30E-07	GFSSGSAVVSGGSR
P35908|K22E_HUMAN	660.7949	76.47	1.20E-07	HGGGGGGFGGGGFGSR
P35908|K22E_HUMAN	871.3759	75.05	7.50E-08	GGSGGGGSISGGGYGSGGGSGGR
P35908|K22E_HUMAN	730.9011	90.81	6.90E-08	VDLLNQEIEFLK
P35908|K22E_HUMAN	730.9003	91.01	6.20E-08	VDLLNQEIEFLK
P35908|K22E_HUMAN	1200.011	80.53	1.50E-08	GGGFGGGSSFGGGSGFSGGGFGGGGFGGGR
P35908|K22E_HUMAN	660.7961	86.71	1.40E-08	HGGGGGGFGGGGFGSR
P35908|K22E_HUMAN	730.9012	97.95	1.30E-08	VDLLNQEIEFLK
P35908|K22E_HUMAN	660.7953	87.49	9.70E-09	HGGGGGGFGGGGFGSR
P35908|K22E_HUMAN	660.795	91.01	4.20E-09	HGGGGGGFGGGGFGSR
P35908|K22E_HUMAN	870.8542	89.07	1.20E-09	GSSSGGGYSSGSSSYGSGGR
P35908|K22E_HUMAN	1200.013	98.92	3.00E-10	GGGFGGGSSFGGGSGFSGGGFGGGGFGGGR
P35908|K22E_HUMAN	1200.009	102.84	8.60E-11	GGGFGGGSSFGGGSGFSGGGFGGGGFGGGR
P35908|K22E_HUMAN	1200.016	116.7	7.10E-12	GGGFGGGSSFGGGSGFSGGGFGGGGFGGGR

P35908|K22E_HUMAN	1200.012	114.76	7.00E-12	GGGFGGGSSFGGGSGFSGGGFGGGGFGGGR
P35908|K22E_HUMAN	1200.009	114.21	6.10E-12	GGGFGGGSSFGGGSGFSGGGFGGGGFGGGR
P35908|K22E_HUMAN	1200.01	121.45	1.10E-12	GGGFGGGSSFGGGSGFSGGGFGGGGFGGGR
P35908|K22E_HUMAN	1200.011	128.15	2.80E-13	GGGFGGGSSFGGGSGFSGGGFGGGGFGGGR
P35908|K22E_HUMAN	1200.011	131.72	1.20E-13	GGGFGGGSSFGGGSGFSGGGFGGGGFGGGR
P35908|K22E_HUMAN	1200.009	141.47	1.10E-14	GGGFGGGSSFGGGSGFSGGGFGGGGFGGGR
P35908|K22E_HUMAN	1200.008	143.5	6.50E-15	GGGFGGGSSFGGGSGFSGGGFGGGGFGGGR
P35908|K22E_HUMAN	1200.011	146.94	3.60E-15	GGGFGGGSSFGGGSGFSGGGFGGGGFGGGR
P35908|K22E_HUMAN	1200.01	146.92	3.30E-15	GGGFGGGSSFGGGSGFSGGGFGGGGFGGGR
P35908|K22E_HUMAN	1200.01	159.19	1.90E-16	GGGFGGGSSFGGGSGFSGGGFGGGGFGGGR
P35908|K22E_HUMAN	1200.01	175.62	4.40E-18	GGGFGGGSSFGGGSGFSGGGFGGGGFGGGR
P38159|RBMX_HUMAN	437.2545	44.57	0.0045	RGPPPPPR
P38159|RBMX_HUMAN	437.2549	46.61	0.0027	RGPPPPPR
P38159|RBMX_HUMAN	806.3416	27.22	0.0026	DRDYSDHPSGGSYR
P38159|RBMX_HUMAN	718.3602	43.77	0.0016	VEQATKPSFESGR
P38159|RBMX_HUMAN	437.2549	49.5	0.0014	RGPPPPPR
P38159|RBMX_HUMAN	718.3597	47.95	0.00061	VEQATKPSFESGR
P38159|RBMX_HUMAN	718.3594	49.22	0.00045	VEQATKPSFESGR
P38159|RBMX_HUMAN	806.3415	35.3	0.0004	DRDYSDHPSGGSYR
P38159|RBMX_HUMAN	718.3729	55.48	0.00014	LFIGGLNTETNEK
P38159|RBMX_HUMAN	718.3727	59.54	5.60E-05	LFIGGLNTETNEK
P38159|RBMX_HUMAN	718.3731	61.47	3.70E-05	LFIGGLNTETNEK
P38159|RBMX_HUMAN	718.3726	66.77	1.10E-05	LFIGGLNTETNEK
P38159|RBMX_HUMAN	718.3721	73.7	2.10E-06	LFIGGLNTETNEK
P38159|RBMX_HUMAN	718.3737	73.93	1.90E-06	LFIGGLNTETNEK
P38159|RBMX_HUMAN	718.3729	78.85	6.50E-07	LFIGGLNTETNEK
P38159|RBMX_HUMAN	718.3724	92.32	2.90E-08	LFIGGLNTETNEK
P38159|RBMX_H	1025.	87.74	1.70E-09	GGHMDDGGYSMNFNMSSSR

UMAN	393			
P38159|RBMX_HUMAN	1025.395	98.68	1.40E-10	GGHMDDGGYSMNFNMSSSR
P38159|RBMX_HUMAN	1025.396	104.21	3.80E-11	GGHMDDGGYSMNFNMSSSR
P38159|RBMX_HUMAN	1025.391	114.49	3.60E-12	GGHMDDGGYSMNFNMSSSR
P38159|RBMX_HUMAN	1025.394	114.71	3.40E-12	GGHMDDGGYSMNFNMSSSR
P38159|RBMX_HUMAN	1025.399	117.18	1.90E-12	GGHMDDGGYSMNFNMSSSR
P38159|RBMX_HUMAN	1025.397	128.01	1.60E-13	GGHMDDGGYSMNFNMSSSR
P38919|IF4A3_HUMAN	587.3253	46.18	0.0022	RDELTLEGIK
P38919|IF4A3_HUMAN	735.3752	48.43	0.00047	LDYGQHVVAGTPGR
P38919|IF4A3_HUMAN	587.3256	53.8	0.00038	RDELTLEGIK
P38919|IF4A3_HUMAN	889.8949	44.48	0.00035	EANFTVSSMHGDMPQK
P38919|IF4A3_HUMAN	702.3654	54.75	0.00019	GRDVIAQSQSGTGK
P38919|IF4A3_HUMAN	735.3791	54.67	0.00011	LDYGQHVVAGTPGR
P38919|IF4A3_HUMAN	587.327	62.85	5.20E-05	RDELTLEGIK
P38919|IF4A3_HUMAN	587.3263	62.55	5.00E-05	RDELTLEGIK
P38919|IF4A3_HUMAN	587.3254	63.14	4.40E-05	RDELTLEGIK
P38919|IF4A3_HUMAN	587.3275	63.01	4.40E-05	RDELTLEGIK
P38919|IF4A3_HUMAN	587.3277	63.25	4.20E-05	RDELTLEGIK
P38919|IF4A3_HUMAN	889.8915	59.35	1.30E-05	EANFTVSSMHGDMPQK
P38919|IF4A3_HUMAN	587.3262	71.8	6.00E-06	RDELTLEGIK
P39019|RS19_HUMAN	852.3871	49.99	7.20E-05	ELAPYDENWFYTR
P39019|RS19_HUMAN	852.3845	50.31	6.40E-05	ELAPYDENWFYTR
P43243|MATR3_HUMAN	889.9582	41.42	0.0049	GAPPSSNIEDFHGLLPK
P43243|MATR3_HUMAN	740.35	35.67	0.0047	DLDELSRYPEDK
P43243|MATR3_HUMAN	985.0407	43.22	0.0045	IGPYQPNVPVGIDYVIPK
P43243|MATR3_HUMAN	810.4899	39.95	0.0044	ITPENLPQILLQLK
P43243|MATR3_HUMAN	810.4896	39.75	0.0044	ITPENLPQILLQLK
P43243|MATR3_HUMAN	813.4614	42.88	0.004	YQLLQLVEPFGVISNHLILNK

P43243|MATR3_HUMAN	889.957	42.56	0.0036	GAPPSSNIEDFHGLLPK
P43243|MATR3_HUMAN	889.9535	43.02	0.0034	GAPPSSNIEDFHGLLPK
P43243|MATR3_HUMAN	889.9565	44.93	0.0021	GAPPSSNIEDFHGLLPK
P43243|MATR3_HUMAN	810.4893	43.02	0.0021	ITPENLPQILLQLK
P43243|MATR3_HUMAN	985.041	46.65	0.002	IGPYQPNVPVGIDYVIPK
P43243|MATR3_HUMAN	810.4882	44.82	0.0017	ITPENLPQILLQLK
P43243|MATR3_HUMAN	985.0416	47.62	0.0016	IGPYQPNVPVGIDYVIPK
P43243|MATR3_HUMAN	1019.037	48.85	0.0012	VIHLSNLPHSGYSDSAVLK
P43243|MATR3_HUMAN	810.4863	47.41	0.00098	ITPENLPQILLQLK
P43243|MATR3_HUMAN	889.9568	48.66	0.00088	GAPPSSNIEDFHGLLPK
P43243|MATR3_HUMAN	896.944	48.48	0.00081	GDADQASNILASFGLSAR
P43243|MATR3_HUMAN	1019.039	51.68	0.00063	VIHLSNLPHSGYSDSAVLK
P43243|MATR3_HUMAN	810.4891	49.53	0.00055	ITPENLPQILLQLK
P43243|MATR3_HUMAN	985.0411	52.82	0.00047	IGPYQPNVPVGIDYVIPK
P43243|MATR3_HUMAN	896.9406	51.25	0.0004	GDADQASNILASFGLSAR
P43243|MATR3_HUMAN	889.9583	53.72	0.00029	GAPPSSNIEDFHGLLPK
P43243|MATR3_HUMAN	810.4879	52.41	0.00029	ITPENLPQILLQLK
P43243|MATR3_HUMAN	810.4879	52.95	0.00025	ITPENLPQILLQLK
P43243|MATR3_HUMAN	1019.039	56.07	0.00023	VIHLSNLPHSGYSDSAVLK
P43243|MATR3_HUMAN	810.4876	53.8	0.00021	ITPENLPQILLQLK
P43243|MATR3_HUMAN	1019.038	56.75	0.0002	VIHLSNLPHSGYSDSAVLK
P43243|MATR3_HUMAN	896.9434	55.05	0.00019	GDADQASNILASFGLSAR
P43243|MATR3_HUMAN	606.291	52.3	8.00E-05	SQAFIEMETR
P43243|MATR3_HUMAN	896.9421	59.38	6.80E-05	GDADQASNILASFGLSAR
P43243|MATR3_HUMAN	896.9456	61.55	3.00E-05	GDADQASNILASFGLSAR
P43243|MATR3_HUMAN	1019.039	65.6	2.80E-05	VIHLSNLPHSGYSDSAVLK
P43243|MATR3_HUMAN	1019.041	65.6	2.70E-05	VIHLSNLPHSGYSDSAVLK
P43243|MATR3_	896.9	62.7	2.50E-05	GDADQASNILASFGLSAR

HUMAN	464			
P43243|MATR3_HUMAN	896.9421	65.86	1.60E-05	GDADQASNILASFGLSAR
P43243|MATR3_HUMAN	896.9437	66.53	1.30E-05	GDADQASNILASFGLSAR
P43243|MATR3_HUMAN	1019.042	70.89	7.60E-06	VIHLSNLPHSGYSDSAVLK
P46777|RL5_HUMAN	593.2781	36.45	0.0017	RFPGYDSESK
P46777|RL5_HUMAN	593.2787	44.36	0.00027	RFPGYDSESK
P46777|RL5_HUMAN	593.2777	47.28	0.00018	RFPGYDSESK
P46777|RL5_HUMAN	593.2776	47.44	0.00017	RFPGYDSESK
P46777|RL5_HUMAN	717.8312	52.56	5.40E-05	HIMGQNVADYMR
P46777|RL5_HUMAN	717.8314	62.73	5.00E-06	HIMGQNVADYMR
P46778|RL21_HUMAN	820.9564	67.85	1.30E-05	VYNVTQHAVGIVVNK
P47914|RL29_HUMAN	689.3763	51.12	0.00047	AQAAAPASVPAQAPK
P50995|ANX11_HUMAN	907.4179	39.52	0.0013	SLYHDISGDTSGDYRK
P51991|ROA3_HUMAN	814.4009	43.15	0.003	LFIGGLSFETTDDSLREHFEK
P51991|ROA3_HUMAN	885.9493	47.54	0.00095	LFIGGLSFETTDDSLR
P51991|ROA3_HUMAN	617.8002	46.48	0.00049	IETIEVMEDR
P51991|ROA3_HUMAN	941.9771	53.06	0.00028	IFVGGIKEDTEEYNLR
P51991|ROA3_HUMAN	941.9784	54.64	0.0002	IFVGGIKEDTEEYNLR
P51991|ROA3_HUMAN	617.8005	55.56	6.60E-05	IETIEVMEDR
P51991|ROA3_HUMAN	617.8007	57.25	4.50E-05	IETIEVMEDR
P51991|ROA3_HUMAN	885.9503	61.38	4.00E-05	LFIGGLSFETTDDSLR
P51991|ROA3_HUMAN	885.9482	61.46	3.70E-05	LFIGGLSFETTDDSLR
P51991|ROA3_HUMAN	617.7998	57.82	3.50E-05	IETIEVMEDR
P51991|ROA3_HUMAN	941.9779	63.36	2.80E-05	IFVGGIKEDTEEYNLR
P51991|ROA3_HUMAN	617.801	63.16	1.00E-05	IETIEVMEDR
P51991|ROA3_HUMAN	617.8015	62.87	1.00E-05	IETIEVMEDR
P51991|ROA3_HUMAN	617.7999	69.96	2.10E-06	IETIEVMEDR
P51991|ROA3_HUMAN	617.8005	70.97	1.90E-06	IETIEVMEDR

P51991|ROA3_HUMAN	617.8011	70.73	1.70E-06	IETIEVMEDR
P51991|ROA3_HUMAN	617.8005	80.81	2.00E-07	IETIEVMEDR
P51991|ROA3_HUMAN	955.897	83.47	8.10E-09	SSGSPYGGGYGSGGGSGGYGSR
P51991|ROA3_HUMAN	955.8956	84.8	5.10E-09	SSGSPYGGGYGSGGGSGGYGSR
P51991|ROA3_HUMAN	955.8968	89.41	1.90E-09	SSGSPYGGGYGSGGGSGGYGSR
P51991|ROA3_HUMAN	955.8967	90.23	1.60E-09	SSGSPYGGGYGSGGGSGGYGSR
P51991|ROA3_HUMAN	955.8962	90.89	1.40E-09	SSGSPYGGGYGSGGGSGGYGSR
P51991|ROA3_HUMAN	955.8969	92.07	1.10E-09	SSGSPYGGGYGSGGGSGGYGSR
P51991|ROA3_HUMAN	955.8952	92.58	8.60E-10	SSGSPYGGGYGSGGGSGGYGSR
P51991|ROA3_HUMAN	955.8965	93.87	7.00E-10	SSGSPYGGGYGSGGGSGGYGSR
P51991|ROA3_HUMAN	955.8972	98.87	2.20E-10	SSGSPYGGGYGSGGGSGGYGSR
P51991|ROA3_HUMAN	955.8956	101.84	1.00E-10	SSGSPYGGGYGSGGGSGGYGSR
P51991|ROA3_HUMAN	955.8967	104.04	6.70E-11	SSGSPYGGGYGSGGGSGGYGSR
P51991|ROA3_HUMAN	955.8962	116.2	4.10E-12	SSGSPYGGGYGSGGGSGGYGSR
P51991|ROA3_HUMAN	955.8973	119.94	1.70E-12	SSGSPYGGGYGSGGGSGGYGSR
P52272|HNRPM_HUMAN	552.2821	38.4	0.0046	ADILEDKDGK
P52272|HNRPM_HUMAN	552.2808	40.38	0.0034	ADILEDKDGK
P52272|HNRPM_HUMAN	692.3083	31.13	0.0034	MGLAMGGGGGASFDR
P52272|HNRPM_HUMAN	632.8477	42.78	0.0031	AFITNIPFDVK
P52272|HNRPM_HUMAN	632.8479	43.76	0.0025	AFITNIPFDVK
P52272|HNRPM_HUMAN	632.8504	44.85	0.0018	AFITNIPFDVK
P52272|HNRPM_HUMAN	632.8478	48.13	0.00091	AFITNIPFDVK
P52272|HNRPM_HUMAN	807.3915	43.6	0.00083	MGPLGLDHMASSIER
P52272|HNRPM_HUMAN	552.2798	47.88	0.00062	ADILEDKDGK
P52272|HNRPM_HUMAN	552.2816	48.4	0.00054	ADILEDKDGK
P52272|HNRPM_HUMAN	1089.526	49.44	0.00042	GIGMGNIGPAGMGMEGIGFGINK
P52272|HNRPM_HUMAN	632.8486	51.07	0.00041	AFITNIPFDVK
P52272|HNRPM_	807.3	46.57	0.00038	MGPLGLDHMASSIER

HUMAN	898			
P52272|HNRPM_HUMAN	807.3892	48.29	0.00027	MGPLGLDHMASSIER
P52272|HNRPM_HUMAN	632.8481	55.62	0.00016	AFITNIPFDVK
P52272|HNRPM_HUMAN	642.8165	51.44	0.00011	QGGGGGGGSVPGIER
P52272|HNRPM_HUMAN	632.8502	58.9	7.40E-05	AFITNIPFDVK
P52272|HNRPM_HUMAN	642.8156	54.44	7.20E-05	QGGGGGGGSVPGIER
P52272|HNRPM_HUMAN	1089.53	58.09	6.20E-05	GIGMGNIGPAGMGMEGIGFGINK
P52272|HNRPM_HUMAN	807.3922	55.79	6.00E-05	MGPLGLDHMASSIER
P52272|HNRPM_HUMAN	642.817	58.44	2.60E-05	QGGGGGGGSVPGIER
P52272|HNRPM_HUMAN	551.2496	51.16	2.40E-05	MGAGLGHGMDR
P52272|HNRPM_HUMAN	807.3907	60.76	1.90E-05	MGPLGLDHMASSIER
P52272|HNRPM_HUMAN	807.3904	60.58	1.90E-05	MGPLGLDHMASSIER
P52272|HNRPM_HUMAN	642.8168	59.62	1.90E-05	QGGGGGGGSVPGIER
P52272|HNRPM_HUMAN	632.8495	65.61	1.60E-05	AFITNIPFDVK
P52272|HNRPM_HUMAN	807.3905	62.76	1.10E-05	MGPLGLDHMASSIER
P52272|HNRPM_HUMAN	1089.525	65.65	1.00E-05	GIGMGNIGPAGMGMEGIGFGINK
P52272|HNRPM_HUMAN	1017.975	67.53	3.70E-06	GNFGGSFAGSFGGAGGHAPGVAR
P52272|HNRPM_HUMAN	1017.976	70.97	1.70E-06	GNFGGSFAGSFGGAGGHAPGVAR
P52272|HNRPM_HUMAN	551.248	62.88	1.60E-06	MGAGLGHGMDR
P52272|HNRPM_HUMAN	807.3916	71.77	1.40E-06	MGPLGLDHMASSIER
P52272|HNRPM_HUMAN	632.8486	77.58	9.10E-07	AFITNIPFDVK
P52272|HNRPM_HUMAN	1017.978	80.79	1.90E-07	GNFGGSFAGSFGGAGGHAPGVAR
P52272|HNRPM_HUMAN	1017.978	82.39	1.30E-07	GNFGGSFAGSFGGAGGHAPGVAR
P52272|HNRPM_HUMAN	1017.978	82.88	1.20E-07	GNFGGSFAGSFGGAGGHAPGVAR
P52272|HNRPM_HUMAN	1017.979	84.3	8.30E-08	GNFGGSFAGSFGGAGGHAPGVAR
P52272|HNRPM_HUMAN	1017.976	84.08	8.10E-08	GNFGGSFAGSFGGAGGHAPGVAR
P52272|HNRPM_HUMAN	1089.526	87.18	7.10E-08	GIGMGNIGPAGMGMEGIGFGINK
P52272|HNRPM_HUMAN	1017.976	94.21	8.50E-09	GNFGGSFAGSFGGAGGHAPGVAR

P52272|HNRPM_HUMAN	1017.976	96.19	5.30E-09	GNFGGSFAGSFGGAGGHAPGVAR
P52272|HNRPM_HUMAN	1017.976	99.34	2.70E-09	GNFGGSFAGSFGGAGGHAPGVAR
P52272|HNRPM_HUMAN	1017.979	100.5	2.00E-09	GNFGGSFAGSFGGAGGHAPGVAR
P52272|HNRPM_HUMAN	1017.977	110.89	1.90E-10	GNFGGSFAGSFGGAGGHAPGVAR
P52597|HNRPF_HUMAN	934.4727	69.18	6.50E-06	ITGEAFVQFASQELAEK
P52597|HNRPF_HUMAN	934.4737	77.81	8.80E-07	ITGEAFVQFASQELAEK
P52597|HNRPF_HUMAN	934.4722	92.25	3.10E-08	ITGEAFVQFASQELAEK
P53999|TCP4_HUMAN	630.8048	36.33	0.0045	EQISDIDDAVR
P53999|TCP4_HUMAN	814.4423	45.05	0.0023	KGISLNPEQWSQLK
P53999|TCP4_HUMAN	630.8046	39.75	0.002	EQISDIDDAVR
P53999|TCP4_HUMAN	630.8054	39.42	0.002	EQISDIDDAVR
P53999|TCP4_HUMAN	630.8059	39.94	0.0019	EQISDIDDAVR
P53999|TCP4_HUMAN	630.8058	39.8	0.0019	EQISDIDDAVR
P53999|TCP4_HUMAN	630.8053	40	0.0018	EQISDIDDAVR
P53999|TCP4_HUMAN	630.8054	39.89	0.0018	EQISDIDDAVR
P53999|TCP4_HUMAN	630.8047	41.41	0.0014	EQISDIDDAVR
P53999|TCP4_HUMAN	814.4401	48.93	0.0012	KGISLNPEQWSQLK
P53999|TCP4_HUMAN	750.3957	49.29	0.00061	GISLNPEQWSQLK
P53999|TCP4_HUMAN	814.4435	52.42	0.00047	KGISLNPEQWSQLK
P53999|TCP4_HUMAN	750.3949	50.81	0.00044	GISLNPEQWSQLK
P53999|TCP4_HUMAN	814.4434	54.2	0.0003	KGISLNPEQWSQLK
P53999|TCP4_HUMAN	814.4432	53.83	0.00028	KGISLNPEQWSQLK
P53999|TCP4_HUMAN	862.8729	41.73	0.00027	EYWMDPEGEMKPGR
P53999|TCP4_HUMAN	814.4418	57.47	0.00015	KGISLNPEQWSQLK
P53999|TCP4_HUMAN	750.3939	56.07	0.00012	GISLNPEQWSQLK
P53999|TCP4_HUMAN	814.442	60	8.30E-05	KGISLNPEQWSQLK
P53999|TCP4_HUMAN	814.4412	61.7	4.80E-05	KGISLNPEQWSQLK
P53999|TCP4_HU	814.4	62.63	4.50E-05	KGISLNPEQWSQLK

MAN	436			
P53999|TCP4_HUMAN	750.3941	61.74	3.30E-05	GISLNPEQWSQLK
P53999|TCP4_HUMAN	750.3944	64.77	1.70E-05	GISLNPEQWSQLK
P53999|TCP4_HUMAN	750.3945	66.62	1.10E-05	GISLNPEQWSQLK
P53999|TCP4_HUMAN	862.8707	53.56	1.00E-05	EYWMDPEGEMKPGR
P53999|TCP4_HUMAN	814.4437	73.82	3.40E-06	KGISLNPEQWSQLK
P53999|TCP4_HUMAN	862.873	62	2.50E-06	EYWMDPEGEMKPGR
P53999|TCP4_HUMAN	750.3947	73.31	2.40E-06	GISLNPEQWSQLK
P53999|TCP4_HUMAN	862.8716	61.84	2.30E-06	EYWMDPEGEMKPGR
P53999|TCP4_HUMAN	862.873	65.82	1.10E-06	EYWMDPEGEMKPGR
P53999|TCP4_HUMAN	862.8751	65.44	1.10E-06	EYWMDPEGEMKPGR
P53999|TCP4_HUMAN	862.8723	69.49	4.00E-07	EYWMDPEGEMKPGR
P53999|TCP4_HUMAN	862.8719	69.34	4.00E-07	EYWMDPEGEMKPGR
P53999|TCP4_HUMAN	750.3943	82.66	3.00E-07	GISLNPEQWSQLK
P53999|TCP4_HUMAN	862.8709	70.1	2.30E-07	EYWMDPEGEMKPGR
P53999|TCP4_HUMAN	750.3956	86.09	1.30E-07	GISLNPEQWSQLK
P55769|NH2L1_HUMAN	729.39	62.86	3.50E-05	QQIQSIQQSIER
P60709|ACTB_HUMAN	566.7653	33.38	0.0032	GYSFTTTAER
P60709|ACTB_HUMAN	1061.873	46.41	0.0024	TTGIVMDSGDGVTHTVPIYEGYALPHAILR
P60709|ACTB_HUMAN	566.7646	35.24	0.0022	GYSFTTTAER
P60709|ACTB_HUMAN	977.5347	50.3	0.00091	VAPEEHPVLLTEAPLNPK
P60709|ACTB_HUMAN	566.7653	38.89	0.0009	GYSFTTTAER
P60709|ACTB_HUMAN	977.5335	52.77	0.0005	VAPEEHPVLLTEAPLNPK
P60709|ACTB_HUMAN	977.5338	52.59	0.00049	VAPEEHPVLLTEAPLNPK
P60709|ACTB_HUMAN	566.7662	42.2	0.00047	GYSFTTTAER
P60709|ACTB_HUMAN	977.5331	54.99	0.00028	VAPEEHPVLLTEAPLNPK
P60709|ACTB_HUMAN	566.7653	51.9	4.50E-05	GYSFTTTAER
P60709|ACTB_HUMAN	1061.874	63.99	4.20E-05	TTGIVMDSGDGVTHTVPIYEGYALPHAILR

P60709|ACTB_HUMAN	977.5335	64.01	3.70E-05	VAPEEHPVLLTEAPLNPK
P60709|ACTB_HUMAN	977.5328	64.3	3.60E-05	VAPEEHPVLLTEAPLNPK
P60709|ACTB_HUMAN	977.5341	64.42	3.10E-05	VAPEEHPVLLTEAPLNPK
P60709|ACTB_HUMAN	977.5333	65.23	2.80E-05	VAPEEHPVLLTEAPLNPK
P60709|ACTB_HUMAN	977.533	65.74	2.60E-05	VAPEEHPVLLTEAPLNPK
P60709|ACTB_HUMAN	977.5342	65.72	2.30E-05	VAPEEHPVLLTEAPLNPK
P60709|ACTB_HUMAN	977.5341	67.08	1.70E-05	VAPEEHPVLLTEAPLNPK
P60709|ACTB_HUMAN	977.534	68.91	1.10E-05	VAPEEHPVLLTEAPLNPK
P60709|ACTB_HUMAN	977.5345	70.92	6.80E-06	VAPEEHPVLLTEAPLNPK
P60709|ACTB_HUMAN	977.5338	72.13	5.20E-06	VAPEEHPVLLTEAPLNPK
P60709|ACTB_HUMAN	1061.873	74.24	3.90E-06	TTGIVMDSGDGVTHTVPIYEGYALPHAILR
P60709|ACTB_HUMAN	1061.872	74.48	3.60E-06	TTGIVMDSGDGVTHTVPIYEGYALPHAILR
P60709|ACTB_HUMAN	1061.874	78.06	1.60E-06	TTGIVMDSGDGVTHTVPIYEGYALPHAILR
P60709|ACTB_HUMAN	1061.874	79.05	1.30E-06	TTGIVMDSGDGVTHTVPIYEGYALPHAILR
P60709|ACTB_HUMAN	1108.037	76.26	1.00E-06	DLYANTVLSGGTTMYPGIADR
P60709|ACTB_HUMAN	977.5335	81.15	7.20E-07	VAPEEHPVLLTEAPLNPK
P60709|ACTB_HUMAN	1061.873	84.13	4.10E-07	TTGIVMDSGDGVTHTVPIYEGYALPHAILR
P60709|ACTB_HUMAN	1108.037	87.74	7.50E-08	DLYANTVLSGGTTMYPGIADR
P60709|ACTB_HUMAN	1108.035	87.83	6.30E-08	DLYANTVLSGGTTMYPGIADR
P60709|ACTB_HUMAN	977.5338	93.46	4.00E-08	VAPEEHPVLLTEAPLNPK
P60709|ACTB_HUMAN	1108.036	93.15	2.10E-08	DLYANTVLSGGTTMYPGIADR
P60709|ACTB_HUMAN	1061.873	103.06	5.10E-09	TTGIVMDSGDGVTHTVPIYEGYALPHAILR
P60709|ACTB_HUMAN	1108.034	103.68	1.70E-09	DLYANTVLSGGTTMYPGIADR
P60709|ACTB_HUMAN	1108.035	105.74	1.00E-09	DLYANTVLSGGTTMYPGIADR
P60709|ACTB_HUMAN	1108.036	112.32	2.50E-10	DLYANTVLSGGTTMYPGIADR
P61978|HNRPK_HUMAN	1295.196	43.66	0.0046	IITITGTQDQIQNAQYLLQNSVK
P61978|HNRPK_HUMAN	670.9028	41.65	0.0046	IILDLISESPIK
P61978|HNRPK_H	527.3	38.99	0.0045	VVLIGGKPDR

UMAN	228			
P61978|HNRPK_HUMAN	579.2717	35.08	0.0041	RPAEDMEEEQAFKR
P61978|HNRPK_HUMAN	959.018	44.09	0.0039	GSYGDLGGPIITTQVTIPK
P61978|HNRPK_HUMAN	579.2732	36.41	0.0034	RPAEDMEEEQAFKR
P61978|HNRPK_HUMAN	959.0176	46.04	0.0028	GSYGDLGGPIITTQVTIPK
P61978|HNRPK_HUMAN	890.9002	36.26	0.0024	TDYNASVSVPDSSGPER
P61978|HNRPK_HUMAN	868.4088	43.23	0.0021	RPAEDMEEEQAFKR
P61978|HNRPK_HUMAN	890.9017	37.17	0.002	TDYNASVSVPDSSGPER
P61978|HNRPK_HUMAN	890.9005	37.66	0.0017	TDYNASVSVPDSSGPER
P61978|HNRPK_HUMAN	868.4075	45.34	0.0012	RPAEDMEEEQAFKR
P61978|HNRPK_HUMAN	579.2736	46.04	0.0011	RPAEDMEEEQAFKR
P61978|HNRPK_HUMAN	868.4031	40.85	0.0011	RPAEDMEEEQAFKR
P61978|HNRPK_HUMAN	579.2717	41.89	0.00084	RPAEDMEEEQAFKR
P61978|HNRPK_HUMAN	959.0187	50.69	0.00082	GSYGDLGGPIITTQVTIPK
P61978|HNRPK_HUMAN	890.8995	41.7	0.0007	TDYNASVSVPDSSGPER
P61978|HNRPK_HUMAN	890.9006	42.06	0.00065	TDYNASVSVPDSSGPER
P61978|HNRPK_HUMAN	670.9038	50.09	0.00057	IILDLISESPIK
P61978|HNRPK_HUMAN	579.272	44.74	0.00045	RPAEDMEEEQAFKR
P61978|HNRPK_HUMAN	579.2721	45.19	0.00043	RPAEDMEEEQAFKR
P61978|HNRPK_HUMAN	527.3231	49.39	0.00041	VVLIGGKPDR
P61978|HNRPK_HUMAN	868.4057	45.75	0.00041	RPAEDMEEEQAFKR
P61978|HNRPK_HUMAN	1295.194	54.39	0.00039	IITITGTQDQIQNAQYLLQNSVK
P61978|HNRPK_HUMAN	959.0169	54.65	0.00038	GSYGDLGGPIITTQVTIPK
P61978|HNRPK_HUMAN	959.018	54.2	0.00038	GSYGDLGGPIITTQVTIPK
P61978|HNRPK_HUMAN	959.0184	54.24	0.00037	GSYGDLGGPIITTQVTIPK
P61978|HNRPK_HUMAN	890.8997	45.08	0.00032	TDYNASVSVPDSSGPER
P61978|HNRPK_HUMAN	868.4062	47.3	0.00027	RPAEDMEEEQAFKR
P61978|HNRPK_HUMAN	890.8992	46.29	0.00024	TDYNASVSVPDSSGPER

P61978|HNRPK_HUMAN	670.9035	54.6	0.00023	IILDLISESPIK
P61978|HNRPK_HUMAN	959.0174	57.35	0.0002	GSYGDLGGPIITTQVTIPK
P61978|HNRPK_HUMAN	630.2894	45.32	0.00016	IDEPLEGSEDR
P61978|HNRPK_HUMAN	759.9691	54.52	0.00015	LLIHQSLAGGIIGVK
P61978|HNRPK_HUMAN	959.0182	58.61	0.00014	GSYGDLGGPIITTQVTIPK
P61978|HNRPK_HUMAN	630.2887	46.79	0.00012	IDEPLEGSEDR
P61978|HNRPK_HUMAN	630.2882	46.29	0.0001	IDEPLEGSEDR
P61978|HNRPK_HUMAN	670.905	57.78	9.90E-05	IILDLISESPIK
P61978|HNRPK_HUMAN	890.9007	51.68	7.10E-05	TDYNASVSVPDSSGPER
P61978|HNRPK_HUMAN	630.2888	49.32	6.80E-05	IDEPLEGSEDR
P61978|HNRPK_HUMAN	959.0189	62	6.50E-05	GSYGDLGGPIITTQVTIPK
P61978|HNRPK_HUMAN	868.4083	58.69	5.80E-05	RPAEDMEEEQAFKR
P61978|HNRPK_HUMAN	670.9057	60.66	4.80E-05	IILDLISESPIK
P61978|HNRPK_HUMAN	890.903	54.43	3.70E-05	TDYNASVSVPDSSGPER
P61978|HNRPK_HUMAN	1295.195	64.77	3.60E-05	IITITGTQDQIQNAQYLLQNSVK
P61978|HNRPK_HUMAN	759.9683	61.59	3.10E-05	LLIHQSLAGGIIGVK
P61978|HNRPK_HUMAN	890.9012	55.59	3.00E-05	TDYNASVSVPDSSGPER
P61978|HNRPK_HUMAN	1295.196	65.93	2.70E-05	IITITGTQDQIQNAQYLLQNSVK
P61978|HNRPK_HUMAN	759.9699	62.69	2.20E-05	LLIHQSLAGGIIGVK
P61978|HNRPK_HUMAN	868.4048	59.05	1.90E-05	RPAEDMEEEQAFKR
P61978|HNRPK_HUMAN	630.2885	54.99	1.80E-05	IDEPLEGSEDR
P61978|HNRPK_HUMAN	959.0167	68.12	1.60E-05	GSYGDLGGPIITTQVTIPK
P61978|HNRPK_HUMAN	868.4083	65.02	1.40E-05	RPAEDMEEEQAFKR
P61978|HNRPK_HUMAN	1295.196	69.48	1.20E-05	IITITGTQDQIQNAQYLLQNSVK
P61978|HNRPK_HUMAN	959.0163	70.76	8.90E-06	GSYGDLGGPIITTQVTIPK
P61978|HNRPK_HUMAN	630.2883	57.42	8.00E-06	IDEPLEGSEDR
P61978|HNRPK_HUMAN	1295.195	73.78	4.70E-06	IITITGTQDQIQNAQYLLQNSVK
P61978|HNRPK_H	1295.	77.05	2.20E-06	IITITGTQDQIQNAQYLLQNSVK

UMAN	195			
P61978|HNRPK_HUMAN	1295.195	79.47	1.20E-06	IITITGTQDQIQNAQYLLQNSVK
P61978|HNRPK_HUMAN	890.9006	69.36	1.20E-06	TDYNASVSVPDSSGPER
P61978|HNRPK_HUMAN	1295.196	81.38	7.80E-07	IITITGTQDQIQNAQYLLQNSVK
P61978|HNRPK_HUMAN	1295.195	85.55	3.10E-07	IITITGTQDQIQNAQYLLQNSVK
P61978|HNRPK_HUMAN	1295.195	85.56	3.00E-07	IITITGTQDQIQNAQYLLQNSVK
P61978|HNRPK_HUMAN	1295.195	85.79	2.80E-07	IITITGTQDQIQNAQYLLQNSVK
P61978|HNRPK_HUMAN	1295.195	95	3.50E-08	IITITGTQDQIQNAQYLLQNSVK
P62158|CALM_HUMAN	922.9479	44.14	0.0011	EAFSLFDKDGDGTITTK
P62158|CALM_HUMAN	922.9473	52.25	0.00018	EAFSLFDKDGDGTITTK
P62158|CALM_HUMAN	877.9388	56.1	0.00011	VFDKDGNGYISAAELR
P62158|CALM_HUMAN	922.9511	54.92	0.00011	EAFSLFDKDGDGTITTK
P62158|CALM_HUMAN	877.9386	87.83	6.90E-08	VFDKDGNGYISAAELR
P62306|RUXF_HUMAN	769.3003	57.73	1.70E-06	GVEEEEEDGEMRE
P62314|SMD1_HUMAN	635.3546	39.71	0.0049	LSHETVTIELK
P62314|SMD1_HUMAN	1105.055	42.51	0.004	NGTQVHGTITGVDVSMNTHLK
P62314|SMD1_HUMAN	635.3548	45.99	0.0012	LSHETVTIELK
P62314|SMD1_HUMAN	1105.055	53.36	0.00036	NGTQVHGTITGVDVSMNTHLK
P62314|SMD1_HUMAN	1144.126	54.85	0.00034	YFILPDSLPLDTLLVDVEPK
P62314|SMD1_HUMAN	1144.126	59.17	0.00012	YFILPDSLPLDTLLVDVEPK
P62314|SMD1_HUMAN	777.9319	59.19	9.20E-05	NREPVQLETLSIR
P62314|SMD1_HUMAN	777.9316	60.43	7.10E-05	NREPVQLETLSIR
P62314|SMD1_HUMAN	777.9318	62.52	4.30E-05	NREPVQLETLSIR
P62314|SMD1_HUMAN	1144.125	66.24	2.50E-05	YFILPDSLPLDTLLVDVEPK
P62314|SMD1_HUMAN	777.9312	65.88	2.00E-05	NREPVQLETLSIR
P62314|SMD1_HUMAN	777.9316	68.72	1.10E-05	NREPVQLETLSIR
P62314|SMD1_HUMAN	1105.057	69.06	9.60E-06	NGTQVHGTITGVDVSMNTHLK
P62314|SMD1_HUMAN	1144.126	71.83	6.60E-06	YFILPDSLPLDTLLVDVEPK

P62314|SMD1_HUMAN	1144.124	72.48	6.00E-06	YFILPDSLPLDTLLVDVEPK
P62314|SMD1_HUMAN	777.9319	73.93	3.10E-06	NREPVQLETLSIR
P62314|SMD1_HUMAN	777.9312	74.29	2.90E-06	NREPVQLETLSIR
P62314|SMD1_HUMAN	1144.127	76.24	2.40E-06	YFILPDSLPLDTLLVDVEPK
P62314|SMD1_HUMAN	777.9316	76.33	1.80E-06	NREPVQLETLSIR
P62314|SMD1_HUMAN	1144.126	79.66	1.20E-06	YFILPDSLPLDTLLVDVEPK
P62314|SMD1_HUMAN	1144.125	82.17	6.20E-07	YFILPDSLPLDTLLVDVEPK
P62316|SMD2_HUMAN	1003.999	62.34	3.20E-05	EEEEFNTGPLSVLTQSVK
P62316|SMD2_HUMAN	1082.046	64.65	2.60E-05	REEEEFNTGPLSVLTQSVK
P62316|SMD2_HUMAN	1003.997	65.78	1.40E-05	EEEEFNTGPLSVLTQSVK
P62316|SMD2_HUMAN	1003.998	67.8	8.50E-06	EEEEFNTGPLSVLTQSVK
P62316|SMD2_HUMAN	1082.047	74.02	3.10E-06	REEEEFNTGPLSVLTQSVK
P62316|SMD2_HUMAN	1082.048	74.73	2.60E-06	REEEEFNTGPLSVLTQSVK
P62316|SMD2_HUMAN	1003.996	80.82	4.10E-07	EEEEFNTGPLSVLTQSVK
P62316|SMD2_HUMAN	1003.998	84.13	2.10E-07	EEEEFNTGPLSVLTQSVK
P62316|SMD2_HUMAN	1082.048	87.64	1.30E-07	REEEEFNTGPLSVLTQSVK
P62316|SMD2_HUMAN	1003.996	89.03	6.20E-08	EEEEFNTGPLSVLTQSVK
P62316|SMD2_HUMAN	1003.996	92.9	2.50E-08	EEEEFNTGPLSVLTQSVK
P62316|SMD2_HUMAN	1003.999	96.58	1.20E-08	EEEEFNTGPLSVLTQSVK
P62316|SMD2_HUMAN	1082.046	110.54	6.50E-10	REEEEFNTGPLSVLTQSVK
P62318|SMD3_HUMAN	545.3201	41.09	0.005	FLILPDMLK
P62318|SMD3_HUMAN	545.3217	44.83	0.0023	FLILPDMLK
P62318|SMD3_HUMAN	609.8447	52.18	0.00053	VAQLEQVYIR
P62318|SMD3_HUMAN	609.8431	65	2.20E-05	VAQLEQVYIR
P62318|SMD3_HUMAN	609.8438	66.97	1.30E-05	VAQLEQVYIR
P62318|SMD3_HUMAN	609.8441	67.62	1.10E-05	VAQLEQVYIR
P62318|SMD3_HUMAN	609.8438	67.82	1.00E-05	VAQLEQVYIR
P62318|SMD3_H	609.8	68.9	9.00E-06	VAQLEQVYIR

UMAN	434			
P62318|SMD3_HUMAN	609.8434	68.93	8.70E-06	VAQLEQVYIR
P62318|SMD3_HUMAN	609.8436	68.99	8.20E-06	VAQLEQVYIR
P62318|SMD3_HUMAN	609.8442	71.19	4.70E-06	VAQLEQVYIR
P62318|SMD3_HUMAN	609.8438	73	3.10E-06	VAQLEQVYIR
P62318|SMD3_HUMAN	609.8444	81.48	6.00E-07	VAQLEQVYIR
P62318|SMD3_HUMAN	609.8448	81.51	5.70E-07	VAQLEQVYIR
P62318|SMD3_HUMAN	609.8434	81.43	5.00E-07	VAQLEQVYIR
P62318|SMD3_HUMAN	609.8431	81.59	4.70E-07	VAQLEQVYIR
P62318|SMD3_HUMAN	609.8439	81.6	4.30E-07	VAQLEQVYIR
P62750|RL23A_HUMAN	562.7855	36.2	0.0049	FPLTTESAMK
P62750|RL23A_HUMAN	562.7853	39.21	0.0024	FPLTTESAMK
P62750|RL23A_HUMAN	532.8015	43.88	0.0021	KLYDIDVAK
P62750|RL23A_HUMAN	532.8027	44.68	0.0016	KLYDIDVAK
P62750|RL23A_HUMAN	532.8011	49.72	0.00053	KLYDIDVAK
P62805|H4_HUMAN	567.7734	34.47	0.005	DAVTYTEHAK
P62805|H4_HUMAN	663.38	40.92	0.0049	DNIQGITKPAIR
P62805|H4_HUMAN	668.8629	39.72	0.0049	RISGLIYEETR
P62805|H4_HUMAN	668.8627	40.44	0.0043	RISGLIYEETR
P62805|H4_HUMAN	663.3772	42.36	0.0041	DNIQGITKPAIR
P62805|H4_HUMAN	489.6062	41.95	0.0041	TVTAMDVVYALKR
P62805|H4_HUMAN	797.9514	42.32	0.004	KTVTAMDVVYALKR
P62805|H4_HUMAN	663.3774	42.62	0.0038	DNIQGITKPAIR
P62805|H4_HUMAN	567.7736	35.66	0.0038	DAVTYTEHAK
P62805|H4_HUMAN	719.8991	41.66	0.0037	KTVTAMDVVYALK
P62805|H4_HUMAN	668.8628	41.02	0.0036	RISGLIYEETR
P62805|H4_HUMAN	668.8632	40.96	0.0036	RISGLIYEETR
P62805|H4_HUMAN	663.38	42.41	0.0035	DNIQGITKPAIR

P62805|H4_HUMAN	489.6053	42.92	0.0033	TVTAMDVVYALKR
P62805|H4_HUMAN	663.38	42.66	0.0033	DNIQGITKPAIR
P62805|H4_HUMAN	663.38	42.61	0.0033	DNIQGITKPAIR
P62805|H4_HUMAN	663.38	43.43	0.0028	DNIQGITKPAIR
P62805|H4_HUMAN	606.3458	43.1	0.0026	GGKGLGKGGAKR
P62805|H4_HUMAN	663.3798	43.87	0.0025	DNIQGITKPAIR
P62805|H4_HUMAN	668.8628	43.74	0.0019	RISGLIYEETR
P62805|H4_HUMAN	495.2905	46.25	0.0017	VFLENVIR
P62805|H4_HUMAN	719.9009	46.17	0.0017	KTVTAMDVVYALK
P62805|H4_HUMAN	663.3774	46.07	0.0017	DNIQGITKPAIR
P62805|H4_HUMAN	663.38	45.85	0.0016	DNIQGITKPAIR
P62805|H4_HUMAN	464.2706	42.32	0.0016	GLGKGGAKR
P62805|H4_HUMAN	464.2708	42.28	0.0016	GLGKGGAKR
P62805|H4_HUMAN	464.2704	42.21	0.0016	GLGKGGAKR
P62805|H4_HUMAN	464.2705	42.18	0.0016	GLGKGGAKR
P62805|H4_HUMAN	590.8138	44.02	0.0014	ISGLIYEETR
P62805|H4_HUMAN	567.7726	40.07	0.0014	DAVTYTEHAK
P62805|H4_HUMAN	464.2712	41.97	0.0013	GLGKGGAKR
P62805|H4_HUMAN	567.7729	40.35	0.0013	DAVTYTEHAK
P62805|H4_HUMAN	567.7731	40.16	0.0013	DAVTYTEHAK
P62805|H4_HUMAN	495.2906	47.47	0.0012	VFLENVIR
P62805|H4_HUMAN	668.8634	46.24	0.0012	RISGLIYEETR
P62805|H4_HUMAN	567.7735	41.01	0.0011	DAVTYTEHAK
P62805|H4_HUMAN	567.7731	41.4	0.001	DAVTYTEHAK
P62805|H4_HUMAN	567.7729	43.05	0.00069	DAVTYTEHAK
P62805|H4_HUMAN	668.8627	48.54	0.00066	RISGLIYEETR
P62805|H4_HUMAN	567.7727	43.3	0.00066	DAVTYTEHAK
P62805|H4_HUM	663.3	50.21	0.00058	DNIQGITKPAIR

AN	8			
P62805|H4_HUMAN	567.7733	44.26	0.00052	DAVTYTEHAK
P62805|H4_HUMAN	567.7733	44.51	0.00049	DAVTYTEHAK
P62805|H4_HUMAN	663.38	51.07	0.00047	DNIQGITKPAIR
P62805|H4_HUMAN	797.9537	51.56	0.00045	KTVTAMDVVYALKR
P62805|H4_HUMAN	495.2903	53.19	0.00033	VFLENVIR
P62805|H4_HUMAN	495.2902	53.26	0.00032	VFLENVIR
P62805|H4_HUMAN	606.3461	51.1	0.00032	GGKGLGKGGAKR
P62805|H4_HUMAN	663.38	53.5	0.00027	DNIQGITKPAIR
P62805|H4_HUMAN	733.9033	55.27	0.00018	TVTAMDVVYALKR
P62805|H4_HUMAN	663.38	55.23	0.00018	DNIQGITKPAIR
P62805|H4_HUMAN	590.8112	53.47	0.00018	ISGLIYEETR
P62805|H4_HUMAN	797.9511	57.22	0.00014	KTVTAMDVVYALKR
P62805|H4_HUMAN	495.2905	58.06	0.00011	VFLENVIR
P62805|H4_HUMAN	532.3026	57.77	0.00011	KTVTAMDVVYALKR
P62805|H4_HUMAN	495.2906	58.4	0.0001	VFLENVIR
P62805|H4_HUMAN	495.2908	58.5	9.90E-05	VFLENVIR
P62805|H4_HUMAN	733.9023	57.82	9.90E-05	TVTAMDVVYALKR
P62805|H4_HUMAN	495.2903	58.57	9.60E-05	VFLENVIR
P62805|H4_HUMAN	495.2903	58.59	9.50E-05	VFLENVIR
P62805|H4_HUMAN	655.8527	56.79	9.20E-05	TVTAMDVVYALK
P62805|H4_HUMAN	495.2912	58.12	8.40E-05	VFLENVIR
P62805|H4_HUMAN	655.853	57.33	8.10E-05	TVTAMDVVYALK
P62805|H4_HUMAN	590.8118	57.08	7.80E-05	ISGLIYEETR
P62805|H4_HUMAN	606.3455	58.54	7.50E-05	GGKGLGKGGAKR
P62805|H4_HUMAN	590.8112	57.69	6.90E-05	ISGLIYEETR
P62805|H4_HUMAN	590.812	57.58	6.90E-05	ISGLIYEETR
P62805|H4_HUMAN	590.8115	57.46	6.70E-05	ISGLIYEETR

P62805|H4_HUMAN	495.2904	60.32	6.50E-05	VFLENVIR
P62805|H4_HUMAN	719.8995	59.2	6.50E-05	KTVTAMDVVYALK
P62805|H4_HUMAN	495.2904	60.46	6.30E-05	VFLENVIR
P62805|H4_HUMAN	495.2904	60.46	6.20E-05	VFLENVIR
P62805|H4_HUMAN	495.2906	60.54	6.10E-05	VFLENVIR
P62805|H4_HUMAN	590.8114	58.5	5.30E-05	ISGLIYEETR
P62805|H4_HUMAN	606.3457	60.68	4.60E-05	GGKGLGKGGAKR
P62805|H4_HUMAN	590.8121	59.02	4.60E-05	ISGLIYEETR
P62805|H4_HUMAN	590.8121	59.1	4.50E-05	ISGLIYEETR
P62805|H4_HUMAN	590.8117	59.39	4.40E-05	ISGLIYEETR
P62805|H4_HUMAN	495.2907	62.23	4.20E-05	VFLENVIR
P62805|H4_HUMAN	719.9005	61.05	4.20E-05	KTVTAMDVVYALK
P62805|H4_HUMAN	590.8115	61.19	2.80E-05	ISGLIYEETR
P62805|H4_HUMAN	532.3026	64.17	2.50E-05	KTVTAMDVVYALKR
P62805|H4_HUMAN	590.8118	62.03	2.50E-05	ISGLIYEETR
P62805|H4_HUMAN	797.9515	64.93	2.20E-05	KTVTAMDVVYALKR
P62805|H4_HUMAN	532.3029	64.61	2.20E-05	KTVTAMDVVYALKR
P62805|H4_HUMAN	590.8124	62.32	2.10E-05	ISGLIYEETR
P62805|H4_HUMAN	495.2905	65.52	2.00E-05	VFLENVIR
P62805|H4_HUMAN	590.8119	63.53	1.80E-05	ISGLIYEETR
P62805|H4_HUMAN	590.812	63.49	1.80E-05	ISGLIYEETR
P62805|H4_HUMAN	590.8117	63.28	1.80E-05	ISGLIYEETR
P62805|H4_HUMAN	719.8992	67.03	1.10E-05	KTVTAMDVVYALK
P62805|H4_HUMAN	590.812	65.62	1.10E-05	ISGLIYEETR
P62805|H4_HUMAN	590.8116	65.75	1.00E-05	ISGLIYEETR
P62805|H4_HUMAN	733.9033	67.97	9.70E-06	TVTAMDVVYALKR
P62805|H4_HUMAN	733.9041	68.51	9.40E-06	TVTAMDVVYALKR
P62805|H4_HUM	733.9	68.52	8.50E-06	TVTAMDVVYALKR

AN	033			
P62805|H4_HUMAN	733.9035	68.13	8.20E-06	TVTAMDVVYALKR
P62805|H4_HUMAN	733.9033	68.78	8.00E-06	TVTAMDVVYALKR
P62805|H4_HUMAN	655.8532	66.66	8.00E-06	TVTAMDVVYALK
P62805|H4_HUMAN	719.9001	68.54	7.50E-06	KTVTAMDVVYALK
P62805|H4_HUMAN	655.853	68.77	5.80E-06	TVTAMDVVYALK
P62805|H4_HUMAN	733.9031	71.18	4.60E-06	TVTAMDVVYALKR
P62805|H4_HUMAN	733.9028	71.28	4.50E-06	TVTAMDVVYALKR
P62805|H4_HUMAN	655.8539	70.69	4.40E-06	TVTAMDVVYALK
P62805|H4_HUMAN	797.9517	72.1	4.20E-06	KTVTAMDVVYALKR
P62805|H4_HUMAN	733.9039	72.55	3.80E-06	TVTAMDVVYALKR
P62805|H4_HUMAN	733.9036	71.45	3.80E-06	TVTAMDVVYALKR
P62805|H4_HUMAN	655.8528	70.68	3.80E-06	TVTAMDVVYALK
P62805|H4_HUMAN	655.8532	70.22	3.50E-06	TVTAMDVVYALK
P62805|H4_HUMAN	733.9039	73.74	2.90E-06	TVTAMDVVYALKR
P62805|H4_HUMAN	655.8532	71.3	2.80E-06	TVTAMDVVYALK
P62805|H4_HUMAN	532.3025	73.89	2.70E-06	KTVTAMDVVYALKR
P62805|H4_HUMAN	532.3026	73.73	2.70E-06	KTVTAMDVVYALKR
P62805|H4_HUMAN	733.9037	74.08	2.60E-06	TVTAMDVVYALKR
P62805|H4_HUMAN	655.8522	73.43	1.90E-06	TVTAMDVVYALK
P62805|H4_HUMAN	655.8526	74.51	1.60E-06	TVTAMDVVYALK
P62805|H4_HUMAN	532.3024	76.79	1.40E-06	KTVTAMDVVYALKR
P62805|H4_HUMAN	655.8532	75.94	9.40E-07	TVTAMDVVYALK
P62805|H4_HUMAN	532.3026	79.1	7.90E-07	KTVTAMDVVYALKR
P62805|H4_HUMAN	532.3019	80.08	7.60E-07	KTVTAMDVVYALKR
P62805|H4_HUMAN	655.8527	78.36	6.40E-07	TVTAMDVVYALK
P62805|H4_HUMAN	655.8529	79.78	4.60E-07	TVTAMDVVYALK
P62805|H4_HUMAN	719.9001	81.23	4.10E-07	KTVTAMDVVYALK

P62805|H4_HUMAN	719.9002	82.02	3.40E-07	KTVTAMDVVYALK
P62805|H4_HUMAN	655.853	81.05	3.40E-07	TVTAMDVVYALK
P62805|H4_HUMAN	532.3024	83.06	3.20E-07	KTVTAMDVVYALKR
P62805|H4_HUMAN	532.3026	83.49	2.90E-07	KTVTAMDVVYALKR
P62805|H4_HUMAN	797.9495	84.74	2.60E-07	KTVTAMDVVYALKR
P62805|H4_HUMAN	532.3022	85.6	1.90E-07	KTVTAMDVVYALKR
P62805|H4_HUMAN	655.853	83.6	1.90E-07	TVTAMDVVYALK
P62805|H4_HUMAN	719.9007	86.77	1.50E-07	KTVTAMDVVYALK
P62805|H4_HUMAN	532.3025	86.51	1.50E-07	KTVTAMDVVYALKR
P62805|H4_HUMAN	797.9503	86.45	1.50E-07	KTVTAMDVVYALKR
P62805|H4_HUMAN	532.3019	87.88	1.30E-07	KTVTAMDVVYALKR
P62805|H4_HUMAN	655.8529	86.47	9.90E-08	TVTAMDVVYALK
P62805|H4_HUMAN	655.8532	86.55	8.20E-08	TVTAMDVVYALK
P62805|H4_HUMAN	719.9008	91.18	5.60E-08	KTVTAMDVVYALK
P62805|H4_HUMAN	719.9	91.45	3.90E-08	KTVTAMDVVYALK
P62805|H4_HUMAN	719.9007	94.18	2.80E-08	KTVTAMDVVYALK
P62805|H4_HUMAN	719.9	95.61	1.50E-08	KTVTAMDVVYALK
P62805|H4_HUMAN	719.9	95.85	1.40E-08	KTVTAMDVVYALK
P62805|H4_HUMAN	719.9005	95.72	1.40E-08	KTVTAMDVVYALK
P62805|H4_HUMAN	719.9	96.49	1.20E-08	KTVTAMDVVYALK
P62805|H4_HUMAN	797.9498	103.83	2.90E-09	KTVTAMDVVYALKR
P62805|H4_HUMAN	797.9509	104.34	2.70E-09	KTVTAMDVVYALKR
P62805|H4_HUMAN	797.9503	103.78	2.70E-09	KTVTAMDVVYALKR
P62805|H4_HUMAN	797.9526	104.48	2.50E-09	KTVTAMDVVYALKR
P62805|H4_HUMAN	719.8996	103.55	2.40E-09	KTVTAMDVVYALK
P62805|H4_HUMAN	719.9003	115.5	1.50E-10	KTVTAMDVVYALK
P62805|H4_HUMAN	797.9506	124.2	2.40E-11	KTVTAMDVVYALKR
P62851|RS25_HU	659.8	54.42	0.00024	DKLNNLVLFDK

MAN	701			
P62851|RS25_HUMAN	659.8687	56.92	0.00015	DKLNNLVLFDK
P62899|RL31_HUMAN	822.9622	44.31	0.0037	LYTLVTYVPVTTFK
P62899|RL31_HUMAN	822.9645	48.3	0.0015	LYTLVTYVPVTTFK
P62899|RL31_HUMAN	822.9639	59.71	0.0001	LYTLVTYVPVTTFK
P62913|RL11_HUMAN	773.9273	42.86	0.0045	VLEQLTGQTPVFSK
P62987|RL40_HUMAN	762.3919	40.59	0.0041	IQDKEGIPPDQQR
P62987|RL40_HUMAN	748.7341	45.31	0.0034	TLSDYNIQKESTLHLVLR
P62987|RL40_HUMAN	762.3927	41.4	0.0034	IQDKEGIPPDQQR
P62987|RL40_HUMAN	894.4651	44.09	0.0028	TITLEVEPSDTIENVK
P62987|RL40_HUMAN	762.3929	42.25	0.0028	IQDKEGIPPDQQR
P62987|RL40_HUMAN	762.3928	42.21	0.0028	IQDKEGIPPDQQR
P62987|RL40_HUMAN	762.3931	42.14	0.0027	IQDKEGIPPDQQR
P62987|RL40_HUMAN	762.3925	42.26	0.0026	IQDKEGIPPDQQR
P62987|RL40_HUMAN	383.2198	37.04	0.0026	MQIFVK
P62987|RL40_HUMAN	762.3924	42.99	0.0024	IQDKEGIPPDQQR
P62987|RL40_HUMAN	762.3929	43.18	0.0023	IQDKEGIPPDQQR
P62987|RL40_HUMAN	894.4648	45.23	0.0022	TITLEVEPSDTIENVK
P62987|RL40_HUMAN	762.3926	43.37	0.0022	IQDKEGIPPDQQR
P62987|RL40_HUMAN	541.2778	41.08	0.0019	TLSDYNIQK
P62987|RL40_HUMAN	894.4648	46.11	0.0018	TITLEVEPSDTIENVK
P62987|RL40_HUMAN	762.3928	44.12	0.0018	IQDKEGIPPDQQR
P62987|RL40_HUMAN	762.3925	43.86	0.0018	IQDKEGIPPDQQR
P62987|RL40_HUMAN	762.3922	45.29	0.0014	IQDKEGIPPDQQR
P62987|RL40_HUMAN	534.312	44.27	0.0013	ESTLHLVLR
P62987|RL40_HUMAN	894.4652	48.16	0.0012	TITLEVEPSDTIENVK
P62987|RL40_HUMAN	534.3114	45.02	0.0012	ESTLHLVLR
P62987|RL40_HUMAN	894.4642	49.17	0.00099	TITLEVEPSDTIENVK

P62987|RL40_HUMAN	762.3922	46.97	0.00095	IQDKEGIPPDQQR
P62987|RL40_HUMAN	541.2778	44.12	0.00094	TLSDYNIQK
P62987|RL40_HUMAN	894.4653	49.28	0.00093	TITLEVEPSDTIENVK
P62987|RL40_HUMAN	762.3925	47.23	0.00088	IQDKEGIPPDQQR
P62987|RL40_HUMAN	534.312	45.91	0.00088	ESTLHLVLR
P62987|RL40_HUMAN	762.3918	47.43	0.00085	IQDKEGIPPDQQR
P62987|RL40_HUMAN	762.3928	47.82	0.0008	IQDKEGIPPDQQR
P62987|RL40_HUMAN	762.3918	47.96	0.00075	IQDKEGIPPDQQR
P62987|RL40_HUMAN	762.3928	48.2	0.00072	IQDKEGIPPDQQR
P62987|RL40_HUMAN	762.3922	48.32	0.0007	IQDKEGIPPDQQR
P62987|RL40_HUMAN	762.3932	48.03	0.00069	IQDKEGIPPDQQR
P62987|RL40_HUMAN	762.3919	48.51	0.00066	IQDKEGIPPDQQR
P62987|RL40_HUMAN	762.3923	48.67	0.00064	IQDKEGIPPDQQR
P62987|RL40_HUMAN	894.465	50.69	0.00061	TITLEVEPSDTIENVK
P62987|RL40_HUMAN	762.3924	48.87	0.00061	IQDKEGIPPDQQR
P62987|RL40_HUMAN	541.2782	46.31	0.00059	TLSDYNIQK
P62987|RL40_HUMAN	762.3923	49.1	0.00058	IQDKEGIPPDQQR
P62987|RL40_HUMAN	762.3928	49.19	0.00057	IQDKEGIPPDQQR
P62987|RL40_HUMAN	894.465	51.88	0.00046	TITLEVEPSDTIENVK
P62987|RL40_HUMAN	762.3927	50.22	0.00045	IQDKEGIPPDQQR
P62987|RL40_HUMAN	894.4644	52.71	0.00044	TITLEVEPSDTIENVK
P62987|RL40_HUMAN	541.2779	47.92	0.00041	TLSDYNIQK
P62987|RL40_HUMAN	894.4652	53.47	0.00036	TITLEVEPSDTIENVK
P62987|RL40_HUMAN	762.3915	51.16	0.00036	IQDKEGIPPDQQR
P62987|RL40_HUMAN	762.3937	50.91	0.00036	IQDKEGIPPDQQR
P62987|RL40_HUMAN	762.3924	51.41	0.00034	IQDKEGIPPDQQR
P62987|RL40_HUMAN	762.3923	51.69	0.00032	IQDKEGIPPDQQR
P62987|RL40_HU	534.3	50.31	0.00032	ESTLHLVLR

MAN	119			
P62987|RL40_HUMAN	762.3929	51.85	0.00031	IQDKEGIPPDQQR
P62987|RL40_HUMAN	762.392	51.94	0.0003	IQDKEGIPPDQQR
P62987|RL40_HUMAN	541.2778	49.4	0.00028	TLSDYNIQK
P62987|RL40_HUMAN	762.3925	52.64	0.00025	IQDKEGIPPDQQR
P62987|RL40_HUMAN	762.392	52.92	0.00024	IQDKEGIPPDQQR
P62987|RL40_HUMAN	762.3919	53.05	0.00023	IQDKEGIPPDQQR
P62987|RL40_HUMAN	894.4642	55.78	0.00022	TITLEVEPSDTIENVK
P62987|RL40_HUMAN	894.4651	55.7	0.00021	TITLEVEPSDTIENVK
P62987|RL40_HUMAN	541.2773	50.76	0.00021	TLSDYNIQK
P62987|RL40_HUMAN	894.465	56.53	0.00016	TITLEVEPSDTIENVK
P62987|RL40_HUMAN	762.3924	54.78	0.00016	IQDKEGIPPDQQR
P62987|RL40_HUMAN	894.4656	57.93	0.00013	TITLEVEPSDTIENVK
P62987|RL40_HUMAN	762.3925	55.41	0.00013	IQDKEGIPPDQQR
P62987|RL40_HUMAN	894.4656	58.89	0.0001	TITLEVEPSDTIENVK
P62987|RL40_HUMAN	541.2776	53.99	9.70E-05	TLSDYNIQK
P62987|RL40_HUMAN	894.4646	59.82	8.60E-05	TITLEVEPSDTIENVK
P62987|RL40_HUMAN	541.2776	55.79	6.40E-05	TLSDYNIQK
P62987|RL40_HUMAN	894.4648	61.33	5.20E-05	TITLEVEPSDTIENVK
P62987|RL40_HUMAN	762.3928	59.74	5.00E-05	IQDKEGIPPDQQR
P62987|RL40_HUMAN	894.4651	63.35	3.60E-05	TITLEVEPSDTIENVK
P62987|RL40_HUMAN	894.4645	65.23	2.50E-05	TITLEVEPSDTIENVK
P62995|TRA2B_HUMAN	905.949	42.27	0.0022	YGPIADVSIVYDQQSR
P62995|TRA2B_HUMAN	811.38	39.28	0.0019	GFAFVYFENVDDAK
P62995|TRA2B_HUMAN	811.3833	42.38	0.0011	GFAFVYFENVDDAK
P62995|TRA2B_HUMAN	905.9492	46.71	0.00077	YGPIADVSIVYDQQSR
P62995|TRA2B_HUMAN	905.9496	54.16	0.00015	YGPIADVSIVYDQQSR
P62995|TRA2B_HUMAN	905.9478	54.01	0.00015	YGPIADVSIVYDQQSR

P62995|TRA2B_HUMAN	905.948	55.94	9.40E-05	YGPIADVSIVYDQQSR
P62995|TRA2B_HUMAN	905.9478	57.43	7.00E-05	YGPIADVSIVYDQQSR
P62995|TRA2B_HUMAN	811.3813	57.06	2.90E-05	GFAFVYFENVDDAK
P62995|TRA2B_HUMAN	811.3831	65.04	5.20E-06	GFAFVYFENVDDAK
P62995|TRA2B_HUMAN	905.9484	68.85	5.00E-06	YGPIADVSIVYDQQSR
P63244|GBLP_HUMAN	895.0054	77.7	1.70E-06	IIVDELKQEVISTSSK
P63244|GBLP_HUMAN	895.0004	90.88	8.70E-08	IIVDELKQEVISTSSK
P63244|GBLP_HUMAN	895.0038	92.31	5.20E-08	IIVDELKQEVISTSSK
P63244|GBLP_HUMAN	894.999	99.66	1.10E-08	IIVDELKQEVISTSSK
P63244|GBLP_HUMAN	894.9996	107.86	1.70E-09	IIVDELKQEVISTSSK
P67809|YBOX1_HUMAN	872.9453	45.29	0.0019	NDTKEDVFVHQTAIK
P67809|YBOX1_HUMAN	872.9431	45.49	0.0017	NDTKEDVFVHQTAIK
P67809|YBOX1_HUMAN	848.4365	55.25	0.00017	GAEAANVTGPGGVPVQGSK
P67809|YBOX1_HUMAN	872.9442	63.6	2.40E-05	NDTKEDVFVHQTAIK
P67809|YBOX1_HUMAN	898.4138	60.23	1.20E-05	SVGDGETVEFDVVEGEK
P67809|YBOX1_HUMAN	898.4131	71.33	9.70E-07	SVGDGETVEFDVVEGEK
P67809|YBOX1_HUMAN	898.4174	74.79	4.60E-07	SVGDGETVEFDVVEGEK
P68032|ACTC_HUMAN	980.9572	38.66	0.0026	YPIEHGIITNWDDMEK
P68032|ACTC_HUMAN	980.9567	39.75	0.002	YPIEHGIITNWDDMEK
P68032|ACTC_HUMAN	980.9564	42.92	0.00096	YPIEHGIITNWDDMEK
P68032|ACTC_HUMAN	980.957	44.74	0.00062	YPIEHGIITNWDDMEK
P68032|ACTC_HUMAN	980.9563	46.96	0.00039	YPIEHGIITNWDDMEK
P68032|ACTC_HUMAN	980.9565	48.77	0.00025	YPIEHGIITNWDDMEK
P68032|ACTC_HUMAN	980.9572	50.68	0.00016	YPIEHGIITNWDDMEK
P68032|ACTC_HUMAN	980.9579	52.56	0.00011	YPIEHGIITNWDDMEK
P68032|ACTC_HUMAN	980.9568	52.44	0.0001	YPIEHGIITNWDDMEK
P68032|ACTC_HUMAN	980.9584	54.27	7.80E-05	YPIEHGIITNWDDMEK
P68032|ACTC_HU	980.9	57.29	3.50E-05	YPIEHGIITNWDDMEK

MAN	573			
P68431|H31_HUMAN	1196.236	41.4	0.0028	FQSSAVMALQEACEAYLVGLFEDTNLCAIHAK
P82979|SARNP_HUMAN	540.2958	50.72	0.00033	FGLNVSSISR
P82979|SARNP_HUMAN	936.4447	61	1.80E-05	FGIVTSSAGTGTTEDTEAK
P82979|SARNP_HUMAN	936.4439	61.39	1.60E-05	FGIVTSSAGTGTTEDTEAK
P82979|SARNP_HUMAN	936.4452	63.63	1.00E-05	FGIVTSSAGTGTTEDTEAK
P82979|SARNP_HUMAN	936.4462	64.93	7.30E-06	FGIVTSSAGTGTTEDTEAK
P82979|SARNP_HUMAN	936.4456	67.84	3.70E-06	FGIVTSSAGTGTTEDTEAK
P82979|SARNP_HUMAN	936.4457	75.04	7.10E-07	FGIVTSSAGTGTTEDTEAK
P82979|SARNP_HUMAN	936.4445	76.13	5.50E-07	FGIVTSSAGTGTTEDTEAK
P82979|SARNP_HUMAN	936.4474	82.8	1.20E-07	FGIVTSSAGTGTTEDTEAK
P82979|SARNP_HUMAN	936.4454	92.4	1.30E-08	FGIVTSSAGTGTTEDTEAK
P82979|SARNP_HUMAN	936.4437	92.75	1.20E-08	FGIVTSSAGTGTTEDTEAK
P82979|SARNP_HUMAN	936.4427	101.05	1.50E-09	FGIVTSSAGTGTTEDTEAK
P82979|SARNP_HUMAN	936.4448	104.87	7.50E-10	FGIVTSSAGTGTTEDTEAK
P84243|H33_HUMAN	675.3837	41.7	0.0044	SAPSTGGVKKPHR
P84243|H33_HUMAN	753.4477	44.24	0.0018	KSAPSTGGVKKPHR
P84243|H33_HUMAN	753.4509	45.97	0.0011	KSAPSTGGVKKPHR
P84243|H33_HUMAN	675.3842	48.47	0.00077	SAPSTGGVKKPHR
P84243|H33_HUMAN	675.3837	49.84	0.00068	SAPSTGGVKKPHR
P84243|H33_HUMAN	753.4474	49.73	0.00046	KSAPSTGGVKKPHR
P84243|H33_HUMAN	753.4476	52.78	0.00025	KSAPSTGGVKKPHR
P84243|H33_HUMAN	753.4481	54.83	0.00016	KSAPSTGGVKKPHR
P84243|H33_HUMAN	753.4477	55.26	0.00014	KSAPSTGGVKKPHR
P84243|H33_HUMAN	753.4472	63.61	2.70E-05	KSAPSTGGVKKPHR
P98179|RBM3_HUMAN	865.8786	30.23	0.0032	YYDSRPGGYGYGYGR
P98179|RBM3_HUMAN	865.8793	35.03	0.0011	YYDSRPGGYGYGYGR
P98179|RBM3_HUMAN	865.8817	39.92	0.0005	YYDSRPGGYGYGYGR

P98179|RBM3_HUMAN	865.8776	42.46	0.00017	YYDSRPGGYGYGYGR
P98179|RBM3_HUMAN	991.4808	77.86	5.30E-07	GFGFITFTNPEHASVAMR
P98179|RBM3_HUMAN	991.48	78.29	5.20E-07	GFGFITFTNPEHASVAMR
P98179|RBM3_HUMAN	991.48	78.58	4.80E-07	GFGFITFTNPEHASVAMR
P98179|RBM3_HUMAN	991.4826	82.4	2.00E-07	GFGFITFTNPEHASVAMR
P98179|RBM3_HUMAN	991.4798	99.11	4.10E-09	GFGFITFTNPEHASVAMR
Q00059|TFAM_HUMAN	769.3835	39.03	0.0037	AEWQVYKEEISR
Q00839|HNRPU_HUMAN	633.8311	38.79	0.0048	LLEQYKEESK
Q00839|HNRPU_HUMAN	633.8303	39.66	0.0044	LLEQYKEESK
Q00839|HNRPU_HUMAN	697.877	41.59	0.0043	LLEQYKEESKK
Q00839|HNRPU_HUMAN	908.7875	43.15	0.0036	EKPYFPIPEEYTFIQNVPLEDR
Q00839|HNRPU_HUMAN	857.9578	44.04	0.0035	SSGPTSLFAVTVAPPGAR
Q00839|HNRPU_HUMAN	857.9572	43.78	0.0035	SSGPTSLFAVTVAPPGAR
Q00839|HNRPU_HUMAN	857.9592	45.42	0.0026	SSGPTSLFAVTVAPPGAR
Q00839|HNRPU_HUMAN	498.7575	39.39	0.0021	DIDIHEVR
Q00839|HNRPU_HUMAN	849.3928	37.38	0.0021	GYFEYIEENKYSR
Q00839|HNRPU_HUMAN	908.7869	45.94	0.0019	EKPYFPIPEEYTFIQNVPLEDR
Q00839|HNRPU_HUMAN	908.7877	46.41	0.0017	EKPYFPIPEEYTFIQNVPLEDR
Q00839|HNRPU_HUMAN	857.96	47.59	0.0016	SSGPTSLFAVTVAPPGAR
Q00839|HNRPU_HUMAN	908.7885	46.76	0.0016	EKPYFPIPEEYTFIQNVPLEDR
Q00839|HNRPU_HUMAN	498.7574	41.09	0.0015	DIDIHEVR
Q00839|HNRPU_HUMAN	498.7575	41.01	0.0015	DIDIHEVR
Q00839|HNRPU_HUMAN	498.7567	41.16	0.0014	DIDIHEVR
Q00839|HNRPU_HUMAN	498.7568	41.12	0.0014	DIDIHEVR
Q00839|HNRPU_HUMAN	498.757	41.06	0.0014	DIDIHEVR
Q00839|HNRPU_HUMAN	498.757	41.22	0.0013	DIDIHEVR
Q00839|HNRPU_HUMAN	849.3927	39.42	0.0013	GYFEYIEENKYSR
Q00839|HNRPU_	498.7	42.17	0.0011	DIDIHEVR

HUMAN	574			
Q00839|HNRPU_HUMAN	498.7576	42.6	0.001	DIDIHEVR
Q00839|HNRPU_HUMAN	498.7573	42.56	0.001	DIDIHEVR
Q00839|HNRPU_HUMAN	498.7576	42.76	0.00099	DIDIHEVR
Q00839|HNRPU_HUMAN	498.7571	44.47	0.00065	DIDIHEVR
Q00839|HNRPU_HUMAN	857.9569	52.05	0.00051	SSGPTSLFAVTVAPPGAR
Q00839|HNRPU_HUMAN	498.7577	45.73	0.00049	DIDIHEVR
Q00839|HNRPU_HUMAN	691.8499	50.1	0.00033	YNILGTNTIMDK
Q00839|HNRPU_HUMAN	498.7576	47.51	0.00033	DIDIHEVR
Q00839|HNRPU_HUMAN	857.9573	54.38	0.00031	SSGPTSLFAVTVAPPGAR
Q00839|HNRPU_HUMAN	908.7877	54.47	0.00026	EKPYFPIPEEYTFIQNVPLEDR
Q00839|HNRPU_HUMAN	646.2961	45.05	0.00022	GYFEYIEENK
Q00839|HNRPU_HUMAN	1362.685	56.4	0.00019	EKPYFPIPEEYTFIQNVPLEDR
Q00839|HNRPU_HUMAN	498.759	50.42	0.00017	DIDIHEVR
Q00839|HNRPU_HUMAN	691.8522	54.05	0.00016	YNILGTNTIMDK
Q00839|HNRPU_HUMAN	849.3911	47.69	0.00016	GYFEYIEENKYSR
Q00839|HNRPU_HUMAN	691.8505	53.79	0.00015	YNILGTNTIMDK
Q00839|HNRPU_HUMAN	1362.675	57.77	0.00012	EKPYFPIPEEYTFIQNVPLEDR
Q00839|HNRPU_HUMAN	691.851	55.51	9.40E-05	YNILGTNTIMDK
Q00839|HNRPU_HUMAN	849.3917	50.85	8.90E-05	GYFEYIEENKYSR
Q00839|HNRPU_HUMAN	691.8514	56.98	7.60E-05	YNILGTNTIMDK
Q00839|HNRPU_HUMAN	646.293	49.56	7.60E-05	GYFEYIEENK
Q00839|HNRPU_HUMAN	849.3928	52.17	6.90E-05	GYFEYIEENKYSR
Q00839|HNRPU_HUMAN	691.851	56.93	6.80E-05	YNILGTNTIMDK
Q00839|HNRPU_HUMAN	908.788	62.19	4.70E-05	EKPYFPIPEEYTFIQNVPLEDR
Q00839|HNRPU_HUMAN	908.7878	62.58	4.10E-05	EKPYFPIPEEYTFIQNVPLEDR
Q00839|HNRPU_HUMAN	1362.682	63.23	3.90E-05	EKPYFPIPEEYTFIQNVPLEDR
Q00839|HNRPU_HUMAN	1042.814	56.72	3.20E-05	LQAALDDEEAGGRPAMEPGNGSLDLGGDSAGR

Q00839|HNRPU_HUMAN	849.3915	55.98	2.70E-05	GYFEYIEENKYSR
Q00839|HNRPU_HUMAN	1362.68	65.62	2.10E-05	EKPYFPIPEEYTFIQNVPLEDR
Q00839|HNRPU_HUMAN	849.392	57.82	1.90E-05	GYFEYIEENKYSR
Q00839|HNRPU_HUMAN	691.8508	63	1.70E-05	YNILGTNTIMDK
Q00839|HNRPU_HUMAN	824.4247	66.97	1.30E-05	NFILDQTNVSAAAQR
Q00839|HNRPU_HUMAN	849.3918	61.8	7.60E-06	GYFEYIEENKYSR
Q00839|HNRPU_HUMAN	849.3922	61.86	7.40E-06	GYFEYIEENKYSR
Q00839|HNRPU_HUMAN	849.3914	61.86	7.00E-06	GYFEYIEENKYSR
Q00839|HNRPU_HUMAN	857.9571	71.4	5.60E-06	SSGPTSLFAVTVAPPGAR
Q00839|HNRPU_HUMAN	691.8513	68.61	5.50E-06	YNILGTNTIMDK
Q00839|HNRPU_HUMAN	824.4253	71.72	3.90E-06	NFILDQTNVSAAAQR
Q00839|HNRPU_HUMAN	849.3915	65.18	3.30E-06	GYFEYIEENKYSR
Q00839|HNRPU_HUMAN	849.392	65.55	3.20E-06	GYFEYIEENKYSR
Q00839|HNRPU_HUMAN	849.3917	66.22	2.60E-06	GYFEYIEENKYSR
Q00839|HNRPU_HUMAN	1042.817	71.64	1.30E-06	LQAALDDEEAGGRPAMEPGNGSLDLGGDSAGR
Q00839|HNRPU_HUMAN	1042.816	73.65	7.90E-07	LQAALDDEEAGGRPAMEPGNGSLDLGGDSAGR
Q00839|HNRPU_HUMAN	824.4233	80.91	4.90E-07	NFILDQTNVSAAAQR
Q00839|HNRPU_HUMAN	857.956	83.1	4.70E-07	SSGPTSLFAVTVAPPGAR
Q00839|HNRPU_HUMAN	824.4246	82.41	3.60E-07	NFILDQTNVSAAAQR
Q00839|HNRPU_HUMAN	1042.816	80.43	1.70E-07	LQAALDDEEAGGRPAMEPGNGSLDLGGDSAGR
Q00839|HNRPU_HUMAN	824.4244	91	5.50E-08	NFILDQTNVSAAAQR
Q00839|HNRPU_HUMAN	824.4249	90.74	5.30E-08	NFILDQTNVSAAAQR
Q00839|HNRPU_HUMAN	824.4239	90.97	5.10E-08	NFILDQTNVSAAAQR
Q00839|HNRPU_HUMAN	824.4244	92.57	3.80E-08	NFILDQTNVSAAAQR
Q00839|HNRPU_HUMAN	824.4239	93.28	3.00E-08	NFILDQTNVSAAAQR
Q00839|HNRPU_HUMAN	824.4232	94	2.40E-08	NFILDQTNVSAAAQR
Q00839|HNRPU_HUMAN	824.4242	95.09	2.10E-08	NFILDQTNVSAAAQR
Q00839|HNRPU_	824.4	95.78	1.70E-08	NFILDQTNVSAAAQR

HUMAN	239			
Q00839|HNRPU_HUMAN	824.4243	96.42	1.60E-08	NFILDQTNVSAAAQR
Q00839|HNRPU_HUMAN	1042.817	92.23	1.20E-08	LQAALDDEEAGGRPAMEPGNGSLDLGGDSAGR
Q00839|HNRPU_HUMAN	824.4242	98.95	8.80E-09	NFILDQTNVSAAAQR
Q00839|HNRPU_HUMAN	824.4247	99.71	6.70E-09	NFILDQTNVSAAAQR
Q00839|HNRPU_HUMAN	1042.815	95.95	4.50E-09	LQAALDDEEAGGRPAMEPGNGSLDLGGDSAGR
Q00839|HNRPU_HUMAN	824.4247	109.88	6.40E-10	NFILDQTNVSAAAQR
Q00839|HNRPU_HUMAN	824.4241	120.25	6.50E-11	NFILDQTNVSAAAQR
Q01130|SRSF2_HUMAN	876.3656	26.19	0.0028	DAEDAMDAMDGAVLDGR
Q01130|SRSF2_HUMAN	876.3625	37.64	0.00017	DAEDAMDAMDGAVLDGR
Q01130|SRSF2_HUMAN	876.36	48.36	1.50E-05	DAEDAMDAMDGAVLDGR
Q01130|SRSF2_HUMAN	876.3636	50.34	9.20E-06	DAEDAMDAMDGAVLDGR
Q01130|SRSF2_HUMAN	876.362	52.27	5.90E-06	DAEDAMDAMDGAVLDGR
Q01130|SRSF2_HUMAN	876.3619	60.25	9.40E-07	DAEDAMDAMDGAVLDGR
Q01130|SRSF2_HUMAN	876.36	62.85	5.20E-07	DAEDAMDAMDGAVLDGR
Q01130|SRSF2_HUMAN	876.3614	72.9	5.10E-08	DAEDAMDAMDGAVLDGR
Q01130|SRSF2_HUMAN	876.3631	74.63	3.80E-08	DAEDAMDAMDGAVLDGR
Q04837|SSBP_HUMAN	996.5321	49.49	0.0011	QATTIIADNIIFLSDQTK
Q04837|SSBP_HUMAN	806.3764	60.57	9.30E-06	SGDSEVYQLGDVSQK
Q04837|SSBP_HUMAN	806.3757	64.87	3.60E-06	SGDSEVYQLGDVSQK
Q04837|SSBP_HUMAN	806.3768	70.26	1.20E-06	SGDSEVYQLGDVSQK
Q04837|SSBP_HUMAN	806.3763	69.55	1.20E-06	SGDSEVYQLGDVSQK
Q04837|SSBP_HUMAN	806.3753	72.67	6.50E-07	SGDSEVYQLGDVSQK
Q04837|SSBP_HUMAN	806.3799	73.51	5.60E-07	SGDSEVYQLGDVSQK
Q04837|SSBP_HUMAN	806.3762	77.89	1.80E-07	SGDSEVYQLGDVSQK
Q04837|SSBP_HUMAN	996.5389	93.32	4.70E-08	QATTIIADNIIFLSDQTK
Q04837|SSBP_HUMAN	996.5358	106.04	2.40E-09	QATTIIADNIIFLSDQTK
Q04837|SSBP_HUMAN	996.5353	108.83	1.20E-09	QATTIIADNIIFLSDQTK

Q07020|RL18_HUMAN	730.9022	68.37	1.10E-05	ILTFDQLALDSPK
Q07020|RL18_HUMAN	730.9033	73.78	3.30E-06	ILTFDQLALDSPK
Q07021|C1QBP_HUMAN	1144.088	49	0.0012	VEEQEPELTSTPNFVVEVIK
Q07021|C1QBP_HUMAN	1144.089	52.67	0.00048	VEEQEPELTSTPNFVVEVIK
Q07021|C1QBP_HUMAN	1144.085	52.72	0.00047	VEEQEPELTSTPNFVVEVIK
Q07021|C1QBP_HUMAN	1144.089	54.36	0.00032	VEEQEPELTSTPNFVVEVIK
Q07021|C1QBP_HUMAN	1144.089	61.28	6.90E-05	VEEQEPELTSTPNFVVEVIK
Q07021|C1QBP_HUMAN	1144.086	66.48	2.00E-05	VEEQEPELTSTPNFVVEVIK
Q07021|C1QBP_HUMAN	849.4202	83.75	1.50E-07	AFVDFLSDEIKEER
Q07955|SRSF1_HUMAN	847.7234	35.37	0.0042	GGPPFAFVEFEDPRDAEDAVYGR
Q07955|SRSF1_HUMAN	782.8721	36.07	0.0037	GGPPFAFVEFEDPR
Q07955|SRSF1_HUMAN	782.8746	37.65	0.0035	GGPPFAFVEFEDPR
Q07955|SRSF1_HUMAN	629.3198	40.97	0.0017	TKDIEDVFYK
Q07955|SRSF1_HUMAN	782.8726	40.5	0.0017	GGPPFAFVEFEDPR
Q07955|SRSF1_HUMAN	581.7753	39.61	0.0014	SHEGETAYIR
Q07955|SRSF1_HUMAN	556.7715	40.26	0.0013	KEDMTYAVR
Q07955|SRSF1_HUMAN	581.7755	39.74	0.0012	SHEGETAYIR
Q07955|SRSF1_HUMAN	581.7755	40.34	0.0011	SHEGETAYIR
Q07955|SRSF1_HUMAN	581.7756	40.3	0.0011	SHEGETAYIR
Q07955|SRSF1_HUMAN	847.7253	42.09	0.001	GGPPFAFVEFEDPRDAEDAVYGR
Q07955|SRSF1_HUMAN	556.772	41.85	0.00089	KEDMTYAVR
Q07955|SRSF1_HUMAN	556.7725	42.13	0.00085	KEDMTYAVR
Q07955|SRSF1_HUMAN	782.8778	44.92	0.00069	GGPPFAFVEFEDPR
Q07955|SRSF1_HUMAN	556.7728	43.05	0.00069	KEDMTYAVR
Q07955|SRSF1_HUMAN	556.7725	44.38	0.0005	KEDMTYAVR
Q07955|SRSF1_HUMAN	556.7719	46.67	0.00029	KEDMTYAVR
Q07955|SRSF1_HUMAN	629.3201	50.61	0.00017	TKDIEDVFYK
Q07955|SRSF1_H	629.3	54.67	8.20E-05	TKDIEDVFYK

UMAN	194			
Q07955|SRSF1_HUMAN	629.3199	54.53	7.10E-05	TKDIEDVFYK
Q07955|SRSF1_HUMAN	629.3203	55.94	5.10E-05	TKDIEDVFYK
Q07955|SRSF1_HUMAN	629.3206	56.59	4.40E-05	TKDIEDVFYK
Q07955|SRSF1_HUMAN	629.3197	59.13	2.60E-05	TKDIEDVFYK
Q07955|SRSF1_HUMAN	556.7719	58.22	2.10E-05	KEDMTYAVR
Q07955|SRSF1_HUMAN	556.772	58.34	2.00E-05	KEDMTYAVR
Q07955|SRSF1_HUMAN	556.7725	58.84	1.80E-05	KEDMTYAVR
Q07955|SRSF1_HUMAN	782.8754	61.51	1.40E-05	GGPPFAFVEFEDPR
Q07955|SRSF1_HUMAN	629.3209	67.11	4.10E-06	TKDIEDVFYK
Q08170|SRSF4_HUMAN	873.4233	47.16	0.00053	KNEGVIEFVSYSDMK
Q08170|SRSF4_HUMAN	873.4204	51.87	0.00017	KNEGVIEFVSYSDMK
Q08211|DHX9_HUMAN	790.4238	41.86	0.005	QPAIISQLDPVNER
Q08211|DHX9_HUMAN	922.0021	43.17	0.0048	KVQSDGQIVLVDDWIK
Q08211|DHX9_HUMAN	611.3635	39.33	0.0044	TPLHEIALSIK
Q08211|DHX9_HUMAN	659.3268	36.8	0.0044	YPSPFFVFGEK
Q08211|DHX9_HUMAN	659.3273	38.39	0.0039	YPSPFFVFGEK
Q08211|DHX9_HUMAN	659.3279	39.56	0.0035	YPSPFFVFGEK
Q08211|DHX9_HUMAN	659.3265	39.76	0.003	YPSPFFVFGEK
Q08211|DHX9_HUMAN	659.3269	38.66	0.0029	YPSPFFVFGEK
Q08211|DHX9_HUMAN	659.3279	40.49	0.0028	YPSPFFVFGEK
Q08211|DHX9_HUMAN	659.3265	40.09	0.0027	YPSPFFVFGEK
Q08211|DHX9_HUMAN	986.0299	46.3	0.0022	AIEPPPLDAVIEAEHTLR
Q08211|DHX9_HUMAN	611.363	43.06	0.0021	TPLHEIALSIK
Q08211|DHX9_HUMAN	857.9527	45.92	0.0019	VQSDGQIVLVDDWIK
Q08211|DHX9_HUMAN	866.5113	44.64	0.0019	GMTLVTPLQLLLFASK
Q08211|DHX9_HUMAN	752.3984	46.02	0.0018	GISHVIVDEIHER
Q08211|DHX9_HUMAN	790.4254	46.98	0.0015	QPAIISQLDPVNER

Q08211|DHX9_HUMAN	659.3271	43.03	0.0014	YPSPFFVFGEK
Q08211|DHX9_HUMAN	752.3983	48.35	0.0011	GISHVIVDEIHER
Q08211|DHX9_HUMAN	1025.514	47.11	0.0011	TTQVPQFILDDFIQNDR
Q08211|DHX9_HUMAN	752.3989	48.94	0.00093	GISHVIVDEIHER
Q08211|DHX9_HUMAN	659.3278	45.99	0.00078	YPSPFFVFGEK
Q08211|DHX9_HUMAN	986.0267	51.4	0.00075	AIEPPPLDAVIEAEHTLR
Q08211|DHX9_HUMAN	986.0278	51.24	0.00074	AIEPPPLDAVIEAEHTLR
Q08211|DHX9_HUMAN	986.0265	52.96	0.00051	AIEPPPLDAVIEAEHTLR
Q08211|DHX9_HUMAN	1025.515	51.5	0.00042	TTQVPQFILDDFIQNDR
Q08211|DHX9_HUMAN	752.4025	52.62	0.00041	GISHVIVDEIHER
Q08211|DHX9_HUMAN	871.4318	50.29	0.00034	ELDALDANDELTPLGR
Q08211|DHX9_HUMAN	986.0279	55.52	0.00028	AIEPPPLDAVIEAEHTLR
Q08211|DHX9_HUMAN	986.0269	55.74	0.00027	AIEPPPLDAVIEAEHTLR
Q08211|DHX9_HUMAN	790.426	55.24	0.00021	QPAIISQLDPVNER
Q08211|DHX9_HUMAN	857.9539	57.05	0.00016	VQSDGQIVLVDDWIK
Q08211|DHX9_HUMAN	1025.515	55.85	0.00016	TTQVPQFILDDFIQNDR
Q08211|DHX9_HUMAN	1081.989	48.6	0.00016	AENNSEVGASGYGVPGPTWDR
Q08211|DHX9_HUMAN	857.9556	58.26	0.00014	VQSDGQIVLVDDWIK
Q08211|DHX9_HUMAN	1081.996	50.49	0.00013	AENNSEVGASGYGVPGPTWDR
Q08211|DHX9_HUMAN	752.3967	57.47	0.00012	GISHVIVDEIHER
Q08211|DHX9_HUMAN	752.3995	57.43	0.00012	GISHVIVDEIHER
Q08211|DHX9_HUMAN	1025.512	57.08	0.0001	TTQVPQFILDDFIQNDR
Q08211|DHX9_HUMAN	1025.514	57.92	8.70E-05	TTQVPQFILDDFIQNDR
Q08211|DHX9_HUMAN	752.3966	58.92	8.60E-05	GISHVIVDEIHER
Q08211|DHX9_HUMAN	752.3973	61.71	5.40E-05	GISHVIVDEIHER
Q08211|DHX9_HUMAN	1081.988	53.62	4.60E-05	AENNSEVGASGYGVPGPTWDR
Q08211|DHX9_HUMAN	857.955	64.47	3.20E-05	VQSDGQIVLVDDWIK
Q08211|DHX9_H	922.0	65.75	3.00E-05	KVQSDGQIVLVDDWIK

UMAN	028			
Q08211|DHX9_HUMAN	790.4259	64.64	2.40E-05	QPAIISQLDPVNER
Q08211|DHX9_HUMAN	752.3972	64.39	2.40E-05	GISHVIVDEIHER
Q08211|DHX9_HUMAN	857.9519	65.23	2.10E-05	VQSDGQIVLVDDWIK
Q08211|DHX9_HUMAN	1470.394	65.99	1.70E-05	SEEVPAFGVASPPPLTDTPDTTANAEGDLPTTMGGPLPPHLALK
Q08211|DHX9_HUMAN	866.506	69.75	8.20E-06	GMTLVTPLQLLLFASK
Q08211|DHX9_HUMAN	752.3972	71.54	4.70E-06	GISHVIVDEIHER
Q08211|DHX9_HUMAN	857.9534	73.04	3.40E-06	VQSDGQIVLVDDWIK
Q08211|DHX9_HUMAN	871.4316	71.75	2.20E-06	ELDALDANDELTPLGR
Q08211|DHX9_HUMAN	857.9501	76.6	1.60E-06	VQSDGQIVLVDDWIK
Q08211|DHX9_HUMAN	871.4315	73.18	1.60E-06	ELDALDANDELTPLGR
Q08211|DHX9_HUMAN	871.43	73.12	1.60E-06	ELDALDANDELTPLGR
Q08211|DHX9_HUMAN	871.4307	73.58	1.50E-06	ELDALDANDELTPLGR
Q08211|DHX9_HUMAN	871.4312	73.71	1.40E-06	ELDALDANDELTPLGR
Q08211|DHX9_HUMAN	857.9557	80.28	8.80E-07	VQSDGQIVLVDDWIK
Q08211|DHX9_HUMAN	1081.988	71.83	7.30E-07	AENNSEVGASGYGVPGPTWDR
Q08211|DHX9_HUMAN	871.4331	77.18	6.90E-07	ELDALDANDELTPLGR
Q08211|DHX9_HUMAN	1081.987	72.04	6.60E-07	AENNSEVGASGYGVPGPTWDR
Q08211|DHX9_HUMAN	1081.99	75.82	3.10E-07	AENNSEVGASGYGVPGPTWDR
Q08211|DHX9_HUMAN	1081.989	80.75	9.10E-08	AENNSEVGASGYGVPGPTWDR
Q08211|DHX9_HUMAN	857.9515	88.96	8.40E-08	VQSDGQIVLVDDWIK
Q08211|DHX9_HUMAN	857.9514	93.78	3.00E-08	VQSDGQIVLVDDWIK
Q08211|DHX9_HUMAN	1081.988	89.7	1.10E-08	AENNSEVGASGYGVPGPTWDR
Q08211|DHX9_HUMAN	1081.989	90.68	9.80E-09	AENNSEVGASGYGVPGPTWDR
Q08211|DHX9_HUMAN	857.9531	99.53	8.20E-09	VQSDGQIVLVDDWIK
Q08211|DHX9_HUMAN	1081.989	92.75	6.00E-09	AENNSEVGASGYGVPGPTWDR
Q08211|DHX9_HUMAN	1081.988	100.27	1.00E-09	AENNSEVGASGYGVPGPTWDR
Q09028|RBBP4_HUMAN	804.3589	42	0.00041	ADKEAAFDDAVEER

Q09028|RBBP4_HUMAN	804.3614	55.03	2.50E-05	ADKEAAFDDAVEER
Q09028|RBBP4_HUMAN	804.3594	54.93	2.20E-05	ADKEAAFDDAVEER
Q12874|SF3A3_HUMAN	758.4099	45.11	0.0029	VKPLQDQNELFGK
Q12874|SF3A3_HUMAN	758.4103	45.83	0.0025	VKPLQDQNELFGK
Q12874|SF3A3_HUMAN	758.4114	49.41	0.00097	VKPLQDQNELFGK
Q12874|SF3A3_HUMAN	758.4118	54	0.00037	VKPLQDQNELFGK
Q12874|SF3A3_HUMAN	758.4122	55.09	0.0003	VKPLQDQNELFGK
Q12874|SF3A3_HUMAN	1207.024	59.4	4.90E-06	ENPSEEAQNLVEFTDEEGYGR
Q12874|SF3A3_HUMAN	1207.022	69.17	4.40E-07	ENPSEEAQNLVEFTDEEGYGR
Q12874|SF3A3_HUMAN	1207.025	80.53	3.90E-08	ENPSEEAQNLVEFTDEEGYGR
Q12874|SF3A3_HUMAN	1207.02	78.88	3.20E-08	ENPSEEAQNLVEFTDEEGYGR
Q12874|SF3A3_HUMAN	1207.022	92.13	2.30E-09	ENPSEEAQNLVEFTDEEGYGR
Q12905|ILF2_HUMAN	1050.049	49.41	0.001	NQDLAPNSAEQASILSLVTK
Q12905|ILF2_HUMAN	1050.049	55.95	0.00023	NQDLAPNSAEQASILSLVTK
Q12905|ILF2_HUMAN	1050.048	61.22	7.10E-05	NQDLAPNSAEQASILSLVTK
Q12905|ILF2_HUMAN	1050.05	61.47	6.50E-05	NQDLAPNSAEQASILSLVTK
Q12905|ILF2_HUMAN	1050.047	64.85	2.90E-05	NQDLAPNSAEQASILSLVTK
Q12905|ILF2_HUMAN	1050.048	84.79	3.00E-07	NQDLAPNSAEQASILSLVTK
Q12905|ILF2_HUMAN	1050.049	87.51	1.60E-07	NQDLAPNSAEQASILSLVTK
Q12906|ILF3_HUMAN	707.881	42.89	0.0032	LFPDTPLALDANK
Q12906|ILF3_HUMAN	684.8442	42.48	0.0017	EDITQSAQHALR
Q12906|ILF3_HUMAN	684.845	42.65	0.0015	EDITQSAQHALR
Q12906|ILF3_HUMAN	684.8447	43.63	0.0013	EDITQSAQHALR
Q12906|ILF3_HUMAN	800.9132	47.48	0.001	SIGTANRPMGAGEALR
Q12906|ILF3_HUMAN	891.0836	43.58	0.00099	HSSVYPTQEELEAVQNMVSHTER
Q12906|ILF3_HUMAN	800.9128	50.73	0.00047	SIGTANRPMGAGEALR
Q12906|ILF3_HUMAN	684.845	47.98	0.00043	EDITQSAQHALR
Q12906|ILF3_HU	707.8	52.61	0.00036	LFPDTPLALDANK

MAN	796			
Q12906|ILF3_HUMAN	955.4974	52.59	0.00034	VLAGETLSVNDPPDVLDR
Q12906|ILF3_HUMAN	955.4996	53.15	0.00032	VLAGETLSVNDPPDVLDR
Q12906|ILF3_HUMAN	891.0827	48.87	0.00029	HSSVYPTQEELEAVQNMVSHTER
Q12906|ILF3_HUMAN	599.2944	48.47	0.00025	EATDAIGHLDR
Q12906|ILF3_HUMAN	955.4979	54.95	0.00023	VLAGETLSVNDPPDVLDR
Q12906|ILF3_HUMAN	891.083	49.88	0.00023	HSSVYPTQEELEAVQNMVSHTER
Q12906|ILF3_HUMAN	707.8806	54.65	0.00022	LFPDTPLALDANK
Q12906|ILF3_HUMAN	684.8445	52.69	0.00017	EDITQSAQHALR
Q12906|ILF3_HUMAN	684.8448	52.31	0.00016	EDITQSAQHALR
Q12906|ILF3_HUMAN	684.845	52.55	0.00015	EDITQSAQHALR
Q12906|ILF3_HUMAN	684.8452	52.25	0.00014	EDITQSAQHALR
Q12906|ILF3_HUMAN	684.8453	52.24	0.00014	EDITQSAQHALR
Q12906|ILF3_HUMAN	707.8799	57.85	0.00011	LFPDTPLALDANK
Q12906|ILF3_HUMAN	707.8808	58.28	9.20E-05	LFPDTPLALDANK
Q12906|ILF3_HUMAN	955.5	59.7	7.90E-05	VLAGETLSVNDPPDVLDR
Q12906|ILF3_HUMAN	684.8452	56.19	5.70E-05	EDITQSAQHALR
Q12906|ILF3_HUMAN	599.2949	54.74	5.60E-05	EATDAIGHLDR
Q12906|ILF3_HUMAN	955.496	61.01	5.50E-05	VLAGETLSVNDPPDVLDR
Q12906|ILF3_HUMAN	955.4974	60.85	5.10E-05	VLAGETLSVNDPPDVLDR
Q12906|ILF3_HUMAN	955.494	62.97	3.30E-05	VLAGETLSVNDPPDVLDR
Q12906|ILF3_HUMAN	707.8808	62.88	3.20E-05	LFPDTPLALDANK
Q12906|ILF3_HUMAN	599.2963	57.9	2.80E-05	EATDAIGHLDR
Q12906|ILF3_HUMAN	891.0837	59.91	2.30E-05	HSSVYPTQEELEAVQNMVSHTER
Q12906|ILF3_HUMAN	707.8799	66.67	1.40E-05	LFPDTPLALDANK
Q12906|ILF3_HUMAN	891.0819	62.25	1.30E-05	HSSVYPTQEELEAVQNMVSHTER
Q12906|ILF3_HUMAN	684.8446	64.68	1.00E-05	EDITQSAQHALR
Q12906|ILF3_HUMAN	891.082	63.45	9.60E-06	HSSVYPTQEELEAVQNMVSHTER

Q12906|ILF3_HUMAN	599.2937	64.24	8.30E-06	EATDAIGHLDR
Q12906|ILF3_HUMAN	955.4959	75.76	1.80E-06	VLAGETLSVNDPPDVLDR
Q13148|TADBP_HUMAN	863.8853	48.18	9.90E-05	FGGNPGGFGNQGGFGNSR
Q13148|TADBP_HUMAN	863.884	61.48	4.00E-06	FGGNPGGFGNQGGFGNSR
Q13148|TADBP_HUMAN	863.8895	65.95	1.90E-06	FGGNPGGFGNQGGFGNSR
Q13148|TADBP_HUMAN	863.8873	67.81	1.20E-06	FGGNPGGFGNQGGFGNSR
Q13148|TADBP_HUMAN	863.8875	74.9	2.20E-07	FGGNPGGFGNQGGFGNSR
Q13151|ROA0_HUMAN	803.8927	39.26	0.0036	AVPKEDIYSGGGGGGSR
Q13151|ROA0_HUMAN	803.891	39.11	0.0034	AVPKEDIYSGGGGGGSR
Q13151|ROA0_HUMAN	803.8928	41.68	0.0021	AVPKEDIYSGGGGGGSR
Q13151|ROA0_HUMAN	858.3937	36.48	0.0021	GFGFVYFQNHDAADK
Q13151|ROA0_HUMAN	803.8953	45.85	0.00071	AVPKEDIYSGGGGGGSR
Q13151|ROA0_HUMAN	858.3925	49.04	0.00011	GFGFVYFQNHDAADK
Q13151|ROA0_HUMAN	858.3931	49.31	9.40E-05	GFGFVYFQNHDAADK
Q13151|ROA0_HUMAN	1089.518	61.22	2.20E-05	GDVAEGDLIEHFSQFGTVEK
Q13151|ROA0_HUMAN	858.3936	60.25	8.80E-06	GFGFVYFQNHDAADK
Q13151|ROA0_HUMAN	1089.521	65.94	8.30E-06	GDVAEGDLIEHFSQFGTVEK
Q13151|ROA0_HUMAN	1089.518	67.58	5.00E-06	GDVAEGDLIEHFSQFGTVEK
Q13151|ROA0_HUMAN	1089.521	69.91	3.30E-06	GDVAEGDLIEHFSQFGTVEK
Q13151|ROA0_HUMAN	1089.518	69.99	3.00E-06	GDVAEGDLIEHFSQFGTVEK
Q13151|ROA0_HUMAN	1089.519	71.98	2.00E-06	GDVAEGDLIEHFSQFGTVEK
Q13151|ROA0_HUMAN	1089.519	74.79	9.80E-07	GDVAEGDLIEHFSQFGTVEK
Q13151|ROA0_HUMAN	845.9563	88.23	1.50E-07	LFIGGLNVQTSESGLR
Q13151|ROA0_HUMAN	1089.518	84.96	9.10E-08	GDVAEGDLIEHFSQFGTVEK
Q13151|ROA0_HUMAN	845.9559	90.72	8.40E-08	LFIGGLNVQTSESGLR
Q13151|ROA0_HUMAN	845.9562	91.01	8.00E-08	LFIGGLNVQTSESGLR
Q13151|ROA0_HUMAN	845.9567	91.49	7.00E-08	LFIGGLNVQTSESGLR
Q13151|ROA0_H	845.9	91.83	5.90E-08	LFIGGLNVQTSESGLR

UMAN	572			
Q13151|ROA0_HUMAN	845.9581	92.86	5.20E-08	LFIGGLNVQTSESGLR
Q13151|ROA0_HUMAN	845.9574	93.99	3.60E-08	LFIGGLNVQTSESGLR
Q13151|ROA0_HUMAN	1089.518	96.82	5.90E-09	GDVAEGDLIEHFSQFGTVEK
Q13151|ROA0_HUMAN	845.9576	103.81	4.10E-09	LFIGGLNVQTSESGLR
Q13185|CBX3_HUMAN	745.3775	51.4	0.00035	WKDSDEADLVLAK
Q13242|SRSF9_HUMAN	577.7788	34.97	0.0043	KEDMEYALR
Q13242|SRSF9_HUMAN	577.7815	44.87	0.00046	KEDMEYALR
Q13243|SRSF5_HUMAN	820.9103	65.4	1.10E-05	LNEGVVEFASYGDLK
Q13243|SRSF5_HUMAN	820.9127	73.1	2.00E-06	LNEGVVEFASYGDLK
Q13243|SRSF5_HUMAN	820.9101	73.67	1.50E-06	LNEGVVEFASYGDLK
Q13243|SRSF5_HUMAN	820.9103	75.29	1.10E-06	LNEGVVEFASYGDLK
Q13243|SRSF5_HUMAN	820.908	75.79	9.00E-07	LNEGVVEFASYGDLK
Q13243|SRSF5_HUMAN	820.9098	86.82	7.30E-08	LNEGVVEFASYGDLK
Q13435|SF3B2_HUMAN	797.3691	35.06	0.0047	EQQAQVEKEDFSDMVAEHAAK
Q13435|SF3B2_HUMAN	565.2944	43.49	0.0014	KPGDLSDELR
Q13435|SF3B2_HUMAN	565.2953	45.8	0.00093	KPGDLSDELR
Q13435|SF3B2_HUMAN	565.2936	45.77	0.00091	KPGDLSDELR
Q13435|SF3B2_HUMAN	565.296	57.74	5.40E-05	KPGDLSDELR
Q13595|TRA2A_HUMAN	783.8958	51.87	0.00026	YGPLSGVNVVYDQR
Q13595|TRA2A_HUMAN	783.8989	53.91	0.00018	YGPLSGVNVVYDQR
Q13595|TRA2A_HUMAN	783.8984	53.52	0.00018	YGPLSGVNVVYDQR
Q13838|DX39B_HUMAN	767.3455	36.28	0.0021	VNIAFNYDMPEDSDTYLHR
Q13838|DX39B_HUMAN	767.3452	42.5	0.00051	VNIAFNYDMPEDSDTYLHR
Q13838|DX39B_HUMAN	767.3455	43.77	0.00038	VNIAFNYDMPEDSDTYLHR
Q13838|DX39B_HUMAN	1150.514	51.64	6.20E-05	VNIAFNYDMPEDSDTYLHR
Q13838|DX39B_HUMAN	922.9048	52.35	3.00E-05	FMQDPMEIFVDDETK
Q13838|DX39B_HUMAN	922.906	64.32	1.80E-06	FMQDPMEIFVDDETK

Q13838|DX39B_HUMAN	1150.514	85.21	2.40E-08	VNIAFNYDMPEDSDTYLHR
Q13838|DX39B_HUMAN	922.9058	83.58	2.20E-08	FMQDPMEIFVDDETK
Q14011|CIRBP_HUMAN	1173.082	46.87	0.0013	LFVGGLSFDTNEQSLEQVFSK
Q14103|HNRPD_HUMAN	744.8795	41.68	0.0034	IFVGGLSPDTPEEK
Q14103|HNRPD_HUMAN	744.8807	49.56	0.0006	IFVGGLSPDTPEEK
Q14103|HNRPD_HUMAN	744.88	51.39	0.00038	IFVGGLSPDTPEEK
Q14103|HNRPD_HUMAN	744.88	55.86	0.00014	IFVGGLSPDTPEEK
Q14103|HNRPD_HUMAN	744.88	62.18	3.20E-05	IFVGGLSPDTPEEK
Q14103|HNRPD_HUMAN	744.8814	64.7	2.00E-05	IFVGGLSPDTPEEK
Q14103|HNRPD_HUMAN	744.8806	64.91	1.70E-05	IFVGGLSPDTPEEK
Q14103|HNRPD_HUMAN	744.8799	67.24	9.80E-06	IFVGGLSPDTPEEK
Q14103|HNRPD_HUMAN	1080.989	66.96	1.90E-06	EYFGGFGEVESIELPMDNK
Q14103|HNRPD_HUMAN	1080.992	69.58	1.10E-06	EYFGGFGEVESIELPMDNK
Q14103|HNRPD_HUMAN	744.88	78.82	6.80E-07	IFVGGLSPDTPEEK
Q14103|HNRPD_HUMAN	1080.99	79.87	1.00E-07	EYFGGFGEVESIELPMDNK
Q14978|NOLC1_HUMAN	518.8088	39.03	0.004	SPAVKPAAAPK
Q14978|NOLC1_HUMAN	973.0305	43.92	0.0039	NKPGPYSSVPPPSAPPPKK
Q14978|NOLC1_HUMAN	518.8104	39.18	0.0039	SPAVKPAAAPK
Q14978|NOLC1_HUMAN	680.8372	39.77	0.003	VREEEIEVDSR
Q14978|NOLC1_HUMAN	973.0297	48	0.0016	NKPGPYSSVPPPSAPPPKK
Q14978|NOLC1_HUMAN	973.0298	49.11	0.0013	NKPGPYSSVPPPSAPPPKK
Q14978|NOLC1_HUMAN	973.0305	48.93	0.0012	NKPGPYSSVPPPSAPPPKK
Q14978|NOLC1_HUMAN	844.4911	49.2	0.0008	VVPSDLYPLVLGFLR
Q14978|NOLC1_HUMAN	844.4904	49.81	0.00073	VVPSDLYPLVLGFLR
Q14978|NOLC1_HUMAN	973.0268	52.83	0.00055	NKPGPYSSVPPPSAPPPKK
Q14978|NOLC1_HUMAN	844.4899	51.9	0.00046	VVPSDLYPLVLGFLR
Q14978|NOLC1_HUMAN	1250.62	52.42	0.00034	ATGATQQDANASSLLDIYSFWLK
Q14978|NOLC1_H	844.4	53.42	0.00032	VVPSDLYPLVLGFLR

UMAN	908			
Q14978|NOLC1_HUMAN	844.4913	53.34	0.00031	VVPSDLYPLVLGFLR
Q14978|NOLC1_HUMAN	973.0304	55.36	0.00028	NKPGPYSSVPPPSAPPPKK
Q14978|NOLC1_HUMAN	844.4911	54.3	0.00025	VVPSDLYPLVLGFLR
Q14978|NOLC1_HUMAN	844.4907	55.09	0.00022	VVPSDLYPLVLGFLR
Q14978|NOLC1_HUMAN	844.491	62.43	3.80E-05	VVPSDLYPLVLGFLR
Q14978|NOLC1_HUMAN	844.4917	63.61	2.80E-05	VVPSDLYPLVLGFLR
Q14978|NOLC1_HUMAN	844.4912	65.25	2.00E-05	VVPSDLYPLVLGFLR
Q14978|NOLC1_HUMAN	844.4908	65.73	1.90E-05	VVPSDLYPLVLGFLR
Q14978|NOLC1_HUMAN	844.4906	66.51	1.60E-05	VVPSDLYPLVLGFLR
Q14978|NOLC1_HUMAN	844.4913	66.39	1.50E-05	VVPSDLYPLVLGFLR
Q14978|NOLC1_HUMAN	1250.62	66.78	1.30E-05	ATGATQQDANASSLLDIYSFWLK
Q14978|NOLC1_HUMAN	844.4894	68.15	1.10E-05	VVPSDLYPLVLGFLR
Q14978|NOLC1_HUMAN	844.4904	68.06	1.10E-05	VVPSDLYPLVLGFLR
Q14978|NOLC1_HUMAN	1250.62	77.16	1.20E-06	ATGATQQDANASSLLDIYSFWLK
Q14978|NOLC1_HUMAN	1250.62	77.21	1.10E-06	ATGATQQDANASSLLDIYSFWLK
Q14978|NOLC1_HUMAN	1250.62	80.47	5.40E-07	ATGATQQDANASSLLDIYSFWLK
Q14978|NOLC1_HUMAN	1250.62	83.83	2.50E-07	ATGATQQDANASSLLDIYSFWLK
Q14978|NOLC1_HUMAN	1250.62	95.25	1.80E-08	ATGATQQDANASSLLDIYSFWLK
Q14978|NOLC1_HUMAN	1250.622	99.92	6.40E-09	ATGATQQDANASSLLDIYSFWLK
Q15029|U5S1_HUMAN	967.5377	43.25	0.0042	VPAGNWVLIEGVDQPIVK
Q15029|U5S1_HUMAN	967.5408	43.58	0.0035	VPAGNWVLIEGVDQPIVK
Q15233|NONO_HUMAN	848.3737	35.3	0.0018	FAQPGSFEYEYAMR
Q15233|NONO_HUMAN	848.3773	37.71	0.0014	FAQPGSFEYEYAMR
Q15233|NONO_HUMAN	930.4606	46.34	0.0011	LFVGNLPPDITEEEMR
Q15233|NONO_HUMAN	930.4606	48.17	0.0007	LFVGNLPPDITEEEMR
Q15233|NONO_HUMAN	930.4607	48.71	0.00067	LFVGNLPPDITEEEMR
Q15233|NONO_HUMAN	1082.042	55.22	0.00021	FGQAATMEGIGAIGGTPPAFNR

Q15233|NONO_HUMAN	848.373	46.99	0.00013	FAQPGSFEYEYAMR
Q15233|NONO_HUMAN	930.4604	56.1	0.00011	LFVGNLPPDITEEEMR
Q15233|NONO_HUMAN	930.4643	57.22	0.0001	LFVGNLPPDITEEEMR
Q15233|NONO_HUMAN	1082.039	59.93	6.10E-05	FGQAATMEGIGAIGGTPPAFNR
Q15233|NONO_HUMAN	930.4623	61.65	3.60E-05	LFVGNLPPDITEEEMR
Q15233|NONO_HUMAN	848.374	53.94	2.70E-05	FAQPGSFEYEYAMR
Q15287|RNPS1_HUMAN	970.8281	58.51	0.00014	HMDGGQIDGQEITATAVLAPWPRPPPR
Q15287|RNPS1_HUMAN	880.8835	50.72	2.40E-05	GYAYVEFENPDEAEK
Q15287|RNPS1_HUMAN	970.8245	69.04	1.20E-05	HMDGGQIDGQEITATAVLAPWPRPPPR
Q15287|RNPS1_HUMAN	880.8826	54.52	9.20E-06	GYAYVEFENPDEAEK
Q15287|RNPS1_HUMAN	970.8254	71.71	6.20E-06	HMDGGQIDGQEITATAVLAPWPRPPPR
Q15287|RNPS1_HUMAN	880.8829	56.92	5.30E-06	GYAYVEFENPDEAEK
Q15287|RNPS1_HUMAN	970.825	72.54	5.20E-06	HMDGGQIDGQEITATAVLAPWPRPPPR
Q15287|RNPS1_HUMAN	970.8272	75.46	2.70E-06	HMDGGQIDGQEITATAVLAPWPRPPPR
Q15287|RNPS1_HUMAN	880.8831	61.82	1.70E-06	GYAYVEFENPDEAEK
Q15287|RNPS1_HUMAN	970.8254	77.96	1.50E-06	HMDGGQIDGQEITATAVLAPWPRPPPR
Q15287|RNPS1_HUMAN	970.8235	79.7	9.60E-07	HMDGGQIDGQEITATAVLAPWPRPPPR
Q15287|RNPS1_HUMAN	880.8824	66.33	5.80E-07	GYAYVEFENPDEAEK
Q15287|RNPS1_HUMAN	880.8821	66.48	5.60E-07	GYAYVEFENPDEAEK
Q15287|RNPS1_HUMAN	970.8265	83.43	4.30E-07	HMDGGQIDGQEITATAVLAPWPRPPPR
Q15287|RNPS1_HUMAN	880.8834	73.11	1.30E-07	GYAYVEFENPDEAEK
Q15287|RNPS1_HUMAN	880.8831	74.07	1.00E-07	GYAYVEFENPDEAEK
Q15393|SF3B3_HUMAN	961.0203	44.18	0.0036	LGAVFNQVAFPLQYTPR
Q15393|SF3B3_HUMAN	961.0222	47.08	0.002	LGAVFNQVAFPLQYTPR
Q15393|SF3B3_HUMAN	927.92	38.24	0.0012	LPPNTNDEVDEDPTGNK
Q15393|SF3B3_HUMAN	927.92	40.8	0.00065	LPPNTNDEVDEDPTGNK
Q15393|SF3B3_HUMAN	927.9189	40.75	0.00064	LPPNTNDEVDEDPTGNK
Q15393|SF3B3_H	841.4	51.65	0.00047	TPVEEVPAAIAPFQGR

UMAN	459			
Q15393|SF3B3_HUMAN	744.8795	53.18	0.00024	TVLDPVTGDLSDTR
Q15393|SF3B3_HUMAN	841.4464	54.97	0.00019	TPVEEVPAAIAPFQGR
Q15393|SF3B3_HUMAN	927.917	47.13	0.00013	LPPNTNDEVDEDPTGNK
Q15393|SF3B3_HUMAN	840.449	57.64	0.00012	HIANYISGIQTIGHR
Q15393|SF3B3_HUMAN	927.9199	48	0.00012	LPPNTNDEVDEDPTGNK
Q15393|SF3B3_HUMAN	963.4739	56.8	8.70E-05	WVTTASLLDYDTVAGADK
Q15393|SF3B3_HUMAN	927.9252	52.32	5.00E-05	LPPNTNDEVDEDPTGNK
Q15393|SF3B3_HUMAN	841.4451	62.2	4.40E-05	TPVEEVPAAIAPFQGR
Q15393|SF3B3_HUMAN	841.4476	62.18	4.20E-05	TPVEEVPAAIAPFQGR
Q15393|SF3B3_HUMAN	841.4472	64.28	2.80E-05	TPVEEVPAAIAPFQGR
Q15393|SF3B3_HUMAN	927.9187	56.65	1.60E-05	LPPNTNDEVDEDPTGNK
Q15393|SF3B3_HUMAN	841.4456	66.99	1.40E-05	TPVEEVPAAIAPFQGR
Q15393|SF3B3_HUMAN	961.0181	68.6	1.20E-05	LGAVFNQVAFPLQYTPR
Q15393|SF3B3_HUMAN	963.4758	68.13	6.80E-06	WVTTASLLDYDTVAGADK
Q15393|SF3B3_HUMAN	961.0203	71.41	6.70E-06	LGAVFNQVAFPLQYTPR
Q15393|SF3B3_HUMAN	961.0181	71.46	6.20E-06	LGAVFNQVAFPLQYTPR
Q15393|SF3B3_HUMAN	927.9211	65.3	2.40E-06	LPPNTNDEVDEDPTGNK
Q15393|SF3B3_HUMAN	961.0183	78.48	1.50E-06	LGAVFNQVAFPLQYTPR
Q15424|SAFB1_HUMAN	1123.026	52.37	0.00014	AIEDEGGNPDEIEITSEGNKK
Q15424|SAFB1_HUMAN	1123.032	57.55	5.60E-05	AIEDEGGNPDEIEITSEGNKK
Q15424|SAFB1_HUMAN	1123.024	73.76	9.00E-07	AIEDEGGNPDEIEITSEGNKK
Q15424|SAFB1_HUMAN	1123.023	75.02	6.70E-07	AIEDEGGNPDEIEITSEGNKK
Q15424|SAFB1_HUMAN	1123.025	79.04	2.90E-07	AIEDEGGNPDEIEITSEGNKK
Q15427|SF3B4_HUMAN	754.8618	92.39	1.20E-08	NQDATVYVGGLDEK
Q15459|SF3A1_HUMAN	768.404	47.6	0.0011	RTDIFGVEETAIGK
Q15459|SF3A1_HUMAN	768.4034	52.53	0.0004	RTDIFGVEETAIGK
Q15459|SF3A1_HUMAN	768.4035	52.57	0.00038	RTDIFGVEETAIGK

Q15459|SF3A1_HUMAN	768.407	61.79	4.30E-05	RTDIFGVEETAIGK
Q15459|SF3A1_HUMAN	768.4039	72.28	3.80E-06	RTDIFGVEETAIGK
Q15717|ELAV1_HUMAN	594.8306	46.75	0.0021	VLVDQTTGLSR
Q15717|ELAV1_HUMAN	594.8301	51.6	0.00088	VLVDQTTGLSR
Q15717|ELAV1_HUMAN	594.8303	53.46	0.00043	VLVDQTTGLSR
Q15717|ELAV1_HUMAN	784.9324	60.67	6.70E-05	NVALLSQLYHSPAR
Q15717|ELAV1_HUMAN	784.9285	68.67	8.60E-06	NVALLSQLYHSPAR
Q15717|ELAV1_HUMAN	1081.546	71.41	4.90E-06	TNLIVNYLPQNMTQDELR
Q15717|ELAV1_HUMAN	677.3517	72.61	2.10E-06	SLFSSIGEVESAK
Q15717|ELAV1_HUMAN	784.9308	77.86	1.00E-06	NVALLSQLYHSPAR
Q15717|ELAV1_HUMAN	1081.548	82.17	4.20E-07	TNLIVNYLPQNMTQDELR
Q15717|ELAV1_HUMAN	784.93	85.63	1.70E-07	NVALLSQLYHSPAR
Q15717|ELAV1_HUMAN	1081.548	107.11	1.30E-09	TNLIVNYLPQNMTQDELR
Q15717|ELAV1_HUMAN	1081.547	107.49	1.20E-09	TNLIVNYLPQNMTQDELR
Q16531|DDB1_HUMAN	822.4498	45.54	0.0032	ALYYLQIHPQELR
Q16531|DDB1_HUMAN	984.8272	44.63	0.003	IEVQDTSGGTTALRPSASTQALSSSVSSSK
Q16531|DDB1_HUMAN	984.8252	64.14	3.30E-05	IEVQDTSGGTTALRPSASTQALSSSVSSSK
Q16531|DDB1_HUMAN	984.8267	73.31	3.90E-06	IEVQDTSGGTTALRPSASTQALSSSVSSSK
Q16629|SRSF7_HUMAN	622.841	43.59	0.0032	VRVELSTGMPR
Q16629|SRSF7_HUMAN	622.8411	44.11	0.0028	VRVELSTGMPR
Q5BKZ1|ZN326_HUMAN	849.9816	44.99	0.0032	ESVLTATSILNNPIVK
Q7L7L0|H2A3_HUMAN	650.8442	55.96	0.00013	NDEELNKLLGR
Q7L7L0|H2A3_HUMAN	650.8472	65.84	1.50E-05	NDEELNKLLGR
Q7L7L0|H2A3_HUMAN	650.8447	65.37	1.40E-05	NDEELNKLLGR
Q7L7L0|H2A3_HUMAN	650.8452	66.55	1.20E-05	NDEELNKLLGR
Q7L7L0|H2A3_HUMAN	650.8443	66.37	1.20E-05	NDEELNKLLGR
Q7L7L0|H2A3_HUMAN	650.845	65.58	1.20E-05	NDEELNKLLGR
Q7L7L0|H2A3_HU	650.8	66.27	1.10E-05	NDEELNKLLGR

MAN	448			
Q7L7L0|H2A3_HUMAN	650.8445	70.71	4.20E-06	NDEELNKLLGR
Q7L7L0|H2A3_HUMAN	650.8448	70.47	4.00E-06	NDEELNKLLGR
Q7L7L0|H2A3_HUMAN	650.8447	72.17	2.70E-06	NDEELNKLLGR
Q7L7L0|H2A3_HUMAN	650.8442	74.91	1.70E-06	NDEELNKLLGR
Q7L7L0|H2A3_HUMAN	650.8442	78.1	8.00E-07	NDEELNKLLGR
Q7L7L0|H2A3_HUMAN	650.8446	83.77	2.10E-07	NDEELNKLLGR
Q7L7L0|H2A3_HUMAN	650.845	88.69	6.00E-08	NDEELNKLLGR
Q7Z7K6|CENPV_HUMAN	769.9246	44.29	0.0021	LLLDTFEYQGLVK
Q7Z7K6|CENPV_HUMAN	769.926	46.21	0.0012	LLLDTFEYQGLVK
Q7Z7K6|CENPV_HUMAN	769.925	56.23	0.00014	LLLDTFEYQGLVK
Q7Z7K6|CENPV_HUMAN	769.9256	57.05	0.0001	LLLDTFEYQGLVK
Q7Z7K6|CENPV_HUMAN	769.9259	58.59	7.00E-05	LLLDTFEYQGLVK
Q86V81|THOC4_HUMAN	938.4825	46.71	0.0022	QYNGVPLDGRPMNIQLVTSQIDAQR
Q86V81|THOC4_HUMAN	616.3061	41.27	0.0016	SLGTADVHFER
Q86V81|THOC4_HUMAN	768.8657	40.65	0.0013	ADKMDMSLDDIIK
Q86V81|THOC4_HUMAN	616.3052	42.25	0.0012	SLGTADVHFER
Q86V81|THOC4_HUMAN	616.3052	43.74	0.00087	SLGTADVHFER
Q86V81|THOC4_HUMAN	768.8648	43.94	0.00064	ADKMDMSLDDIIK
Q86V81|THOC4_HUMAN	768.8655	43.88	0.00063	ADKMDMSLDDIIK
Q86V81|THOC4_HUMAN	590.7802	43.59	0.00039	MDMSLDDIIK
Q86V81|THOC4_HUMAN	768.8657	47.89	0.00025	ADKMDMSLDDIIK
Q86V81|THOC4_HUMAN	616.3052	54.34	7.60E-05	SLGTADVHFER
Q86V81|THOC4_HUMAN	768.8663	55.19	5.80E-05	ADKMDMSLDDIIK
Q86V81|THOC4_HUMAN	768.8651	54.93	5.00E-05	ADKMDMSLDDIIK
Q86V81|THOC4_HUMAN	616.306	58.58	3.60E-05	SLGTADVHFER
Q86V81|THOC4_HUMAN	616.3055	58.49	3.50E-05	SLGTADVHFER
Q86V81|THOC4_HUMAN	616.3062	58.43	3.20E-05	SLGTADVHFER

Q86V81|THOC4_HUMAN	616.3055	58.43	3.00E-05	SLGTADVHFER
Q86V81|THOC4_HUMAN	590.7819	56.09	2.70E-05	MDMSLDDIIK
Q86V81|THOC4_HUMAN	616.3059	62.65	1.40E-05	SLGTADVHFER
Q86V81|THOC4_HUMAN	616.3054	62.24	1.20E-05	SLGTADVHFER
Q86V81|THOC4_HUMAN	616.3055	62.76	1.10E-05	SLGTADVHFER
Q86V81|THOC4_HUMAN	768.8657	63.28	7.20E-06	ADKMDMSLDDIIK
Q86V81|THOC4_HUMAN	1017.989	100.02	3.30E-09	QQLSAEELDAQLDAYNAR
Q86V81|THOC4_HUMAN	1017.994	101.62	2.70E-09	QQLSAEELDAQLDAYNAR
Q86V81|THOC4_HUMAN	1017.99	101.75	2.10E-09	QQLSAEELDAQLDAYNAR
Q86V81|THOC4_HUMAN	1017.989	102.43	1.90E-09	QQLSAEELDAQLDAYNAR
Q86V81|THOC4_HUMAN	1017.991	104.85	1.20E-09	QQLSAEELDAQLDAYNAR
Q86V81|THOC4_HUMAN	1017.989	104.6	1.10E-09	QQLSAEELDAQLDAYNAR
Q86V81|THOC4_HUMAN	1017.992	105.54	1.00E-09	QQLSAEELDAQLDAYNAR
Q86V81|THOC4_HUMAN	1017.992	106.82	7.80E-10	QQLSAEELDAQLDAYNAR
Q86V81|THOC4_HUMAN	1017.987	106.93	6.70E-10	QQLSAEELDAQLDAYNAR
Q86V81|THOC4_HUMAN	1017.991	113.2	1.60E-10	QQLSAEELDAQLDAYNAR
Q86V81|THOC4_HUMAN	1017.99	117.11	6.60E-11	QQLSAEELDAQLDAYNAR
Q86V81|THOC4_HUMAN	1017.991	117.33	6.50E-11	QQLSAEELDAQLDAYNAR
Q86YZ3|HORN_HUMAN	792.8616	33.42	0.0028	GPYESGSGHSSGLGHR
Q86YZ3|HORN_HUMAN	792.8599	40.42	0.00042	GPYESGSGHSSGLGHR
Q86YZ3|HORN_HUMAN	792.8625	81.92	4.80E-08	GPYESGSGHSSGLGHR
Q8IUE6|H2A2B_HUMAN	418.7577	34.85	0.005	HLQLAVR
Q8IYB3|SRRM1_HUMAN	916.4832	53.06	0.00047	VKEPSVQEATSTSDILK
Q8IYB3|SRRM1_HUMAN	916.4902	53.32	0.00046	VKEPSVQEATSTSDILK
Q8IYB3|SRRM1_HUMAN	916.485	59.94	0.0001	VKEPSVQEATSTSDILK
Q8IYB3|SRRM1_HUMAN	916.4835	62.02	6.10E-05	VKEPSVQEATSTSDILK
Q8IYB3|SRRM1_HUMAN	916.4843	64.85	3.30E-05	VKEPSVQEATSTSDILK
Q8IYB3|SRRM1_H	916.4	73.12	4.70E-06	VKEPSVQEATSTSDILK

UMAN	832			
Q8IYB3|SRRM1_HUMAN	916.4832	73.06	4.70E-06	VKEPSVQEATSTSDILK
Q8IYB3|SRRM1_HUMAN	916.4849	76.05	2.50E-06	VKEPSVQEATSTSDILK
Q8IYB3|SRRM1_HUMAN	916.4852	78.25	1.50E-06	VKEPSVQEATSTSDILK
Q8IYB3|SRRM1_HUMAN	916.4824	79.52	1.10E-06	VKEPSVQEATSTSDILK
Q8IYB3|SRRM1_HUMAN	916.4829	90.19	9.20E-08	VKEPSVQEATSTSDILK
Q8IYB3|SRRM1_HUMAN	916.4827	91.29	7.20E-08	VKEPSVQEATSTSDILK
Q8IYW5|RN168_HUMAN	859.91	37.11	0.0049	SQFGSASHSEAVQEVR
Q8IYW5|RN168_HUMAN	687.8393	40.14	0.0029	LLAEEEEEEKR
Q8IYW5|RN168_HUMAN	641.8403	42.07	0.0027	SAHSLQPSISQK
Q8IYW5|RN168_HUMAN	687.8386	40.71	0.0026	LLAEEEEEEKR
Q8IYW5|RN168_HUMAN	687.8391	41.25	0.0023	LLAEEEEEEKR
Q8IYW5|RN168_HUMAN	687.8396	41.38	0.0021	LLAEEEEEEKR
Q8IYW5|RN168_HUMAN	687.8387	42.65	0.0017	LLAEEEEEEKR
Q8IYW5|RN168_HUMAN	699.3945	50.7	0.00053	LIDLEHLLFER
Q8IYW5|RN168_HUMAN	537.2552	45.17	0.00021	GSPDEYHLR
Q8IYW5|RN168_HUMAN	537.2527	45.03	0.00015	GSPDEYHLR
Q8IYW5|RN168_HUMAN	956.4358	49.25	0.00013	ASEEEENKASEEYIQR
Q8IYW5|RN168_HUMAN	537.2518	45.58	0.00013	GSPDEYHLR
Q8IYW5|RN168_HUMAN	537.2545	46.7	0.00012	GSPDEYHLR
Q8IYW5|RN168_HUMAN	859.9061	54.32	8.30E-05	SQFGSASHSEAVQEVR
Q8IYW5|RN168_HUMAN	956.4302	52.54	4.30E-05	ASEEEENKASEEYIQR
Q8IYW5|RN168_HUMAN	859.9058	69.29	2.50E-06	SQFGSASHSEAVQEVR
Q8IYW5|RN168_HUMAN	859.9048	71.27	1.50E-06	SQFGSASHSEAVQEVR
Q8IYW5|RN168_HUMAN	859.9063	73.09	1.10E-06	SQFGSASHSEAVQEVR
Q8IYW5|RN168_HUMAN	859.9061	75.24	6.50E-07	SQFGSASHSEAVQEVR
Q8IYW5|RN168_HUMAN	1082.997	83.06	7.80E-08	VSPESSPDQEETEINFTQK
Q8IYW5|RN168_HUMAN	1082.995	86.56	2.90E-08	VSPESSPDQEETEINFTQK

Q8NC51|PAIRB_HUMAN	628.3204	43.15	0.0014	RPDQQLQGEGK
Q92522|H1X_HUMAN	666.3554	41.75	0.005	GAPAAATAPAPTAHK
Q92522|H1X_HUMAN	666.3547	41.31	0.0047	GAPAAATAPAPTAHK
Q92522|H1X_HUMAN	666.3555	43.32	0.0035	GAPAAATAPAPTAHK
Q92522|H1X_HUMAN	604.3351	45.66	0.0016	YSQLVVETIR
Q92522|H1X_HUMAN	604.337	47.83	0.00085	YSQLVVETIR
Q92522|H1X_HUMAN	604.3354	49.31	0.00062	YSQLVVETIR
Q92522|H1X_HUMAN	666.3547	50.92	0.00052	GAPAAATAPAPTAHK
Q92522|H1X_HUMAN	666.3557	53.96	0.00032	GAPAAATAPAPTAHK
Q92522|H1X_HUMAN	604.3349	54.96	0.0002	YSQLVVETIR
Q92522|H1X_HUMAN	666.3555	56.1	0.00018	GAPAAATAPAPTAHK
Q92522|H1X_HUMAN	604.3358	57.01	9.90E-05	YSQLVVETIR
Q92522|H1X_HUMAN	604.336	58.34	6.80E-05	YSQLVVETIR
Q92522|H1X_HUMAN	604.3367	59.54	5.80E-05	YSQLVVETIR
Q92522|H1X_HUMAN	666.3549	65.95	1.60E-05	GAPAAATAPAPTAHK
Q92522|H1X_HUMAN	671.3887	70.01	8.40E-06	ALVQNDTLLQVK
Q92522|H1X_HUMAN	671.3885	70.6	7.40E-06	ALVQNDTLLQVK
Q92522|H1X_HUMAN	671.3878	73.43	4.40E-06	ALVQNDTLLQVK
Q92522|H1X_HUMAN	671.3882	73.57	3.80E-06	ALVQNDTLLQVK
Q92522|H1X_HUMAN	671.3882	73.51	3.80E-06	ALVQNDTLLQVK
Q92522|H1X_HUMAN	671.3881	79.39	1.10E-06	ALVQNDTLLQVK
Q92522|H1X_HUMAN	671.3883	79.01	1.10E-06	ALVQNDTLLQVK
Q92522|H1X_HUMAN	671.389	79.63	7.90E-07	ALVQNDTLLQVK
Q92804|RBP56_HUMAN	719.8423	35.15	0.0043	GPMTGSSGGDRGGFK
Q92804|RBP56_HUMAN	719.8414	36.51	0.0033	GPMTGSSGGDRGGFK
Q96A72|MGN2_HUMAN	1163.064	47.34	0.00096	IIDDSEITKEDDALWPPPDR
Q96A72|MGN2_HUMAN	1163.067	49.78	0.00061	IIDDSEITKEDDALWPPPDR
Q96A72|MGN2_H	1163.	49.79	0.00057	IIDDSEITKEDDALWPPPDR

UMAN	065			
Q96A72|MGN2_HUMAN	1163.064	63.67	2.20E-05	IIDDSEITKEDDALWPPPDR
Q96A72|MGN2_HUMAN	1163.07	66.81	1.30E-05	IIDDSEITKEDDALWPPPDR
Q96A72|MGN2_HUMAN	1163.068	67.16	1.20E-05	IIDDSEITKEDDALWPPPDR
Q96A72|MGN2_HUMAN	1163.069	70.83	5.10E-06	IIDDSEITKEDDALWPPPDR
Q96PK6|RBM14_HUMAN	804.919	45.74	0.0018	ASYVAPLTAQPATYR
Q96PK6|RBM14_HUMAN	1233.096	59.93	5.00E-05	TQSSASLAASYAAQQHPQAAASYR
Q96PK6|RBM14_HUMAN	1233.092	69.59	4.90E-06	TQSSASLAASYAAQQHPQAAASYR
Q99729|ROAA_HUMAN	664.3192	37.76	0.0019	MFVGGLSWDTSK
Q99729|ROAA_HUMAN	728.3669	43.91	0.0012	MFVGGLSWDTSKK
Q99729|ROAA_HUMAN	728.3658	43.7	0.0012	MFVGGLSWDTSKK
Q99729|ROAA_HUMAN	728.3655	45.52	0.00078	MFVGGLSWDTSKK
Q99729|ROAA_HUMAN	1107.516	46.16	0.0005	EYFGEFGEIEAIELPMDPK
Q99729|ROAA_HUMAN	899.4901	54.12	0.00037	GFVFITFKEEEPVKK
Q99729|ROAA_HUMAN	464.7668	45.9	0.00035	GFGFILFK
Q99729|ROAA_HUMAN	728.3677	49.55	0.00034	MFVGGLSWDTSKK
Q99729|ROAA_HUMAN	464.7664	52.45	0.00024	GFGFILFK
Q99729|ROAA_HUMAN	664.3193	46.48	0.00023	MFVGGLSWDTSK
Q99729|ROAA_HUMAN	664.3198	48.3	0.00021	MFVGGLSWDTSK
Q99729|ROAA_HUMAN	728.3663	52.07	0.00018	MFVGGLSWDTSKK
Q99729|ROAA_HUMAN	464.766	55.15	0.00013	GFGFILFK
Q99729|ROAA_HUMAN	664.3195	49.09	0.00013	MFVGGLSWDTSK
Q99729|ROAA_HUMAN	1107.517	57.38	3.80E-05	EYFGEFGEIEAIELPMDPK
Q99729|ROAA_HUMAN	728.3672	63.89	1.20E-05	MFVGGLSWDTSKK
Q99729|ROAA_HUMAN	664.3197	63.15	6.40E-06	MFVGGLSWDTSK
Q99729|ROAA_HUMAN	1107.516	66.37	4.80E-06	EYFGEFGEIEAIELPMDPK
Q99729|ROAA_HUMAN	664.3204	66.44	3.30E-06	MFVGGLSWDTSK
Q99729|ROAA_HUMAN	664.3194	65.91	2.60E-06	MFVGGLSWDTSK

Q99729|ROAA_HUMAN	1107.517	88.74	2.80E-08	EYFGEFGEIEAIELPMDPK
Q9BRT6|LLPH_HUMAN	761.9438	40.67	0.0044	DVQEIATVVVPKPK
Q9BRT6|LLPH_HUMAN	761.944	40.91	0.0042	DVQEIATVVVPKPK
Q9BRT6|LLPH_HUMAN	761.9447	42.25	0.0027	DVQEIATVVVPKPK
Q9BRT6|LLPH_HUMAN	761.9458	43.23	0.0022	DVQEIATVVVPKPK
Q9BRT6|LLPH_HUMAN	761.9437	48.11	0.0008	DVQEIATVVVPKPK
Q9BRT6|LLPH_HUMAN	761.9448	47.94	0.00073	DVQEIATVVVPKPK
Q9BRT6|LLPH_HUMAN	761.9426	53.56	0.00023	DVQEIATVVVPKPK
Q9NVP1|DDX18_HUMAN	721.3507	47	0.00041	VPLSEFDFSWSK
Q9NX24|NHP2_HUMAN	1078.075	58.4	0.00015	TYQELLVNQNPIAQPLASR
Q9NX24|NHP2_HUMAN	1078.081	68.28	1.60E-05	TYQELLVNQNPIAQPLASR
Q9NX24|NHP2_HUMAN	1078.08	82.79	5.50E-07	TYQELLVNQNPIAQPLASR
Q9NYF8|BCLF1_HUMAN	854.4692	43.07	0.0044	LKETGYVVERPSTTK
Q9NYF8|BCLF1_HUMAN	854.4664	45.82	0.0021	LKETGYVVERPSTTK
Q9NYF8|BCLF1_HUMAN	1040.982	60.84	1.30E-05	SSATSGDIWPGLSAYDNSPR
Q9NYF8|BCLF1_HUMAN	961.3638	71.56	7.00E-08	FNDSEGDDTEETEDYR
Q9NYF8|BCLF1_HUMAN	961.363	77.03	2.00E-08	FNDSEGDDTEETEDYR
Q9P0M6|H2AW_HUMAN	1000.521	43.3	0.0035	SQGPLEVAEAAVSQSSGLAAK
Q9P0M6|H2AW_HUMAN	1000.515	50.12	0.00074	SQGPLEVAEAAVSQSSGLAAK
Q9P0M6|H2AW_HUMAN	1000.516	52.26	0.00049	SQGPLEVAEAAVSQSSGLAAK
Q9P0M6|H2AW_HUMAN	1000.515	63.94	2.90E-05	SQGPLEVAEAAVSQSSGLAAK
Q9P0M6|H2AW_HUMAN	768.3732	65.35	7.30E-06	AISAHFDDSSASSLK
Q9P0M6|H2AW_HUMAN	1000.514	72.26	4.70E-06	SQGPLEVAEAAVSQSSGLAAK
Q9P0M6|H2AW_HUMAN	1000.514	80.28	6.70E-07	SQGPLEVAEAAVSQSSGLAAK
Q9UKM9|RALY_HUMAN	667.3129	33.88	0.005	GYAFVQYSNER
Q9UKM9|RALY_HUMAN	577.3085	45.33	0.00082	KSDVETIFSK
Q9UMS4|PRP19_HUMAN	799.4369	41.35	0.0049	TVPEELVKPEELSK
Q9UMS4|PRP19_	799.4	43.1	0.0038	TVPEELVKPEELSK

HUMAN	367			
Q9UMS4|PRP19_HUMAN	1357.675	47.1	0.0015	YIAENGTDPINNQPLSEEQLIDIK
Q9UMS4|PRP19_HUMAN	1357.673	46.9	0.0015	YIAENGTDPINNQPLSEEQLIDIK
Q9UMS4|PRP19_HUMAN	1357.677	47.49	0.0014	YIAENGTDPINNQPLSEEQLIDIK
Q9Y221|NIP7_HUMAN	787.9288	49.25	0.0012	LHVTALDYLAPYAK
Q9Y221|NIP7_HUMAN	787.9299	58.69	0.00012	LHVTALDYLAPYAK
Q9Y221|NIP7_HUMAN	787.9288	63.12	4.90E-05	LHVTALDYLAPYAK
Q9Y221|NIP7_HUMAN	787.9322	63.4	4.80E-05	LHVTALDYLAPYAK
Q9Y221|NIP7_HUMAN	787.931	65.69	2.30E-05	LHVTALDYLAPYAK
Q9Y221|NIP7_HUMAN	787.9299	67.98	1.40E-05	LHVTALDYLAPYAK
Q9Y221|NIP7_HUMAN	787.931	72.69	4.60E-06	LHVTALDYLAPYAK
Q9Y221|NIP7_HUMAN	787.9308	73.23	4.00E-06	LHVTALDYLAPYAK
Q9Y221|NIP7_HUMAN	787.9314	75.36	2.30E-06	LHVTALDYLAPYAK
Q9Y2W1|TR150_HUMAN	765.3917	42	0.0028	SIFQHIQSAQSQR
Q9Y2W1|TR150_HUMAN	560.7836	41.11	0.002	YKDDPVDLR
Q9Y2W1|TR150_HUMAN	1027.97	45.42	0.00033	ASESSKPWPDATYGTGSASR
Q9Y2W1|TR150_HUMAN	811.8774	46.26	0.00028	KTEELEEESFPER
Q9Y2W1|TR150_HUMAN	765.3926	53.37	0.00022	SIFQHIQSAQSQR
Q9Y2W1|TR150_HUMAN	765.3925	54.09	0.00018	SIFQHIQSAQSQR
Q9Y2W1|TR150_HUMAN	765.3922	54.64	0.00015	SIFQHIQSAQSQR
Q9Y2W1|TR150_HUMAN	1027.97	52.6	6.30E-05	ASESSKPWPDATYGTGSASR
Q9Y2W1|TR150_HUMAN	765.3917	59.34	5.10E-05	SIFQHIQSAQSQR
Q9Y2W1|TR150_HUMAN	765.3938	60.43	4.30E-05	SIFQHIQSAQSQR
Q9Y2W1|TR150_HUMAN	811.8815	56.57	3.70E-05	KTEELEEESFPER
Q9Y2W1|TR150_HUMAN	811.8807	57.52	2.40E-05	KTEELEEESFPER
Q9Y2W1|TR150_HUMAN	765.3925	63.44	2.10E-05	SIFQHIQSAQSQR
Q9Y2W1|TR150_HUMAN	811.8791	68.28	2.10E-06	KTEELEEESFPER
Q9Y2W1|TR150_HUMAN	811.8803	72.4	7.40E-07	KTEELEEESFPER

Q9Y3B4|SF3B6_HUMAN	708.8399	76.46	3.20E-07	ITAEEMYDIFGK
Q9Y3Y2|CHTOP_HUMAN	723.8596	51.57	0.00025	ASMQQQQQLASAR
Q9Y3Y2|CHTOP_HUMAN	723.8612	54.02	0.00014	ASMQQQQQLASAR
Q9Y5S9|RBM8A_HUMAN	1111.967	34.21	0.00072	MREDYDSVEQDGDEPGPQR
Q9Y5S9|RBM8A_HUMAN	1111.963	32.87	0.00062	MREDYDSVEQDGDEPGPQR
Q9Y5S9|RBM8A_HUMAN	1111.964	39.71	0.00016	MREDYDSVEQDGDEPGPQR
Q9Y5S9|RBM8A_HUMAN	1111.967	44.97	6.00E-05	MREDYDSVEQDGDEPGPQR
Q9Y5S9|RBM8A_HUMAN	1111.963	44.69	4.40E-05	MREDYDSVEQDGDEPGPQR
Q9Y5S9|RBM8A_HUMAN	1111.963	44.83	3.90E-05	MREDYDSVEQDGDEPGPQR
Q9Y5S9|RBM8A_HUMAN	1111.964	46.78	3.00E-05	MREDYDSVEQDGDEPGPQR
Q9Y5S9|RBM8A_HUMAN	1111.967	49.38	2.20E-05	MREDYDSVEQDGDEPGPQR
Q9Y5S9|RBM8A_HUMAN	1111.97	55.33	6.60E-06	MREDYDSVEQDGDEPGPQR
Q9Y5S9|RBM8A_HUMAN	1111.969	58.07	3.40E-06	MREDYDSVEQDGDEPGPQR
Q9Y5S9|RBM8A_HUMAN	1111.968	62.52	1.10E-06	MREDYDSVEQDGDEPGPQR
Q9Y5S9|RBM8A_HUMAN	1111.962	66.15	2.70E-07	MREDYDSVEQDGDE PGPQR

Appendix Table 4. List of peptides identified by MS following streptavidin pull-down.

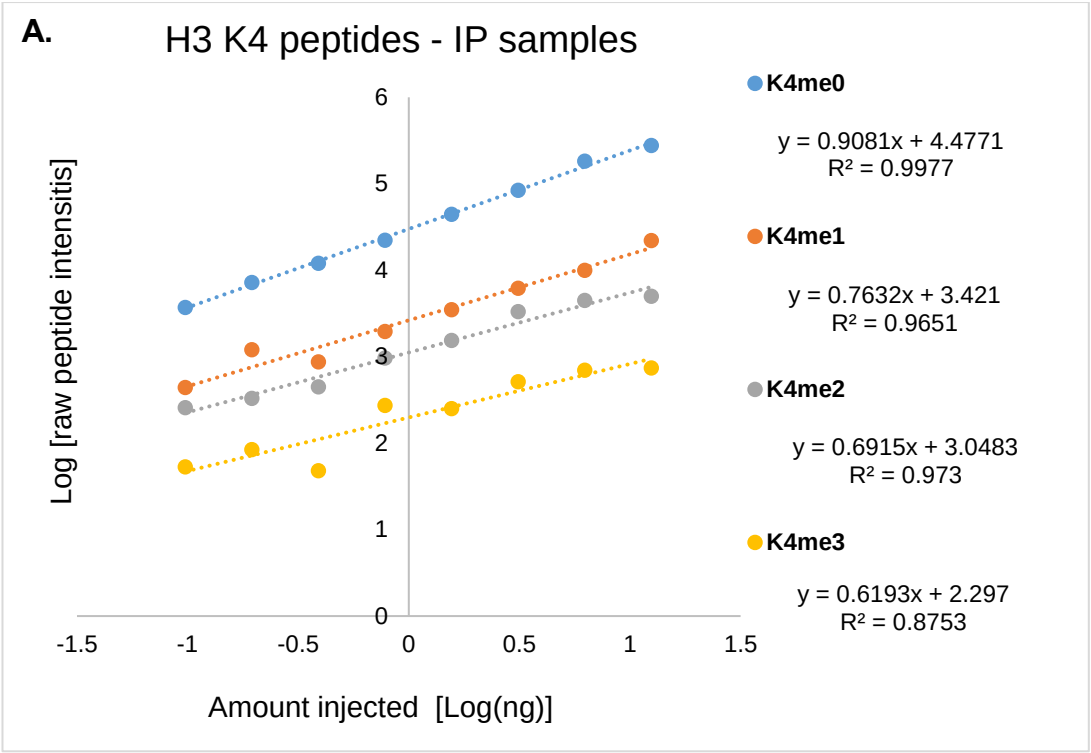
A.
H3 K4 peptides - IP samples
Log [raw peptide intensitis]
Amount injected [Log(ng)]
K4me0
y = 0.9081x + 4.4771
R² = 0.9977
K4me1
y = 0.7632x + 3.421
R² = 0.9651
K4me2
y = 0.6915x + 3.0483
R² = 0.973
K4me3
y = 0.6193x + 2.297
R² = 0.8753

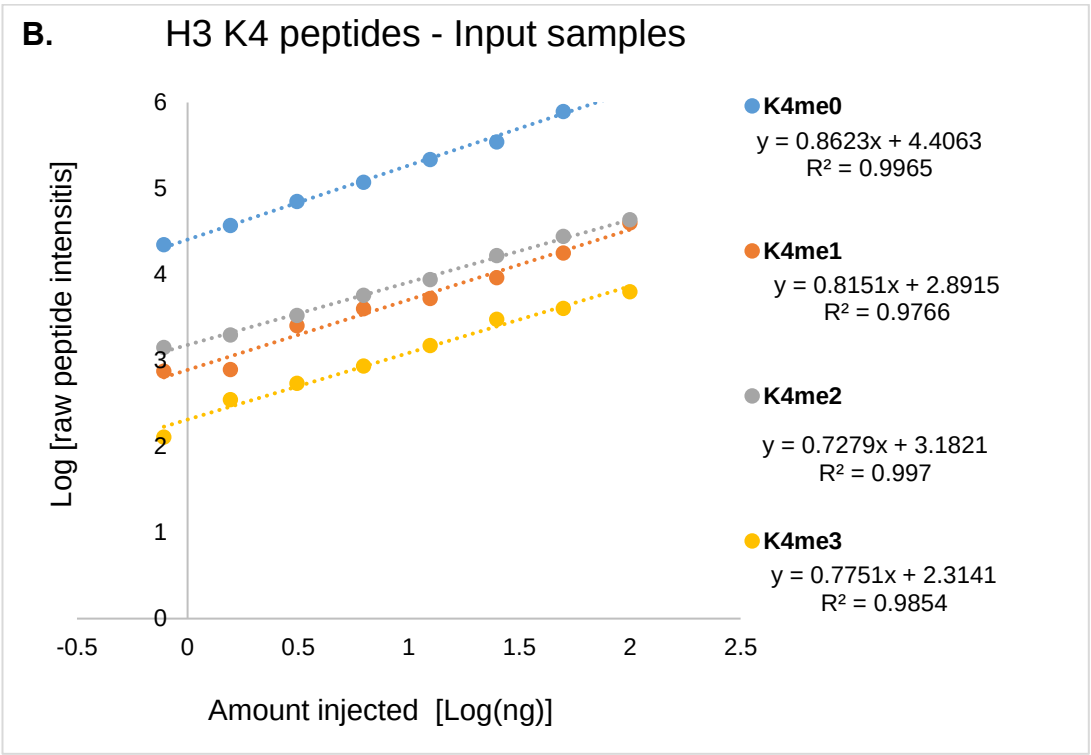
B.
H3 K4 peptides - Input samples
Log [raw peptide intensitis]
Amount injected [Log(ng)]
K4me0
y = 0.8623x + 4.4063
R² = 0.9965
K4me1
y = 0.8151x + 2.8915
R² = 0.9766
K4me2
y = 0.7279x + 3.1821
R² = 0.997
K4me3
y = 0.7751x + 2.3141
R² = 0.9854

C.

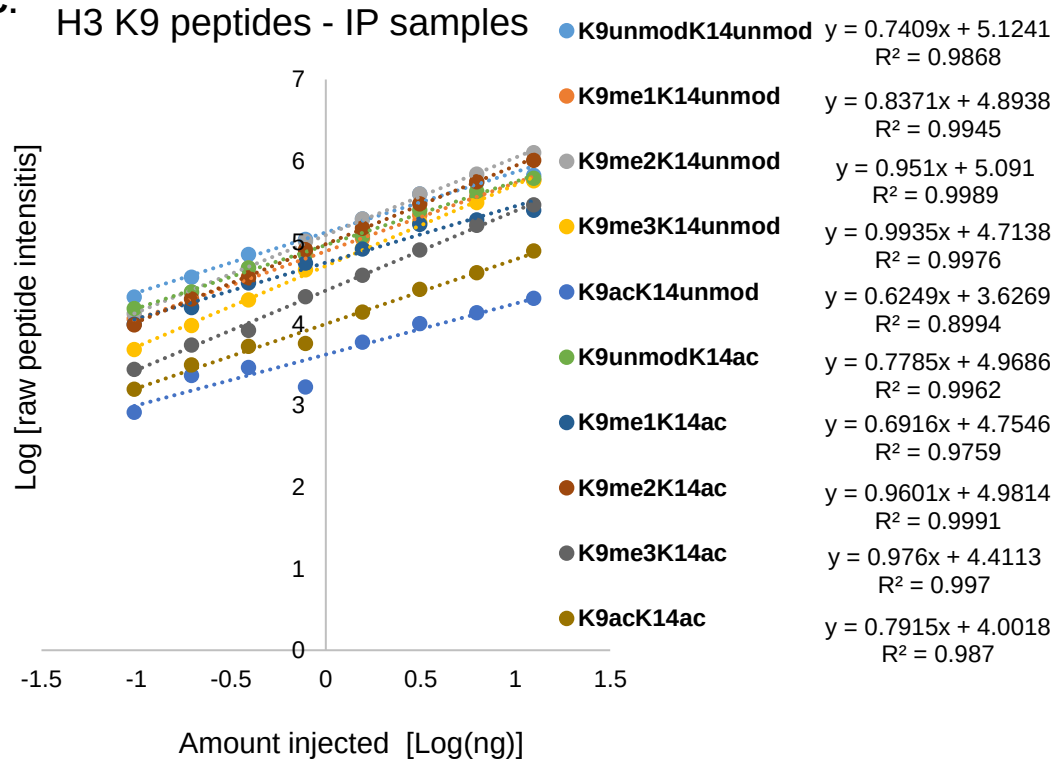
H3 K9 peptides - IP samples
Log [raw peptide intensitis]
Amount injected [Log(ng)]
K9unmodK14unmod y = 0.7409x + 5.1241 R² = 0.9868
K9me1K14unmod y = 0.8371x + 4.8938 R² = 0.9945
K9me2K14unmod y = 0.951x + 5.091 R² = 0.9989
K9me3K14unmod y = 0.9935x + 4.7138 R² = 0.9976
K9acK14unmod y = 0.6249x + 3.6269 R² = 0.8994
K9unmodK14ac y = 0.7785x + 4.9686 R² = 0.9962
K9me1K14ac y = 0.6916x + 4.7546 R² = 0.9759
K9me2K14ac y = 0.9601x + 4.9814 R² = 0.9991
K9me3K14ac y = 0.976x + 4.4113 R² = 0.997
K9acK14ac y = 0.7915x + 4.0018 R² = 0.987

D.

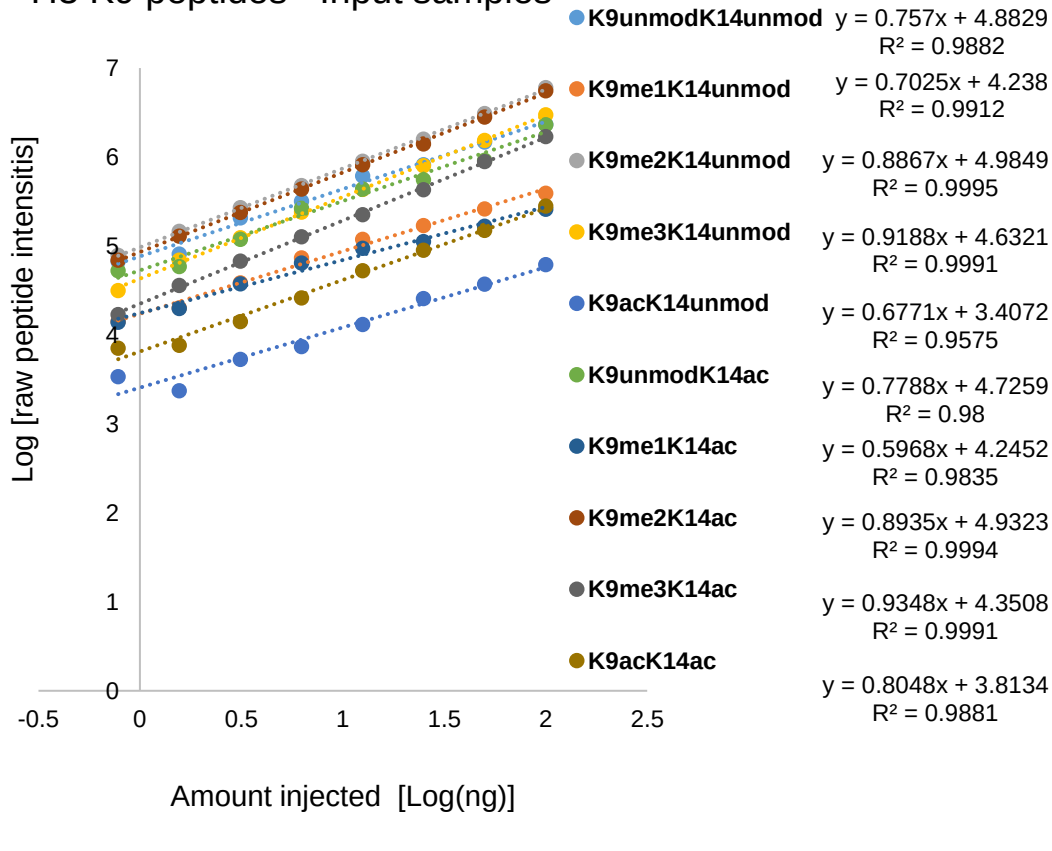
H3 K9 peptides - Input samples
Log [raw peptide intensitis]
Amount injected [Log(ng)]
K9unmodK14unmod y = 0.757x + 4.8829 R² = 0.9882
K9me1K14unmod y = 0.7025x + 4.238 R² = 0.9912
K9me2K14unmod y = 0.8867x + 4.9849 R² = 0.9995
K9me3K14unmod y = 0.9188x + 4.6321 R² = 0.9991
K9acK14unmod y = 0.6771x + 3.4072 R² = 0.9575
K9unmodK14ac y = 0.7788x + 4.7259 R² = 0.98
K9me1K14ac y = 0.5968x + 4.2452 R² = 0.9835
K9me2K14ac y = 0.8935x + 4.9323 R² = 0.9994
K9me3K14ac y = 0.9348x + 4.3508 R² = 0.9991
K9acK14ac y = 0.8048x + 3.8134 R² = 0.9881

E. H3 K27unmodK36 peptides - IP samples

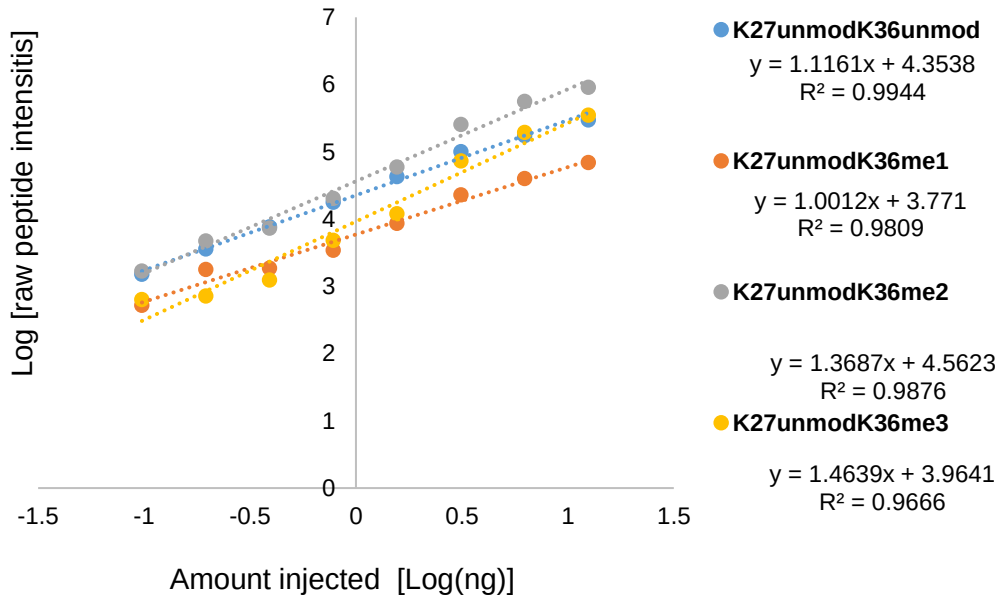

F. H3 K27unmodK36 peptides - Input samples

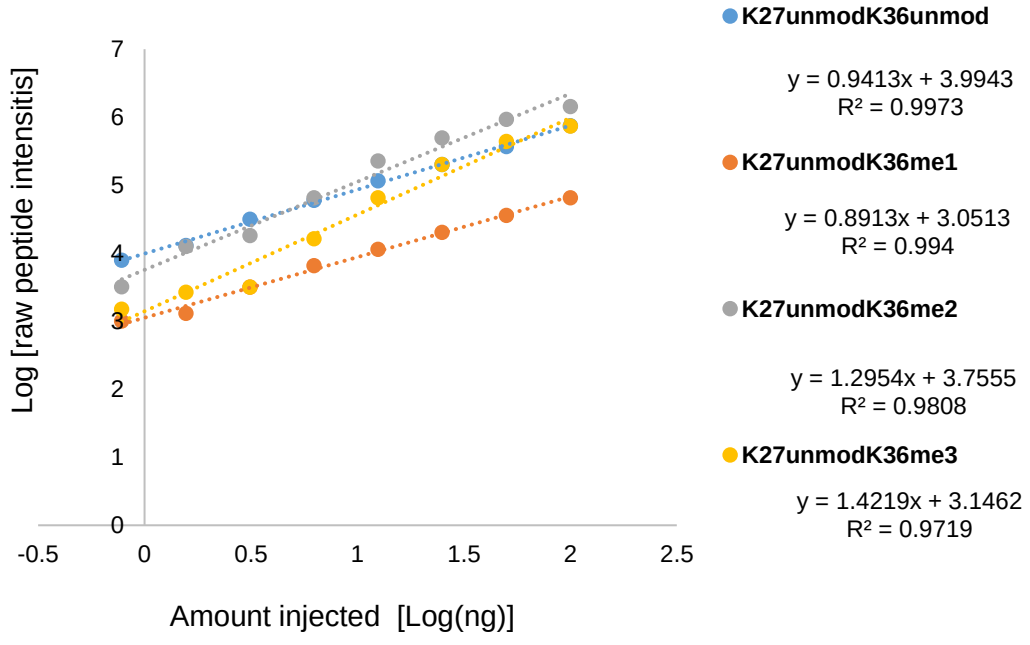

G H3 K27me1K36 peptides - IP samples

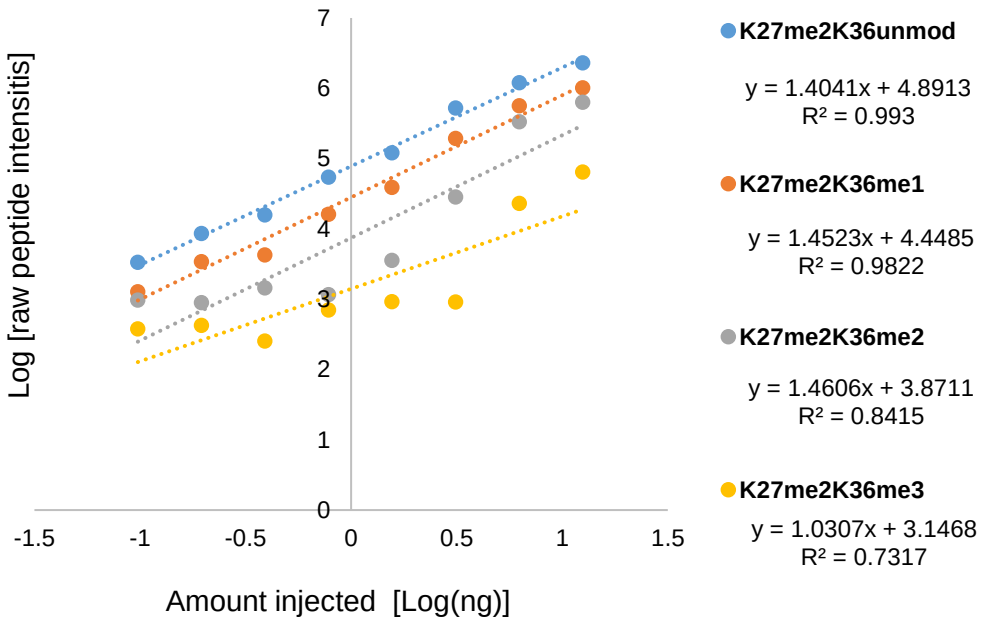

H. H3 K27me1K36 peptides - Input samples

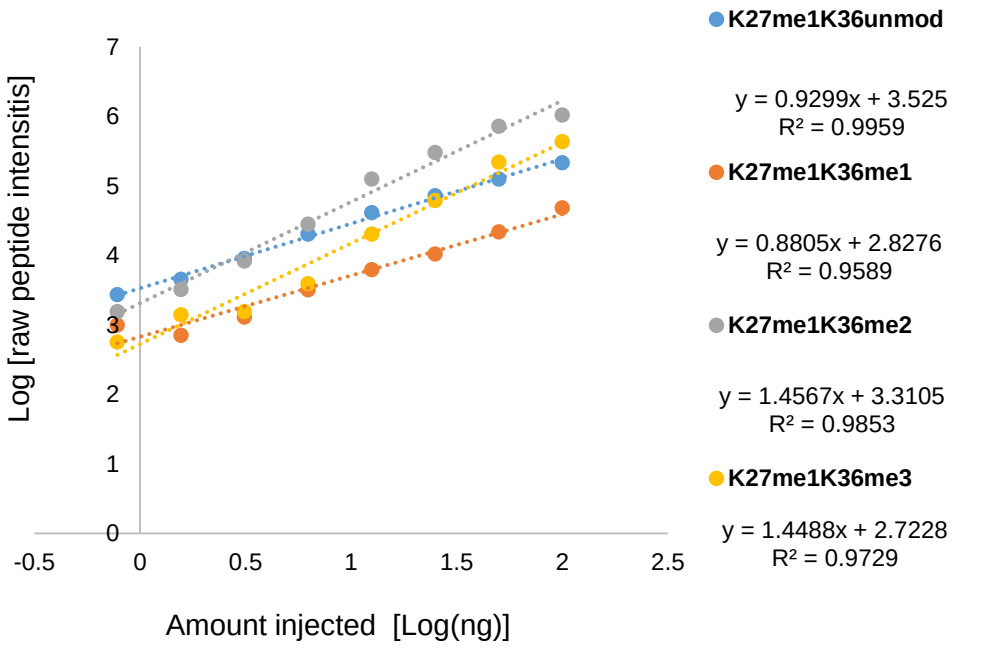

I.

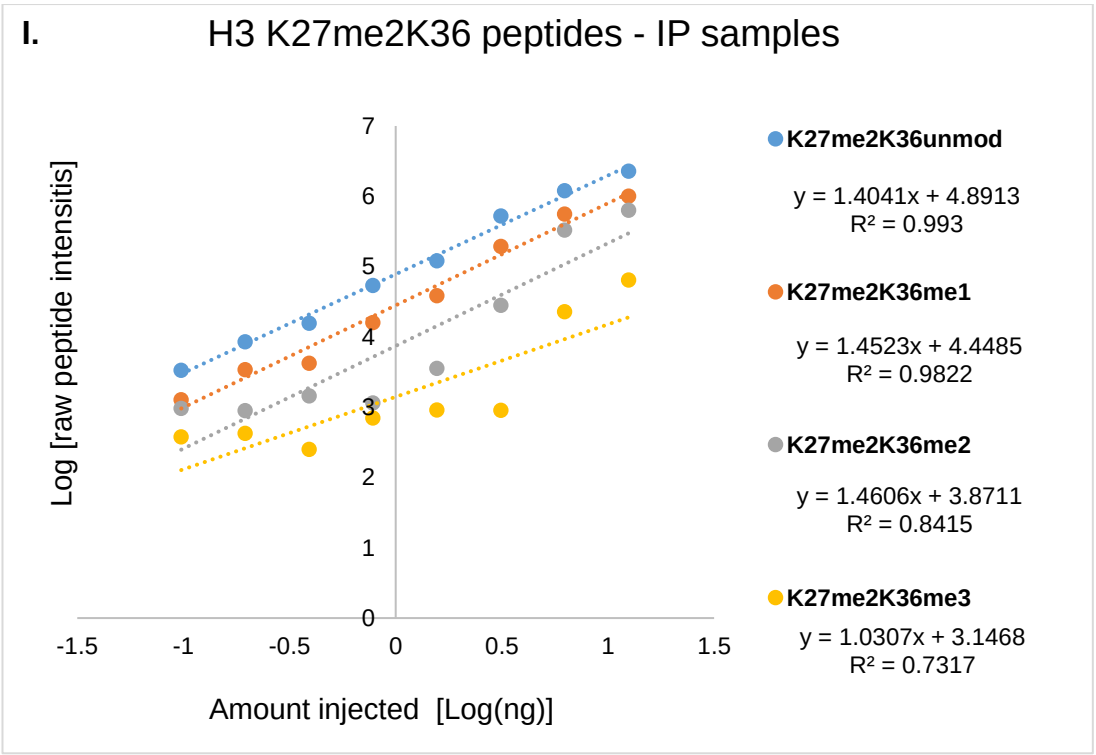
H3 K27me2K36 peptides - IP samples
Log [raw peptide intensitis]
Amount injected [Log(ng)]
K27me2K36unmod
y = 1.4041x + 4.8913
R² = 0.993
K27me2K36me1
y = 1.4523x + 4.4485
R² = 0.9822
K27me2K36me2
y = 1.4606x + 3.8711
R² = 0.8415
K27me2K36me3
y = 1.0307x + 3.1468
R² = 0.7317

J.

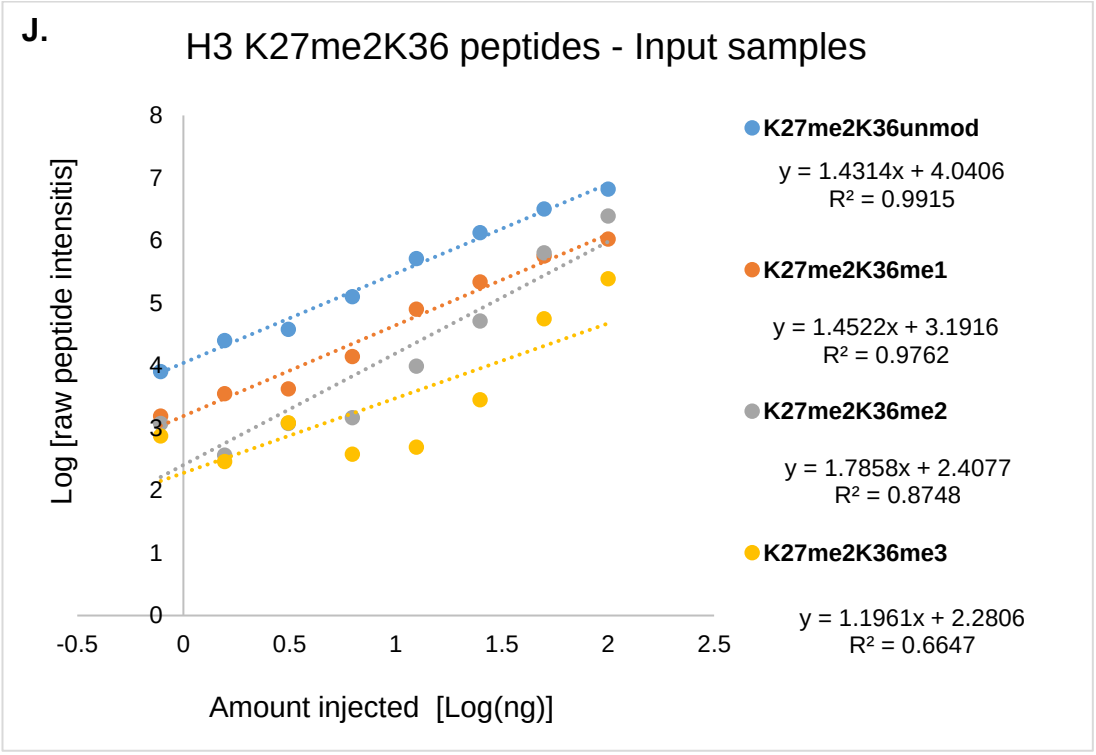
H3 K27me2K36 peptides - Input samples
Log [raw peptide intensitis]
Amount injected [Log(ng)]
K27me2K36unmod
y = 1.4314x + 4.0406
R² = 0.9915
K27me2K36me1
y = 1.4522x + 3.1916
R² = 0.9762
K27me2K36me2
y = 1.7858x + 2.4077
R² = 0.8748
K27me2K36me3
y = 1.1961x + 2.2806
R² = 0.6647

K.

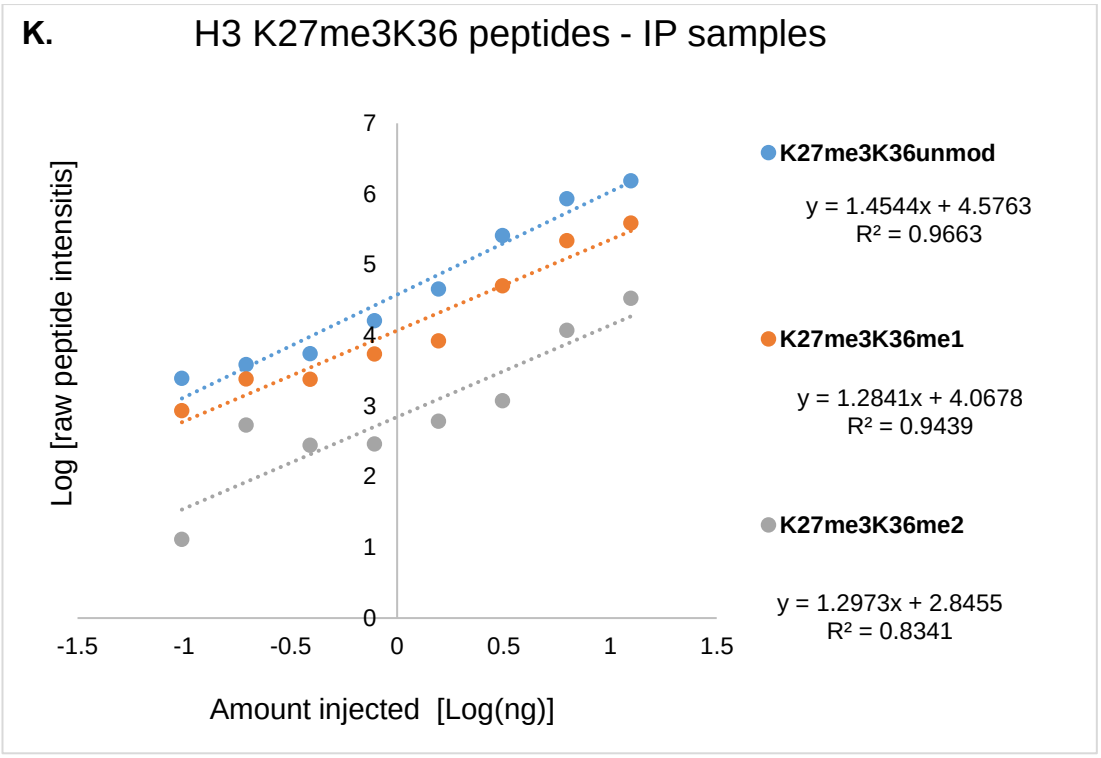
H3 K27me3K36 peptides - IP samples
Log [raw peptide intensitis]
Amount injected [Log(ng)]
K27me3K36unmod
y = 1.4544x + 4.5763
R² = 0.9663
K27me3K36me1
y = 1.2841x + 4.0678
R² = 0.9439
K27me3K36me2
y = 1.2973x + 2.8455
R² = 0.8341

L.

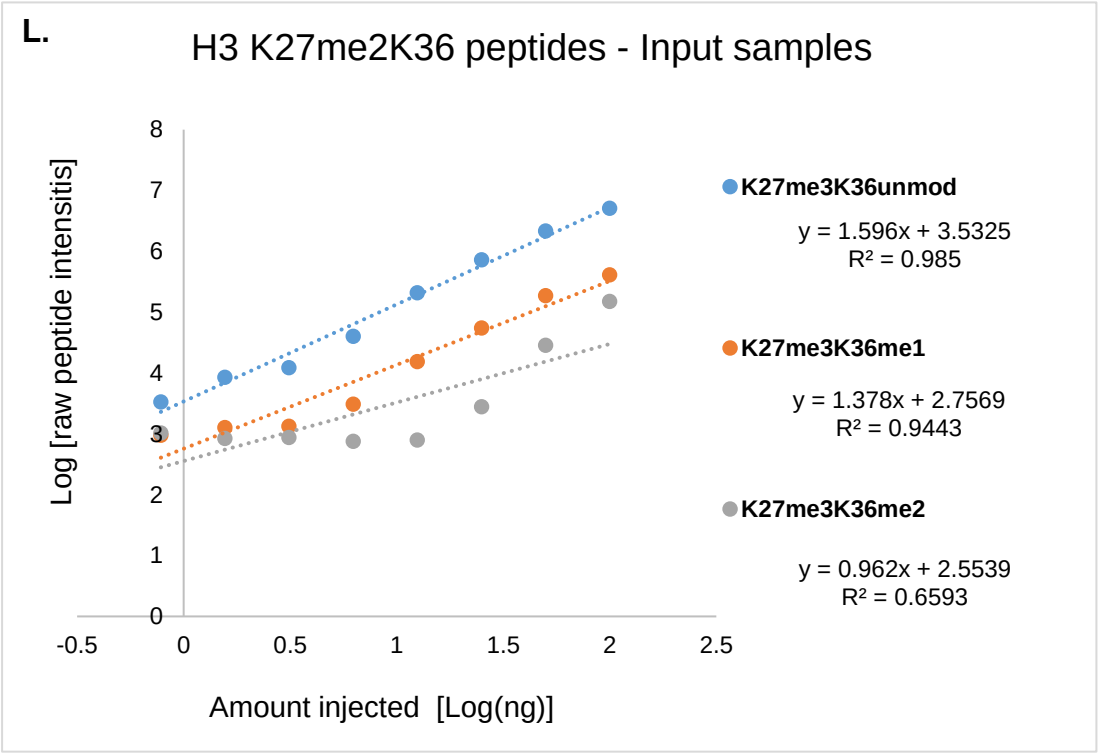
H3 K27me2K36 peptides - Input samples
Log [raw peptide intensitis]
Amount injected [Log(ng)]
K27me3K36unmod
y = 1.596x + 3.5325
R² = 0.985
K27me3K36me1
y = 1.378x + 2.7569
R² = 0.9443
K27me3K36me2
y = 0.962x + 2.5539
R² = 0.6593

M

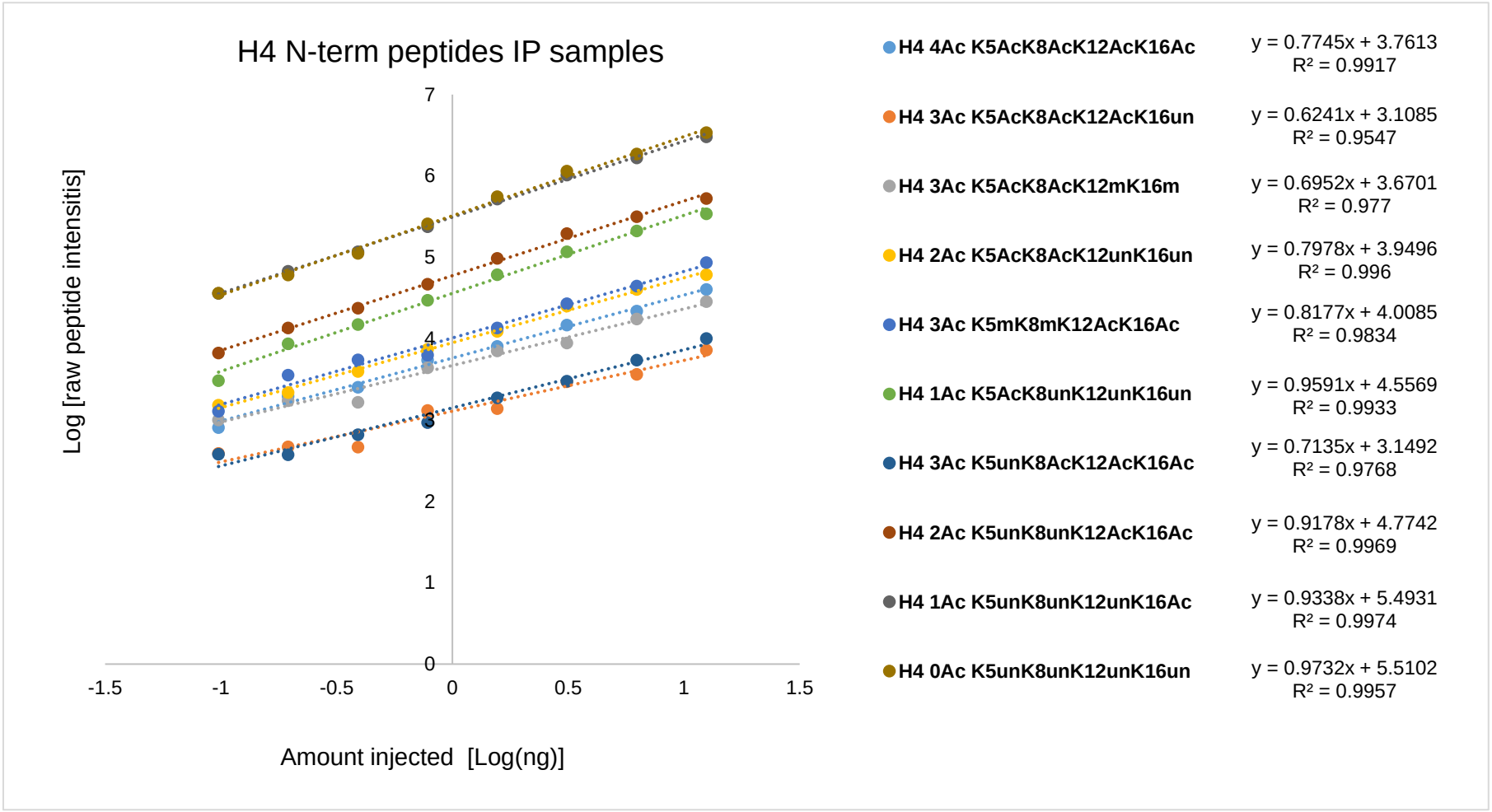
H4 N-term peptides IP samples
Log [raw peptide intensitis]
Amount injected [Log(ng)]
7
6
5
4
3
2
1
0
-1.5
-1
-0.5
0
0.5
1
1.5
H4 4Ac K5AcK8AcK12AcK16Ac
y = 0.7745x + 3.7613
R² = 0.9917
H4 3Ac K5AcK8AcK12AcK16un
y = 0.6241x + 3.1085
R² = 0.9547
H4 3Ac K5AcK8AcK12mK16m
y = 0.6952x + 3.6701
R² = 0.977
H4 2Ac K5AcK8AcK12unK16un
y = 0.7978x + 3.9496
R² = 0.996
H4 3Ac K5mK8mK12AcK16Ac
y = 0.8177x + 4.0085
R² = 0.9834
H4 1Ac K5AcK8unK12unK16un
y = 0.9591x + 4.5569
R² = 0.9933
H4 3Ac K5unK8AcK12AcK16Ac
y = 0.7135x + 3.1492
R² = 0.9768
H4 2Ac K5unK8unK12AcK16Ac
y = 0.9178x + 4.7742
R² = 0.9969
H4 1Ac K5unK8unK12unK16Ac
y = 0.9338x + 5.4931
R² = 0.9974
H4 0Ac K5unK8unK12unK16un
y = 0.9732x + 5.5102
R² = 0.9957

N.

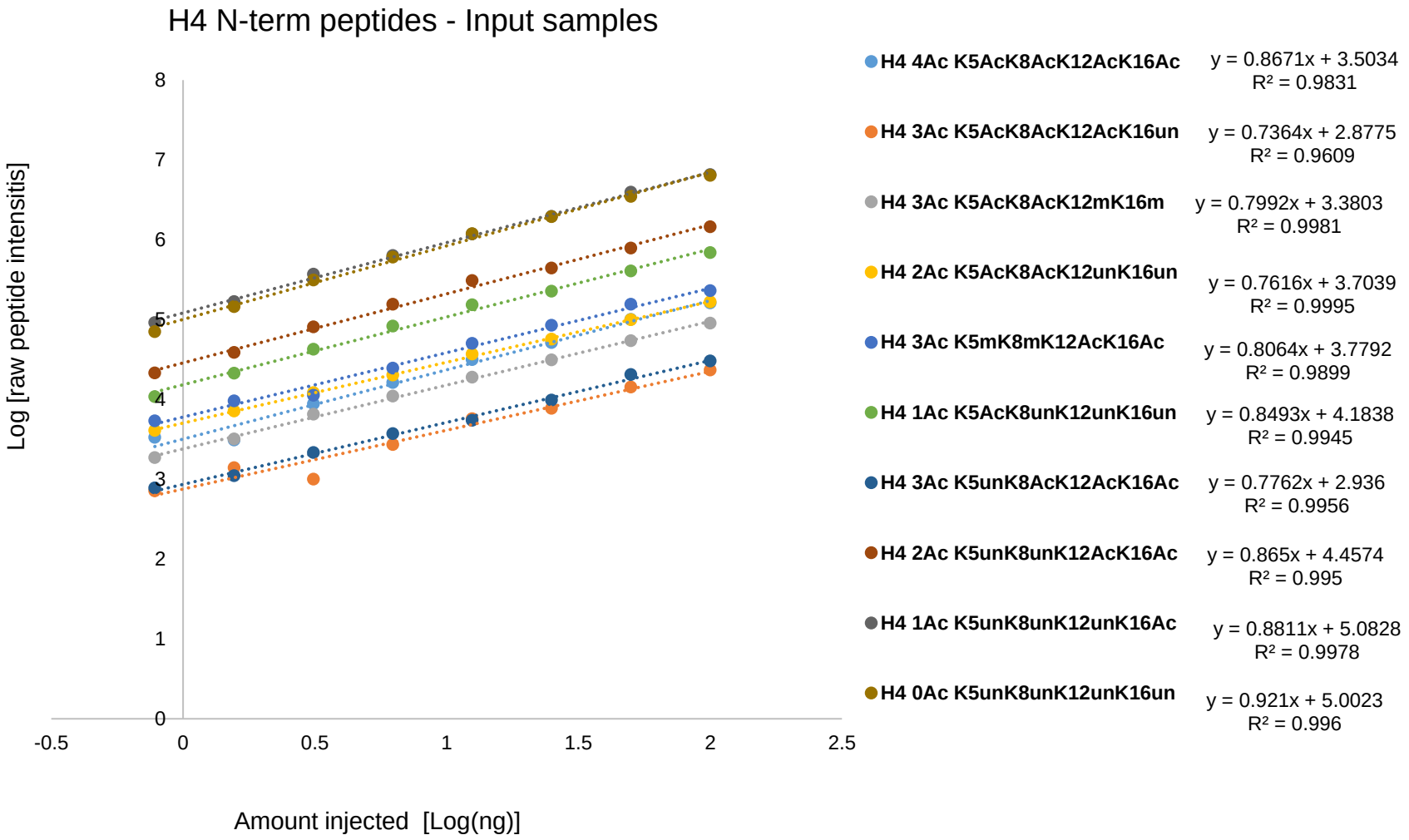
H4 N-term peptides - Input samples
Log [raw peptide intensitis]
Amount injected [Log(ng)]
-0.5
0
0.5
1
1.5
2
2.5
0
1
2
3
4
5
6
7
8
H4 4Ac K5AcK8AcK12AcK16Ac
y = 0.8671x + 3.5034
R² = 0.9831
H4 3Ac K5AcK8AcK12AcK16un
y = 0.7364x + 2.8775
R² = 0.9609
H4 3Ac K5AcK8AcK12mK16m
y = 0.7992x + 3.3803
R² = 0.9981
H4 2Ac K5AcK8AcK12unK16un
y = 0.7616x + 3.7039
R² = 0.9995
H4 3Ac K5mK8mK12AcK16Ac
y = 0.8064x + 3.7792
R² = 0.9899
H4 1Ac K5AcK8unK12unK16un
y = 0.8493x + 4.1838
R² = 0.9945
H4 3Ac K5unK8AcK12AcK16Ac
y = 0.7762x + 2.936
R² = 0.9956
H4 2Ac K5unK8unK12AcK16Ac
y = 0.865x + 4.4574
R² = 0.995
H4 1Ac K5unK8unK12unK16Ac
y = 0.8811x + 5.0828
R² = 0.9978
H4 0Ac K5unK8unK12unK16un
y = 0.921x + 5.0023
R² = 0.996

O.

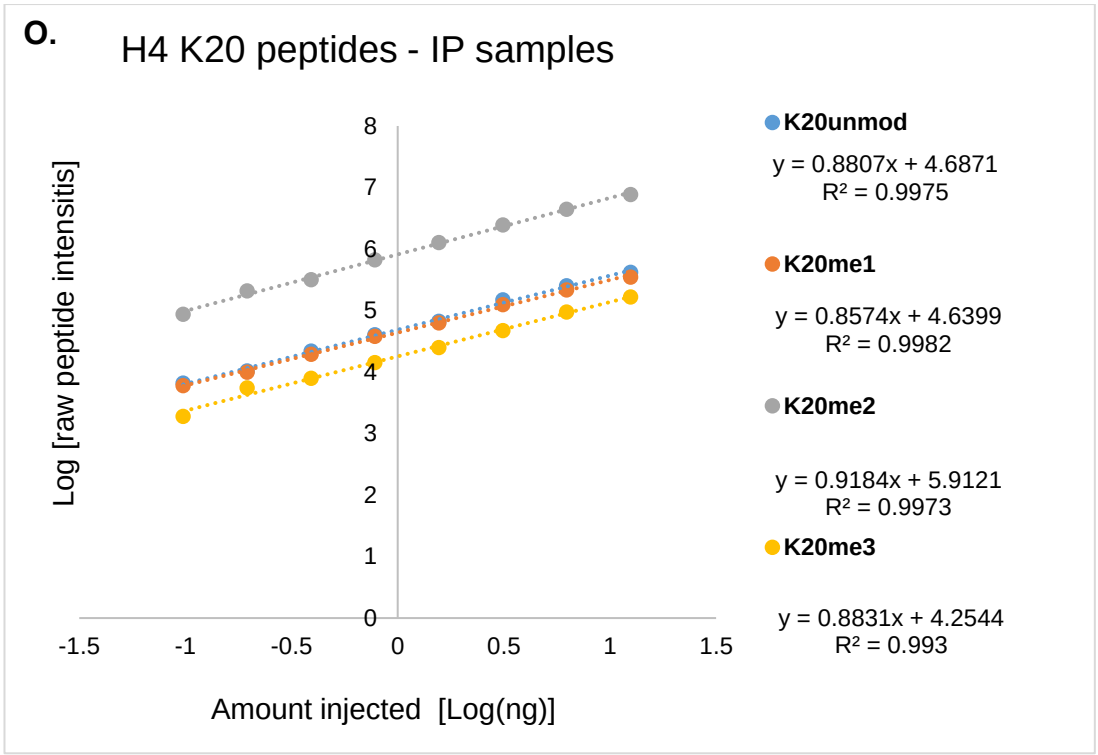
H4 K20 peptides - IP samples
Log [raw peptide intensitis]
Amount injected [Log(ng)]
K20unmod
y = 0.8807x + 4.6871
R² = 0.9975
K20me1
y = 0.8574x + 4.6399
R² = 0.9982
K20me2
y = 0.9184x + 5.9121
R² = 0.9973
K20me3
y = 0.8831x + 4.2544
R² = 0.993

P.

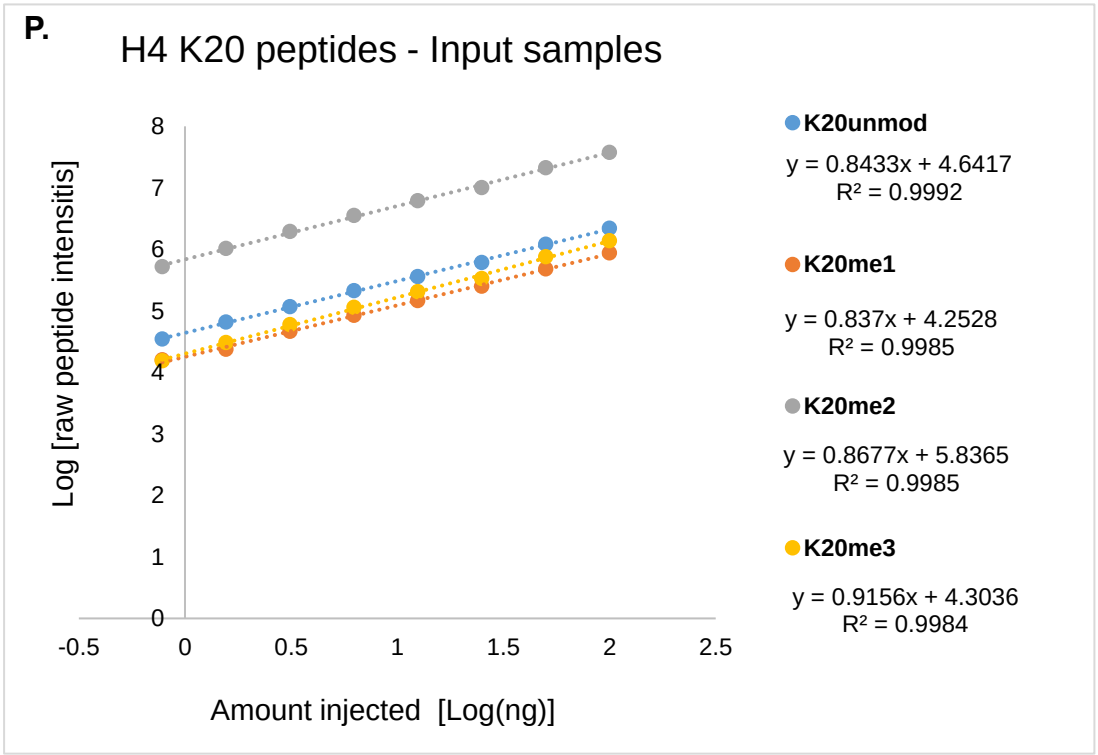
H4 K20 peptides - Input samples
Log [raw peptide intensitis]
Amount injected [Log(ng)]
K20unmod
y = 0.8433x + 4.6417
R² = 0.9992
K20me1
y = 0.837x + 4.2528
R² = 0.9985
K20me2
y = 0.8677x + 5.8365
R² = 0.9985
K20me3
y = 0.9156x + 4.3036
R² = 0.9984

Q.

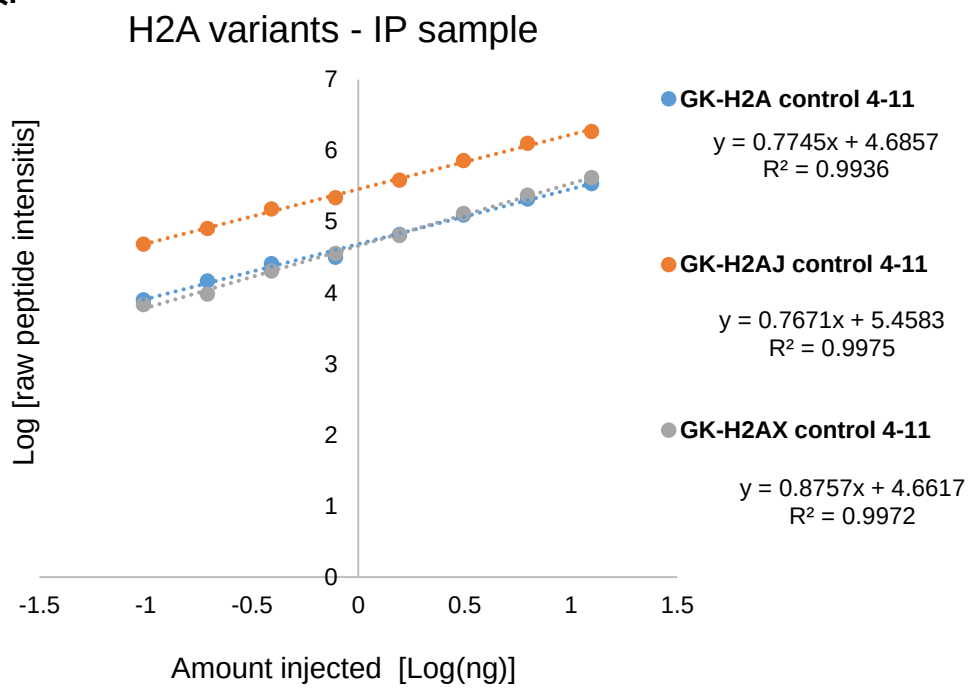
H2A variants - IP sample
Log [raw peptide intensitis]
Amount injected [Log(ng)]
GK-H2A control 4-11
y = 0.7745x + 4.6857
R² = 0.9936
GK-H2AJ control 4-11
y = 0.7671x + 5.4583
R² = 0.9975
GK-H2AX control 4-11
y = 0.8757x + 4.6617
R² = 0.9972

R.

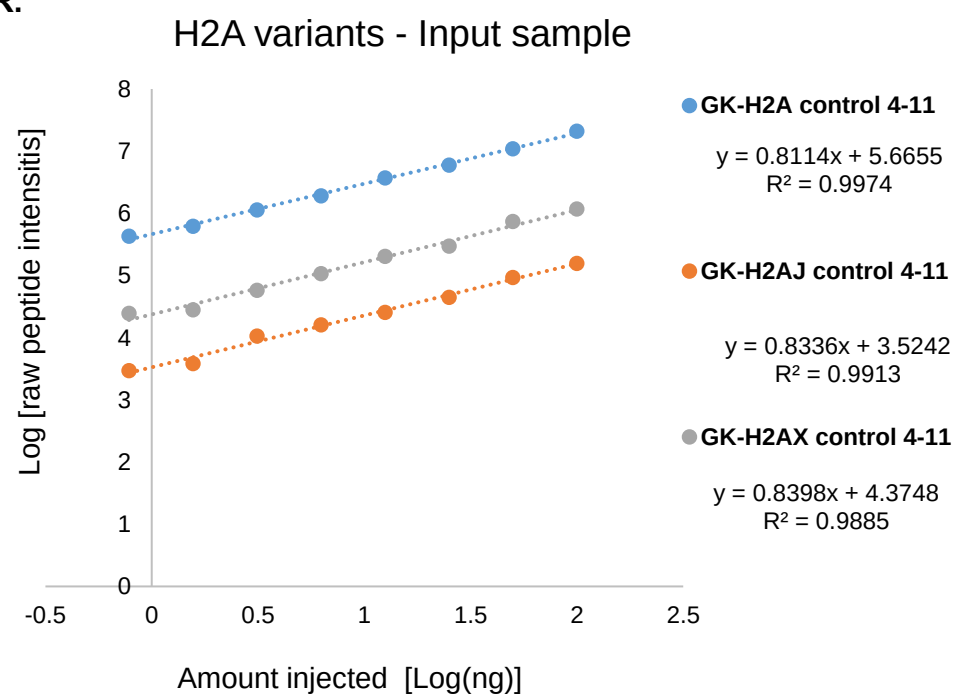
H2A variants - Input sample
Log [raw peptide intensitis]
Amount injected [Log(ng)]
GK-H2A control 4-11
y = 0.8114x + 5.6655
R² = 0.9974
GK-H2AJ control 4-11
y = 0.8336x + 3.5242
R² = 0.9913
GK-H2AX control 4-11
y = 0.8398x + 4.3748
R² = 0.9885

Appendix Figure 1. Peptide response curve. The input samples linearly increasing from 0.8 – 100 ng and B) IP samples linearly increasing from 0.1 – 12.5 % of IP samples were injected into chromatography column and analysed by mass spectrometry. The raw intensities for each peptide were plotted on the double-Log scale. R^2 and slope of the linear trendline for each peptide was displayed on the graph**.**

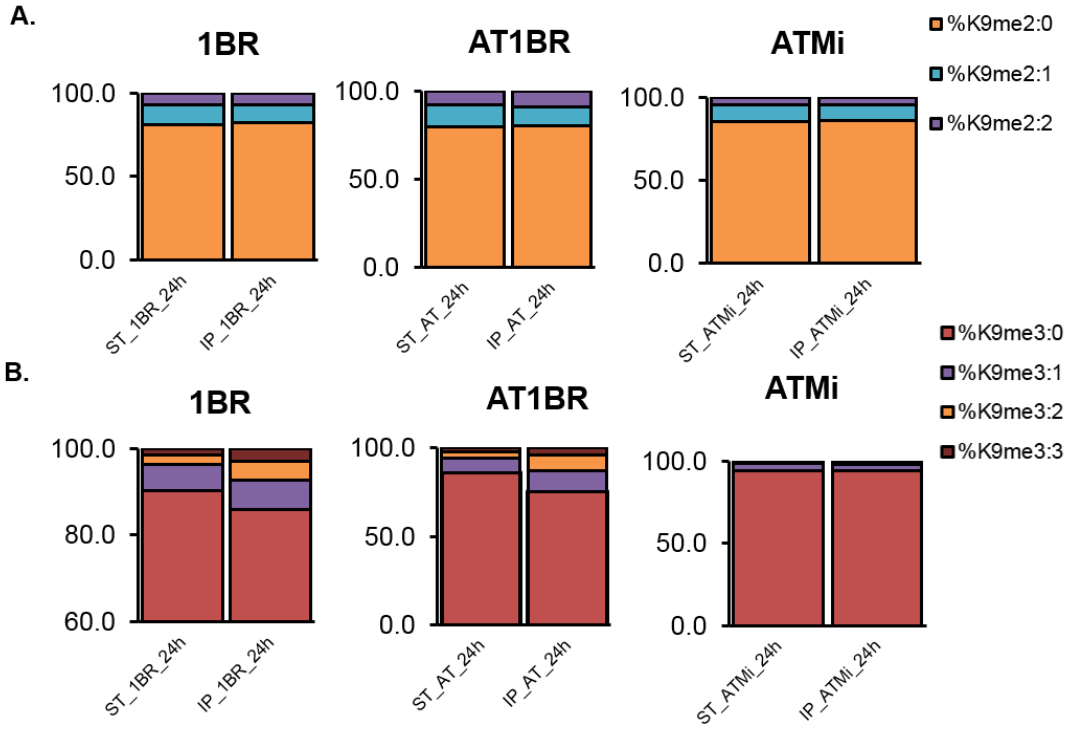

Appendix Figure 2. Heavy methyl SILAC labelling shows no significant difference in the turnover of H3K9me2/3 marks at the site of DSBs compared to global turnover. A) Turnover of H3K9me2 and B) H3K9me3 globally (ST) and on γH2AX-containing nucleosomes (IP) 24 h after 10 Gy of IR in 1BR, AT1BR and ATM-inhibited (ATMi) fibroblast. ST = starting material or input, IP = γH2AX IP.

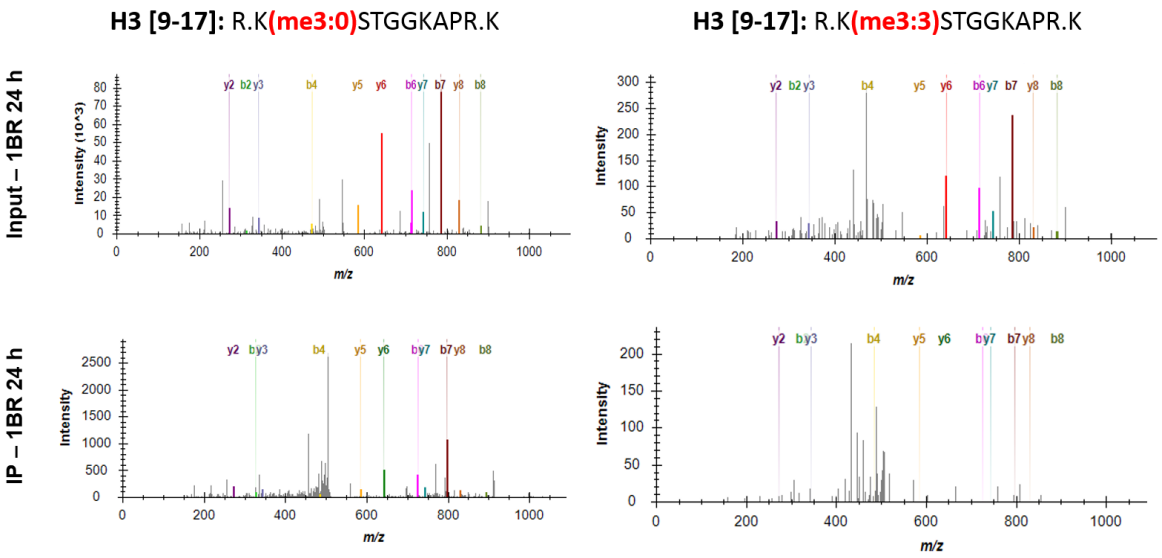

Appendix Figure 3. Analysis of histone H3K9me3 methylation labelled with heavy methionine. Example of extracted ion spectrum showing matched fragment ions of H3K9me3-peptide containing three light methyl (me3:0) or three heavy methyl (me3:3) groups.

nature COMMUNICATIONS

ARTICLE

Received 3 Oct 2015 | Accepted 4 Mar 2016 | Published 11 Apr 2016

DOI: 10.1038/ncomms11242 OPEN

The Ku-binding motif is a conserved module for recruitment and stimulation of non-homologous end-joining proteins

Gabrielle J. Grundy[1,*], Stuart L. Rulten[1,*], Raquel Arribas-Bosacoma[1,2], Kathryn Davidson[1], Zuzanna Kozik[1], Antony W. Oliver[1,2], Laurence H. Pearl[1,2] & Keith W. Caldecott[1]

The Ku-binding motif (KBM) is a short peptide module first identified in APLF that we now show is also present in Werner syndrome protein (WRN) and in Modulator of retrovirus infection homologue (MRI). We also identify a related but functionally distinct motif in XLF, WRN, MRI and PAXX, which we denote the XLF-like motif. We show that WRN possesses two KBMs; one at the N terminus next to the exonuclease domain and one at the C terminus next to an XLF-like motif. We reveal that the WRN C-terminal KBM and XLF-like motif function cooperatively to bind Ku complexes and that the N-terminal KBM mediates Ku-dependent stimulation of WRN exonuclease activity. We also show that WRN accelerates DSB repair by a mechanism requiring both KBMs, demonstrating the importance of WRN interaction with Ku. These data define a conserved family of KBMs that function as molecular tethers to recruit and/or stimulate enzymes during NHEJ.

[1] Genome Damage and Stability Centre, School of Life Sciences, University of Sussex, Brighton BN1 9RQ, UK. [2] Cancer Research UK DNA Repair Enzymes Group, Genome Damage and Stability Centre, School of Life Sciences, University of Sussex, Brighton BN1 9RQ, UK. * These authors contributed equally to this work. Correspondence and requests for materials should be addressed to K.W.C. (email: k.w.caldecott@sussex.ac.uk).

DNA double-strand breaks (DSBs) arise as a consequence of both endogenous and exogenous DNA damage and during normal cellular processes such as the generation of antibody diversity[1,2]. DSB repair pathways exist to ensure that chromosomal integrity is maintained but mis-regulation or inappropriate engagement of such pathways can lead to potentially oncogenic translocations, mutagenesis or cell death[3]. Moreover, loss or mutation of non-homologous end joining (NHEJ) factors in mice or humans can result in a range of phenotypes including immunodeficiency, cancer predisposition, neurological defects and embryonic lethality[4,5]. Mammalian cells possess two major types of DSB repair pathway; homologous recombination and NHEJ[6]. Homologous recombination employs sister chromatids as a template for accurate repair during S/G_2 phase of the cell cycle, whereas NHEJ ligates DSB termini directly and can occur throughout the cell cycle.

The core protein factors involved in NHEJ are DNA protein kinase (DNA–PK), XRCC4-like factor (XLF) and XRCC4/DNA ligase IV[7–9]. While these core factors are sufficient to repair DSBs with ligatable termini the repair of most physiologically relevant DSBs require additional protein factors to process the DSB termini before ligation, including nucleases, DNA polymerases and polynucleotide kinase/phosphatase. An increasing number of accessory protein factors have been implicated in NHEJ, many of which appear to interact with DNA–PK[10]. DNA–PK is comprised of a protein kinase catalytic subunit (DNA–PKcs) and Ku heterodimer; the latter being composed of Ku70 and Ku80. Recently, we and others identified a novel Ku-binding peptide motif (now denoted the KBM) of 10–15 amino acids in the accessory protein Aprataxin-and-polynucleotide kinase/phosphatase-like Factor (APLF), which we showed interacts directly with a hydrophobic pocket in the vWA domain of Ku80 (refs 11,12). Here we have identified and characterized analogous KBMs in two additional NHEJ proteins, revealing this motif to be an evolutionary conserved Ku-binding module. In particular, we identify two KBMs in the exonuclease/helicase mutated in Werner syndrome (WRN) and show that these motifs are employed by WRN to accelerate chromosomal DSB repair, defining the functional importance of these motifs *in vitro* and in cells.

Results

A conserved KBM. The interaction between APLF and Ku80 was previously mapped to a conserved motif in APLF of 10–15 amino acids, denoted the KBM[11,12]. PSI-BLAST[13] analysis using this sequence, and subsequent additional searching by eye, suggested that similar KBMs are present at the N terminus and C terminus of WRN protein; the DNA helicase and exonuclease mutated in Werner syndrome and an established partner of Ku (Fig. 1a)[14,15]. We also identified a putative KBM in Modulator of retroviral infection homologue (MRI, C7orf49); a poorly characterized protein that we recovered in a yeast two-hybrid screen using the Ku80 vWA-like domain as bait (Fig. 1a). MRI was reported previously to interact with Ku and to stimulate NHEJ, *in vitro*[16]. Similar to the KBM in APLF[11], the putative KBMs in WRN and MRI are conserved among vertebrate species (Supplementary Fig. 1). Our analyses also revealed a distinct but related motif at the C terminus of XLF, Paralog of XRCC4 and XLF (PAXX), WRN and MRI, which we denoted the XLF-like motif (Fig. 1a, right). Interestingly, the XLF-like motif in WRN is present in tandem with the putative C-terminal KBM, raising the possibility that these motifs function cooperatively.

APLF-like KBMs bind Ku by a common mechanism. To examine Ku binding by the putative KBMs and XLF-like motifs, we employed recombinant Ku heterodimer and fluorescent peptides spanning these domains in fluorescence polarization assays. We employed recombinant Ku70/Ku80ΔC heterodimer (denoted KuΔC) lacking the flexible Ku80 C-terminal helical domain for these experiments, since KuΔC exhibits greater structural homogeneity than does full-length Ku heterodimer[11,17–19]. Similar to the KBM in APLF, which binds Ku with an affinity of ~0.6 μM (ref. 11), peptides spanning the APLF-like KBMs from WRN or MRI bound KuΔC with K_d values of 0.5–1.7 μM (Fig. 1b, top panels). Mutation of the conserved tryptophan in the APLF-like KBMs greatly reduced or ablated KuΔC interaction, suggesting that these motifs share a common mechanism of Ku80 binding (Fig. 1b, top panels). Indeed, a peptide encoding the APLF KBM competed efficiently in KuΔC binding assays with peptides encoding each of the three APLF-like KBMs from WRN and MRI, suggesting that these motifs compete for the same hydrophobic pocket in the Ku80 vWA-like domain that binds APLF[11] (Fig. 1b, bottom right). In contrast to the APLF-like KBMs none of the peptides spanning the XLF-like motifs interacted with KuΔC heterodimer in fluorescence polarization assays (Supplementary Fig. 2a), and the XLF-like motif in WRN also failed to improve KuΔC binding by the adjacent C-terminal KBM (Fig. 1b, bottom left).

To examine whether the APLF-like KBMs are sufficient to bind Ku in cells, we employed UVA laser microirradiation. With the exception of the N-terminal KBM from WRN ('WRN-nA') each of the green fluorescent protein (GFP)-tagged KBMs accumulated at sites of UVA-induced chromosome damage in U2-OS cells, albeit with different efficiencies, and did so with similar kinetics to red fluorescent protein (RFP)-Ku80 (Fig. 2a and Supplementary Fig. 3). The XLF-like motifs from XLF and PAXX also accumulated at sites of UVA-induced chromosome damage, albeit relatively weakly, despite their inability to bind Ku in fluorescence polarization assays (Supplementary Fig. 2b). In contrast, the XLF-like motifs from MRI and WRN were unable to accumulate at sites of UVA laser damage (Supplementary Fig. 2b), although the latter did increase accumulation of the adjacent C-terminal KBM (Fig. 2a; compare 'WRN-cA' and 'WRN-cAX'). Importantly, recruitment of the GFP-tagged APLF-like KBMs to sites of UVA laser damage was reduced by mutation of the Ku80 vWA-like domain (L68R) that we showed previously binds the APLF KBM[11] (Fig. 2b), further suggesting that each of the KBMs interact with the same site in Ku80.

The WRN C-terminal tandem domains bind Ku cooperatively. Mutations in WRN protein result in Werner syndrome, a rare genetic disease characterized by genome instability, premature ageing and cancer[20,21]. WRN is a member of the RecQ family of helicases and is involved in multiple DNA repair processes[20]. Since WRN possesses multiple KBMs and also an XLF-like motif, we addressed the role and relative importance of these for Ku binding. Once again, as described above, the C-terminal KBM targeted GFP to sites of UVA laser-induced damage when expressed in cells as a fusion peptide and did so more efficiently if present together with the adjacent XLF-like motif (Fig. 3b, compare 'WRN-cA' and 'WRN-cAX'). Moreover, this accumulation was reduced if either the C-terminal KBM or XLF-like motif were mutated, further suggesting that these two motifs function cooperatively. Similar results were observed in pull-down experiments, in which GFP-tagged KBM co-precipitated Ku protein complexes from cell extract more efficiently if present in tandem with the XLF-like motif, despite the latter being unable to co-precipitate Ku complexes by itself (Fig. 3a). In addition, whereas co-precipitation of Ku by full-length GFP–WRN was reduced by only ~30% by mutation of either the C-terminal KBM or the XLF-like motif separately

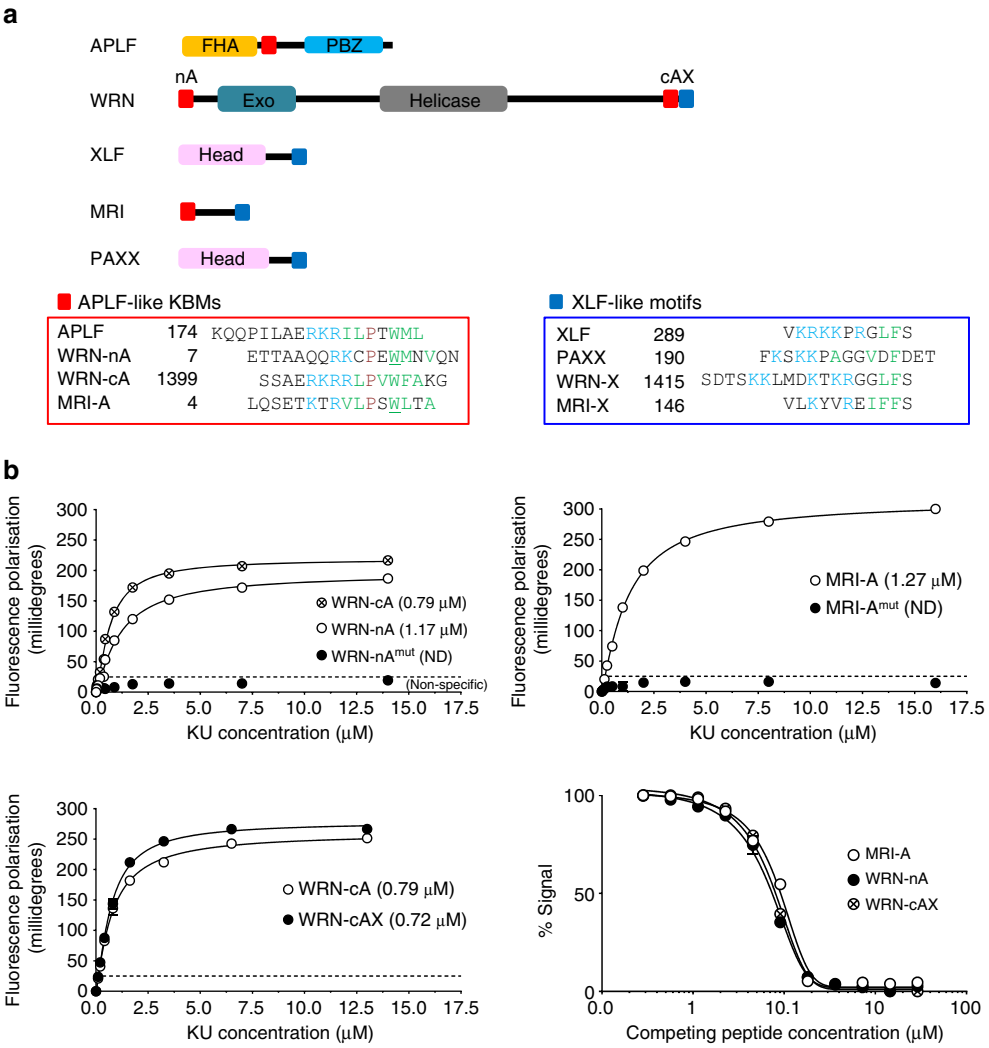

Figure 1 | Conserved Ku-binding motifs (KBMs). (**a**) Cartoon of NHEJ proteins containing putative APLF-like KBMs (red squares) and/or the related XLF-like motif (blue squares). Peptide sequences (lower panels) highlight the conserved basic (blue), hydrophobic (green), proline (purple), and tryptophan/phenylalanine (green bold) residues characteristic of these motifs. The tryptophan residues mutated for the fluorescence polarization (FP) assays described below are underlined. (**b**) Top and bottom left panels, FP assays measuring direct interaction between synthetic fluorescein-labeled peptides (100 nM) encoding the indicated KBMs and the indicated concentration of Ku heterodimer (KuΔC). Peptide sequences are those shown in **a**, but additionally preceded at the N terminus by fluorescein-GGYG. Mutant peptides have alanine instead of tryptophan at the positions underlined in **a**. WRN-cAX peptide encodes both the APLF-like KBM (residues 1,399–1,414) and XLF-like motif (residues 1,415–1,432) from the WRN C terminus. Bottom right panel, MRI-A, WRN-nA or WRN-cAX peptides (2.1 μM) were employed in FP competition assays with KuΔC (1 μM) and the indicated concentration (X-axis) of unlabeled APLF KBM peptide. All data points are the mean of three independent experiments (±1 s.d.). K_d values are indicated in parentheses (±1 s.d.) unless too weak to be determined ('ND').

(Fig. 3c, lane 7 and Fig. 3d, lane 10), it was reduced by >95% by deletion of the entire C-terminal tandem domain (Fig. 3d, lane 8). Notably, recombinant Ku was also co-precipitated by purified full-length recombinant Strep-tagged WRN *in vitro*, and this co-precipitation was again greatly reduced by deletion of the C-terminal tandem domain (Fig. 3e). This experiment confirms that WRN and Ku interact directly and do so in a manner that is mediated primarily by the C-terminal tandem domain.

The N-terminal KBM cooperates with WRN exonuclease. In contrast to the C-terminal KBM, the N-terminal KBM was unable to accumulate at sites of UVA laser-induced chromosome damage or co-precipitate Ku protein complexes if over-expressed by itself as a GFP-fusion protein (Figs 2a and 3a; 'WRN-nA'). Mutation of the N-terminal KBM reduced Ku co-precipitation by full-length GFP–WRN by only ~10% (Fig. 3c, lane 6), and reduced Ku co-precipitation by Strep-tagged WRN *in vitro* to a lesser extent than deletion of the C-terminal tandem domain (Fig. 3e). Nevertheless, mutation of the N-terminal KBM further reduced Ku co-precipitation to ~7% of normal if combined with mutation of the C-terminal KBM (Fig. 3d, lane 7), and to almost undetectable levels if combined with deletion of the C-terminal tandem domain (Fig. 3d, lane 9). We thus conclude that both the N-terminal KBM and the C-terminal tandem domain contribute to the stable interaction of WRN with Ku, with the C-terminal tandem domain contributing the most.

Given the close proximity of the N-terminal KBM and exonuclease domain (Fig. 1a), we considered the possibility that these domains might function cooperatively. In support of this, in contrast to GFP-tagged N-terminal KBM alone (see above), a GFP-tagged fragment encoding both the KBM and the

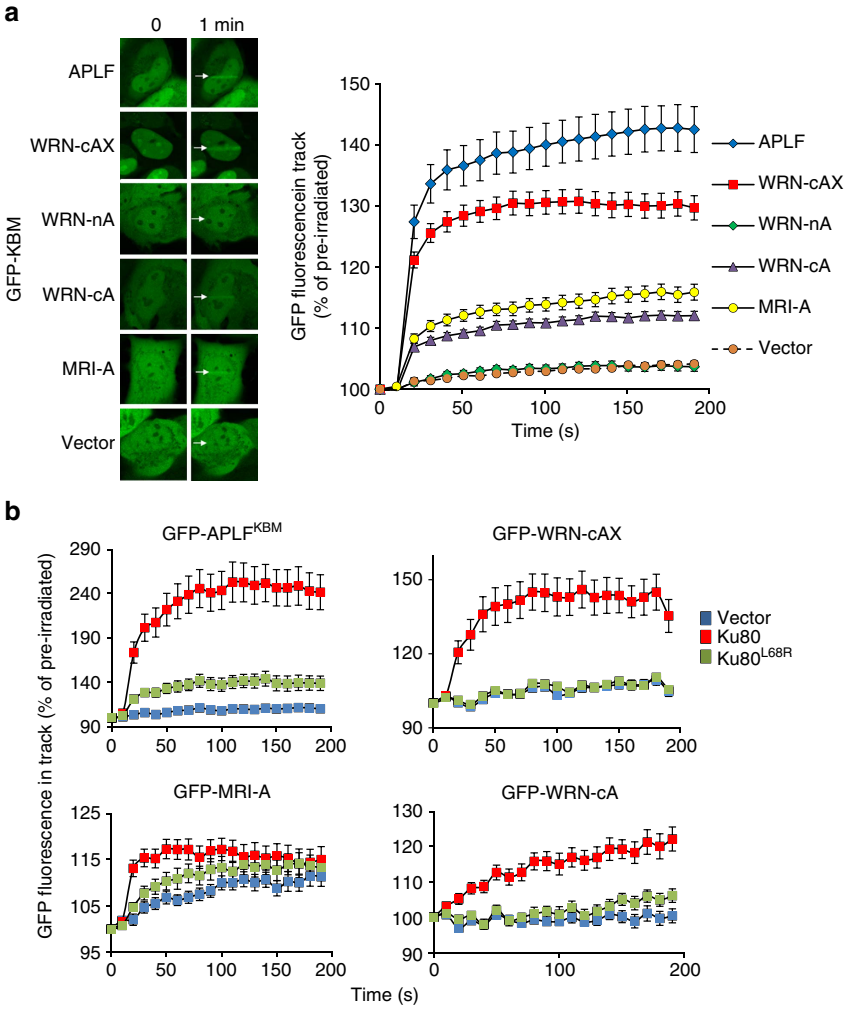

Figure 2 | KBM accumulation at sites of UVA laser-induced chromosome damage. (**a**) U2-OS cells were transiently transfected with expression constructs encoding GFP alone (Vector) or the indicated GFP-tagged KBM and subjected to UVA laser-induced micro-irradiation. The expressed peptide sequences for each KBM were APLF (177–193), WRN-cAX (1,399–1,432), WRN-nA (10–23), WRN-cA (1,399–1,414), MRI-A (6–19). Images were captured immediately before and at 10 s intervals following treatment. Representative images are shown on the left and quantified data on the right. (**b**) *Ku80*$^{-/-}$ mouse embryonic fibroblasts (MEFs) were co-transfected with expression constructs encoding the GFP-tagged KBM from APLF or the indicated GFP-tagged APLF-like KBMs from WRN or MRI, mRFP-Ku70, and either mRFP ('vector'), mRFP-Ku80 or mRFP-Ku80^{L68R}. Cells were micro-irradiated with UVA as above. All data are the mean GFP fluorescence (±s.e.m.) in the laser track relative to the mean GFP fluorescence before irradiation (set at 100%) from >20 cells per experiment.

exonuclease domain (WRN$^{1-236}$; denoted 'WRN-Exo') accumulated at sites of UVA laser-induced chromosome damage in human U2-OS cells (Fig. 4a, left and middle). Importantly, however, WRN-Exo accumulation was diminished by the mutation of either the N-terminal KBM (Fig. 4a, middle) or the KBM-binding site in Ku80 (Fig. 4a, right), indicating that KBM-mediated interaction with Ku was required for WRN-Exo accumulation at chromosome damage. Similarly, GFP-tagged WRN-Exo co-precipitated Ku protein complexes in pull-down experiments, and this required the KBM because the W18G mutation greatly reduced or ablated Ku co-precipitation (Fig. 4b). Notably, WRN-Exo co-precipitated Ku even in the presence of DNAse and RNAse in these experiments, suggesting that the interaction between these proteins is not mediated by nucleic acid. Similar results were observed in yeast two-hybrid assays, in which WRN-Exo transactivated a β-galactosidase reporter gene if co-expressed with Ku80 (but not Ku70) in a manner dependent on both the KBM in WRN-Exo and the KBM-binding site in Ku80 (Supplementary Fig. 4).

Next, we examined the role of the N-terminal KBM in the stimulation of WRN exonuclease activity by Ku[14,15]. WRN-Exo was stimulated by either full-length Ku heterodimer or the truncated KuΔC heterodimer employed in our fluorescence polarization assays, and this stimulation was greatly reduced by mutation of either the KBM (Fig. 4c) or the KBM-binding site in Ku80 (Fig. 4d). This did not reflect a non-specific effect of the KBM mutation on WRN exonuclease activity; however, because wild-type and mutant WRN-Exo were equally active if stimulated independently of Ku by replacing magnesium with manganese in the assay (Supplementary Fig. 5)[22]. Finally, fusion of the tandem peptide from the C terminus of WRN to the C terminus of WRN-Exo^{W18G} rescued stimulation by Ku, suggesting that the KBM stimulates WRN exonuclease by acting as a position-independent molecular tether (Fig. 4e).

The WRN KBMs accelerate chromosomal DSB repair. WRN has previously been implicated in NHEJ by various

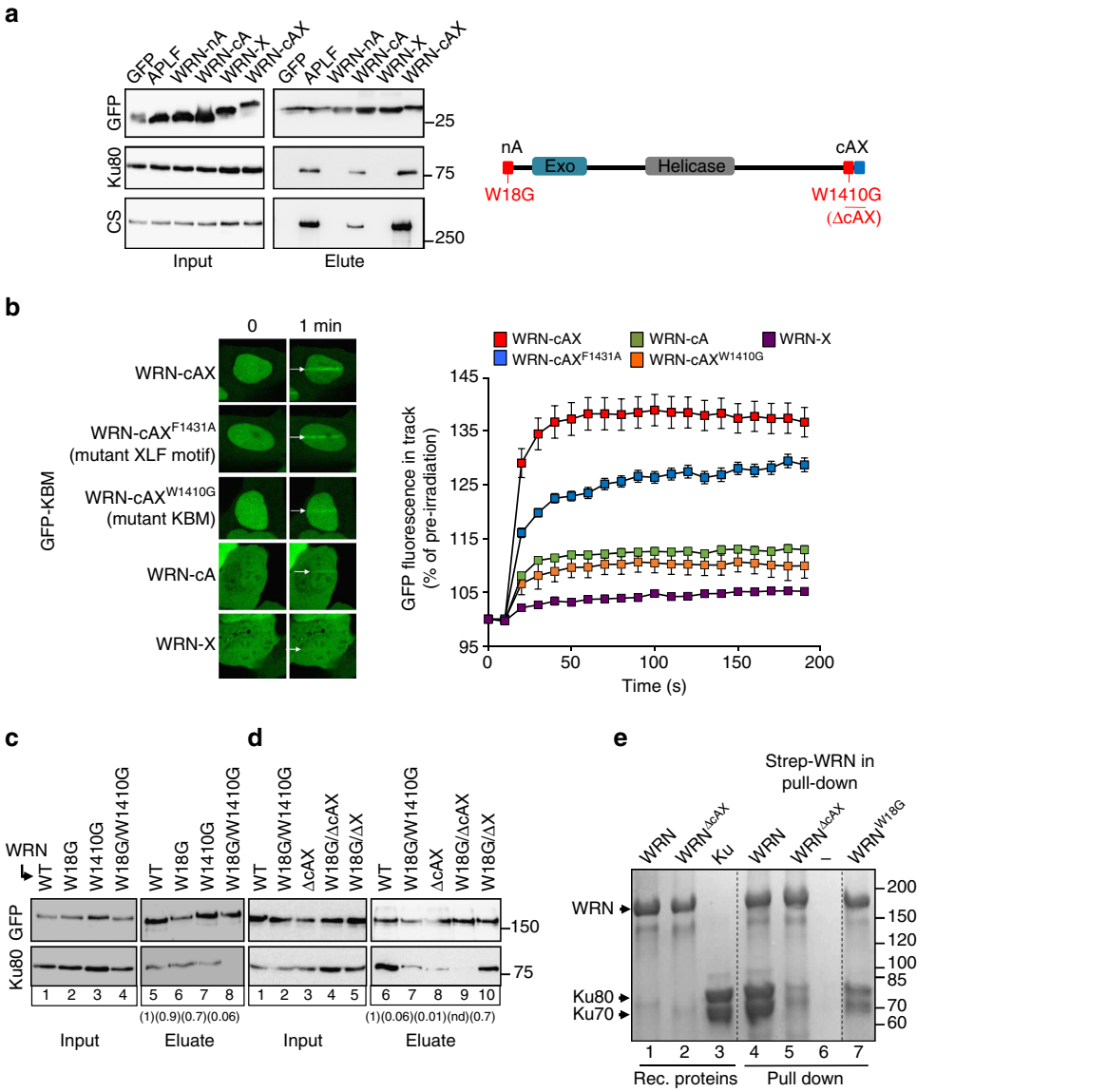

Figure 3 | The WRN C-terminal KBM and XLF-like motif bind Ku protein complexes cooperatively. (**a**) HEK293T cells were co-transfected with expression constructs encoding GFP or the indicated GFP-tagged KBMs and GFP-tagged proteins recovered using GFP-TRAP beads. Aliquots of the input and eluate samples were fractionated by SDS–PAGE and immunoblotted for GFP, Ku80 and DNA-PKcs (CS). Right, cartoon depicting WRN and the position of the KBMs and XLF-like motif and the mutations employed in these experiments. (**b**) HEK293T cells were transfected with expression constructs encoding the indicated wild-type or mutated GFP-tagged WRN C-terminal KBM, XLF-like motif ('X'), or KBM plus XLF-like motif in tandem. Cells were micro-irradiated with UVA as in Fig. 2. Representative images (left) and quantification (right) are shown. All quantified data are the mean GFP fluorescence (±s.e.m.) in the laser track relative to the mean GFP fluorescence before irradiation (set at 100%) from >20 cells per experiment. (**c**,**d**) Expression constructs encoding full-length wild-type ('WT') GFP–WRN or derivatives harbouring the indicated point mutations in the N-terminal KBM (W18G), C-terminal KBM (W1410G) or deleted C-terminal tandem domain (ΔcAX) or XLF-like motif (ΔX) were transfected into HEK293T cells and recovered using GFP-TRAP beads. Input and eluates were immunoblotted for GFP and Ku80. Numbers in parentheses are the fraction of Ku co-precipitated by the indicated GFP-tagged WRN protein, relative to wild-type WRN, quantified by ImageJ. Data are from two to six independent experiments, except for W18G/ΔcAX in which Ku recovery was too low to be determined ('nd'). (**e**) Direct interaction of purified full-length Strep-tagged WRN with recombinant human Ku. Recombinant Strep-tagged WRN, WRN$^{\Delta cAX}$ or WRN^{W18G} was immobilized on Streptavidin Mag sepharose beads and incubated with recombinant Ku heterodimer. Aliquots of the recombinant proteins employed in the experiment are shown on the left (lanes 1–3) and proteins pulled down by the indicated Strep-tagged WRN protein are shown on the right (lanes 4–7). Lane 6 contains the proteins recovered in a control pull-down that lacked Strep-tagged WRN. Proteins were fractioned by SDS–PAGE and stained with Coomassie Blue.

biochemical and cellular assays[14,15,23–26], but a role in promoting chromosomal DSB repair has not been demonstrated. We showed recently that the interaction of the APLF KBM with Ku accelerates NHEJ, as measured using γH2AX as a surrogate marker of DSBs[11]. Given the similarity of the APLF-like KBMs, we examined whether this was also the case for WRN. Indeed, we observed a small but significant reduction in NHEJ rate in Werner Syndrome cells arrested in G_0, as suggested by the slower loss of γH2AX foci in these cells following ionizing radiation (Fig. 5a). We employed cells arrested in G_0 in these experiments to avoid measuring DSBs induced in S/G2 phase, which are

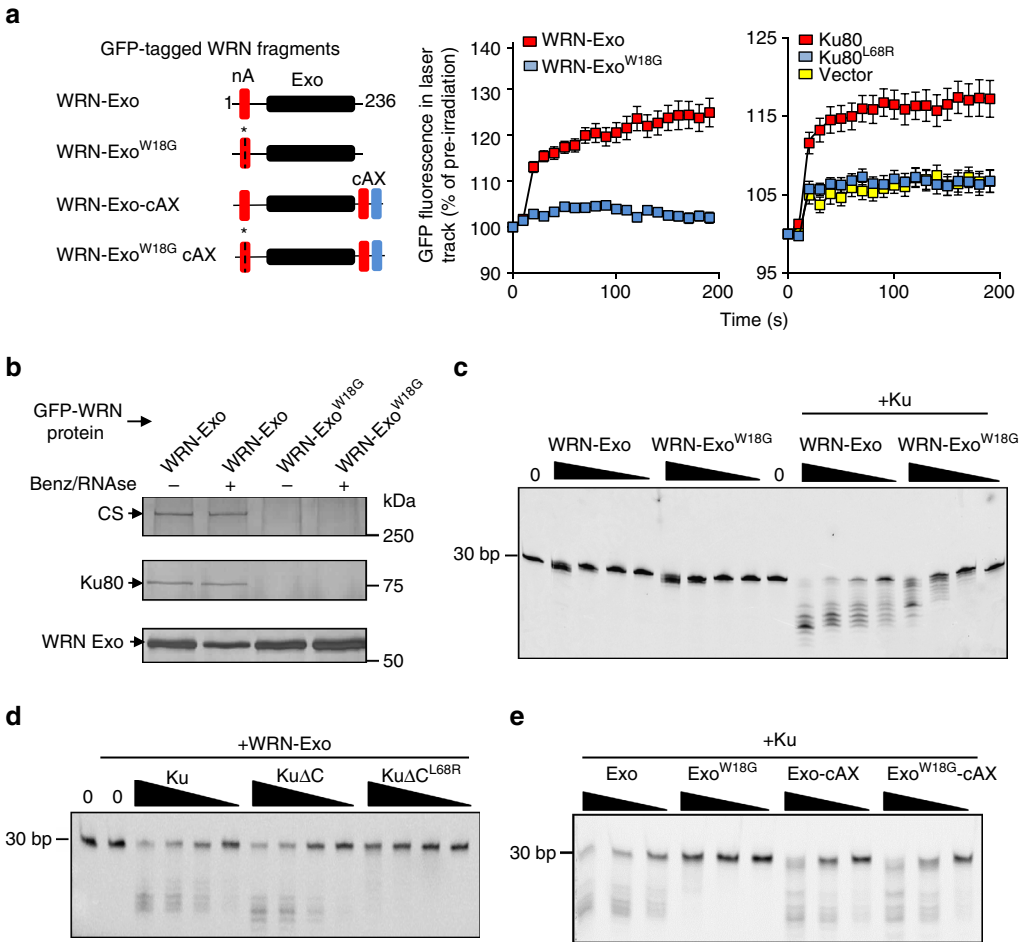

Figure 4 | The WRN N-terminal KBM promotes WRN exonuclease activity. (**a**) Left, cartoon illustrating the GFP-tagged truncated recombinant WRN proteins employed in these experiments. The WRN N-terminal ('nA') and C-terminal ('cA') KBMs are indicated by red boxes and XLF-like motif ('X') by a blue box. The exonuclease domain is indicated by a black box, and the position of the KBM mutation (W18G) by an asterisk and dotted line. Middle, U2-OS cells transiently expressing the indicated recombinant GFP-tagged WRN protein were imaged for GFP before and after UVA microirradiation, as in Fig. 2. Right, *Ku80*$^{-/-}$ MEFs transiently co-expressing GFP-tagged WRN-Exo, RFP-Ku70, and either RFP (vector), RFP-Ku80 or RFP-Ku80^{L68R} as indicated were micro-irradiated as in Fig. 1. Data are the mean GFP fluorescence (±s.e.m.) in the laser track relative to the mean GFP fluorescence before irradiation (set at 100%) from >20 cells per experiment. (**b**) The indicated GFP-tagged WRN proteins were recovered from transiently transfected HEK293T cell lysates pre-treated or not as indicated with Benzonase and RNAse in pull-down assays using GFP-TRAP beads. Aliquots of the bead eluate were fractionated by SDS-PAGE and silver stained to detect GFP-WRN, GFP-WRNW18G, Ku80, and DNA-PKcs ('CS'). (**c**) Cy3-labeled 30 bp duplex oligonucleotide (20 nM) with a 5′ overhang was incubated with 500, 100, 20 or 5 nM His-tagged WRN-Exo or WRN-Exo^{W18G} in the absence or presence of 100 nM Ku heterodimer (Ku70/Ku80, 'Ku') and 5 mM $MgCl_2$. Exonuclease products were resolved on a 16% TBE-Urea gel. (**d**) Exonuclease assays were conducted as above in the presence of 5 mM $MgCl_2$ using 10 nM His-tagged WRN-Exo and 100, 20, 4 or 0.8 nM of either Ku heterodimer (Ku70/Ku80; 'Ku'), KuΔC heterodimer (Ku70/Ku80ΔC; 'KuΔC'), or mutant KuΔC heterodimer harbouring the Ku80 mutation, L68R (KuΔC^{L68R}). (**e**) Exonuclease assays were conducted as above using 100, 20 and 4 nM of the indicated His-tagged WRN protein and 10 nM wild-type Ku heterodimer (Ku70/Ku80; 'Ku') in 5 mM Mg^{2+}.

substrates for homologous recombination-mediated repair. To our knowledge this is the first report of a reduced rate of chromosomal NHEJ in Werner Syndrome cells. The slower loss of γH2AX foci reflected the loss of WRN because it was complemented by expression of wild-type recombinant human WRN (Fig. 5b,c). In contrast, this defect was not complemented by recombinant WRN protein harbouring mutations in either of the two KBMs, confirming the importance of these motifs for WRN functionality during NHEJ (Fig. 5b,c). However, WRN protein harbouring a mutated exonuclease or helicase domain was still able to complement the defect, suggesting that the acceleration of NHEJ detected here reflects the scaffolding function of WRN[23] rather than its catalytic activity.

Discussion

The NHEJ accessory factor APLF possesses a short conserved peptide motif denoted the KBM that interacts with the vWA-like domain in Ku80 (refs 11,12). Here we show that the KBM is present and conserved in several other NHEJ proteins, including two in WRN protein and one in MRI; a poorly characterized protein that interacts with Ku and promotes NHEJ by an unclear mechanism[16,27]. Each of these KBMs interact with Ku heterodimer with sub/low micromolar affinity *in vitro*, and do so by interacting with the same hydrophobic pocket in the Ku80 vWA domain that binds APLF. Each of the KBMs also accumulate at cellular sites of laser-induced chromosome damage in a Ku80- and vWA-dependent manner when expressed as a GFP-tagged peptide, with the exception of the KBM present at the

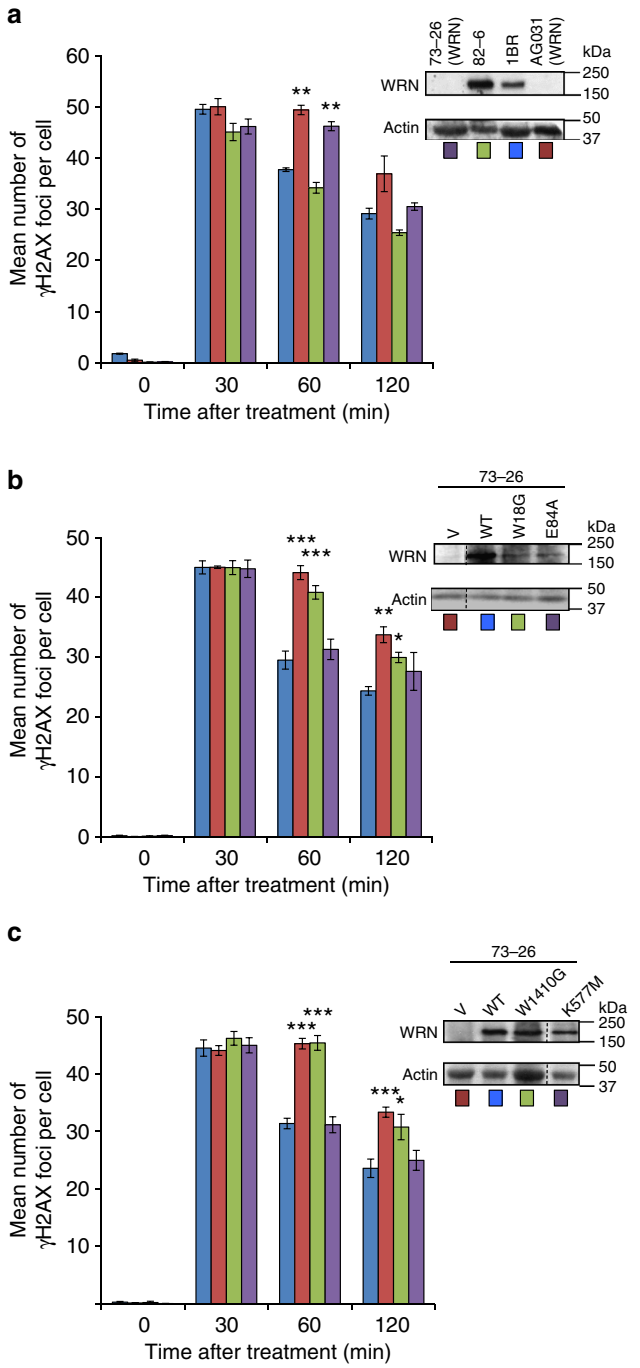

Figure 5 | WRN KBMs accelerate DSB repair. (**a**) Confluence-arrested (G0/G1) hTERT-immortalised fibroblasts from two WRN patients (73–26 and AG03141) and normal controls (82–6 and 1BR) were treated with γ-rays (2 Gy) and γH2Ax foci counted at the time-points indicated. Inset, Actin and WRN protein levels in the indicated cell lines. (**b**) WRN cells (73–26) stably transduced with empty vector (V) or vector encoding wild-type (WT) WRN, WRN^{W18G} harbouring a mutated N-terminal KBM (W18G), or WRN harbouring a mutated exonuclease domain WRN^{E84A} (E84A), were examined for DSB repair rates as described above. (**c**) Werner syndrome cells (73–26) stably transduced with empty vector (V) or vector encoding WT WRN, WRN^{W1410G} harbouring a mutated C-terminal KBM (W1410G), or WRN harbouring a mutated helicase domain (WRN^{K577M}) were examined as above. Data points are the mean (± s.e.m.) number of foci per cell from four independent experiments. $^{*}P<0.05$, $^{**}P<0.01$, $^{***}P<0.001$ by paired *t*-test when compared with WT cells.

N terminus of WRN, which accumulates at these sites cooperatively with the adjacent exonuclease domain. Intriguingly, database searches using Pattinprot and the core minimal KBM sequence (R-X-X-P-X-W) identified more than 600 proteins with this motif (Supplementary Data 1). More sophisticated bioinformatic analyses and experimental validation are needed to identify which of these are true KBMs.

We also identified a motif in XLF, WRN, PAXX and MRI that is similar in sequence to the KBM but which is structurally and functionally distinct, and which we denoted the XLF-like motif. KBMs and XLF-like motifs are similar in sequence in that both are comprised of a basic patch followed by a highly conserved aromatic residue, but they differ in several key respects. Whereas KBMs possess a highly conserved proline and tryptophan the XLF-like motifs possess a conserved phenylalanine. In addition, whereas KBMs are found at different locations the XLF-like motifs are typically present at protein C termini. Finally, in contrast to KBMs, none of the XLF-like motifs interacted measurably with Ku heterodimer in fluorescence polarization assays. This is surprising, because the XLF and PAXX motifs promote accumulation of the full-length proteins at sites of laser-induced chromosome damage in a Ku-dependent manner and/or associate with Ku complexes *in vitro*[28–30]. Consequently, we suggest that XLF-like motifs associate with Ku complexes only in the presence of DNA and/or other cellular protein/s. This idea is consistent with a previous report that mutation of this motif in XLF influences binding to DNA[31].

Werner syndrome is a progeroid disease characterized by premature ageing, genetic instability and predisposition to cancer[20,21], and WRN protein is implicated in multiple aspects of DNA metabolism including telomere maintenance, base-excision repair, homologous recombination, replication fork processing and NHEJ (reviewed in ref. 20). Intriguingly, WRN protein possesses two KBMs and an XLF-like motif, with the N-terminal KBM located next to the exonuclease domain and the C-terminal KBM located in tandem with the XLF-like motif. WRN interacts with multiple protein components of these pathways including MRN nuclease, RAD51, XPG and Ku heterodimer[14,15,32–34]. The interaction with Ku was reported to occur towards both the N and C termini of WRN[14,15,35], and our identification of N- and C-terminal KBMs has fine-mapped these interactions and allowed us to disrupt them individually or together. All of the KBM interactions with Ku detected to date are with the vWA-like domain of Ku80. This is in agreement with two of the above reports, which also concluded that the N and C termini of WRN interact with Ku80 (ref. 15), but disagrees with the study of Karmakar *et al.*[35] in which the WRN N terminus was reported to interact with Ku70. The source of this discrepancy is not clear but our conclusion that Ku80 is the partner of both the N-terminal and C-terminal KBMs is based on a variety of biochemical, cellular and yeast two-hybrid experiments.

Whereas mutation of the individual KBMs in full-length WRN did not greatly reduce the interaction with Ku, as measured by co-immunoprecipitation experiments, pair-wise mutation or deletion greatly reduced or ablated it. However, only the C-terminal KBM was able by itself to accumulate at sites of chromosomal damage or efficiently co-precipitate Ku from cell extract, suggesting that this KBM is the major contributor to stable Ku binding by WRN. It is not clear why this was not reflected in our fluorescence polarization assays *in vitro*, in which the two KBMs interacted with Ku with similar affinities. Importantly, the adjacent XLF-like motif functioned cooperatively with the C-terminal KBM, greatly enhancing Ku interaction and accumulation at chromosome damage. It is possible that the XLF-like motif simply promotes Ku binding by the adjacent KBM, although we note that it did not increase the affinity of the

KBM for Ku in fluorescence polarization assays, *in vitro*. Rather, we suggest that the XLF-like motif interacts with another component of DNA–PK complexes that is positioned near the KBM-binding site in Ku80, such as DNA–PKcs. An interaction between WRN and DNA–PKcs has been reported previously[24], and in our experiments the XLF-like motif promoted co-precipitation of DNA–PKcs to a greater extent than Ku when present either in tandem with the C-terminal KBM (Figs 3a). While more experiments are required to confirm this idea, we suggest that the XLF-like motif in WRN interacts directly with the catalytic subunit of DNA–PK, thereby promoting the assembly of more stable DNA–PK protein complexes.

The N-terminal KBM in WRN was unable by itself to accumulate at sites of chromosome damage or to precipitate Ku from cell extract, despite the affinity of this KBM for Ku *in vitro* being similar to that of the C-terminal KBM. However, the N-terminal KBM both accumulated at sites of UVA laser damage and promoted co-precipitation of Ku if present together with the adjacent exonuclease domain. These data suggest that while the N-terminal KBM possesses intrinsic Ku-binding activity it requires the adjacent exonuclease domain for Ku binding in cells and for accumulation at sites of chromosome damage. The reason for this difference between *in vitro* and cellular functionality is currently unclear, but nevertheless the cooperativity between the KBM and exonuclease domain extended to the activity of the latter, which was stimulated by Ku in a largely KBM-dependent manner. Intriguingly, fusion of the C-terminal KBM to the C terminus of the WRN exonuclease domain also supported Ku-dependent stimulation of WRN exonuclease activity, even in the absence of a functional N-terminal KBM. This suggests that the KBMs act in an orientation-independent but proximity-dependent manner to tether the WRN exonuclease domain to Ku–DNA complexes.

WRN has been implicated in NHEJ previously. For example, the interaction with Ku stimulates WRN exonuclease activity on a variety of DSB termini, including those harbouring different types of recessed termini and termini harbouring oxidized nucleotides[14,15,36]. This is consistent with a role for WRN in processing DSB termini during NHEJ in advance of gap filling and DNA ligation. A number of phenotypes are also consistent with aberrant NHEJ in WRN syndrome cells, such as mild hypersensitivity to ionizing radiation[24], reduced accuracy and joining efficiency at plasmid-borne DSBs[23,25], and elevated deletion sizes at the chromosomal *HPRT* locus[37]. However, to our knowledge, the current work is the first in which an impact of WRN on the rate of chromosomal NHEJ has been observed. While this phenotype is similar to that reported for APLF, another KBM-mediated partner of Ku80, it is unique in that it was detected only in cells arrested in G_0. We do not yet understand the reason for this observation, but one possibility is that the role detected here for WRN is redundant with other proteins in other cell cycle phases. Surprisingly, although both WRN KBMs were required for acceleration of NHEJ, the catalytic activity of WRN was not required. This does not rule out an involvement of WRN catalytic activity during NHEJ, because it is possible that the fraction of DSBs requiring this activity is too small to detect or that other enzymes can also provide this activity. Nevertheless, our data suggest that the acceleration of NHEJ that we have detected in this work reflects an impact of WRN on the structure and stability of NHEJ protein complexes. Such a structural role for WRN has been suggested previously, in which WRN stabilizes DNA–PK complexes and protects DSB termini from excessive degradation by other nucleases[23].

On the basis of these data, we propose the following model (Fig. 6). We suggest that the N- and C-terminal KBMs enable WRN to interact with Ku80 and thereby promote the stability of DNA–PK protein complexes. The two KBMs may interact with Ku80 simultaneously, sequentially or both. For example, a high-affinity interaction of the C-terminal KBM tandem domain could tether WRN to DNA–PK, with the N-terminal KBM either displacing the C-terminal KBM from Ku80 when exonuclease activity is required for end processing (Fig. 6, left) or, alternatively, interacting with a second molecule of Ku on the opposite DSB terminus to bridge the break (Fig. 6, right). Either of these possibilities can explain the need to mutate or delete both KBMs to greatly reduce or ablate Ku interaction, and the requirement for both KBMs for normal rates of NHEJ.

Methods

WRN cells. The hTERT-immortalised fibroblast cell lines '73–26' (Werner syndrome)[24] and wild-type sibling control ('82–6')[24] were kindly provided by Judy Campisi (Buck Institute, CA), and the Werner syndrome cell line AG03141 (ref. 38) was kindly provided by David Kipling (Cardiff University). Retroviruses encoding wild-type or mutant human WRN protein were packaged in GP2–293 cells using the Retro-X Universal Packaging System (Clontech) according to the manufacturer's instructions. GP2–293 supernatants were used to transduce 73–26 hTERT cells in the presence of 4 μg ml^{-1} hexadimethrine bromide (Polybrene, Sigma) for 24 h. Following three successive rounds of transduction, cells were selected in 0.5 mg ml^{-1} G418 for 4–6 weeks. Resulting cultures were screened for WRN expression by western blotting using mouse anti-WRN (Abcam 66601, 1:500). All cell lines were tested and found to be mycoplasma-free before use.

Plasmids. Primers employed for cloning and mutagenesis are detailed in Supplementary Table 1. pET16b-WRN-Exo, encoding WRN residues 1–236 (UniProt accession number Q14191) and including a C-terminal octahistidine tag, was generated by PCR using pEGFP-C3-WRN (a gift from Will Bohr) as a template and subsequent subcloning of the PCR product into the *Nco*I and *Xho*I sites of pET16b. GST-fusion or enhanced GFP (eGFP)-fusion peptides encoding the KBMs or XLF-like motifs WRN-nA (KBM sequence; LETTAAQQRKCPEWMNVQ), WRN-cA (KBM sequence: TSSAERKRRLPVWFAK), WRN-X (KBM sequence: SKKLMDKTKRGGLFS), MRI-A (KBM sequence: SETKTRVLPSWLTA), MRI-X (KBM sequence; VLKYVREIFFS), XLF (KBM sequence; VKRKKPRGLFS) and PAXX (KBM sequence; FKSKKPAGGVDFDET) were generated by annealing appropriate complementary oligonucleotides and ligation into the *Bam*HI/*Xho*I sites of pGEX6p1 or the *Bgl*II/*Sal*I sites of pEGFP-C1, respectively. For GST-fused and eGFP-fused WRN-cAX, residues 1,399–1,432 (SSAERKRRLPVWFAKSKKLMDK TKRGGLFS) were amplified by PCR and subcloned as above. GFP-tagged WRN-Exo-cAX was generated by PCR amplification of WRN-Exo (see above) and insertion of the resulting *Bgl*II fragment into the *Bam*HI site of pGEX6-cAX. To generate pEGFP-WRN encoding full-length WRN, a stop codon was introduced by site-directed mutagenesis of pEGFP-C3-WRN after S1432, to remove exogenous plasmid-derived C-terminal residues present in pEGFP-C3-WRN (see above)[39]. Alternatively, to generate pGFP-WRN$^{\Delta cAX}$, a stop codon was introduced at position S1399. Derivatives harbouring point mutations were generated by site-directed mutagenesis using the primers in Supplementary Table 1. pmRFP-Ku70, pmRFP-Ku80 and pmRFP-Ku80^{L68R} were generated by subcloning from pGFP-Ku70, pGFP-Ku80 and pGFP-Ku80^{L68R} (ref. 11). pLXSN, pLXSN-WRN, pLXSN-WRN^{E84A} and pLXSN-WRN^{K577M} were kind gifts from Junko Oshima[23]. For yeast two-hybrid plasmids, the *Nco*I/*Xho*I fragments from pET16b-WRN-Exo and pET16b-WRN-Exo^{W18G} were ligated into the *Nco*I/*Sal*I sites of pGBKT7. pACT2-Ku80 vWA (encoding residues 1–258) was constructed using the *Xho*I fragment from pACT Clone 5, which was recovered from a previous pACT human complementary DNA library screen using APLF as bait[11]. pACT2-Ku80 vWA^{L68R} mutant was also subcloned in this way. pACT2-Ku70 vWA was cloned by PCR amplification of a fragment encoding amino acids 1–272 of Ku70 and insertion into the *Bam*HI and *Xho*I restriction sites of pACT2.

Yeast two-hybrid experiments. For interaction analysis, yeast Y190 cells were co-transformed with the indicated pACT2 and pGBKT7 plasmids and selected on minimal media plates lacking leucine and tryptophan. Transformed cells were screened for activation of the LacZ reporter gene by β-galactosidase filter lift assays[11].

Recombinant proteins. Strep-tagged WRN, Ku, KuΔC and KuΔC^{L68R} were expressed and purified from insect cells using a baculovirus expression system and purified using immobilized metal-chelate chromatography and gel filtration[11]. Strep-tagged WRN was purified using an affinity Strep-Tactin Superflow Plus cartridge (Qiagen) followed by Superose 6 gel filtration. KuΔC is comprised of full-length Ku70 and Ku80ΔC lacking the C-terminal residues 591–732. His-tagged WRN-Exo was expressed from pET16b-WRN-Exo in BL21(DE3) (pLysS) by induction with 1 mM IPTG in 0.5 l cultures in LB containing

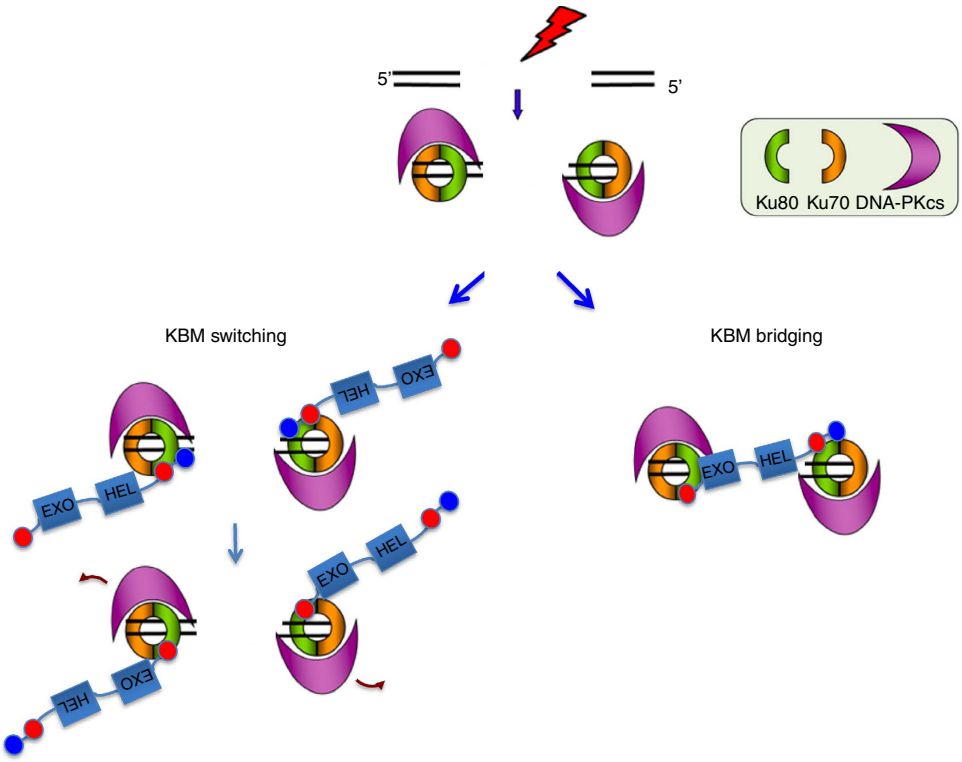

Figure 6 | A Model for WRN KBM function during NHEJ. Top, DNA-PK holoenzyme binds to a DSB. Bottom left, WRN is recruited into DNA-PK complexes by high affinity interaction between the C-terminal KBM (red circle) and the hydrophobic pocket in the vWA domain of Ku80. The XLF-like motif (blue circle) functions cooperatively, perhaps stabilizing the association of Ku with DNA-PKcs. Following autophosphorylation, DNA-PKcs dissociates and the C-terminal KBM is replaced by the N-terminal KBM to stimulate WRN 3′-exonucease activity. Bottom right, The N-terminal and C-terminal KBMs bind two Ku molecules simultaneously, bridging the DSB. Note that WRN may fulfil both enzymatic and structural roles during NHEJ.

50 μg ml^{-1} ampicillin, and 30 μg ml^{-1} chloramphenicol for 16 h at 16 °C. Harvested cells were frozen and subsequently lysed in 20 mM Tris-HCl pH 7.5, 0.5 M NaCl, 5% glycerol, 1.4 mM β-mercaptoethanol, 1% Triton X-100, 1 mM phenylmethylsulphonyl fluoride, 10 mM imidazole, pH 8.0. Cells were sonicated (3 × 20 s) and the cell extracts clarified by centrifugation 12,000*g* for 30 min. The supernatant was incubated with 0.5 ml pre-washed Ni-agarose beads (Qiagen) for 20 min at 4 °C and the beads washed twice with 10 ml wash buffer (lysis buffer lacking detergent) before being transferred to a gravity-flow column. The resin was washed with a further 10 ml wash buffer containing 50 mM imidazole and proteins then eluted with wash buffer containing 250 mM imidazole. Fractions containing WRN-Exo were pooled and purified further by gel filtration using Superdex 200 equilibrated with 20 mM Tris-HCl pH 7.5, 0.3 M NaCl, 10% glycerol, 1 mM DTT. GST-tagged KBMs were expressed as above and purified using glutathione sepharose affinity chromatography.

Fluorescence polarization assays. 100 nM fluorescein-labeled peptides (Peptide Protein Research) were incubated at room temperature for 10 min with the indicated concentrations of Ku70/Ku80ΔC (KuΔC) in 20 mM HEPES pH 7.5, 200 mM NaCl, and 0.5 mM TCEP. Fluorescence polarization was measured in a POLARstar Omega microplate reader (BMG Labtech GmbH, Ortenberg, Germany). Fifty flashes were recorded for each well with an excitation wavelength of 485nm, and simultaneous detection of emission at 520 nm with parallel and perpendicular polarizers in-line. Background fluorescence in wells containing only buffer was subtracted from all values obtained for the samples. Polarization data were analysed using GraphPad Prism 5.0 by non-linear fitting with a one-site total binding model. All data represent the mean of at least three separate experiments and error bars represent 1 s.d. Peptide sequences are those depicted in Fig. 1a, in each case additionally preceded with fluorophore and four amino acid linker (Flu-GGYG). For competition assays, 1 μM KuΔC was incubated with 2.1 μM fluorescently labeled WRN-nA, WRN-cAX or MRI-A peptides for 10 min at room temperature followed by the indicated concentration of unlabeled APLF peptide (highest concentration; 29 μM).

Laser microirradiation. 2 × 10^5 U2-OS cells or *Ku80*$^{-/-}$ mouse embryonic fibroblasts[40] were seeded in glass-bottomed 35-mm dishes (Mattek) in DMEM (+10% FCS) and 2 days later transfected with either (U2-OS cells) 1 μg plasmid DNA and 3 μl Genejuice (Merck Millipore) or (*Ku80*$^{-/-}$ mouse embryonic fibroblasts) 7.5 μl GeneJuice and 0.5 μg of the indicated GFP-KBM plasmid, 1 μg of pmRFP-Ku70, and 1 μg of either pmRFP-C1 vector, pmRFP-Ku80 or pmRFP-Ku80^{L68R}. 24 h after transfection, cells were pre-treated with 10 μg ml^{-1} Hoechst 34580 (Sigma) and micro-irradiated (210 nJ μm^{-2}) with a 405 nm laser focused through a ×60 oil objective (Intelligent Imaging Innovations). Images were captured at 10 s intervals after treatment and image analysis was carried out using Slidebook software.

GFP pull-down assays. HEK293T cells were cultured in DMEM supplemented with 10% FCS, glutamine and antibiotics in 15 cm culture dishes and at ~70% confluence the media was replaced with 18 ml Hybridoma-SFM media (supplemented with 1% FCS and antibiotics) and supplemented with 2 ml transfection mix containing PEI (80 μg) and the appropriate plasmid (20 μg). Cells were harvested 48 h later, washed with cold PBS and flash frozen. Thawed pellets (5 × 10^6 cells) were lysed in 400 μl lysis buffer (25 mM Tris-HCl pH 7.5, 150 mM NaCl, 10% glycerol, 0.5% Triton X-100, 1 mM DTT) containing protease and phosphatase inhibitors (Sigma) for 20 min at 4 °C. Samples were sonicated in water-bath sonicator for 10 min at 30 s intervals (30 s on/30 s off). Cell extracts were clarified by centrifugation (13,000*g*, 10 min, 4 °C) and 40 μl removed for the 'input' sample. GFP-TRAP beads (20 μl; Chromotek) were washed three times with lysis buffer then incubated with the supernatant for 1 h at 4 °C. Unbound proteins were recovered by gentle centrifugation (2,700*g*, 2 min, 4 °C) and the beads were washed with 3 × 500 μl lysis buffer. Proteins were then eluted from the beads using SDS–PAGE loading buffer, heated at 95 °C for 5 min, and aliquots fractionated by 10% SDS–PAGE and transferred to Hybond-C membrane (GE Healthcare). Proteins were detected by immunoblotting using anti-GFP (Cell Signalling #2555S, 1/1,000 dilution), anti Ku80 (Abcam Ab80592, 1/10,000 dilution), anti DNA–PKcs (Abcam Ab80514, 1/1,000 dilution) or anti-RFP (Abcam, Ab62341, 1:1,000) antibodies. Pictures of the full membranes containing the blotted eluates from these experiments are shown in Supplementary Figs 6–8.

Strep-tag pull-down assays. Streptavidin Mag Sepharose beads (100 μl; GE Healthcare) were washed three times with sample buffer (20 mM Hepes pH 7.5, 150 mM NaCl, 5% glycerol, 0.5 mM TCEP, 0.05% IGEPAL-CA640) then incubated with Strep-tagged 50 nM WRN, WRN$^{\Delta cAX}$ or WRN^{W18G} for 1 h at 4 °C. Unbound

protein was recovered by applying magnetic force to the slurry, and the beads washed with 3 × 500 µl sample buffer. Recombinant untagged Ku protein (50 nM) was then incubated with the beads for 1 h at 4 °C, the unbound fraction removed and washes performed as above. Bound proteins were eluted from the beads using SDS–PAGE loading buffer, heated at 95 °C for 5 min, and aliquots fractionated by 10% SDS–PAGE and stained with Instant Blue (Expedeon).

Exonuclease assays. A 5′ Cy3-labeled 30-bp oligonucleotide (5′ cy3-CCGTTTCG CTCAAGTTAGTATGTCAAAGCA-3′) was annealed to a complementary unlabeled 30-bp oligonucleotide (5′-CGTTGAAGCCTGCTTTGACATACT AACTTG-3′) to produce a 20-bp duplex with 10 nucleotide 5′ overhangs. 20 nM of DNA duplex was incubated at 37 °C for 30 min with 10 nM or the indicated titration of WRN-Exo or WRN-Exo^{W18G} in reaction buffer (20 mM Tris-HCl, pH 7.5, 50 mM KCl, 10 mM $MgCl_2$, 1 mM DTT and 0.1 mg ml^{-1} BSA). Where indicated, reactions also contained 10 nM or the indicated titration of Ku, Ku70/Ku80ΔC or Ku70/Ku80ΔC^{L68R} and where indicated 5 mM of either $MgCl_2$ or $MnCl_2$. Reactions were stopped using 90% (v/v) Formamide/TBE and heated at 95 °C for 5 min. Products were fractionated on 16% TBE-Urea gels in 1 × TBE (89 mM Tris, 89 mM Boric Acid, 2 mM EDTA) and imaged on a Fuji imager using a Cy3 filter.

γH2Ax assays. 3×10^5 of the indicated cells were seeded and grown on coverslips in 35-mm dishes and grown to confluence for 1 week. Cells were then treated with 2 Gy γIR, fixed with paraformaldehyde at the time-points indicated, and immunolabeled as previously described[41]. Cells were co-labeled with CENPF to confirm that cell populations were confluence-arrested.

References

1. Cannan, W. J. & Pederson, D. S. Mechanisms and consequences of double-strand DNA break formation in chromatin. *J. Cell. Physiol.* **231,** 3–14 (2016).
2. Soulas-Sprauel, P. *et al.* V(D)J and immunoglobulin class switch recombinations: a paradigm to study the regulation of DNA end-joining. *Oncogene* **26,** 7780–7791 (2007).
3. Bunting, S. F. & Nussenzweig, A. End-joining, translocations and cancer. *Nat. Rev. Cancer* **13,** 443–454 (2013).
4. McKinnon, P. J. & Caldecott, K. W. DNA strand break repair and human genetic disease. *Annu. Rev. Genomics Hum. Genet.* **8,** 37–55 (2007).
5. Woodbine, L., Gennery, A. R. & Jeggo, P. A. The clinical impact of deficiency in DNA non-homologous end-joining. *DNA Repair (Amst)* **16,** 84–96 (2014).
6. Chapman, J. R., Taylor, M. R. G. & Boulton, S. J. Playing the end game: DNA double-strand break repair pathway choice. *Mol. Cell* **47,** 497–510 (2012).
7. Mahaney, B. L., Meek, K. & Lees-Miller, S. P. Repair of ionizing radiation-induced DNA double-strand breaks by non-homologous end-joining. *Biochem. J.* **417,** 639–650 (2009).
8. Davis, A. J., Chen, B. P. C. & Chen, D. J. DNA-PK: a dynamic enzyme in a versatile DSB repair pathway. *DNA Repair (Amst)* **17,** 21–29 (2014).
9. Ochi, T. *et al.* Structural biology of DNA repair: spatial organisation of the multicomponent complexes of nonhomologous end joining. *J. Nucleic Acids* **2010,** pii: 621695 (2010).
10. Grundy, G. J., Moulding, H. A., Caldecott, K. W. & Rulten, S. L. One ring to bring them all-The role of Ku in mammalian non-homologous end joining. *DNA Repair (Amst)* **17,** 30–38 (2014).
11. Grundy, G. J. *et al.* APLF promotes the assembly and activity of non-homologous end joining protein complexes. *EMBO J.* **32,** 112–125 (2013).
12. Shirodkar, P., Fenton, A. L., Meng, L. & Koch, C. A. Identification and functional characterization of a Ku-binding motif in Aprataxin polynucleotide kinase/phosphatase-like factor (APLF). *J. Biol. Chem.* **288,** 19604–19613 (2013).
13. Altschul, S. F. *et al.* Gapped BLAST and PSI-BLAST: a new generation of protein database search programs. *Nucleic Acids Res.* **25,** 3389–3402 (1997).
14. Cooper, M. P. *et al.* Ku complex interacts with and stimulates the Werner protein. *Genes Dev.* **14,** 907–912 (2000).
15. Li, B. & Comai, L. Functional interaction between Ku and the werner syndrome protein in DNA end processing. *J. Biol. Chem.* **275,** 28349–28352 (2000).
16. Slavoff, S. A., Heo, J., Budnik, B. A., Hanakahi, L. A. & Saghatelian, A. A human short ORF-encoded peptide that stimulates DNA end joining. *J. Biol. Chem.* **C113,** 533968 (2014).
17. Harris, R. *et al.* The 3D solution structure of the C-terminal region of Ku86 (Ku86CTR). *J. Mol. Biol.* **335,** 573–582 (2004).
18. Rivera-Calzada, A., Spagnolo, L., Pearl, L. H. & Llorca, O. Structural model of full-length human Ku70-Ku80 heterodimer and its recognition of DNA and DNA-PKcs. *EMBO Rep.* **8,** 56–62 (2007).
19. Walker, J. R., Corpina, R. A. & Goldberg, J. Structure of the Ku heterodimer bound to DNA and its implications for double-strand break repair. *Nature* **412,** 607–614 (2001).
20. Rossi, M. L., Ghosh, A. K. & Bohr, V. A. Roles of Werner syndrome protein in protection of genome integrity. *DNA Repair (Amst)* **9,** 331–344 (2010).
21. Muftuoglu, M. *et al.* The clinical characteristics of Werner syndrome: molecular and biochemical diagnosis. *Hum. Genet.* **124,** 369–377 (2008).
22. Perry, J. J. P. *et al.* WRN exonuclease structure and molecular mechanism imply an editing role in DNA end processing. *Nat. Struct. Mol. Biol.* **13,** 414–422 (2006).
23. Chen, L. *et al.* WRN, the protein deficient in Werner syndrome, plays a critical structural role in optimizing DNA repair. *Aging Cell* **2,** 191–199 (2003).
24. Yannone, S. M. *et al.* Werner syndrome protein is regulated and phosphorylated by DNA-dependent protein kinase. *J. Biol. Chem.* **276,** 38242–38248 (2001).
25. Oshima, J., Huang, S., Pae, C., Campisi, J. & Schiestl, R. H. Lack of WRN results in extensive deletion at nonhomologous joining ends. *Cancer Res.* **62,** 547–551 (2002).
26. Li, B. & Comai, L. Requirements for the nucleolytic processing of DNA ends by the Werner syndrome protein-Ku70/80 complex. *J. Biol. Chem.* **276,** 9896–9902 (2001).
27. Agarwal, S. *et al.* Isolation, characterization, and genetic complementation of a cellular mutant resistant to retroviral infection. *Proc. Natl Acad. Sci. USA* **103,** 15933–15938 (2006).
28. Ochi, T. *et al.* DNA repair. PAXX, a paralog of XRCC4 and XLF, interacts with Ku to promote DNA double-strand break repair. *Science* **347,** 185–188 (2015).
29. Xing, M. *et al.* Interactome analysis identifies a new paralogue of XRCC4 in non-homologous end joining DNA repair pathway. *Nat. Commun.* **6,** 6233 (2015).
30. Yano, K.-I., Morotomi-Yano, K., Lee, K.-J. & Chen, D. J. Functional significance of the interaction with Ku in DNA double-strand break recognition of XLF. *FEBS Lett.* **585,** 841–846 (2011).
31. Andres, S. N. *et al.* A human XRCC4-XLF complex bridges DNA. *Nucleic Acids Res.* **40,** 1868–1878 (2012).
32. Cheng, W.-H. *et al.* Linkage between Werner syndrome protein and the Mre11 complex via Nbs1. *J. Biol. Chem.* **279,** 21169–21176 (2004).
33. Otterlei, M. *et al.* Werner syndrome protein participates in a complex with RAD51, RAD54, RAD54B and ATR in response to ICL-induced replication arrest. *J. Cell Sci.* **119,** 5137–5146 (2006).
34. Trego, K. S. *et al.* The DNA repair endonuclease XPG interacts directly and functionally with the WRN helicase defective in Werner syndrome. *Cell Cycle* **10,** 1998–2007 (2011).
35. Karmakar, P., Snowden, C. M., Ramsden, D. A. & Bohr, V. A. Ku heterodimer binds to both ends of the Werner protein and functional interaction occurs at the Werner N-terminus. *Nucleic Acids Res.* **30,** 3583–3591 (2002).
36. Orren, D. K. *et al.* A functional interaction of Ku with Werner exonuclease facilitates digestion of damaged DNA. *Nucleic Acids Res.* **29,** 1926–1934 (2001).
37. Fukuchi, K., Martin, G. M. & Monnat, R. J. Mutator phenotype of Werner syndrome is characterized by extensive deletions. *Proc. Natl Acad. Sci. USA* **86,** 5893–5897 (1989).
38. Wyllie, F. S. *et al.* Telomerase prevents the accelerated cell ageing of Werner syndrome fibroblasts. *Nat. Genet.* **24,** 16–17 (2000).
39. Kobbe, von C. *et al.* Colocalization, physical, and functional interaction between Werner and Bloom syndrome proteins. *J. Biol. Chem.* **277,** 22035–22044 (2002).
40. Löser, D. A. *et al.* Sensitization to radiation and alkylating agents by inhibitors of poly(ADP-ribose) polymerase is enhanced in cells deficient in DNA double-strand break repair. *Mol. Cancer Ther.* **9,** 1775–1787 (2010).
41. Rulten, S. L. *et al.* PARP-3 and APLF function together to accelerate nonhomologous end-joining. *Mol. Cell* **41,** 33–45 (2011).

Acknowledgements

This work was funded by a CR-UK Programme grants to K.W.C (C6563/A16771), L.H.P. and A.W.O. (C302/A14532).

Author contributions

S.L.R. and G.J.G. conducted all cell biology experiments, pull-down experiments from cell extracts, and exonuclease assays. K.D. and Z.K. contributed to early experiments in the study. R.A.-B. conducted FP assays and pull-down experiments with purified proteins. A.W.O. and L.H.P. supervised and designed the FP assay, biophysical and structural aspects of the project with R.A.-B., and K.W.C. supervised and designed the cell biology and biochemical aspects of the project with S.L.R. and G.J.G. K.W.C. conceived and managed the overall project. K.W.C. wrote the manuscript with input and editing from all of the authors.

Additional information

Supplementary Information accompanies this paper at http://www.nature.com/naturecommunications

Competing financial interests: The authors declare no competing financial interests.

How to cite this article: Grundy, G. J. *et al.* The Ku-binding motif is a conserved module for recruitment and stimulation of non-homologous end-joining proteins. *Nat. Commun.* 7:11242 doi: 10.1038/ncomms11242 (2016).

SCIENTIFIC REPORTS

OPEN

Large XPF-dependent deletions following misrepair of a DNA double strand break are prevented by the RNA:DNA helicase Senataxin

Received: 26 October 2017
Accepted: 9 February 2018
Published online: 01 March 2018

Julien Brustel[1], Zuzanna Kozik[1], Natalia Gromak[2], Velibor Savic[3,4] & Steve M. M. Sweet[1,5]

Deletions and chromosome re-arrangements are common features of cancer cells. We have established a new two-component system reporting on epigenetic silencing or deletion of an actively transcribed gene adjacent to a double-strand break (DSB). Unexpectedly, we find that a targeted DSB results in a minority (<10%) misrepair event of kilobase deletions encompassing the DSB site and transcribed gene. Deletions are reduced upon RNaseH1 over-expression and increased after knockdown of the DNA:RNA helicase Senataxin, implicating a role for DNA:RNA hybrids. We further demonstrate that the majority of these large deletions are dependent on the 3′ flap endonuclease XPF. DNA:RNA hybrids were detected by DNA:RNA immunoprecipitation in our system after DSB generation. These hybrids were reduced by RNaseH1 over-expression and increased by Senataxin knock-down, consistent with a role in deletions. Overall, these data are consistent with DNA:RNA hybrid generation at the site of a DSB, mis-processing of which results in genome instability in the form of large deletions.

DNA is the target of numerous genotoxic attacks that result in different types of damage. DNA double-strand breaks (DSBs) occur at low frequency, compared with single-strand breaks and other forms of DNA damage[1], however DSBs pose the risk of translocations and deletions and their repair is therefore essential to cell integrity. The majority of DSBs are repaired by either homologous recombination (HR) or non-homologous end-joining (NHEJ), with a smaller fraction repaired by non-canonical alternative end joining and single-strand annealing pathways[2–5]. In order to study the repair of a DSB at a known site in the genome, rare-cutting endonucleases such as I-SceI are employed[6]. DSBs generated by endonucleases have 'clean' ends, i.e. intact 5′-phosphate and 3′-hydroxyl groups, and are in most cases repaired without end-processing and associated deletions[7,8].

R-loops consist of an RNA:DNA hybrid, with the RNA displacing the non-transcribed DNA strand[9]. R-loops are a source of genome instability[9,10]. Indeed, collisions between replication or transcription machineries with R-loops can result in DSBs. It has recently been shown that Fanconi anemia proteins prevent instability resulting from replication fork progression and R-loops[11,12]. Furthermore, the displaced single-stranded DNA resulting from R-loop formation is susceptible to damage or processing. For example it has been shown that the transcription-coupled nucleotide excision repair (TC-NER) pathway, including flap endonucleases XPF/ERCC4 and XPG/ERCC5, can generate DSBs after R-loop formation[13]. Recently it has been demonstrated in *S. pombe* that DNA:RNA hybrids can occur in a DSB-dependent manner, associated with PolII recruitment to the DSB region[14]. These DNA:RNA hybrids are presumed to originate from transcription from the DSB and the displaced DNA strand is either resected or free-floating. DNA damage-dependent DNA:RNA hybrids have also been detected in human cells[15]. Transcription initiated from DSBs in human, *Drosophila* and plant cells has been reported[16–19].

[1]Genome Damage and Stability Centre (GDSC), University of Sussex, Brighton, BN1 9RQ, UK. [2]Sir William Dunn School of Pathology, University of Oxford, Oxford, South Parks Road, OX1 3RE, UK. [3]Brighton and Sussex Medical School (BSMS), University of Sussex, Brighton, BN1 9RQ, UK. [4]Present address: Horizon Discovery Ltd, 8100 Cambridge Research Park, Cambridge, CB25 9TL, UK. [5]Present address: NantOmics, 9600 Medical Center Drive, Rockville, MD, 20850, USA. Correspondence and requests for materials should be addressed to S.M.M.S. (email: stephen.sweet@nantomics.com)

To prevent the formation of R-loops, RNA-binding proteins interact with the RNA transcript, preventing it from invading the DNA duplex[10]. In parallel, topoisomerase enzymes resolve R-loop-promoting negative supercoiling, generated behind polymerases[10,20]. In addition, the cell possesses two different mechanisms to remove R-loops: the DNA-associated RNA can be specifically digested by enzymes of the RNase H family; the DNA:RNA hybrid can be dissociated by DNA:RNA helicases such as Senataxin, Aquarius and others[13,21,22]. Removing the protective function of Senataxin results in an increase in DNA strand breakage and γH2AX: these effects are reduced with overexpression of RNaseH1, implicating increased R-loops in the damage[23].

In this report, we have established a new system to study the deleterious consequences of DSBs utilising a proximal transcription unit as a marker. We show that targeted DSB induction and repair is correlated with an appearance of a subpopulation where the neighbouring gene is lost due to a large deletion. Knockdown of the DNA:RNA helicase Senataxin increases deletions, while RNaseH1 over-expression and knockdown of the 3′ flap endonuclease XPF/ERCC4 has the opposite effect. DNA:RNA hybrids were only detected after DSB induction. These results suggest a role of DNA:RNA hybrids in DSB processing, defects in which can result in genome instability in the form of large deletions.

Results

A two-component system to study the long-term effect of DNA damage on a neighbouring gene. To study the long-term and inherited effect of DNA DSB repair on gene expression, we established a two-component system allowing the quantification of long-term loss of gene expression close to DNA damage. The U2OS cell line was created by stable integration of two independent sequences (Fig. 1A and S1A). The first insertion is composed of a restriction endonuclease (RE) site array (containing recognition sites for the rare-cutter enzymes I-SceI, I-PpoI and I-AniY2) localized 2 kb upstream of an actively transcribed bicistronic cassette coding for the TetR and Neomycin-Resistance (NeoR) genes under control of the CMV promotor. The second component is a bicistronic cassette coding for a nuclear GFP and the Puromycin-Resistance (PuroR) genes under the control of a TetO cassette. The TetR protein, expressed by the first component, represses the GFP and the PuroR (Figure S1B). This system is reversible either by doxycycline disruption of the TetR:TetO interaction (Figure S1B) or by loss of the TetR protein.

To induce the site-specific DSB, cells are transiently transfected with a plasmid coding for a nuclear-localisation inducible form of I-SceI (I-SceI-GR-LBD)[24]: the nuclease is re-localized from the cytoplasm to the nucleus upon triamcinolone acetonide (TA) hormone treatment (2 hours) (Figure S1C). Nuclear entry is associated with activation of the local DNA damage response, as indicated by γH2AX and 53BP1 foci adjacent to the lacO array (Figure S1D). To evaluate the percentage of breaks occurring after I-SceI nuclear induction, the genomic DNA was extracted and the RE array amplified by qPCR, alongside a genomic control region. A DSB is associated with a lack of amplification of the RE array. Under our experimental conditions, around 35% of cells contain an unrepaired DSB at the I-SceI sites two hours after DSB induction (Figure S1E). This new two-component system allows the quantification and characterization of long-term loss of gene expression induced by a DSB.

A double-strand break induces loss of TetR expression. Strikingly, following site-specific DSB and repair, a new population of cells characterized by the expression of the bicistronic cassette GFP-IRES-PuroR appears. This GFP-positive population was quantified by fluorescence-activated cell sorting (FACS) analysis seven days after I-SceI-induced DSB (Fig. 1B), or by a clonogenic survival assay, following puromycin selection (Fig. 1C). It is important to note that this phenomenon appears to be independent of the chromosomal insertion location of the cassette, as this result has been reproduced in six different polyclonal cell lines (independently established) as well as in thirteen different monoclonal cell lines (Figure S1F,G). It is also independent of the LacO repeat sequences (Figure S1H). Furthermore, the appearance of this subpopulation is dependent on RE cutting: it was not observed in a cell line where the RE array was deleted (Figure S1F). We obtained similar results with other site-specific endonucleases: I-PpoI (Figure S2) and I-AniIY2 (Fig. 1D). Interestingly, the expression of the nickase mutant I-AniIY2-K227M which can induce only a single-strand break[25,26] was not associated with the appearance of this GFP-expressing subpopulation (Fig. 1D).

All together, these data suggest that after DSB and repair, a subset of cells (<10%) lose the expression of the neighbouring gene. This could be due to long-term silencing mediated by a change of the local chromatin state[27] or simply by a large deletion including the neighbouring gene[28,29].

A double-strand break induces large deletions. In order to investigate the mechanism of loss of expression after DSB, puromycin selection was employed to isolate the subpopulation of cells expressing GFP-IRES-PuroR after DNA damage. Antibiotic selection after DSB induction gave polyclonal cell lines characterized by expression of GFP and the absence of the TetR protein (Fig. 1E). Genomic DNA was extracted and sites proximal to the DSB site were compared to a distant control region by quantitative PCR (qPCR) assay (sites annotated in Fig. 1A)[30]. The qPCR signals obtained for each set of primers were normalized to the signal from the parental cell line, i.e. the cell line without DSB induction and puromycin selection. Interestingly, the results from three independently established polyclonal cell lines show a near complete loss of DNA template around the DSB site (Fig. 1F), demonstrating that the loss of TetR is caused predominantly by large deletions of at least 9 kb. To confirm this result, we also isolated clones showing GFP appearance after DSB by limited dilution, without antibiotic selection, into 96 well plates. After plating, GFP-expressing clones (≤1 per well) were selected through puromycin resistance and colonies derived from single cells (Figure S3A) were investigated for deletions. The qPCR assay was carried out as above and a similar pattern of loss of DNA was observed on 43 different GFP-positive clones (Figure S3B,C).

Our data indicate that we have established a new tool to study the mechanism behind large, DSB-dependent, deletions, in contrast to the majority of I-SceI systems which are only designed to monitor deletions up to a certain

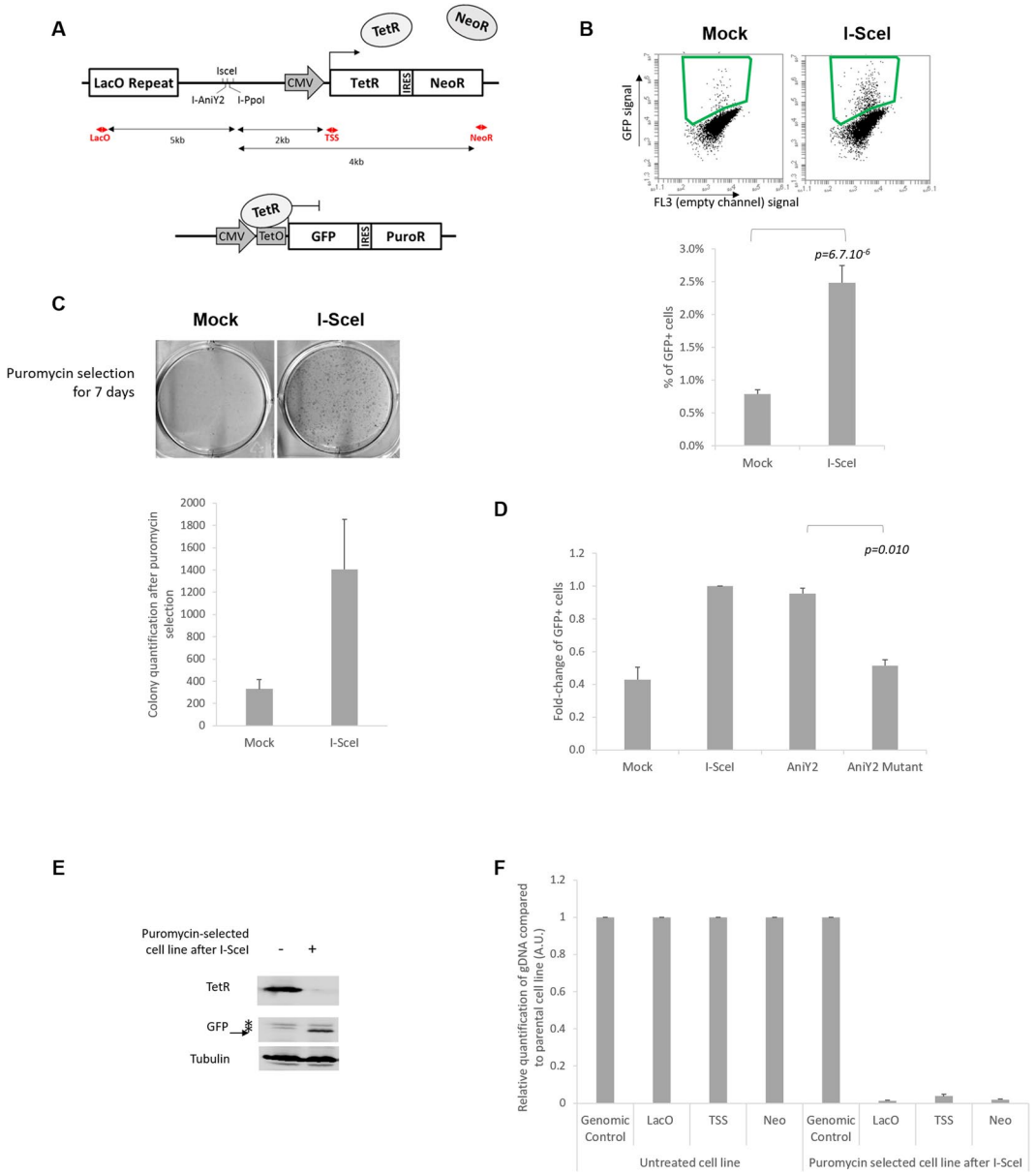

Figure 1. Two-component system to study large deletions following a DSB: (**A**) Schematic representation of the cell line, named U2OS-RE-TetR-GFP. Two components have been stably integrated in the U2OS cell line: the first (top panel) is composed of LacO repeats, an array with specific RE sites for I-SceI, I-PpoI and I-AniY2, and a TetR-IRES-NeoR gene under control of a CMV promotor; the second component (bottom panel) is a bicistronic GFP-IRES-PuroR cassette under the control of two TetO sites. The red arrows indicate the location of the primers used in F, and the black arrows the distance to the RE array. (**B**) Flow cytometry analysis of the GFP-positive subpopulation seven days after I-SceI induction. Top panel: representative dot plots of FACS analysis seven days after I-SceI induction in I-SceI-transfected or in control cells (Mock). The green square indicates the gate used to quantify the percentage of positive cells. Bottom panel: quantification of the percentage of GFP-positive cells seven day after I-SceI induction (n = 11 for a single U2OS-RE-TetR-GFP clone (mc#5). (**C**) Clonogenicity assay: 3 days after I-SceI induction cells were treated with puromycin for one week, then fixed and stained with brilliant blue (top panel). Bottom panel: ImageJ quantification of colony numbers (n = 3). (**D**) The loss of TetR expression is dependent on DSB: fold-change of GFP-positive cells induced by different RE, as indicated (I-SceI, I-AniY2 wt and the nickase mutant I-AniY2-K227M) normalised to I-SceI (n = 3). (**E**) Immunoblot analysis of a polyclonal cell line selected by puromycin treatment following I-SceI induction, with specific antibodies directed against TetR, GFP and tubulin (as a loading control). (**F**) Relative quantification of genomic DNA in 3 independently established puromycin-selected cell lines evaluated by qPCR using specific primers localized around the break site (as indicated in A), compared to a genomic control region (Genomic control #1) and normalized to the signal from untreated cells (n = 3). All *p*-values are from two-tailed, paired T-tests. All error bars represent the standard error of the mean, unless stated otherwise.

size, e.g. 500 bp from the I-SceI cut site[31]. Given that we never observed GFP-positive cells without a corresponding deletion, for brevity we refer to I-SceI-dependent increases in GFP-positive cells as 'I-SceI-dependent deletions'.

The DSB-induced large deletions are independent of ATM, ATR and DNA-PK activation and cell cycle stage at the time of damage. We first tested if this deletion requires activation of early damage response kinases. Using inhibitors of the kinases ATM, DNA-PK and ATR (Figure S4A,B) we did not observe significant changes in the levels of large deletions (inhibition from one hour before I-SceI nuclear localization until 24 h after damage induction for ATM and DNA-PK inhibitors or 4 h after for the ATR inhibitor; Fig. 2A). This observation suggests that the activation of these canonical kinases at the time of the DSB is not required for this phenomenon.

Secondly, we hypothesized that collision between DSB repair and DNA replication could be a cause of this genomic instability. To test the role of replication fork progression in the appearance of DSB-induced deletions, the I-SceI cutting was carried out in arrested cells. Cells were arrested either at the G1/S phase boundary by thymidine treatment, or in G2 phase by CDK1 inhibitor treatment (Fig. 2B). TA treatment of arrested cells allowed I-SceI nuclear localisation and, after 4 hours to allow damage and repair, cells were released. After seven days, we did not observe any significant change in the population of I-SceI-dependent GFP-positive cells that were arrested at the time of damage, compared to asynchronous cells (Fig. 2C). This suggests that the deletions are not restricted to cells undergoing DNA replication at the time of damage.

R-loop modulators alter DSB-induced deletion frequencies. R-loop structures, associated with transcription, have been identified as an important source of genetic instability[9,10]. We hypothesised that these molecular structures could be one of the causes of our deletions. To test the hypothesis that DNA:RNA hybrid are involved in DSB-dependent large deletions we employed three approaches. We first asked whether knockdown of Senataxin, an DNA:RNA helicase, capable of resolving DNA:RNA hybrid[21], would alter the level of deletions. After depletion of Senataxin I-SceI-dependent deletions are significantly increased (Fig. 3A, S5A,B). We next over-expressed RNaseH1 (Figure S5C), an enzyme capable of removing transcription-associated DNA:RNA hybrids[11,32,33]. This resulted in a strong (80%) reduction in I-SceI-dependent deletions (Fig. 3B, S5D). To control for possible confounding effects, we confirmed that RNaseH1 over-expression did not reduce the cutting efficiency of I-SceI (Figure S1E), or alter the level of transcription of the TetR-IRES-Neo gene (Figure S5E). Finally, we inhibited TopI to increase negative supercoiling behind the transcription complex, an approach that has previously been shown to increase R-loops[34,35]. TopI inhibition with camptothecin (CPT) induced a two-fold increase in DSB-associated deletions (Fig. 3C, S5C,F). In addition to increasing negative supercoiling, CPT-stabilised TopI-cleavage complexes lead to DSBs upon collision with the DNA replication machinery[36]. To control for a possible CPT damage-dependent effect on I-SceI-dependent deletions, we carried out TopI knockdown; this is expected to increase transcription-generated negative supercoiling in the absence of stabilised TopI-cleavage complex damage. TopI knockdown (Figure S5G) also resulted in an increase in DSB-dependent deletions, similar to that seen with CPT (compare Figure S5F and G).

R-loops are a 3-stranded structure: it has been shown that this structure can be a target for structure-specific endonucleases such as XPF/ERCC4 and XPG/ERCC5[13,37], as part of the transcription-coupled nucleotide excision repair (TC-NER) pathway. To study the influence of these endonucleases, XPF and XPG were depleted by siRNA in our DSB deletion reporter system. The depletion of XPF led to a significant decrease in deletions, suggesting a role for this endonuclease in the DSB deletion mechanism (Fig. 3D and S5A,H). By contrast, the depletion of XPG by siRNA did not prevent DSB-induced deletion (Fig. 3E and S5A,I). In addition, the depletion of ERCC8, a subunit of CSA[38], involved in the early stages of TC-NER upstream of XPF/XPG activity, did not affect the DSB-induced deletion (Figure S5J). These data suggest an NER-independent role of XPF, which also has roles in alternative error-prone and deletion associated DSB repair pathways, namely alternative end joining (Alt-NHEJ) and single strand annealing (SSA)[5,39–42].

Overall, the SETX, RNaseH1 and TopI data are consistent with a role for R-loops in our DSB-dependent deletions. We next asked whether inhibiting transcription reduced the level of DSB-dependent deletions and whether R-loops could be detected locally by DNA:RNA immunoprecipitation (DRIP).

Deletions are unaffected by modulation of transcription and R-loops are not detected by DRIP in undamaged cells. To test the influence of transcriptional activity on our phenotype, cells were first treated with an inhibitor of transcription elongation, DRB, one hour before and concomitant with DSB induction (2 h)[43]. This short and global transcription elongation inhibition did not significantly reduce the level of deletions (Fig. 4A; S6A).

Transient global inhibition of transcription is a crude tool: to more selectively study the potential role of local transcriptional activity on deletion, our two-component system was modified by integration of two TetO cassettes between the CMV promotor and the TetR-IRES-PuroR gene (Fig. 4B). This modification allows regulation of the gene transcription activity: in the presence of doxycycline, the interaction between TetR and the TetO cassette is prevented, and consequently the TetR gene is highly expressed, as is the GFP gene. In contrast, when doxycycline is removed, there is an auto-repression of TetR transcription by the TetR protein (schematic in Figure S6B, GFP expression in both condition Figure S6C); this results in a 60% decrease of TetR protein level (Fig. 4C) and a corresponding drop in mRNA level (Fig. 4D). This system allows deletion quantification with the same cell line, in a context of high (+Dox) or low (−Dox) transcription. It is important to note that for the high expression level condition, the doxycycline was removed 24 h after TA induction. This allows a high level of transcription during the break and the repair, and subsequent repression of GFP over the next six days, prior to scoring GFP-positive cells (Fig. 4B). Induction of DSBs in the context of high or low transcription is equally efficient (Figure S6D) and led to similar levels of deletions (Fig. 4E). This result suggests that the level of expression of the neighbouring gene does not play a major role in misrepair deletions, in concordance with the literature[44].

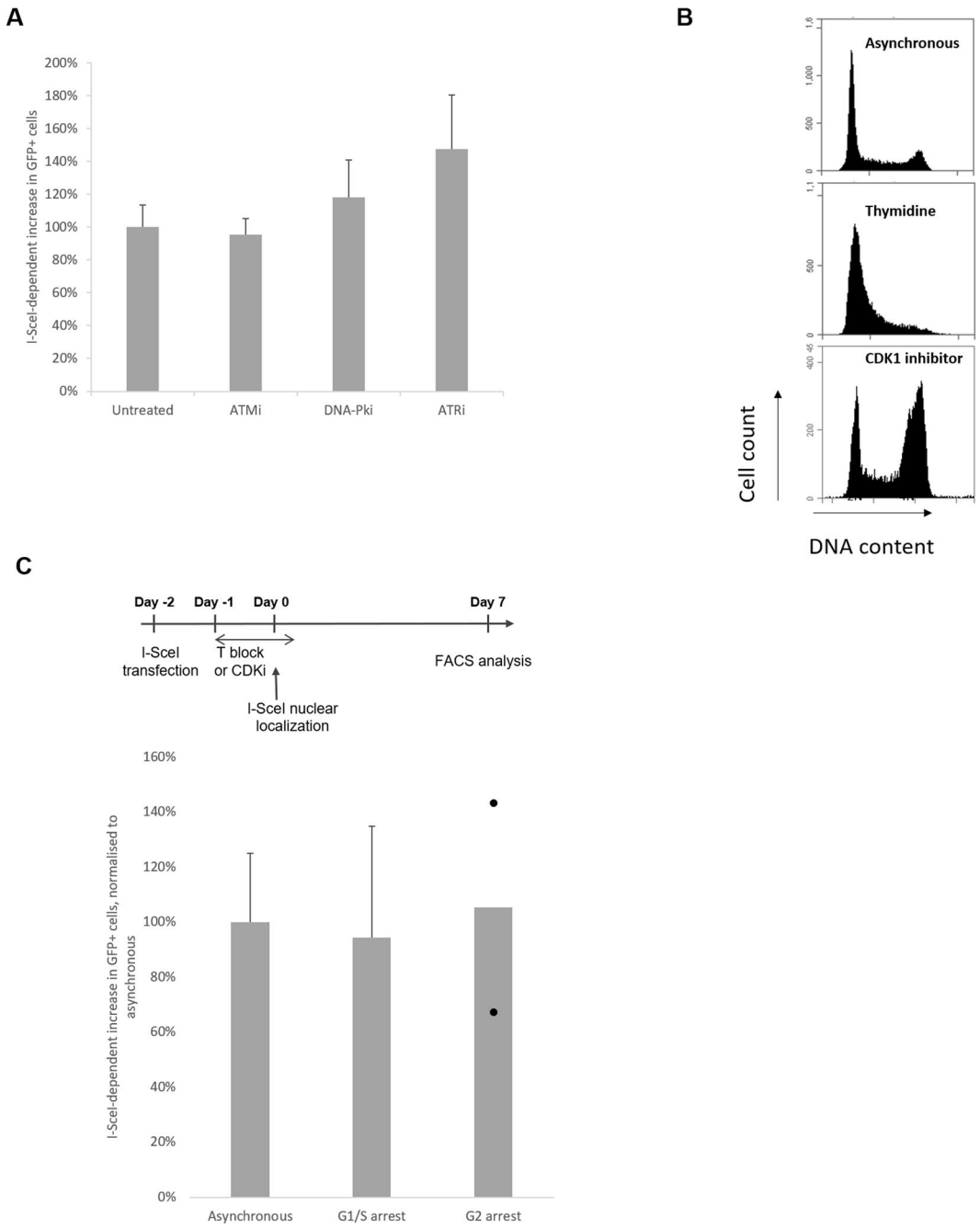

Figure 2. The DSB-induced deletions are independent of ATM, ATR and DNA-PK activation and DNA replication at the time of damage: (**A**) I-SceI-dependent increase in deletions in cells treated with or without inhibitors from 1 h before DSB induction (and until 24 h after for ATM and DNA-PK inhibitors, 4 h after for ATRi), normalised to control cells (n = 3 for ATMi and DNA-PKi, n = 4 for ATRi). (**B**) Cell cycle profile quantifying PI-stained DNA of proliferating cells (top panel), thymidine-arrested cells (G1/S; middle panel) or CDK1-I-treated cells (RO-3306; G2; bottom panel); (**C**) DSB-induced deletions are independent of cell-cycle stage at the time of damage. Top panel: experimental design to study the impact of cell-cycle stage at the time of DSB induction on deletion: after I-SceI transfection, cells are arrested with 18 h treatment with the drug pre-I-SceI induction, as indicated. During the arrest, I-SceI nuclear localisation is induced. Cells are released 4 hours after the induction. Bottom panel: I-SceI-dependent increase in deletions normalised to asynchronous cells (asynchronous n = 5; G1/S arrested (thymidine) n = 3; G2 arrested (CDKi) n = 2, each dot represents one experiment).

To evaluate the presence of DNA:RNA hybrids at the highly expressed TetR-IRES-NeoR gene, immunoprecipitation with the DNA:RNA specific antibody S9.6 followed by qPCR analysis (DRIP-qPCR) was performed (cell line in Fig. 1). While we detect a specific R-loop signal at the APOE positive control locus[12,33], we did not detect

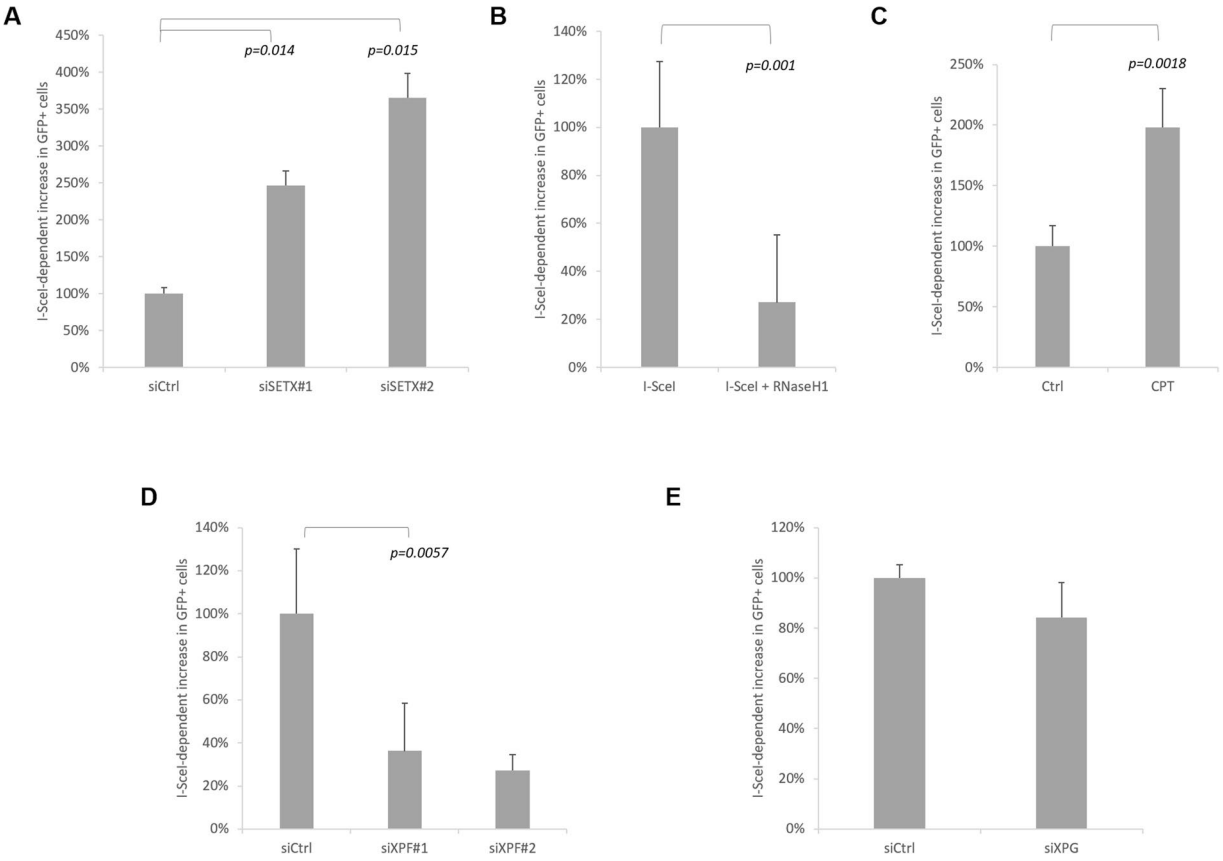

Figure 3. R-loop modulators alter DSB-induced deletion frequencies: (**A**) Knockdown of the helicase Senataxin increases the level of DSB-induced deletions. I-SceI-dependent increase in deletions in Senataxin-depleted cells normalised to siCtrl cells (n = 3). (**B**) RNAseH1 expression prevents DSB-induced deletions: I-SceI-dependent increase in deletions in RNaseH1-expressing cells normalised to control cells (n = 4). (**C**) Camptothecin (CPT) treatment increases DSB-induced deletions: I-SceI-dependent increase in deletions in CPT treated cells normalised to control cells (n = 7). (**D**,**E**) Knockdown of the endonucleases XPF/ERCC4 (**D**) and XPG/ERCC5 (**E**). I-SceI-dependent increase in deletions four days after I-SceI induction in XPF/ERCC4-depleted cells (siXPF) normalised to control cells (siCtrl) (n = 6 for siXPF#1; n = 3 for siXPF#2, siXPG). Knockdown efficiencies shown in Figure S5A.

R-loop levels above background at the TetR gene (background estimated by treatment with RNaseH *in vitro*, pre-IP; Fig. 4F). Based on the transcription-level independent nature of the deletions, and the lack of detectable R-loops, we conclude that canonical R-loop processing is not responsible for the DSB-dependent deletions.

DNA:RNA hybrids occur at the break site. We next considered the possibility that DNA:RNA hybrids were generated as a consequence of local transcription occurring after the I-SceI DSB. Two hours after I-SceI induction, cells were collected and DRIP was performed. We detected an increase in DNA:RNA signal after I-SceI cleavage adjacent to the I-SceI array and at the TetR gene but not at the intergenic control region or APOE gene (Fig. 5A). The DSB-dependent DRIP signal was increased further after Senataxin knockdown (Fig. 5A, IsceI + siSETX condition). By contrast, DNA:RNA hybrids at the break site were prevented by RNaseH1 over-expression (Fig. 5A, IsceI + RNaseH1 condition). These trends, while not statistically significant, due to large variability in the DRIP signal, are consistent with a role for DSB-dependent DNA:RNA hybrids in the deletion process.

Discussion

In this report, we have established a cell line to study DSB-induced large deletions based on the loss of a gene in the proximity of an RE array. The fact that TetR sequence was missing in all the clones analysed (Figure S3) strongly suggests that silencing due to epigenetic changes, as previously described for a system utilising a promoter known to undergo DNA methylation-dependent silencing[27], does not account for the loss of TetR expression in our system. Large deletions induced by I-SceI have previously been observed[28,29]. However the requirement for selection to observe these large deletions usually precludes an estimate of frequency and the mechanism resulting in these large deletions has not been determined[28,29]. The gain of GFP-expression associated with deletions in our system allows the quantification of rare events. We observe the frequency of DSB-induced large deletions to vary between 0.3% and 22% of transfected cells, across nineteen independently integrated cell lines (Figure S1F; taking into account background, I-SceI independent loss and transfection efficiency of ~35%

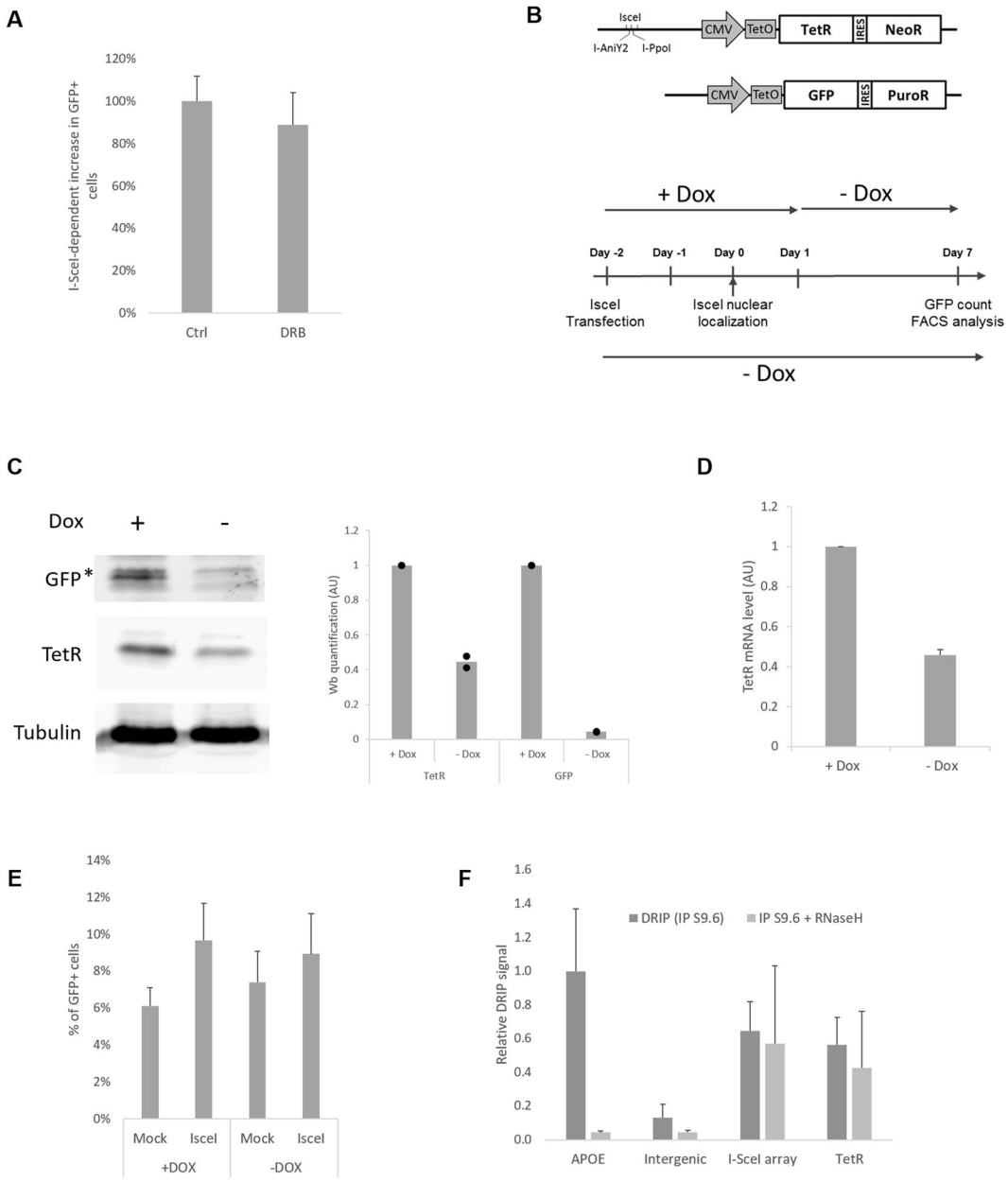

Figure 4. DSB-dependent deletions are unaffected by modulation of transcription: (**A**) I-SceI-dependent increase in deletions seven days after I-SceI induction in cells treated with the transcription inhibitor DRB compared to control cells (n = 7). (**B**) Schematic representation of the transcription regulation system. Upper panel: two TetO cassettes are inserted in front of TetR-IRES-NeoR. Lower panel: experimental design to study deletions in a context of high (+Dox) or low (−Dox) transcriptional activity, indicating I-SceI transfection and induction, doxycycline treatment and FACS analysis. (**C**) Immunoblot analysis of the cell line treated with or without doxycycline for six days, using antibodies against TetR, GFP and tubulin (as a loading control) (left panel). Right panel: relative quantification (n = 2). (**D**) TetR mRNA quantification by RT-qPCR, normalized to GAPDH mRNA level (n = 4). (**E**) Percentage of GFP-positive cells after I-SceI induction in high (+Dox) or low (−Dox) transcriptional activity context (n = 3). (**F**) DRIP-qPCR analysis of DNA:RNA hybrid structure at TetR-IRES-NeoR gene in undamaged cells (no I-SceI induction). Primers targeting the APOE gene are used as a positive control for R loop formation, and primers specific to an intergenic region are used as a negative control. The values, corresponding to the signal following S9.6 IP of isolated DNA (dark grey bar) or of *in vitro* RNaseH-treated DNA (clear grey bar), are represented as fold increase normalised to the APOE positive control (n = 7).

(Figure S1D). These frequencies are not per DSB: I-SceI will cut repeatedly, until a misrepair event removes the cleavage motif, therefore the rate of deletion per DSB will be lower than the rate per transfected cell.

LacO repeats, in the presence of LacI repressor, have been shown to act as fragile sites, generating DSBs[45]. In our system we are confident that the lacO repeats are not playing a significant role in the DSB-induced deletion

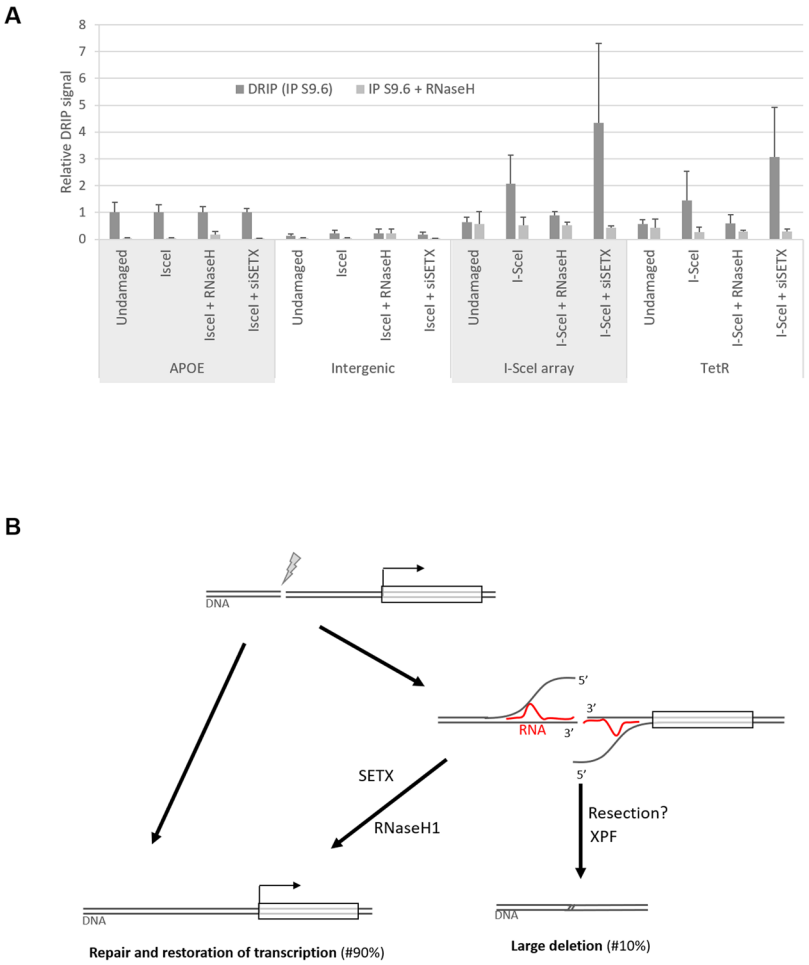

Figure 5. DNA:RNA hybrids occur at the break site: (**A**) DRIP-qPCR analysis of DNA:RNA hybrid structure at TetR-IRES-NeoR gene in undamaged cells or after DSB induction. Primers targeting the APOE gene are used as a positive control for R loop formation, and primers specific to an intergenic region are used as a negative control. The values, corresponding to the signal following S9.6 IP of isolated DNA (dark grey bar) or of *in vitro* RNaseH-treated DNA (clear grey bar), are represented as fold increase normalised to the APOE positive control (Undamaged, n = 7 (from Fig. 4(F)); I-SceI, n = 7; I-SceI + RNaseH1, n = 3; I-SceI + siSETX, n = 4). (**B**) Model of DSB-induced large deletion dependent on a DNA:RNA hybrid associated with transcription from the DSB: Generally a DSB occurring in close proximity to a gene is efficiently repaired, either by HR or NHEJ, and the transcription program is not affected over the long term (left side). Alternatively (right side), transcription and DNA:RNA hybrid generation displaces the 5′ DNA strand. Senataxin is shown reversing this, promoting correct repair. ERCC1/XPF is required to cleave the displaced 3′ DNA strands.

for three reasons: (i) our experiments are carried out in the absence of LacI protein (with the exception of the co-localization experiment with γH2AX and 53BP1 in S1C); (ii) we inserted only 59 LacO repeats, fewer than the 256 repeats shown to generate a fragile site[45]; (iii) the DSB-induced large deletions are independent of replication fork progression at the time of I-SceI cleavage (Fig. 2C). Furthermore, we generated a cell line without LacO repeats and found the frequency of DSB-induced deletions to be unchanged compared to the original cell line, as expected (Figure S1H).

The detection of DNA:RNA hybrid formation at a DSB is in agreement with a recent observation in fission yeast[14], and laser-stripe damage-dependent accumulation of DNA:RNA hybrid in mammalian cells[15]. DNA:RNA hybrids formation at the break site could be explained by the previously documented local initiation of transcription in response to the DSB[16–18]. The lack of effect of transient DRB treatment on the observed deletions may indicate a delayed or non-canonical transcriptional activity at the DSB: DRB acts by inhibiting the CDK9-dependent transition of PolII from initiation to elongation[46]. Ohle *et al*. found that efficient removal of RNA:DNA hybrids was required for homologous recombination repair and viability after DSB induction in fission yeast[14]. This shared link between RNA:DNA hybrid removal and DSB repair is intriguing, however while controlled levels of RNA:DNA hybrids in the *S. pombe* system appear to promote repair, it is unclear what physiological role RNA:DNA hybrids play in the repair of our I-SceI DSB.

A DSB flanked by homologous sequences may undergo single-strand annealing (SSA), including XPF cleavage, generating a deletion[5,47]. The speculative model we propose involves mis-repair of a targeted DSB associated

with DNA:RNA hybrid processing. Transcription from the DSB end will displace the 5′ end of the DNA, promoting SSA. SSA entails resection of the 5′ end until homologous sequences are revealed. This is followed by annealing and subsequent cleavage of 3′ overhangs by XPF to complete the deletion (Fig. 5B). Alternatively, Senataxin can reverse the DNA:RNA hybrid at an early stage, before resection occurs. While the model involving SSA has the advantage of linking XPF activity with a DSB-linked deletion, we have no evidence that SSA occurs in our system, and other models are possible. For instance, it is possible that the subset of breaks generating a large deletion are repaired slowly[48,49], and loss of Senataxin may be destabilising DNA replication forks[50], promoting deletions at these sites of repair. Genetic instability is a common feature of most types of cancer[51]. Deletions of between 1–100 kb are a signature of BRCA1 and 2-negative breast cancers[52]. Deletions may in most cases be tolerable to a cell, as indicated by the surprisingly high proportion of post-mitotic neurons containing Mb-scale deletions, revealed by single-cell sequencing[53]. Nonetheless, loss of DNA repair or tumour-suppressor genes will contribute to the development of further genetic instability or cancer.

Altogether, data from our two-component system suggests DSB-induced DNA:RNA hybrid formation may be mechanistically associated with a minor mis-repair pathway generating large deletions.

Experimental Procedures

Plasmids. The plasmid pcDNA4-GFP-IRES-PuroR was generated by insertion of the bicistronic cassette GFP-IRES-PuroR (amplified from pGIPZ-GFP(nls)-IRES-PURO (Murray lab, University of Sussex)) in pcDNA4-CMV-TetO (Invitrogen).

The plasmid pIRES-LacOR-REsites-TetR-IRES-NeoR was generated in three steps: (i) TetR gene (amplified from pcDNA6 (Invitrogen) was inserted in pIRESneo3 (Clontech) (ii) The LacO repeats were integrated: 16 LacO repeats (amplified from the plasmid Holo16 (Sweet lab, University of Sussex)) and 43 LacO repeats (from PLAU43[54]) were inserted in pIRESneo3-TetR (iii) The RE sites array containing specific sequence for I-SceI (3 times), AniI-Y2 and Ppo-I (synthesized by Invitrogen) was integrated in the plasmid obtained at step (ii).

The pIRES-LacOR-REsites-TetO-TetR-IRES-Neo was generated by integration of two TetO cassettes (generated by Thermofisher) in pIRES-LacOR-REsites-TetR-IRES-Neo.

All primer sequences and cloning details are available on request.

Other plasmids used in this study are pdsRED-I-SceI[24], pCVL-HA.NLS.I-AniIY2wt, pCVL-HA.NLS.I-AniIY2-K227M[25], pBABE-IPpoI (Puromycin resistant gene was removed.), pCMV6-AC-RNaseH1 (O. Wells, University of Sussex), pLacI-GFP (Savic Lab, University of Sussex).

Cell culture, DNA transfection, establishment of stable cell lines, siRNA transfection and drug treatment. U2OS cells were obtained from ATCC, tested for mycoplasma contamination and grown in Dulbecco's modified Eagle's medium (Gibco) supplemented with 10% foetal bovine serum (PAN biotech), Penicillin/Streptomycin (Corning) and L-Glutamin (Gibco). All plasmid transfections utilised the Jet-Pei transfection reagent (Polyethylenimine 25000, PolyScience) as previously described[30].

The "*U2OS RE-Sites TetR GFP*" cell line was generated in two steps: (i) stably integration of pcDNA4-GFP-IRES-Puromycin through transfection followed by a Puromycin selection (Sigma, 2.5 μg/ml) then (ii) stably integration of HpaI-linearized pIRES-LacOR-REsites-TetR-IRES-Neo through G418 selection (200 μg/ml). Monoclonal cell lines were generated by limited dilution.

Cells expressing PpoI were established after transduction with retroviral vectors. Virus production and cell infection were performed as previously described[30].

Smart-pool siRNA (siCtrl, siSETX#1, siTOP1, siXPF#1, siERCC8) and individual siRNA (siSETX#2, siXFP#2, siXPG) were ordered from Dharmacon (see Supp. Table 1: references and sequences). All siRNA transfections were done with Lipofectamine RNAimax (Invitrogen) following the manufacturer's instructions.

The chemical compounds (and their final concentrations) used in this study were: ATMi: Ku-55933 (Abcam; 10 μM), ATRi: VE-822 (STRATECH SCIENTIFIC; 10 μM), Camptothecin (Sigma; 5 μM), CDK1i: RO-3306 (Sigma; 10 μM) DNA-PKi: NU-7026 (Abcam; 20 μM), Doxycycline cyclate (Sigma; 2 μg/ml), 4OH-Tamoxifene (Sigma; 25 μM), Triamcinolone acetonide, TA (Sigma; 1 μM), and thymidine (Sigma; 2.5 mM).

Fluorescence-activated cell sorting (FACS) analysis. For quantification of GFP-positive cell populations, cells were trypsinized and re-suspended in complete media. Samples were run on a FACS-accuri (Beckton Dickinson) and data analysed with the BD accuri software. Briefly single cells were gated, first on their size (FLH) and their granularity (SSC) to exclude debris, and then on the linearity between FLH-H and FLH-A signal to exclude doublets. GFP-positive cells were quantified on the signal read on FL1 detector (GFP) vs FL3 (empty channel).

For cell-cycle analysis, cells were fixed with cold ethanol 70%, washed with PBS and re-suspended in PBS containing propidium iodide (PI, Sigma, 5 ug/ml) and RNAse A (Sigma, 50 ug/ml) overnight at 4 °C. Samples were run and single cell gated as described above. PI signal (correlating with DNA content) was read on FL2 detector.

DSB-dependent deletion reporter system. The "*U2OS RE-Sites TetR GFP*" cell lines were seeded at 70% confluency and transfected with I-SceI-GR-LBD plasmid, as described above. DMEM media phenol-free (Gibco) with charcoal-stripped serum (Gibco) was used to prevent premature nuclear-localisation of I-SceI-GR-LBD. Two days after transfection, cells were treated with the drug triamcinolone acetonide (TA) (Sigma, 1 μM) for 2 to 4 hours. After TA induction, cell were kept in culture, collected at different days (Day 4 and 7), and GFP-positive cells quantified by FACS, as described above. For the analysis of the GFP-positive subpopulation, data can be represented either by the raw percentage of GFP-positive cells, or by the fold increase of the GFP subpopulation normalised to undamaged cells $\left(Fold\ increase = \frac{[\%\ of\ GFP\ sample\ ]}{[average\ \%\ of\ GFP\ untreated\ condition]}\right)$, or by percentage of

GFP-positive cells with subtraction of background levels (mock), normalised to a reference condition, $\left(\mathrm{I-SceI-dependent\ increase\ in\ GFP+cells} = \frac{([\%\ \mathrm{of\ GFP\,I-SceI\ sample}]-[\%\ \mathrm{of\ GFPMock\ sample}])}{(\mathrm{average\ of}\,[[\%\ \mathrm{of\ GFP\,I-SceI\ reference}]-[\%\ \mathrm{of\ GFPMock\ reference}]])} * 100\right)$.

siRNA depletion in DSB-induced deletion reporter system: cells were first transfected with siRNA overnight (as described above), the day after, cells were washed and transfected with I-SceI-GR-LBD, 48 h later TA induction was as described above. The quantification of a GFP-positive subpopulation was as described above.

Kinase inhibition (ATM, ATR, DNA-PK): 48 h after I-SceI transfection, cells were pre-treated for 1 h with the chemical inhibitor (as described above), then I-SceI nuclear localisation was induced (as described above) in the presence of the inhibitor and the inhibitor was maintained for 24 h after I-SceI nuclear localisation induction (TA). The GFP-positive subpopulation was analysed as described above.

CPT: 48 h after I-SceI transfection, cells were pre-treated for 1 h with the drug (as described above), then I-SceI nuclear-localisation was induced (as described above) in the presence of the inhibitor. After induction of I-SceI nuclear localisation, cells were washed and inhibitor removed. The GFP-positive subpopulation was analysed as described above.

Replication assay: 24 h after I-SceI transfection, thymidine was added (2.5 mM) for 18 h, and I-SceI nuclear localisation was induced (as described above) in the presence of thymidine. Then cells were washed 3 time with PBS and released. The GFP-positive subpopulation was analysed as described above. Cell cycle arrest and release were monitored by FACS as described above.

Immunoblot analysis. Proteins were resolved by Mini Gel SDS-PAGE (Bio-Rad system) and transferred to nitrocellulose membrane (GE Healthcare) as previously described[30]. All the blocking and antibody incubations were done in TBS −0.2% Tween-20 5% BSA (Fisher). The following primary antibodies were used: anti-53BP1 (1:1000, Millipore), anti-ATM (1:1000, Abcam), anti-Chk1-phS317 (1:1000, Cell Signalling Technology), anti-GFP (1:1000), anti-HA (1:1000, Sigma), anti-H2AX-P (1:1000, Abcam), anti-p53 (1:1000, DO-1, SantaCruz), anti-p53-phS15 (1:1000, NEB), anti-RNaseH1 (1:1000, Abcam), anti-TetR (1:1000, TETO2, MoBiTec), anti-tubulin (1:5000, Abcam), and appropriate HRP-conjugated secondary antibodies were used: anti-mouse (1:10000, Cell Signalling Technology), anti-rabbit (1:10000, Cell Signalling Technology) and anti-rat (1:10000, Abcam). Immuno-reactive bands were detected by chemoluminescence induced by Supersignal reagent and detected with the ImageQuant LAS 4000 machine (GE Healthcare). Quantification was performed using ImageJ.

DNA extraction, RNA extraction, qPCR and RT qPCR. Total genomic DNA was isolated using the DNeasy kit (Qiagen). Total RNA was extracted using the RNeasy kit (Qiagen). Reverse transcription was performed by using the Super Script III reverse transcriptase (Invitrogen) and random hexamers (Invitrogen).

The list of primers used for qPCR are available in Supp. Table 2. Quantitative PCR was performed with goTaq qPCR master mix (Promega) and Mx3005-P qPCR machine (Stratagene). The data was analysed with MX-Pro software (Stratagene).

Immunofluorescence microscopy. Images of GFP-positive live cells were acquired with the AMG-Evos inverted microscope. Immunofluorescence microscopy was performed as described[30], with antibody dilutions: HA (1/500, Sigma), γH2AX (1/500, Millipore), GFP (1/500, Roche). Samples were examined either with a microscope (Zeiss) equipped with a 10X, a 40X dry objective and a 100X oil immersion objective and a Hamamatsu Orca ER camera, or a confocal microscope (Olympus IX71) equipped with a 40X, 60X and 100X oil immersion objective and a CoolSNAP HQ2 camera. Pictures were analysed with ImageJ software.

Clonogenicity assay. Two days after I-SceI induction, cells were counted and plated in 6 well plates (200 000 per well). One day after plating GFP+/PuroR clones were selected through puromycin treatment (2.5 µg/ml) for one week. Then the cells were fixed with formaldehyde 3% (FISHER) and stained with Brilliant blue 0.5% (Sigma) in PBS overnight. After PBS washing, drying and scanning, the clones were counted by ImageJ.

DNA:RNA hybrid Immunoprecipitation (DRIP-qPCR). After treatment as indicated, cells were collected, and lysed with the lysis buffer (200 mM NaCl, 10 mM Tris pH7.5, 2 mM EDTA, 0.2% SDS and proteinase K 20 µg/ml (Sigma P2308) at 56 °C for 3 h. Then, DNA and associated RNA are precipitated by addition of one volume of isopropanol, washed with ethanol 70%, and resuspended in TE buffer (Tris-HCl pH 7.5, 0.5 mM EDTA). After sonication to obtain DNA fragments less than 800 bp, 50 µg of DNA was treated with recombinant RNaseH (NEB) and used as a negative control. 50 µg of digested DNA was immuno-precipitated with 3 µg of S9.6 antibody[12] (Kerafast) coupled to IgG magnetic beads (Invitrogen). Washing utilised five buffers (W1: Tris pH8 10 mM, KCl 150 mM, NP40, 0.5%, EDTA 1 mM; W2: Tris pH8 10 mM, NaCl 100 mM, NaDoc 0.1%, TritonX100 0.5%; W3: Tris pH8 10 mM, NaCl 400 mM, NaDoc 0.1%, TritonX100 0.5%; W3b: Tris pH8 10 mM, NaCl 500 mM, NaDoc 0.1%, TritonX100 0.5%; W4: Tris pH8 10 mM, LiCl 250 mM, NaDoc 0.5%, NP40 0.5%, EDTA 1 mM; W5: Tris pH8 10 mM, EDTA 1 mM). After washing, DNA:RNA hybrid associated structures are eluted with SDS buffer and the DNA purified with a Nucleospin Extract II kit (MACHEREY NAGEL). qPCR analyses of DRIP DNAs were performed as described above. The amount of DNA in DRIP samples was extrapolated from analysis of DNA before immunoprecipitation (input) and values were represented as fold increase compared to the positive control.

DNA break efficiency assay. The U2OS I-SceI TetR GFP cell line was transfected with I-SceI GR-LBD plasmid and its nuclear localisation was induced as described above. Two hours after induction, total genomic DNA was isolated, as described above. For quantification of I-SceI induced cutting efficiency, qPCR was performed (as described above), with amplification across the I-SceI sites. The data was normalised to an unconnected genomic

control locus (Genomic control #2), and then expressed as a ratio relative to the undamaged sample. Primer sequences available in Supp. Table 2.

Statistics. All *p*-values are from two-tailed, paired T-tests. All error bars represent the standard error of the mean, unless stated otherwise.

Data availability. All datasets generated during and/or analysed during the current study are available from the corresponding author on reasonable request.

References

1. Mehta, A. & Haber, J. E. Sources of DNA Double-Strand Breaks and Models of Recombinational DNA Repair. *Cold Spring Harbor Perspectives in Biology* **6** (2014).
2. Chang, H. H. Y., Pannunzio, N. R., Adachi, N. & Lieber, M. R. Non-homologous DNA end joining and alternative pathways to double-strand break repair. *Nat Rev Mol Cell Biol* **18**, 495–506 (2017).
3. Shanbhag, N. M., Rafalska-Metcalf, I. U., Balane-Bolivar, C., Janicki, S. M. & Greenberg, R. A. ATM-Dependent Chromatin Changes Silence Transcription In cis to DNA Double-Strand Breaks. *Cell* **141**, 970–981 (2010).
4. Sancar, A., Lindsey-Boltz, L. A., Ünsal-Kaçmaz, K. & Linn, S. Molecular Mechanisms of Mammalian DNA Repair and the DNA Damage Checkpoints. *Anne. Rev. Biochem.* **73**, 39–85 (2004).
5. Bhargava, R., Onyango, D. O. & Stark, J. M. Regulation of Single-Strand Annealing and its Role in Genome Maintenance. *Trends in Genetics* **32**, 566–575 (2016).
6. Plessis, A., Perrin, A., Haber, J. E. & Dujon, B. Site-specific recombination determined by I-SceI, a mitochondrial group I intron-encoded endonuclease expressed in the yeast nucleus. *Genetics* **130**, 451–460 (1992).
7. Liang, F., Han, M., Romanienko, P. J. & Jasin, M. Homology-directed repair is a major double-strand break repair pathway in mammalian cells. *Proceedings of the National Academy of Sciences* **95**, 5172–5177 (1998).
8. Moynahan, M. E. & Jasin, M. Loss of heterozygosity induced by a chromosomal double-strand break. *Proceedings of the National Academy of Sciences* **94**, 8988–8993 (1997).
9. Sollier, J. & Cimprich, K. A. Breaking bad: R-loops and genome integrity. *Trends in Cell Biology* **25**, 514–522 (2015).
10. Aguilera, A. & García-Muse, T. R Loops: From Transcription Byproducts to Threats to Genome Stability. *Molecular Cell* **46**, 115–124 (2012).
11. Schwab, R. A. *et al*. The Fanconi Anemia Pathway Maintains Genome Stability by Coordinating Replication and Transcription. *Molecular Cell* **60**, 351–361 (2015).
12. García-Rubio, M. L. *et al*. The Fanconi Anemia Pathway Protects Genome Integrity from R-loops. *PLoS Genet* **11**, e1005674 (2015).
13. Sollier, J. *et al*. Transcription-Coupled Nucleotide Excision Repair Factors Promote R-Loop-Induced Genome Instability. *Molecular Cell* **56**, 777–785 (2014).
14. Ohle, C. *et al*. Transient RNA-DNA Hybrids Are Required for Efficient Double-Strand Break Repair. *Cell* **167**, 1001–1013.e1007 (2016).
15. Britton, S. *et al*. DNA damage triggers SAF-A and RNA biogenesis factors exclusion from chromatin coupled to R-loops removal. *Nucleic Acids Research* **42**, 9047–9062 (2014).
16. Francia, S. *et al*. Site-specific DICER and DROSHA RNA products control the DNA-damage response. *Nature* **488**, 231–235 (2012).
17. Francia, S., Cabrini, M., Matti, V., Oldani, A. & d'Adda di Fagagna, F. DICER, DROSHA and DNA damage response RNAs are necessary for the secondary recruitment of DNA damage response factors. *Journal of Cell Science* **129**, 1468–1476 (2016).
18. Wei, W. *et al*. A Role for Small RNAs in DNA Double-Strand Break Repair. *Cell* **149**, 101–112 (2012).
19. Michalik, K. M., Böttcher, R. & Förstemann, K. A small RNA response at DNA ends in Drosophila. *Nucleic Acids Research* **40**, 9596–9603 (2012).
20. Liu, L. F. & Wang, J. C. Supercoiling of the DNA template during transcription. *Proceedings of the National Academy of Sciences* **84**, 7024–7027 (1987).
21. Skourti-Stathaki, K., Proudfoot, Nicholas, J. & Gromak, N. Human Senataxin Resolves RNA/DNA Hybrids Formed at Transcriptional Pause Sites to Promote Xrn2-Dependent Termination. *Molecular Cell* **42**, 794–805 (2011).
22. Mischo, H. E. *et al*. Yeast Sen1 Helicase Protects the Genome from Transcription-Associated Instability. *Molecular Cell* **41**, 21–32 (2011).
23. Hatchi, E. *et al*. BRCA1 Recruitment to Transcriptional Pause Sites Is Required for R-Loop-Driven DNA Damage Repair. *Molecular Cell* **57**, 636–647 (2015).
24. Soutoglou, E. *et al*. Positional stability of single double-strand breaks in mammalian cells. *Nature Cell Biology* **9**, 675–682 (2007).
25. Certo, M. T. *et al*. Tracking genome engineering outcome at individual DNA breakpoints. *Nat Meth* **8**, 671–676 (2011).
26. McConnell Smith, A. *et al*. Generation of a nicking enzyme that stimulates site-specific gene conversion from the I-AniI LAGLIDADG homing endonuclease. *Proceedings of the National Academy of Sciences* **106**, 5099–5104 (2009).
27. O'Hagan, H. M., Mohammad, H. P. & Baylin, S. B. Double Strand Breaks Can Initiate Gene Silencing and SIRT1-Dependent Onset of DNA Methylation in an Exogenous Promoter CpG Island. *PLoS Genet* **4**, e1000155 (2008).
28. Honma, M. *et al*. Deletion, rearrangement, and gene conversion; genetic consequences of chromosomal double-strand breaks in human cells. *Environmental and Molecular Mutagenesis* **42**, 288–298 (2003).
29. Varga, T. & Aplan, P. D. Chromosomal aberrations induced by double strand DNA breaks. *DNA Repair* **4**, 1038–1046 (2005).
30. Tardat, M. *et al*. The histone H4 Lys 20 methyltransferase PR-Set7 regulates replication origins in mammalian cells. *Nat Cell Biol* **12**, 1086–1093 (2010).
31. Soong, C.-P. *et al*. Development of a novel method to create double-strand break repair fingerprints using next-generation sequencing. *DNA Repair* **26**, 44–53 (2015).
32. Chon, H. *et al*. RNase H2 roles in genome integrity revealed by unlinking its activities. *Nucleic Acids Research* **41**, 3130–3143 (2013).
33. Bhatia, V. *et al*. BRCA2 prevents R-loop accumulation and associates with TREX-2 mRNA export factor PCID2. *Nature* **511**, 362–365 (2014).
34. El Hage, A., French, S. L., Beyer, A. L. & Tollervey, D. Loss of Topoisomerase I leads to R-loop-mediated transcriptional blocks during ribosomal RNA synthesis. *Genes & Development* **24**, 1546–1558 (2010).
35. Sordet, O. *et al*. Ataxia telangiectasia mutated activation by transcription- and topoisomerase I-induced DNA double-strand breaks. *EMBO reports* **10**, 887–893 (2009).
36. Ryan, A. J., Squires, S., Strutt, H. L. & Johnson, R. T. Camptothecin cytotoxicity in mammalian cells is associated with the induction of persistent double strand breaks in replicating DNA. *Nucleic Acids Research* **19**, 3295–3300 (1991).
37. Tian, M. & Alt, F. W. Transcription-induced Cleavage of Immunoglobulin Switch Regions by Nucleotide Excision Repair Nucleases *in Vitro*. *Journal of Biological Chemistry* **275**, 24163–24172 (2000).
38. Henning, K. A. *et al*. TheCockayne syndrome group A gene encodes a WD repeat protein that interacts with CSB protein and a subunit of RNA polymerase II TFIIH. *Cell* **82**, 555–564.
39. Ciccia, A., McDonald, N. & West, S. C. Structural and Functional Relationships of the XPF/MUS81 Family of Proteins. *Anne. Rev. Biochem.* **77**, 259–287 (2008).

40. Bennardo, N., Cheng, A., Huang, N. & Stark, J. M. Alternative-NHEJ Is a Mechanistically Distinct Pathway of Mammalian Chromosome Break Repair. *PLoS Genet* **4**, e1000110 (2008).
41. Ma, J.-L., Kim, E. M., Haber, J. E. & Lee, S. E. Yeast Mre11 and Rad1 Proteins Define a Ku-Independent Mechanism To Repair Double-Strand Breaks Lacking Overlapping End Sequences. *Molecular and Cellular Biology* **23**, 8820–8828 (2003).
42. Ahmad, A. *et al*. ERCC1-XPF Endonuclease Facilitates DNA Double-Strand Break Repair. *Molecular and Cellular Biology* **28**, 5082–5092 (2008).
43. Yankulov, K., Yamashita, K., Roy, R., Egly, J.-M. & Bentley, D. L. The Transcriptional Elongation Inhibitor 5,6-Dichloro-1-β-D-ribofuranosylbenzimidazole Inhibits Transcription Factor IIH-associated Protein Kinase. *Journal of Biological Chemistry* **270**, 23922–23925 (1995).
44. Allen, C., Miller, C. A. & Nickoloff, J. A. The mutagenic potential of a single DNA double-strand break in a mammalian chromosome is not influenced by transcription. *DNA Repair* **2**, 1147–1156 (2003).
45. Jacome, A. & Fernandez-Capetillo, O. Lac operator repeats generate a traceable fragile site in mammalian cells. *EMBO reports* **12**, 1032–1038 (2011).
46. Wang, S. & Fischer, P. M. Cyclin-dependent kinase 9: a key transcriptional regulator and potential drug target in oncology, virology and cardiology. *Trends in Pharmacological Sciences* **29**, 302–313 (2008).
47. Al-Minawi, A. Z., Saleh-Gohari, N. & Helleday, T. The ERCC1/XPF endonuclease is required for efficient single-strand annealing and gene conversion in mammalian cells. *Nucleic Acids Research* **36**, 1–9 (2008).
48. Goodarzi, A. A. *et al*. ATM Signaling Facilitates Repair of DNA Double-Strand Breaks Associated with Heterochromatin. *Molecular Cell* **31**, 167–177 (2008).
49. Löbrich, M. & Jeggo, P. A Process of Resection-Dependent Nonhomologous End Joining Involving the Goddess Artemis. *Trends in Biochemical Sciences* **42**, 690–701.
50. Alzu, A. *et al*. Senataxin Associates with Replication Forks to Protect Fork Integrity across RNA-Polymerase-II-Transcribed Genes. *Cell* **151**, 835–846 (2012).
51. Hanahan, D. & Weinberg, R. A. Hallmarks of Cancer: The Next Generation. *Cell* **144**, 646–674 (2011).
52. Nik-Zainal, S. *et al*. Landscape of somatic mutations in 560 breast cancer whole-genome sequences. *Nature* (2016).
53. McConnell, M. J. *et al*. Mosaic Copy Number Variation in Human Neurons. *Science* **342**, 632–637 (2013).
54. Lau, I. F. *et al*. Spatial and temporal organization of replicating Escherichia coli chromosomes. *Molecular Microbiology* **49**, 731–743 (2003).

Acknowledgements

We thank J.A. Downs (Institute for Cancer Research) for helpful discussions during the project and for critical reading of the manuscript, K. Caldecott, S. Rulten, H. Hochegger, N. Hegarat, A. Macpherson, J. Murray, O. Wells, P. Jeggo, M. O'Driscoll (University of Sussex), E. Julien, C Sardet (INSERM, Université de Montpellier) for providing reagents and members of SMMS lab and VS lab for discussions. NG is supported by the Royal Society University Research Fellowship. This work was supported by an MRC career development award G1100257.

Author Contributions

S.M.M.S. and V.S. conceptualized the two component system; J.B., V.S. and S.M.M.S. designed the experiments and analysed the data; J.B. carried out all experiments and statistical analyses; J.B. and Z.K. carried out the cutting efficiency assay; N.G. assisted with DRIP experiments; J.B. and S.M.M.S. wrote the manuscript. All authors reviewed the manuscript.

Additional Information

Supplementary information accompanies this paper at https://doi.org/10.1038/s41598-018-21806-y.

Competing Interests: The authors declare no competing interests.

Publisher's note: Springer Nature remains neutral with regard to jurisdictional claims in published maps and institutional affiliations.